AN *IN VITRO* STUDY OF THE PROPERTIES OF GICs WITH BIOACTIVE BIOMATERIAL MODIFICATION

Riaan Mulder

A dissertation submitted in the fulfilment of the requirements for the degree of PhD in Paediatric Dentistry, University of the Western Cape

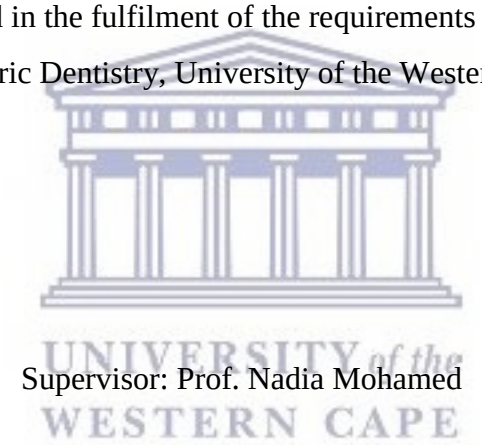

Supervisor: Prof. Nadia Mohamed

2019

AN *IN VITRO* STUDY OF THE PROPERTIES OF GICs WITH BIOACTIVE BIOMATERIAL MODIFICATION

R Mulder

KEYWORDS

Glass Ionomer Restorative Cement

Hand-mix

Capsule

Biomaterial modification

Chitosan

Nanodiamonds

Physical properties

Ion release

Gradient weight potential percentage

Streptococcus Mutans

Cell viability

Neutral Sodium Fluoride

ABSTRACT

AN *IN VITRO* STUDY OF THE PROPERTIES OF GICs WITH BIOACTIVE BIOMATERIAL MODIFICATION

PhD Candidate: R Mulder

Dissertation tendered for the degree: PhD Paediatric Dentistry

Department of Orthodontics and Paediatric Dentistry, University of the Western Cape.

Introduction

The fluoride release and chemical adherence to tooth structure remain the most desirable features of glass ionomer restorative cements (GICs). Although the physical properties for multi-surface restorations are well-defined, even with the introduction of newer GICs not all demands have been met. Yet, increased use of GICs will only be possible if clinicians change their perceptions of the low survival rate of GICs. The lower clinical success rate of GICs is partly due to the marginal integrity and wear over time, which has often been recorded in the literature as restoration failure. The current, well-established restorative options for the primary dentition are Resin Modified Glass Ionomers (RMGICs) and Compomer resins. There is a paradigm shift towards materials that are more biologically favourable. Areas of research for dental materials include antibacterial properties in conjunction with ion release to maintain healthy restored teeth. If a GIC can provide adequate physical properties with the inclusion of the aforementioned features, GICs might become a more viable permanent restorative solution.

Current research

There is no research on GICs where bioactive biomaterials such as chitosan or nanodiamonds have been incorporated into the powder of the GICs. In addition, the cell viability of modified GICs has not been assessed (3T3 cell-line). The interaction with ion release and fluoride absorbance is also unknown. The interaction with *Streptococcus mutans* growth has been

established for chitosan incorporated into the liquid (Petri *et al*., 2007; Ibrahim *et al*., 2017) of GICs, but not for nanodiamonds. Likewise, moduli of elasticity, flexural strength and micro-hardness have been studied for modified GICs where chitosan has been incorporated into the liquid of GICs (Petri *et al*., 2007). However, GICs modified with nanodiamonds have not been studied.

Aim of this research

To evaluate the effect on the physical- and bioactive properties of GICs, when a commercially available biomaterial is added to the powder phase of GICs.

Objectives of this investigation

- To investigate various clinical techniques to improve the surface hardness of a commercial GIC.
- To investigate the accuracy of three hand-mix commercial GIC powder/liquid ratios.
- To investigate the accuracy of the powder/liquid ratios of capsulated GICs and a carbomer.
- To investigate and compare the effect of the bioactive modifications on the various physical properties of three modified commercial GICs i.e. elemental analysis (gradient weight potential percentage), surface hardness, water sorption, water contact angle, surface tension, compressive strength, proportional limit and surface roughness.
- To investigate and compare the effect that the bioactive modifications have to further induce the bioactivity of the three modified commercial GICs i.e. ion release, neutral sodium fluoride absorbance, tooth/restoration ion-diffusion zone, microbial effect (*S. mutans*) and cell viability (3T3 cell-line).

Materials

Three modified commercial hand-mix GICs were used: FN: Fuji IX GP (*GC Corp*), KU: Ketac Universal (*3M ESPE*) and RSC: Riva Self Cure (*SDI Ltd*) modified with two biomaterials namely chitosan (*Merck*) and nanodiamonds (*PlasmaChem*).

Conclusions

The recommended powder liquid ratio of the manufacture should be used for nanodiamond and chitosan modifications in order to obtain the largest compressive strength. Overall, incorporation of chitosan (in its commercially available powder form) into restorative materials is not suitable due to the low physical properties. The modified nano-chitosan modifications (Senthil Kumar *et al*., 2017) and chitosan modification within the liquid (Petri *et al*., 2007; Ibrahim *et al*., 2017) is a more viable technique for incorporating chitosan into GICs.

Overall the 5% nanodiamond modifications presented with physical properties close to that of the control and for that reason the 10% nanodiamond (10%ND) modifications are not a suitable modification. The cell viability was increased and the biofilm integrity disrupted with GICs that contained a 5% nanodiamond (5%ND) modification. A 5% nanodiamond addition presented with ion release (aluminium, lanthanum, silicon, sodium and strontium) into the de-ionised water that increased significantly for most ions in KU and RSC, but displayed no significant difference with FN. The fluoride release as assessed with TISAB III in the GIC-diluents of the DMEM liquid was improved for KU and RSC with a 5% nanodiamond modification but no significant effect was noted for the fluoride release of FN. The ion movement into healthy dentine for the 5% nanodiamond-modified materials presented with the highest weight percentages of each ion for all three GIC materials (FN, KU and RSC). The surface fluoride percentage increased for the 5% nanodiamond GICs, but

did not increase the surface fluoride percentage significantly in relation to their control materials.

There is no perfect material but there are however advantages to using FN and RSC depending on the aspects considered and the intended rationale for use. Based on the following categories: physical properties, all the ions released, cell viability compared to the control 3T3 cells, *S. mutans* biofilm disruption and the ion movement from the GIC to the dentine, it is the conclusion of the author that only Ketac Universal modified with 5% nanodiamond particles (KU5%ND) is a viable option as a restorative material. This 5% nanodiamond modification of KU meets all the criteria for an improvement in the above-mentioned categories. The only current disadvantage would be the greyer appearance of the material and whether that is acceptable to the patient or not.

2019

DECLARATION

I declare that "AN *IN VITRO* STUDY OF THE PROPERTIES OF GICs WITH BIOACTIVE BIOMATERIAL MODIFICATION" is my own work. It has not been submitted before for any degree or examination at any other university and that all the sources I have used or quoted have been indicated and acknowledged as complete references. I declare that I have no competitive interest in any of the companies that manufacture any of the materials used in this study. No shares and or stocks are held nor will I have any financial gain or loss with the publication of any manuscript and articles pertaining to this research.

The research in this dissertation was funded by Dr. Riaan Mulder, Prof. Nadia Mohamed, Dentistry Development Foundation Trust (DDFT) (The South African Dental Association) and the UWC postgraduate research office with Senate Research Funds.

Riaan Mulder

Student number: 2382119 Date: April 2019

Signed: 

ACKNOWLEDGEMENTS

I would like to thank my supervisor Prof. Nadia Mohamed for her continued support and guidance for the completion of this dissertation.

I would like to acknowledge the staff at The University of Stellenbosch Central Analytical Facilities (US CAF). The ICP-MS and SEM-EDS analysis was completed at US-CAF. The technical assistance and guidance with the use of the specialised equipment was essential for these projects.

To my wife, Dr. Suné Mulder van Staden – your unwavering support and encouragement has been a pillar of strength and the cornerstone that gave me focus to complete this dissertation.

CONTENTS

FIGURES

AN *IN VITRO* STUDY OF THE PROPERTIES OF GICS WITH BIOACTIVE BIOMATERIAL MODIFICATION	
	Page numbers:
CHAPTER 2	
2.1. Vickers Hardness indentations at a minimum of 500µm apart	9
2.2. Average Vickers Hardness with Standard Deviation (SD) for each technique	10
2.3. Log_e (Surface Hardness) of the six techniques	11
CHAPTER 3	
3.1. Flowchart of capsule distribution for specimen preparations	24
3.2. Capsule systems with a posterior plunger	24
3.3. Capsules with an external diaphragm	25
3.4. Chamber and plunger with liquid visible	27
3.5. Dried liquid chamber under 1.75 magnification	28
3.6. No weight change due to evaporation of the liquid after 3 minutes	29
3.7. Powder/liquid ratio distribution of two batches with ± 10% ratio of the manufacturers' recommendations	34
3.8. Mean Vickers Hardness values of batches for days 1, 7 and 180	38
3.9. Mean compression strength values (MPa) of batches for days 1, 7, 180	39
CHAPTER 4	
4.1. Powder, liquid and PLR observations achieved by the operator	59

TABLES

AN *IN VITRO* STUDY OF THE PROPERTIES OF GICS WITH BIOACTIVE BIOMATERIAL MODIFICATION

TABLES

CHAPTER 1

INTRODUCTION TO DISSERTATION

1.1 Introduction

This dissertation will explore various aspects of Glass Ionomer Restorative Cements (GICs). The known literature will be used as a departure point to explore the modification of three commercially available GICs. The GICs are well known. Fuji IX GP hand-mix (*GC Corp, Tokyo, Japan*) has a comprehensive base of established research and has been used extensively as an atraumatic restorative treatment (ART) restoration. Ketac Universal hand-mix (*3M ESPE, Seefeld, Germany*) is a relatively newly launched GIC with expanded clinical indications and nearly no publications in the literature. There are currently two articles available for Ketac Universal. Both articles explored the increase of physical properties with different light emitting diode curing lights. The last GIC that will be explored is Riva Self Cure hand-mix (*SDI Limited, Australia*) - one of the most popular GICs in South African private dental practices. There are a few studies on Riva Self Cure, but most only explore the physical properties. With the continuous search to improve or enhance the various properties of GICs, this dissertation explored two GIC modifications. The modifications were formulated by either substituting a 5% or a 10% weight per weight percentage of the powder phase of the GICs. The two modifications added to the GICs were commercially available chitosan (*Merck, 75% deacethylation, item 448877, CAS: 9012-76-4*) and nanodiamonds (*PlasmaChem, item: PL-D-G01, CAS: 7782-40-3*). This dissertation is comprised of various studies which are reported on in separate chapters. Due to the depth and volume of information, these individual chapters are presented in an article style, each with its own abstract, introduction, methods, results, discussion, conclusion and reference list. Presenting the dissertation in an article format allowed for a more structured

approach. The sequence of the chapters has been arranged based on the progression of knowledge from the chitosan and nanodiamond literature, as well as the discoveries made during the course of this dissertation. The sequence presented in the dissertation is essential to building the relevant knowledge base, as the investigations become more integrated and follow on from the preceding chapters. Some concepts may be repeated to provide context to a particular study and to fully explain the results. The final chapter will draw on the key findings and conclusions from each chapter to round off the dissertation and highlight where future research would be required.

1.2. General GIC introduction and orientation of the chapters

Glass ionomer cements (GICs) are multi-component materials consisting of a powder and a liquid phase that requires the clinician to mix the components in a prescribed ratio (Chapter 4). The setting process of a conventional GIC is characterised by an interaction between a weak acid (polyacrylic acid) and a glass powder (fluoro-alumina-silicate glass) upon mixing. Some attempts have been made to increase the surface hardness of GICs. All the articles explore merely two or three techniques and the true effect on the GICs are difficult to conclude. This dissertation explored all the best techniques and the most practical combinations that a clinician could use in their general dental practice for various clinical scenarios on the same material (Chapter 2). Both the manipulation techniques and the material modifications present with interaction of the powder and the liquid, directly influencing the acid–base reaction. Upon ion release from the glass particle, “salt bridge formation” occurs over a period of minutes to form the immature GIC restoration. Simultaneously, the ion exchange interaction with the chitosan or nanodiamonds occurs (Chapter 6). The maturity of the restoration during water sorption plays a role in the physical properties as well as with the interaction with various ions (aluminium,

fluoride, lanthanum, silicon, sodium and strontium) (Chapter 6) that commence upon contact with moisture (Chapter 7). The most important ion to dentists, namely fluoride, is also released (Chapter 8). Fluoride adsorption into the restoration after professional neutral sodium fluoride application was also explored in this dissertation (Chapter 12). GICs interact readily with tooth structure and the ion exchange with the dentine of primary teeth. This interaction gives rise to the formation of the inter-diffusion zone (Chapter 11). The antibacterial activities of GICs have been established in the literature and are further explored with *Streptococcus Mutans* (Chapter 10). The biocompatibility is an important aspect of dental materials, especially since GICs are considered as biomaterials. The addition of chitosan and the nanodiamonds showed increased GIC activity and it was therefore important to explore the cell viability of 3T3 Balb/c mouse fibroblasts (3T3) to the diluents made from the GICs that were aged in growth medium (Chapter 9).

The conclusion (Chapter 13) summarises the key results and provides evidence for the potential modifications of the three commercial GICs with chitosan and/or nanodiamonds.

CHAPTER 2

TECHNIQUES THAT ALTER THE SURFACE HARDNESS OF A GLASS IONOMER RESTORATIVE CEMENTS

2.1. Abstract

Background and objective: The purpose of this *in vitro* study was to compare the effect of different manipulation techniques on the surface hardness of a glass ionomer restorative cements (GICs).

Methods: Six techniques were evaluated with ten samples prepared (per technique) using a Teflon mould under laboratory conditions (n = 60). The six techniques evaluated in this study included: Standard set as the control, finger pressure set, electronic piezo producing a high frequency set, air piezo producing a low frequency set, heat set achieved with a curing light and the last technique was a combination of electronic piezo followed by heat set. The surface micro-hardness was measured in Vickers Hardness (VH) with a diamond indenter.

Results: The average surface hardness for the standard set was 49.5VH. No statistical differences were demonstrated when the means of each test group were compared for finger pressure set (49.2VH) or the air piezo set (48.49VH) with standard set. The electronic piezo (54.21VH) and the heat set (57.5VH) had an increased mean surface micro-hardness when compared to the other techniques. Heat set had the highest surface hardness demonstrating a significant statistical difference when compared with standard set, finger pressure set, air piezo set as well as the combination of electronic piezo followed by heat set ($p < 0.05$).

Conclusion: The surface hardness of the glass ionomer in this study can be predictably improved by applying the heat set technique. A command set can be achieved with the electronic piezo or

the air piezo; however, the surface hardness will only increase with the use of the electronic piezo.

Keywords: Glass ionomer cement, electronic piezo, air piezo, curing light, finger press, Vickers Hardness.

Abbreviations and acronyms:

Ap: Air piezo producing a low frequency set

Ep: Electronic piezo producing a high frequency set

Ep & Ht: Electronic piezo followed by heat set

Fpre: Finger pressure set

GICs: Glass ionomer restorative cements

Ht: Heat set achieved with curing light

LED: Light emitting diode

RMGI: Resin Modified Glass Ionomer restorative material

SD: Standard Deviation

Sts: Standard set

VH: Vickers Hardness measurement for the surface micro-hardness

2.2. Graphical abstract

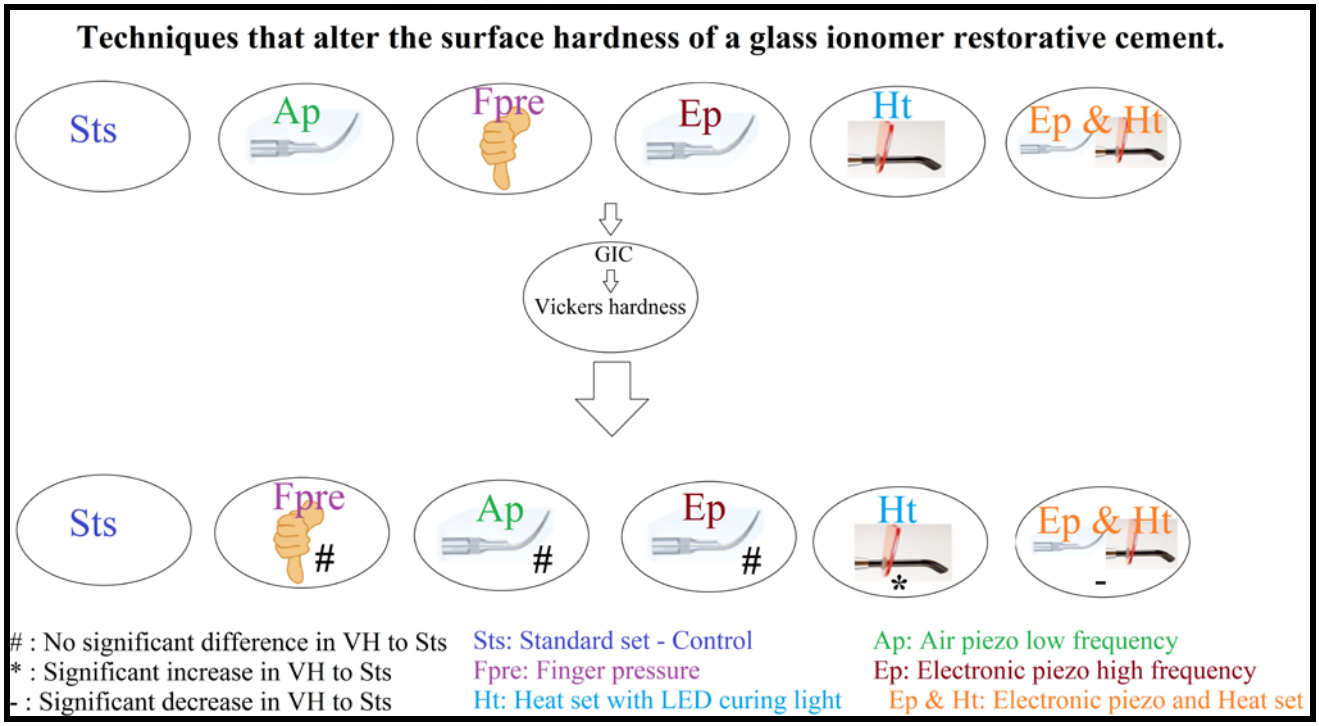

2.3. Introduction

Glass ionomer restorative materials (GICs) are advantageous in paediatric restorative dentistry. The main advantages of GICs include fluoride release up to 50µg/cm^2 and a chemical adhesion to the tooth structure (Berg, 2002; Hübel and Mejàre, 2003; Khoroushi *et al.*, 2012). The drawback of GICs is the relatively poorer mechanical properties, compared to resin composites and resin modified glass ionomer materials (RMGIs).

Numerous techniques have been evaluated in the literature to improve the properties of GICs. Pre-warming the material capsules of RMGIs for 90 seconds at 40°C is one technique that has been found to be effective in increasing the surface hardness. This technique however, had no effect on the shear bond strength to enamel or dentine (Khoroushi *et al*., 2012). This technique of pre-heating the capsule was not included in the present *in vitro* study, since very few clinicians have access to a heating device like the Therma-Flo™ composite warmer (*Vista dental, USA)* or an appropriate water bath. The literature on ultrasonic excitation and heat application to GICs showed a significant increase in the mechanical properties compared with the control materials (Towler, 2001; Kleverlaan *et al*., 2004; Qvist *et al.*, 2004; Twomey *et al.*, 2004; O'Brien *et al*., 2010; Menne-Happ and Ilie, 2013). Heat generated from a curing light and the ultrasonic vibrations from an electronic piezo have been reported to enhance the surface hardness of GICs (Baloch *et al*., 2010). All the techniques evaluated in the literature achieved improved material properties due to the manipulation of the salt bridge formation (Kleverlaan *et al*., 2004; Algera *et al.*, 2005; Barata *et al*., 2008; Gorseta *et al*., 2012). Early application of heat after the placement of the restoration has been shown to improve the mechanical properties (Towler, 2001; Kleverlaan *et al*., 2004). The application of the electronic piezo resulted in an improved marginal adaptation of the GIC to the cavity wall. In turn, a lower microleakage for the GICs exposed to electronic piezo set versus the control group (Gorseta *et al.*, 2012).

Due to the varied methodologies used in the literature related to the *in vitro* manipulation of GICs, a comparison of available techniques under similar conditions was required. The objective of this study was therefore to compare the changes in the surface hardness of a GIC after using different, readily available techniques from the literature as a basis for the experiments.

2.4. Materials and methods

2.4.1. Specimen preparation

Ten samples of Chemfil Rock (*Dentsply Sirona, Konstanz, Germany*) prepared from capsules (n = 60) were produced for each of the six techniques (test groups). Chemfil Rock was chosen as the material for assessment, as no reported literature investigated the increase of the surface hardness for this material. A Teflon mould with a cylindrical space of 6±1mm in height and 4±1mm in diameter was used. Each of the moulds were randomly assigned to a test group and marked accordingly on the underside. Various steps followed in the study methodology were based on published literature. The Chemfil Rock capsules were kept at room temperature and the moulds were stored in a temperature-controlled incubator (37±1°C) prior to testing (Menne-Happ and Ilie, 2013). A single experienced operator performed the application of the six techniques at a constant room temperature (23±1°C) with a relative humidity of 50±5% (Twomey *et al*., 2001; ISO, 2007). Chemfil Rock was mixed for 15 seconds at 4000-4500 oscillations per minute in an amalgamator (in accordance with manufacturer's instructions). Hand instruments were used to remove the excess GIC from the mould that was slightly overfilled. A thin layer of petroleum jelly was applied to the back of the electronic and air piezo tips to prevent adherence to the GIC when in contact with the piezo tip. A LED curing light (*Bonart ART-L3, Taipei City, Taiwan*) served as the heat source and was applied at a distance of 1mm from the surface of the GIC. A red cap eye shield was modified to a 1mm thickness (*Bonart LD5003-001, Taipei City, Taiwan*).

2.4.2. Six techniques / test groups

Control group (Sts): Setting time of 3 minutes in accordance with the manufacturer's instructions.

Electronic piezo high frequency set (Ep): An electric piezo (*Bonart ART-PB3, Taipei City, Taiwan*) was set at 29 kHz for 15 seconds (Fagundesa *et al*., 2006) without water coolant (Coldebella *et al.*, 2010).

Air piezo low frequency set (Ap): The air piezo (*Kavo Sonic flex 2000N, tip no 7, Biberach an der Riss, Germany*) was set at 6 kHz for 15 seconds (Fagundesa *et al*., 2006) without water coolant (Coldebella *et al*., 2010).

Heat set (Ht): The heat was provided by a LED curing light (*Bonart ART-L3, Taipei City, Taiwan*) at 1450±50 mW/cm² for 40 seconds (Gorseta *et al*., 2012).

Electronic piezo combined with heat set (Ep & Ht): The electronic piezo (29 kHz) was applied to the surface of the GIC for 15 seconds without water coolant. This was followed immediately by heat provided by the LED curing light at 1450±50 mW/cm² for 40 seconds.

Finger pressure set (Fpre): The mould was placed on a desktop analytical balance (*Ohaus Precision Standard, Model TS400D, Ohaus Corp, Florham Park, N.J, USA*) and 3kg±100g (0.238kgf/mm² = 2.3411N/mm²) of pressure was applied with a latex-free gloved thumb covered with a thin layer of petroleum jelly. The pressure was maintained on the sample for two minutes immediately after placement on a desktop analytical balance to ensure a standardised pressure during the entire setting process.

After completion of each technique, a layer of petroleum jelly was placed on the surface of the specimens to protect them against dehydration and moisture contamination during the initial setting (Hattab and Amin, 2001). Each specimen was left for six minutes after the initial

technique application (as per the manufacturer's instructions) and then completely submerged in distilled water at 37±1°C.

2.4.3. Surface micro-hardness analysis

Forty-eight hours after the specimens were submerged in distilled water; the surface of the sample was treated with 2500 grit wet silicon carbide paper, followed by 4000 grit (*3M, Massachusetts, USA*). The polishing ensured an adjustment to the surface of ±100µm, as measured with a micrometer prior to the surface hardness evaluation. This simulates the restoration polishing that would occur in the clinical setting (Menne-Happ and Ilie, 2013). A second and blinded operator completed the surface hardness evaluation with a Vickers Hardness (VH) diamond indenter (*Zwick-Roell durometer, ZHV1/2 Micro-Vickers, Italy*) set at HV0.5 (load of 500gf) and a dwell time of ten seconds. Three Vickers Hardness (VH) measurements were recorded 500µm apart on each sample to obtain a mean value per specimen (Figure 2.1).

Figure 2.1: Vickers Hardness indentations at a minimum of 500µm apart

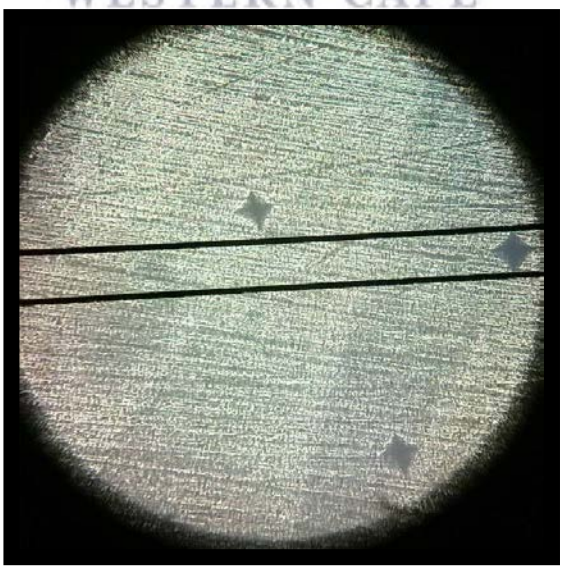

The mean values from the ten samples per test group (O'Brein *et al.*, 2010; Ellakuria *et al.*, 2003; Yap *et al.*, 2003) were calculated with the standard deviation (Figure 2.2). The mean values of the Vickers Hardness measurements were converted to Logarithms$_e$ and these values were noted as "Log$_e$ (Surface Hardness)" for each test group. ANOVA t-tests were carried out for statistical comparisons of the various values obtained from the Log$_e$ (Surface Hardness), at a significance level of $p < 0.05$ (Figure 2.3).

2.5. Results

Only the Ht technique demonstrated an increased surface hardness that was significantly different when compared to the control (Sts). No significant difference was noted when applying the Fpre (49.2VH) and the Ap (48.49VH) techniques in comparison to Sts. Furthermore, the average of the VH of the Ep & Ht (39.73VH) technique was statistically lower than Sts (49.5VH). The technique that resulted in the greatest surface hardness was Ht technique (57.5VH). The second best technique was Ep (54.21VH) (Figure 2.2 and 2.3).

Figure 2.2: Average Vickers Hardness with Standard Deviation (SD) for each technique

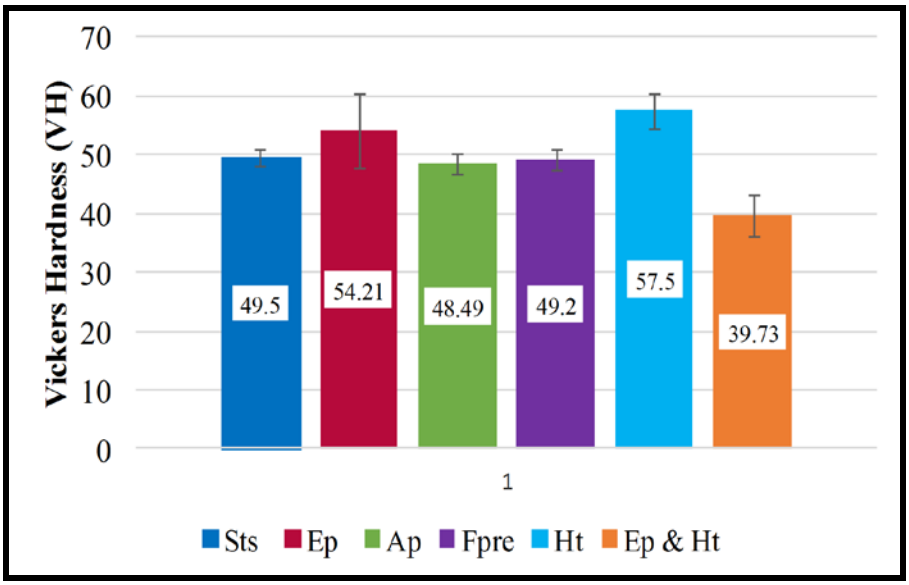

Figure 2.3 demonstrates the observed spread of the Log_e (Surface Hardness) values. Ep as well as the Ep & Ht demonstrated the greatest spread. A Bartlett test of homogeneity of variances confirmed that a significant difference was present ($p < 0.001$) between the homogeneity of the various treatments.

The Welch version of the ANOVA t-test therefore allows for the appropriate evaluation of these differences in homogeneity between the six techniques. When no overlap of the upper and lower limits occurs with the Welch version of the ANOVA t-test, it illustrates a significant difference between techniques at a level of $p < 0.05$ (Figure 2.3). There is therefore no significant difference between the VH of the Ht and the Ep techniques in Figures 2.2 and 2.3.

Figure 2.3: Log_e (Surface Hardness) of the six techniques

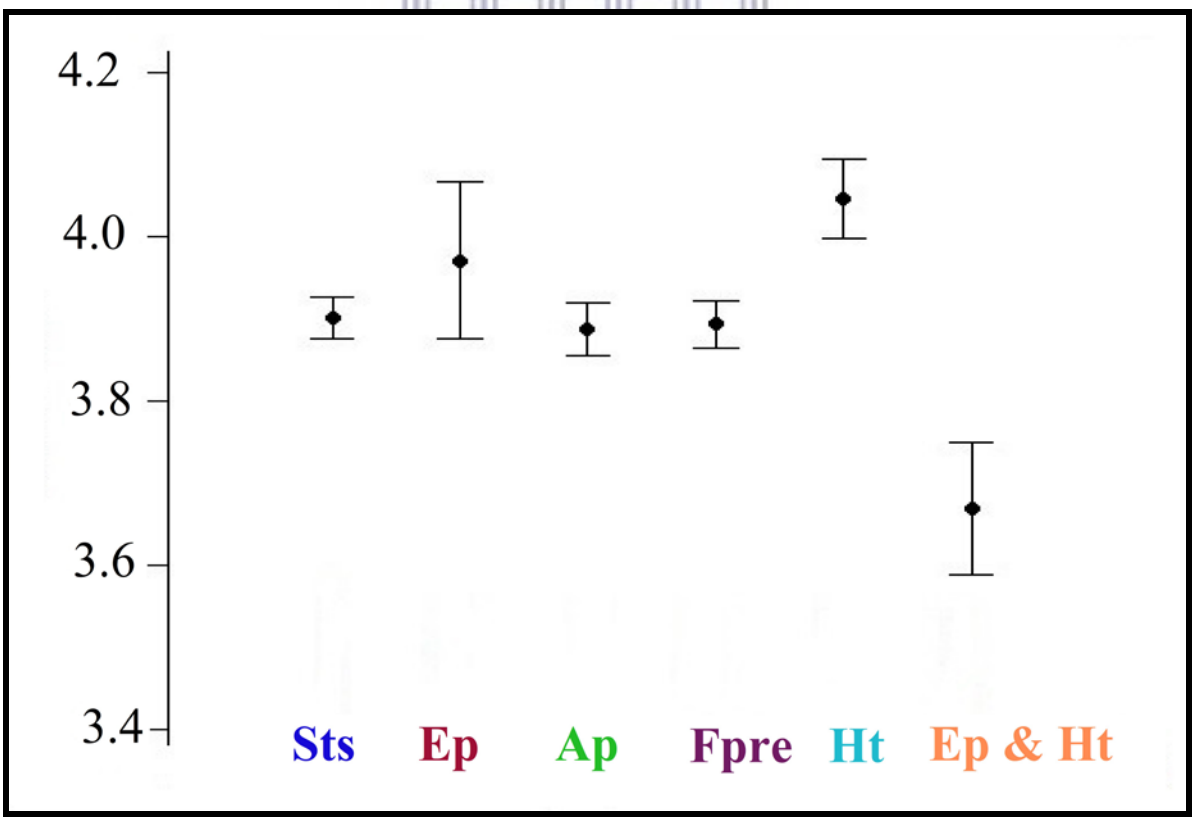

2.6. Discussion

Manipulation of the "salt bridge" formation results in a faster or slower setting of the material. The liquid phase of Chemfil Rock consists of polycarboxylic- and tartaric acid. The powder phase contains zinc modified fluoro-alumino-silicate glass filler particles. During the first mixing phase in the amalgamator, the polycarboxylic acid ($R\text{-}COOH^-$) in the liquid hydrates the glass particles of the powder. This is the start of the acid-base reaction and results in the exchange of protons from the glass filler particles causing the release of the cations from aluminium, calcium, strontium and zinc (Al^{3+}, Ca^{2+}, Sr^{2+}, Zn^{2+}). While this reaction takes place, the water content in the Chemfil Rock causes the polycarboxylic acid to neutralize and form a carboxylate ($R\text{-}COO^-$) molecule. The cations aluminium, calcium, strontium and zinc cross-link ionically to the carboxylate. Water is then released during the binding of cations with the carboxylate molecule. The application of ultrasonic excitation from Ep and the Ap techniques improves the reactivity of this aforementioned process (Algera *et al*., 2005). This excitation causes the movement of the cations and the liquid of the Chemfil Rock to the surface, where the cations join with the neutralised carboxylate chains resulting in an accelerated binding of the carboxylate to the various cations to form the salt bridge. This results in the rapid command set from Ep and the Ap techniques when compared to Ht, where no ultrasonic excitation was present. The resultant surface hardness of the Ep was greater, but not statistically different from the control (Sts) due to the surface hardness values having a greater standard deviation (Figures 2.2 and 2.3). Ultrasonic stimulation of both the Ep and Ap techniques therefore resulted in a rapid set (salt bridge formation) within 15 seconds of excitation.

The ultrasonic vibrations enhance the reaction rate of the salt bridge formation and improve the mechanical properties of GICs (Kleverlaan *et al*., 2004; Algera *et al*., 2005; Fagundesa *et al*.,

2006). Although the Ap ultrasonic vibrations at 6 kHz resulted in a command set, it did not improve the surface hardness compared to the control (Sts). This result confirmed that when an ultrasonic device is used, the minimum frequency of 17 kHz (Fagundesa *et al*., 2006) or higher is required to obtain the additional increase in the surface hardness of GICs.

According to Gorseta *et al*. (2012), the addition of heat generated by the Ht, Ap and the Ep techniques result in a relatively small temperature increase of 2-3°C. In contrast, a temperature increase of 13°C was cited by Algera *et al*. (2005). Both Ht (Barata *et al*., 2008) and the Ep applications are considered sufficient to increase the reactivity of the GIC molecules to rearrange and achieve a greater zone of ionic exchange during salt bridge formation in the surface of the GIC, resulting in an increased surface hardness. It is thought that the Ht and the Ep result in decreased susceptibility of the restoration to hydrolysis in the early setting stage with the polycarboxylic acid becoming more reactive (Algera *et al*., 2005; Khoroushi *et al*., 2012). Furthermore, a more consistent and predictable surface hardness was achieved in the present *in vitro* study and a previously confirmed study by Menne-Happ and Ilie (2013) where heat (Ht) was generated by a LED curing light.

During the salt bridge formation, loosely bound water is present in the GIC (Hattab and Amin, 2001). The decreased surface hardness observed with Ep combined with Ht (Ep & Ht) was visually explained by surface dehydration and crack formation of the loosely bound water as seen under 10x stereomicroscope magnification (*Carl Zeiss AG, Stemi508 stereomicroscope, Oberkochen, Germany*). The temperature rise in the samples of Ep & Ht was greater than when Ep and Ht were applied individually. Ep & Ht resulted in small droplets of moisture becoming visible around the margin of the material under magnification.

The materials subjected to the finger pressure (Fpre) technique were standardised at 3kg±100g (0.238kgf/mm² = 2.3411N/mm²) for two minutes to ensure a standardised pressure during the setting process. This standardisation had to be ensured, since previous studies conducted on the application of intra-oral finger pressure during crown cementation resulted in the subjective application of forces (Black and Amoore, 1993; Zortuk *et al*., 2010). The surface hardness obtained from the Fpre group (49.2VH) was not significantly different from the control (49.5VH). The Fpre technique will not contribute to an increase in the surface hardness of GICs.

2.7. Conclusion

In clinical scenarios where compliance and moisture control can be difficult, the clinician could make use of the Ht technique to increase the surface hardness of Chemfil Rock. A reduction in the setting time of GICs is desirable for paediatric restoration placement (Guglielmi *et al*., 2011). In such cases, the Ep and the Ap techniques could be advantageous in preventing moisture contamination due to the command set effect of the ultrasonic vibrations. The use of the Ep technique will induce the material to set within 15 seconds, preventing premature dissolution of the GIC (O'Brein *et al*., 2010) and improving the surface hardness to a greater extent than the Ap technique. Clinicians should not combine the two techniques (Ep & Ht) as this will lead to a significantly lower surface hardness.

2.8. References

Algera, T., Kleverlaan, C., de Gee, A., Prahl-Andersen, B. and Feilzer, A. (2005). The influence of accelerating the setting rate by ultrasound or heat on the bond strength of glass ionomers used as orthodontic bracket cements. *European Journal of Orthodontics*, 27(5), pp.472-476.

Baloch, F., Mirza, A. and Baloch, D. (2010). An in-vitro study to compare the microhardness of glass ionomer cement set conventionally versus set under ultrasonic waves. *International Journal of Health Sciences (Qassim),* 4(2), pp.149-155.

Barata, T., Bresciani, E., Adachi, A., Fagundes, T., Carvalho, C. and Navarro, M. (2008). Influence of ultrasonic setting on compressive and diametral tensile strengths of glass ionomer cements. *Materials Research,* 11(1), pp.57-61.

Berg, J. (2002). Glass ionomer cements. *Pediatric Dentistry,* 24, pp.430-438.

Black, S. and Amoore, J. (1993). Measurement of forces applied during the clinical cementation of dental crowns. *Physiological Measurement,* 14(3), pp.387-392.

Coldebella, C., Santos-Pinto, L. and Zuanon, A. (2010). Effect of ultrasonic excitation on the porosity of glass ionomer cement: A scanning electron microscope evaluation. *Microscopy Research and Technique*, 74(1), pp.54-57.

Ellakuria, J., Triana, R., Mínguez, N., Soler, I., Ibaseta, G., Maza, J. and García-Godoy, F. (2003). Effect of one-year water storage on the surface microhardness of resin-modified versus conventional glass-ionomer cements. *Dental Materials*, 19(4), pp.286-290.

Fagundesa, T., Barataa, J., Bresciania, T., Cefalyb, D., Carvalhoa, C. and Navarroc, M. (2006). Influence of Ultrasonic Setting on Tensile Bond Strength of Glass-ionomer Cements to Dentin. *Journal of Adhesive Dentistry,* 8, pp.401-407.

Gorseta, K., Glavina, D. and Skrinjaric, I. (2012). Influence of ultrasonic excitation and heat application on the microleakage of glass ionomer cements. *Australian Dental Journal,* 57(4), pp.453-457.

Guglielmi, C., Mohana, A., Hesse, D., Lenzi, T., Bonini, G. and Raggio, D. (2011). Influence of ultrasound or halogen light on microleakage and hardness of enamel adjacent to glass ionomer cement. *International Journal of Paediatric Dentistry*, 22(2), pp.110-115.

Hattab, F. and Amin, W. (2001). Fluoride release from glass ionomer restorative materials and the effects of surface coating. *Biomaterials*, 22(12), pp.1449-1458.

Hübel, S. and Mejàre, I. (2003). Conventional versus resin-modified glass-ionomer cement for Class II restorations in primary molars. A 3-year clinical study. *International Journal of Paediatric Dentistry*, 13(1), pp.2-8.

International Organization for Standardization (2007). *ISO 9917-1- Dentistry-Water based cements Part 1: Powder/liquid acid-base cements*, 1st ed.; (pages1–21).

Khoroushi, M., Karvandi, T. and Sadeghi, R. (2012). Effect of Prewarming and/or Delayed Light Activation on Resin-Modified Glass Ionomer Bond Strength to Tooth Structures. *Operative Dentistry*, 37(1), pp.54-62.

Kleverlaan, C., van Duinen, R. and Feilzer, A. (2004). Mechanical properties of glass ionomer cements affected by curing methods. *Dental Materials*, 20(1), pp.45-50.

Menne-Happ, U. and Ilie, N. (2013). Effect of heat application on the mechanical behaviour of glass ionomer cements. *Clinical Oral Investigations*, 18(2), pp.643-650.

O'Brien, T., Shoja-Assadi, F., Lea, S., Burke, F. and Palin, W. (2010). Extrinsic energy sources affect hardness through depth during set of a glass-ionomer cement. *Journal of Dentistry*, 38(6), pp.490-495.

Qvist, V., Laurberg, L., Poulsen, A. and Teglers, P. (2004). Eight-year study on conventional glass ionomer and amalgam restorations in primary teeth. *Acta Odontologica Scandinavica*, 62(1), pp.37-45.

Towler, M. (2001). A preliminary comparison of the mechanical properties of chemically cured and ultrasonically cured glass ionomer cements, using nano-indentation techniques. *Biomaterials*, 22(11), pp.1401-1406.

Twomey, E., Towler, M., Crowley, C., Doyle, J. and Hampshire, S. (2004). Investigation into the ultrasonic setting of glass ionomer cements Part II Setting times and compressive strengths. *Journal of Materials Science*, 39(14), pp.4631-4632.

Yap, A., Pek, Y. and Cheang, P. (2003). Physico-mechanical properties of a fast-set highly viscous GIC restorative. *Journal of Oral Rehabilitation*, 30(1), pp.1-8.

Zortuk, M., Bolpaca, P., Kilic, K., Ozdemir, E. and Aguloglu, S. (2010). Effects of Finger Pressure Applied By Dentists during Cementation of All- Ceramic Crowns. *European Journal of Dentistry*, 4, pp.383-388.

CHAPTER 3

VARIATION OF POWDER/LIQUID RATIOS OF CAPSULATED GLASS-IONOMER RESTORATIVE CEMENTS

3.1. Abstract

Purpose: Besides hand-mixed formulations, glass-ionomer restorative cements (GICs) are also available in sealed capsules. The main advantage of capsulated materials is that the clinician cannot alter the powder/liquid ratio. Subsequent to the investigation of hand-mix GICs, the present research study was conducted to investigate the consistency of the recommended powder/liquid ratios inside the capsules stated by the manufacturers compared to the actual powder/liquid content. The study additionally assessed the surface micro-hardness and compressive strength of randomly selected capsules.

Materials and Methods: Two different batch numbers for five glass-ionomer restorative cements and one carbomer were evaluated. Twenty specimens were selected from each batch of materials: Chemfil Rock (*Dentsply Sirona*), Fuji Equa Forte (*GC Corp*), Glass Fill (*GCP dental*), Ionofil Molar AC (*Voco*) and Ketac Universal (*3M ESPE*) and Riva Self Cure (*SDI Limited*). The capsules were deconstructed and the powder and liquid were weighed. Additionally, five specimens were prepared for each time interval (days 1, 7 and 180) and the compressive strength assessed. The surface micro-hardness (Vickers Hardness) was completed on five specimens per batch and assessed sequentially at days 1, 7 and 180 on the same specimen after the lapsed time intervals.

Results: The results showed that there were significant differences between the two batches for the powder and liquid content for Chemfil Rock ($p < 0.001$), Ketac Universal ($p = 0.029$) and Riva Self Cure ($p < 0.001$). There were no significant differences for surface micro-hardness or

compressive strength between the two batches for any of the assessed time intervals (days 1, 7 and 180).

Conclusion: This research demonstrated that there were differences between the various batches from the same manufacturer where the powder/liquid ratio content was concerned. The actual content of powder and liquid from the two batches differed when compared to the manufacturers' recommended powder/liquid ratios on the package inserts for most of the manufacturers. The difference in powder/liquid ratios between batches did not significantly influence the Vickers Hardness or the compressive strength for the material over the same time period.

Keywords: Capsule, Glass ionomer, Carbomer, powder/liquid ratio, Vickers Hardness, compressive strength, powder weight, liquid weight.

Abbreviations and acronyms:

CR: Chemfil Rock

Batch: B

FEF: Fuji Equa Forte Fil

GF: GCP Glass Fill

IM: Ionofil Molar AC

KU: Ketac Universal

PLR: Powder/liquid ratio

RSC: Riva Self Cure

RMGIC: Resin modified glass-ionomer

3.2. Introduction

The favourable bioactive properties of glass-ionomer restorative materials (GICs) lie in their ability to form a physicochemical bond to the tooth structure (Glasspoole *et al*., 2002). This physicochemical bond is primarily due to ion exchange and integration with moist tooth structure (Wilson *et al*., 1983; Yoshida *et al*., 2000). GICs also have a thermal compatibility, since the coefficient of thermal expansion is similar to that of dentine (Nassan and Watson, 1998). The anicariogenic properties of GICs due to the release of fluoride (Xie *et al*., 2000; Chau *et al*., 2015) and other ions are advantageous to both sound tooth structure and compromised tooth structure (Ngo *et al*., 2006). GICs can be technique sensitive and two key disadvantages may include low early strength and moisture sensitivity during the initial setting process (Pelka *et al*., 1996; Xie *et al*., 2000). The setting process of conventional GICs is characterised by an acid-base reaction between the powder and the liquid. Powder/liquid ratios (PLR) were therefore shown to play an important role in the early stages of material placement and maturation (Eames *et al*., 1977). Initially, when GICs were launched, the method of mixing was by spatulation and capsulated versions were not readily available. The clinical manipulation by clinicians is based on two main variables namely: 1) variation in the volume of incorporated powder and 2) the speed of spatulation. The speed of spatulation has been well documented for hand-mix materials (Billington *et al*., 1990; Cattani-Lorente *et al*., 1993). The challenge that clinicians face with hand spatulation of GICs in daily dental practice is to abide by the manufacturer's mixing time and PLR instructions.

The capsulated materials should have an advantage over hand-mixed preparations as the manufacturer controls the PLR of the components. Hand-mixed materials are vulnerable to variability of mixing and PLR (Nomoto, 2004; Mulder, 2018). Mechanical mixing together with the pre-proportioned PLR by the manufacturer should allow the various functional properties of the mixed material to be less susceptible to operator-induced variability.

The use of capsulated GICs is considered to be less time-consuming, as it is ready for immediate use by expressing the GICs into the preparation directly from the capsule and a cleaner clinical area is maintained than when hand-mixed GICs are used (Nomoto and McCabe, 2001). With capsulated materials, mixing speed (Gee and Pearson, 1993) and duration of mixing (Fleming *et al*., 2006) can be influenced by the clinician. Manipulation of the mixing speed and duration of the GICs in capsulated form can either increase or decrease the setting time. This could however result in a decreased PLR, especially if the mixing speed is lower than 3000 oscillations (Rupp *et al*., 1996). The decreased PLR is due to the powder not achieving a sufficient mix with the liquid. As a result, the non-reacted powder decreases the PLR that can take part in the acid-base reaction. The alteration of the PLR can result in the GIC having insufficient liquid for wetting and interaction with the powder. The polyalkenoic acid portion of the liquid interacts with the powder to allow various metallic ions to release from the glass particles to form the primary polysalt matrix (Maeda *et al*., 1999). Subsequent to metallic ion release, a siliceous hydrogel is left on the glass particle surface (Hatton & Brook, 1992; Nicholson, 1998). Therefore, the interaction of the liquid with the powder influences the number of ions released and directly influences the matrix formation. Although GICs continue to absorb water from the moist dentine, it allows additional acid-base reactions to take place over time (Ten Bosch *et al*., 2000). This absorbed moisture is essential for the gradual maturation and increase of compressive strength, due to the hydration of the silicate phase that contributes to the increase of compressive strength (Matsuya *et al*., 1996). In order to assess the effect of maturation and variations in the PLR of capsulated GICs, the specimens were matured in de-ionised water and assessed over time. It has been shown that GICs mature over time and this subsequently changes the physical properties (Zanata *et al*., 2011; Zoergiebel and Ilie, 2013).

The bond strength of GICs to both healthy and carious tooth structure has been studied with shear bond testing (McInnes-Ledoux *et al*., 1989; Burke and Lynch, 1994). The use of GIC restorations for the atraumatic restorative technique have been shown to be clinically successful in single surface restorations after a three-year period (Frenken *et al*., 1998; Holmgren *et al*., 2000), with the bond strengths of GICs reported to be in the range of 3±4MPa (Hewlett *et al*., 1991; Ewoldsen *et al*., 1997). The newer high viscosity glass-ionomers assessed in the present study have shown improved physical properties, such as Ketac Universal (*3M ESPE*) and Fuji Equa Forte Fill (*GC Corp*) which have expanded indications for restorative treatment. The manufacturer (*GCP Dental*) classifies Glass Fill as a Glass Carbomer due to the filler particles in the material. The claimed improvement in the physical properties of the carbomer by the manufacturer is attributed to the nano-sized apatite filler particles. The material should be thermocured with a light emitting diode (LED) curing light through the surface protective gloss (Arita *et al*., 2011) in order to increase the setting reaction.

The accuracy of the PLR in GICs has been questioned. A study using three GICs with a PLR of -11%, +3% and +6% of the manufacturer's recommendations respectively, was identified (Gee and Pearson, 1993). Variations in PLR of approximately 6% have been reported in capsulated materials (Azillah *et al*., 1998). The rationale was that as GICs mature over time, it was uncertain how the possible variation in PLR would influence it. In the present study, the time intervals for assessment of the Vickers Hardness and compressive strength were completed on days 1, 7, and 180. Ionofil Molar AC (*Voco*) was only assessed for powder/liquid ratios, due to insufficient capsules per batch. The purpose of assessing the compressive strength and Vickers Hardness at different time intervals was to evaluate whether the consistency of the PLR in the capsules of the assessed GICs and carbomer in relation to the manufacturers' recommendations, would influence the results. It was important to assess two different batch numbers from each

manufacturer and compare it to the manufacturer's recommended capsulated content. This allowed insight into any differences in the batches from each manufacturer compared to the manufacturer's PLR recommendation as stated on the packaging. The subsequent research question was whether a variation in the PLR between batches and/or the manufacturers' recommendations would influence the Vickers Hardness and compressive strength. As the material matures, the Vickers Hardness and compressive strength change, moisture is absorbed and ions are released (De Caluwe *et al*., 2017). The compressive strength specimens were different for days 1, 7 and 180. The same surface hardness specimens were assessed with Vickers Hardness on days 1, 7 and 180 to evaluate how the surface hardness changed over time.

The hypothesis was that the PLR would be similar with no variance between batches of the two capsulated GIC materials. Additionally, no significant difference would exist between the batches for the Vickers Hardness and compressive strength for the different time periods of 1, 7 and 180 days.

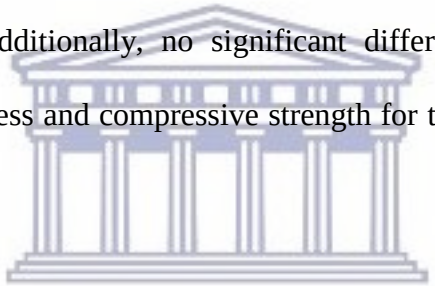

3.3. Materials and methods

3.3.1. Capsule selection criteria

Figure 3.1 provides an outline of the capsule distribution for the powder/liquid assessment and comparison of the compressive strength and surface microhardness of the two batches of materials. IM could not be assessed for Vickers Hardness or compressive strength due to insufficient capsules per batch.

Figure 3.1: Flowchart of capsule distribution for specimen preparations

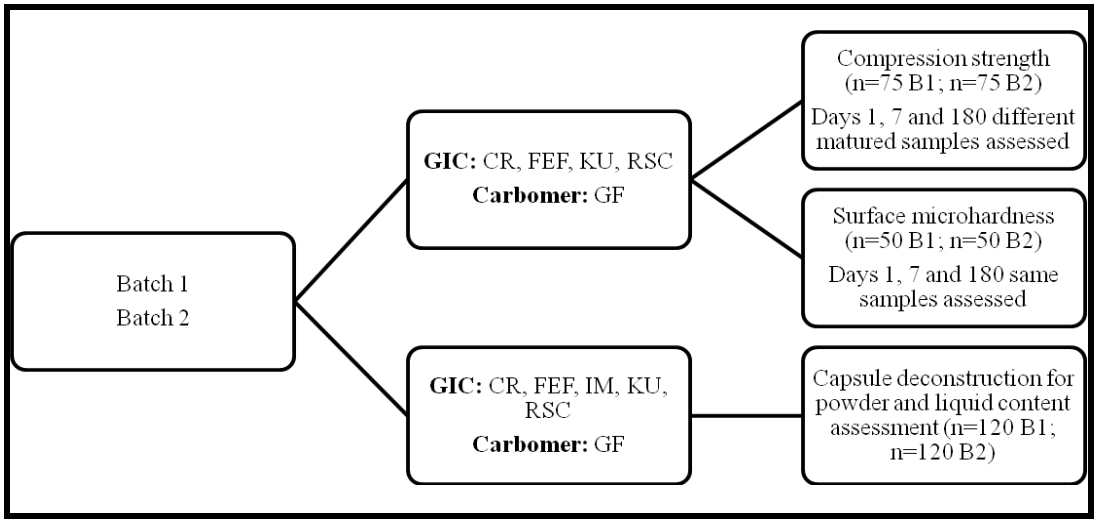

Two different batches (B1, B2) from each manufacturer were assessed. Five encapsulated GIC materials and one carbomer were assessed for the powder and liquid content (Figures 3.2 and 3.3).

Figure 3.2: Capsule systems with a posterior plunger

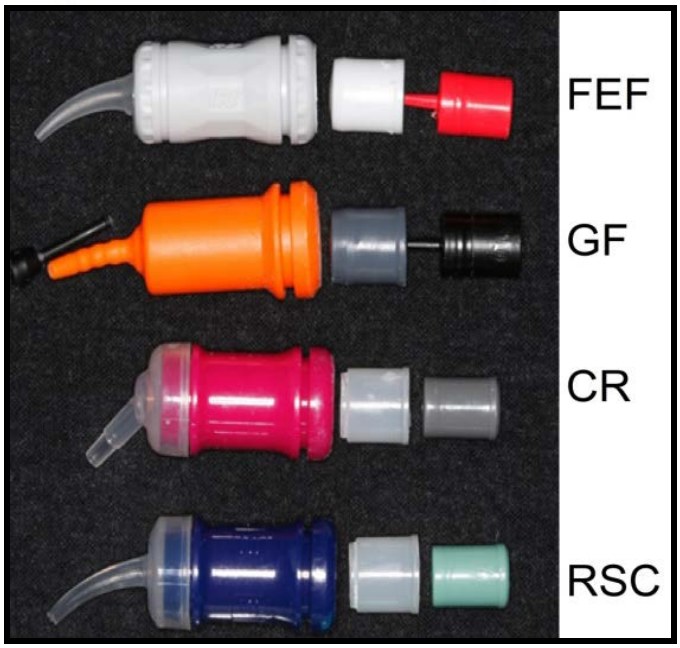

Figure 3.3: Capsules with an external diaphragm

Twenty capsules were randomly selected from each of the two different batch numbers (n = 240) for the PLR assessment (Table 3.1).

The capsules were deconstructed in order to assess the individual liquid and powder weight. The techniques used to deconstruct the capsules were based on the capsule design. Figure 3.2 shows the posterior plunger system for Chemfil Rock (CR), Fuji Equa Forte (FEF), Riva Self Cure (RSC) and the carbomer namely GCP Glass Fill (GF). The remaining GICs namely Ketac Universal (KU) and Voco Ionofil Molar AC (IM) had the liquid in a compressible diaphragm located on the superior aspect of the capsule under the activation cover (Figure 3.3).

Table 3.1: Material abbreviation, batch numbers and the recommended manufacturer PLR

Material and manufacturer	Material abbreviation	Recommended powder (g)	Manufacturer recommended liquid (g)	Manufacturer recommended PLR
CR: Chemfil Rock (*Dentsply Sirona, Konstanz, Germany*). B1: 1511000724 B2: 1502008003	CR B1 CR B2	0.442	0.12	3.683 : 1
FEF: Fuji Equa Forte (*GC Corp, Tokyo, Japan).* B1: 1508265 B2: 151118A	FEF B1 FEF B2	0.4	0.13	3.076 : 1
GF: Glass Fill (*GCP dental, Netherlands*). B1:7511350 B2:75114444	GF B1 GF B2	0.5	0.15	3.333 : 1
KU: Ketac Universal (*3M ESPE, Seefeld, Germany).* B1: 614726 B2: 606207	KU B1 KU B2	0.339	0.106	3.198 : 1
RSC: Riva Self Cure (*SDI Limited, Australia*). B1: B1506291F B2: B1508193F	RSC B1 RSC B2	0.45	0.14	3.214 : 1
IM: Ionofil Molar AC (*Voco, Germany*). B1: 1530546 B2: 1526687	IM B1 IM B2	0.43	0.125	3.440 : 1

3.3.2. Deconstruction of the posterior plunger capsule

Capsule deconstruction of CR, FEF, GF, and RSC (n = 160): The capsules were stored with the dispensing tips down for 30 minutes prior to capsule deconstruction. This storage position

allowed the dispensable liquid that had varying viscosities due to differences in chemistry, sufficient time to pool at the bottom of the liquid chamber. The plunger (Figure 3.4) was removed carefully with pliers. Liquid present on the plunger was wiped off with one of three discs of filter paper, to ensure that no liquid adhered to the plunger due to surface tension.

Figure 3.4: Chamber and plunger with liquid visible

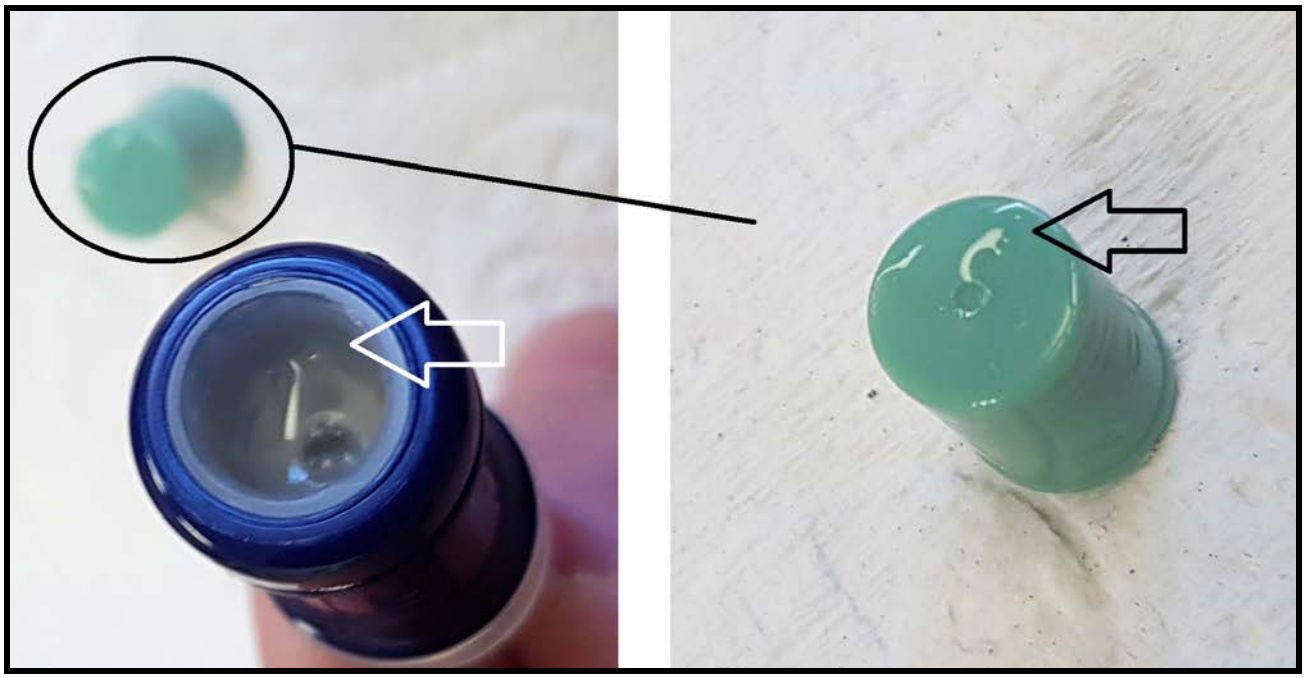

The liquid was absorbed from the chamber with three identical pieces of Whitman filter paper (*Whitman no1, GE Healthcare, Illinois, USA*) which was punched with a 25mm paper punch (*Upikit HCP-110 craft punch, circle shape size one, Upikit International PTY Ltd, Tainan, Taiwan*). The three filter paper discs of known weight were held with a stainless steel tweezer and the liquid was absorbed from the liquid chamber. The chamber was dried with the filter paper until all the liquid was absorbed and visual inspection under 1.75x fluorescent

magnification (*Start International, Dallas, Texas, USA*) ensured that no liquid remained in the chamber (Figure 3.5).

Figure 3.5: Dried liquid chamber under 1.75 magnification

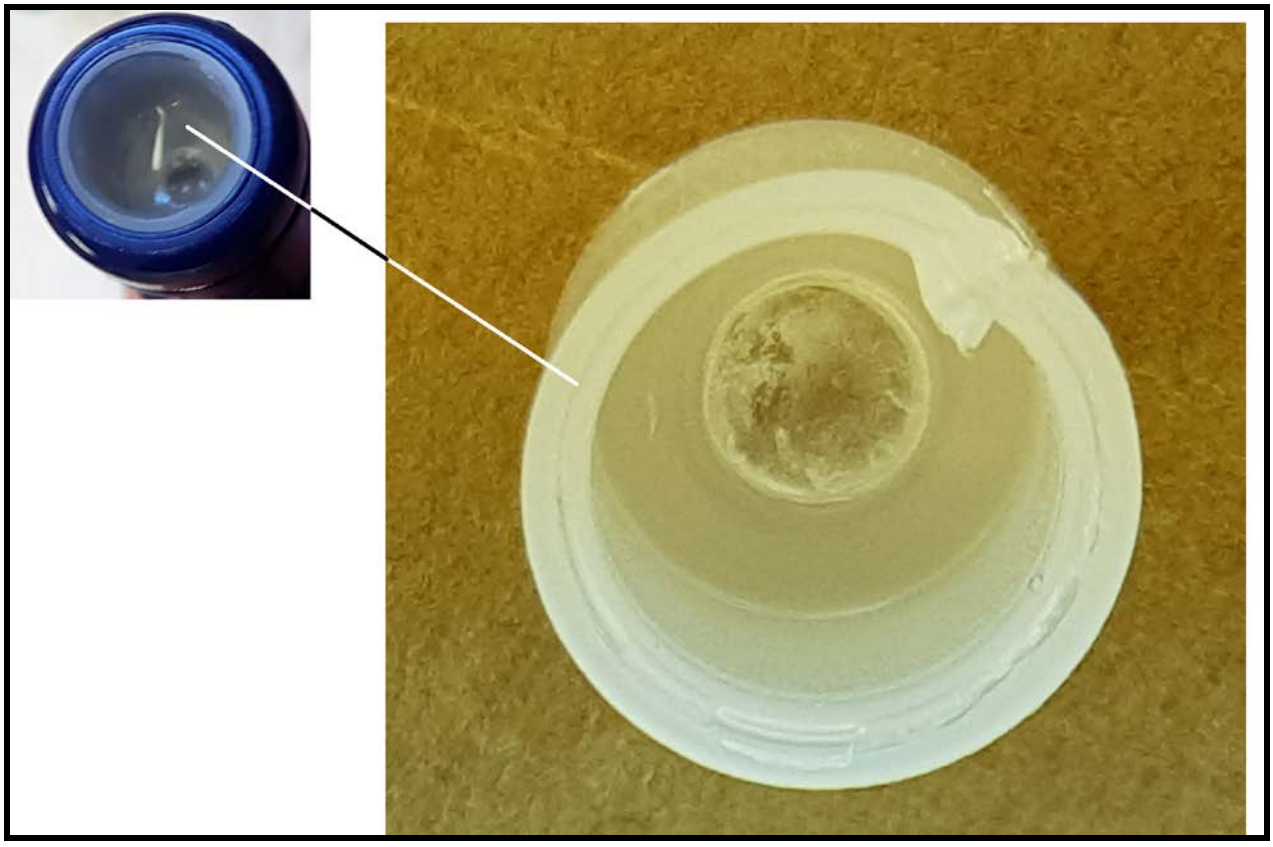

The liquid content was calculated by deducting the known weight of the three filter paper discs from the final weight after the liquid was absorbed. The chamber that housed the liquid was subsequently removed with a carbon surgical blade (*Swann-Morton, Sheffield, England, UK*) to expose the powder chamber. The powder was placed in a small specimen jar of known weight. A visual inspection under magnification (as previously stated) was performed to ensure that no powder was retained on the capsule walls.

In order to ensure that no liquid was lost due to evaporation, the liquid was exposed to room temperature for 3 minutes. Figure 3.6 illustrates that there was no weight change to the fourth decimal.

Figure 3.6: No weight change due to evaporation of the liquid after 3 minutes

3.3.3. Deconstruction of the diaphragm capsule

KU, IM (n = 80): These capsules were not stored with the dispensing tip down for 30 minutes, as the liquid component was pre-packed in a silver compressible diaphragm on the superior aspect of the capsule under the activation cover (Figure 3.3). The various plungers were removed carefully with pliers to gain access to the powder chamber. The powder was placed in a small specimen jar of known weight. Visual inspection under magnification as previously described, ensured that no powder was retained on the capsule walls. Subsequently the silver compressible diaphragm was weighed with the liquid content. The dispensable liquid was determined by using a surgical blade (*Swann-Morton carbon steel surgical blade no.15, Sheffield, United Kingdom*)

to cut the diaphragm and weighing the liquid on the three filter paper discs. The silver diaphragm was visually inspected as previously described. The liquid weight was additionally confirmed by deducting the initial weight of the diaphragm from the end weight of the empty diaphragm.

After deconstruction, the weight of the powder and the liquid were established on a desktop analytical balance (*Ohaus Precision Standard, Model TS400D, Ohaus Corp, Florham Park, N.J, USA*). The PLR was calculated by dividing the powder weight by the liquid weight and comparing it to the manufacturers' recommendations (Table 3.1).

3.3.4. Compressive strength

Four GICs (except IM) and the carbomer were assessed for compressive strength. Five cylindrical test specimens were prepared for each material per batch for the various time intervals (days 1, 7 and 180). The specimens were prepared and assessed as per the ISO for Dentistry-Water-based cements - Part 1: Powder/liquid acid-base cements (ISO 9917-1). For the mixing of the materials, the ISO 9917-1 standard indicated a relative humidity of 50±10%. The mould and clamp used to prepare the specimens were kept in a temperature-controlled cabinet (37±1ºC) with a 30% relative humidity. The capsules were mixed with a Rotomix (*3M ESPE, Seefeld, Germany*) according to the manufacturers' instructions, except for GF. The only deviation was where the surface protective gloss was not applied to GF. This was also not followed by thermocuring with a LED curing unit through the gloss directly after material placement into the mould. This step was omitted, since the mould and clamp set-up outlined in the ISO 9917-1 was not conducive to carrying out those two steps. All the specimens were prepared at room temperature (23±1ºC). The cylindrical test specimens were made by placing the mixed materials into a Teflon split mould between stainless-steel plates (height 6±0.1 mm, diameter 4±0.1 mm). The mould was slightly overfilled and a cellulose strip was placed between

the material and the plates. The specimens were removed from the moulds after one hour of bench-setting and immediately submerged in 5ml de-ionized water grade 3 (37±1°C), as defined in ISO 3696:1987. The specimens were stored in this medium for 1, 7 and 180 days (in a temperature-controlled cabinet). The compressive force (p) was measured in Newton with a universal material testing machine (*H10KT-0293 Tinus Olsen, Redhill, England*) at a cross-head speed of 0.75mm/min. The software of the universal tester was used for analysis of the results (*QMat Testzone, version 4.5.37, Tinus Olsen, Redhill, England*). The specimens (with moist filter paper on either side) were placed with their flat ends between the plates on the testing machine, so that the progressively increasing compressive load was applied along the 6mm long axis of the specimen.

The compressive strength was calculated in megapascals (MPa), using the following equation:

$$C = 4p/\pi d^2$$

C: Compressive strength in MPa

p: Compressive force/maximum force applied

d: Diameter of the specimen, in millimeters

π: Constant for pie used as 3.14

3.3.5. Surface micro-hardness analysis

The surface micro-hardness of four GICs (except IM) and one carbomer (Figure 3.2 and 3.3) were assessed with a Vickers Hardness indenter. Five specimens were constructed and assessed at the various time intervals (days 1, 7 and 180).

Storage was completed as described for the specimens for compressive strength. Forty-eight hours after the specimens were submerged in distilled water, the surface of all the specimens for Vickers Hardness testing were smoothened with 2500 grit wet silicon carbide paper, followed

with 4000 grit (*3M, Massachusetts, USA*). The polishing ensured an adjustment to the surface of ±100µm (as measured within a micrometer). The application of the silicon carbide paper simulates the restoration polishing that would occur in the clinical setting (Menne-Happ and Ilie, 2013). This smoothed surface allowed accurate evaluation of the pyramidal indentation on the surface of the material. A second, blinded operator completed the surface hardness evaluation with a Vickers Hardness indenter (*Zwick-Roell durometer, ZHV1/2 Micro-vickers, Italy*) set at HV0.5 (load of 500gf) and a dwell (indentation) time of ten seconds. The instrument automatically calculated the Vickers Hardness after the diagonals were selected. Three Vickers Hardness (VH) measurements were recorded 500µm apart on each specimen to obtain a mean value per specimen. The mean values from the five specimens of each batch per time period (days 1, 7 and 180) (Ellakuria *et al*., 2003; Yap *et al*., 2003; O'Brein *et al*., 2010) were calculated with a standard deviation and compared per batch within the same material group.

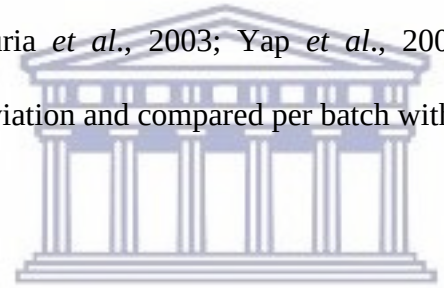

3.4. Statistical analysis

The collected data was tabulated in a Microsoft Excel® spreadsheet (2012); (*Microsoft® Corp., Richmond, VA, USA*) and analysed. The statistical analysis included the calculation of p-values at a significance level of $p < 0.05$ for all analyses. The powder/liquid ratio was assessed using the Bartlett's test for homogeneity of variances within the standard deviation (SD). The mean values of B1 and B2 for each material was analysed with the Welch version of the two-sample t-test, which took the differences in the variances into account to establish the significance of the differences. For the Vickers Hardness and compression test, the Welch t-test was completed to establish if there was a significant difference between the two batches. In order to consider the changes in the physical properties as the glass ionomers and the carbomer mature, the difference in the two batches for Vickers Hardness and compressive strength were assessed at days 1, 7 and 180.

3.5. Results

3.5.1. Powder/liquid assessment of the capsules

The statistical analysis between B1 and B2 within the material groups are represented in Table 3.2 for the mean PLR and standard deviation (SD) of the twenty capsules from each batch number.

Table 3.2: Mean powder/liquid ratio per batch

Material	Mean PLR B1	Mean PLR B2	p–value
CR	3.4712(±0.05767)	3.6238(±0.07146)	<0.001
FEF	3.4483(±0.08895)	3.4336(±0.09109)	=0.607
GF	3.5665(±0.14918)	3.5062(±0.08779)	=0.129
KU	3.2145(±0.04234)	3.1680(±0.08004)	=0.029
RSC	3.4788(±0.04625)	3.2368(±0.05712)	<0.001
IM	3.6068(±0.03131)	3.5849(±0.05384)	=0.126

Significant differences were found between the mean values of the PLR from the 20 specimens from B1 and B2 within the material for CR ($p < 0.001$), KU ($p = 0.029$) and RSC ($p < 0.001$). The variances of the observed PLR inside the capsules were assessed in terms of the SD for the batches. The Bartlett's test indicated significant differences between the SD B1 and SD B2 for GF ($p = 0.012$), IM ($p = 0.011$) and KU ($p = 0.004$). GF B1, IM B2 and KU B2 had the largest SD within their respective manufacturer batches, resulting in significant differences between the batches of the particular manufacturer. This aforementioned variance can be seen in the spread within each batch between the 20 PLR observations represented in Figure 3.7.

Figure 3.7: Powder/liquid ratio distribution of two batches with ± 10% ratio of the manufacturers' recommendation

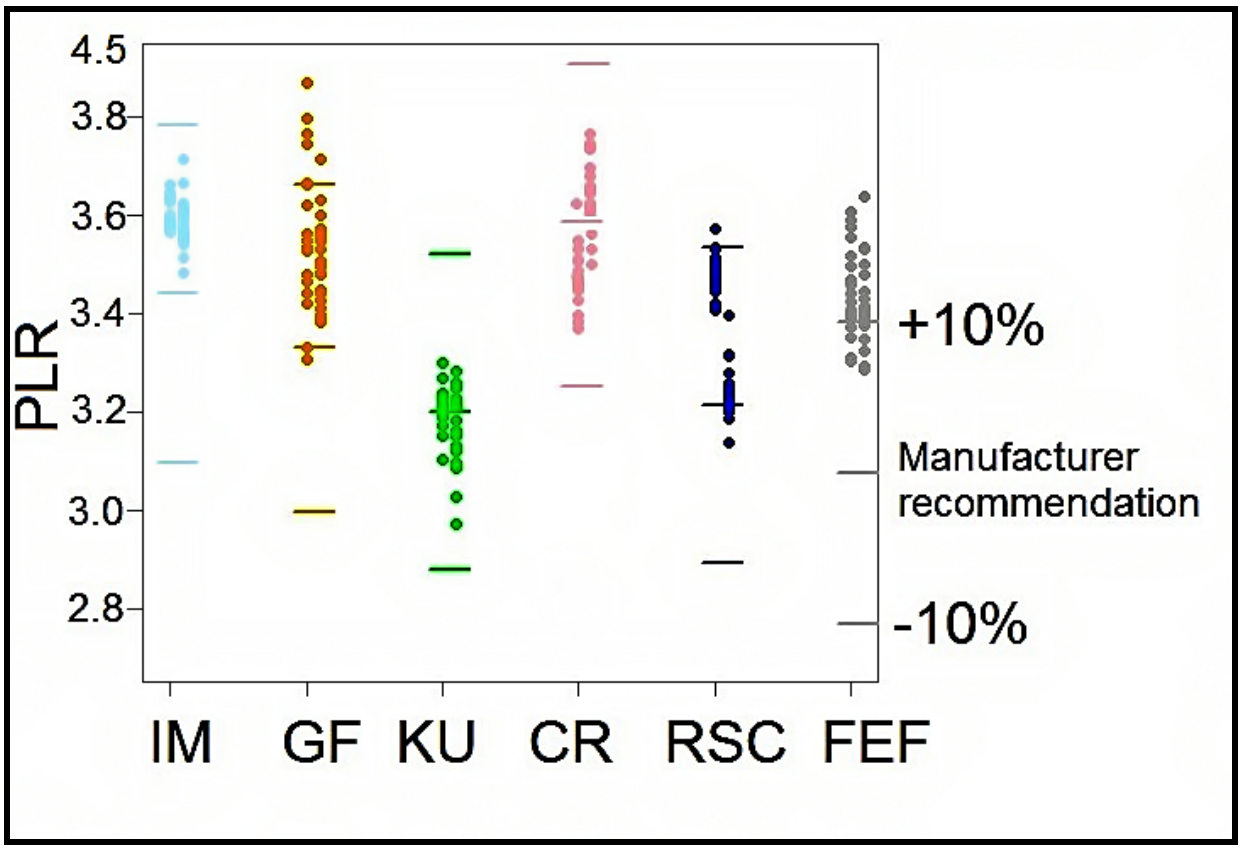

Differences were present between batches shown in Table 3.3 based on the PLR mean values of the observation. The smallest difference between the two batches from the same manufacturer were FEF (0.42%) followed by IM (0.60%). The greatest difference between the actual mean PLR per batch and the manufacturer's recommendation on the packaging was FEF (B1:10.79%. B2:10.41%).

Table 3.3: PLR comparative difference between batches versus the manufacturers' recommendations

Material	Mean powder in capsule	% Powder difference between batch and manufacturer recommendation	Mean liquid in capsule	% Liquid difference between batch and manufacturer recommendation	Mean PLR capsules	PLR % difference between B1 and B2	PLR % difference between batch and manufacturer recommendation
CR B1	0.4516	+2.17	0.1301	+8.41	3.4712 : 1	4.39	-5.75*
CR B2	0.4569	+3.37	0.1261	+5.08	3.6238 : 1		-1.60*
FEF B1	0.3986	-0.35	0.1156	-11.07	3.4483 : 1	0.42	+10.79
FEF B2	0.3928	-1.8	0.1144	-12	3.4336 : 1		+10.41
GF B1	0.4115	-17.7	0.1151	-23.06	3.5665 : 1	1.69	+6.63
GF B2	0.4123	-17.54	0.1176	-21.60	3.5062 : 1		+5.02
KU B1	0.3384	-0.17	0.1053	-0.66	3.2145 : 1	1.48	+0.52*
KU B2	0.3339	-1.50	0.1051	-0.56	3.1680 : 1		-0.94*
RSC B1	0.4129	-8.24	0.1187	-15.21	3.4788 : 1	6.95	+7.61*
RSC B2	0.4143	-7.93	0.1280	-8.57	3.2368 : 1		+0.63*
IM B1	0.4256	-1.02	0.1180	-5.6	3.6068 : 1	0.60	+4.62
IM B2	0.4240	-1.39	0.1183	-5.36	3.5849 : 1		+4.04

"+" indicates greater than manufacturer's recommendation. "-" indicates less than manufacturer's recommendation.
"*" significant difference between the two batches from the same manufacturer.

The 240 PLR observations were plotted for each manufacturer; B1 on the left and B2 on the right (Figure 3.7). The upper (10%) and lower horizontal bars (-10%) represent the variation of the PLR from the manufacturers' instructions that ensure no significant change to the setting time, compression strength or flexural strength. The actual PLR recommendation of the manufacturer has been placed as the horizontal bar between the -10 to 10% bars (Table 3.4 and Figure 3.7). Table 3.4 additionally illustrates the distribution of the PLR observations located

between -10% and 10% of the PLR recommended by the manufacturer. The batches of CR-, KU B1 and CR-, KU- and RSC B2 had observations that were well distributed around the PLR of the respective manufacturer's recommendation. IM-, CR-, KU B1/B2 and RSC B2 were the only material batches with all 20 PLR observations between the -10% and 10% range of the manufacturers' recommended PLR (Table 3.4 and Figure 3.7).

This does however not illustrate that the silver diaphragm is superior in terms of liquid accuracy compared to a liquid chamber. When Tables 3.1 and 3.3 are evaluated on how the mean values of powder and/or liquid can vary individually from the manufacturers' recommendation, it becomes clear that the PLR as a standalone value must not be misinterpreted, as the final PLR is close to the ratio recommended by the manufacturer, despite the individual variation from the manufacturer's individual powder and liquid values. Therefore, CR-, KU B1 and CR-, KU B2 were the material manufacturers that displayed individual powder, individual liquid and combined PLR closest to the manufacturers' recommendations. The spread of the observations that were significantly different can be considered irrelevant for IM and KU, since the observations are all within the -10% to 10% PLR from that of the manufacturer.

Table 3.4: Variation between the capsules' PLR distribution versus the manufacturers' recommendations

Material	Number of capsules with a PLR -10% to 0%	Number of capsules with a PLR 0% to 10%	Number of capsules with a PLR >10%
IM B1	0	20	0
IM B2	0	20	0
GF B1	0	15	5
GF B2	0	19	1
KU B1	5	15	0
KU B2	10	10	0
CR B1	20	0	0
CR B2	16	4	0
RSC B1	0	19	1
RSC B2	0	20	0
FEF B1	0	4	16
FEF B2	0	5	15
0% represents the exact manufacturer recommended PLR			

3.5.2. Surface micro-hardness

The Vickers Hardness values between the batches of the same material and the same specimens were compared for each time interval to assess how it differed as the material matured (Figure 3.8). The Vickers Hardness for the materials with the exception of RSC B2 on day 7, showed an increase in surface hardness over the progression of 1, 7 and 180 days. The statistical analysis revealed no significant differences for each manufacturer between Batch 1 and Batch 2 for any of the materials tested within the same time period of 1, 7 and 180 days ($p > 0.05$).

Figure 3.8: Mean Vickers Hardness values of batches for days 1, 7 and 180

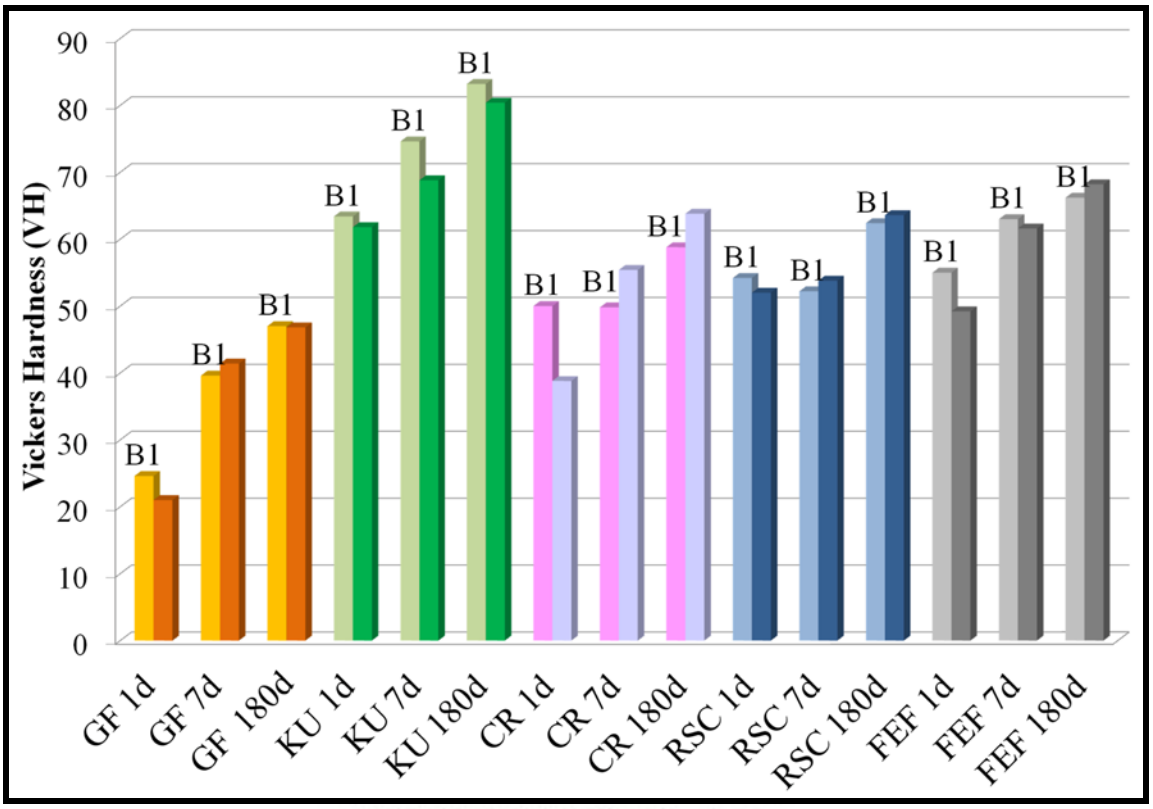

3.5.3. Compressive strength

The compression strength values between the batches of the same material, but different specimens for days 1, 7 and 180 were compared (Figure 3.9). All the materials indicated an increase in compressive strength over the progression of 1, 7 and 180 days, with the exception of KU B1 on day 7; CR B1 on day 7; CR B2 on day 7; RSC B1 on day 7 and RSC B2 on day 7. There is no clear explanation for this finding as the specimens were all produced at the same point in time prior to storage. These specimens interestingly all had a lower mean compressive strength on day 7 compared to the comparative compressive strength values at days 1 and 180. The aim of study was however still achieved since this decrease on day 7 for the aforementioned batches did not show any statistical differences between the batches for each manufacturer.

Figure 3.9: Mean compression strength values (MPa) of batches for days 1, 7, 180

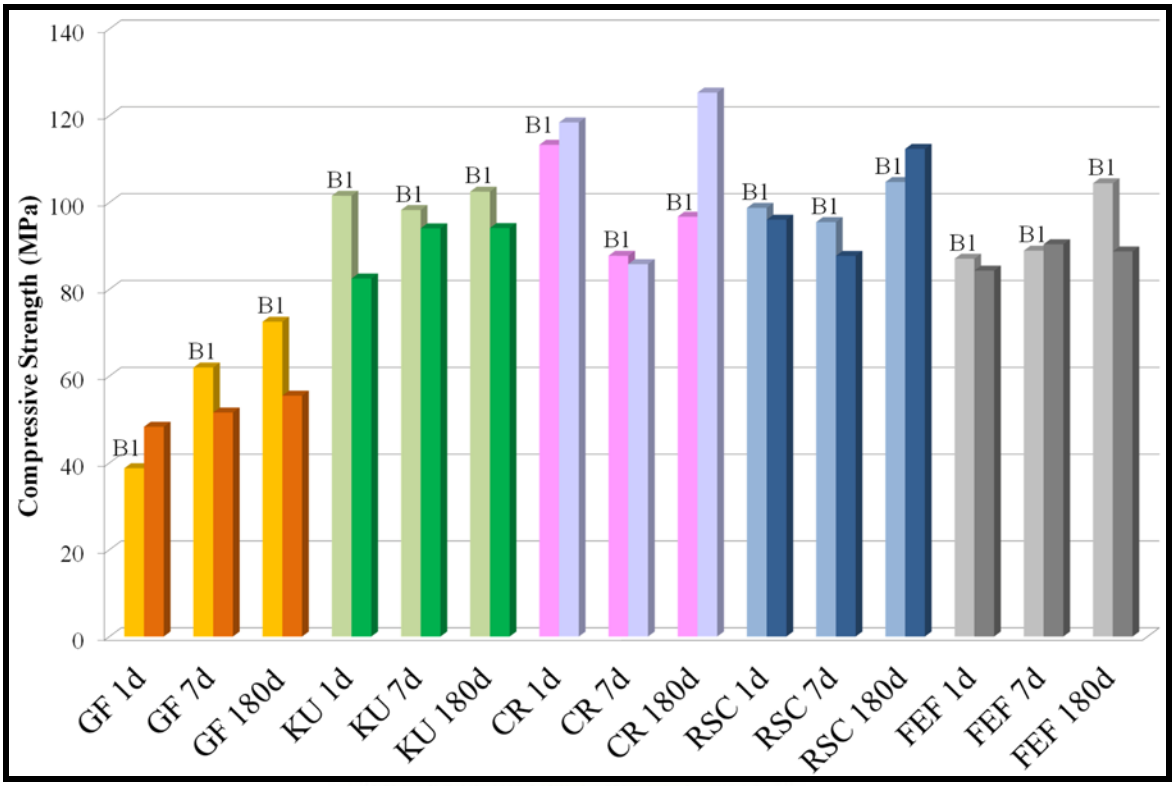

3.6. Discussion

The present study rejected the hypothesis that the PLR would be similar between the two materials batches for CR, KU and RSC. Furthermore, the hypothesis that the variance in the PLR of the capsules between the batches would not differ for GF was also rejected. For IM and KU, the hypothesis that the variances would not differ significantly was accepted, since all the observations from B1 and B2 were within the -10% to 10% range. However, the hypothesis that no significant difference would exist between the batches for the Vickers Hardness and compressive strength were accepted for the days 1, 7 and 180. The PLR of GICs is pivotal to the strength and longevity of these dental restorations (Fleming, 2003). Previous studies done on the GF carbomer have not assessed a PLR variation of that suggested by the manufacturer. The

present study however only focussed on the PLR differences between batches and their effect on the Vickers Hardness and compressive strength.

The PLR has an effect not only on the physical properties of the material, but also impacts the setting time (Eames *et al*., 1977). A greater amount of powder and/or less liquid decreases the setting time and increases the compressive strength. Decreases in PLR negatively impact on various properties of the material and acid erosion of the restoration is more likely to occur (Zahra *et al*., 2011). The material has to resist the stresses that occur during mastication in posterior teeth (Dowling and Fleming, 2008), since this is the area in which the material is utilised in most clinical scenarios. When the optimal PLR relationship is maintained for GIC and carbomer materials, the material should perform as the manufacturer intended if the clinical scenario permits. The PLR influences the way the GIC internally counters the compressive strength and elastic modulus during function (White and Yu, 1993). *In vitro* compressive strength provides insight into the properties of a material, since masticatory forces are partly compressive (Craig, 1997). Additionally, the surface micro-hardness parameters provide insight into the material's resistance to penetration of the surface. The recommended PLR, which appears on the manufacturer's packaging, is therefore the "gold standard" to which the powder and liquid of capsulated materials should adhere. Each manufacturer sets their own PLR in accordance with their internal research and development of the material. Subsequently, the manufacturers compile their internal testing data from this premise of the recommended PLR in the capsule.

The greater powder ratios in both GICs and RMGICs have resulted in accelerated setting reactions. This therefore reduces the working time for the clinician (Quackenbush *et al*., 1998; Fleming *et al*., 2012). Inconsistencies in the PLR were observed between batches of the same

GIC material and carbomer in this study and a PLR above the 10% of the manufacturer's recommendation resulted in an increased viscosity, which can influence the clinical handing. This was evident in a study where clinicians mixed GICs to their preference (Billington *et al*., 1990).

From the results of the present study, it was apparent that FEF had the most individual capsule observations with PLRs above 10% of the manufacturer's recommendations. It was expected that B1 and B2 from each material would have no difference in the PLR between the capsules from that manufacturer. This study illustrated that there were differences based on the SD between the batches of the materials in relation to the manufacturers' recommendation for the PLR of the GICs capsules. The spread of the observations is illustrated in Figure 3.7, but are only relevant if there are capsules with a PLR above the 10% perimeter. The degree to which these variations of the PLR between the manufacturer's recommendation and the actual content of the PLR in the capsule influences the Vickers Hardness and the compressive strength, were determined to have no significant influence between the two batches for the same time periods. Variations between capsulated materials are expected, but the manufacturer placed an exact value in grams on the material brochures and not a range/estimated powder and liquid weight. There were various ranges presented in the literature on the permissible percentage that the PLR can vary below the manufacturer's recommendation before the properties are negatively affected (Fleming, 2003; Behr *et al*., 2008, Torabzadeh *et al*., 2011). The present study assessed the PLR in the capsules and illustrated that most observations were found to be above, but also within the 10% PLR recommended by the manufacturer. The literature cited in this Chapter on PLR mainly focused on the reduction of the PLR below that of the manufacturer's recommendation. In the present study, the negative effects of too much liquid or too little powder resulted in a PLR value below that of the manufacturer's recommendation. The effective reduction of the powder weight

that serves as the filler particle and the ion donor reduces the ability to achieve an optimal compressive strength. GIC specimens from the literature were unable to withstand the *in vitro* analysis where the powder was kept constant and the liquid was increased to the level where the PLR was 17% below the manufacturer's recommendation (PLR -17%) (Behr *et al*., 2008). The physical properties of GIC specimens with various PLRs were assessed by Fleming *et al*, (2003) at PLRs of -10%, -20% and -50% powder to a constant volume of liquid as per the manufacturer's mixing recommendation. The -20% group presented with significantly lower compressive strengths and significantly longer setting times. The variation in the study of -10% PLR resulted in compressive strength variation not significantly different from the manufacturer's recommended PLR (Fleming, 2003) and was confirmed by this assessment of the GICs and carbomer. All the aforementioned articles indicated that when the PLR of the GIC ranges between the -10% and 0% ratio of the manufacturer's recommendation, the compressive strength and setting time should be within the suggested features as outlined in the material brochures of the manufacturer. It was concluded that in order to maintain the compressive strength of GICs, the PLR should not differ by more than -10% to 10% of the manufacturer's recommended PLR. An increase in the powder will result in a higher viscosity of the GIC, as noted during specimen production for this PLR study. The low Vickers Hardness and compressive strength values of GF carbomer could be because the specimen device could not accommodate the surface protective gloss and subsequent thermocuring with the LED application. It has been shown that the glass phase of the carbomer has fewer network modifying ions available than regular aluminosilicate glass (Zainuddin *et al*., 2012). Another study concluded that the compressive strength was not significantly increased during thermocuring with the LED through the gloss (De Caluwe *et al*., 2017). Therefore, omitting the gloss and LED thermocured steps did not necessarily cause the lower compressive strength values.

Although there were differences in the individual weights of the powder and the liquid for the GICs and the carbomer, the Vickers Hardness and compressive strength were not significantly affected.

The viscosity of some of the capsulated GICs and the carbomer did not really change as the PLR remained close to the manufacturer's recommended PLR. FEF was the only exception, where extrusion difficulty was noticeable with most of the capsules. Based on Table 3.3, the net ratio between the powder and the liquid weight resulted in lower weights than those recommended by the manufacturer. In Figure 3.7 and Table 3.4, the PLR variation of -10% to 10% illustrated that most of the observations for CR, GF, IM, KU and RSC were within this parameter. Considering that the compressive strength assessed in this study did not indicate a significant difference between the two batches within a material group, it would support the theory that a PLR between -10% and 10% PLR deviation from the manufacturer's PLR recommendation would be acceptable. Figure 3.7 illustrates that CR, KU and RSC B2 were the only materials that were well distributed around the manufacturers' recommendations. The SD between observations from a particular manufacturer represents the significant difference in the spread between various observations of B1 and B2 (Table 3.4). Although the SD of the mean showed significant differences for some materials, all the SDs from a clinical and *in vitro* testing perspective were still well below the -10% to 10% variation of the mean PLR value. The p-values for the mean of B1 versus B2, as well as the SD of B1 versus B2 indicated that the filling of the capsules with powder and/or liquid were relatively consistent and close together, although the PLR was above the recommended PLR of the manufacturer. The manufacturers consistently over-filled the capsules with powder and/or liquid with the exception of CR B1/B2, KU B1/B2 (Figure 3.7). When Table 3.3 is considered for RSC B2, the significant role that the powder and/or liquid weights play in the final PLR becomes clear. Figure 3.7 illustrates the PLR of the 20 capsules of

RSC B2 being well distributed around the manufacturer's PLR (i.e. only a +0.63% difference from manufacturer's recommended PLR, Table 3.3). However, when the individual powder (-7.93%) and liquid (-8.57%) mean values for RSC B2 were below the weight stated by the manufacturer, the PLR was very close to the manufacturer's PLR. The KU B1 mean powder (-0.17%) and liquid (-0.66%) compared to RSC B2 further illustrated this individual powder and liquid importance (Table 3.3). Considering the consistently overfilled capsules, it was essential to evaluate the magnitude in terms of the effect on the PLR. Essentially the PLR is an important influencing factor on the Vickers hardness and compressive strength. When assessing the PLR from B1 and B2, it became clear that if the mean PLR values of the capsules per batch was considered - CR, GF, IM, KU and RSC had mean PLR values that differed less than -10% to 10% from the manufacturer's PLR (Table 3.3). The majority of the FEF B1/B2 PLR was well above the manufacturer's PLR.

The complex nature of the PLR becomes clear when the various combinations of the powder and liquid weight determines the PLR. The same mean PLR could be achieved with both a high powder/low liquid weight or vice versa. The B1 and B2 mean values as shown in Table 3.3 do not have large percentage differences when compared with the manufacturer's recommended PLR. Only FEF B1 (+10.79) and FEF B2 (+10.41) had a PLR higher than 10% of that recommended by the manufacturer. Table 3.3 shows the role that the powder and the liquid play towards the resultant PLR in the capsules. This role explains the significant difference found between CR B1/B2, as well as KU B1/B2. The batches from CR and KU showed the best distribution of observations around the manufacturer's recommendation (Figure 3.4) as well as a relatively small percentage variation in relation to the other GIC powder and liquid weights. The mean value above the manufacturer's recommendation for CR B1 (-5.75) and CR B2 (-5.75) as well as for KU B1 (+0.52) and KU B2 (-0.94) were the reason for the significant difference

between the mean batch PLRs. There was a large difference between the GF powder and liquid content from the evaluated capsules compared to the manufacturer's recommendation (on the side of the packaging). Nevertheless, during statistical analysis of the evaluated PLR, only a very small difference between the manufacturer's recommended PLR and the mean PLR of GF B1 (+6.32) and GF B2 (+5.02) were noted. This clearly illustrates that the combination of the powder and the liquid values can offset one another to have a PLR that is closer to the manufacturer's recommendation. Therefore, three things should be considered when assessing the effect of PLR in the capsules in relation to the manufacturer recommendation: 1) the internal data of the manufacturer is accepted as correct with the premise that the powder and liquid are the same as the actual capsule PLR content, based on the provided individual powder and liquid weights 2) the physical properties must not differ significantly and 3) a PLR range must be within -10% to 10% of the manufacturer's recommendation.

The literature further indicated that capsulated GICs have an advantage due to ease of mixing, reduction in variation of the PLR and the ease of clinical application. Additionally, capsulated GICs are mechanically mixed and therefore the mix is clinically reproducible.

3.7. Conclusion

Although the capsule PLR of the GIC materials was shown to be well distributed around the manufacturer's PLR recommendation, the spread of the individual capsule PLR can influence the overall mean value. It is therefore essential that the -10% to 10% PLR for each manufacturer be used to assess the individual GIC capsule for consistency. The results concluded that the physical properties with regard to Vickers Hardness and compressive strength were not negatively affected as none of the materials had values below the -10% PLR. The small difference between the manufacturer's recommended mean values and the total observations

from this study illustrated that GIC capsules are still a predictable dispensing format, provided the manufacturer stays within a -10% to 10% range of their recommended PLR.

3.8. Limitations

IM could not be assessed for Vickers Hardness or compressive strength due to insufficient capsules per batch. The liquid content of the KU and IM groups were additionally confirmed by weight determination of the silver diaphragm as well. This could have also been completed for the plunger group and for capsules with liquid housing chambers.

Acknowledgement:

This chapter was published in the New Zealand Dental Journal

https://www.nzda.org.nz/assets/files/Archives/NZDJ_Articles/2019/June_2019/Variation_of_powder:liquid_ratios_of_capsulated_glass-ionomer_materials.pdf

3.9. References

Arita, K., Yamamoto, A., Shinonaga, Y., Harada, K., Abe, Y., Nakagawa, K. and Sugiyama, S. (2011). Hydroxyapatite particle characteristics influence the enhancement of the mechanical and chemical properties of conventional restorative glass-ionomer cement. *Dental Materials Journal*, 30(5), pp.672-683.

Azillah, M., Anstice, H. and Pearson, G. (1998). Long-term flexural strength of three direct aesthetic restorative materials. *Journal of Dentistry*, 26(2), pp.177-182.

Behr, M., Rosentritt, M., Loher, H., Kolbeck, C., Trempler, C., Stemplinger, B., Kopzon, V. and Handel, G. (2008). Changes of cement properties caused by mixing errors: The therapeutic range of different cement types. *Dental Materials*, 24(9), pp.1187-1193.

Billington, R., Williams, J. and Pearson, G. (1990). Variation in powder/liquid ratio of a restorative glass-ionomer cement used in dental practice. *British Dental Journal*, 169(6), pp.164-167.

Burke, F. and Lynch, E. (1994). Glass polyalkenoate bond strength to dentine after chemomechanical caries removal. *Journal of Dentistry*, 22(5), pp.283-291.

Cattani-Lorente, M., Godin, C. and Meyer, J. (1993). Early strength of glass ionomer cements. *Dental Materials*, 9(1), pp.57-62.

Chau, N., Pandit, S., Cai, J., Lee, M. and Jeon, J. (2015). Relationship between fluoride release rate and anicariogenic biofilm activity of glass ionomer cements. *Dental Materials*, 31(4), pp.e100-e108.

Craig, R. (1997). *Mechanical Properties. In: Restorative dental materials.*. 10th ed. St. Louis: Mosby, pp.56-103.

De Caluwe, T., Vercruysse, C. and Martens, L. (2017). Mechanical and Bioactive Properties of a Commercial Glass Carbomer: GCP Glass Fill. *Avicenna Journal of Dental Research*, 9(4).

Dowling, A. and Fleming, G. (2008). Is encapsulation of posterior glass-ionomer restoratives the solution to clinically induced variability introduced on mixing? *Dental Materials*, 24(7), pp.957-966.

Eames, W., Monroe, S., Roan, J. and O'Neal, S. (1977). Proportioning and mixing of cements: a comparison of working times. *Operative Dentistry*, 2(3), pp.97-104.

Ellakuria, J., Triana, R., Mínguez, N., Soler, I., Ibaseta, G., Maza, J. and García-Godoy, F. (2003). Effect of one-year water storage on the surface micro-hardness of resin-modified versus conventional glass-ionomer cements. *Dental Materials*, 19(4), pp.286-290.

Ewoldsen, N., Covey, D. and Lavin, M. (1997). The physical and adhesive properties of dental cements used for atraumatic restorative treatment. *Special Care in Dentistry*, 17(1), pp.19-24.

Fleming, G. (2003). Influence of powder/liquid mixing ratio on the performance of a restorative glass-ionomer dental cement. *Biomaterials*, 24(23), pp.4173-4179.

Fleming, G., Dowling, A. and Addison, O. (2012). The crushing truth about glass ionomer restoratives: Exposing the standard of the standard. *Journal of Dentistry*, 40(3), pp.181-188.

Fleming, G., Kenny, S. and Barralet, J. (2006). The optimisation of the initial viscosity of an encapsulated glass-ionomer restorative following different mechanical mixing regimes. *Journal of Dentistry*, 34(2), pp.155-163.

Frencken, J., Makoni, F. and Sithole, W. (1998). ART restorations and glass ionomer sealants in Zimbabwe: survival after 3 years. *Community Dentistry and Oral Epidemiology*, 26(6), pp.372-381.

Gee, D. and Pearson, G. (1993). Effect of mixing speed on mechanical properties of encapsulated glass-ionomer cements. *British Dental Journal*, 174(2), pp.65-68.

Glasspoole, E., Erickson, R. and Davidson, C. (2002). Effect of surface treatments on the bond strength of glass ionomers to enamel. *Dental Materials*, 18(6), pp.454-462.

Hatton, P. and Brook, I. (1992). Characterisation of the ultrastructure of glass-ionomer (poly-alkenoate) cement. *British Dental Journal*, 173(8), pp.275-277.

Hewlett, E., Caputo, A. and Wrobele, D. (1991). Glass ionomer bond strength and treatment of dentin with polyacrylic acid. *The Journal of Prosthetic Dentistry*, 66(6), pp.767-772.

Holmgren, C., Lo, E., Hu, D. and Wan, H. (2000). ART restorations and sealants placed in Chinese school children - results after three years. *Community Dentistry and Oral Epidemiology*, 28(4), pp.314-320.

Maeda, T., Mukaeda, K., Shimohira, T. and Katsuyama, S. (1999). Ion Distribution in Matrix Parts of Glass-Polyalkenoate Cement by SIMS. *Journal of Dental Research*, 78(1), pp.86-90.

Matsuya, S., Maeda, T. and Ohta, M. (1996). IR and NMR Analyses of Hardening and Maturation of Glass-ionomer Cement. *Journal of Dental Research*, 75(12), pp.1920-1927.

McInnes-Ledoux, P., Weinberg, R. and Grogono, A. (1989). Bonding glass-ionomer cements to chemomechanically-prepared dentin. *Dental Materials*, 5(3), pp.189-193.

Menne-Happ, U. and Ilie, N. (2013). Effect of heat application on the mechanical behaviour of glass ionomer cements. *Clinical Oral Investigations*, 18(2), pp.643-650.

Mulder, R. (2018). Variation in the Dispersions of Powder Liquid Ratios in Hand-Mix Glass Ionomers. *The Open Dentistry Journal*, 12(1), pp.647-654.

Nassan, M. and Watson, T. (1998). Conventional glass-ionomers as posterior restorations. A status report for the Am Journal of Dentistry. *American Journal of Dentistry*, 11, pp.36-45.

Ngo, H., Mount, G., Mc Intyre, J., Tuisuva, J. and Von Doussa, R. (2006). Chemical exchange between glass-ionomer restorations and residual carious dentine in permanent molars: An in vivo study. *Journal of Dentistry*, 34(8), pp.608-613.

Nicholson, J. (1998). Chemistry of glass-ionomer cements: a review. *Biomaterials*, 19(6), pp.485-494.

Nomoto, R. and McCabe, J. (2001). Effect of mixing methods on the compressive strength of glass ionomer cements. *Journal of Dentistry*, 29(3), pp.205-210.

Nomoto, R. (2004). Effect of mixing method on the porosity of encapsulated glass ionomer cement. *Dental Materials*, 20(10), pp.972-978.

O'Brien, T., Shoja-Assadi, F., Lea, S., Burke, F. and Palin, W. (2010). Extrinsic energy sources affect hardness through depth during set of a glass-ionomer cement. *Journal of Dentistry*, 38(6), pp.490-495.

Pelka, M., Ebert, J., Schneider, H., Kramer, N. and Petschelt, A. (1996). Comparison of two-and three-body wear of glass-ionomers and composites. *European Journal of Oral Sciences*, 104(2), pp.132-137.

Quackenbush, B., Donly, K. and Croll, T. (1998). Solubility of resin-modified glass-ionomer cement. *American Society of Dentistry for Children*, 65, pp.310-312.

Rupp, D., Hernesch, C. and Charlton, D. (1996). Effect of triturator speed variation on physical properties of encapsulated glass-ionomer luting cements. *Operative Dentistry*, 21(3), pp.96-102.

Ten Bosch, J., Fennis-le, Y. and Verdonschot, E. (2000). Time-dependent Decrease and Seasonal Variation of the Porosity of Recently Erupted Sound Dental Enamel in vivo. *Journal of Dental Research*, 79(8), pp.1556-1559.

Torabzadeh, H., Ghasemi, A., Shakeri, S., Baghban, A. and Razmavar, S. (2011). Effect of powder/liquid ratio of glass-ionomers cements on flexural and shear bond strengths to dentin. *Brazilian Journal of Oral Sciences*, 10(3), pp.204-207.

White, S. and Yu, Z. (1993). Compressive and diametral tensile strengths of current adhesive luting agents. *The Journal of Prosthetic Dentistry*, 69(6), pp.568-572.

Wilson, A., Prosser, H. and Powis, D. (1983). Mechanism of Adhesion of Polyelectrolyte Cements to Hydroxyapatite. *Journal of Dental Research*, 62(5), pp.590-592.

Xie, D., Brantley, W., Culbertson, B. and Wang, G. (2000). Mechanical properties and microstructures of glass-ionomer cements. *Dental Materials*, 16(2), pp.129-138.

Yap, A., Pek, Y. and Cheang, P. (2003). Physico-mechanical properties of a fast-set highly viscous GIC restorative. *Journal of Oral Rehabilitation*, 30(1), pp.1-8.

Yoshida, Y., Van Meerbeek, B., Nakayama, Y., Snauwaert, J., Hellemans, L., Lambrechts, P., Vanherle, G. and Wakasa, K. (2000). Evidence of Chemical Bonding at Biomaterial-Hard Tissue Interfaces. *Journal of Dental Research*, 79(2), pp.709-714.

Zahra, V., Kohen, S. and Macchi, R. (2011). Powder-liquid ratios and properties of two restorative glass-ionomer cements. *Acta Odontologica Latinoamericana*, 24(2), pp.200-204.

Zainuddin, N., Karpukhina, N., Law, R. and Hill, R. (2012). Characterisation of a remineralising Glass Carbomer® ionomer cement by MAS-NMR Spectroscopy. *Dental Materials*, 28(10), pp.1051-1058.

Zanata, R., Magalhães, A., Lauris, J., Atta, M., Wang, L. and Navarro, M. (2011). Micro-hardness and chemical analysis of high-viscous glass-ionomer cement after 10 years of clinical service as ART restorations. *Journal of Dentistry*, 39(12), pp.834-840.

Zoergiebel, J. and Ilie, N. (2013). An *in vitro* study on the maturation of conventional glass ionomer cements and their interface to dentin. *Acta Biomaterialia*, 9(12), pp.9529-9537.

CHAPTER 4

VARIATIONS IN THE DISPERSION OF POWDER/LIQUID RATIOS IN HAND-MIX GLASS IONOMER RESTORATIVE CEMENTS

4.1. Abstract

Background: The influence of powder/liquid ratios (PLRs) and the available literature on the handling and physical properties of glass ionomer restorative cements (GICs) were investigated.

Objective: The objective of the study was to compare the PLR variability and magnitude in hand-mix GICs, as dispensed for clinical use. From the recorded individual powder and liquid weights, additional comparisons could be made by pairing the various "extreme" outer observations in relation to the manufacturer's PLR.

Study design: The materials assessed were Ketac Universal hand-mix (KU), Riva Self Cure hand-mix (RSC) and Fuji IX GP hand-mix (FN). Twenty scoops of powder were paired with twenty drops of liquid, as would be the case in a clinical scenario. Statistical analysis was completed using the Kruskal Wallis H test, intraclass correlation (ICC) and straight line regressions with One-way ANOVA and the post-hoc Tukey HSD Test ($p < 0.05$ was considered significant).

Results: The powder and liquid observations indicated a lack of consistency in both the powder and liquid dispersions. The volume remained "one drop" but the weights were much lower than the manufacturer's recommended drop weight for some observations, due to the presence of air in the liquid drop. The Kruskal-Wallis H test indicated significant differences ($p = 0.0001$) between the three materials for the paired PLRs. The One-way ANOVA and post-hoc Tukey

HSD Test were used to compare the recommended PLR to the results and the significant differences ($p < 0.01$).

Conclusion: The recommended manufacturers' powder and liquid weights were KU 0.150/0.05g, RSC 0.165/0.035 and FN 0.18/0.05, respectively. KU, FN and RSC liquid had powder and liquid dispersions above the manufacturers' recommendations. FN had the most paired PLR observations within the ±10% range followed by KU. This means that extreme powder and liquid combinations could occur in the clinical scenario and these combinations could influence the physical properties of the restoration that the clinician places.

Keywords: Hand-mix, powder/liquid ratio, glass ionomer, liquid weight, powder weight, manufacturer's recommendation.

Abbreviations and acronyms:

FN: Fuji IX GP hand-mix

GIC: Glass ionomer restorative cement

ICC: Intraclass correlation

KU: Ketac Universal hand-mix

PLR: Powder liquid ratio

RSC: Riva self cure hand-mix

4.2. Introduction

The literature shows that capsulated glass ionomer restorative cements (GICs) stay superior to the hand-mixed versions with regard to the consistent mixing regime and physical properties (Fleming, 2003; Nomoto *et al*., 2004). The capsulated GIC powder/liquid ratio (PLR) is not influenced as severely as the variation in PLR of hand-mix GIC preparations (Fleming, 2003). Besides an increased fluoride release (Verbeeck *et al*., 1993) the capsules have a definite advantage due to the decrease in operator variability (Nomoto *et al*., 2004) and increased ease of dispension into the cavity preparation (Hatrick and Eakle, 2016). The clinician-induced variation in PLR in relation to the manufacturer's recommendation, results in the compressive- and diametral tensile strength being influenced (Billington *et al*., 1990). The reduction in the physical properties also has clinical relevance with regard to the wear resistance. Hand-mix GICs are more regularly used in clinical practice compared to capsulated GICs. The clinical manipulations of hand-mix GICs by clinicians are based on personal preference of the material consistency (Cattani-Lorente *et al*., 1993). This preferred consistency does not necessarily reflect the manufacturer's PLR recommendation, with the speed of spatulation and the powder content being manipulated by clinicians (Billington *et al*., 1990; Cattani-Lorente *et al*., 1993). Clinician variability markedly reduces the powder content of the GIC to below the manufacturer's recommendation to as much as -50%. A large reduction in the PLR of hand-mix GICs were noted when anterior teeth were restored. The use of capsulated GICs was suggested as a suitable alternative (Dowling and Fleming, 2009).

The hypothesis of the present study was that the powder and the liquid dispensed would be the same as the manufacturer's recommendation. The aim of this study was therefore to assess the PLR variability and the extent of the variability for hand-mix GIC formulations as dispensed for clinical use. From the recorded individual powder and liquid weights, additional comparisons

could be made by pairing the various "extreme" outer observations in relation to the manufacturer's PLR.

4.3. Materials and methods

This *in vitro* comparative study of three GIC hand-mix restorative materials was completed in accordance with the manufacturers' recommendations.

4.3.1. Specimen preparation

Three GIC materials were used (Table 4.1). A total of 20 powder scoops and 20 liquid drops from the materials were dispensed (n = 60 powder; n = 60 liquid drops). The research assistant randomly allocated materials to the researcher for assessment, thereby ensuring that the researcher was blinded to the type of material being assessed. The researcher dispensed the powder and liquid in accordance with the manufacturers' instruction sheets. The liquid bottle was kept perpendicular to the paper pad. The excess powder in the scoop was removed by levelling it against the plastic margin present in the lid of the powder bottle. This technique is in accordance with the manufacturer's instruction sheet and simulates the technique that clinicians should follow. The weight determination of the powder and the liquid were completed on a desktop analytical balance to an accuracy of 0.0001g *(Metler AE240 analytical balance, Columbus, Ohio, USA)* at a constant room temperature (23±1°C) with a relative humidity of 50±5% (Twomey *et al*., 2004).

4.3.2. Test parameters

One scoop of powder and one drop of liquid was dispensed under standardised laboratory conditions to be "paired" as an observation of the PLR. The powder and liquid pairing was done in order to calculate the PLR as would have been the case in a clinical setting.

4.4. Statistical analysis

The observed powder and liquid values were paired as initially dispensed. These results were assessed with the Kruskal Wallis H test, intraclass correlation (ICC) and straight line regressions. The twenty paired observations were firstly compared with a Kruskal-Wallis H test to determine if there were differences in the PLR score between the three groups: Ketac Universal hand-mix (KU), Riva Self Cure hand-mix (RSC) and Fuji IX GP hand-mix (FN). In order to determine the difference between and correlation with the manufacturer's PLR recommendation, an intraclass correlation was done with the two-way mixed-effect model at a 95% confidence interval ($p < 0.05$ as significant).

The values obtained in this observational study were further compared as a percentage difference between the manufacturer's PLR recommendation and the observed dispersion of powder and liquid. A graphical representation of the straight-line regression of the observations was made with a ±10% limit from the observed value as well at the manufacturer's recommendation. The PLR recommended by the manufacturer was compared with the PLR of this observational study. The statistical analysis was completed after the straight-line regression with One-way ANOVA and the post-hoc Tukey HSD Test (Statistical analysis with R Core Team (2013); (R: A language and environment for statistical computing. R Foundation for Statistical Computing, Vienna, Austria).

4.5. Results

The Kruskal-Wallis H test indicated the differences in the paired PLR to determine the extent of the variability for hand-mix GIC formulations between the three materials. Mean PLR scores had statistically significant differences between materials, $p = 0.0001$.

Upon analysis of the intraclass correlation (ICC), no degree of reliability was present between the paired PLR ratio and the manufacturers' recommended PLR for KU, RSC or FN. The confidence interval included zero and the $p > 0.05$. The ICC was not regarded as statistically significant.

The manufacturers' recommended PLRs are represented in Table 4.1.

Table 4.1: Manufacturer supplied PLR recommendations

Material and manufacturer	Material abbreviation	Recommended powder (g)	Manufacturer recommended liquid (g)	Manufacturer recommended PLR
Fuji IX GP hand-mix (*GC Corp, Tokyo, Japan, Batch: 1503231*).	FN	0.18	0.05	3.6:1
Ketac Universal hand-mix (*3M ESPE, Seefeld, Germany, Batch: 583514*).	KU	0.150	0.05	3:1
Riva Self Cure hand-mix (*SDI Limited, Australia, Batch: 62657V*).	RSC	0.165	0.035	4.7:1

Figure 4.1 represents the observations of the powder, liquid and the recommended PLR of the three manufacturers' PLRs. The horizontal lines indicate the ±10% allowable variation in order to retain the physical properties of the GIC (Figure 4.1). The graphs illustrate that all the paired KU and FN ratios are greater than the manufacturers' recommended PLRs. The opposite was found for the RSC ratios.

Figure 4.1: Powder, liquid and PLR observations achieved by the operator

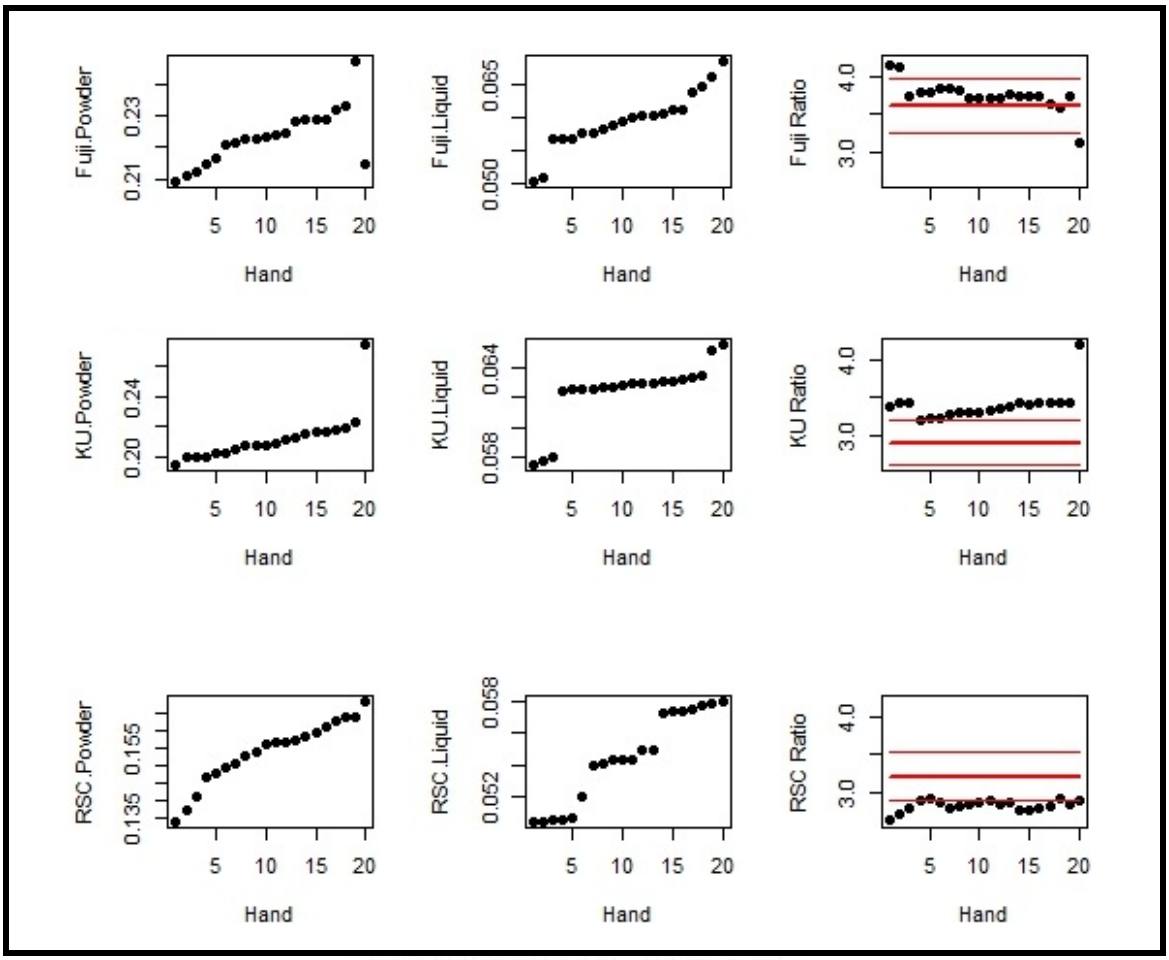

The powder and liquid observations shown in the graph indicate the lack of consistency of both the powder and liquid dispensing (Figure 4.1). The trend from the first 19 observations is nearly linear with random variations. The standard deviation obtained from a straight-line regression was 0.00111. According to this regression, the expected value at observation number 20 should have been 0.2227. This means that the observed KU powder observation number 20 was 0.275, resulting in a difference from the expected value of (0.275-0.2227)/0.00111=47.1 standard deviations. This illustrates that the KU powder observation number 20 can be considered an outlier.

Based on the random error standard deviation for FN, the successive difference of the first 18 observations was 0.00134. The estimated standard deviation of the difference between two observations for FN was $0.00134\sqrt{2} = 0.00190$. The observed difference between observations 18 and 19 was 0.0139, i.e. 7.3 standard deviations, denoting 18 and 19 as outliers. Similarly, the difference between FN observation 20 and 19 was 0.0324, with 17.1 standard deviations.

It was therefore appropriate to perform a comparison between the manufacturers' PLR recommendations *versus* the twenty-paired PLR observations. The One-way ANOVA and post-hoc Tukey HSD tests indicated significant differences with $p < 0.01$ between the KU, FN and RSC manufacturers' PLR in relation to the PLR of each glass ionomer assessed.

Table 4.2 illustrates the individual observations as they were paired: one powder to be mixed with one liquid, as would be the case for the clinical setting. The paired observations for KU, FN and RSC liquid had observations above the +10% mark. KU and FN had the most paired PLR observations for both powder and liquid observations above the +10% ratio in relation to the manufacturers' recommendations. Although the paired powder and liquid weights were different from the manufacturer's recommended PLR for each scoop or drop, the final PLR remained within the ±10% range of the manufacturers' recommendations for FN (17) and KU (7). RSC showed all 20 paired observations below the -10% PLR of the manufacturer's recommendation even though the RSC powder had 15 of the observations within the ±10% of the manufacturer's recommendation.

Table 4.2: Paired observations distribution between the ±10% limits of the manufacturer's recommendation

Material	Observations within ±10%	Observations below -10%	Observations above +10%	Paired observation PLR within ±10%	Paired observation PLR below -10%	Paired observation PLR above +10%
FN powder	0	0	20	17	1	2
FN liquid	2	0	18			
KU powder	0	0	20	7	0	13
KU liquid	0	0	20			
RSC powder	15	5	0	0	20	0
RSC liquid	0	0	20			

Table 4.3 shows the various combinations for the smallest and largest values of the powder and the liquid observations. Although the 20 powder observations were paired with the 20 liquid observations in Table 4.2 for statistical purposes, in order to simulate the clinical scenario, other "extreme" combinations are possible. It was plausible to consider that any combination of the powder and liquid observations could have occurred in the clinical scenario. The variation of the PLR in the dispensing stage can occur due to the variation of the powder and/or the liquid. Table 4.3 illustrates the extremes of PLR variation, e.g. largest powder in combination with smallest liquid observation.

For the most part, the PLR percentage difference in Table 4.3 illustrates that all three manufacturers had variations from the recommended PLR when the smallest and largest combinations were evaluated. RSC PLR combinations of the powder and liquid had all the extreme combinations of the PLR well below the manufacturer's recommendation (Table 4.3). The comparison of the extreme PLR values for KU and FN had PLR both above and below the manufacturers' PLR. The percentage difference between the various extreme values ranged

between 22.11% (RSC), 33.97% (FN) and 42.08% (KU) (Table 4.3). For RSC, on the other hand, the value of the liquid being above the +10% mark and the powder within or below the manufacturer's recommendation, resulted in the PLR in Table 4.3 being well below the manufacturer's PLR recommendation. FNH, interestingly had values above the +10% for the powder and the liquid (Table 4.2), but the PLR presented values either above or below the manufacturer's PLR (Table 4.3). Based on the results, the hypothesis that the powder and the liquid dispensed would be the same as the manufacturer's recommendation was rejected.

Table 4.3: Extreme powder/liquid combinations from the operator observations

Material	"Extreme" observations				
	Mean P or Mean L	**Highest P or Highest L**	**Lowest P or Lowest L**	**Highest P or Lowest L**	**Lowest P or Highest L**
FN powder	0.223165^{+}	0.2147^{+}	0.2089^{+}	0.2147^{+}	0.2089^{+}
FN liquid	0.05958^{+}	0.0686^{+}	0.0503^{+}	0.0503^{+}	0.0686^{+}
FN PLR	3.7456:1	$3.1297{:}1^{-}$	$4.153{:}1^{+}$	$4.2683{:}1^{+}$	$3.0451{:}1^{-}$
FN PLR % different to manufacturer's recommendation	+1.04%	-13.06%	+15.36%	+18.56%	-15.41%
KU powder	0.2119^{+}	0.275^{+}	0.1938^{+}	0.275^{+}	0.1938^{+}
KU liquid	0.0623^{+}	0.0655^{+}	0.0575^{+}	0.0575^{+}	0.0655^{+}
KU PLR	$3.3987{:}1^{+}$	$4.1984{:}1^{+}$	$3.3704{:}1^{+}$	$4.7826{:}1^{+}$	2.9587:1
KU PLR % different to manufacturer's recommendation	+13.29%	+39.94%	+12.34%	+40.71%	-1.37%
RSC powder	0.15384	0.1684	0.1335^{-}	0.1684	0.1335^{-}
RSC liquid	0.05446^{+}	0.058^{+}	0.0504^{+}	0.0504^{+}	0.058^{+}
RSC PLR	$2.8249{:}1^{-}$	$2.9034{:}1^{-}$	$2.6488{:}1^{-}$	$3.3412{:}1^{-}$	$2.3017{:}1^{-}$
RSC PLR % different to manufacturer's recommendation	-39.89%	-38.22%	-43.64%	-28.91%	-51.02%
The "+" indicates a value above +10% and "-" below -10%, of the manufacturer's powder weight per scoop or liquid weight per drop recommendation in Table 4.1.					

4.6. Discussion

The powder densities determine the weight per volume of the powder present in the scoop (Billington *et al*., 1990; Fleming *et al*., 1999; Fleming, 2003; Mount *et al*., 2016). The hygroscopic nature of the powder was not relevant for this study, since the materials were opened at the commencement of the study and the observations immediately completed. The room temperature, angle and the finger pressure applied to the bottle during liquid dispensing play a role in the amount of liquid that is dispensed (Billington *et al*., 1990; Fleming *et al*., 1999; Fleming, 2003; Mount *et al*., 2016). It was noted that air bubbles were present in some drops of liquid from all manufacturers. The volume remained "one drop" but the weight was much lower than the manufacturer's recommended drop weight. These factors impact on the powder and liquid weight and can therefore influence the handling and physical properties of the materials.

Compressive strengths obtained due to variation in the PLR of hand-mix GICs indicated that a 100% PLR ratio was not significantly different from a 90% PLR ratio, but was significantly different from 80% ratio. An 80% PLR ratio (20% less than the manufacturer's recommendation) also resulted in statistically significant longer setting times as less powder was incorporated into the constant volume of liquid (Fleming, 2003). For this reason, 10% less than the manufacturer's recommendation is acceptable as a PLR variation. A decreased PLR affects the physical properties and increases the setting time (Eames *et al*., 1977). The decrease in filler particles result in a weaker material. With GICs being more active in the presence of an acidic environment (Asmussen and Peutzfeldt, 2002), the decrease in pH will result in an increased acid erosion of the restoration (Zahra *et al*., 2011). This poses a problem if one considers that GICs are specifically indicated in higher caries risk patients. The Vickers Hardness (VH) and the three body wear tests for a GIC luting cement illustrated that when the GIC liquid content increased to 17% more than the manufacturer's recommended PLR, there was a 50% decrease in both the VH and wear resistance of the GIC luting cement. The increase of the powder to 17%

above the manufacturer's recommendation did not negatively affect the VH and the wear resistance. An increase in liquid greater than the aforementioned 17% resulted in samples that could not withstand wear cycles (Behr *et al*., 2008). The higher the amount of powder incorporated, the greater the mechanical properties of GICs (Yap *et al*., 2001). The amount of powder correlates with the compressive strength and wear resistance. The solubility, setting and working time is indirectly correlated with the amount of powder incorporated (Crisp *et al*., 1975; Fleming, 2003).

The dispensing of powder and liquid prior to mixing should be aimed at being as close to the manufacturer's recommendation as possible to prevent changes in the physical properties. If clinicians are made aware of the impact of variation from the recommended PLR, one might find a greater acceptance of GIC materials. A study performed with a hand-mixed GIC (Fleming, 2003), assessed the physical properties with various powder ratios to a constant liquid ratio that was maintained at 1g. This aforementioned study found that powder ratios of 50% and 80% less than the manufacturer's instructions statistically decreased the compressive strength as well as the setting time of the GIC tested (Fleming, 2003). This decrease in powder led to a lower concentration of reinforced glass particles which in turn, resulted in a decreased load-bearing capacity. The clinician should therefore attempt to mix GICs with as high a powder content as possible, provided that there is still enough liquid for the gelation to occur. This would translate well to the RSC materials that were well below the -10% value for the PLR extremes. GICs with high powder content would be more resistant to the effects of moisture, have a shorter working time and a higher compressive strength. GICs with increased powder content can be a clinically identified as a viscous paste (Crisp *et al*., 1975). Results from the present study indicated that the largest powder and the smallest liquid ratio should result in a higher PLR (Table 4.3). It was noted that the extreme ranges of KU (+40.71%) and FN (+18.56%) had values well above the

+10% range. RSC extreme ranges still obtained a -28.91% below the recommended PLR of the manufacturer. If the powder ratio was more than what the liquid can effectively hydrate, a faster setting reaction will take place and the material will set before the restoration is placed in the prepared cavity (Fleming, 2003). The variability in the liquid to powder ratio will affect the clinical handling and physical properties of the GIC (Zahra *et al*., 2011). In general, FN seemed to be the closest to the manufacturer's recommendation, although the ICC was not significant. This could explain why the FN hand-mix GICs performed better than the capsulated version in a previous study from 2007 (Ilie and Hickel, 2007).

FN hand-mix and Fuji IX Fast Capsules have the same PLR according to the manufacturer's recommendation. The short capsule titration versus the 40s hand-mix was suggested as the reason why the hand-mix formulation could have had more homogeneity of the powder and liquid mix (Dowling and Fleming, 2008). This explains why the FN hand-mix had a significantly higher compressive strength compared to the Fuji IX Fast Capsule group. The spatulation time for hand-mix was 40 seconds, resulting in a greater interaction between the liquid and the powder of FN hand-mix GICs. The mixing time of capsulated GICs is usually reduced compared to hand-mix versions. The Fuji IX Fast Capsule group which has a mixing time of 10s (*3M ESPE, Capmix*^{TM}) or 11s is completed with the *Rotomix*^{TM} (the mixing time is 8s with 3s of centrifuging; (*3M ESPE, Rotomix*^{TM}) in accordance with the manufacturer's instructions.

4.7. Conclusion

An increase in powder above the manufacturer's recommendation with a constant liquid will result in a PLR above the manufacturer's recommendation. This will result in an increased setting time and increased physical properties. In the clinical setting, consistent dispersion of

powder and liquid is ideal. Irregularities in dispersions have contributed to the possibility of various extreme PLR combinations. The presence of air bubbles in the liquid when dispensing was not a significant contributor to variations in PLR. Increasing the scoop size per dispension could be a strategy to mitigate the low PLR for RSC. Although the FN powder and liquid weights were greater than the recommended manufacturer's PLR recommendation, the observations from FN were the closest to the manufacturer's recommendation. The reality is that extreme powder and liquid combinations could occur in the clinical environment. The clinical implications are that too little liquid with too much powder will also have an increased PLR. Too much powder, or too little liquid will result in an insufficient acid-base reaction with a decrease in the physical properties, change in the working time and an altered manipulation ability of the clinician during restoration placement.

Acknowledgement:

This chapter was published in The Open Journal of Dentistry, Betham publishers.

DOI: 10.2174/1745017901814010647

4.8. References

Asmussen, E. and Peutzfeldt, A. (2002). Long-term fluoride release from a glass ionomer cement, a compomer, and from experimental resin composites. *Acta Odontologica Scandinavica*, 60(2), pp.93-97.

Behr, M., Rosentritt, M., Loher, H., Kolbeck, C., Trempler, C., Stemplinger, B., Kopzon, V. and Handel, G. (2008). Changes of cement properties caused by mixing errors: The therapeutic range of different cement types. *Dental Materials*, 24(9), pp.1187-1193.

Billington, R., Williams, J. and Pearson, G. (1990). Variation in powder/liquid ratio of a restorative glass-ionomer cement used in dental practice. *British Dental Journal*, 169(6), pp.164-167.

Billington, R., Williams, J. and Pearson, G. (1990). Variation in powder/liquid ratio of a restorative glass-ionomer cement used in dental practice. *British Dental Journal*, 169(6), pp.164-167.

Billington, R., Williams, J. and Pearson, G. (1990). Variation in powder/liquid ratio of a restorative glass-ionomer cement used in dental practice. *British Dental Journal*, 169(6), pp.164-167.

Cattani-Lorente, M., Godin, C. and Meyer, J. (1993). Early strength of glass ionomer cements. *Dental Materials*, 9(1), pp.57-62.

Dowling, A. and Fleming, G. (2008). Is encapsulation of posterior glass-ionomer restoratives the solution to clinically induced variability introduced on mixing? *Dental Materials*, 24(7), pp.957-966.

Dowling, A. and Fleming, G. (2009). Are encapsulated anterior glass-ionomer restoratives better than their hand-mixed equivalents? *Journal of Dentistry*, 37(2), pp.133-140.

Fleming, G. (2003). Influence of powder/liquid mixing ratio on the performance of a restorative glass-ionomer dental cement. *Biomaterials*, 24(23), pp.4173-4179.

Fleming, G., Marquis, P. and Shortall, A. (1999). The influence of clinically induced variability on the distribution of compressive fracture strengths of a hand-mixed zinc phosphate dental cement. *Dental Materials*, 15(2), pp.87-97.

Hatrick, C. and Eakle, W. (2016). *Dental materials. Clinical applications for dental assistants and dental hygienists.* 3rd ed. St. Louis, Missouri: Saunders, p.87.

Ilie, N. and Hickel, R. (2007). Mechanical Behavior of Glass Ionomer Cements as a Function of Loading Condition and Mixing Procedure. *Dental Materials*, 26(4), pp.526-533.

Mitchell, C., Orr, J. and Russell, M. (1998). Capsulated versus hand-mixed glass-ionomer luting cements for post retention. *Journal of Dentistry*, 26(1), pp.47-51.

Mount, G., Hume, W., Ngo, H. and Wolff, M. (2016). *Preservation and Restoration of Tooth Structure, 3rd Edition*. 3rd ed. John Wiley & Sons.

Skinner, E. and Phillips, R. (1982). *Skinner's science of dental materials*. 8th ed. Philadelphia: Saunders, pp.480-481.

Verbeeck, R., De Moor, R., Van Even, D. and Martens, L. (1993). The Short-term Fluoride Release of a Hand-mixed vs. Capsulated System of a Restorative Glass-ionomer Cement. *Journal of Dental Research*, 72(3), pp.577-581.

CHAPTER 5

POWDER AND LIQUID RATIO OPTIMISATION OF MODIFIED GICs

5.1. Abstract

Purpose: Optimisation of the powder and liquid ratio is essential to achieve the largest possible compressive strength. The objective was to determine the ideal powder/ liquid ratio of the modified GICs that would achieve sufficient physical properties in line with the ISO standard (ISO 9917-1, 2007).

Materials and Methods: The clinician's preference was used to mix the GICs to a "workable smooth mix". This workable smooth mix is subjective between clinicians. As the GIC material modifications were to be investigated by the PhD candidate, his perspective on a "workable smooth mix" was to incorporate as much powder possible without clumping of particles, while still retaining a shiny surface of the mixed GIC. The compressive strength of the GICs mixed in accordance with the clinician's preference was assessed in relation to the manufacturers' recommended powder/liquid ratio on a universal testing machine in MPa.

Results: There were significant differences between the compressive strength obtained from the GICs mixed according to the clinician's preference versus the GICs mixed according to the manufacturers' recommended powder/liquid ratio.

Conclusion: The chitosan- and nanodiamond-modified GIC materials have to be mixed in accordance with the powder/liquid ratio of the respective manufacturers.

Keywords: Powder liquid ratio, clinician's preference, compressive strength, manufacturers' recommendation.

5.2. Introduction

With clinicians and chair side assistants mixing glass ionomer restorative cements (GICs) to their own preference (Cattani-Lorente *et al*., 1993) the present study postulates that an accurate assessment regarding the properties of these restorations cannot be made. The powder/liquid ratios (PLR) play an important role in the physical properties of GICs (Fleming, 2003). It is generally accepted that the maximum amount of powder needs to be added to the GIC in order to obtain sufficient glass particles, thereby increasing its strength (Billington *et al*., 1990).

Fleming *et al*., (2003) showed that decreasing the powder and keeping the liquid constant or an increase in liquid with a constant amount of powder will result in a smaller powder/liquid ratio (Fleming *et al*., 2003). This proves that the physical properties are influenced by the change in the PLR percentage in relation to the manufacturers' recommendations.

The aim of this powder liquid optimisation study was to assess whether the compressive strength would differ between PLRs as mixed according to the clinician's preference versus the PLR as recommended by the manufacturer.

The hypothesis was that the properties of the samples prepared from the smooth mix will have improved physical properties, compared to the manufacturer's powder/ liquid ratio.

5.3. Materials and Methods

Three commercial GICs were modified with the addition of chitosan (CH) or nanodiamonds (ND) in either a 5 or 10% weight by weight percentage (w/w%) substitution. The compressive strength was investigated by comparing the effect of the clinician's preference of powder incorporation to that recommended by the manufacturer.

The approach of determining a "workable PLR" with the chitosan and nanodiamond modifications for this study was initially simply based on obtaining a "smooth mix" according to the clinician's preference, since the chitosan in particular had to dissolve in the liquid of the GIC during mixing. The clinician's preference was used to mix the GICs to a "workable smooth mix".

This concept was obtained from previous studies where GICs modified with the addition of bioactive glasses were evaluated. Two studies cited a methodology where the powder incorporation into a constant liquid was maintained. The author of this dissertation added as much powder as possible, provided that the modified GICs "workable". This approach was also followed for GICs and RMGICs by Yli-Urpo *et al*., (2005) and De Caluwe *et al*., (2017). The clinician's preference was used to incorporate the chitosan- and nanodiamond-modified GIC powders into their respective constant liquid measures.

5.3.1. Powder preparation of modified GICs

The powder of the GICs was modified with chitosan or nanodiamond particles using a previously published methodology (Mulder, 2018). Three commercially available GICs namely FN: Fuji IX GP hand-mix (*GC Corp, Tokyo, Japan; Batch: 1503231*); KU: Ketac Universal hand-mix; (*3M ESPE, Seefeld, Germany; Batch: 583514*) and RSC: Riva Self Cure hand-mix (*SDI Limited, Australia; Batch: 62657V*) were used in this study. In addition to this, each of the three GICs were modified with 5% and 10% w/w chitosan (*Merck, item 448877*) or nanodiamond particles *(PlasmaChem; Item PL-D-G01*) incorporated into the powder phase of the GICs. The GIC powder and nanodiamond particles were placed in an airtight high density polyethylene (HDPE) container and clamped in a beaker shaker for two hours to ensure complete mixing of the GIC powder and the chitosan or nanodiamond particles (Mulder, 2018).

5.3.2. Sample preparation

Samples were prepared from each material and assessed as per the ISO for Dentistry-Water-based cements - Part 1: Powder/liquid acid-base cements (ISO 9917-1, 2007). Five samples were prepared by adding the powder from the selected GICs, according to the clinician's preference for obtaining a "smooth mix" (Group A). Five samples were prepared for the GICs as per the manufacturers' powder and liquid recommendations (Table 5.1) (Mulder, 2018). The weight determination for both the powder and the liquid were determined on a desktop analytical balance to an accuracy of 0.0001g *(Metler AE240 analytical balance, Columbus, Ohio, USA).* The manufacturer's PLR (Group B) was completed after sample production of Group A so as not to influence the clinician by producing the samples of Group B first. The mixed GIC materials were placed in cylindrical Teflon split moulds (height 6±0.1mm, diameter 4±0.1mm). Weight determination of a known amount of powder was added into the manufacturer's recommended liquid measure, until the clinician's preference was achieved. The powder weight incorporated into the known liquid was established by deducting the unused powder from the initial powder weight, to determine the used PLR for Group A.

5.3.3. Compressive strength

The compressive force was measured in Newton (N) with a universal material testing machine (*H10KT-0293 Tinus Olsen, Redhill, England*) at a cross-head speed of 0.75mm/min. The software of the universal tester was used to analyse the results (*QMat Testzone, version 4.5.37, Tinus Olsen, Redhill, England*). The compressive strength was calculated in megapascals (MPa) (Chapter 3).

5.4. Statistical analysis

In order to assess the compressive strength of the sample mixed according to the clinician's PLR choice and compare it to the compressive strength obtained using the manufacturer's PLR, the

Mann Whitney test for unpaired data (also known as Wilcoxon rank sum test) with a confidence level of 0.95 and significance $p < 0.05$ was used.

5.5. Results

The powder/ liquid ratio achieved by the clinician for the assessment Group A was achieved once the GIC was a "smooth workable mix". The resultant powder /liquid ratio is represented in Table 5.1. The manufacturers' recommended PLR was used as the comparative PLR (Group B) and the compressive strengths obtained indicated the presence of significant differences ($p < 0.05$) between materials. All the PLRs from Group A had less powder than the manufacturers' recommendations (Table 5.1).

Table 5.1: Clinicians' preferred PLR in relation the manufacturers' PLR

Material	Powder	Liquid	Ratio	Percentage difference from the manufacturer recommendation
Fuji IX GP hand-mix (*GC Corp, Tokyo, Japan, Batch: 1503231*).	**0.18**	**0.05**	**3.6:1**	**0**
FN5%ND	0.15	0.05	3:1	-16.6
FN10%ND	0.15	0.05	3.1	-16.6
FN5%CH	0.135	0.05	2.7:1	-25
FN10%CH	0.12	0.05	2.4	-33.33

Ketac Universal hand-mix (*3M ESPE, Seefeld, Germany, Batch: 583514*).	**0.15**	**0.05**	**3:1**	**0**
KU5%ND	0.115	0.05	2.3:1	-23.33
KU10%ND	0.115	0.05	2.3:1	-23.33
KU5%CH	0.115	0.05	2.3:1	-23.33
KU10%CH	0.1	0.05	2:1	-66.66
Riva Self Cure hand-mix (*SDI Limited, Australia, Batch: 62657V*).	**0.165**	**0.035**	**4.7:1**	**0**
RSC5%ND	0.126	0.035	3.6:1	-23.4
RSC10%ND	0.101	0.035	2.9:1	-38.29
RSC5%CH	0.098	0.035	2.8	-40.42
RSC10%CH	0.070	0.035	2:1	-57.44

Figure 5.1: Compressive strength of the clinician's preferred PLR in relation the manufacturers' PLR

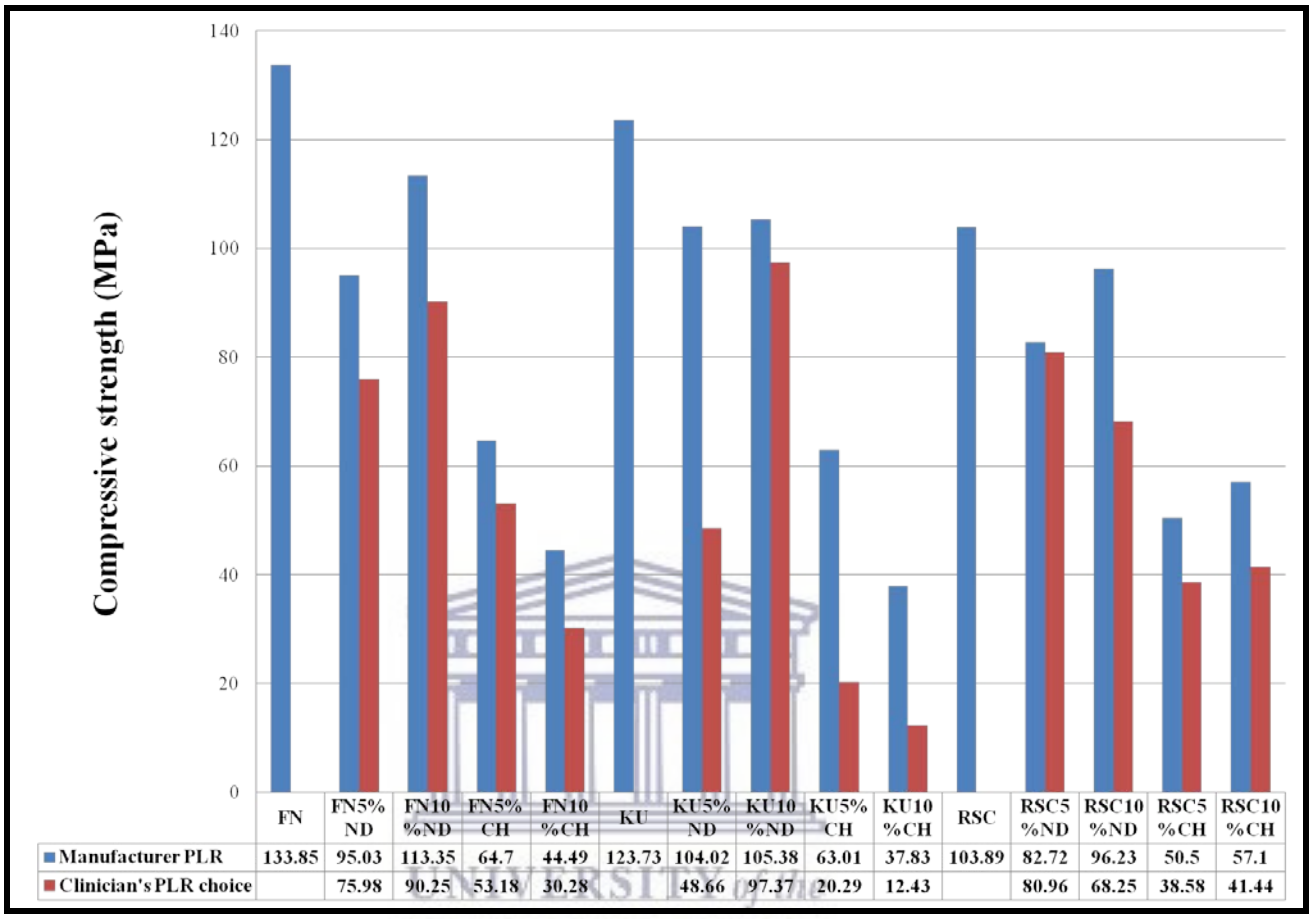

	FN	FN5% ND	FN10 %ND	FN5% CH	FN10 %CH	KU	KU5% ND	KU10 %ND	KU5% CH	KU10 %CH	RSC	RSC5 %ND	RSC10 %ND	RSC5 %CH	RSC10 %CH
Manufacturer PLR	133.85	95.03	113.35	64.7	44.49	123.73	104.02	105.38	63.01	37.83	103.89	82.72	96.23	50.5	57.1
Clinician's PLR choice		75.98	90.25	53.18	30.28		48.66	97.37	20.29	12.43		80.96	68.25	38.58	41.44

Table 5.2: Significance between clinician's preferred PLR in relation the manufacturers' PLR

Material	Clinicians' PLR	Manufacturer PLR
FN5%ND	p = 0.15	
FN10%ND	p = 0.03*	
FN5%CH	p = 0.01*	
FN10%CH	p = 0.01*	
KU5%ND	p = 0.01*	
KU10%ND	p = 0.22	
KU5%CH	p = 0.01*	
KU10%CH	p = 0.01*	
RSC5%ND	p = 1	
RSC10%ND	p = 0.05*	
RSC5%CH	p = 0.01*	
RSC10%CH	p = 0.01*	
(*) indicates p < 0.05		

5.6. Discussion

The hypothesis was rejected, since the properties of the samples prepared by the smooth mix as mixed by the clinician, presented reduced physical properties, compared to the manufacturer's powder/ liquid ratio.

The chitosan and nanodiamonds were added to the GICs in either a 5 or 10% weight by weight percentage (w/w%) and substituted by removing that percentage of powder from the GIC

containers. In order to assess the achievable compressive strength that the clinician could obtain in Group A, five samples were prepared with a standard liquid content into which the powder was incorporated. It is clear from Table 5.1 that the clinician mixed much less powder into the liquid with percentages less than that recommended by the respective manufacturers and ranging from -16.6 to as much as -66.66%. This is consistent with a study for GICs on anterior teeth where a marked reduction in the powder content of GICs by as much as -50% below the manufacturer's recommendation was noted (Dowling and Fleming, 2009).

The variability in the powder ratio (to a constant liquid) affects the clinical handling of GICs (Zahra *et al*., 2011). This would explain why the percentage of powder not incorporated into the liquid increased in the present study as the percentage of chitosan or nanodiamonds increased from 5 to 10%. The amount of powder incorporated for the chitosan-modified GICs was much less than for the nanodiamond materials with the same respective percentages. This was due to the fact that the chitosan particles that were used in its commercially supplied form is relatively large and has a low weight per volume ratio. One chitosan particle replaces multiple GIC powder particles per volume. The "popcorn effect" between the GIC powder and the commercially available chitosan also plays a role in the relatively lower weight of powder in relation to the chitosan replacement of the powder in a weight by weight percentage ratio.

Figure 5.1 illustrates that all the materials in Group A obtained a lower compressive strength compared to the samples in Group B. Table 5.2, therefore illustrates the significant findings that Group A had a lower compressive strength than the samples from Group B was directly related to the lower PLR of Group A versus Group B. Only FN5%ND and RSC5%ND compressive strengths from Group A were not significantly different from Group B; $p = 0.15$ and $p = 1$ respectively. Although the percentage of powder was -16.66 and 23.4% less than the manufacturers', these results were well in line with compressive strengths obtained when variation in the PLR of hand-mix GICs to -20% from the manufacturer's recommendation were

assessed (Fleming, 2003). Although the powder was significantly reduced in Group A, the setting time was not reduced since the chitosan and nanodiamonds have active participation in the acid base reaction, due to the active surface chemistries. In Group B, the setting time was reduced by about 50% as an anecdotal observation with a stopwatch. The setting time was not a priority for this thesis, as further modification with tartaric acid will produce the ideal working and setting time for the material modification(s) that prove most effective in this thesis.

5.7. Conclusion

In this study it was confirmed that the greater the amount of powder incorporated into the liquid of the GICs, the better the mechanical properties of GICs (Yap *et al*., 2001). Hence, for the GICs in this study which were modified with chitosan and nanodiamond particles, it is advisable to dispense the powder and liquid ratio as close to the manufacturers' recommendations as possible to prevent a significant reduction in the compressive strength due to operator failure.

5.8. References

Billington, R., Williams, J. and Pearson, G. (1990). Variation in powder/liquid ratio of a restorative glass-ionomer cement used in dental practice. *British Dental Journal*, 169(6), pp.164-167.

Cattani-Lorente, M., Godin, C. and Meyer, J. (1993). Early strength of glass ionomer cements. *Dental Materials*, 9(1), pp.57-62.

De Caluwé, T., Vercruysse, C., Ladik, I., Convents, R., Declercq, H., Martens, L. and Verbeeck, R. (2017). Addition of bioactive glass to glass ionomer cements: Effect on the physico-chemical properties and biocompatibility. *Dental Materials*, 33(4), pp.e186-e203.

Dowling, A. and Fleming, G. (2009). Are encapsulated anterior glass-ionomer restoratives better than their hand-mixed equivalents? *Journal of Dentistry*, 37(2), pp.133-140.

Fleming, G. (2003). Influence of powder/liquid mixing ratio on the performance of a restorative glass-ionomer dental cement. *Biomaterials*, 24(23), pp.4173-4179.

International Organization for Standardization (2007). *ISO 9917-1- Dentistry-Water based cements Part 1: Powder/liquid acid-base cements*, 1st ed.; (pages1–21).

Mulder, R. (2018). Variation in the Dispersions of Powder Liquid Ratios in Hand-Mix Glass Ionomers. *The Open Dentistry Journal*, 12(1), pp.647-654.

Yap, A., Mudambi, S., Chew, C. and Neo, J. (2001). Mechanical properties of improved visible light-cured resin-modified glass ionomer cement. *Operative Dentistry*, 26(3), pp.295-301.

Yli-Urpo, H., Lassila, L., Närhi, T. and Vallittu, P. (2005). Compressive strength and surface characterization of glass ionomer cements modified by particles of bioactive glass. *Dental Materials*, 21(3), pp.201-209.

Zahra, V., Kohen, S. and Macchi, R. (2011). Powder-liquid ratio and properties of two restorative glass ionomer cements. *Acta Odontológica Latinoamericana*, 24(2).

CHAPTER 6

PHYSICAL PROPERTIES AND WEIGHT CHANGE BEHAVIOUR OF CHITOSAN OR NANODIAMOND-MODIFIED GLASS IONOMER RESTORATIVE CEMENTS

6.1. Abstract

*Purpose***:** The aim of the study was to assess selected physical properties of glass ionomer restorative cements (GICs) after chitosan or nanodiamond modification. The hypothesis was that the water sorption, surface roughness, surface micro-hardness, compressive strength and the proportional limit of the modified GICs would be improved in relation to their respective commercial materials.

Background: The compressive strength assessment was based on the International Organization for Standardization Standard (ISO) for water-based dental cements (2007; 9917-1).

Materials and Methods: Three different commercially available hand-mix GICs were used in this study: Fuji IX GP (FN), Ketac Universal (KU) and Riva Self Cure (RSC). The three GICs were modified in the powder phase per weight percentage (w/w%) by adding 5% or 10% of a commercially available chitosan (CH) powder (*Merck, item 448877*) or nanodiamond (ND) particles (*PlasmaChem, item: PL-D-G01*) to the GICs. The specimens were prepared using a standard powder liquid ratio in a Teflon mould and polished with 1200 grit wet silicon carbide paper, weighed and subsequently stored in neutral de-ionised water at 37ºC for 24 hours after which the experiments were completed.

Results: The one way ANOVA test for homogeneity of the mean values of FN, KU, RSC and their respective chitosan or nanodiamond modifications indicated the presence of significant differences ($p < 0.00001$) for compressive strength, proportional limit and surface micro-hardness. For weight gain due to water sorption, the control materials increased significantly less

($p < 0.05$) than the chitosan and nanodiamond modifications. The chitosan modifications had a significant difference when compared with the control materials ($p < 0.01$) for the water contact angle. FN10%ND was significantly lower than FN. KU5%ND was higher than KU ($p < 0.01$). The chitosan modifications resulted in a significant ($p < 0.01$) increase in surface roughness over the control and nanodiamond GIC materials.

Significance: The chitosan modifications presented with the lowest compressive strength, proportional limit and surface micro-hardness values. The chitosan particles mixed with the GIC powder became completely encapsulated by the GICs and this phenomenon was referred to as "popcorn effect", as it was a key role player in the poor performance of the chitosan-modified GICs.

Overall, the nanodiamond particles had no significant differences and did not perform significantly worse than their respective control materials. In accordance with the ISO 9917-1, the compressive strength (CS) in MPa above 100MPa was only observed for FN, KU, RSC, FN10%ND and KU5%ND.

Key words: Glass ionomer, compressive strength, micro-hardness, surface roughness, proportional limit, water contact angle, weight gain, surface tension, nanodiamond and chitosan.

Abbreviations and acronyms

FN: Fuji IX GP

CH: Chitosan

GICs: Glass-ionomer restorative cements

CS: Compressive strength

KU: Ketac Universal

ND: Nanodiamond (s)

RSC: Riva Self Cure

ICPMS: Inductively coupled plasma mass spectrometer

MPa: Megapascals

N: Newton

SEM-EDS: Scanning Electron Microscopy and Energy Dispersive X-Ray Spectrometry Microanalysis

VH: Vickers Hardness / surface micro-hardness

w/w%: weight by weight percentage

wt%: weight percentage

6.2. Introduction

The linear coefficient of thermal expansion is a clinically relevant property of GIC materials, since it is similar to that of enamel (11.4 CTE [ppm]) and relatively close to dentine (8.3 CTE [ppm]). This CTE has been measured during *in vitro* studies at a temperature between 20ºC to 60ºC (Esser *et al*., 1998; Craig, 2002). GICs have a CTE [ppm] property that is close to that of tooth structure with a linear coefficient of thermal expansion (CTE [ppm]) at 10.2-11.4 CTE [ppm]. GICs consist of a powder phase of aluminosilicate glass and a liquid phase with a water soluble organic polymer of poly-carboxylic acid (Nicholson, 1999). GICs are considered to be "high-viscosity GICs" when the powder: liquid ratio is at least 3.6 powder: 1 liquid (Nicholson, 2018). Using this as a guide, FN with a powder of 3.6 to a liquid of 1 and RSC (4.7:1) are high viscosity GICs. KU had the lowest powder to liquid ratio (3:1) and is therefore a medium viscosity GIC (Mulder, 2018).

The initial setting reaction in the first 10 minutes is followed by a continued setting or maturation process that occurs over days to months. Some of the important changes that occur during maturation are: 1) the steady increase of compressive strength (CS), that results in a higher compressive strength as the material matures over weeks and months compared to the

initial 24-hour compressive strength (Crisp *et al*., 1975). 2) Increase in brittleness due to the toughness that declines. 3) Declining opacity and an increased translucency. 4) Change in weight as moisture interactions with the GICs occur and 5) the formation of the inter-diffusion zone as the GICs are incorporated into tooth structure (Nicholson, 2018).

The "surface roughness" (Ra) has received attention from various spheres of dental material research, but has never been assessed with the weight change of a GIC exposed to moisture. The surface roughness also influences the water contact angle on the surface of the materials. The investigation of the water contact angle on the surfaces that were prepared according to a similar technique should therefore provide additional information regarding the interaction of the GICs with a moist environment. The properties that change due to maturation of GICs are dependent upon moisture ingress into the GICs (Wasson and Nicholson, 1993), but to the opposite effect, exposure to excessive moisture contamination in the early salt-bridge formation stage results in a significantly weakened material (Gemalmaz *et al*., 1998). On the contrary, there are also negative effects from dehydration, resulting in the fraying and cracking of the GICs (Naasan and Watson, 1998).

The aims of this study were to assess the effect of the modification of GICs with chitosan (CH) and nanodiamonds (ND) on the physical properties of materials. The rationale was that various functional groups are introduced by chitosan and nanodiamond particles into the GICs and these interactions with the ions released from the glass filler particles and the functional groups of the carboxylic acid play a role in the moisture ingress of modified GICs. Due to the change in the composition of the GIC matrix and the GICs' surface topography, the water contact angle on the restoration as well as the surface roughness would be influenced. This is why the surface roughness had to be standardised and prepared with the same method. The hypothesis was

therefore that the weight gain, compressive strength, proportional limit and surface micro-hardness would increase with chitosan and nanodiamond modifications to the GICs.

6.3. Materials and Methods

6.3.1. Materials

Three different commercially available hand-mix GICs were used in this study: Fuji IX GP (FN: *GC Corp, Tokyo, Japan, Batch: 1503231*), Ketac Universal (KU: *3M ESPE, Seefeld, Germany, Batch: 583514*) and Riva Self Cure (RSC: *SDI Limited, Australia, Batch: 62657V*). The three GICs were modified in the powder phase per weight (w/w%) by adding 5% or 10% of a commercially available chitosan powder (*Merck, item 448877*) or nanodiamond particles (*PlasmaChem, item: PL-D-G01*) to the GICs. The modified experimental materials were prepared by placing the GIC powder in an airtight high density polyethylene (HDPE) container. The container was subsequently clamped in a beaker shaker for two hours to ensure complete mixing of the two powders prior to dispensing the powder with a level manufacturer's spoon and a drop of liquid. The modification of the GIC powder was done with chitosan or nanodiamond particles to a 5-weight% modification GIC powder or a 10%-weight modification. Therefore, the final w/w% was 95% commercial GIC and 5%CH or 5%ND per weight. The powder/liquid ratio prescribed by the manufacturer was followed and confirmed on a desktop analytical balance (*Metler AE240 analytical balance, Columbus, Ohio, USA*) by first dispensing the powder followed by the liquid. This ensured that the manufacturer's recommended powder/liquid ratio was maintained (Mulder, 2018).

Fifteen powders were prepared: (1) FN GIC powder [FN]; (2) FN GIC powder modified with 5-wt% chitosan powder [FN5%CH]; (3) FN10%CH; (4) FN5%ND; (5) FN10%ND; (6) KU; (7)

KU5%CH; (8) KU10%CH; (9) KU5%ND; (10) KU10%ND; (11) RSC; (12) RSC5%CH; (13) RSC10%CH; (14) RSC10%ND; (15) RSC5%ND.

6.3.2. Sample distribution

Group A: Five samples (height 6±0.1mm, diameter 4±0.1mm) for the weight change determination, proportional limit and compressive strength.

Proportional limit is defined as the maximum point just before the sample fractures, where if the force is removed, the material could return to its original form. Below the fracture point the maximum proportional limit value will have a linear relationship between applied force and the materials' compression (Giancoli, 1998:253).

Group B: Five samples (height 6±0.1mm, diameter 4±0.1mm) were produced for surface micro-hardness.

Group C: Ten samples (diameter 5±0.1mm and thickness 2±0.1mm) were made to determine the subsequent surface roughness and the water contact angle.

Figure 6.1: Flow diagram of methods applied to Group A, B and C

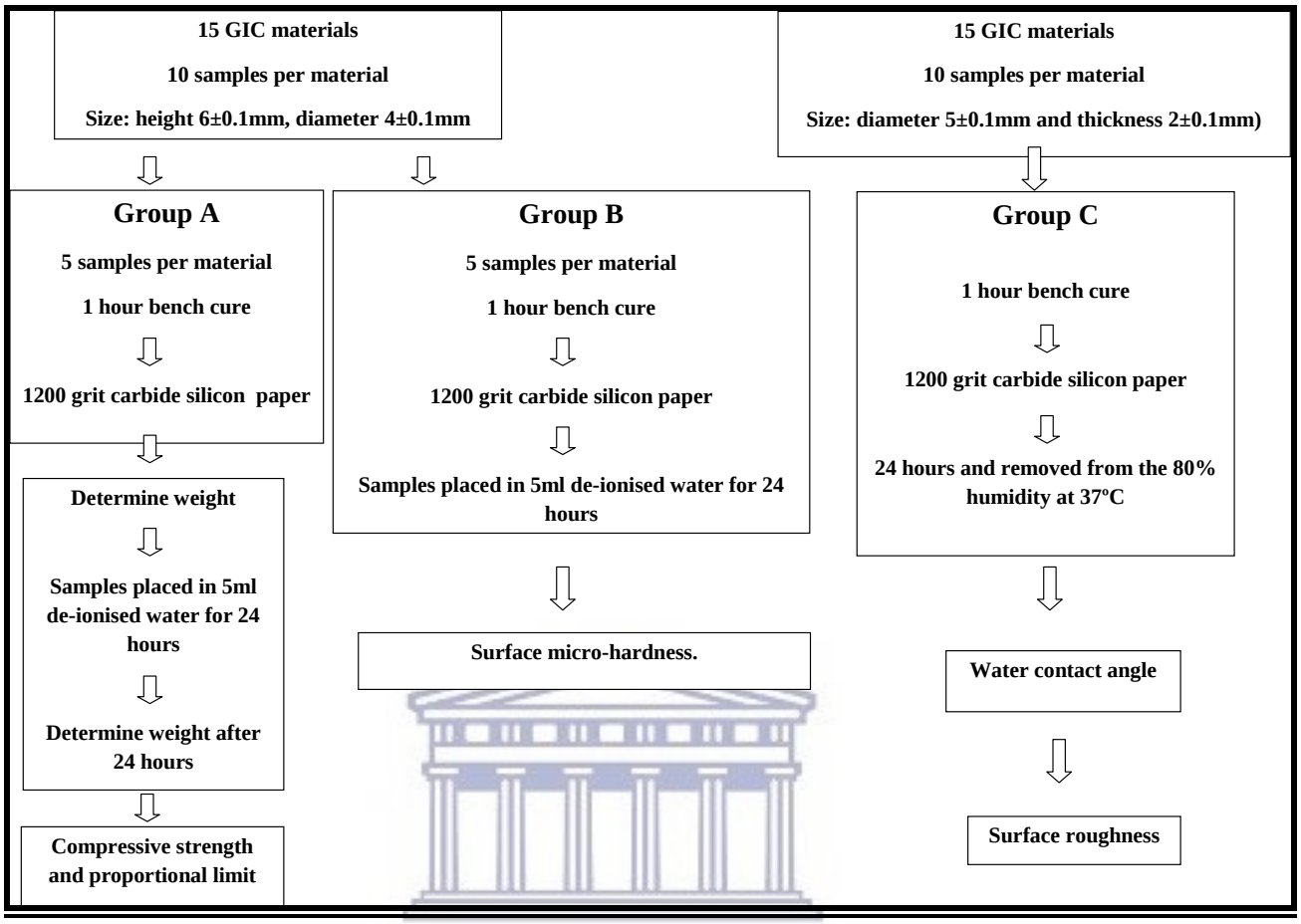

6.3.3. General sample preparation and GIC handling protocols

The materials were kept at room temperature (23±1°C) with a relative humidity of 50±5% and the moulds were stored in a temperature-controlled incubator (37±1°C) prior to testing (Twomey *et al*., 2004; ISO 9917-1, 2007; Menne-Happ and Ilie, 2013). After 1 hour of bench curing, the 150 samples for group A and B were prepared with 1200 grit (*3M, Massachusetts, USA*) wet silicon carbide paper and placed in 5ml of de-ionised water for maturation. The 75 samples for Group A were prepared with 1200 grit wet silicon carbide paper, the weight was assessed for Group A and then the samples were placed in 5ml of de-ionised water. Group C received 1200 grit as per the ISO 9917-1, 2007 for acid erosion. After 24 hours, the weight, followed by

compression strength and proportional limit determination was completed for Group A and the surface micro-hardness was assessed for Group B.

6.3.4. Group A: Weight change determination

Group A: weight change determination was completed to the fourth decimal on an analytical balance (*Metler AE240 analytical balance, Columbus, Ohio, USA*) one hour after bench curing and wet silicon carbide paper preparation prior to placing the 75 samples from group A in the 5ml de-ionised water. After 24 hours, the samples were blot dried and weighed again. The percentage change in weight was calculated for statistical analysis. The stability of GICs in water has been noted to be acceptable (McKenzie *et al*., 2003; ISO 9917-1, 2007).

6.3.5. Compressive strength and proportional limit

The 75 samples from Group A were assessed for compressive strength and proportional limit, 24 hours after their placement in the de-ionised water. Five cylindrical test specimens were prepared and assessed as per the ISO for Dentistry-Water-based cements - Part 1: Powder/ liquid acid-base cements (ISO 9917-1, 2007). For the mixing of the materials, the ISO 9917-1 standard indicated a relative humidity of 50±10%. The mould and clamp used to prepare the specimens were kept in a temperature-controlled cabinet (37±1ºC) with a 30% relative humidity. All the specimens were prepared at room temperature (23±1ºC). The cylindrical test specimens were made by placing the mixed materials into a Teflon split mould with stainless steel plates (height 6±0.1 mm, diameter 4±0.1 mm). The mould was slightly overfilled and a cellulose strip was placed between the material and the plates. The specimens were removed from the moulds after one hour of bench-setting and immediately submerged in individual containers of 5ml de-ionized water grade 3 (37±1°C), as defined in ISO 3696:1987. The specimens were stored in this medium for 1 day (in a temperature-controlled cabinet). The compressive force (p) was measured in Newton with a universal material testing machine (*H10KT-0293 Tinus Olsen*,

Redhill, England) at a cross-head speed of 0.75mm/ min. The software of the universal tester was used for analysis of the results (*QMat Testzone, version 4.5.37, Tinus Olsen, Redhill, England*). The specimens (with moist filter paper on either side) were placed with their flat ends between the plates on the testing machine, so that the progressively increasing compressive load was applied along the 6 mm long axis of the specimen.

The compressive strength was calculated in megapascals (MPa), using the following equation: $C = 4p/\pi d^2$, where C: Compressive strength in MPa, p: Compressive force/maximum force applied in Newton (N), d: Diameter of the specimen, in millimeters and π: Constant for pie used as 3.14. The proportional limit (σ) was determined by assessing the curve of the compressive strength test for each sample in the QMat Testzone. The software used the formula σ = Force in Newton /Area.

6.3.6. Group B: Surface micro-hardness analysis

Group B: The surface micro-hardness of the samples prepared from the three commercial GICs and their modifications were assessed on five prepared samples with the Vickers Hardness indenter (*Zwick-Roell durometer, ZHV1/2 Micro-vickers, Italy*) after 24 hours.

The sample dimensions, preparation and storage were completed as described for the specimens for compressive strength. Twenty four hours after the specimens were submerged in de-ionised water, the surface of all the specimens for surface micro-hardness testing were prepared with 1200 grit wet silicon carbide paper (*3M, Massachusetts, USA*). The wet silicon carbide paper ensured an adjustment to the surface of ±100µm (as measured with a micrometer). The application of the wet silicon carbide paper simulated the restoration polishing that would occur in the clinical setting (Menne-Happ and Ilie, 2013). This wet silicon carbide paper-prepared surface allowed for accurate evaluation of the surface micro-hardness by evaluating the pyramidal indentation from the Vickers Hardness (VH) indenter on the surface of the GIC

material. A second and blinded operator completed the surface micro-hardness evaluation with a Vickers Hardness indenter set at HV0.5 (load of 500gf) and a dwell (indentation) time of ten seconds. The instrument automatically calculated the VH after the diagonals were selected by the operator. Three surface micro-hardness indentations were repeated 500µm apart from one another on each specimen to obtain a mean value per specimen (Figure 6.2) (Ellakuria *et al*., 2003; Yap *et al*., 2003; O'Brien *et al*., 2010).

Figure 6.2: Surface micro-hardness indentations 500µm apart

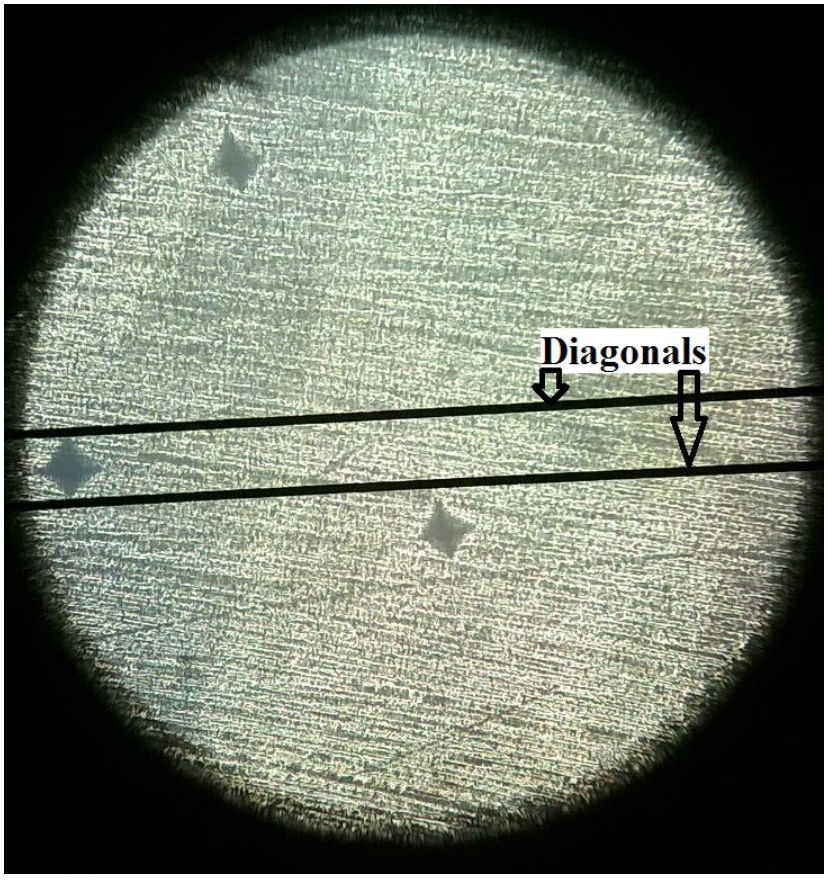

6.3.7. Group C: Water contact angle and surface roughness

6.3.7.1. Water contact angle

The water contact angle measurement method has been cited as the most definitive method to determine an average value for hydrophobicity (wettability) of a material surface (Doyle, 2000).

The GIC specimens for wettability and surface roughness were made in a Teflon mould (diameter 5±0.1mm and thickness 2±0.1mm). Five samples per material were made. The samples were stored in 80% humidity at 37ºC for 24 hours and then removed. The surface was prepared using 1200 grit wet silicon carbide paper, followed by it being blot-dried with filter paper and the water contact angle assessed with a stereomicroscope (*Zeiss Stemi880, GmbH*). The stereomicroscope was positioned perpendicularly +1-2º, in order to achieve the correct position to view the sessile water drop and the sample surface. This allowed the near edge of the sample stage to be slightly out of focus to the line of sight. This position of +1-2º allows for a more accurate representation of the drop bottom (Bracco and Holst, 2013). The contact angle of the 10µl of de-ionised water sessile drop was placed with a fixed volume micropipette (Namen *et al*., 2008). Five samples per material received one drop, where the contact angle was measured on the left and right of the drop, with the average per drop used as the water contact angle. The micropipette was suspended perpendicularly in an adjustable angle clamp 3mm above the sample with the tip 5mm from the edge of the sample, to allow the water drop to interact with the GIC sample surface, without falling onto the surface. The micropipette was removed and after 20 seconds of drop stabilization (Kasraei and Azarsina, 2012), a photo (*Zeiss Axiocam ERc5s digital camera, GmbH*) was taken with a stereomicroscope at 25 X magnification. The sample was turned and the next drop was placed. The software (*Zen 2.3 blue ed, Carl Zeiss Microscope 2011, GmbH*) was used to measure the liquid-solid surface interface for five different drops around the margin of the sample. The average contact angle was calculated per

material and the following equation was used to determine the water adhesion tension: $\tau^o = \cos \theta \times \gamma^o$.

τ^o is water adhesion tension, γ^o is the water interfacial tension = 72.8 dyn/cm and θ is the water adhesion contact angle. If $\theta > 65^o$ *and* $\tau^o < 30$ *dyn/cm,* then the surface of the GICs are hydrophobic. When $\theta < 65$ *and* $\tau^o > 30$ *dyn/cm,* the surface of the GIC is hydrophilic (Vogler, 1998).

6.3.7.2. Surface roughness

The contact surface roughness (Ra) of the materials was measured on the five samples used for the aforementioned water angle determination with a Leeb contact surface roughness tester. A standard sensor (*Model Leeb432, Chongqing Leeb Instrument co Ltd*) was used and the Ra meter had a measuring range of 0.005-16μm for Ra. The testing parameters were: surface roughness (Ra), Filter set at Gauss, the assessment length (λc) at 0.8mm x n5 (assessment length (*L*n=*l*r x n); *L*n=3.2mm) (ISO 4288, 1998) and the range at ±80μm. The standard stylus has a natural diamond at a 90º cone angle with a 5 μm tip radius. The stylus applied a force to the sample of <4mN. The travelling speed (Vt) for the above parameters was 0.135mm/s and the measurement accuracy ±10%.

Two parallel lines were recorded 2mm apart and two lines perpendicular to that (n = 4) per sample. The average of the four measurements was used as the mean Ra per specimen.

6.4. Statistical analysis

Statistical analysis of the results was performed with R Core Team (2013) (*R: A language and environment for statistical computing; R: Foundation for Statistical Computing, Vienna, Austria*). Group A: The mean values from the surface micro-hardness samples per material (Ellakuria *et al*., 2003; Yap *et al*., 2003; O'Brein *et al*., 2010) were calculated with the standard

deviation (Table 6.1). For Group A, the surface micro-hardness was assessed with the one way ANOVA test for homogeneity of the mean values. Upon statistical analysis of the compressive strength and the proportional limit for Group B, the variances within-groups were different. In order to apply the correct statistical analysis, a variance stabilising transformation of the data was completed to overcome the difference in variance within the groups. This was achieved by transforming the original readings to their logarithms: Y=log (Compressive strength in MPA) and Y=log (Proportional limit in N). The one way ANOVA test of homogeneity was confirmed with the t-test between the two means and the analysis of variance was performed for all the results from Group A and B. For Group C, the p-value corresponding to the one-way ANOVA was lower than 0.05, suggesting that one or more water contact angles from the GICs were considered significantly different. The Tukey HSD test with the Bonferroni multiple comparison test identified which of the contact angle pairs were significantly different in relation to the control GIC (Kasraei and Azarsina, 2012).

6.5. Results

The one way ANOVA test for homogeneity of the mean values of FN, KU, RSC and their chitosan and nanodiamond modifications indicated the presence of significant differences ($p < 0.00001$) for compressive strength, proportional limit and surface micro-hardness. The data analysis was conducted through the variances. Each control material was first compared with its four modifications. The standard deviations were kept in mind when comparing the means in Table 6.1 of the modifications to their respective control materials. The pooled within material standard deviation (SD) and standard error (SE) that were used to determine if there was any significance between the results were: ±SD0.0535:SE0.023 for compressive strength, ±SD0.0671:SE0.03 for the proportional limit and ±SD11.5033:SE5.144 for the surface micro-hardness. Non-overlap of a pair of limits indicated a statistically significant difference between the means at a significance level of $p < 0.05$ (Figures 6.6, 6.8 and 6.10). The figures represent

the comparison of the modifications per control group, followed by a figure with all the materials present per material group.

Table 6.1. Summary of the mean values with significant differences in relation to the control material for the various physical properties

Group	*In vitro* analysis	Commercial material	Modification			
			5%ND	10%ND	5%CH	10%CH
		FN				
Group A	Weight Change (%)	1.2161	1.6667	2.5076*	1.6249	2.1030*
	Log(Compressive strength MPA)	2.12	1.97	2.04	1.81	1.64
	Compressive strength (MPA)	133.85	95.03-	113.35-	64.70-	44.49-
	Log(Proportional limit N)	2.25	2.12	2.18	1.91	1.7
	Proportional limit (N)	178.52	134.74-	154.38	83.24-	50.72-
Group B	Surface micro-hardness (VH)	95.8	88	74.6-	66-	39.8-
Group C	Water contact angle (θ)^o	64.74	61.22	56.01*	0*	0*
	Water adhesion tension (τ^o)	30.93	34.90	40.53*	72.8*	72.8*
	Surface roughness	1.037	1.360*	0.980	1.201	1.621*
(*) and (^) indicates a significant difference $p < 0.01$ and $p < 0.05$ respectively with control (FN).						
"-"indicates other p-values. (See statistical results for values).						

Group	*In vitro* analysis	Commercial material	Modification			
			5%ND	10%ND	5%CH	10%CH
		KU				
Group A	**Weight determination (%)**	2.3931	2.5898	3.4453*	2.9694	3.6827*
	Log(Compressive strength MPA)	2.085	2.015	1.98	1.79	1.57
	Compressive strength (MPA)	123.73	104.2	97.37-	63.01-	37.81-
	Log(Proportional limit N)	2.21	2.13	2.11	1.89	1.68
	Proportional limit (N)	167.68	135.85	129.82-	77.96-	49.53-
Group B	**Surface micro-hardness (VH)**	67.8	59.4	51-	67	36.6-
Group C	**Water contact angle (θ)°**	53.08	63.8*	52.87	0*	0*
	Water adhesion tension (τ^o)	43.55	32*	43.76	72.8*	72.8*
	Surface roughness	0.859	0.758	0.877	1.251*	1.470*

(*) and (^) indicates a significant difference $p < 0.01$ and $p < 0.05$ respectively with control (KU)

"-"indicates other p-values. (See statistical results for values).

Group	*In vitro* analysis	Commercial material	Modification			
		RSC	5%ND	10%ND	5%CH	10%CH
Group A	**Weight determination (%)**	2.0995	3.0100	3.5169*	3.1260^	3.8162*
	Log(Compressive strength MPA)	2.01	1.91	1.98	1.69	1.61
	Compressive strength (MPA)	103.89	82.72-	96.23	50.50-	44.14-
	Log(Proportional limit N)	2.16	2.06	2.13	1.77	1.73
	Proportional limit (N)	148.88	116.84	136.76	60.33-	55.23-
Group B	**Surface micro-hardness (VH)**	66.8	55.2	57.4	59	37.8-
Group C	**Water contact angle (θ)º**	66.72	70.52	70.74	0*	0*
	Water adhesion tension (τ^{o})	28.65	24.17	23.91	72.8*	72.8*
	Surface roughness	1.322	1.120	1.225	1.715*	1.675*

(*) and (^) indicates a significant difference $p < 0.01$ and $p < 0.05$ respectively with control (RSC).

"-"indicates other p-values. (See statistical results for values).

Weight change

Figure 6.3 illustrates that FN and KU had significantly less water sorption ($p < 0.01$) than their respective 10% modifications with chitosan and nanodiamonds (FN10%ND and FN10%CH).

FN5%ND had significantly less water sorption ($p < 0.01$) than FN5%CH.

KU5%ND had significantly less water sorption ($p < 0.01$) than KU10%ND. KU5%ND had significantly less water sorption ($p < 0.01$) than KU10%CH. KU5%CH had significantly less water sorption ($p < 0.05$) than KU10%CH.

RSC had significantly less water sorption than RSC10%ND ($p < 0.01$), KU5%CH ($p < 0.05$) and RSC10%CH ($p < 0.01$) (Figure 6.3).

Figure 6.3: Weight change percentage of GICs over 24 hours

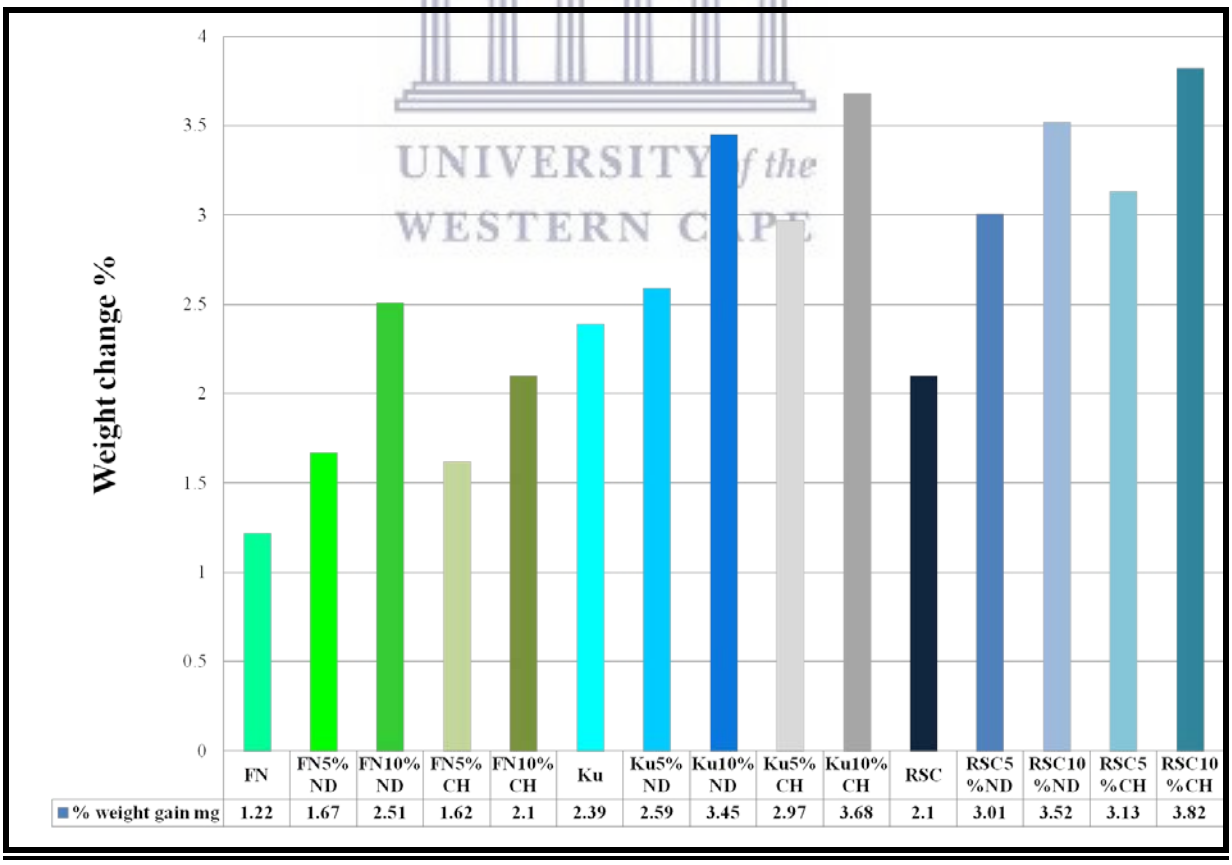

Compressive strength

Figure 6.4: The log (Compressive strength in MPA) vs log (Proportional limit in N) illustrates that the variables were closely correlated to one another. One outlier per control material (FN, KU and RSC) was present, but did not make any difference to the significance of the analysis. Table 6.1 shows the mean values and standard deviations (SD) for the compressive strength.

Figure 6.4: The log (Compressive strength in MPA) vs log (Proportional limit in N) of all fifteen materials

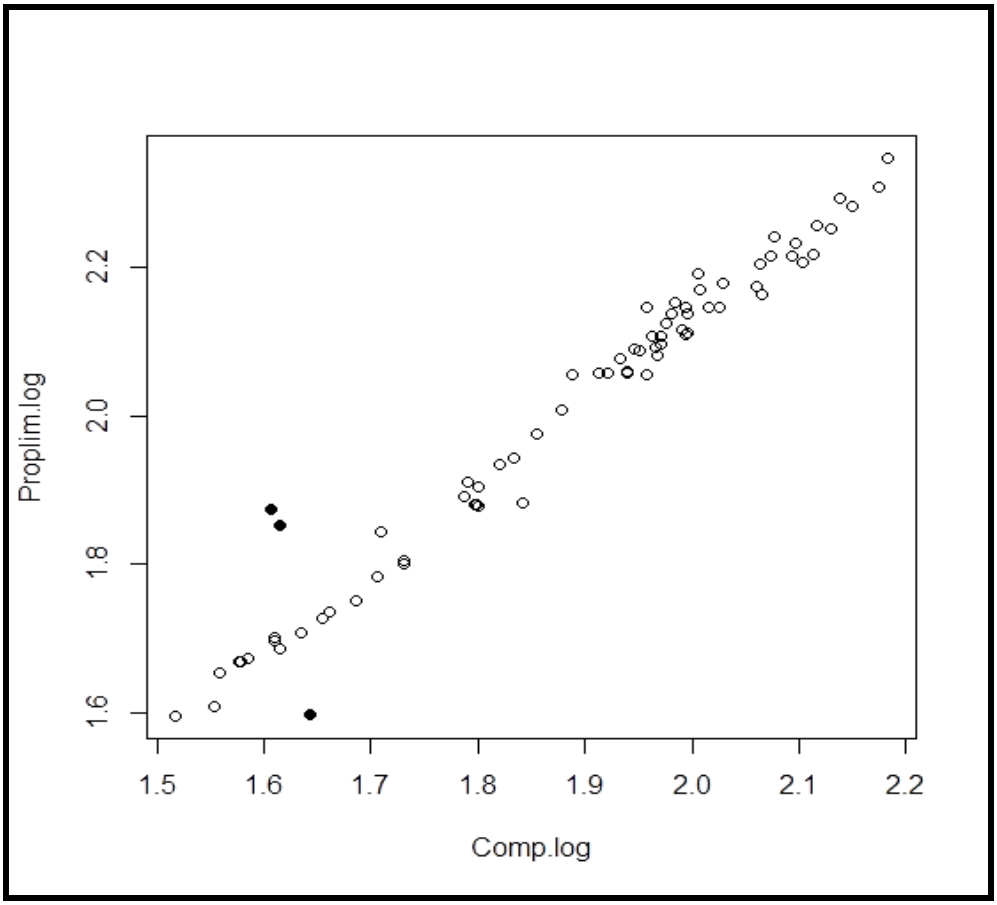

Figure 6.5: Mean values of compressive strength in relation to proportional limit

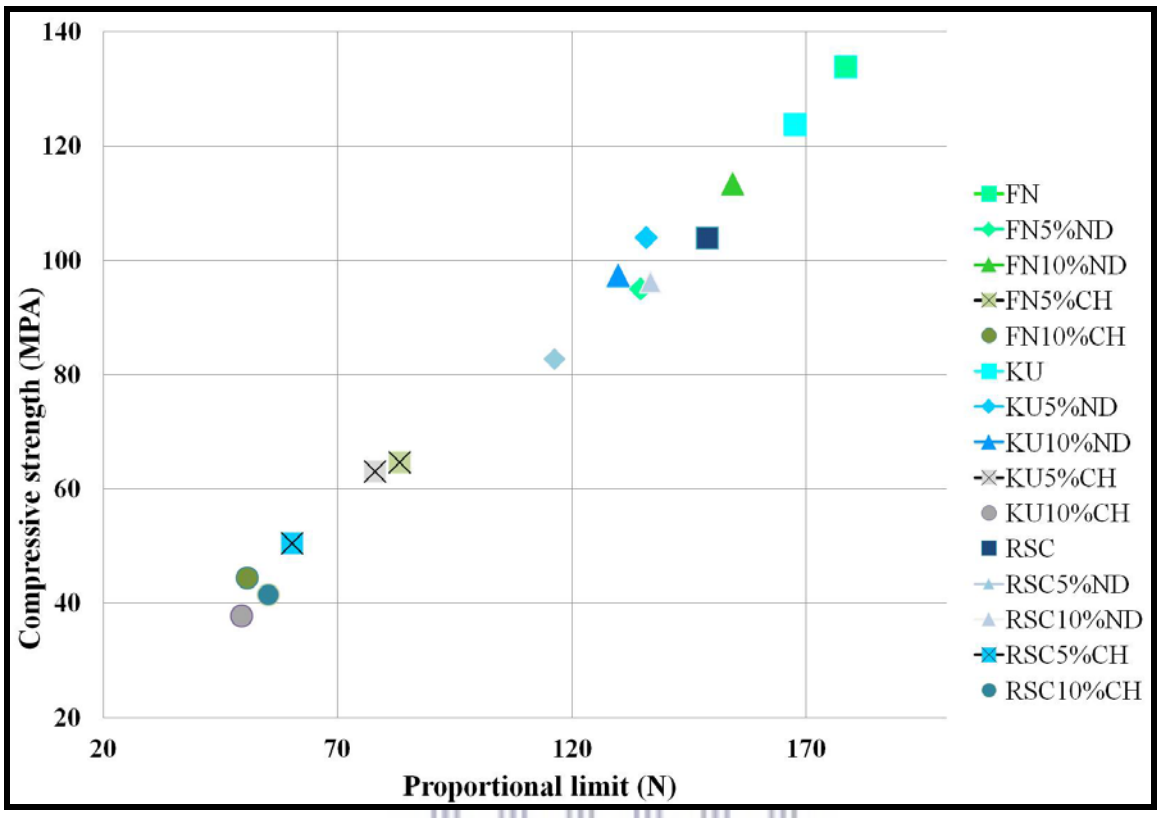

Figure 6.6 illustrates that for the modified materials with nanodiamonds, a significant decrease in the mean compressive strength was found for FN5%ND and FN10%ND ($p = 0.0003$) compared to FN. The same trend was present for FN5%CH and FN10%CH compared to the FN control ($p < 0.0001$) as well as for the FN-chitosan modifications compared to the FN-nanodiamond modifications ($p < 0.0009$).

No significant difference was found in the mean compressive strength between KU and KU5%ND. There was a significant decrease ($p = 0.033$) in the mean compressive strength between the KU and KU10%ND. The same trend was present for KU5%CH and KU10%CH ($p < 0.0001$).

There was a significant decrease ($p = 0.041$) in the mean compressive strength values between RSC and RSC5%ND. The same trend was present for RSC5%CH and RSC10%CH ($p < 0.0001$) (Figure 6.6).

Figure 6.6: Comparison of the log (Compressive strength in MPa) of the control materials to their modifications

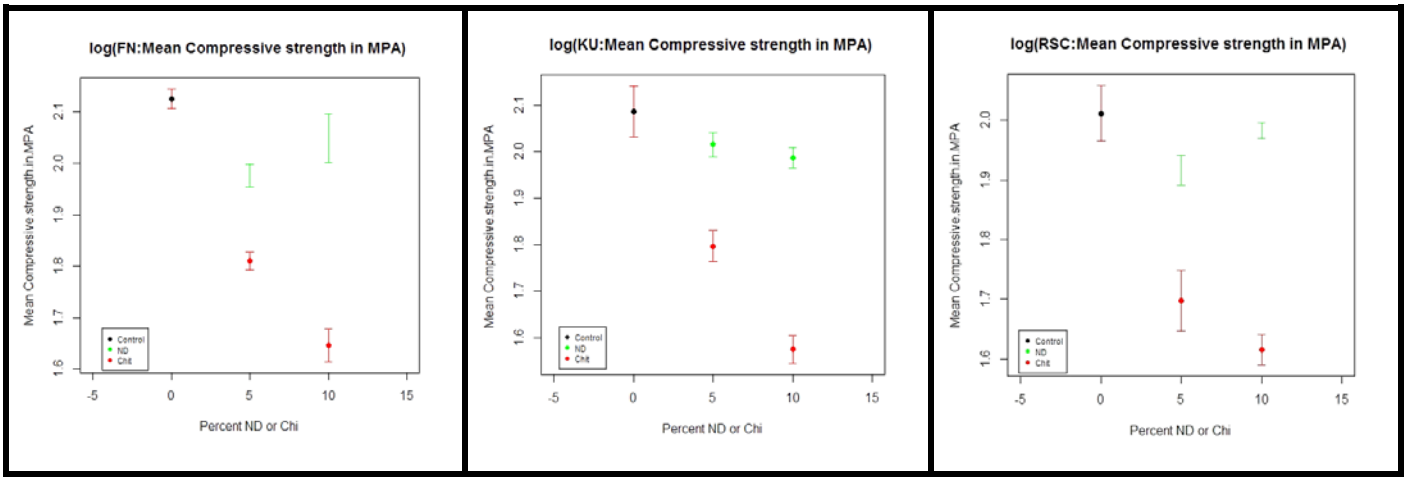

With the comparison of the compressive strength in MPA of all 15 materials, significant differences were represented by a non-overlap of the mean (±SE) values ($p < 0.05$) (Figure 6.7).

Based on the overall within-group variance, the standard error of any two means (Figure 6.7) was 0.0339, which is useful when calculating the significance as illustrated by Figure 6.7. An example of this manual calculation for RSC5%CH mean (1.697202) was significantly smaller than the KUC5%CH mean (1.796942). The statistician provided the following formula to illustrate how the statistical software calculated the p-value from the material means: t (60) = (1.796942-1.697202)/0.0339=2.942, p-value=0.0046.

The one way ANOVA test for homogeneity of the mean values illustrated that RSC had a significant decrease ($p = 0.047$) in the mean compressive strength when compared with FN and KU. FN and KU had no difference ($p = 0.0603$). With regard to the ND modifications FN5%ND, KU10%ND and RSC5%ND performed the best. The 5%CH modifications performed

better than the 10%CH, but performed significantly worse than the nanodiamond modifications for all three materials (0.0002) (Figure 6.7).

Figure 6.7: Comparison of the log (Compressive strength in MPA) of the control materials to their modifications

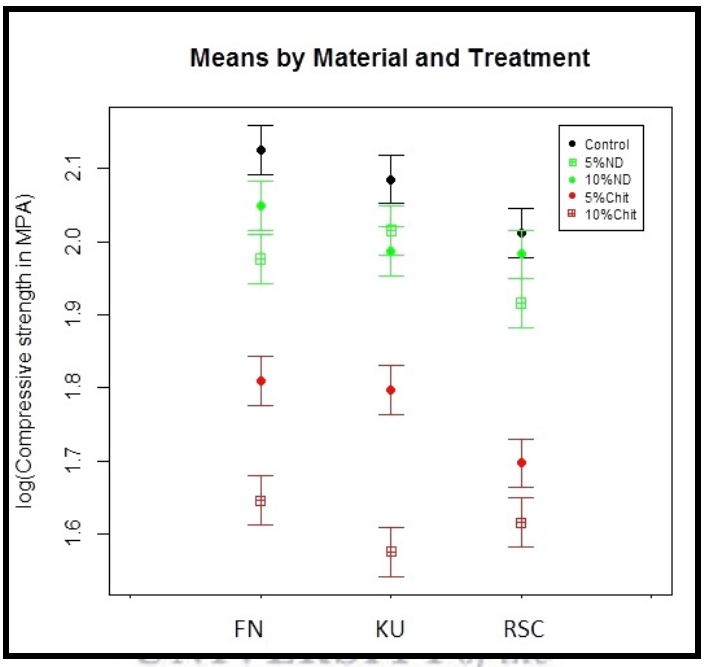

Proportional limit

An analysis of variance showed significant differences between the 15 material means ($p < 0.00001$). The pooled within-material standard deviation was 0.0671. This standard deviation was kept in mind when comparing means. The standard error of a mean of 5 observations was 0.03.

Non-overlap of a pair of limits indicates a statistically significant difference between the means ($p < 0.05$).

Figure 6.8 illustrates that FN had higher proportional limit values, which were significant for FN5%ND ($p = 0.012$). There was a significant decrease in the proportional limit when FN was modified with chitosan ($p < 0.0001$).

KU had a significantly higher proportional limit for KU10%ND ($p = 0.0001$). There was a significant decrease of the proportional limit when KU was modified with chitosan ($p < 0.0001$).

RSC had higher proportional limit values, but this was not significant for 10%ND ($p = 0.068$). There was a significant decrease in the proportional limit when RSC was modified with CH ($p < 0.0001$).

Figure 6.8: Comparison of the log (Proportional limit in N) of the control materials to their modifications

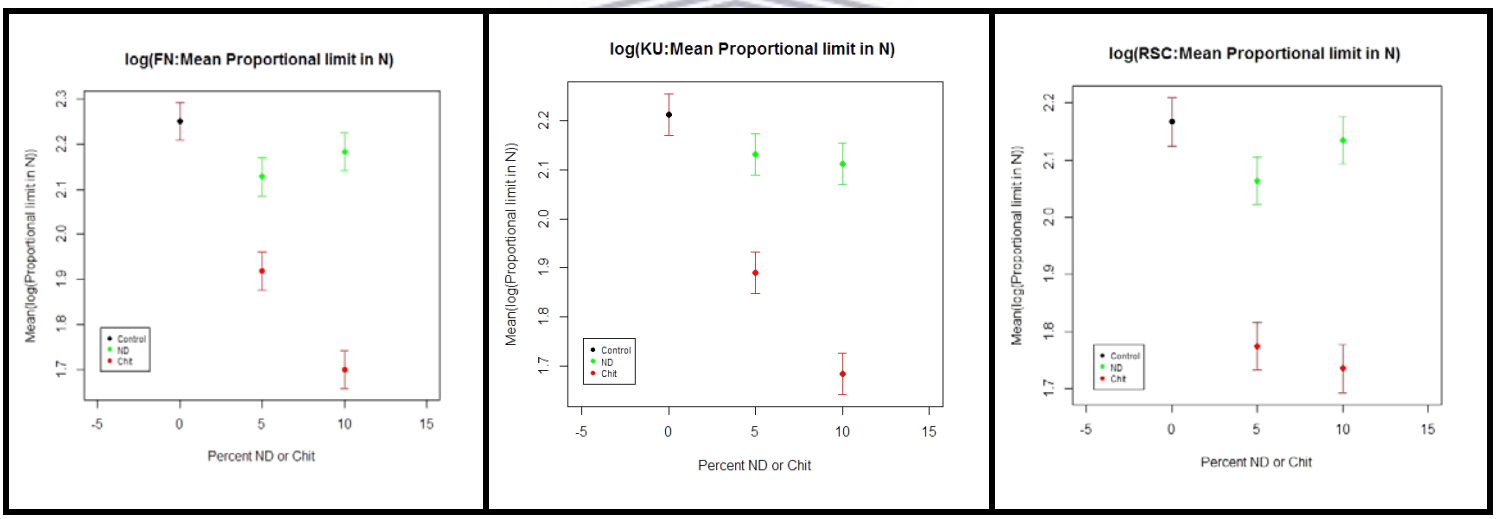

When comparing the proportional limit of all 15 materials (Figure 6.9), significant differences ($p < 0.05$) are represented by non-overlap of the mean (±SE) values.

Based on the overall mean values of the proportional limits within-group variance of the 15 materials compared to one-another, the standard error of any two means in Table 6.2 was 0.0425, which is useful when checking the significance of a difference indicated by Figure 6.9.

The one way ANOVA test for homogeneity of the mean values of FN, KU and RSC indicated the presence of no significant differences (p = 0.31) for their proportional limit values. For the FN10%ND modification a significantly higher proportional limit (p = 0.134) was found when compared with RSC5%ND. FN5%CH and KU5%CH had a significantly higher proportional limit (p = 0.0006) than FN10%CH, KU10%CH, RSC5%CH and RSC10%CH (Figure 6.9).

Figure 6.9: Comparison of the log (Proportional limit in N) of the control materials to their modifications

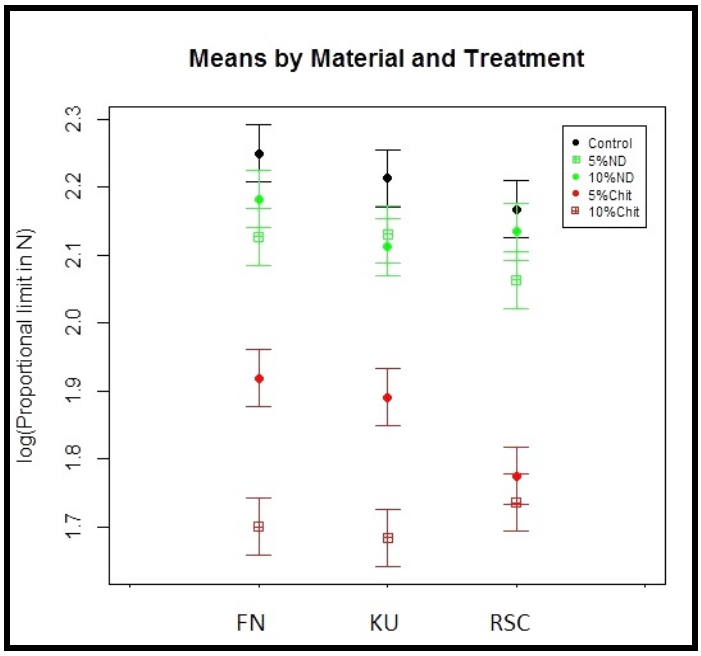

Surface micro-hardness (Vickers Hardness)

For the 15 materials, an analysis of variance showed significant differences between the material means (p < 0.00001). The pooled within-material standard deviation was 11.5. This standard deviation was kept in mind when comparing means. The standard error of a mean of 5 observations was 5.14.

Non-overlap of a pair of limits indicates a statistically significant difference between the means ($p < 0.05$).

Figure 6.10 illustrates that FN had higher Vickers Hardness values, but this was not significant for FN5%ND ($p > 0.05$). There was a significant decrease ($p = 0.028$) in the mean VH between FN and FN10%ND. There was also a significant decrease of the Vickers Hardness when FN was modified with chitosan ($p < 0.0001$).

KU had no significant difference in Vickers Hardness compared with KU5%ND ($p = 0.07$). There was however a significant decrease in the Vickers Hardness when KU was modified with KU10%CH ($p < 0.0002$).

There were no significant differences present in the Vickers Hardness of RSC, RSC5%ND, RSC10%ND and RSC5%CH ($p > 0.054$). There was a significant decrease ($p = 0.003$) in the mean VH between the RSC and RSC10%CH (Figure 6.10).

Figure 6.10: Comparison of the Vickers Hardness of the control materials to their modifications

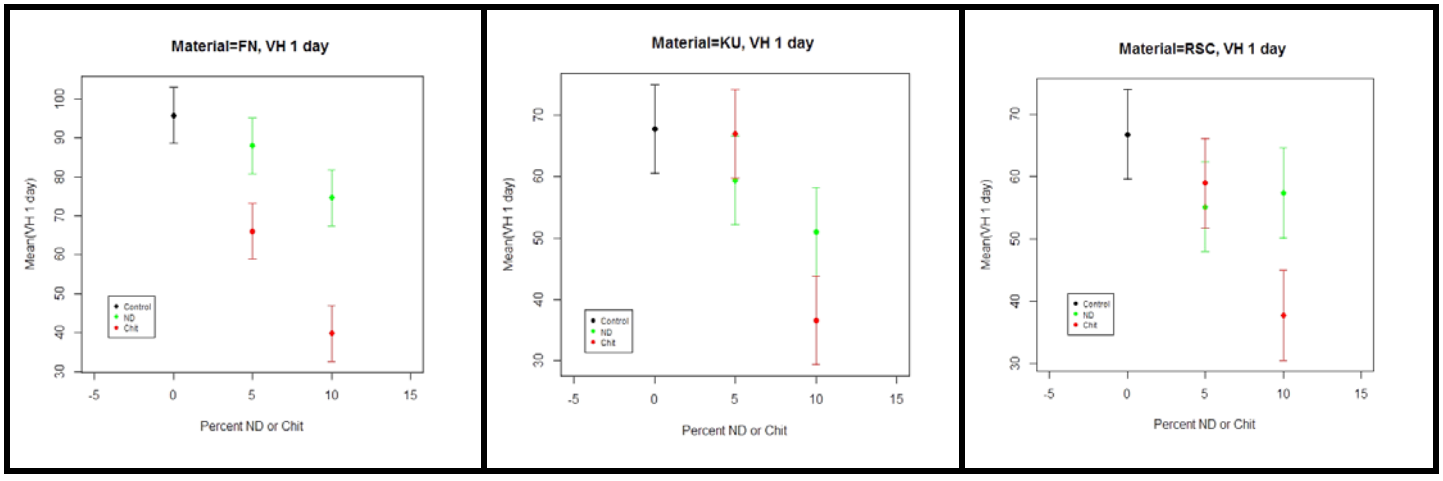

The one way ANOVA test for homogeneity in Figure 6.11 illustrates the mean values indicated the presence of significant differences between FN ($p = 0.0008$) and FN5%ND ($p = 0.002$) with lower Vickers Hardness values for all the KU and RSC materials. FN10%ND showed no significant difference in the Vickers Hardness compared to KU, KU5%CH and RSC ($p = 0.002$) (Figure 6.11).

Figure 6.11: Comparison of the Vickers Hardness of the control materials to their modifications

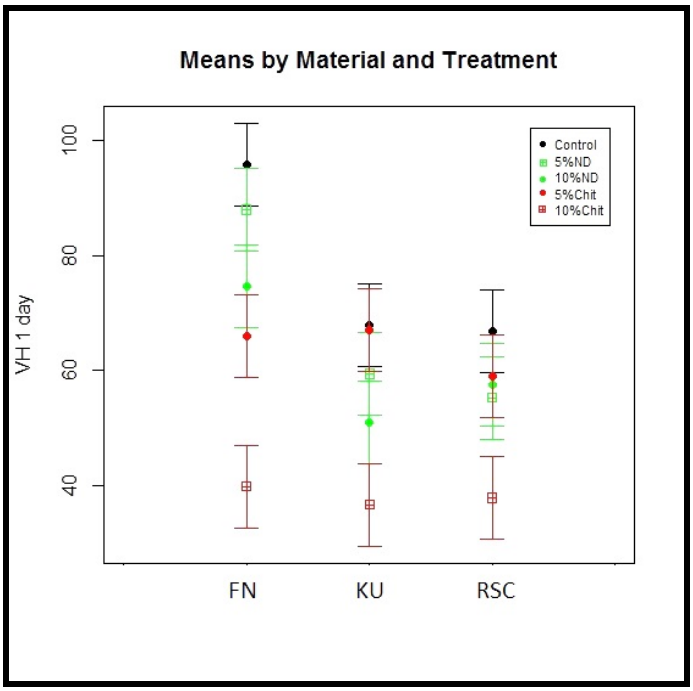

Water surface contact angle

The average water contact angles are represented in Table 6.1. The water contact angles were presented in degrees (θ°). The chitosan modifications demonstrated a significant difference for the water contact angle of the control materials ($p < 0.01$). FN10%ND was significantly lower than FN. KU5%ND was higher than KU ($p < 0.01$) (Table 6.2).

Table 6.2: Multiple comparison summary of the significantly larger contact angles between materials

	FN	FN5%ND	FN10%ND	FN5%CH	FN10%CH
FN			$p < 0.01$	$p < 0.01$	$p < 0.01$
FN5%ND			$p < 0.01$	$p < 0.01$	$p < 0.01$
FN10%ND				$p < 0.01$	$p < 0.01$
FN5%CH					
FN10%CH					
	KU	**KU5%ND**	**KU10%ND**	**KU5%CH**	**KU10%CH**
KU		$p < 0.01$		$p < 0.01$	$p < 0.01$
KU5%ND			$p < 0.01$	$p < 0.01$	$p < 0.01$
KU10%ND				$p < 0.01$	$p < 0.01$
KU5%CH					
KU10%CH					
	RSC	**RSC 5%ND**	**RSC10%ND**	**RSC5%CH**	**RSC10%CH**
RSC				$p < 0.01$	$p < 0.01$
RSC5%ND	$p < 0.01$			$p < 0.01$	$p < 0.01$
RSC10%ND	$p < 0.01$			$p < 0.01$	$p < 0.01$
RSC5%CH					
RSC10%CH					

$p < 0.01$ indicates significantly larger contact angle **"grey blocks"** indicate no significant difference

Figure 6.12: Correlation between the materials with the length of the drop in relation to the contact angle

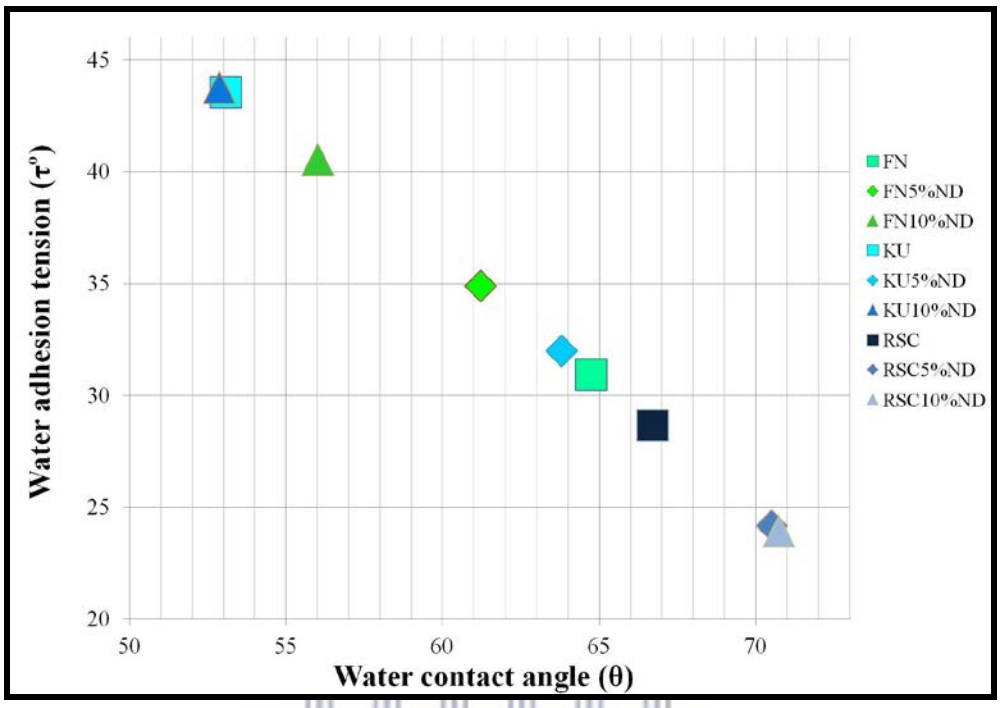

Water adhesion

The water adhesion (τ^o) values are represented in Table 6.1. All the GICs presented with a high wettability (i.e. surface wetting that is favourable). A larger contact angle (θ°) results in a smaller adhesion tension.

Surface roughness

FN5%ND and FN10%CH had significantly higher surface roughness than FN ($p < 0.01$). The chitosan modifications of KU and RSC resulted in a significantly higher surface roughness ($p < 0.01$) compared to their respective control materials.

Figure 6.13: Surface roughness of GICs prepared with 1200 grit silicon carbide paper

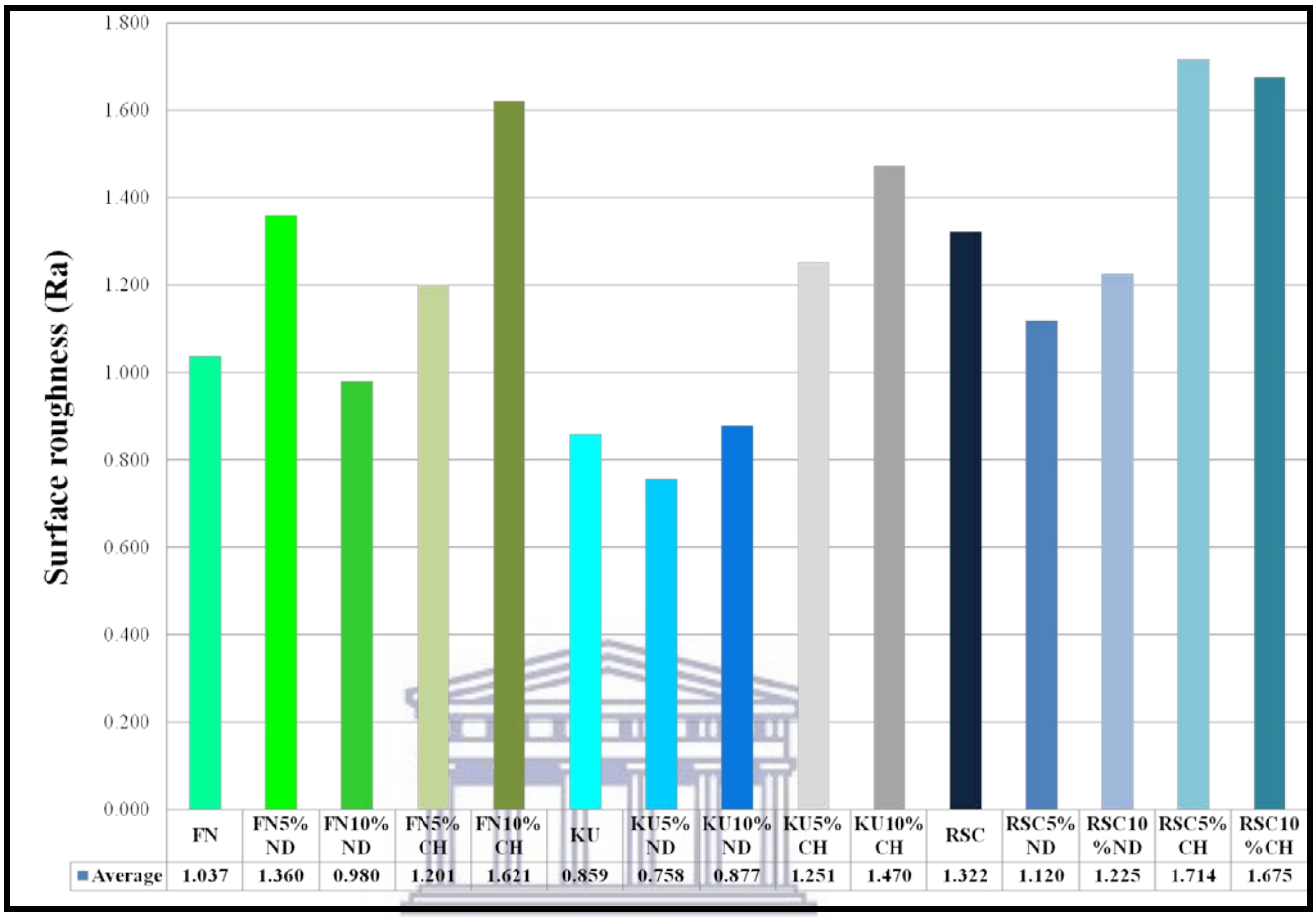

6.6. Discussion

The hypothesis that the chitosan- and nanodiamond-modified GICs would have improved properties for compressive strength, proportional limit and surface micro-hardness was rejected.

Contact angle and weight change

According to Yuan and Lee (2013): "The contact angle is defined as the angle formed by the intersection of the liquid-solid interface and the liquid-vapor interface (geometrically acquired by applying a tangent line from the contact point along the liquid-vapor interface in the droplet

profile)". The interface where solid, liquid and vapour co-exist is referred to as the "three phase contact line" (Yuan and Lee, 2013). Yuan and Lee (2013) further indicated that contact angles <90° are considered small contact angles and correspond to a high wettability (i.e. surface wetting is favourable). With contact angles >90° it is considered large and corresponds to a low wettability. There are as yet no general guidelines regarding how smooth a solid surface must be for surface roughness not to have an obvious impact on the contact angle. It is therefore recommended that the solid surface should be prepared as smooth as possible (Yuan & Lee, 2013). The ISO 9917-1, 2007 for lactic acid erosion of GICs indicated a surface preparation with a 1200 grit wet silicon carbide paper. This surface preparation was used as standardisation for the samples. The standardisation of the 1200 grit wet silicon carbide paper applied to all the materials allowed assessment of the achieved surface roughness.

Figure 6.14 represents the exact point where the sessile drop and the GIC material meet and from which the measurement was recorded for the surface contact angle. The conventional technique for calculating the water contact angle of a sessile drop, using a device named a "telescope-goniometer" was employed (Bigelow *et al.*, 1946). Subsequent to that, an improvement of the accuracy was achieved with the use of a camera at right angles to the sessile water drop. Photos were taken to measure the contact angle manually (Leja and Poling, 1960). Usually, a background light assists the observation of the sessile drop, but the Zeiss Stemi 880 stereomicroscope used in this dissertation has a LED ring light and the digital camera that allowed reproducible observations from the front. The LED ring light provided the added advantage that no heat was generated from the light source. The images recorded with the digital camera are presented in Figure 6.14 as three sessile drops. Based on the water contact angle (θ) below 65º and the calculated water adhesion tension (τ^o) above 30dyn/cm for FN and KU with their respective chitosan and nanodiamond modifications, they were all considered hydrophilic.

However, RSC and its nanodiamond-modified versions were hydrophobic. The chitosan samples for all the control materials (FN, KU and RSC) had a $\theta = 0^{o}$ and the $\tau^{o} = 72.8$dyn/cm. This characteristic was partly due to the inconsistency of the surface texture and the spaces between the GIC matrix and the chitosan particles that allowed the water to flow through the irregularities of the CH within the 20 seconds that the sessile drop requires for stabilization (Figure 6.15).

Figure 6.14: Stereomicroscope images of water contact angle

RSC

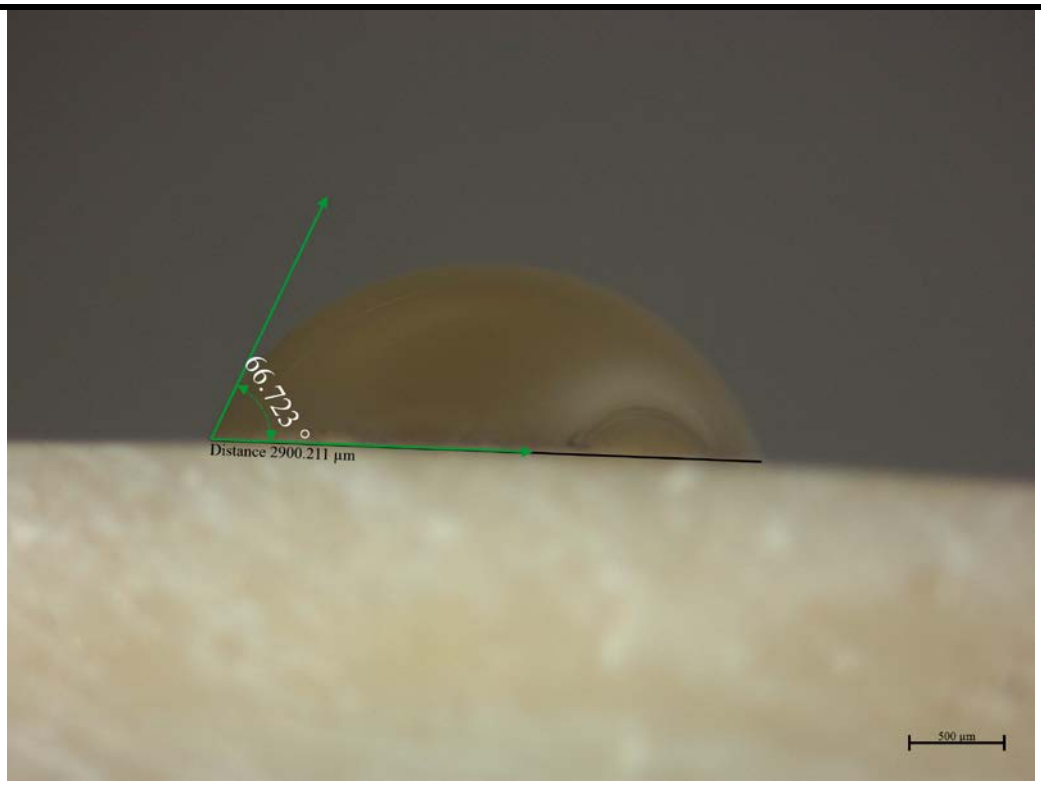

RSC5%ND

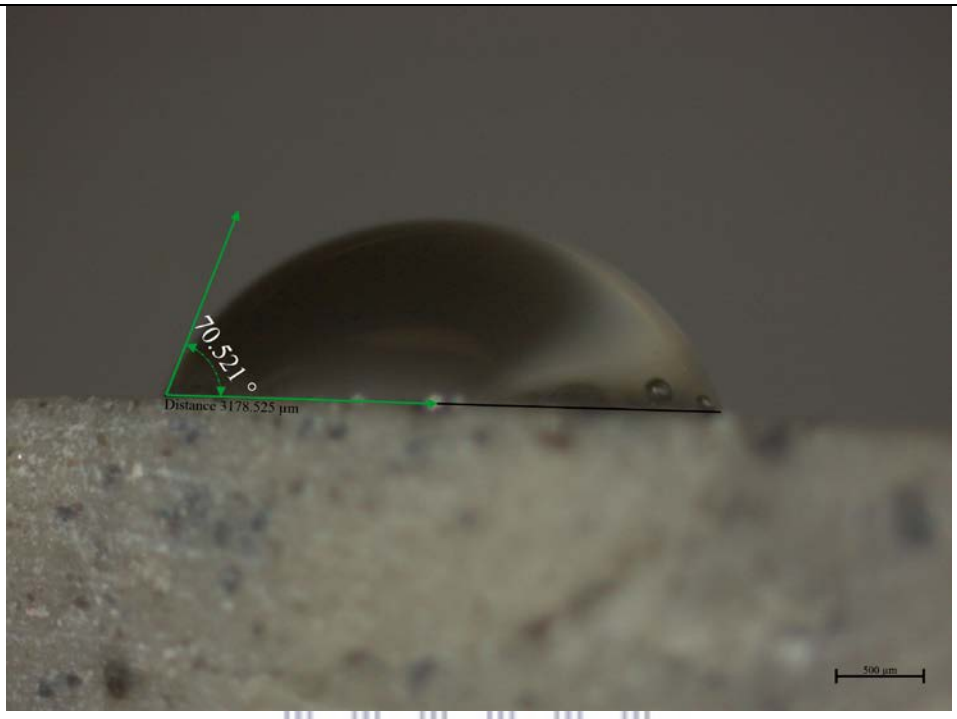

RSC10%ND

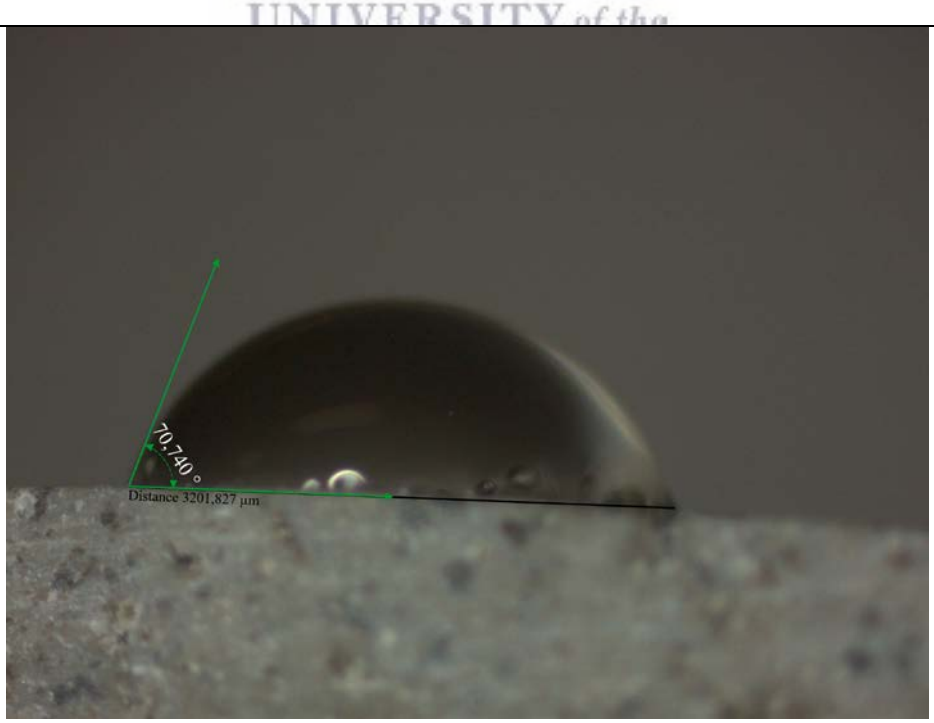

Figure 6.15: SEM image of the FN10%CH surface illustrating the irregular surface and chitosan as a macro-filler

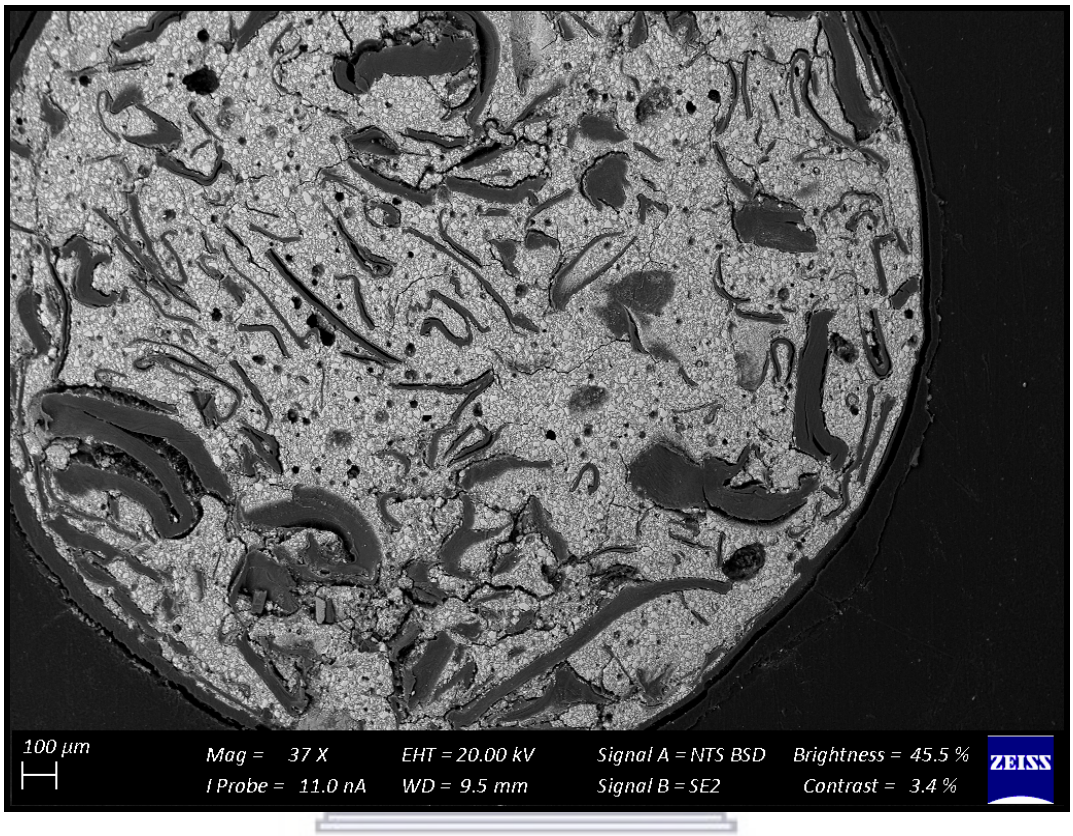

The surface activity of the GIC material was determined by Voelkel *et al*. (2005) to have both dispersive (non-polar) and specific (polar, acid–base) interactions with water. GICs have inorganic structures (glass filler particles) in the matrix. These structures are present and integrated into the matrix as a direct result of the reaction of the ion-donor species from the glass filler particles that serve as the ion donors (Voelkel *et al*., 2005).

The surface activity of GICs have not been explored by many researchers, but Voelkel *et al*. (2005) successfully used Inverse gas chromatography (IGC) to determine the dispersive properties of FN (Voelkel *et al*., 2005).

The surface properties change as the material is subjected to modifications. It has been noted that the addition of silver micro-particles to a composite, influenced the surface contact angle measurements in relation to the control material (Bürgers *et al*., 2009).

Both the chitosan- and nanodiamond-modified GICs showed a greater weight gain than their respective control materials. The hydrophobic effect is a phenomenon dominated by the strong self-association of water molecules. This strong self-association of water can occur independently of solubilisation of non-polar solutes (Tanford, 1973; Oss *et al*., 1980; Israelachvili and Pashley, 1982; Lyklema, 1991).

When GICs are stored in water, ionic exchange reactions first occur between the water and the GIC. Thereafter, the polar functional groups on the surface of the GICs develop. As part of the water sorption process, the newly developed functional groups, may have both active acidic (e.g. carboxylic) and basic sites (e.g. carboxylate). The observed increase in the number of acidic and basic sites of the matrix that are exposed to the surface allows the free energy to change over time during the storage in water (Andrzejewska *et al*., 2005). The surface activity of the GICs have been recorded to gradually increase in the water for up to 6 months, indicating that the GICs have a continuous on-going setting reaction and interaction with water (Voelkel et al., 2005). This means that KU5%ND will have less degradation and change of the surface over time compared to KU. This is applicable as it would suggest that the chitosan-modified GICs will have a greater interaction with water/moisture over time than their respective control materials. Due to the chitosan also increasing in size as it is exposed to water and the poor integration with the GIC matrix material, it can be predicted that in prolonged storage or moisture contact, the chitosan restorations can disintegrate, as was seen in Chapter 10. The chitosan-modified GICs with 5% and 10% particles are therefore a restorative option that could only be used as a temporary measure, e.g. for two-step caries removal procedures where re-entry is required. Besides the maturation of GICs being proven by the aforementioned change in the surface free

energy, the variation in the samples also suggested that the powder: liquid ratio of GICs and the accuracy of sample production was an essential component to the reaction of the GICs' interaction with water over time (Andrzejewska *et al.*, 2005). As the PLR was consistent in this study, the water contact angle and the water adhesion tension are accurate predictors of the water interaction of the chitosan- and nanodiamond-modified GICs. The wettability of the GICs is the most relevant for the first 24 hours, until a biofilm is established on the restoration. After the established biofilm has formed, the wettability will change as well (Doyle, 2000). The chitosan- and nanodiamond-modified GICs have an advantage in the first 10 minutes after mixing, considering there is an accelerated salt bridge formation period. The faster setting time enhances the water degradation resistance in the initial ±10 minutes. This is important, as when GICs are exposed to water too soon without the presence of a surface protective material, the material will present with a chalky appearance. These restorations with chalky appearance will be weaker due to dissolution of the salt bridge matrix and the propagation of micro-cracks (Nicholson, 2018). However, in the present study, this did not limit the volume of water ingress into the chitosan- and nanodiamond-modified GICs (Table 6.1 and Figure 6.3). GICs have been shown to have a water uptake of 5% within the first six months (Small *et al.*, 1998). The materials FN and FN5%ND should have the same rate of maturation over time, since the weight gain was similar. However, as the moisture (water) enters the GICs and binds to the anhydrous aluminium, sodium and strontium ions, changes occur e.g. aluminium forms $Al(H_20)_6^{3+}$ (Schweitzer and Pesterfield, 2010). This ingress of water also facilitates the increase in ion release as water ingress occurs. The ion release can also occur as the free aluminium and strontium bind to the hydroxide group from the absorbed moisture and then bind loosely to the carboxylate anions (Nicholson, 2018). Due to FN5%ND having agglomerated nanodiamond particles, a larger volume of water was absorbed into the modified materials. This result links to the larger ion release (mg/L) when compared to FN in Chapter 7.

Chitosan and nanodiamond particles as well as the carboxylic acid are able to interact with the water due to the fact that they contain many alkenes. An alkene is an unsaturated hydrocarbon that contains at least one carbon–carbon double bond (C=C) (Wade, 2006). Hildebrand (1979) indicated that there was no "real" hydrophobia between water and alkenes. Just enough hydrophilia exists between the alkene and the water to pry apart the hydrogen bonds of the water and allow the alkene to move into solution without assistance from the attached polar groups (Hildebrand, 1979). In order for a material that is hydrophobic to absorb water, two aspects should be considered, namely, the material's hydrophobicity and the self association of water that is in contact with the non-polar surface of the material (Hildebrand, 1979; Vogler, 1998). In order to simplify the concept we can sketch a comparison: "It is like a mobile phone battery that is 80% charged. The mobile has a battery containing energy of 80% and the capacity to retain 20% energy". If this principle is followed and applied to an alkene that is predominantly hydrophobic, it is also true that to some extent it also has the capacity to be hydrophilic. Thus, the interaction of the functional groups (in the GICs) and the chitosan or nanodiamond-modifications with the water, determine the volume of water ingress i.e. the weight gain and potential to release ions. The polar groups on the surface of the GICs allow the water to wet the surface of the alkenes due to the Lewis sites interacting with the water (Vogler, 1998). A Lewis site accepts electrons and as a result, the hydrocarbon transforms to a carbon molecule that has three formal bonds and carries a positive charge (carbocation). This explains why the RSC materials that presented as being a material that should be hydrophobic, still increased in weight upon exposure to water.

The very large surface area of nanodiamonds increases the amount of interfacial water molecules (Petit *et al*., 2015). Additionally, the nanodiamonds have a negative Zeta potential that results in the hydrogen (H) atoms pointing towards the negatively-charged nanodiamond particles. The

unique surface chemistry of the nanodiamond particles (and especially the carboxylate groups) promotes the electrostatic breaking of hydrogen bonds between the water molecules. The interaction of water molecules with the carboxylate group results in a reduction in water molecules in the double hydrogen bond (donor) configuration and an increase in water molecules in a single hydrogen bond configuration (Tristan Petit *et al*., 2015). The physical structure of the nanodiamond particle has colloidal aggregates with small mesopores exhibiting a hydrophobic behaviour for water vapour. The spaces between the agglomerated nanodiamond particles are known as ultra-micropores and work as hydrophilic sites (Pina-Salazar *et al*., 2017), further enhancing the increased hygroscopic nature of the GICs modified with nanodiamonds. The white arrows in Figure 6.16 illustrate the interaction of the nanodiamond agglomerated particles once they come into contact with the water. The nanodiamond agglomerated particles form small bubbles towards the centre of the nanodiamond agglomerated particle as water ingress occurs.

Figure 6.16: Nanodiamond-modified GIC surface interaction with de-ionised water

Sample surface before 10µl placed (50x magnification)

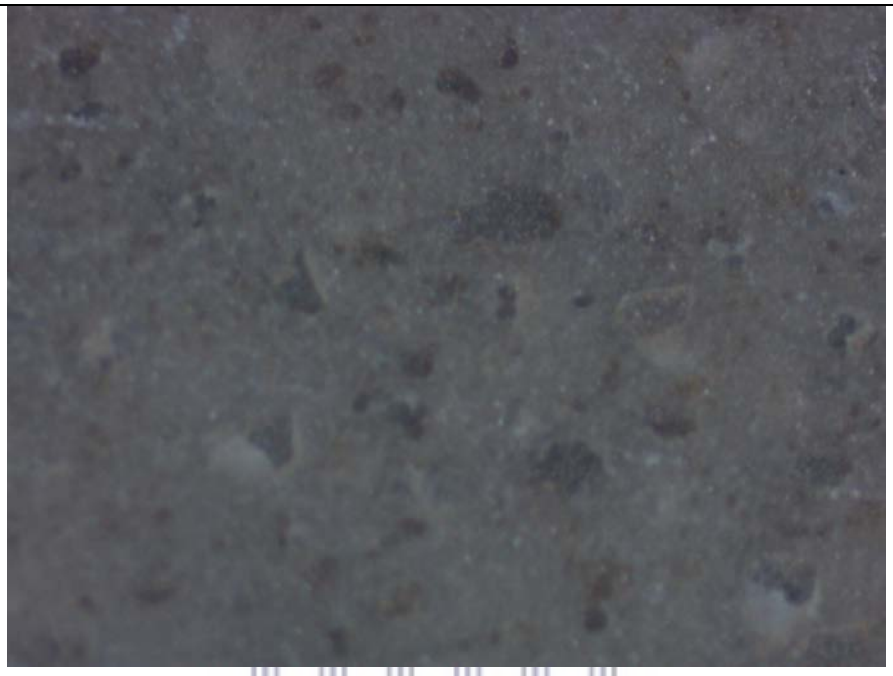

5 seconds after 10µl placed

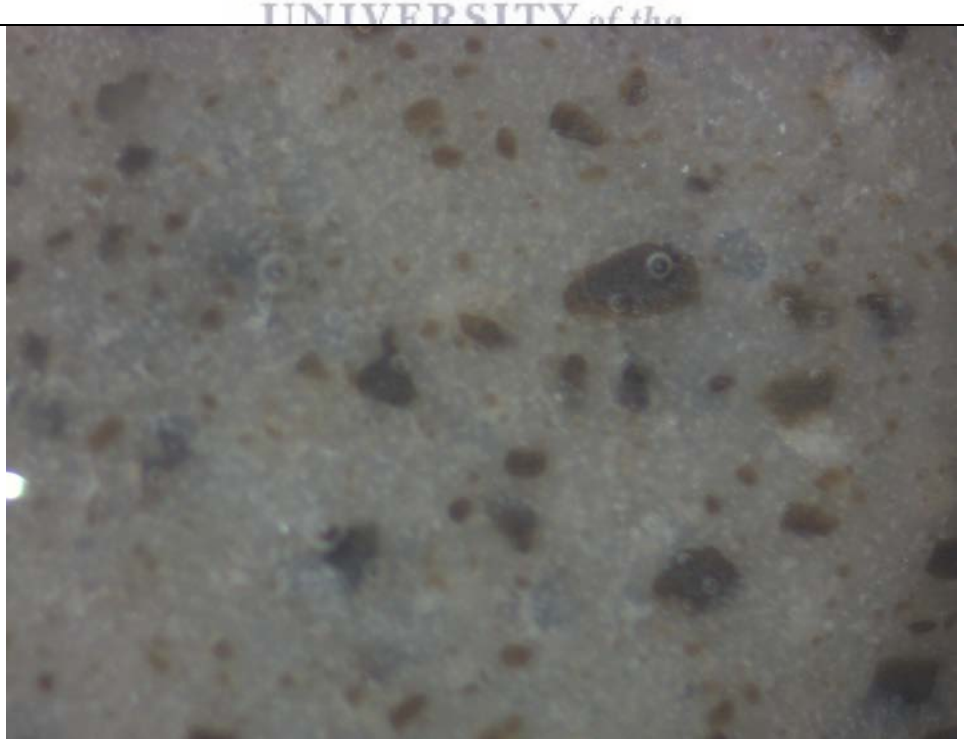

20 seconds after 10µl placed – top view of water drop edge

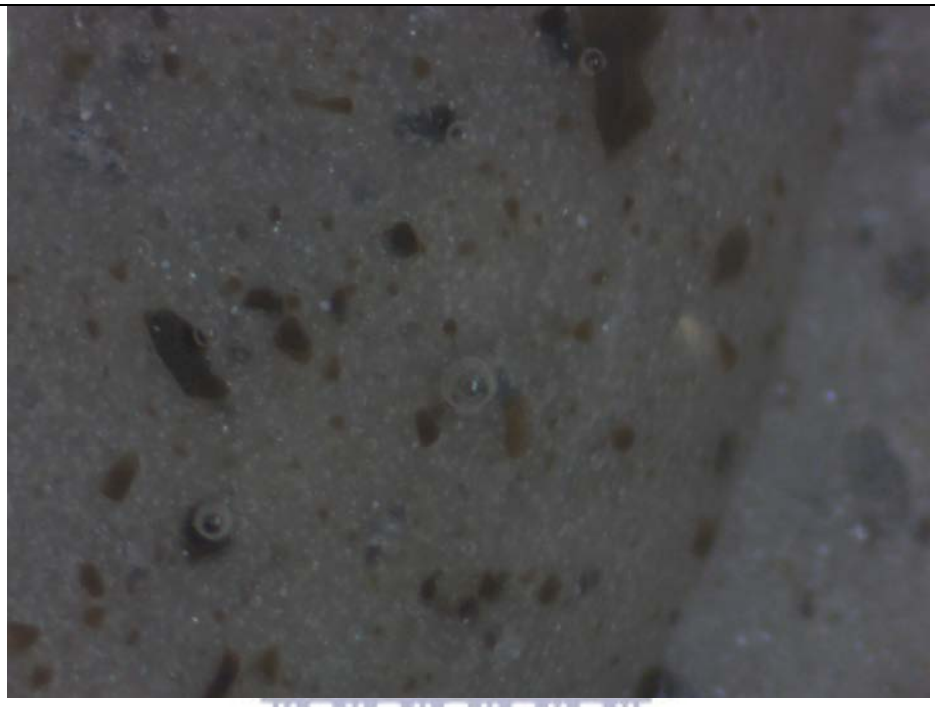

20 seconds after 10µl placed

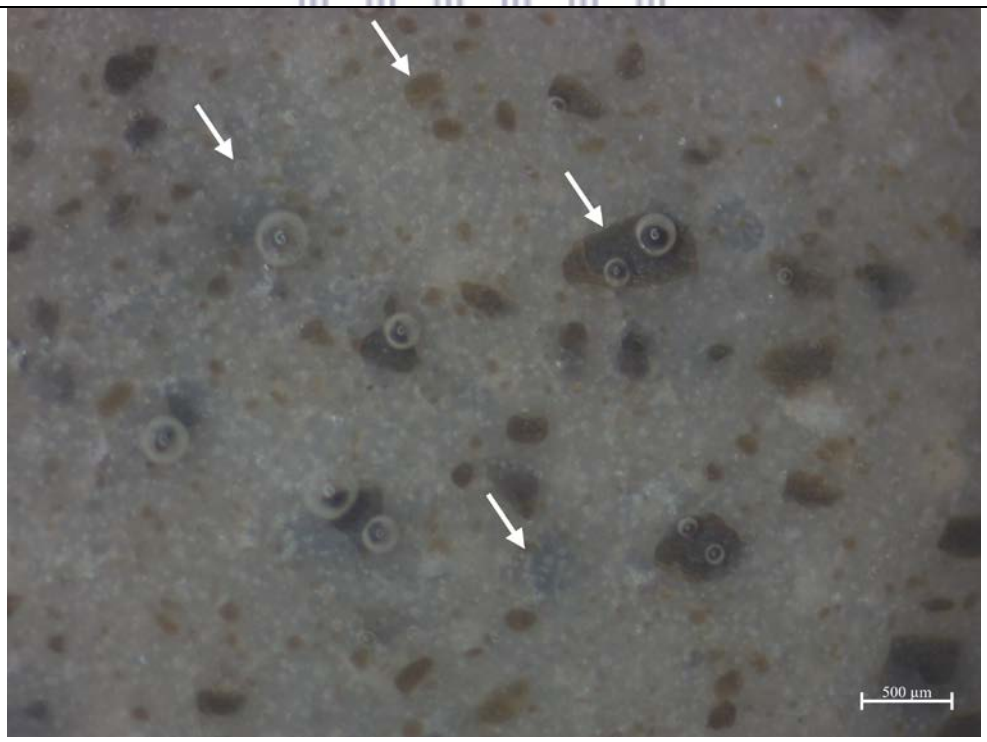

Surface roughness

The build-up of plaque on the surface of a restoration has a correlation with the superficial surface roughness (Ra) (Bollen *et al*., 1997) and the physiochemical properties of the material (Doyle, 2000). The surface roughness also influences the contact angles of the water on the surface of a restoration (Almeida *et al*., 2003). The clinically relevant surface roughness of the specimens should ideally be less than 1µm as presented by Sidhu and Henderson (1993). Only FN10%ND, KU, KU5%ND and KU10%ND materials from Table 6.1 and Figure 6.13 presented with Ra values below 1µm. None of the GICs finished to a standard 1200 grit wet silicon carbide paper would therefore achieve the Ra < 0.2µm to limit bacterial adhesion as suggested by Bollen *et al*. (1996). Even though this finishing method did not produce a similar surface roughness in the various GICs studied, standardisation of the surface finishing was essential to the interpretation of the results and linking of the studies in this dissertation across all the investigations for surface roughness, water contact angle, ion release, *S. mutans* adhesion, cell viability of 3T3 Balb/c mouse fibroblasts (3T3) and ion diffusion into tooth structure. In addition to the ISO 9917-1, 2007 advocating the 1200 grit wet silicon carbide paper, the surface roughness of the GICs were close when finished with Soflex discs (*3M ESPE*) (Ra 0.629) compared to a carbide bur (Ra 0.727) with no significant difference noted (p = 0.452) between the two modalities (Miličević *et al*., 2018). The surface roughness using the 1200 grit wet silicon carbide paper resulted in a Ra of 0.859 for KU but no significant difference was noted for KU5%ND (Ra 0.758) and KU10%ND (Ra 0.877). As the Ra is below 1µm, it is quite acceptable. The use of 1200 grit silicon carbide paper (ISO 9917-1, 2007) as well as the circular motion technique employed for finishing of all chitosan- and nanodiamond-modified GIC samples provided the consistency required throughout the various studies reported on in this dissertation and facilitated the deduction of clinically relevant conclusions. At the end of the

surface roughness investigation, the results indicated that the GICs modified with chitosan and nanodiamond particles played a role in the resultant surface roughness, essentially due to the interaction of the chitosan and nanodiamond particles changing the filler distribution of the GICs due to the unreacted chitosan and nanodiamond also acting as filler particles. This directly influences the finishing roughness of the surface and is in line with Bala *et al*. (2012) who stated that the particle size plays a role in the polishing performance of restorative materials (Bala *et al*., 2012). This explains why the chitosan-modified GICs all had a significant increase in surface roughness when compared with the control materials (Figure 6.15 and 6.17). Based on Senthil Kumar *et al*. (2017), the nano-chitosan powder incorporated into Fuji II GIC produced a much more uniform surface with the matrix of the GIC well bound to the nano-chitosan molecules. For the nanodiamond modifications, there were no significant changes in surface roughness except for FN5%ND where the Ra was significantly increased. On the other hand, FN10%ND had no significant difference in Ra when compared with FN. This is mainly due to the fact that the larger nanodiamond agglomerated particles were found in the FN5%ND material and the agglomerated nanodiamond particles in FN10%ND were smaller. The materials from FN5%ND had small crack formations through the agglomerated nanodiamond agglomerates, resulting in the increased surface roughness for FN and FN10%ND (Figure 6.18).

Figure 6.17: RSC10% chitosan-modified sample with chitosan particles visible as whitish flakes

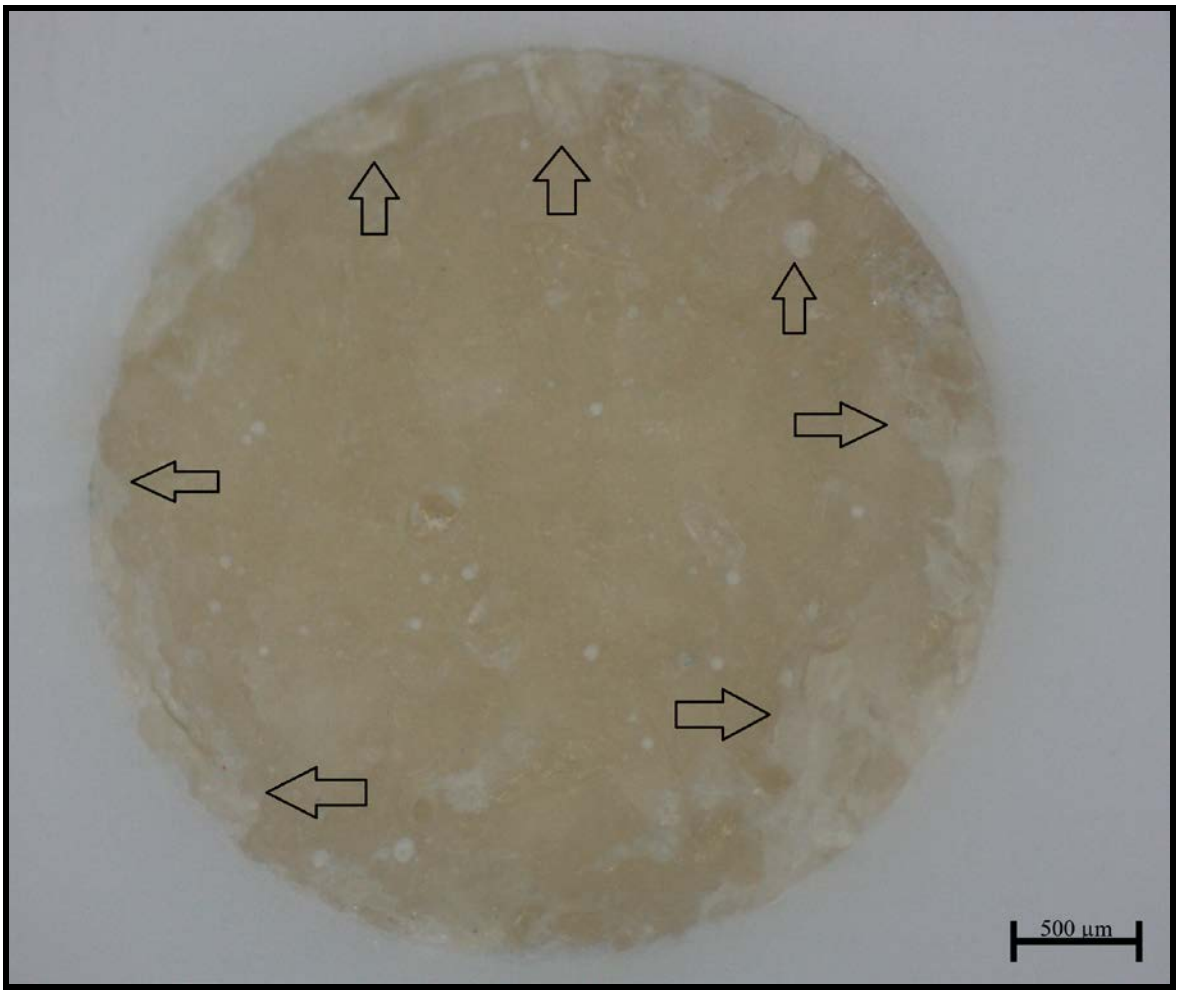

Figure 6.18: SEM of cracks through the larger nanodiamond agglomerates of FN5%ND

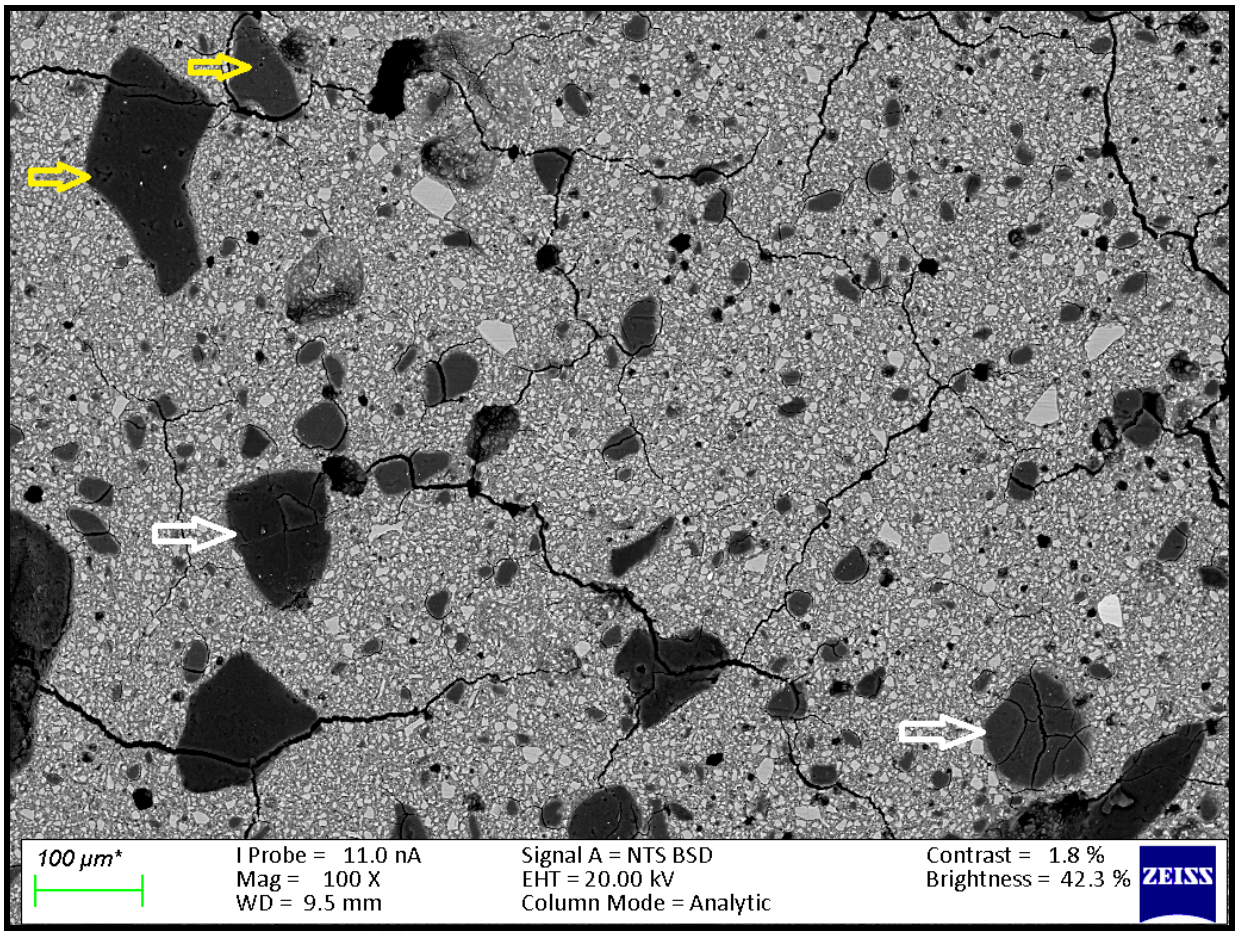

Compressive strength

It is well established that the PLR influences the mechanical properties of a GIC (Fennell and Hill, 2001; Lohbauer, 2010; Moshaverinia *et al*., 2011). This variable has been addressed in the powder/liquid optimisation Chapter 5. The manufacturers' PLR was retained as it provided sufficient wetting and the best results with the chitosan- and nanodiamond-modified powder. A clinically relevant observation is therefore that the material should retain its workable limits in order to obtain the best outcome (Prentice *et al*., 2005; Nagaraja, Upadaja and Kishore, 2015.) The reduction in the physical properties of the nanodiamond-modified GICs was explored with evidence from other investigations. As the relative amounts of aluminium and/or silicon

decrease based on the SEM-EDS elemental gradient wt% potential (Table 6.3), there was a marked decrease in physical properties.

Table 6.3: Elemental analysis of all GICs to determine the gradient wt% potential

	Aluminium	Barium	Calcium	Fluoride	Iron	Lanthanum	Phosphorus	Silicon	Sodium	Strontium	Zinc
FN	11.2	0.1	0.2	13.3	0	0	3.1	10.2	0.9	3.9	0.1
FN5 %ND	10.7	0.2	0.2	11.9	0	0	3	9.9	0.8	3.7	0
FN10 %ND	9.5	0.1	0.2	12.3	0	0	2.7	8.5	0.8	3.2	0
FN5 %CH	19.6	0.2	0.2	8.68	0.06	0	3.3	5.7	0.2	29.3	0.07
FN10 %CH	23	0.5	0.2	10.45	0.07	0	6.5	6.5	0.2	35	0.06
KU	8.2	0.1	0.2	11.4	0	2.6	2.5	10.5	1.8	2.8	0
KU5 %ND	7.8	0	0.2	9.8	0.1	2.6	2.4	10.1	1.6	2.7	0
KU10 %ND	7.7	0.1	0.2	10.2	0	2.5	2.3	9.8	1.6	2.6	0
KU5 %CH	21.6	0.2	0.2	11.8	0.08	8.3	4.6	6.2	0.9	28.3	0.05
KU10 %CH	22.8	0.3	0.07	12.4	0.06	9.2	4.9	6.5	1	31.2	0.075
RSC	9.8	0.5	0.1	11.7	0	0	2.3	9.9	1.3	3	0
RSC5 %ND	10.4	0.5	0.1	10.9	0	0	2.6	10.6	1.2	3.3	0
RSC10%ND	9.3	0.4	0.1	11.1	0	0	2.3	9.3	1.1	3	0
RSC5 %CH	23.9	1.1	0.07	9.6	0.02	0	4.2	7.1	0.5	35.2	0.2
RSC10%CH	21.8	1	0.07	9.9	0.07	0	3.7	6.3	0.4	31	0.05

The literature also states that when sodium is added as a network modifier to the GICs, less aluminium will bind to form in the matrix (De Caluwe *et al*., 2017). Table 6.3 indicates a larger wt% reduction in the ions (aluminium, silicon, and strontium) compared to sodium. These ions were absorbed into the nanodiamond agglomerates and became shielded from the polyacrylic acid interaction. This initial matrix formation is essential, as the ions present in this matrix will then, upon maturation, have ion exchange with the free ions to mature the GICs. This will be explored further in Chapter 7 where the siloxane group dissociates into a silanol group.

The role of fluoride in the production of the GIC powder, and setting reaction play a role in the strength of the GICs. It has been postulated than the addition of fluoride to GICs increases the compressive strength as well as the setting time. The aforementioned processes are due to the formation of Al–F–Ca(n), F–Ca(n) and possibly Si–F–Ca(n) species with the tooth as part of the ion diffusion zone. Most GICs however have calcium substituted for strontium, therefore these binding sites become Al–F–Sr(n), F–Sr(n) and Si–F–Sr(n) in the GIC material itself. These species increase the reactivity of the glass, resulting in fewer bonds being hydrolyzed during the setting reaction, thereby increasing its resistance to early moisture damage (Hill *et al*., 1999; De Barra and Hill, 2000; Matsuya *et al*., 2007). After the acid-base reaction is completed, fluoride serves as a free ion that moves through the GICs. A decrease in compressive strength was noted as the percentages of chitosan and nanodiamond particles increased from 5% to 10%. This confirms that a physical change of the filler-matrix stability of the GIC occurs (Figure 6.19), as the chitosan and the agglomerated nanodiamond particles change the matrix considerably to the chitosan and the nanodiamond agglomerates being much larger than the GIC glass filler particles. In Chapter 8, the fluoride release from the modified GICs are also influenced by the larger chitosan and nanodiamond agglomerates and will be discussed further.

Figure 6.19: FN10%CH sample with fracture lines and force dissipation (illustrated with black arrows)

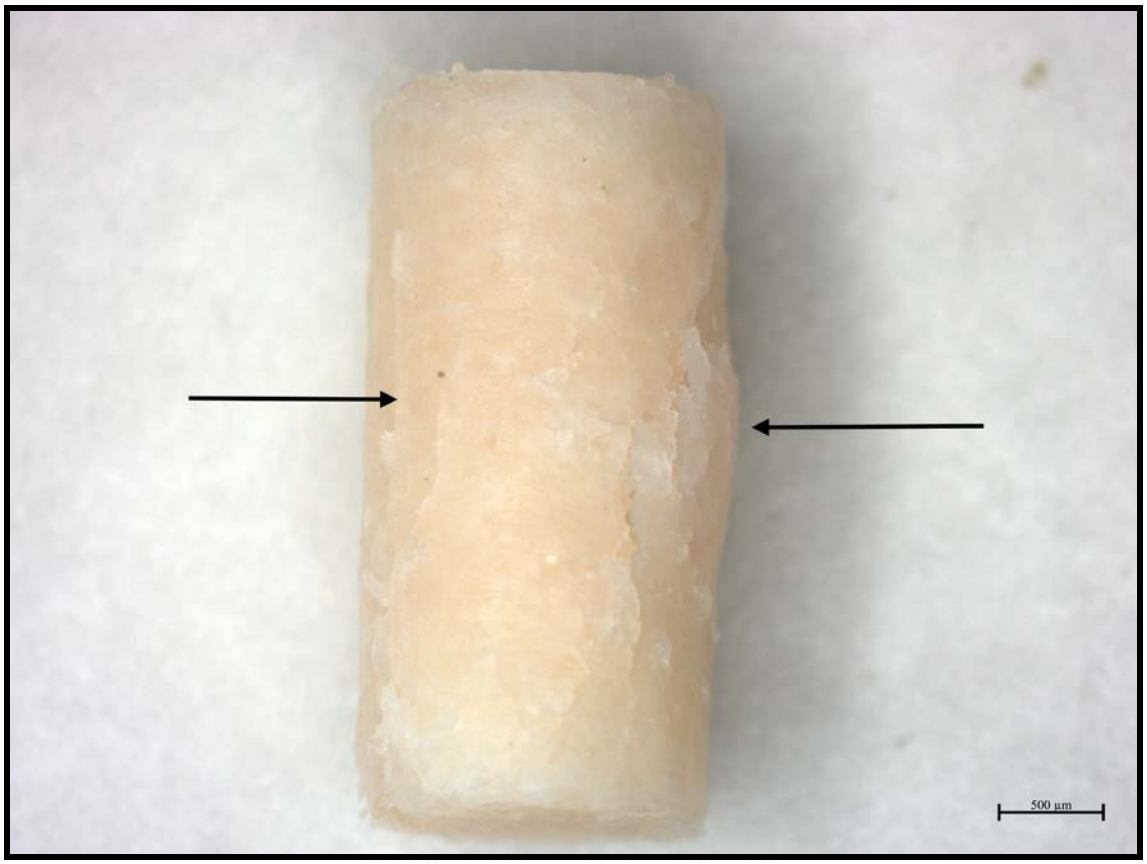

The composition of the glass phases (glass filler particle and the matrix of the GICs) play a role in the dissolution rate of the ions from the filler particle and the matrix during salt bridge formation. GICs with increased $A1_2O_3/SiO_2$ result in these GICs becoming more alkaline and therefore more susceptible to acid attack from the liquid during the acid-base reaction. These GICs will therefore have greater ion dissolution (Wilson and McLean, 1988). Alkaline ions like sodium also increase the release of fluoride ions by serving as a soluble counter-ion (Billington *et al*., 1998). The addition of sodium influences the solubility, hydrolytic stability and the physical properties of the GICs. Sodium is released and exchanged for a hydrogen ion in the

GIC. Based on the gradient wt% potential in Table 6.3, the nanodiamond and chitosan particles did not have an affinity for the sodium ions, as the drop in wt% potential was negligible.

A greater proportion of sodium was released from the GICs in this study compared to the other cations (aluminium, silicon and strontium). This result was in line with De Barra and Hill (1998) where the sodium competes for binding sites to the carboxylic groups in the polyacid chain during mixing with aluminium, calcium and strontium. As previously mentioned, the larger the amount of aluminium and silicon that take part in the salt bridge formation, the better the physical properties of the GICs.

The chitosan and nanodiamond modifications also prevent the aluminium and strontium from integrating strongly within the matrix due to fewer hydrolised bonds forming as moisture ingress occurs (Chapter 7).

It is this polyacid chain with the cations that results in the salt bridge formation. As the sodium occupies the carboxylic group before the aluminium, calcium and strontium are released from the glass filler particle, a weaker matrix will form. This is more sensitive to a damaging hydrolysis effect, thereby decreasing the proportional limit of the GIC. This result was confirmed by Griffin and Hill, (1998). The nanodiamond agglomerated particles with varying crack formations within the particle play a role in the small variation between the compressive strength and proportional limits of the 5% and 10% nanodiamond modifications. This, coupled with the relatively greater volume of water ingress, adds to the large ingress of moisture that also reduces the compressive strength and the proportional limit properties.

As the pH is well below (pH < 6.5), the liquid from the GICs (FN, KU and RSC) can, to a limited extent, dissolve the chitosan. The acid would normally dissolve the amino groups of the chitosan particle. The glucosamine then becomes a molecule in its protonated form i.e. ammonia (NH_3^+). In this NH_3^+ form, the chitosan used in this study behaves both like a cationic polymer

reacting with negatively charged organic species (Peniche & Arguelles-Monal, 2001) as well as inorganic species (Kang *et al*., 2006) in both the solid state and gel phase of the chitosan. The interaction of the liquid during the spatulation of the chitosan- modified GICs was however peculiar. Figures 6.20 to 6.24 illustrate a newly seen phenomenon where the powders of the GICs encapsulate the chitosan particles completely. This encapsulation of the chitosan particle in the modified chitosan is said to have a "popcorn effect" with the chitosan particle being the kernel and the powder the puffed starch. This occurrence is due to the chitosan particles being integrated with the powder phase of the GICs in the flask shaker with a tipping action as well as the electrostatic nature of the powder and the chitosan particles. These figures shed light on why the chitosan particles have such a poor dissolution with the liquid i.e. 1) the setting time does not allow prolonged exposure to the chitosan particles to allow it to dissolve and become part of the liquid and matrix chemistry. 2) The particles are large, so a greater size will require a longer interaction period and 3) the chitosan is covered with the powder of the GICs.

Figure 6.20: "Popcorn effect" of KU powder encapsulating the chitosan particle (black arrow illustrates chitosan)

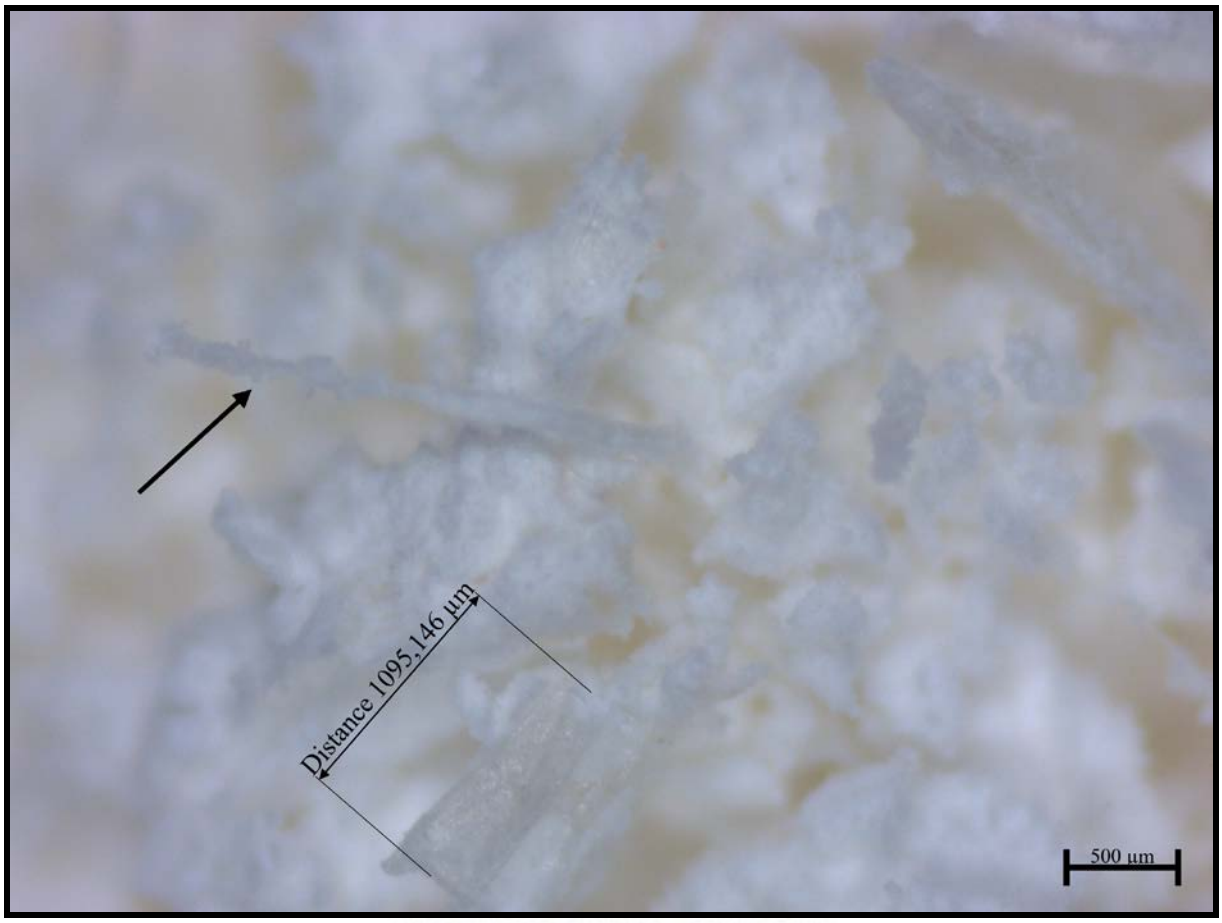

Figure 6.21: "Popcorn effect" of KU powder partly encapsulating the chitosan particle (black arrow illustrates chitosan)

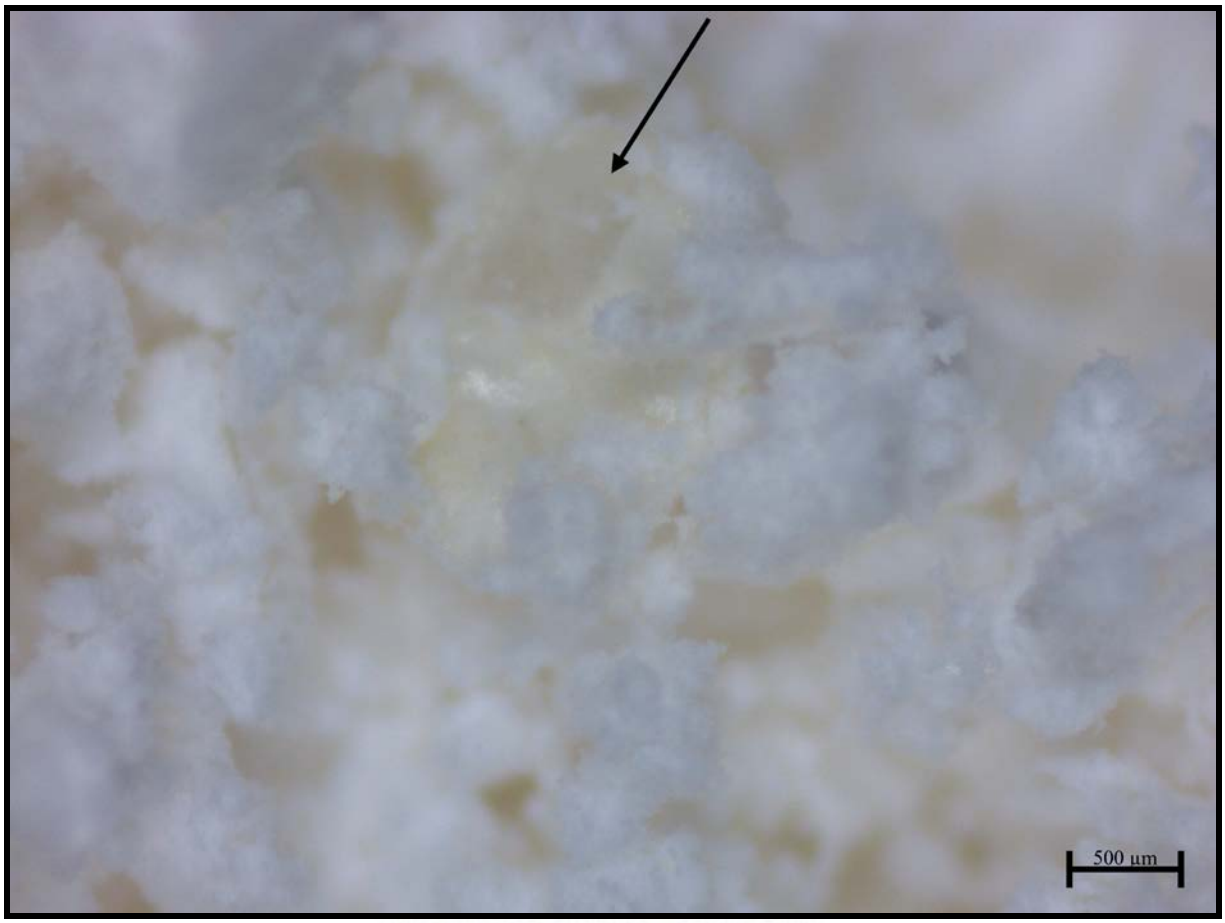

The "popcorn effect" of the powder around the chitosan particle is so severe that the volume of powder around the chitosan particles was removed by the researcher for illustrative purposes (illustrated sequentially from Figures 6.22 to 6.24).

Figure 6.22: KU powder encapsulated chitosan particle (black arrow indicates chitosan particle)

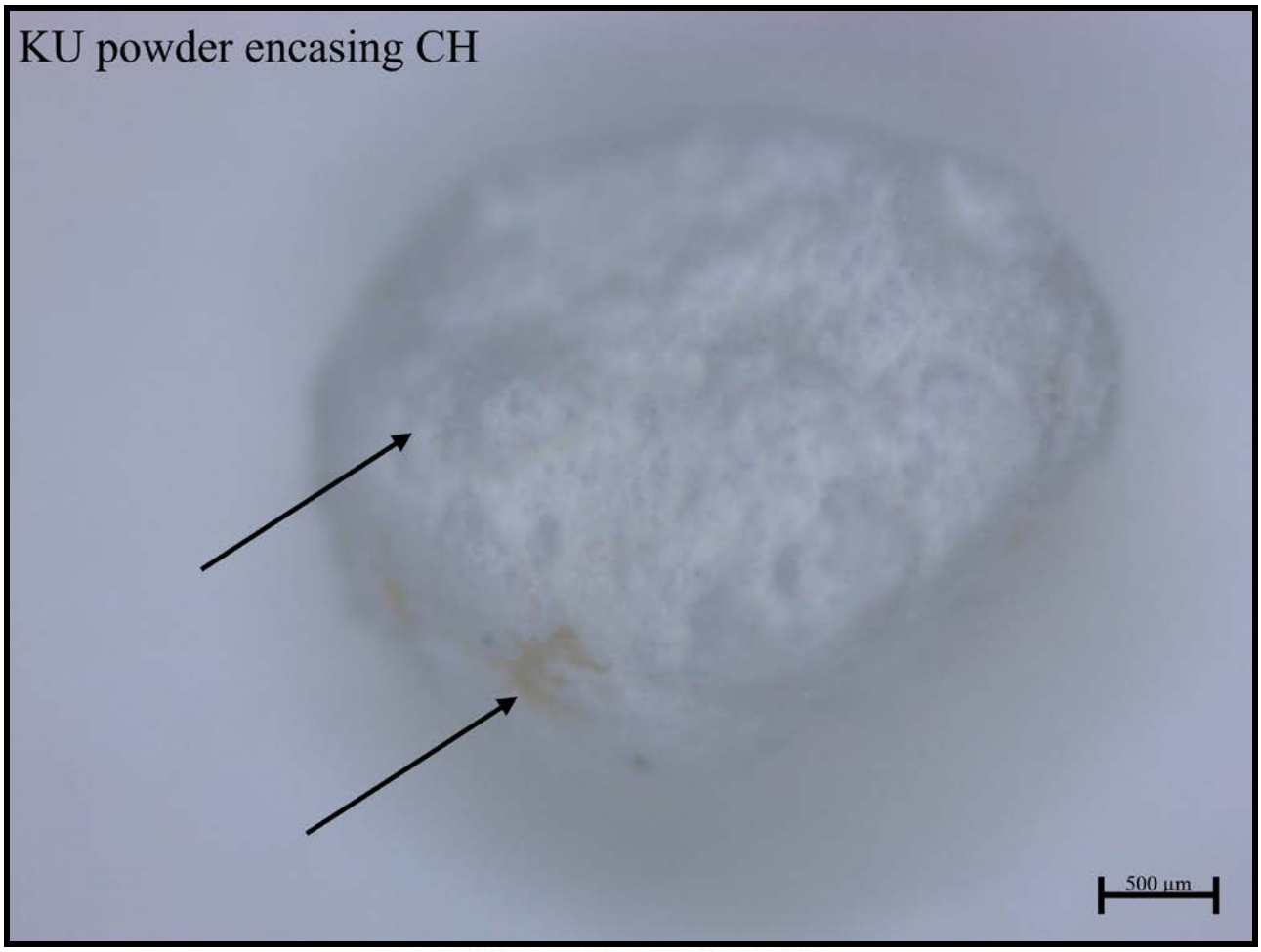

Figure 6.23: Chitosan particle agitated by researcher to remove powder, chitosan becomes visible (black arrow illustrating chitosan and powder)

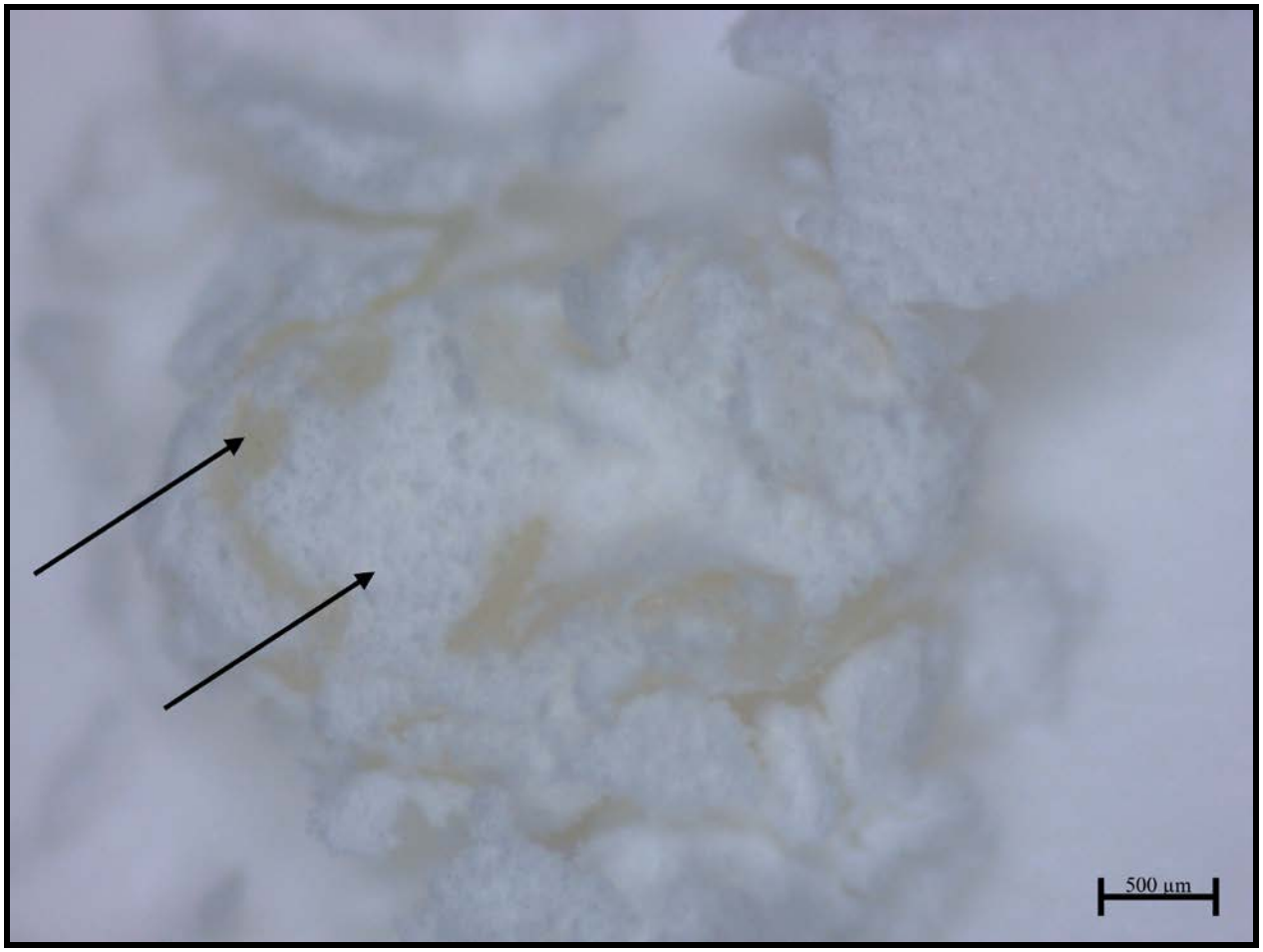

Figure 6.24: Chitosan particle visible after more agitation from previous image, chitosan particle is visible (black arrows showing chitosan and powder)

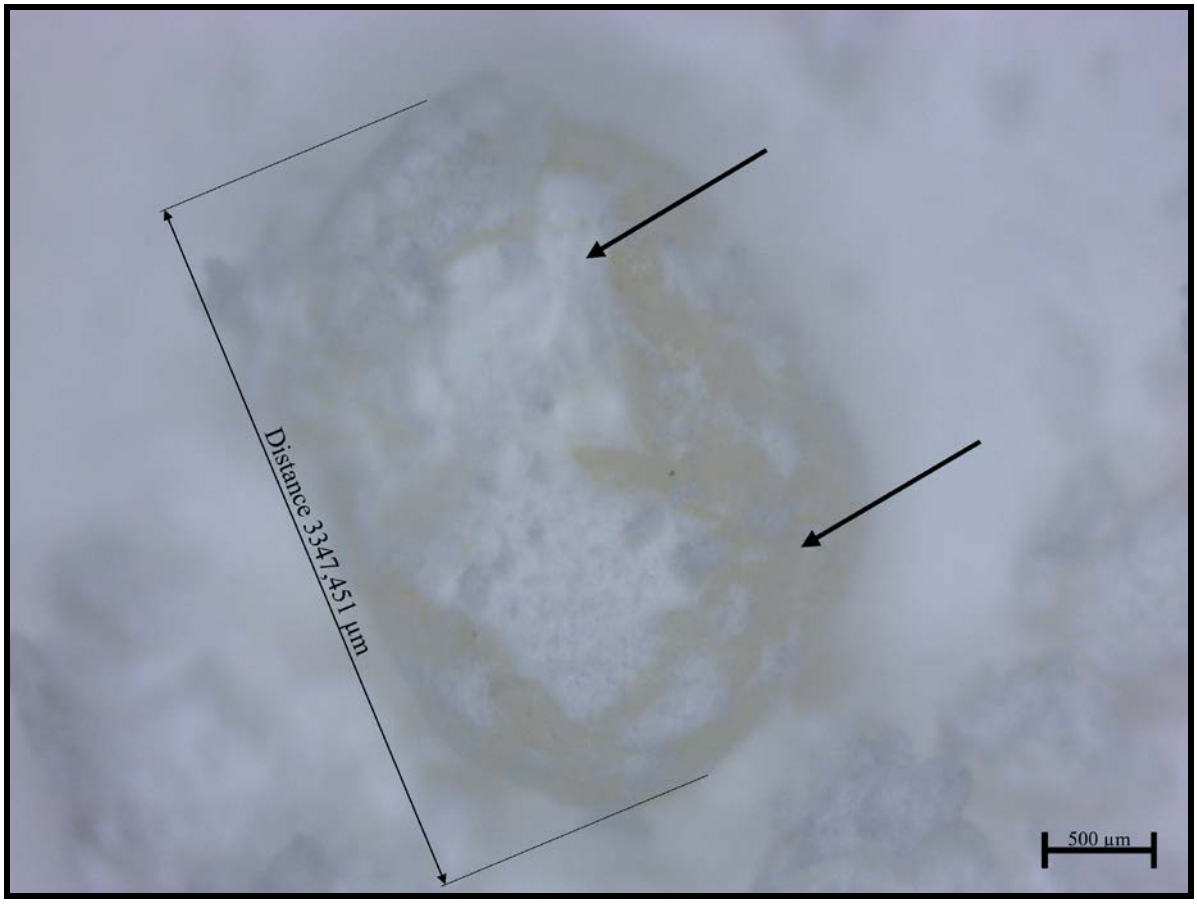

During the mixing of the chitosan-modified GIC, there is initially a low pH environment and the chitosan has a positive charge. The chitosan particle subsequently reacts through self-assembly with the negative carboxylic part of the occurring acid-base reaction. The interactions between the polymeric chains of the chitosan with the liquid and the powder (freeze dried polyacrylic acid in the powder) lead to the formation of a polyelectrolyte complex network. This network is not a permanent structure, since there are no covalent cross-linkers. Therefore, once the pH has stabilised after the initial setting of the chitosan- modified GIC, the ion exchange with positive ions can occur. This is why the chitosan-modified GIC has a low compressive strength and

proportional limit. No proper salt bridge formation occurs and the aluminium and silicon that strengthen the GIC do not interact with the negative carboxylic acid that is supposed to bind to the positive aluminium, silicon, sodium and strontium ions. In the next chapter, the ion release will be discussed in detail, but the larger ppm ion release from the chitosan-modified GICs also indicate that there was not sufficient integration of the aluminium, silicon, sodium and strontium ions into the carboxylate groups of the liquid to form a proper matrix. Additionally, the chitosan particle has a great affinity for the carboxylic group of the liquid and the aluminium, silicon, sodium and strontium ions that are released in the acid-base reaction. The carboxylic group is occupied as soon as the chitosan particle comes into contact with it. The aluminium, silicon, sodium and strontium released from the glass filler particles are therefore left to serve as free ions in the matrix and subsequently only bind ionically to the hydroxide groups of the carboxylic acid and the chitosan particle. Upon water sorption, the ion release starts to occur as the GIC material gets hydrolised (Chapter 7).

The decrease in the compressive strength and the proportional limit is therefore further explained on the level of the chitosan particle not integrating and binding to the matrix and the glass filler particles. The chitosan particles do not integrate with the matrix due to the reduced dissolving process of the chitosan particles when mixed with the liquid of the GICs. The chitosan particles essentially became non-bound macro-molecules (Figure 6.15). The force from the universal tester dissipates quickly after the start of the force application around the non-bound chitosan particles, based on the proportional limits. The typical fracture pattern of the chitosan-modified GICs were consistent where the lateral walls of the cylindrical samples pushed outwards as the force did not build up in the sample, but rather dissipated laterally based on the low proportional limit and the eventual low compressive strength reading (Figure 6.19).

Research by Ibrahim *et al.* (2017) and Petri *et al.*, (2007) where the chitosan was dissolved into the GIC liquid to become part of the liquid chemistry, is therefore justified and the best route for

the use of chitosan in GICs (Ibrahim *et al*., 2017; Petri *et al*., 2007). One study showed a significant increase in compressive strength with 10% nano-chitosan particles added to the powder. Forces on the control GIC (115MPa) and nano-chitosan (180MPa) were significantly different (Senthil Kumar *et al*., 2017). The results of the physical properties investigation however illustrate a lack of chitosan binding to the matrix (Figure 6.15). This translates into a poor integration with the matrix of the GIC and supports the results obtained by the compressive strength assessment (Figure 6.19) as well as that from the surface roughness analysis (Figure 6.17). The chitosan particle is integrated into the GIC's powder phase and serves as a macro-filler particle.

For the nanodiamond particles, the general integration of the nanodiamond particles that were not in an agglomerated state (Figure 6.25) dispersed well and gave the GIC the general grey appearance. When there were no or few agglomerated nanodiamond particles and only small or loose nanodiamond particles, the dispersion is well distributed and the nano size will then have its intended function of packing a greater density of particles within the GIC (De Caluwe *et al*., 2014). The larger agglomerated particles were much larger (Figures 6.26 and 6.27) than the glass filler particles of the GICs and did not readily break up during mixing to a size less than 50µm agglomerated particles.

Figure 6.25: Very well integrated nanodiamond particles of the GICs matrix

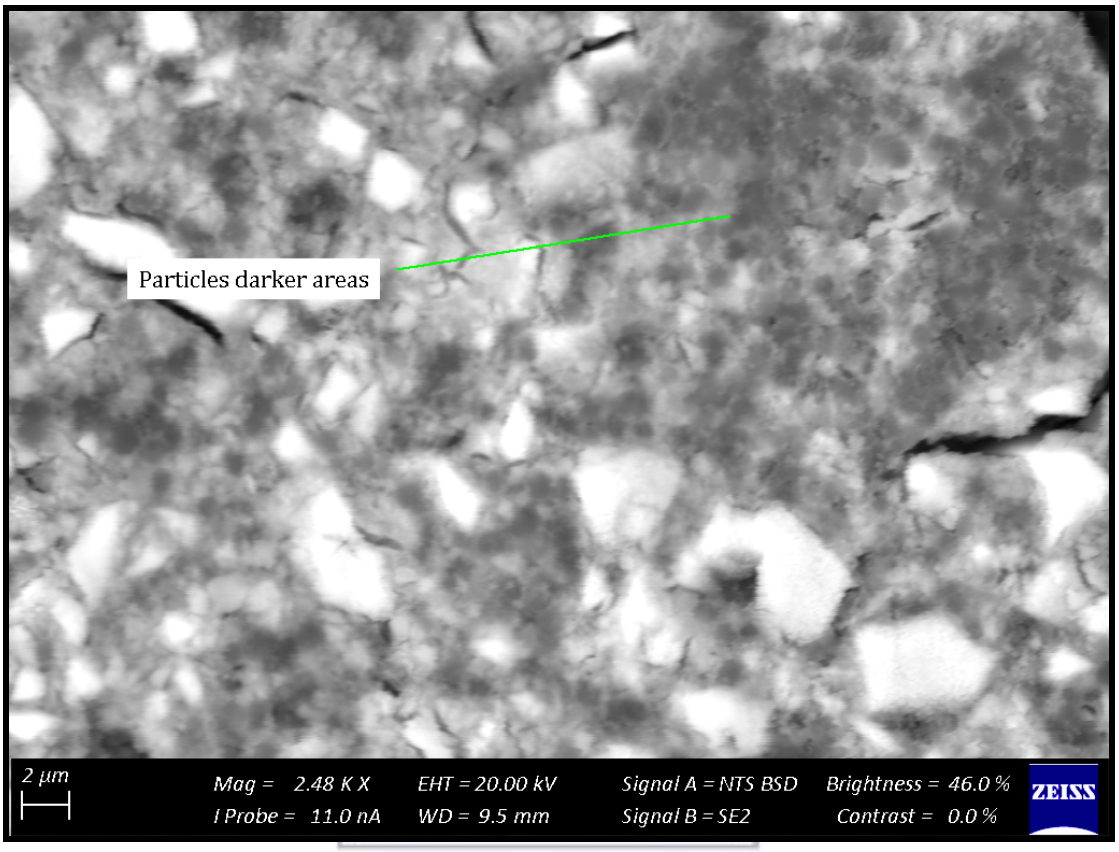

Figure 6.26: Typical agglomerated nanodiamond particles due to van der Waals forces

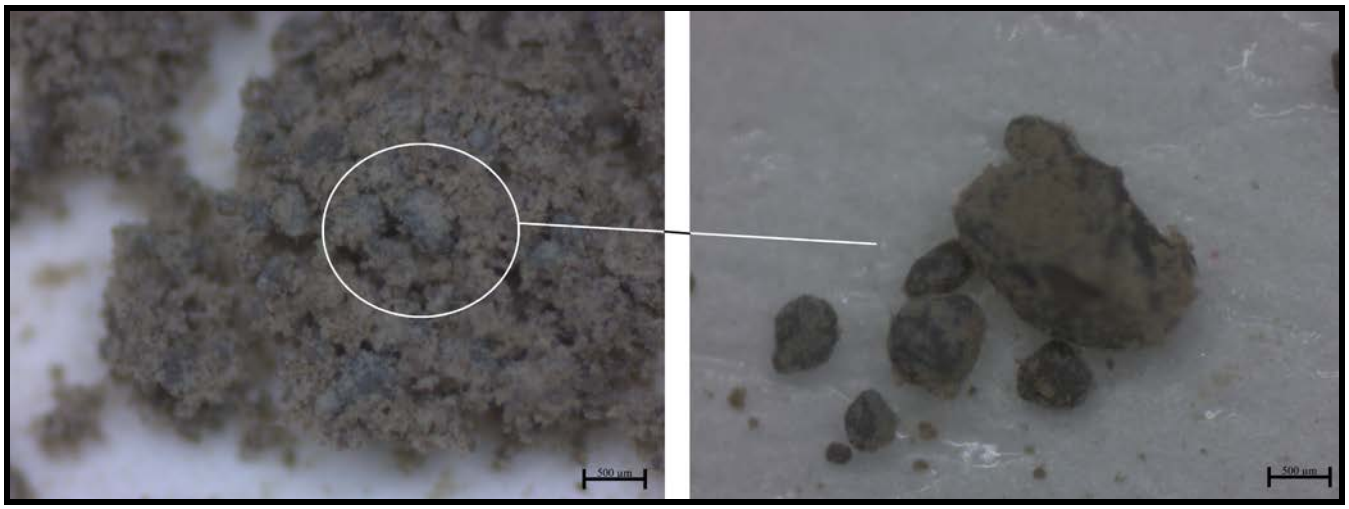

Figure 6.27: SEM image of nanodiamond agglomerated particles due to van der Waals forces

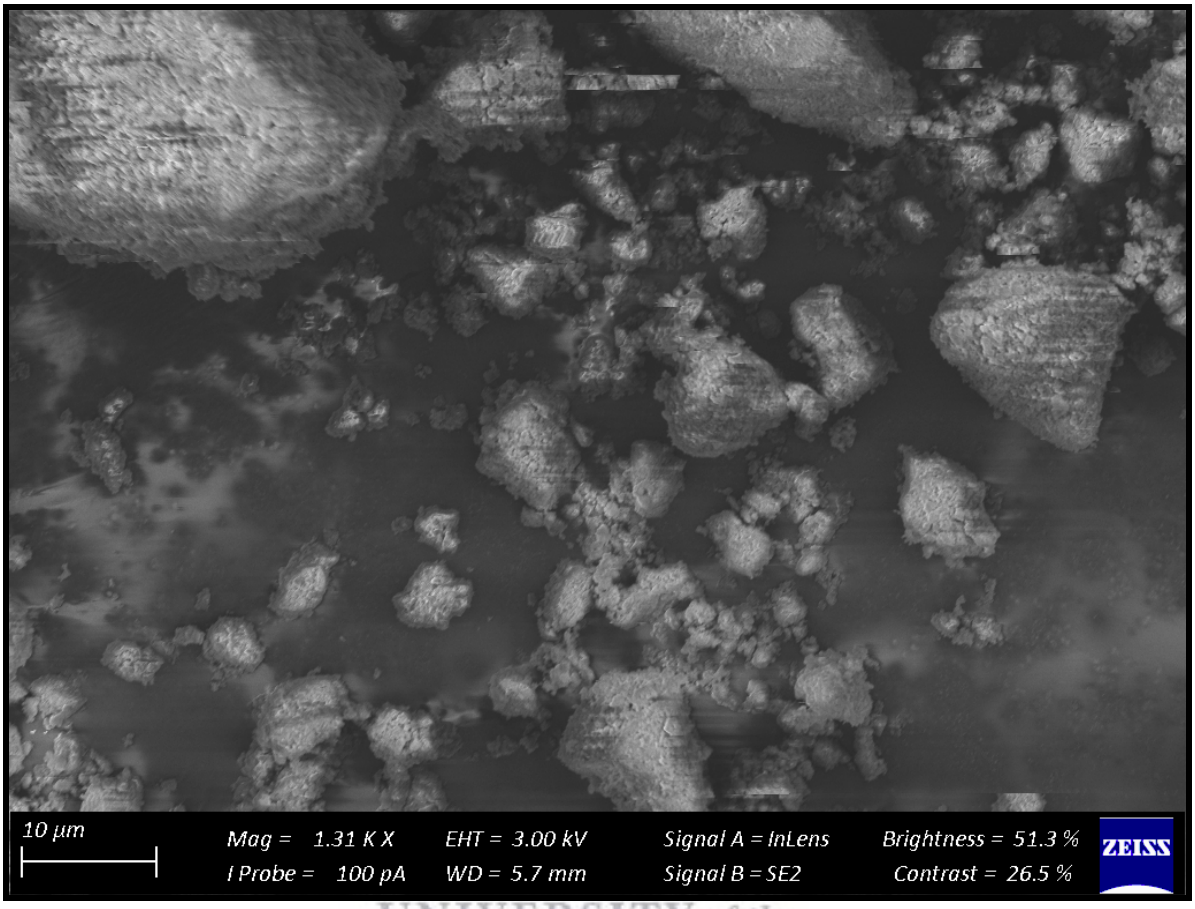

The reduction in compressive strength for GICs modified with nanodiamond particles was noted for the 5% and 10% modifications. It has been reported that the addition of silver compounds in percentages greater than 10%, significantly reduced the compressive strength in composite (Yoshida *et al*., 1999; Bürgers *et al*., 2009).

The agglomerated particles that did not disperse functioned as a macro-filler particles (Figure 6.28), reducing the strength.

Figure 6.28: Fractured agglomerated particles within the RSC10%ND modified GIC during the compressive strength test (white arrow indicating nanodiamond agglomerated particle)

The RSC fractured sample (Figure 6.29), illustrates smooth fracture lines through the sample. Although the RSC10%ND looked similar to RSC (Figure 6.30), there was a reduction in the compressive strength as well as the proportional limit. Upon larger magnification it becomes clear that the agglomerated nanodiamond particles do not easily disperse into smaller agglomerated particles or even singular nanodiamond particles during mixing. The fact that these nanodiamond particles are initially nano-sized at manufacture therefore becomes redundant for GIC modification if the nanodiamond particles form agglomerated particles. The larger agglomerated particles serve as a macro-filler and reduce the compressive and proportional limit

as found in this dissertation. Even if the nanodiamond particles are well integrated with the powder of the GICs, over time, self-agglomeration could very well occur since the GIC powder does not encapsulate the nanodiamond particles like the chitosan particles. During the acid-base reaction, the moisture from the matrix adsorbs into the nanodiamond agglomerated particles with the dissolved ions from the dissolving glass filler particle. These nanodiamond agglomerated particles with adsorbed matrix ion rich moisture are distributed throughout the material and therefore reduces the surface micro-hardness (Figure 6.18 and 6.28). This decrease in surface micro-hardness was due to the nanodiamond agglomerated particles not achieving the same strength or the ability to distribute forces like a glass filler particle. The normal formation of the GIC matrix with filler integration and adherence to the matrix is clearly more uniform with the smaller original GIC filler particles. When the surface micro-hardness is determined with the diamond indenter in an area where a nanodiamond agglomerated particle is exposed to the surface or slightly below the GIC surface, a reduction in the surface micro-hardness is recorded. As the chitosan and nanodiamond percentages increased from 5% to 10% the reduction in the VH was noted.

Figure 6.29: RSC sample from the compressive strength test (balck arrow indicates fracture line)

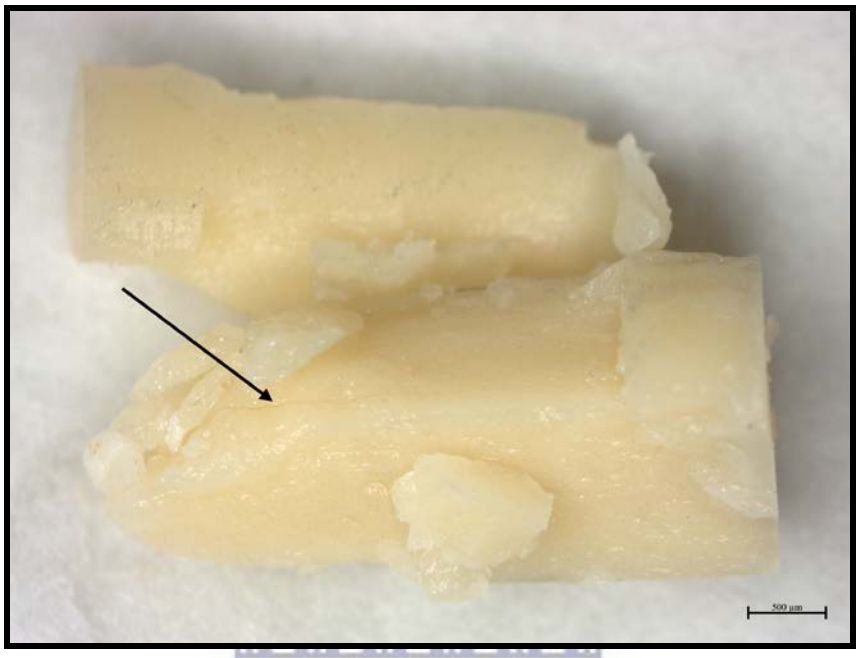

Figure 6.30: RSC10%ND-modified GIC sample from the compressive strength test with agglomerated nanodiamond particles visible

The agglomerated particles were noted through the fractured portion of the cylindrical sample. The appearance of the RSC10%ND sample in Figure 6.30 was due to the agglomeration of the nanodiamond particles (Figure 6.26) that did not disperse into smaller nanodiamond agglomerated particles upon mixing. The agglomeration is unavoidable since the nanodiamonds have an intrinsic tendency to minimize their surface energy. This is achieved when the individual nanodiamond particles of 4-6nm in size, structurally self-organize into small 20-30nm clusters. From this point, these clusters form larger agglomerated particles that range from nanometers to micrometers (Figure 6.27). This agglomeration is likely facilitated even further by the various surface functional groups (carboxylic acid (COOH), hydroxide (OH), sulfonic acid (SO_3H), and amino radical (NH_2)) and the negative Zeta potential that play a role in this agglomeration process (Jiang *et al*., 1996; Shenderova *et al*., 2002.)

The dispersion of the nanodiamond particles in the powder is much better compared to that of chitosan. At 16x magnification the smaller nanodiamond clusters and even the nanodiamond agglomerated particles dispersed with the GIC powder to form a very light grey powder (Figure 6.31: black arrows). The green arrow indicates an area of powder with no nanodiamond particles and the red arrow indicates a large nanodiamond agglomerated particle. Upon larger magnification (Figure 6.32) it becomes clear that all the small nanodiamond clusters (e.g. 21.78µm) and the agglomerated particles (480.86µm) are not covered by GIC powder, but are rather in close proximity.

Figure 6.31: Incorporation of nanodiamond particles at 16x magnification (KU10%ND)

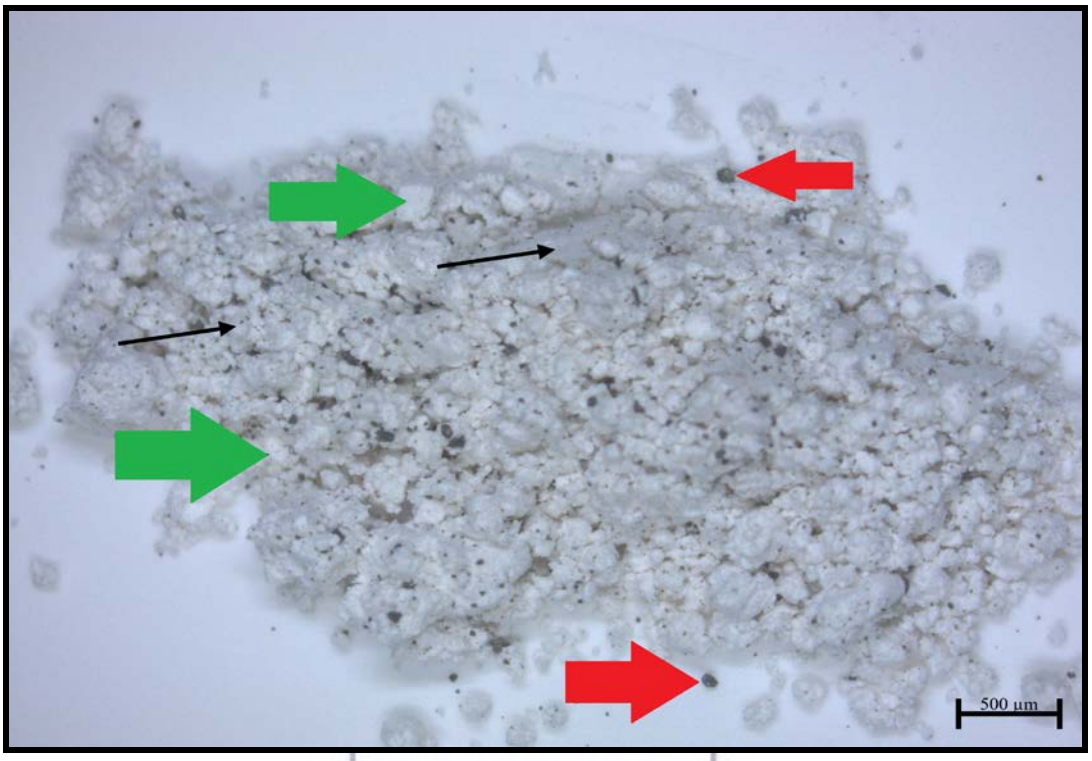

Figure 6.32: Incorporation of nanodiamond particles at 50x magnification (KU10%ND)

6.7. Conclusion

All the GIC material samples showed a high wettability based on the contact angles being below 90° (i.e. surface wetting was favourable). The greatest contributor to the weight gain was the water ingress into the agglomerated nanodiamond particles and for chitosan, the non-integration of the large chitosan particles allowed spaces for easier water ingress and swelling to occur. The chitosan-modified GICs were plagued with difficulties due to the chitosan particles being added to the powder of the GICs. During the mixing of the chitosan-modified powder with the liquid, the powder that encapsulated the chitosan continued with the initial interaction, followed by the newly exposed chitosan surface under the powder. The outer surface of the chitosan therefore had a limited exposure and interaction time with the low pH of the liquid. As a direct result, not many of the chitosan particles dissolved and could not integrate with the matrix of the GIC. The big drawback that was discovered for chitosan clearly illustrated that the chitosan particle integration into the GIC matrix as a macro-filler particle was not advantageous to the force distribution through the specimen. The functional groups on the surface of the chitosan did not provide sufficient interaction to bond to the matrix of the GIC, as it immediately occupied the building blocks of the matrix (the carboxylic acid, aluminium, silicon and the strontium ions). The chitosan modifications presented with the lowest compressive strength, proportional limit and surface micro-hardness values. The ISO 9917-1, 2007 state that the compressive strength must be above 100 MPa. Overall, the nanodiamond particles neither had non-significant differences nor did they perform significantly worse than their respective control materials although the CS above 100MPa were only observed for FN, KU, RSC, FN10%ND and KU5%ND. The GIC material has to resist the stresses that occur during mastication in posterior teeth (Dowling and Fleming, 2008) as this is the area in which the material is used in most clinical situations. From a clinical perspective, only GICs above 100MPa can be advised for clinical use.

6.8. References

Almeida, L., Namen, F., Galan, J. and Filho, F. (2003). Wettability of some dental aesthetic materials containing fluoride after surface finishing treatments. *STOMA*, 68, pp.5-11.

Andrzejewska, E., Voelkel, A., Andrzejewski, M. and Limanowska-Shaw, H. (2005). Dispersive surface properties of glass-ionomer cements determined by inverse gas chromatography. *Applied Surface Science*, 245(1-4), pp.135-140.

Anstice, H. and Nicholson, J. (1999). The Chemistry of Modern Dental Filling Materials. *Journal of Chemical Education*, 76(11), p.1497.

Bala, O., Arisu, H., Yikilgan, I., Arslan, S. and Gullu, A. (2012). Evaluation of surface roughness and hardness of different glass ionomer cements. *European Journal of Dentistry*, 6(1), pp.79-86.

Bigelow, W., Pickett, D. and Zisman, W. (1946). Oleophobic monolayers. *Journal of Colloid Science*, 1(6), pp.513-538.

Billington, R., Towler, M., Hadley, P. and Pearson, G. (1998). Effects on the glass ionomer of NaF addition. *Journal of Dental Research*, 77, p.1226.

Bollen, C., Papaioanno, W., Van Eldere, J., Schepers, E., Quirynen, M. and van Steenberghe, D. (1996). The influence of abutment surface roughness on plaque accumulation and peri-implant mucositis. *Clinical Oral Implants Research*, 7(3), pp.201-211.

Bollenl, C., Lambrechts, P. and Quirynen, M. (1997). Comparison of surface roughness of oral hard materials to the threshold surface roughness for bacterial plaque retention: A review of the literature. *Dental Materials*, 13(4), pp.258-269.

Bracco, G. and Holst, B. (2013). *Surface science Techniques (Chapter 1)*. 51st ed. New York Dordrecht: Springer Heidelberg -Springer series in surface sciences.

Bürgers, R., Eidt, A., Frankenberger, R., Rosentritt, M., Schweikl, H., Handel, G. and Hahnel, S. (2009). The anti-adherence activity and bactericidal effect of microparticulate silver additives in composite resin materials. *Archives of Oral Biology*, 54(6), pp.595-601.

Craig, R. (2002). *Restorative Dental Materials*. 11th ed. London, UK: Mosby.

Crisp, S., Lewis, B. and Wilson, A. (1975). Characterization of glass ionomer cements: Effect of powder:liquid ratios on physical properties. *Journal of Dentistry*, 6, pp.287-290.

De Barra, E. and Hill, R. (2000). Influence of glass composition on the properties of glass polyalkenoate cements. Part III: influence of fluorite content. *Biomaterials*, 21(6), pp.563-569.

De Caluwe, T., Vercruysse, C. and Martens, L. (2017). Mechanical and Bioactive Properties of a Commercial Glass Carbomer: GCP Glass Fill. *Avicenna Journal of Dental Research*, 9(4).

De Stefano, C., Gianguzza, A., Piazzese, D. and Sammartano, S. (2010). Speciation of chitosan–phosphate and chitosan–nucleotide systems in NaCI aqueous solution. *Chemical Speciation & Bioavailability*, 22(2), pp.99-107.

Doyle, R. (2000). Contribution of the hydrophobic effect to microbial infection. *Microbes and Infection*, 2(4), pp.391-400.

Esser, M., Tinschert, J. and Marx, R. (1998). Material characteristics of the hard tissues of bovine versus human teeth. *Deutsche Zahnärztliche. Zeitschrift*, 53(713), p.717.

Fennell, B. and Hill, R. (2001). The influence of poly(acrylic acid) molarmass and concentration on the properties of polyalkenoate cements. Part I- compressive strength. *Journal of Materials Science*, 36(21), pp.193-202.

Germalmaz, D., Yoruc, B., Ozcan, M. and Alkumru, H. (1998). Conventional glass ionomers as posterior restorations: A status report for the American Journal of Dentistry. *American Journal of Dentistry*, 11, pp.36-45.

Giancoli, D. (1998). *Physics*. Upper Saddle River, N.J.: Prentice Hall.

Hickel, R., Manhart, J. and Garcia-Godoy, F. (2000). Clinical results and new developments of direct posterior restorations. *American Journal of Dentistry*, 13, pp.41-54.

Hildebrande, J. (1979). Is there a "hydrophobic effect"?. *Proceedings of the National Academy of Science of the United States of Ameica.*, [online] 76(1), p.94. Available at: https://www.ncbi.nlm.nih.gov/pmc/articles/PMC382903/ [Accessed 21 Apr. 2019].

Hill, R., Wood, D. and Thomas, M. (1999). Trimethylsilylation analysis of the silicate structure of fluoro-alumino-silicate glasses and the structural role of fluorine. *Jornal of Materials Science*, 34(8), pp.1767-1774.

Ibrahim, M., Meera Priyadarshini, B., Neo, J. and Fawzy, A. (2017). Characterization of Chitosan/TiO2 Nano-Powder Modified Glass-Ionomer Cement for Restorative Dental Applications. *Journal of Esthetic and Restorative Dentistry*, 29(2), pp.146-156.

International Organization for Standardization (2007). *ISO 9917-1- Dentistry-Water based cements Part 1: Powder/liquid acid-base cements*, 1st ed.; (pages1–21).

Israelachvilli, J. and Pashley, R. (1982). The hydrophobic interaction is long range, decaying exponentially with distance. *Nature 300*, pp.341-342.

Jiang, T., Xu, K. and Ji, S. (1996). FTIR studies on the spectral changes of the surface functional groups of ultradispersed diamond powder synthesized by explosive detonation after treatment in hydrogen, nitrogen, methane and air at different temperatures. *Journal of the Chemical Society, Faraday Transactions*, 92, pp.3401-3406.

Kang, H., Cai, Y., Deng, J., Zhang, H., Tang, Y. and Liu, P. (2006). Synthesis and aqueous solution behavior of phosphonate-functionalized chitosans. *European Polymer Journal*, 42(10), pp.2678-2685.

Kasraei, S. and Azarsina, M. (2012). Addition of silver nanoparticles reduces the wettability of methacrylate and silorane-based composites. *Brazilian Oral Research*, 26(6), pp.505-510.

Klinge, S., Kunstmann, K., Frankenberger, R. and Krämer, N. (1999). Clinical behaviour of viscous glass ionomer cement in classes I and II cavities. *Journal of Dental Research*, 78, p.2285.

Leja, J. and Poling, G. (1960). "On the Interpretation of Contact Angle." *Proceedings of the Fifth International Mineral Processing Congress*, pp.325-332.

Lohbauer, U. (2009). Dental Glass Ionomer Cements as Permanent Filling Materials? – Properties, Limitations and Future Trends. *Materials*, 3(1), pp.76-96.

Lyklema, J. (2000). *Fundamentals of Interface and Colloid Science*. 1st ed. Burlington: Elsevier.

Matsuya, S., Stamboulis, A., Hill, R. and Law, R. (2007). Structural characterization of ionomer glasses by multinuclear solid state MAS-NMR spectroscopy. *Journal of Non-Crystalline Solids*, 353(3), pp.237-243.

McKenzie, M. (2003). The physical properties of conventional and resin-modified glass-ionomer dental cements stored in saliva, proprietary acidic beverages, saline and water. *Biomaterials*, 24(22), pp.4063-4069.

Menne-Happ, U. and Ilie, N. (2013). Effect of heat application on the mechanical behaviour of glass ionomer cements. *Clinical Oral Investigations*, 18(2), pp.643-650.

Miličević, A., Goršeta, K., van Duinen, R. and Glavina, D. (2018). Surface Roughness of Glass Ionomer Cements after Application of Different Polishing Techniques. *Acta Stomatologica Croatica*, 52(4), pp.314-321.

Moshaverinia, A., Roohpour, N., Chee, W. and Schricker, S. (2011). A review of powder modifications in conventional glass-ionomer dental cements. J*ournal of Material Chemistry*, 21(5), pp.1319-1328.

Mulder, R. (2018). Variation in the Dispersions of Powder Liquid Ratios in Hand-Mix Glass Ionomers. *The Open Dentistry Journal*, 12(1), pp.647-654.

Naasan, M. and Watson, T. (1998). Effect of early water contact on solubility of glass ionomer luting cements. *The Journal of Prosthetic Dentistry*, 80(4), pp.474-478.

Nagaraja Upadja, P. and Kishore, G. (2015). Glass ionomer cement - the different generations. *Trends Biomaterials and Artificial Organs*, pp.158-165.

Namen, F., Galan, J., De Deus, G., Cabreira, R. and Filho, F. (2008). Effect of pH on the Wettability and Fluoride Release of an Ion-releasing Resin Composite. *Operative Dentistry*, 33(5), pp.571-578.

Nicholson, J. (1998). Chemistry of glass-ionomer cements: a review. *Biomaterials*, 19(6), pp.485-494.

Nicholson, J. (2018). Maturation processes in glass-ionomer dental cements. *Acta Biomaterialia Odontologica Scandinavica*, 4(1), pp.63-71.

Peniche, C. and Argüelles-Monal, W. (2001). Chitosan based polyelectrolyte complexes. *Macromolecular Symposia*, 168(1), pp.103-116.

Petit, T., Yuzawa, H., Nagasaka, M., Yamanoi, R., Osawa, E., Kosugi, N. and Aziz, E. (2015). Probing Interfacial Water on Nanodiamonds in Colloidal Dispersion. *The Journal of Physical Chemistry Letters*, 6(15), pp.2909-2912.

Petri, D., Donegá, J., Benassi, A. and Bocangel, J. (2007). Preliminary study on chitosan-modified glass ionomer restoratives. *Dental Materials*, 23(8), pp.1004-1010.

Pina-Salazar, E., Urita, K., Hayashi, T., Futamura, R., Vallejos-Burgos, F., Włoch, J., Kowalczyk, P., Wiśniewski, M., Sakai, T., Moriguchi, I., Terzyk, A., Osawa, E. and Kaneko, K. (2017). Water Adsorption Property of Hierarchically Nanoporous Detonation Nanodiamonds. *Langmuir*, 33(42), pp.11180-11188.

Prentice, L., Tyas, M. and Burrow, M. (2005). The effect of particle size distribution on an experimental glass-ionomer cement. *Dental Materials*, 21(6), pp.505-510.

Reis, A., Giannini, M., Lovadino, J. and Dos santos dias, C. (2002). The effect of six polishing systems on the surface roughness of two packable resin based composites. *American Journal of Dentistry*, 15(3), pp.193-197.

Ryba, T., Dun, N. and Murchison, D. (2002). Surface roughness of various packable composites. *Operative Dentistry*, 27(3), pp.243-247.

Schweitzer, G. and Pesterfield, L. (2010). *The aqueous chemistry of the elements*. Oxford (UK): Univeristy Press.

Senthil Kumar, R., Ravikumar, N., Kavitha, S., Mahalaxmi, S., Jayasree, R., Sampath Kumar, T. and Haneesh, M. (2017). Nanochitosan modified glass ionomer cement with enhanced mechanical properties and fluoride release. *International Journal of Biological Macromolecules*, 104, pp.1860-1865.

Shenderova, O., Zhirnov, V. and Brenner, D. (2002). Carbon Nanostructures. *Critical Reviews in Solid State and Materials Sciences*, 27(3-4), pp.227-356.

Sidhu, S. and Henderson, L. (1993). The surface finish of light-cured composite site resin materials. *Clinical Materials*, 12(1), pp.11-15.

Small, I., Watson, T., Chadwick, A. and Sidhu, S. (1998). Water sorption in resin-modified glass-ionomer cements: An *in vitro* comparison with other materials. *Biomaterials*, 19(6), pp.545-550.

Tanford, C. (1973). *The Hydrophobic Effect: Formation of Micelles and Biological Membranes*. New York, London, Sydney, Toronto: John Wiley and Sons, pp.https://doi.org/10.1002/food.19760200449.

Twomey, E., Towler, M., Crowley, C., Doyle, J. and Hampshire, S. (2004). Investigation into the ultrasonic setting of glass ionomer cements Part II Setting times and compressive strengths. *Journal of Materials Science*, 39(14), pp.4631-4632.

Van Oss, C., Absolom, D. and Neuman, A. (1980). The "Hydrophobic Effect" : Essentially a van der Waals interaction. *Journal of Colloid and Interface Science*, 15, pp.424-427.

Voelkel, A., Andrzejewska, E., Limanowska-Shaw, H. and Andrzejewski, M. (2005). Acid–base surface properties of glass-ionomers determined by IGC. *Applied Surface Science*, 245(1-4), pp.149-154.

Vogler, E. (1998). Structure and reactivity of water at biomaterial surfaces. *Advances in Colloid and Interface Science*, 74(1-3), pp.69-117.

Wade, L. (2006). *Wade Organic Chemistry*. 6th ed. Pearson Prentice Hall, p.279.

Wasson, E. and Nicholson, J. (1993). New Aspects of the Setting of Glass-ionomer Cements. *Journal of Dental Research*, 72(2), pp.481-483.

Wilson, A. and McLean, J. (1988). *Glass ionomer cement*. Chicago: Quintessence Publishing Co.

Yoshida, K., Tanagawa, M. and Atsuta, M. (1999). Characterization and inhibitory effect of antibacterial dental resin composites incorporating silver-supported materials. *Journal of Biomedical Materials Research*, 47(4), pp.516-522.

Yuan, Y. and Lee, T. (2013). Contact Angle and Wetting Properties - Chapter 1. *Surface Science Techniques*, Springer publishing.

CHAPTER 7

ION RELEASE BEHAVIOUR OF GLASS IONOMER RESTORATIVE CEMENTS MODIFIED WITH CHITOSAN OR NANODIAMONDS

7.1. Abstract

Purpose: Ion release from glass ionomer restorative cements (GICs) play an important role in GICs. The ion release from chitosan- and nanodiamond-modified glass ionomers was assessed.

Materials and Methods: Three different glass ionomer restorative cements Fuji IX (FN: *GC Corp, Tokyo, Japan, Batch: 1503231*), Ketac Universal (KU: *3M ESPE, Seefeld, Germany, Batch: 583514*) and Riva Self Cure (RSC: *SDI Limited, Australia, Batch: 62657V*) served as the control materials. These three GICs were modified in the powder phase per weight by adding 5% or 10% of a commercially available chitosan powder (CH) or nanodiamond (ND) powder to the GICs. The specimens with dimensions 6±0.1mm height and 4±0.1mm diameter manufactured from the 15 GIC formulations were placed in neutral de-ionised water after 1 hour of bench-setting. The specimens were stored at 37ºC for 24 hours after which the released ions were assessed using Inductively Coupled Plasma Mass Spectrometer (ICP-MS) to determine the elemental release. Additionally, three different disc-shaped specimens (3±0.1mm in diameter and 1±0.1mm thick) were constructed from each material for Scanning Electron Microscopy (SEM) and Energy Dispersive X-Ray Spectrometry (EDS) Microanalysis (SEM-EDS) to establish a baseline ion concentration (gradient weight percentage potential).

Results: There were no significant differences in the ion release between the control materials for aluminium, silicon and strontium. The ion release from chitosan and most nanodiamond-modified GICs were significantly ($p < 0.00001$) increased compared to the control materials.

Chitosan modifications significantly increase the ion release of aluminium, silicon, sodium and strontium for all three control materials (with the exception of KU5%CH for strontium).

Conclusion: Ion release influences the mineralization of tooth structure and alters the bacterial growth. Ion release can therefore be advantageous due to the interaction of chitosan with the GIC chemistry and moisture during maturation. The chitosan and nanodiamond modified GICs presented with ion release up to five times greater than the control material.

Keywords: Glass ionomer, chitosan, nanodiamond, ICP-MS, SEM-EDS, aluminium, strontium, silicon.

Abbreviations and acronyms:

FN: Fuji IX GP

CH: Chitosan

GICs: Glass ionomer restorative cements

ICP-MS: Inductively coupled plasma mass spectrometer

KU: Ketac Universal

ND: Nanodiamond (s)

RSC: Riva Self Cure

SEM-EDS: Scanning Electron Microscopy (SEM) and Energy Dispersive X-Ray Spectrometry (EDS) Microanalysis

w/w%: weight/weight%

Baseline ion concentration: Gradient weight percentage potential.

7.2. Introduction

Fuji IX (*GC Corp*) and Ketac Universal (*3M ESPE*) are glass ionomer restorative cements (GICs) that are indicated as restorative materials for use in the atraumatic restorative treatment (ART) technique. FN has been well established as a restorative material for ART, since it has been shown to be durable with satisfying results over several years (Frenken *et al*., 2012).

Glass ionomer success for the ART technique is partly attributed to the fact that GICs bind well to tooth structure, potentially reducing the risk of micro-leakage between the restoration and the tooth interface (Fucio *et al*., 2008).

The activity of GICs by way of ion release is essential to the mineralization of carious dentine (Ngo *et al*., 2006). Upon mixing the two components of a GIC (powder and liquid), the acid-base reaction continues until neutralization of the acidic liquid by the basic ions released from the powder are completed (Sidhu *et al*., 2016). This acid-base reaction forms calcium polyacrylate (or strontium polyacrylate in more modern GICs) immediately followed by aluminium polyacrylate as the reaction continues (Nicholson *et al*., 1988). The glass particles in the GICs serve as ion donors and the filler particles. Together they interlock with the matrix of the GICs (Nicholson, 2018). The modification of GICs with chitosan (CH) or nanodiamond (ND) particles may result in different material surface properties compared to unmodified GICs that could be advantageous to the ion release properties. Chitosan is derived from chitin, which results from shell fish being partly deacetylated. The amino-polysaccharide that develops due to this process is known as chitosan (Muzzarelli, 1973). Chitosan contains a large number of repeating units of ß-(1-4)-linked glucosamines. This unit has various amino (NH_3) and hydroxide (OH^-) functional groups (De Stefano *et al*., 2010). The cationic amino groups of chitosan are of particular interest in GIC modification, since it can interact electrostatically with the carboxylic acid group (Hamman, 2010) of the GIC liquid to form various polyelectrolyte complexes.

Nanodiamond (ND) particles on the other hand have a negative Zeta potential due to the presence of multiple carboxylic groups on the surface of the nanodiamond particles (Osswald *et al*., 2006). The cation ions derived from the glass filler particles of GICs (aluminium, silicon, sodium and strontium) have the potential to attach to the nanodiamond particle.

Billington *et al*. (2006) stated that traditionally the ion release from GICs was thought to have originated from the exposure of the glass filler particles to the polymeric and tartaric acid present in the GIC liquid (Billington *et al*., 2006). It has been shown that ions can release soluble ions into neutral water. From the literature reviewed, it is clear that the ion release from GICs is of importance. Inductively Coupled Plasma Mass Spectrometer (ICP-MS) analysis has previously successfully been used in an acidic medium to assess the ion release from GICs (Wasson and Nicholson, 1990). The only limitation is that fluoride analysis is not possible with this method (Wasson and Nicholson, 1990). When a restoration is placed in a tooth or ion release is assessed *in vitro* the ions present in GICs move from the matrix into the liquid-moist environment and vice versa (Williams *et al*., 2002). This is why de-ionised water is a successful medium to assess the ion release behaviour of modified glass ionomers for a 24-hour period.

The aim of the present study was to assess the ion release of GICs after chitosan or nanodiamond modification. The hypothesis was that the ion release of the modified GICs would be improved in relation to the respective commercial materials.

7.3. Materials and Methods

Three different commercially available hand-mix GICs were used in this study: Fuji IX GP (FN: *GC Corp, Tokyo, Japan, Batch: 1503231*), Ketac Universal (KU: *3M ESPE, Seefeld, Germany, Batch: 583514*) and Riva Self Cure (RSC: *SDI Limited, Australia, Batch: 62657V*). The three GICs were modified in the powder phase per weight percentage (w/w%) by adding 5% or 10%

of a commercially available chitosan powder (*Merck, item 448877*) or nanodiamond particles (*PlasmaChem, item: PL-D-G01*) to the GICs. The modified experimental materials were produced by placing the GIC powder in an airtight high density polyethylene (HDPE) container. The container was subsequently clamped in a beaker shaker for two hours to ensure complete mixing of the two powders prior to being dispensed using a level manufacturer's powder spoon per drop of liquid. Upon dispensing with the manufacturer's spoon, the chitosan or nanodiamond particle incorporation of 5-weight% modification to the GIC powder consisted of 95% commercial GIC and 5%CH or 5%ND per weight. The powder/liquid ratio prescribed by the manufacturer was followed and confirmed on a desktop analytical balance (*Metler AE240 analytical balance, Columbus, Ohio, USA*) by first dispensing the powder followed by the liquid. This ensured that the manufacturer's recommended powder/liquid ratio was maintained for all the GICs used in this study (Mulder, 2018).

Fifteen GICs were prepared: (1) FN GIC powder [FN]; (2) FN GIC powder modified with 5-wt% chitosan powder [FN5%CH]; (3) FN10%CH; (4) FN5%ND; (5) FN10%ND; (6) KU; (7) KU5%CH; (8) KU10%CH; (9) KU5%ND; (10) KU10%ND; (11) RSC; (12) RSC5%CH; (13) RSC10%CH; (14) RSC5%ND; (15) RSC10%ND.

7.3.1. Sample size and experimental sequence

Five samples of each GIC material were produced using a Teflon mould with a cylindrical space of 6±0.1mm in height and 4±0.1mm in diameter. The materials were kept at room temperature (23±1°C) with a relative humidity of 50±5% and the moulds were stored in a temperature-controlled incubator (37±1°C) prior to testing (ISO, 2003; Twomey *et al*., 2004; Menne-Happ and Ilie, 2013). After 1 hour of bench curing, the 75 samples were prepared with 4000 grit silicon carbide paper on the top and bottom sides of the cylindrical sample and placed in 5ml of de-ionised water. After being stored in a temperature-controlled incubator (37±1°C) for 24 hours, the GIC material was removed and the de-ionised water used for ICP-MS analysis.

7.3.2. ICP-MS analysis

Trace and major analysis of ions was completed using an Inductively Coupled Plasma Mass Spectroscopy (ICP-MS) unit (*Agilent 7900, Santa Clara, CA, USA*). This is a suitable method for trace ion analysis of liquids as samples ranging from sub-parts per billion to mid-parts per million levels can be assessed. The lowest detection limits for the instrument were aluminium 2.51µg/L; lanthanum 0.02µg/L; sodium 0.15mg/L; phosphorus 0.02mg/L; silicon 0.01mg/L and strontium 0.08µg/L;. The control sample of de-ionised water and the de-ionised water sample with the unknown ions that leached from the GICs were analysed against NIST traceable standards and independent quality control solutions. Sample preparation of the liquids was completed after the calibration acceptance criterion of R2 > 0.9995 was achieved. Water samples were acidified with Ultra pure nitric acid (HNO_3) to a 2% final acid concentration. Particulates were left to settle out prior to analysis. The results obtained were therefore a dissolved fraction of the sample. The instrument conditions were a RF Power of 1600W, 0.83L/min Argon carrier gas, and 10mm sample depth. The make-up gas flowed at 0.15L/min; helium (He) at 5ml/min, hydrogen (H_2) at 6ml/min and the nebuliser was set at 0.4mL/min micro mist.

The water sample passed through the nebuliser which produced a fine aerosol. The large droplets were removed by a spray chamber and the small droplets passed through the plasma. In the ICP-MS analysis, the plasma torch was positioned horizontally and used to generate positively charged ions rather than photons. In fact, every attempt was made to stop the photons reaching the detector because they had the potential to increase signal noise. It is the production and detection of large quantities of these ions that gives ICP-MS its characteristic ultra trace detection capability.

Once the ions are produced in the plasma, they are directed into the mass spectrometer via the interface region which was maintained at a vacuum of 1 - 2 torr with a mechanical roughing

pump. This interface region consisted of two metallic cones (usually made of nickel) called the sampler and skimmer cone. Each cone featured a small (0.6 - 1.2mm) orifice that allowed the ions through to the ion optics, where they were guided into the mass separation device.

The interface region is one of the most critical areas of an ICP-MS. Its role is to help the ion transport to occur efficiently (and retain the electrical integrity) from the plasma which is at atmospheric pressure (760 torr), to the mass spectrometer analyzer region at approximately 10^6 torr. Unfortunately, there was capacitive coupling between the radiofrequency coil and the plasma that produced a potential difference of a few hundred volts. If this wasn't eliminated, an electrical discharge (called a secondary discharge or pinch effect) would appear between the plasma and the sampler cone. This discharge could increase the formation of an interfering ion species and also dramatically affect the kinetic energy of the ions entering the mass spectrometer, making optimisation of the ion optics very erratic and unpredictable. For this reason, the secondary charge was eliminated using a radiofrequency coil grounding mechanism and this was successfully achieved.

Once the ions have been successfully extracted from the interface region, they were directed into the main vacuum chamber by a series of electrostatic lenses (ion optics). A turbo-molecular pump maintained the operating vacuum in this region at about 10^2 torr. The ion optic region serves to electrostatically focus the ion beam towards the mass separation device and to stop photons, particulates, and neutral ion species from reaching the detector.

The ion beam that contained all the analyte and matrix ions exited the ion optics and passed into the mass spectrometer (mass separation device) where a second turbo-molecular pump maintained an operating vacuum of approximately 10^6 torr. The mass separation device allowed the analyte ions of a particular mass-to-charge ratio (m/z) through to the detector and filtered out all the non-analyte, interfering ions and matrix ions. In the final process, the ion detector

converted the ions into an electrical signal. This signal was expressed as counts using Masshunter software for calculating the weight of the present per µg/L. For analysis purposes, all values were converted to mg/L.

7.3.3. SEM-EDS micro-analysis

Scanning Electron Microscopy (SEM) and Energy Dispersive X-Ray Spectrometry (EDS) Microanalysis (SEM-EDS) was completed on the three commercial GICs to establish the baseline percentage of elements. Five spectrums were taken on filler particles and five in the matrix. This is essential to allow for sufficient quantification, since it has been shown that the glass filler particle and matrix have different ion concentrations (Hatton and Brook, 1992). In order to increase the electrical conductivity of the GIC specimens for SEM analysis, the specimens were first gold sputter-coated (*Edwards S150A Sputter Coater*) at 40 mA. SEM-EDS of the outer surfaces was then performed (*Zeiss MERLIN Field Emission SEM; Carl Zeiss Microscopy, Jena, Germany*) at 200x magnification. Five points were chosen in the central field of view on the filler particles and five points in the matrix of the GIC for EDS analysis (generating ten spectrums per specimen). This was essential since it has been shown that ions in GICs vary. The EDS spectrums were collected from the central field of view for each specimen under the following conditions: The accelerating voltage of 20kV and a working distance of 9.5mm, an 11nA beam current at 10^6 Torr pressure (high-vacuum) with a 10s acquisition time and 30-45% detector dead time were used for this application. The elemental analyses (in weight percentage) of the specimens were performed in non-standard analysis mode, applying the PROZA (*Phi-Rho-Z*) correction method. A Zeiss 5-diode Back Scattered Electron (BSE) Detector (*Zeiss NTS BSD*) and Zeiss Smart SEM software generated the BSE images. The Semi-quantitative Energy Dispersive X-Ray Spectrometry (EDS) using an X-Max 20mm^2 detector (*Oxford Instruments, Abingdon, UK*) and Oxford Aztec software were used to chemically quantify the specimens. Images were obtained at 200 and 500nm.

7.4. Statistical analysis

Statistical analysis of the results was performed with R Core Team (2013). R: A language and environment for statistical computing. R Foundation for Statistical Computing (*Vienna, Austria*). The one way ANOVA test for homogeneity was used and confirmed with the t-test between the various means, with an analysis of variance ($p < 0.05$).

7.5. Results

ICP-MS analysis of ion release into de-ionised water over a 24-hour period.

The one way ANOVA test for homogeneity of the mean values of FN, KU, RSC and their chitosan or nanodiamond modifications indicated the presence of significant differences. The data analysis was conducted across the variances. First, each control material was compared with its four modifications. Significant differences between the ion release for the control materials and the means of their chitosan or nanodiamond modifications for aluminium, silicon, sodium and strontium ($p < 0.00001$) were identified. The standard deviation (SD): standard error (SE) for each element was aluminium (±SD1.42:SE0.063); sodium (±2.33:1.04); silicon (±3.48:1.55) and strontium (±0.2:0.09). This standard deviation was kept in mind when comparing means from Table 7.1 for the control materials and their respective chitosan or nanodiamond modifications. It is important to note that 1mg/L is equal to 1part per million (ppm).

Table 7.1: Mean ion release (mg/L) of the commercial materials and their respective modifications

Ion released	Commercial material	Modification			
		5%ND	10%ND	5%CH	10%CH
FN					
Al^{3+}	2.22	2.5	3.29	5.22*	10.8*
Na^{+}	11.03	11.77	14.62*	19.27*	29.72*
Si^{4+}	4.16	5.42	4.78	10.29*	23.70*
Sr^{+}	0.4	0.4	0.49	1.33*	2.09*
(*): Indicates significant increase of ion release compared to FN.					
KU					
Al^{3+}	2.86	7.56^	8.84^	6.44^	14.04^
Na^{+}	15.91	22.07^	26.95^	27.61^	41.72^
Si^{4+}	8.61	18^	19.65^	12.41^	26.39^
Sr^{+}	0.09	0.23	0.18	0.3	0.48^
La^{3+}	0.000261	0.003517^	0.004199^	0.01048^	0.015138^
(^): Indicates significant increase of ion release compared to KU.					
RSC					
Al^{3+}	5.16	8^{+}	9.03^{+}	9.85^{+}	8.85^{+}
Na^{+}	20.04	25.55^{+}	28.54^{+}	31.20^{+}	30.34^{+}
Si^{4+}	8.05	11.52	12.58	12.64^{+}	13.35^{+}
Sr^{+}	0.32	0.7	0.63	1.31^{+}	1.99^{+}
($^{+}$): Indicates significant increase of ion release compared to RSC.					

Figure 7.1: Mean ion release (mg/L) of the commercial materials and their respective modifications

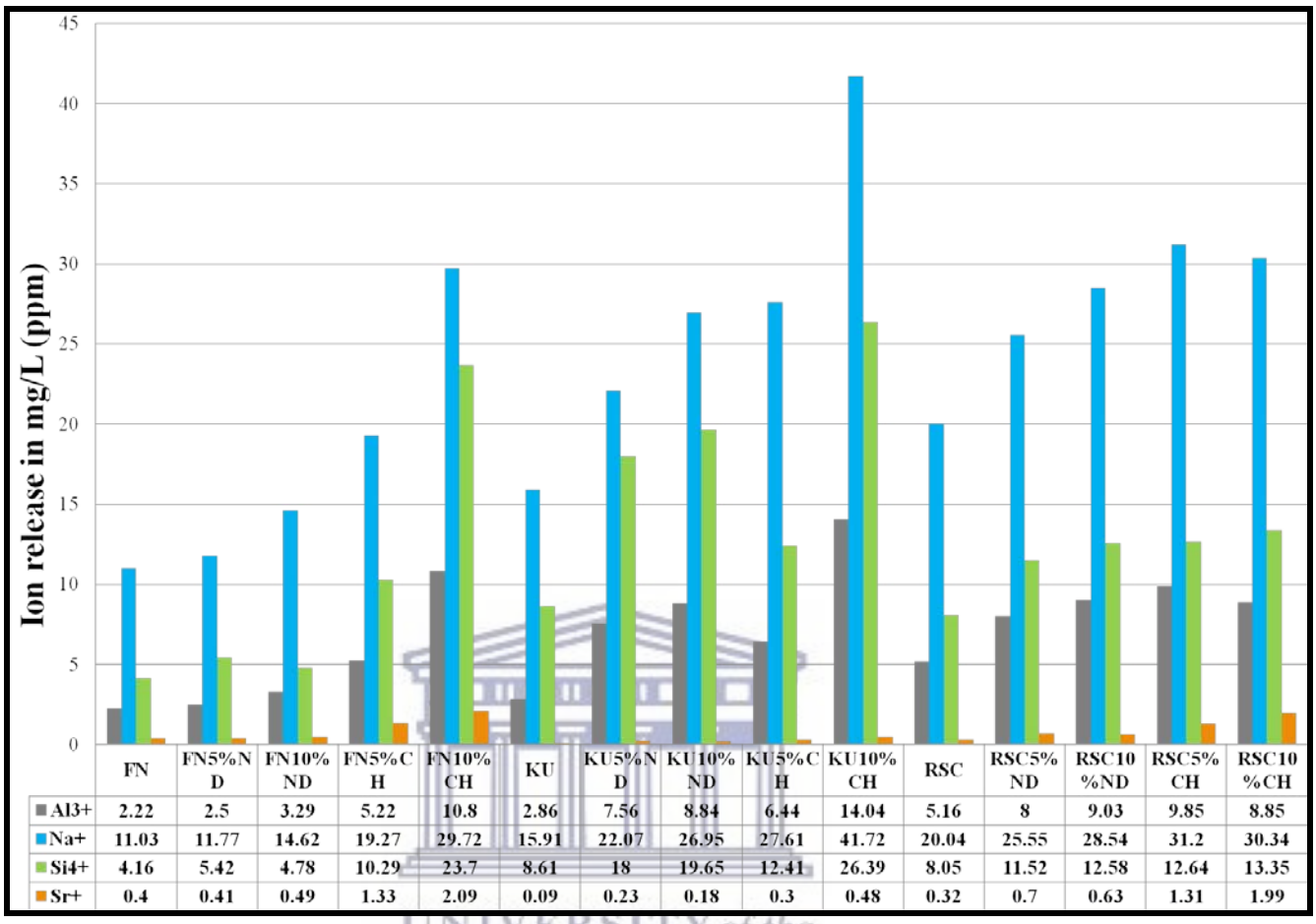

	FN	FN5%ND	FN10%ND	FN5%CH	FN10%CH	KU	KU5%ND	KU10%ND	KU5%CH	KU10%CH	RSC	RSC5%ND	RSC10%ND	RSC5%CH	RSC10%CH
Al3+	2.22	2.5	3.29	5.22	10.8	2.86	7.56	8.84	6.44	14.04	5.16	8	9.03	9.85	8.85
Na+	11.03	11.77	14.62	19.27	29.72	15.91	22.07	26.95	27.61	41.72	20.04	25.55	28.54	31.2	30.34
Si4+	4.16	5.42	4.78	10.29	23.7	8.61	18	19.65	12.41	26.39	8.05	11.52	12.58	12.64	13.35
Sr+	0.4	0.41	0.49	1.33	2.09	0.09	0.23	0.18	0.3	0.48	0.32	0.7	0.63	1.31	1.99

When the comparison of all fifteen materials to one another were completed, significant differences between the material means of aluminium ($p < 0.0001$); sodium ($p < 0.0001$); silicon ($p = 0.0008$) and strontium ($p < 0.0001$) were noted once again. The pooled within-material standard error difference between any two means was aluminium±1.47; sodium±1.47; silicon±2.2 and strontium±0.13. This standard deviation was kept in mind when comparing means from Table 7.1 and Figure 7.1.

Aluminium release (Al^{3+})

The comparison within a material (FN, KU and RSC) and their respective chitosan and nanodiamond modifications (Figure 7.2) provided insight as to how the chitosan or nanodiamond modifications influenced the aluminium ion release. The chitosan modification of FN released significantly more aluminium ($p < 0.0001$) than the FN control material. There was no significant release difference between FN, FN5%ND and FN10%ND over the 24-hour period ($p = 0.265$) (Figure 7.2).

The nanodiamond ($p = 0.0004$) and chitosan modifications ($p < 0.0001$) of KU released significantly more aluminium than the KU control. KU5%ND did not release more aluminium than KU10%ND ($p = 0.056$) or KU5%CH ($p > 0.056$). KU10%CH however released significantly more aluminium ($p = 0.005$) than KU5%ND, KU10%ND and KU5%CH.

The chitosan and nanodiamond modifications of RSC released significantly more aluminium ($p < 0.0001$). There was no significant aluminium release difference between any of the chitosan and nanodiamond modifications ($p > 0.09$) when RSC was modified (Figure 7.2).

Figure 7.2: Comparison of aluminium release from the control materials to their modifications

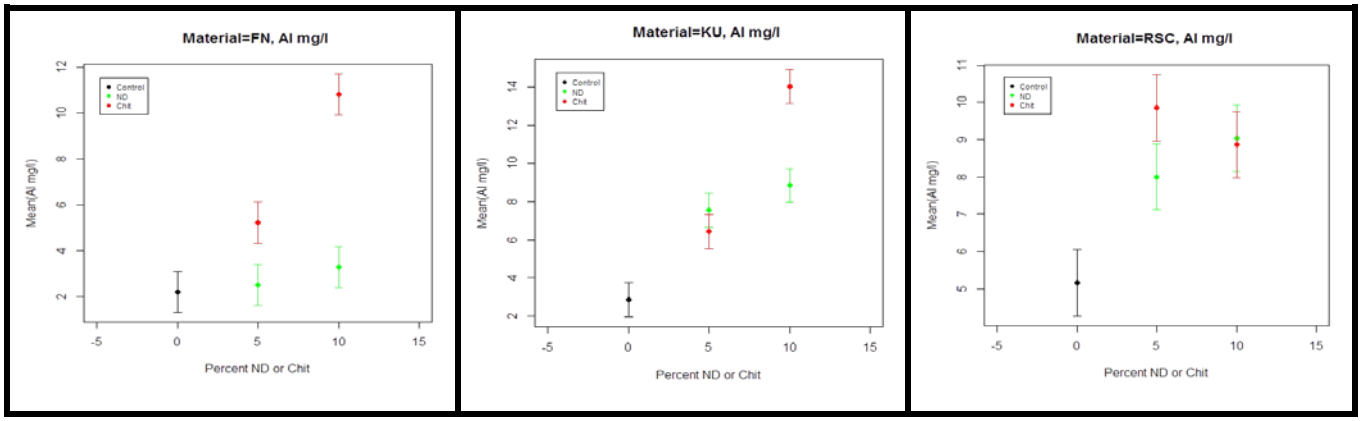

The comparison of all fifteen materials to one another (Figure 7.3) provided insight into how the aluminium release from the three control materials and their chitosan or nanodiamond modifications influenced the aluminium ion release. There was no difference ($p > 0.05$) between the aluminium releases of the three control materials. There was however a general increasing trend of aluminium ion release from the control materials (FN to KU to RSC) and their 5% to 10% modifications with chitosan and nanodiamonds, with the exception of RSC10%CH. KU10%CH was the chitosan-modified material with a significantly greater aluminium ion release ($p < 0.00015$) than any one of the remaining fourteen materials. For nanodiamonds, the materials KU5%ND and RSC5%ND released more aluminium ($p < 0.00024$) than FN5%ND (Figure 7.3).

Figure 7.3: Comparison of aluminium release from the control materials to their modifications

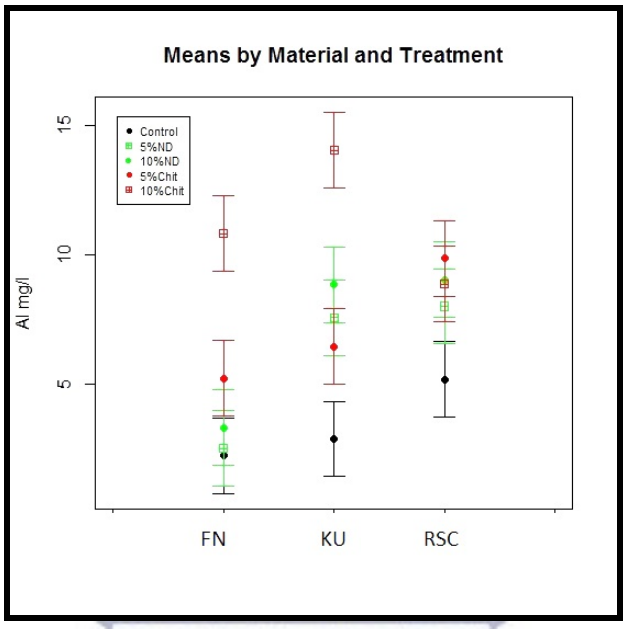

Sodium release (Na^+)

The comparison within the material group and the respective modifications (Figure 7.4) provided insight as to how the sodium ion release was influenced by the chitosan and nanodiamond modifications. The sodium release for FN5%CH, FN10%CH ($p < 0.0001$) and FN10%ND ($p = 0.022$) was significantly higher than for the FN control material. There was no significant difference between FN and FN5%ND over the 24-hour period ($p > 0.05$) (Figure 7.4).

The chitosan and nanodiamond modifications ($p = 0.0001$) of KU released significantly more sodium than the KU control. No significant difference was noted between KU5%CH and KU10%ND ($p > 0.05$).

RSC modified with chitosan and nanodiamonds released significantly more sodium than the RSC control ($p < 0.0001$). There was no significant sodium release difference between RSC5%ND and RSC10%ND or RSC5%CH and RSC10%CH ($p > 0.054$) (Figure 7.4).

Figure 7.4: Comparison of sodium release of the control materials and their modifications

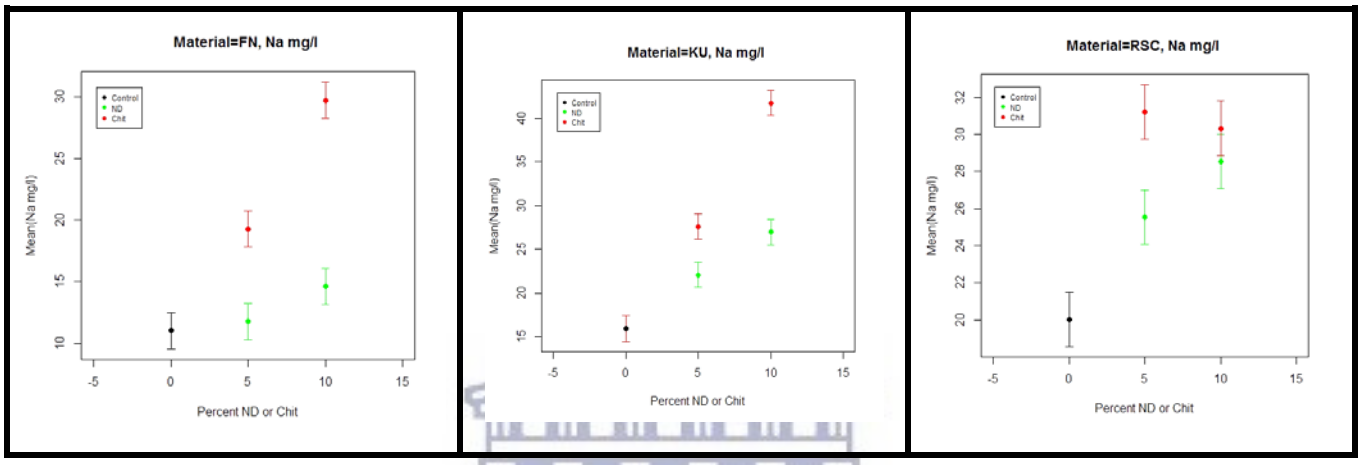

Comparing all fifteen materials to one another (Figure 7.5) provided insight as to how the sodium release from the three control materials and their chitosan or nanodiamond modifications influenced the sodium ion release. There was a significant difference ($p < 0.0001$) between the control materials with sodium release increasing from FN to KU to RSC.

Figure 7.4 illustrates that there was a general increasing trend for sodium ion release from the control materials (FN to KU to RSC) and their 5% to 10% modifications with chitosan and nanodiamonds, with the exception of RSC10%CH. KU10%CH was the chitosan-modified material which had a significantly ($p < 0.00021$) higher sodium ion release than any one of the remaining fourteen materials. For nanodiamonds, the materials KU5%ND, RSC5%ND and RSC10%ND released more sodium ($p < 0.00024$) than FN5%ND, FN5%ND and FN10%ND (Figure 7.5).

Figure 7.5: Comparison of sodium release from the control materials and their modifications

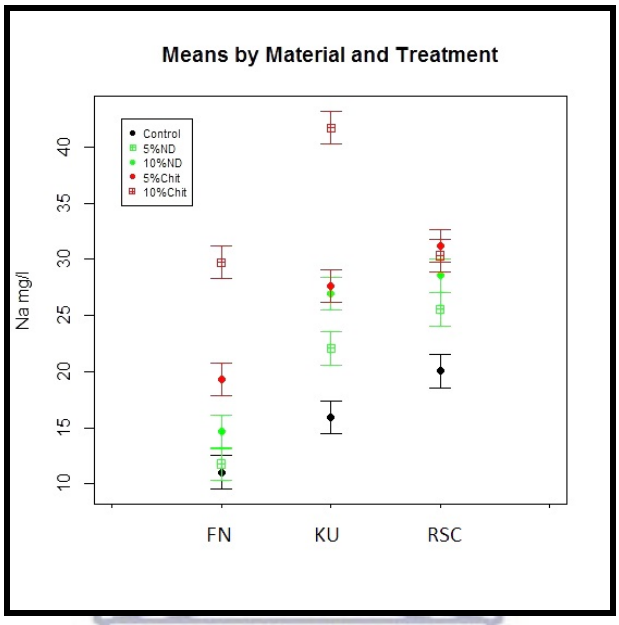

Silica release (Si^{4+})

The comparison of materials and their respective modifications within each group (Figure 7.6) made it possible to assess how the chitosan and nanodiamond modifications influenced the silicon ion release. The chitosan-modified FN material released significantly more silicon ($p < 0.0001$) when compared to the FN control material. FN10%CH released significantly more ($p = 0.003$) Si than FN5%CH. There was no significant silicon release difference between FN, FN5%ND and FN10%ND over the 24-hour period ($p = 0.867$) (Figure 7.6).

The nanodiamond modification of KU released significantly more silicon than the KU control ($p = 0.0002$) as well as KU5%CH and KU10%CH ($p = 0.012$ and $p = 0.0001$). KU5%ND did not release more silicon than KU10%ND ($p = 0.79$). KU10%CH however released significantly more silicon ($p = 0.012$) than KU5%ND, KU10%ND and KU5%CH.

The RSC10%ND and RSC10%CH modifications of RSC released significantly more silicon ($p < 0.0002$) than the RSC control. There was no significant silicon release difference between any of the chitosan and nanodiamond modifications ($p > 0.802$) of RSC (Figure 7.6).

Figure 7.6: Comparison of silicon release from the control materials and their modifications

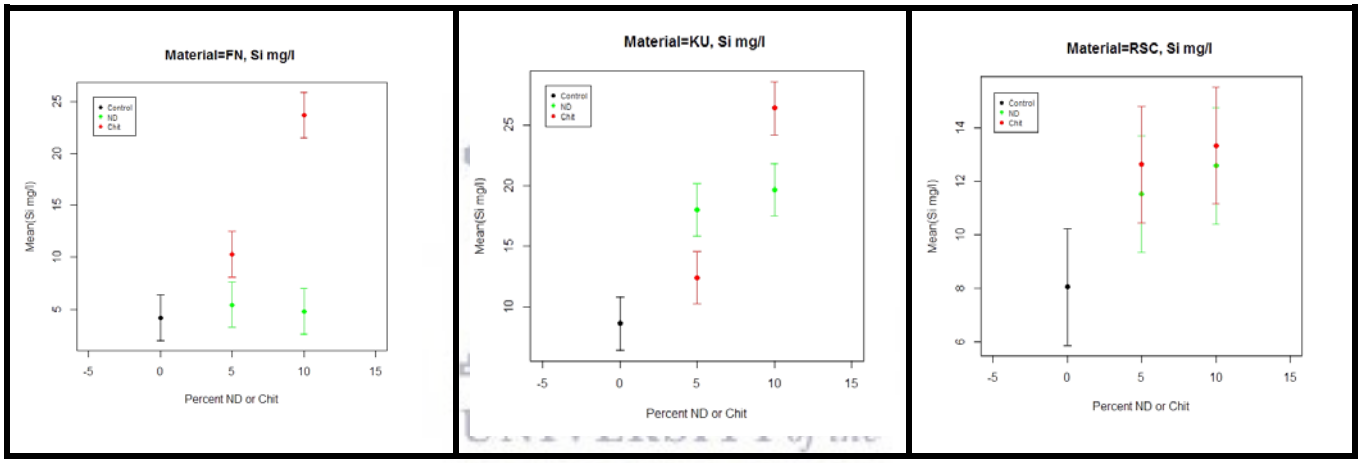

There was no difference ($p > 0.05$) between the silicon releases of the control materials. Figure 7.7 illustrates a general increasing trend of silicon ion release from the control materials (FN to RSC to KU) and their 5% to 10% modifications with chitosan and nanodiamonds. FN 10%CH and KU10%CH displayed a significantly greater silicon ion release ($p < 0.008$) than any one of the remaining thirteen materials. For nanodiamonds, the materials KU5%ND and KU10%ND released more silicon ($p < 0.008$) than the FN and RSC modifications with chitosan and nanodiamonds (Figure 7.7).

Figure 7.7: Comparison of silicon release from the control materials and their modifications

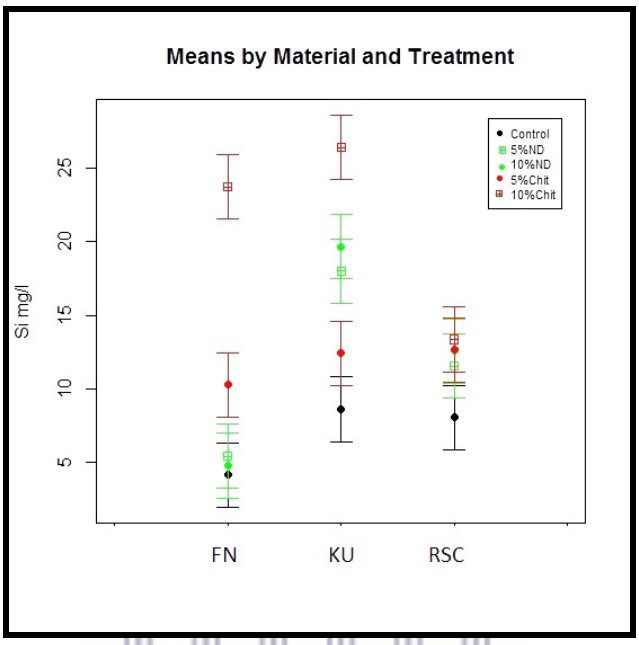

Strontium release (Sr^{+})

Figure 7.8 illustrates the chitosan modification of FN released significantly more strontium ($p < 0.0001$) than the FN control material, FN5%ND and FN10%ND ($p > 0.014$). FN, FN5%ND and FN10%ND showed no difference ($p = 0.788$) in strontium release over the 24-hour period. FN10%CH released significantly more strontium ($p = 0.003$) than the FN5%CH.

The KU5%CH and nanodiamond modifications of the KU control did not release significantly more strontium than the KU control ($p > 0.05$). The KU5%ND did not release significantly more strontium than KU10%ND ($p = 0.12$). KU10%CH however released significantly more strontium ($p < 0.0001$) than KU and KU10%ND ($p = 0.009$).

No difference in strontium release was noted for RSC5%ND and RSC10%ND ($p = 0.059$) when compared with the RSC control. RSC5%CH and RSC10%CH released significantly more strontium ($p < 0.0001$) than the RSC control group. There was a significant strontium release between the chitosan and nanodiamond modifications ($p < 0.008$) (Figure 7.8).

Figure 7.8: Comparison of strontium release from the control materials and their modifications

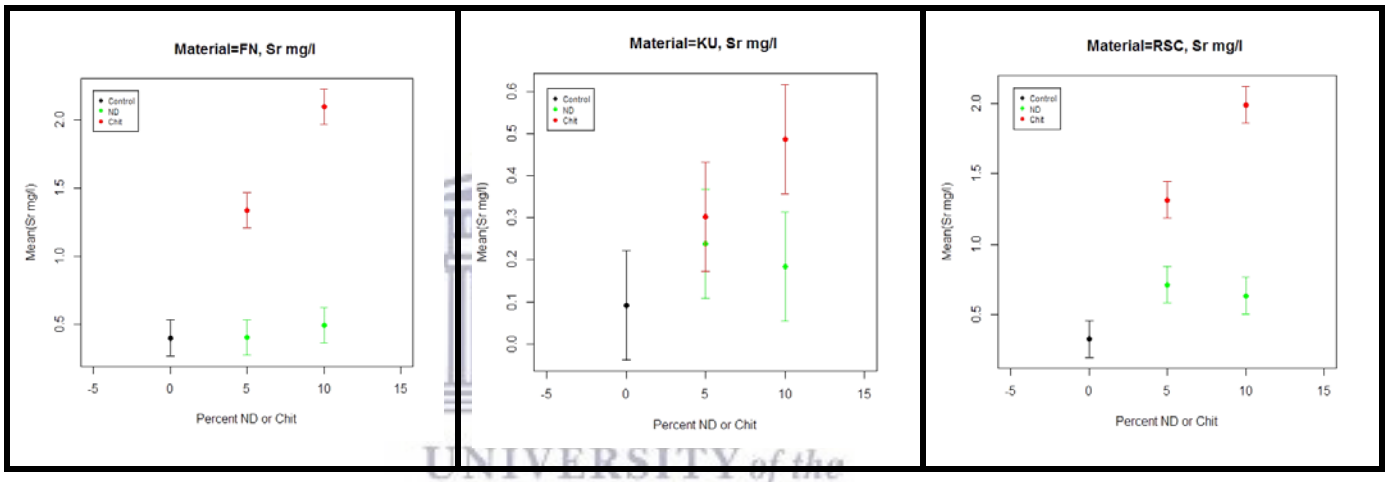

Figure 7.9: Comparison of strontium release from the control materials and their modifications

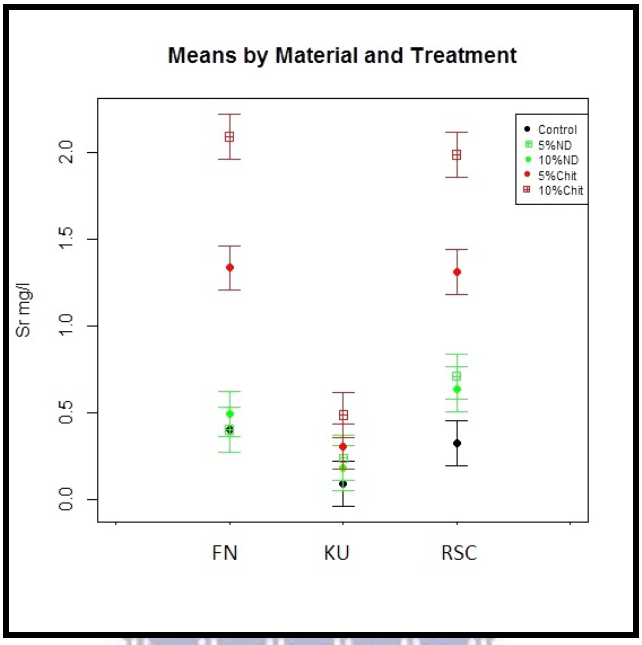

FN released significantly more strontium ($p < 0.0002$) than KU. There was no difference ($p > 0.05$) in strontium release between FN and RSC as well as between KU and RSC. There was however a general increasing trend of strontium ion releases from the control materials (KU to RSC to FN) and their 5% to 10% modifications with chitosan and nanodiamonds. FN10%ND was the only exception. The FN10%CH and KU10%CH modifications had greater strontium ion release ($p < 0.0059$) when compared to the remaining thirteen materials. For nanodiamonds, the materials RSC5%ND and RSC10%ND released more strontium ($p < 0.004$) than KU (Figure 7.9).

In order to evaluate the ICP-MS results, the ion potential of the commercial materials must be known. The elements present in FN, KU and RSC are presented in Table 7.2.

The results of the elemental analysis for the three commercial materials are presented in Table 7.2.

Table 7.2: SEM-EDS Elemental analysis of the commercial GICs expressed in percentages

	Aluminium (%)	Sodium (%)	Silica (%)	Strontium (%)
FN	11.181	0.906	10.183	3.854
KU	8.151	1.813	10.464	2.782
RSC	9.793	1.266	9.911	3.048

7.6. Discussion

The release of ions from GICs was assessed for chitosan and nanodiamond modifications of three commercially available GICs. The hypothesis was accepted as all the chitosan- and nanodiamond-modified GICs were shown to release more ions than their respective control materials.

Aluminium has been shown to be antibacterial (Oppermann and Rölla, 1980) so its release is important as it contributes to the antibacterial properties of GICs. Aluminium is also an essential contributor to GIC strength as the Al^{3+} ion changes to Al(IV) and Al(VI). After the powder and liquid components of a material have been mixed, the aluminium present in the GICs (without chitosan or nanodiamond particles), usually interacts with a variety of ion species and functional groups within the GICs matrix. The carboxylate groups of the GIC liquid are the primary functional groups that interact with the aluminium (Nicholson, 2018). Between the three commercially available materials (without any chitosan or nanodiamond modification), the release of aluminium and silicon was not significantly different, illustrating that the aluminium and silicon took part in the acid-base reaction and the subsequent integration with the carboxylic matrix. Silicon forms a layer around the glass filler particles during the setting process of the acid-base reaction and continues this formation at the initial stage of GIC maturation. This

silicon layer around the glass filler particles is composed of siloxane groups (-Si-O-Si-). Upon exposure to water and after the setting of the GICs is complete, the siloxane group dissociates into a silanol group (-Si-OH) (Czarnecka *et al*., 2015). The silanol group renders the GICs more hydrophilic and a subsequent increase in the percentage of water absorbed is noted. The water that is absorbed by the GIC results in the silicon developing the ability to be released from the GICs more readily, compared to when the silicon remains in the siloxane group. When the three GICs were modified with chitosan or nanodiamond particles, many more hydroxide (OH^-) functional groups were introduced to these modified GICs. For example, the hydroxide surface functional groups present on the nanodiamonds used in this study consist of 35% hydroxide functional groups (*PL-D-G01*). The result of so many hydroxide functional groups added to the GIC chemistry is an increased substitution of silicon with water, as many silanol groups were formed with the nanodiamond and even more with the chitosan particles once the material matured in a moist environment.

The addition of the nanodiamond particles to the GICs also allows the silicon from the GICs to bind to the carbon of the nanodiamond and form silicon carbide bonds (Si–C). These new bonds are located on the nanodiamond surface namely nanodiamond silicon carbide (ND–SiC) (Mochalin *et al*., 2011). Based on the SEM-EDS elemental analysis (Table 7.2), the three commercial GICs (FN, KU and RSC) assessed in this study are considered to be high in aluminium, silicon and strontium. Therefore, during mixing, the silicon dioxide (SiO_2) network forms readily within the three GICs. The aluminium released from the glass filler particles partly replaces the silicon (from the silicon dioxide) to form the Si-O-Al bonds upon the acid-base reaction. These silicon substitutions with aluminium lead to the GIC becoming more basic (closer to a pH of 7) and the development of negative sites. The results from the negative sites render the glass particles more susceptible to acid attack of the liquid during mixing. In the non-modified GICs, the network dweller ion namely sodium (Na) is also attracted to these negative

sites (Hill *et al*., 1992) that form when aluminium replaces the silicon. Sodium can also form Si-O-Na bonds, breaking down the silica network and rendering the glass more basic (De Maeyer *et al*., 1998). The sodium release increased significantly from FN to KU to RSC. With the sodium ionically bound to the chitosan and nanodiamond functional groups, it is readily released upon water sorption.

Chitosan is a weak base and it does not readily dissolve in water (De Stefano *et al*., 2010). Ibrahim *et al*. (2017) incorporated a small percentage of chitosan into the liquid of a GIC and found significant improvement of various GIC properties. Chitosan particles had a peculiar reaction when they were incorporated into the GIC powder, as in the present study. The commercial chitosan used in this study also required an acidic medium to "dissolve". The weight percentage of chitosan was taken at 10% of the manufacturer's powder weight and the 10%CH was mixed with the liquid of the respective GICs, as per the manufacturers' recommendations (Mulder, 2018). The result was that, during mixing, much of the GIC liquid became occupied for the purpose of dissolving the chitosan particles (as depicted in Figure 7.10).

Figure 7.10: Illustration of 10% chitosan particles mixed with the respective FN, KU and RSC liquids

FN	KU	RSC
		

In a low pH environment, the chitosan has a positive charge (Hamman, 2010). Initially during the mixing of the GIC liquid, this positive charge of the chitosan subsequently reacts by way of self-assembly with the negative carboxylic part of the GIC liquid during the acid-base reaction with the powder. The interactions between the polymeric chains of the chitosan with the GIC liquid (and freeze-dried polyacrylic acid in the powder) lead to the formation of a polyelectrolyte complex network. Hamman (2010) cited that polyelectrolyte complex networks were not permanent structures, since there were no covalent cross-linkers (Hamman, 2010). Therefore, aluminium, sodium and silicon which are responsible for the pH to stabilise are ionically bound to the chitosan. This results in a decreased interaction of the aluminium, silicon and sodium with the matrix of the GIC to form a viable restoration. Additional ion exchange with positive ions can occur after the pH has stabilised (Hamman, 2010). Besides the aluminium, sodium and silicon being bound to the chitosan, the increased activity of the GIC liquid with the chitosan functional groups during the mixing of the chitosan-modified GICs therefore sped up the setting process of the chitosan-modified GICs, leaving more aluminium, sodium, silicon and strontium loosely bound with ionic bonds that became vulnerable to being displaced upon water sorption. This results in a significant ion increase from the control materials (Table 7.1, Figure 7.1).

Nanodiamond particles contain impurities originating from the manufacture and purification processes. These impurities can be chemically bonded to the nanodiamond at any of the various functional groups such as carboxylate (COO^-), carboxylic acid (COOH), hydroxide (OH^-) and imidogen (NH) or the impurities could be absorbed into the graphite part of the nanodiamond. The nanodiamonds used for the GIC modification in this study had various impurities: 10500ppm for aluminium, 25ppm for sodium, 1260ppm for silicon and 3ppm for strontium (Volkov *et al*., 2014). Although the nanodiamond particles had these impurities bound to the nanodiamond, in general the ion release for chitosan modifications was greater than the

nanodiamond modifications and both the modifications had a greater release than the control materials.

For KU and RSC, the nanodiamond modifications increased the amount of aluminium and the sodium release when compared to the two commercial materials. The nanodiamond modification for FN released the same amount of aluminium as the commercial material. For FN, the aluminium and silicon release was similar to the FN-nanodiamond modifications, suggesting that aluminium and silicon are integrated into the matrix of the GIC without changing the material's response to the de-ionised water sorption and subsequent ion release from the material. The same could not be said for the FN modified with chitosan.

The aluminium and silicon continued to take part in the acid-base reaction for the GIC component. Some of the aluminium, sodium, silicon and strontium were bound ionically to the functional groups of the nanodiamond particle during mixing of the GIC due to their high activity and many binding sites. The additional carboxylate groups on the nanodiamond resulted in the nanodiamond-modified GICs having a greater capacity for water sorption, than the non-modified GIC materials. When the water entered the nanodiamond-modified GICs (after the GIC completed the acid-base reaction), the water interacted with the carboxylate (COO^-), carboxylic acid (COOH), hydroxide (OH^-) groups of the nanodiamond to release the aluminium, sodium and strontium from their binding sites on the nanodiamond particle.

Sodium is a relatively small and mobile ion that initially neutralises the carboxylic acid (COOH) groups of GICs as the gel phase completes, causing ionic cross-linking in the chitosan- and nanodiamond-modified GICs. Subsequent to the acid-base reaction being completed and exposure to the de-ionised water, the aluminium replaces the sodium, providing the subsequent cross-links (Billington *et al*., 2006).

Aluminium, silicon and strontium can be reduced as aging occurs and forms a thin layer around the nanodiamond particle (Mochalin *et al*., 2011). The carboxylic groups on the nanodiamond can also form salts (Panich *et al*., 2011) by way of ion exchange with the aluminium, calcium, silicon and strontium ions. This is therefore the reason why nanodiamond-modified GICs release a greater amount of ions than the control materials.

The nanodiamond modifications of FN and KU released the same strontium as their respective control materials. For RSC, both the chitosan and nanodiamond modifications resulted in significantly greater strontium release. Strontium can inhibit *Streptococcus Mutans* growth, but it is unlikely for the strontium released from the GICs to achieve this. This is because the strontium release was only 2.09mg/L (FN10%CH) and 10000mg/L would be required to move into the dental biofilm (Gallagher and Cutress, 1981).

7.7. Conclusion

For the chitosan- and nanodiamond-modified GICs, the aluminium can co-ordinate and interact with carboxylate groups of the polymer liquid, as well as with the functional groups of chitosan and nanodiamonds. The chitosan-modified GICs react with the liquid of the GICs to a much larger extent than the nanodiamond-modified GICs due to the polyelectrolyte complex network that forms. The ion release from chitosan- and most nanodiamond-modified GICs are therefore significantly increased compared to the control materials. Chitosan modifications significantly increase the ion release of aluminium, sodium, silicon and strontium (with the exception of KU5%CH for strontium) for all three control materials. The nanodiamond modifications increased ion release, although not significantly for some ions.

7.8. References

Billington, R., Williams, J. and Pearson, G. (2006). Ion processes in glass ionomer cements. *Journal of Dentistry*, 34(8), pp.544-555.

Czarnecka, B., Klos, J. and Nicholson, J. (2015). The effect of ionic solutions on the uptake and water-binding behaviour of glass-ionomer dental cements. *Ceramics - Silikaty*, 59, pp.102–108.

De Maeyer, E., Verbeeck, R. and Vercruysse, C. (1998). Reactivity of Fluoride-containing Calcium Aluminosilicate Glasses Used in Dental Glass-ionomer Cements. *Journal of Dental Research*, 77(12), pp.2005-2011.

De Stefano, C., Gianguzza, A., Piazzese, D. and Sammartano, S. (2010). Speciation of chitosan–phosphate and chitosan–nucleotide systems in NaCI aqueous solution. *Chemical Speciation & Bioavailability*, 22(2), pp.99-107.

Frencken, J., Leal, S. and Navarro, M. (2012). Twenty-five-year atraumatic restorative treatment (ART) approach: a comprehensive overview. *Clinical Oral Investigations*, 16(5), pp.1337-1346.

Fúcio, S., Carvalho, F., Sobrinho, L., Sinhoreti, M. and Puppin-Rontani, R. (2008). The influence of 30-day-old Streptococcus mutans biofilm on the surface of esthetic restorative materials—An *in vitro* study. *Journal of Dentistry*, 36(10), pp.833-839.

Gallagher, I. and Cutress, T. (1977). The effect of trace elements on the growth and fermentation by oral Streptococci and Actinomyces. *Archives of Oral Biology*, 22(10-11), pp.555-562.

Hamman, J. (2010). Chitosan Based Polyelectrolyte Complexes as Potential Carrier Materials in Drug Delivery Systems. *Marine Drugs*, 8(4), pp.1305-1322.

Hatton, P. and Brook, I. (1992). Characterisation of the ultrastructure of glass-ionomer (poly-alkenoate) cement. *British Dental Journal*, 173(8), pp.275-277.

Hill, R., Goat, C. and Wood, D. (1992). Thermal Analysis of a $SiO_2Al_2O_3CaOCaF_2$ Glass. *Journal of the American Ceramic Society*, 75(4), pp.778-785.

Ibrahim, M., Meera Priyadarshini, B., Neo, J. and Fawzy, A. (2017). Characterization of Chitosan/TiO2 Nano-Powder Modified Glass-Ionomer Cement for Restorative Dental Applications. *Journal of Esthetic and Restorative Dentistry*, 29(2), pp.146-156.

International Organization for Standardization (2007). *ISO 9917-1- Dentistry-Water based cements Part 1: Powder/liquid acid-base cements*, 1st ed.; (pages1–21).

Menne-Happ, U. and Ilie, N. (2013). Effect of heat application on the mechanical behaviour of glass ionomer cements. *Clinical Oral Investigations*, 18(2), pp.643-650.

Mochalin, V., Shenderova, O., Ho, D. and Gogotsi, Y. (2011). The properties and applications of nanodiamonds. *Nature Nanotechnology*, 7(1), pp.11-23.

Mulder, R. (2018). Variation in the Dispersions of Powder Liquid Ratios in Hand-Mix Glass Ionomers. *The Open Dentistry Journal*, 12(1), pp.647-654.

Muzzarelli, R. (1973). *Natural chelating polymers*. Oxford: Pergamon Press.

Ngo, H., Mount, G., Mc Intyre, J., Tuisuva, J. and Von Doussa, R. (2006). Chemical exchange between glass-ionomer restorations and residual carious dentine in permanent molars: An in vivo study. *Journal of Dentistry*, 34(8), pp.608-613.

Nicholson, J. (2018). Maturation processes in glass-ionomer dental cements. *Acta Biomaterialia Odontologica Scandinavica*, 4(1), pp.63-71.

Nicholson, J., Brookman, P., Lacy, O. and Wilson, A. (1988). Fourier Transform Infrared Spectroscopic Study of the Role of Tartaric Acid in Glass-ionomer Dental Cements. *Journal of Dental Research*, 67(12), pp.1451-1454.

Oppermann, R. and Rölla, G. (1980). Effect of Some Polyvalent Cations on the Acidogenicity of Dental Plaque in vivo. *Caries Research*, 14(6), pp.422-427.

Osswald, S., Yushin, G., Mochalin, V., Kucheyev, S. and Gogotsi, Y. (2006). Control of sp2/sp3Carbon Ratio and Surface Chemistry of Nanodiamond Powders by Selective Oxidation in Air. *Journal of the American Chemical Society*, 128(35), pp.11635-11642.

Panich, A., Altman, A., Shames, A., Osipov, V., Aleksenskiy, A. and Vul', A. (2011). Proton magnetic resonance study of diamond nanoparticles decorated by transition metal ions. *Journal of Physics D: Applied Physics*, 44(12), p.125303.

Plasmachem.com. (2019). *NanoDiamonds, purified, grade G01 - PlasmaChem GmbH*. [online] Available at: http://www.plasmachem.com/shop/en/nanodiamonds-purified-grade-g01/49-pl-d-g01-nanodiamonds-g01.html [Accessed 17 Feb. 2019].

Sidhu, S. and Nicholson, J. (2016). A Review of Glass-Ionomer Cements for Clinical Dentistry. *Journal of Functional Biomaterials*, 7(3), p.16.

Twomey, E., Towler, M., Crowley, C., Doyle, J. and Hampshire, S. (2004). Investigation into the ultrasonic setting of glass ionomer cements Part II Setting times and compressive strengths. *Journal of Materials Science*, 39(14), pp.4631-4632.

Volkov, D., Proskurnin, M. and Korobov, M. (2014). Elemental analysis of nanodiamonds by inductively-coupled plasma atomic emission spectroscopy. *Carbon*, 74, pp.1-13.

Wasson, E. and Nicholson, J. (1990). A study of the relationship between setting chemistry and properties of modified glass-poly(alkenoate) cements. *British Polymer Journal*, 23(1-2), pp.179-183.

Williams, J., Billington, R. and Pearson, G. (2002). The glass ionomer cement: the sources of soluble fluoride. *Biomaterials*, 23(10), pp.2191-2200.

CHAPTER 8

DETERMINATION OF FLUORIDE RELEASE FROM CHITOSAN- AND NANODIAMOND-MODIFIED GLASS IONOMER RESTORATIVE CEMENTS

8.1. Abstract

Background: Total Ionic Solubility Acid Buffer in the forms of TISAB III and IV are the most widely used buffer mediums for fluoride determination. The accurate investigation of fluoride released from chitosan (CH) and nanodiamond (ND)-modified GICs provide insight regarding the diluents released into the cellular growth medium for interaction with the materials and the buffer mediums.

Materials and methods: Three different glass ionomer restorative cements Fuji IX GP (FN: *GC Corp, Tokyo, Japan, Batch: 1503231*), Ketac Universal (KU: *3M ESPE, Seefeld, Germany, Batch: 583514*) and Riva Self Cure (*RSC: SDI Limited, Australia, Batch: 62657V*) served as the control materials. These three GICs were modified in the powder phase per weight by adding 5% or 10% of a commercially available chitosan powder (CH) or nanodiamond (ND) powder to the GICs. The specimens with dimensions 6±0.1mm height and 4±0.1mm diameter were manufactured from the 15 GIC formulations, sterilised and placed in 15ml of DMEM growth medium. The specimens were subsequently stored at 4ºC for 0-1 days, 1-7 days and 7-21 days. These specimens were then removed with a sterile tweezer and placed in another 15ml of DMEM for the subsequent time periods to allow elution of the ions to form the final diluent that would be assessed for fluoride release. A fluoride ion selective electrode with a calibration curve was used to determine the free- and total fluoride. TISAB III or TISAB IV was used for this after the volume of GIC DMEM diluent was equally divided between the two buffer mediums.

Results: The one-way ANOVA with post-hoc Tukey HSD was used for the three control materials and indicated significantly more fluoride release for FN>RSC>KU. KU had significantly lower fluoride release than the other control materials for all three time periods. The one-way ANOVA with post-hoc and Holm interference were used to assess the statistical significance between the chitosan- and nanodiamond-modified materials with their respective control material. The chitosan modifications released significantly more fluoride than their control materials.

Conclusion: The high pH of the GIC-diluents did not provide accurate free fluoride results due to hydroxide interferences. Therefore, only the total fluoride could be determined as the de-complexed fluoride can only be calculated if the free fluoride and total fluoride values are accurate. TISAB III provided the most accurate total fluoride results, although aluminium, strontium and sodium interfered with the ionic strength (Frenzel and Bratter, 1986). TISAB IV was not an ideal buffer medium for the nanodiamond- and chitosan-modified GICs due to the final pH of 9-9.1 and hydroxide ion interference when the pH is above 8.1.

Keywords: Glass ionomer, chitosan, nanodiamonds, TISAB III, TISAB IV, free fluoride, de-complexed fluoride, lanthanum, aluminium, strontium, silicon, sodium.

8.2. Introduction

Glass ionomers have been well documented to have an initial rapid fluoride release phase, followed by a second, more prolonged phase (Castioni *et al*., 1998). The resistance to secondary caries around the GIC/tooth interface could be reduced as time passes (Itota *et al*., 2005). Additionally, the release of fluoride from GICs influences the extra-cellular polysaccharide structure of cariogenic biofilm (Koo *et al*., 2010). The extra-cellular polysaccharide structure is important, since it contributes to the bulk, physical integrity and stability of the bacterial biofilm (Koo *et al*., 2010). This was confirmed based on the fact that GIC biofilms had a lower weight

due to the release of higher amounts of fluoride from the GICs (Chau *et al*., 2015). Fluoride cannot function alone and is dependent upon other ions, many of which have not always been assessed in the majority of the fluoride studies conducted to date. Smith (1982) identified that the fluoride release from GICs results in the absorption of calcium and phosphate ions to maintain electrolytic balance. Due to the retention of electrolytic balance, it was additionally established that as the sodium release increases, the fluoride release also increases (Wilson *et al*., 1985). Fluoride released from GICs can be present in ionic form (F^-) i.e. free fluoride and in complexed forms with aluminium, iron, silicon and any other polyvalent electron (Orion Research Incorporated, 2001; Okte *et al*., 2012). The complexed fluoride is calculated by subtracting the total fluoride from the free fluoride. The free fluoride is assessed without adding any chelating agents like TISAB (Total Ionic Solubility Acid Buffer). The determination of the total fluoride requires the use of TISAB. The total fluoride is measured with the fluoride ion selective electrode after the TISAB medium has de-complexed the fluoride and stabilised the pH and ionic strength. This de-complexing of the fluoride is an essential step to ensure that all the complexed fluoride is released into the measured diluent. In order to establish the presence of fluoride in the diluents, GICs were exposed to a selective ion fluoride electrode (Torabzadeh *et al*., 2015). The selective ion fluoride electrode determines the mV potential of the medium and this mV value is related to the mV readings obtained with the calibration of the electrode with known fluoride standards in the calibration curve (Section 8.3.8).

There are essentially four main TISAB versions recommended by Orion Research Incorporated (2001) for use with their selective fluoride ion electrode. The first is “low level TISAB” where no aluminium or iron is present with fluoride concentrations <0.4ppm, TISAB II, III have the same function and can de-complex 5ppm of aluminium for every 1ppm of fluoride. TISAB IV has the ability to de-complex more than 100ppm of aluminium for every 1ppm of fluoride (Orion research Incorporated, 2001).

The biggest confounding factor in the detection of fluoride is the pH and its direct influence on the development of interfering species like hydrogen and hydroxides. Hydrogen interferes with the detection of fluoride at a pH<5 (Orion Research Incorporated, 2001), as the electrode detects hydrogen ions and measures it as fluoride. The hydroxide ions can increase or decrease the perceived fluoride. The pH must therefore be buffered between 5 and 5.5. This can be achieved with TISAB II and III. The use of TISAB II or III will prevent the hydroxide complexes of fluoride from forming provided that the temperature of the measurements does not differ more than ±1ºC, as this prevents millivolt (mV) differences from influencing the readings. At the pH between 5 and 5.5, there are no hydroxide ions present. TISAB III can de-complex 5ppm of aluminium for every 1ppm fluoride and TISAB IV de-complexes more than 100ppm of aluminium for every 1ppm fluoride (Orion research Incorporated, 2001).

The hypothesis of the study was that, due to its high aluminium de-complexing ability, TISAB IV would be a more appropriate buffer than TISAB III for use with chitosan- and nanodiamond-modified GICs.

8.3. Materials and Methods

8.3.1. Sample preparation

Three different glass ionomer restorative cements Fuji IX GP (FN: *GC Corp, Tokyo, Japan, Batch: 1503231*), Ketac Universal (KU: *3M ESPE, Seefeld, Germany, Batch: 583514*) and Riva Self Cure (RSC: *SDI Limited, Australia, Batch: 62657V*) served as the control materials. These three GICs were modified in the powder phase per weight by adding 5% or 10% of a commercially available chitosan powder (CH) (*Merck, item 448877*) or nanodiamond (ND) powder (*PlasmaChem, item: PL-D-G01*) to the GICs. Cylindrical specimens with the same dimensions (6±0.1mm height and 4±0.1mm) were manufactured from the 15 GIC formulations

(Ariffin *et al*., 2006). Surface preparation was carried out as for the compressive strength in Chapter 6.

8.3.2. Sterilization

Sterilization with ethylene oxide gas (*Steri-Vac 4XL gas sterilizer, Model 400DGP, 3M centre, St Paul, MN, USA*) was completed for all the samples before they were placed in the DMEM growth medium. The sterilization was essential, since the same DMEM were to be used for the cell viability study in Chapter 9.

8.3.3. GIC-diluent preparation from sterile DMEM liquid

Diluent preparation for fluoride assessment

Five ethylene oxide gas sterilized GIC specimens (per material) were placed in sterile centrifuge tubes with 5mL of sterile DMEM growth medium liquid (*Hyclone, GE Healthcare Sciences, Utah, USA, Lot AD16496263*) at specified intervals i.e. 0-1 days, 1-7 days and 7-21 days. The DMEM growth medium liquid with the material inside it was kept at 4^0C in a temperature-controlled fridge throughout the duration of the experiment.

At the end of day 1, the centrifuge tube containing the DMEM and the material samples were vortexed for 3 seconds, the material sample removed with sterile tweezers and placed into another sterile centrifuge tube with 5ml of DMEM growth medium liquid for the next time period of 1 to 7 days. This process was repeated for the 7 to 21 day time period. The DMEM medium of day 1, 7 and 21 where the materials were stored and subsequently removed would be known as the GIC-diluent. The 3 second vortex prior to every step is to ensure that no ions have settled in the medium, resulting in a non-representative diluent being used for cell viability or fluoride determination.

8.4.4. GIC-diluent use for fluoride determination

The fluoride release study of this dissertation was completed after the cell viability (Chapter 9), in order to prevent contaminated DMEM diluents being used during cell viability testing.

For the cell viability in Chapter 9, 1mL of the GIC-diluent was removed after a 3 second vortex for assessment of the 3T3 cells.

The remaining 4mL (free of TISAB agents) was used in three steps: 1) the 4mL was vortexed for 3 seconds and the pH determined. A calibrated fluoride selective electrode was used to measure the electrode potential (mV) of every GIC-diluent. 2) Thereafter, the 4mL was split into two equal amounts. 2mL was mixed with 0.2mL of TISAB III chelating/buffer agent for total fluoride determination. 3) The last 2mL was mixed with TISAB IV chelating/buffer agent for total fluoride determination. The "complexed fluoride" can be calculated by "total fluoride" - "free fluoride".

The TISAB IV was made in accordance with the recommendation by Orion research (Orion Research Incorporated, 2001):

- 500mL of distilled water was placed in a 1-litre volumetric flask. In a fume cupboard, 84mL of concentrated HCL (36-38%) was added to the distilled water.
- The volumetric flask was placed on a magnetic stirrer on the maximum speed. Added to this was 242g of TRIS (hydroxymethyl) aminomethane.
- The last powder added was 230g of Sodium Tartrate ($Na_2C_4H_4O_6 - 2H_2O$). Once the medium reached room temperature, additional distilled water was added to the 1-litre volumetric mark.
- The TISAB IV medium was left on the magnetic stirrer until all the powder was dissolved.

8.3.5. pH determination

The pH of the DMEM medium from the manufacturer, all the GIC-diluents made from ion elution of the GIC sample into the DMEM as well as the GIC-diluents combined with either TISAB III or IV were determined. An Ohaus pH meter (*Ohaus Corporation, model Starter 3100, USA*) was used after calibration with pH 4 and pH 7 standards.

8.3.6. Fluoride ion selective electrode operation

The use of the fluoride selective electrode and the calibration was completed in accordance with the manufacturer's instructions (Orion Research Incorporated, 2001). Prior to use, the protective cap was removed from the fluoride ion selective electrode and assembly completed by adding electrode filling solution (*Model 94-09, item 900-001, Orion*) to minimise the junction potentials and fluoride ion contamination of the sample. The electrode was pre-soaked by immersion in a 10ppm fluoride solution for 10 minutes (Orion Research Incorporated, 2001). Following immersion, the electrode was rinsed with distilled water and the samples blot dried with a soft paper towel that did not disintegrate upon becoming moist. Electrode memory (hysteresis) of the fluoride ion selective electrode can occur when individual samples are assessed and rinsed with de-ionised water. In order to prevent the electrode memory from developing, rinsing of the electrode was done between different sample groups (e.g. between KU and KU5%ND). In order to prevent transfer and contamination between samples within the same group, the electrode was blot dried with a soft paper towel.

The operation of the electrode was assessed with the development of a slope difference of 54-60 mV/decade indicating that the electrode is functioning correctly at 25ºC.

The aforementioned procedure was completed by mixing 90mL of distilled water with 10ml of TISAB III in a 150mL polycarboxylate beaker. A magnetic stirrer was used on the slowest

rotation of the 10mm magnet and the electrode placed in the liquid. 1mL of a 100ppm fluoride solution (*Orion research, item 940-907*) was pipetted into the beaker and once the reading in mV stabilised, it was recorded (within 2 minutes). Then, 10mL of the fluoride standard was pipetted into the beaker and the stabilised mV reading was recorded. The difference in mV was within the prescribed 54-60 mV/decade. The same procedure was completed with the DMEM growth medium liquid to assess if the functioning of the fluoride selective electrode was within the prescribed mV/decade (Orion Research Incorporated, 2001).

8.3.7. Rationale for comparing TISAB III to TISAB IV

The results from Chapter 7 determined that Low Level TISAB would not be suitable for this particular GIC study as the fluoride is complexed with aluminium (Orion Research Incorporated, 2001). TISAB II, III and IV would therefore be more appropriate choices (Orion Research Incorporated, 2001). This is because TISAB III de-complexes 5ppm of aluminium for every 1ppm of fluoride present in the GIC-diluent being assessed. Aluminium levels above this 5ppm would require TISAB IV to de-complex all the fluoride from the aluminium if the fluoride is increased above the aluminium5ppm:fluoride1ppm ratio. Chapter 7 revealed that for the 1-day result, the aluminium release from the GIC specimens (of the same dimensions) ranged from 2.22ppm (FN) to 14.04ppm (mg/L) (KU10%CH). The fluoride could however not be assessed in Chapter 7, since the equipment used for the ion detection cannot measure fluoride. There was no de-ionised diluent available for fluoride determination, since the methods used with the ICP-MS unit in Chapter 7 required the full 5mL of diluent for ion assessment. Therefore, it is very likely that the chitosan-modified GICs especially, could have aluminium concentrations at or above the 14.04ppm as determined after 24 hours for KU10%CH in Chapter 7.

Further to the use of TISAB IV, hydrogen and/or hydroxide ions, are interfering ions and could cause errors with the fluoride ion selective electrode. Hydrogen ions present in the diluent will complex with fluoride and form HF or HF_2^- when the pH is less than 5. When there is a low level of fluoride (< 1.9ppm (10^{-4}M)) present in the diluent and a pH > 9.5 the combination of the hydrogen and the fluoride ions will cause the electrode to react with both the hydroxide and fluoride ions (Orion Research Incorporated, 2001), providing an inaccurate representation of the fluoride concentration.

8.3.8. Calibration curve

Once the fluoride selective electrode has been established to function correctly (with a slope difference of 54-60 mV/decade), the calibration curve must be determined before the fluoride of the unknown diluents are assessed. The calibration curve must be established with the same DMEM growth medium liquid that had no exposure to the GICs. The TISAB chelating/buffer agent that will be used to de-complex the DMEM growth medium liquid diluent with an unknown fluoride concentration can be assessed in relation to the calibration curve. Additionally, the DMEM growth medium liquid diluents for fluoride determination as well as the fluoride standards would all have had a 24-hour exposure to the TISAB III or IV. This would allow the TISAB medium to de-complex the maximum fluoride that the TISAB is able to de-complex. If the ionic strength is buffered and the fluoride de-complexed, then the results would be transferrable between the known fluoride standards used to set-up the calibration curve and the fluoride concentrations in the GIC-diluents, which had to be assessed. From the recorded electrode potential readings in mV, the fluoride concentration is determined based on the logarithmic calibration curve in Microsoft Excel. Tables 8.1 and 8.2 indicate the fluoride standard formulas and the combination of GIC-diluent and TISAB used to set-up the calibration curve for the 2mL volume of GIC-diluent assessed in this study.

Table 8.1: Fluoride standard preparatory table for calibration curve

	Measurement to be done		
	A	**B**	**C**
	Calibration curve standards	**Total fluoride with TISAB III**	**Total fluoride with TISAB IV**
Desired ppm for calibration curve	**Ratio required**	**TISAB III**	**TISAB IV**
100ppm	5mL 100ppm standard + 0mL DMEM.	TISAB III 1:10 Fluoride standard/DMEM.	TISAB IV 1:1 Fluoride standard/DMEM.
50ppm	2.5mL 100ppm standard + 2.5mL DMEM.		
30ppm	1.5mL of 100ppm standard + 3.5mL DMEM.		
20ppm	1mL of 100ppm standard + 4mL DMEM.		
10ppm	0.5mL of 100ppm standard + 4.5mL DMEM.		
5ppm	0.25mL 100ppm standard + 4.75mL DMEM.		
4ppm	0.2mL 100ppm standard + 4.8mL DMEM.		
3ppm	0.15mL 100ppm standard + 4.85mL DMEM.		
2ppm	0.1mL 100ppm standard + 4.9mL DMEM.		
1ppm	0.05mL 100ppm standard + 4.95mL DMEM.		
0.5ppm	0.025mL 100ppm standard + 4.975mL DMEM.		
0.2ppm	0.01mL 100ppm standard + 4.99mL DMEM.		

For calibration curve determination with the use of TISAB III, the combination was Column A plus Column B: 10 parts DMEM/fluoride standard (A) and 1 part TISAB III (B).

For calibration curve determination with the use of TISAB IV, the combination was Column A plus Column B: 1 part DMEM/fluoride standard (A) and 1 part TISAB IV (C).

8.3.9. Determination of fluoride ion in the GIC-diluent

The GIC-diluent with unknown fluoride content was allowed to reach room temperature before the pH and the various fluoride measurements were recorded. The room temperature was (25±1ºC) and the pH was determined as previously described. The fluoride assessment was completed with a fluoride ion selective electrode (*Orion research electrode, Orion Research Inc, Boston, USA*) with a minimum detection limit of 0.02ppm. The electrode was connected to an ion analyzer (*Ion 85 Radiometer, Copenhagen, Denmark*). The 2mL of GIC-diluent with the unknown fluoride content was mixed with one of the two TISABs. The electrode potential readings (mV) were completed 24 hours after the TISABs were added to the GIC-diluents to allow the maximum de-complexing of the fluoride values (Nicholson & Duff, 1981). The GIC-diluent and TISAB was vortexed for 3 seconds after 24 hours and the fluoride ion selective electrode inserted into the GIC-diluent/TISAB. The mV reading was recorded upon stabilisation of the mV reading or after 2 minutes. The mV value was placed in the logarithmic calibration curve and the mV converted to ppm.

8.3.10. Free fluoride

For the determination of the free fluoride, the GIC-diluents were vortexed for 3 seconds to allow any ions that might have settled to be dispersed in the diluent. The fluoride ion selective electrode was placed in the 4mL of GIC-diluent to determine the free fluoride reading.

8.3.11. Total fluoride determination with TISAB III and IV

4mL of DMEM growth medium diluent was divided equally after it was vortexed for 3 seconds. TISAB III (*Orion research, item 940-911*) was used in a 10:1 TISABIII/ 2mL GIC-diluent. TISAB IV was used in a 1:1 ratio with 2mL GIC-diluent.

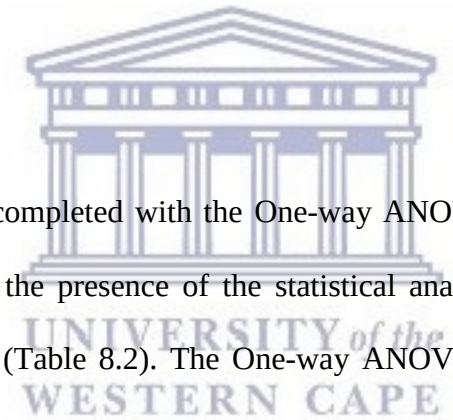

8.4. Statistical analysis

The statistical analysis was completed with the One-way ANOVA with post-hoc Tukey HSD. Results were used to assess the presence of the statistical analysis between the three control materials FN, KU and RSC (Table 8.2). The One-way ANOVA with post-hoc and the Holm interference were used to assess the statistical significance at $p < 0.05$ between the chitosan- and nanodiamond-modified materials and their respective control materials (Table 8.3).

8.5. Results

Figures 8.1, 8.2 and 8.3 illustrate the pH ranges for the GIC-diluent. The pH of DMEM growth medium from the manufacturer was 7. The GIC-diluent had a pH range from 7.77 for KU5%CH at 21days to 9.10 for RSC5%ND at 21days. After TISAB III was added to the GIC-diluent, the pH varied between 5 and 5.5. With regard to TISAB IV, the pH ranged between 9 and 9.10, irrespective of the time period i.e. 1, 7 or 21 days.

Figure 8.1: Average pH measurements of the FN diluents for days 1, 7 and 21

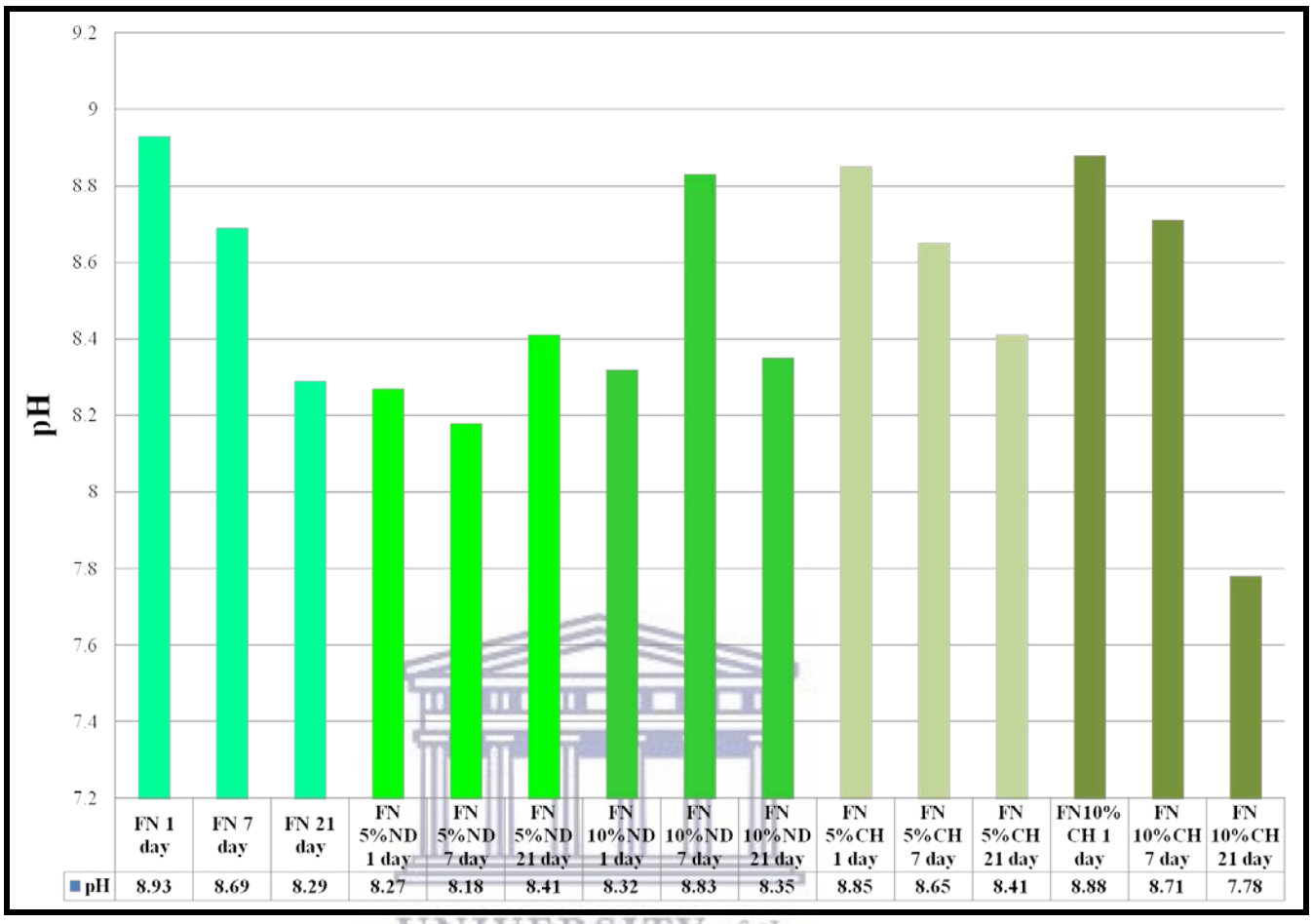

Figure 8.2: Average pH measurements of the KU diluents for days 1, 7 and 21

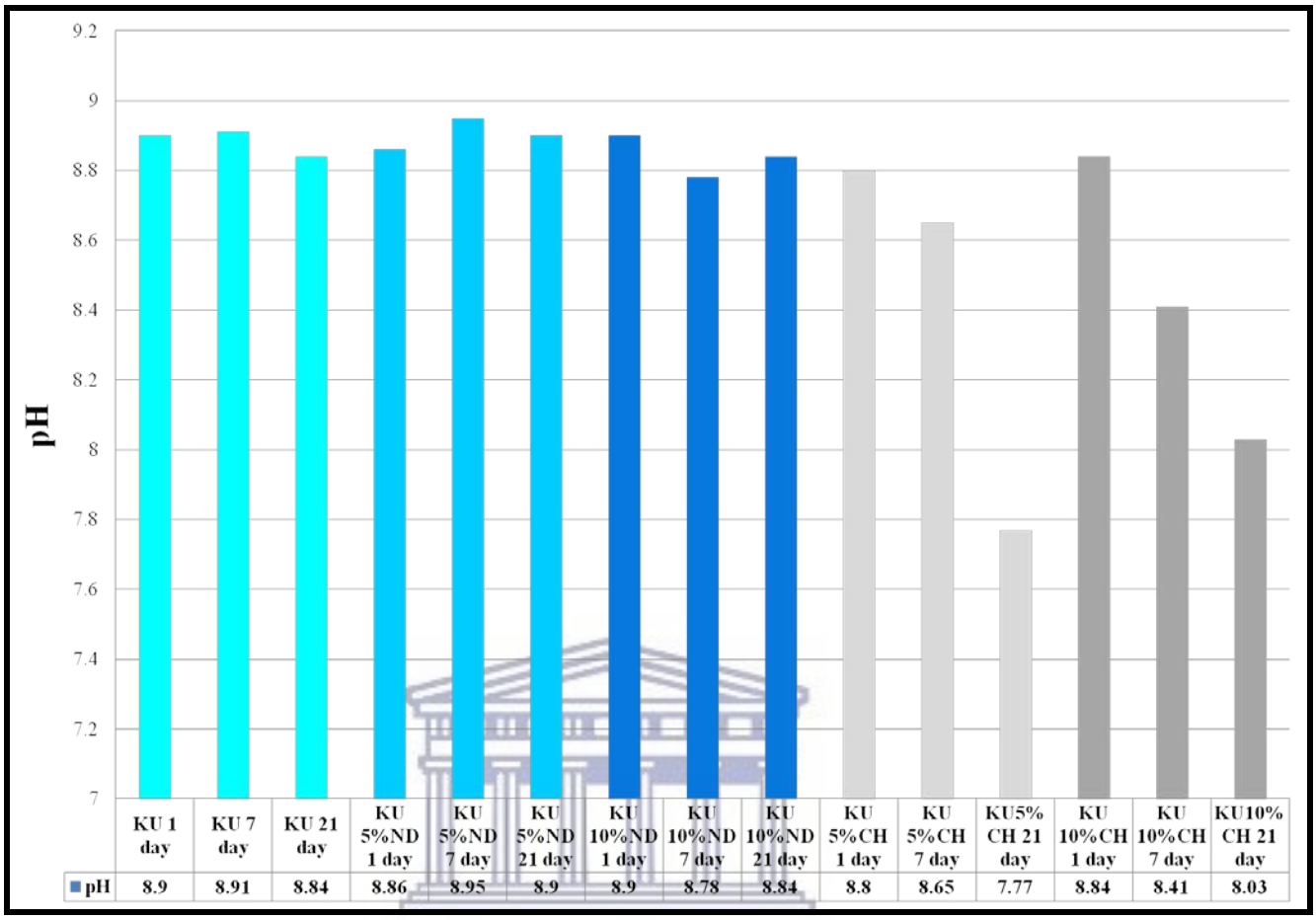

Figure 8.3: Average pH measurements of the RSC diluents for days 1, 7 and 21

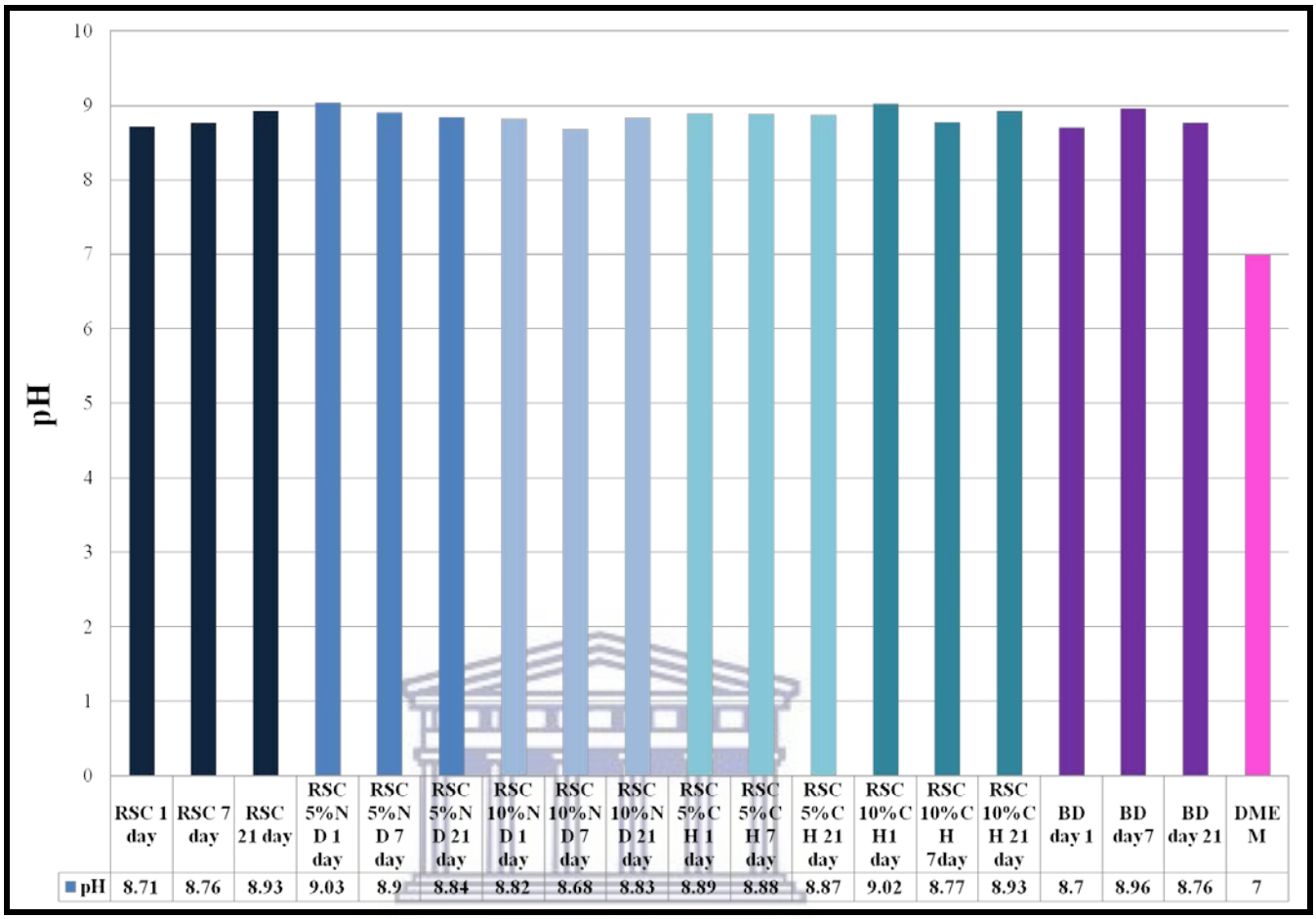

	RSC 1 day	RSC 7 day	RSC 21 day	RSC 5%ND 1 day	RSC 5%ND 7 day	RSC 5%ND 21 day	RSC 10%ND 1 day	RSC 10%ND 7 day	RSC 10%ND 21 day	RSC 5%CH 1 day	RSC 5%CH 7 day	RSC 5%CH 21 day	RSC 10%CH1 day	RSC 10%CH 7day	RSC 10%CH 21 day	BD day 1	BD day7	BD day 21	DMEM
pH	8.71	8.76	8.93	9.03	8.9	8.84	8.82	8.68	8.83	8.89	8.88	8.87	9.02	8.77	8.93	8.7	8.96	8.76	7

The one-way ANOVA illustrated the presence of a significant difference ($p < 0.01$) for the fluoride release assessment. The Tukey HSD indicated where the significant differences were between the three controls materials (Table 8.2). The Holm interference was used as the post hoc test for the difference in fluoride concentration between the chitosan or nanodiamond modifications and their respective control materials (Table 8.3).

Table 8.2: Significance of mean free fluoride release (ppm) of the commercial materials

Material	Day 1			Day 7			Day 21		
	Free F	TISAB III	TISAB IV	Free F	TISAB III	TISAB IV	Free F	TISAB III	TISAB IV
FN vs KU	*	*	^	*	*	*	^	*	^
FN vs RSC	p = 0.274	^	*	^	*	*	*	*	*
KU vs RSC	*	*	*	*	*	*	*	*	*

(*): Indicates a significant difference ($p < 0.01$) between free fluoride ion release of the control materials.

(^): Indicates a significant difference ($p < 0.05$) between free fluoride ion release of the control materials.

Free fluoride release

The free fluoride (Table 8.3) present in the samples for FN10%CH, released significantly more free fluoride than FN ($p < 0.01$) for the analysis on days 1, 7 and 21. FN5%CH only released significantly more free fluoride than FN ($p < 0.01$) for the analysis on day 21.

Neither the chitosan nor nanodiamond-modifications of KU presented with significantly more free fluoride for the analysis on day 1. KU5%CH and KU10%CH however released significantly more free fluoride than FN ($p < 0.01$) for the analysis on days 7 and 21.

RSC5%ND released significantly less free fluoride than RSC ($p < 0.05$) for the analysis on day 1. RSC10%CH released significantly more free fluoride than RSC ($p < 0.01$) for the analysis on days 1, 7, 21. RSC5%CH only released significantly more free fluoride than RSC ($p < 0.01$) for days 7 and 21.

TISAB III fluoride release

The fluoride release assessed from the TISAB III de-complexing agent indicated significantly more fluoride release than the respective control materials for:

- FN5%CH at days 1 and 21;
- FN10%CH, KU5%CH, KU10%CH, RSC5%CH at days 1, 7 and 21;
- KU5%ND, KU10%ND at days 1 and 7;
- RSC5%ND at day 21 and
- RSC10%CH at days 7 and 21 (Figures 8.4, 8.5 and 8.6; Table 8.3).

TISAB IV fluoride release

For TISAB IV on days 1 and 21, there was a significantly increased fluoride reading ($p < 0.01$) between FN5%CH, FN10%CH and FN. At day 7, only FN10%CH had a significantly increased fluoride reading ($p < 0.01$) compared to FN.

On day 1, KU10%ND, KU5%CH and KU10%CH had a significantly increased fluoride reading ($p < 0.01$) compared to KU. At day 7, the same trend was observed for KU5%CH and KU10%CH with only a difference in p-value for KU10%ND ($p < 0.05$). At day 21, only the chitosan modifications of KU had a significantly increased fluoride reading ($p < 0.01$) in relation to KU.

On day 1, RSC5%ND had a significantly lower fluoride reading than RSC ($p < 0.01$), with RSC10%CH having a larger fluoride reading ($p < 0.01$). At day 7, RSC10%CH had a significantly larger fluoride ($p < 0.01$) reading than RSC. On day 21, RSC5%CH ($p < 0.05$) and

RSC10%CH ($p < 0.01$) displayed a significant difference in fluoride release when compared with RSC.

Table 8.3: Mean fluoride release (ppm) of the commercial materials and their respective modifications

Fluoride ion	Commercial material	Modification			
		5%ND	10%ND	5%CH	10%CH
FN					
Free fluoride day 1	0.766	0.882	0.864	1	1.548*
Free fluoride day 7	1.182	1.198	1.066	2.048	8.632*
Free fluoride day 21	1.182	1.098	1.148	3.082*	9.164*
TISAB III fluoride day 1	1.232	1.282	1.33	1.546*	1.964*
TISAB III fluoride day 7	1.532	1.548	1.514	2.55	9.032*
TISAB III fluoride day 21	1.048	1.096	1.164	3.416*	10.45*
TISAB IV fluoride day 1	0.45	0.51	0.654	1.626*	2.82*
TISAB IV fluoride day 7	1.148	1.548	1.166	3.098	10.214*
TISAB IV fluoride day 21	0.764	0.778	0.764	2.548*	11.096*
(*): Indicates a significant difference between free F ion release compared to FN.					

Fluoride ion	Commercial material	Modification			
		5%ND	10%ND	5%CH	10%CH
KU					
Free fluoride day 1	0.2	0.21	0.564	2.916	3.35
Free fluoride day 7	0.412	0.632	0.714	6.364^	11.882^
Free fluoride day 21	0.648	0.582	0.716	8.414^	13.864^
TISAB III fluoride day 1	<0.2	0.748^	1.348^	1.566^	3.564^
TISAB III fluoride day 7	0.26	0.812^	1.364^	5.982^	12.896^
TISAB III fluoride day 21	0.262	0.482	0.782	9.496^	13.916^
TISAB IV fluoride day 1	<0.2	<0.2	1.314^	1.516^	3.65^
TISAB IV fluoride day 7	<0.2	0.21	1.332^	7.446^	13.896^
TISAB IV fluoride day 21	<0.2	<0.2	0.554	9.148^	15.932^
(^): Indicates a significant difference between free F ion release compared to KU.					

Fluoride ion	Commercial material	Modification			
		5%ND	10%ND	5%CH	10%CH
RSC					
Free fluoride day 1	0.9	0.598^{+}	0.714	1.248^{+}	1.73^{+}
Free fluoride day 7	1.582	1.116	1.598	2.4^{+}	4^{+}
Free fluoride day 21	2.164	1.58	1.948	3.082^{+}	5.346^{+}
TISAB III fluoride day 1	1.43	1.264	1.398	1.832^{+}	1.902^{+}
TISAB III fluoride day 7	2.012	1.446^{+}	1.72	2.414	4^{+}
TISAB III fluoride day 21	2.316	1.6^{+}	1.932	3.514^{+}	6.232^{+}
TISAB IV fluoride day 1	1.614	1.166^{+}	1.466	1.866	2.232^{+}
TISAB IV fluoride day 7	1.964	1.498	1.664	2.632	4.298^{+}
TISAB IV fluoride day 21	2.446	1.798	1.98	3.296^{+}	5.85^{+}
($^{+}$): Indicates a significant difference between free F ion releases compared to RSC.					

Figure 8.4: Fluoride measurements in ppm for Day 1

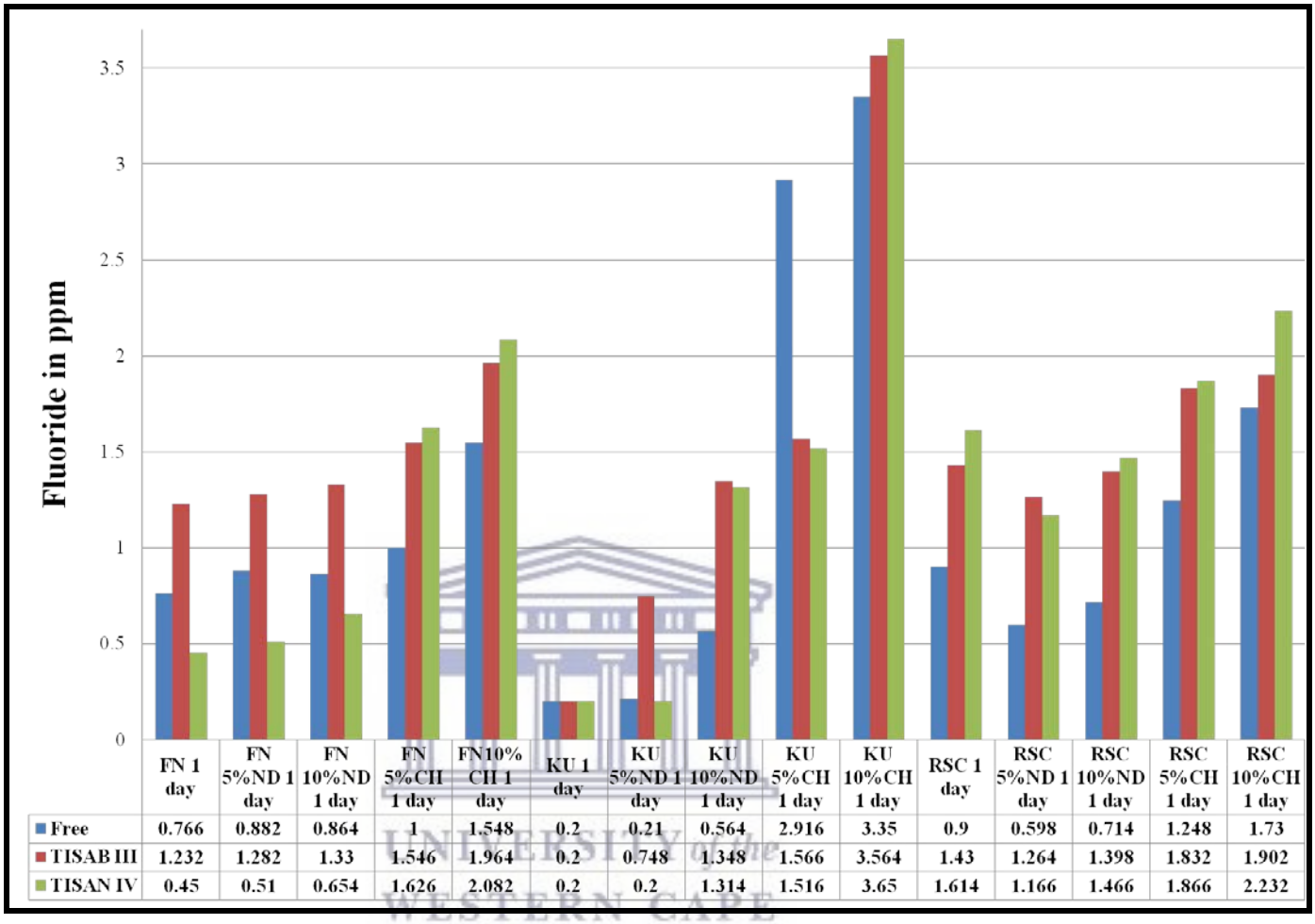

	FN 1 day	FN 5%ND 1 day	FN 10%ND 1 day	FN 5%CH 1 day	FN10% CH 1 day	KU 1 day	KU 5%ND 1 day	KU 10%ND 1 day	KU 5%CH 1 day	KU 10%CH 1 day	RSC 1 day	RSC 5%ND 1 day	RSC 10%ND 1 day	RSC 5%CH 1 day	RSC 10%CH 1 day
Free	0.766	0.882	0.864	1	1.548	0.2	0.21	0.564	2.916	3.35	0.9	0.598	0.714	1.248	1.73
TISAB III	1.232	1.282	1.33	1.546	1.964	0.2	0.748	1.348	1.566	3.564	1.43	1.264	1.398	1.832	1.902
TISAN IV	0.45	0.51	0.654	1.626	2.082	0.2	0.2	1.314	1.516	3.65	1.614	1.166	1.466	1.866	2.232

Figure 8.5: Fluoride measurements in ppm for Day 7

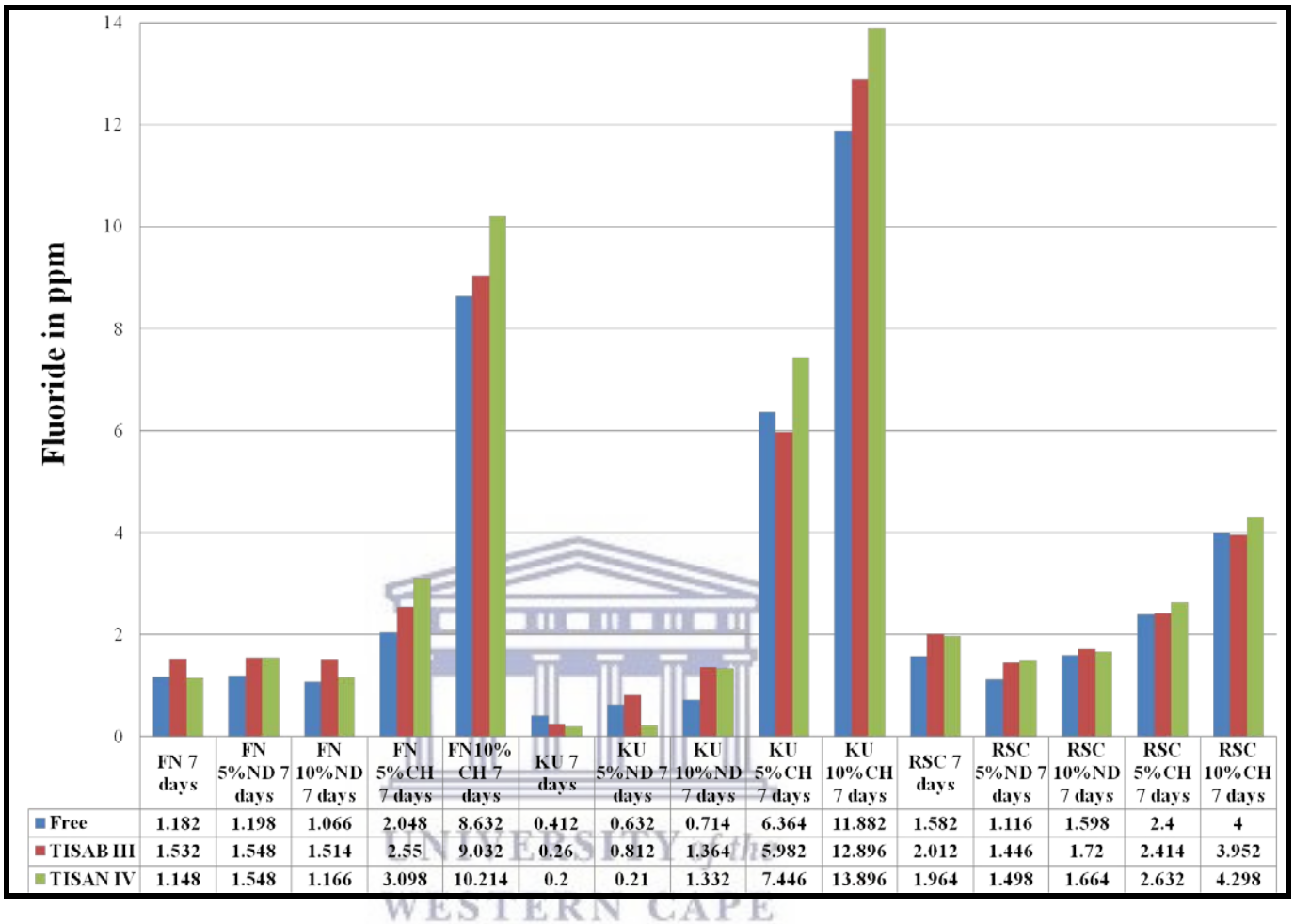

	FN 7 days	FN 5%ND 7 days	FN 10%ND 7 days	FN 5%CH 7 days	FN10% CH 7 days	KU 7 days	KU 5%ND 7 days	KU 10%ND 7 days	KU 5%CH 7 days	KU 10%CH 7 days	RSC 7 days	RSC 5%ND 7 days	RSC 10%ND 7 days	RSC 5%CH 7 days	RSC 10%CH 7 days
Free	1.182	1.198	1.066	2.048	8.632	0.412	0.632	0.714	6.364	11.882	1.582	1.116	1.598	2.4	4
TISAB III	1.532	1.548	1.514	2.55	9.032	0.26	0.812	1.364	5.982	12.896	2.012	1.446	1.72	2.414	3.952
TISAN IV	1.148	1.548	1.166	3.098	10.214	0.2	0.21	1.332	7.446	13.896	1.964	1.498	1.664	2.632	4.298

Figure 8.6: Fluoride measurements in ppm for Day 21

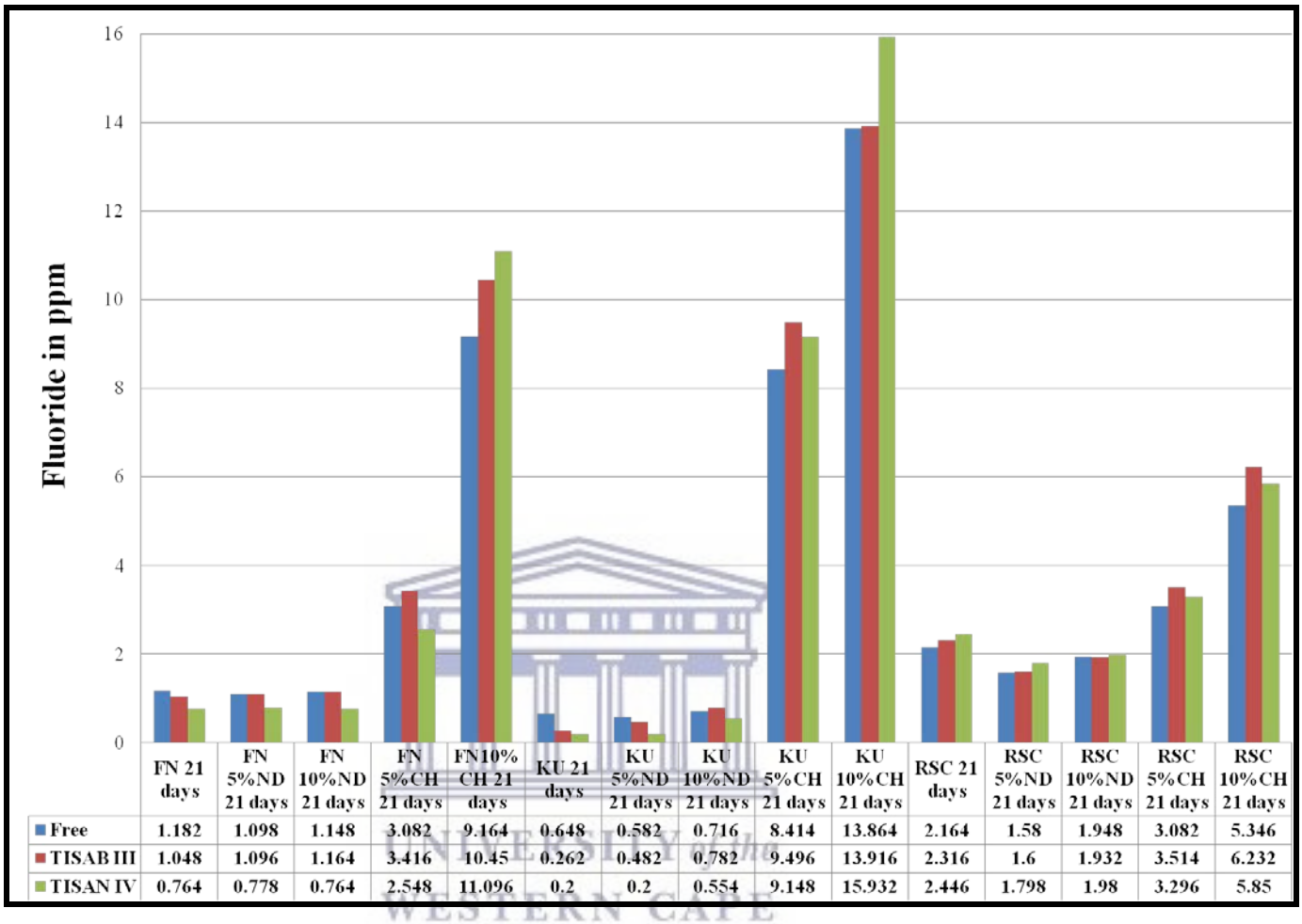

	FN 21 days	FN 5%ND 21 days	FN 10%ND 21 days	FN 5%CH 21 days	FN10% CH 21 days	KU 21 days	KU 5%ND 21 days	KU 10%ND 21 days	KU 5%CH 21 days	KU 10%CH 21 days	RSC 21 days	RSC 5%ND 21 days	RSC 10%ND 21 days	RSC 5%CH 21 days	RSC 10%CH 21 days
Free	1.182	1.098	1.148	3.082	9.164	0.648	0.582	0.716	8.414	13.864	2.164	1.58	1.948	3.082	5.346
TISAB III	1.048	1.096	1.164	3.416	10.45	0.262	0.482	0.782	9.496	13.916	2.316	1.6	1.932	3.514	6.232
TISAN IV	0.764	0.778	0.764	2.548	11.096	0.2	0.2	0.554	9.148	15.932	2.446	1.798	1.98	3.296	5.85

General trends between materials and the type of fluoride assessed

The recorded ppm of free fluoride, TISAB III and TISAB IV fluoride for days 1, 7 and 21 had a clear trend in fluoride release in decreasing order i.e. RSC had the highest release followed by FN and then KU. Higher fluoride readings were recorded for chitosan modifications compared to the nanodiamond modifications within the group. Days 7 and 21 showed similar fluoride release measurements except for the FN10%ND at day 7 that had lower fluoride readings than FN5%ND (Figures 8.4, 8.5 and 8.6). The free fluoride values should be less than the de-complexed values.

This was the general trend except for:

- FN, FN5%ND on day 21;
- KU, RSC10%CH on days 7 and 21;
- KU5%ND on day 21 and
- KU5%CH on days 1 and 7.

The ionic strength of the solutions is determined by the dissolved ions. Additionally, the de-complexing ability of TISAB III is directly proportional to a ratio of 5Al:1F. Table 8.4 represents the maximum ability of TISAB III to de-complex the fluoride from the DMEM growth medium diluent, based on the aluminium release in ppm (Chapter 7).

Table 8.4: Maximum fluoride de-complexing ability of TISAB III in ppm

Ion released	Commercial material	Modification			
		5%ND	10%ND	5%CH	10%CH
	FN				
Al from ICPMS chapter	2.22	2.5	3.29	5.22	10.8
Maximum fluoride that can be de-complexed by TISAB III	0.444	0.5	0.658	1.044	2.16
	KU				
Al from ICPMS chapter	2.86	7.56	8.84	6.44	14.04
Maximum fluoride that can be de-complexed by TISAB III	0.572	1.512	1.768	1.288	2.88
	RSC				
Al from ICPMS chapter	5.16	8	9.03	9.85	8.85
Maximum fluoride that can be de-complexed by TISAB III	1.032	1.6	1.806	1.97	1.77

8.6. Discussion

The hypothesis that TISAB IV would be a more appropriate buffer than TISAB III for the assessment of nanodiamond- and chitosan-modified GICs was rejected, even though TISAB IV can de-complex more fluoride from the aluminium than TISAB III.

Glass ionomer restorative cements (GICs) have been cited to be important materials for paediatric dentistry as they contain various ions including fluoride. Fluoride has been shown to

be relatively biocompatible with the pulp (Pameijer, 2012) provided that there is at least 1 to 1.5mm of dentine above the pulp chamber (Wilson and McLean, 1988). Fluoride released from GICs has shown evidence for a positive contribution towards the antibacterial properties (Hamilton, 1990). Some studies have however shed doubt on the true effect of the fluoride released from the GICs (Featherstone *et al*., 1987; Damato *et al*., 1990; Forss *et al*, 1991; Massara *et al*., 2002). In a systematic review with a meta-analysis, it was noted that secondary caries and demineralisation were reduced with the use of GICs when compared to amalgam for secondary teeth, but not necessarily for primary teeth (Mickenautsch and Yengopal, 2011). An *in vivo* study on primary teeth illustrated that teeth treated using the Atraumatic restorative treatment (ART) technique showed an 18% increase in calcium after 3 months but no increase in fluoride in the demineralised or decomposed dentine under the GICs. The activity of fluoride for remineralisation and the antibacterial activity of FN could not be concluded with certainty (Massara *et al*., 2002). This result and conclusion was in line with the *in vitro* evaluation of healthy dentine and the very low to no fluoride penetration for GICs in Chapter 11. The results from the literature for fluoride in preparations of neutral sodium fluoride gel, acidulated fluoride gel, fluoride solutions, varnishes and dentifrices cannot be transferred to the presence of fluoride in restorative materials. Additionally, three key articles can be seen to cast doubt on the true effect of the fluoride released from GICs: 1) an exploration of the role of fluoride for the prevention of *in vitro* demineralisation on dentine (Featherstone *et al*., 1987) illustrated that when compared to enamel, a much higher level of fluoride was needed to prevent demineralisation of dentine. In order to inhibit demineralisation and enhance remineralisation a fluoride concentration of 100mg/L (100ppm) is required for dentine (Featherstone *et al*., 1987). 2) The second article (Damato *et al*., 1990) focussed on the ability of the fluoride to re-mineralise artificial carious enamel *in vitro.* It was determined that a concentration of 500ppm sodium fluoride solution significantly remineralised the enamel when compared to the 250ppm.

Even when the fluoride concentration was increased to 2500ppm, no significant difference was detected (Damato *et al*., 1990). 3) A comparison of the amount of bacterial protein that grew on a GIC material versus a composite *in vivo* indicated no significant difference between days 0, 14 and 28 although there was significantly more fluoride present in the bacterial samples collected from the GICs, compared to the composites (Forss *et al.*, 1991). The process of fluoride entering tooth structure is however by partial substitution of the hydroxyl group in the hydroxyapatite. This phenomenon results in a more stable apatite structure, reducing the surface area of the hydroxyapatite exposed to the action of the acids produced by the bacteria (Rošin-Grget and Linčir, 2001). A study from 1993 illustrated a clear encouragement of the fluoride rich hydroxyapatite formation that is resistant to acid dissolution (Wahab *et al*., 1993). Wilson *et al*. (1985) postulated that the fluoride release was principally based on the positively charged counter-ion release mechanism of sodium. It was also suggested that if an increased fluoride from GICs is desired, the formulation must allow for an increased gradient percentage potential of sodium. It was suggested that when a greater amount of fluoride release is required, more sodium can be added to the GIC (Wilson *et al*., 1985). The association between an increased fluoride release in this Chapter and an increased sodium release as the counter-ion from Chapter 7 was confirmed based on the increased sodium release for the chitosan- and nanodiamond-modifications. To date, there have been no publications that reported on the fluoride release of KU. Therefore, the fluoride release profiles based on TISAB III and TISAB IV was the first evidence of release. The results from Chapter 7 for sodium and this Chapter on fluoride release indicated that for KU and its respective nanodiamond modifications, the sodium release as the counter-ion did not match the fluoride release that was recorded. This was the first indication that there is something amiss with the KU and nanodiamond-modified GICs. Hill *et al*. (1995) confirmed that the fluoride release from GICs was complex and originated from the three material phases within the GIC as will be discussed in Chapter 11. These areas of the GIC are: 1)

areas of glass clusters (glass), 2) areas of dissolved glass (silica gel) and the 3) areas of less glass and more polyacrylic acid/ glass slurry dominated by polyacrylic acid (polysalt matrix).

It was postulated by Crisp and Wilson (1974) that fluoride release from GICs was not only as free fluoride, but also as complexed fluoride with aluminium (Al-F) (Crisp and Wilson, 1974). It is well known that the majority of fluoride is released as free fluoride ions under neutral conditions (pH 7) and as complexed fluoride under acidic conditions (Lewis *et al.*, 2013).

This is why the fluoride ion selective electrode was placed in the DMEM diluent after the various time periods to measure the free fluoride (Figures 8.4, 8.5 and 8.6; Table 8.3) without buffering the pH (Figures 8.1, 8.2 and 8.3) of the medium. The release of free fluoride from GICs is not always effective against bacteria, since free fluoride does not have the ability to cross the bacterial cell wall (Sutton *et al.*, 1987). The free fluoride would need to interact with H^+ to form HF. In this form it can easily move into the bacteria and starts to dissociate, disrupting the glycolytic enzyme enolase as well as the proton-releasing adenosine triphosphatase enzymatic activity (Sutton *et al.*, 1987). The chitosan modifications of all the GICs presented with the highest recorded free fluoride for all three time periods. It is however important to note that HF only forms at a pH<5. In terms of the free fluoride determination, the hydroxide interferences become more prominent with a pH>8.4 as seen in Figure 8.7 illustrating the variation in mV as the pH changes (Frant and Ross, 1966; Kauranen, 1977). When the ion selective fluoride electrode is influenced by the hydroxide ions, this interference with the mV readings is called a Nerstian response to the hydroxide ions as well as the residual fluorides (Frenzel and Bratter, 1986) (Figure 8.7). With the hydroxide ions interfering at pre-determined fluoride values from the TISAB III assessment of below 0.2ppm, the interferences have been cited as being considerable with the fluoride selective probe. Therefore, the fluoride readings of the KU materials below 0.2ppm were presented as >0.2ppm.

Figure 8.7: Hydroxide interference occurs when line deviates from the horizontal plane

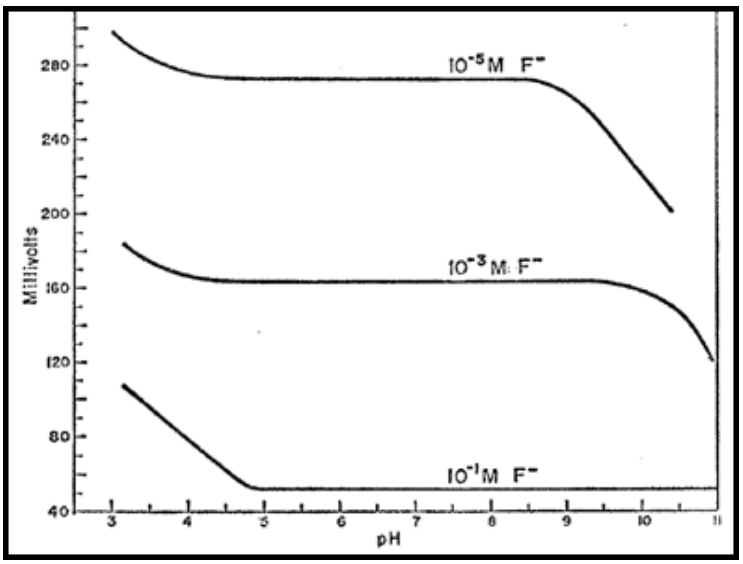

Image used with permission from: Frant and Ross, 1966

Various intrinsic and extrinsic factors determine the amount of fluoride release (Hattab and Amin, 2001; Upadhyay *et al.*, 2013). The intrinsic factors include the relevant factors that were either standardised or assessed in various studies in this dissertation namely: the material composition, powder/ liquid ratio, temperature, specimen geometry, permeability, surface treatment/ finishing of the materials (Hattab & Amin, 2001; Upadhyay *et al.*, 2013). The extrinsic factors influencing the fluoride release include pH and temperature of the medium that the sample is exposed to (Yan *et al.*, 2007; Upadhyay *et al.*, 2013).

The release of fluoride from the GIC materials into the DMEM medium occurred at 4°C, as the instructions of the manufacturer indicated that storage of DMEM should be between 4 -8°C. A study by Yan *et al*. (2007) determined the fluoride release from GICs finished with 1200 wet silicon carbide paper and stored in 5ml of de-ionised water at various temperatures (4, 37 and 55°C). Their study concluded that the release of fluoride was diffusion-controlled over time and based on the temperature that the sample was exposed to. The fluoride release increased

significantly as the temperature increased (Yan *et al.*, 2007). In the present dissertation, it was concluded that the DMEM medium also plays a role in how the materials interact with regard to their ion release. This could be concluded based on the fact that all the mediums with specimens of the same size were stored at 4ºC for Ariffin *et al*. (2006) as well as in this dissertation. The results from this Chapter where the fluoride release for FN was assessed in the DMEM growth medium with the same method used by Ariffin *et al*. (2006) were quite different. Ariffin *et al*. (2006) used de-ionised water (pH 6.5) and recorded 0.11ppm (day 1); 0.36 (day 9) using TISAB IV. Using de-ionised water (pH 7), Ariffin *et al*. (2006) recorded 0.0016ppm (day 1) and 0.0016 (day 7). Therefore the 4ºC temperature did not seem to limit the fluoride release in this Chapter 8 with regard to the control material FN. The author of this dissertation did however realise that Ariffin *et al*. (2006) did not assess the pH values of the TISAB IV/GIC-diluent mixture. Ariffin *et al*. (2006) also did not explicitly state that readings were taken 24 hours after the combination of TISAB IV and the GIC-diluent. Therefore, no final comparison between fluoride release due to temperature or the DMEM medium can be made, as this would merely be speculation. The fluoride release recorded in the DMEM medium with the TISAB III was 1.232ppm (day 1); 1.532ppm (day 7) and 1.048 (day 21). For FN, the TISAB IV fluoride release was 0.45 (day 1); 1.148 (day 7) and 0.764 (day 21) (Figures 8.4, 8.5 and 8.6; Table 8.3).

Figures 8.1, 8.2 and 8.3 illustrate the variation in pH at the time of free fluoride determination. There were many GICs with a pH>8.5. The pH of 8.5 should be considered as the upper limit of acceptable pH for free fluoride determinations according to the manufacturer of the fluoride ion selective probe (Orion research. 2001). This is based on the fact that, the mV potential difference between 7 and 8.1 is small, but between 8.1 and 8.9 as well as between 9.5 and 10.2 there were marked interferences by the hydroxides (Frenzel and Bratter, 1986). The results presented in Figure 8.8 were achieved by adjusting the pH with either sodium hydroxide or nitric acid as part of their experimental design. The results presented in Figure 6 illustrate the same fluoride

concentration and the mV potential differences in relation to the pH (Frenzel and Bratter, 1986). Thus, based on the pH guidelines stated by Frenzel and Bratter, (1986) the only free fluoride values that could be considered accurate were FN, FN10%CH, KU5%CH at day 21; FN5%ND at days 1, 7 and 21; FN5%CH, KU10%CH at days 7 and 21, provided the ionic strength did not influence the fluoride ion selective probe. The ionic strength interaction of the combination of ions released into the GIC-diluents as determined in Chapter 7 has never been determined in any previous literature.

When the chemistry of the chitosan modification of GICs is considered, the fluoride readings become more difficult to accept as correct. This is because chitosan has various functional groups namely: NH_3 and OH groups (De Stefano *et al*., 2010). Figures 8.1, 8.2 and 8.3 illustrate how the pH dropped for the chitosan-modified GICs due to the free fluoride that was released starting to form HF_2 with the hydroxide component. As the pH dropped, the fluoride release increased as complexed fluoride was also released.

Figure 8.8: pH variation where the hydroxides cause significant mV potentials

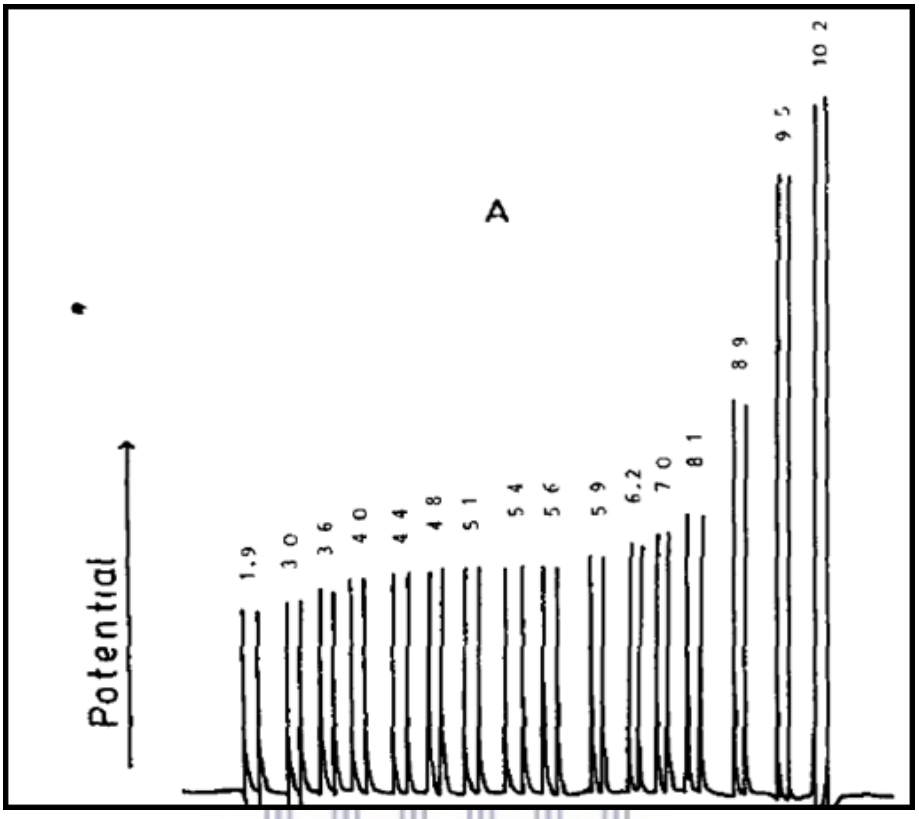

Image used with permission from: Frenzer and Bratter, 1986.

For the determination of the total amount of fluoride, a de-complexing agent was required. TISAB III and IV were used in this dissertation for the assessment of the fluoride released by the GICs into the DMEM growth medium diluents. TISAB IV was chosen additionally to TISAB III, as it was unknown to what extent the chitosan-modified GICs would release the ratio of aluminium to fluoride ions and whether it would be free or complexed. The well-established complexes of aluminium with fluoride are: Al(OH)m(F)n , $Al(OH)F_3^-$ and $Al(OH)_2F$ (Sanjuan and Michard, 1987).

When TISAB IV was used to de-complex the fluoroaluminate complexes (Al-F), the adjustment of the pH to 8.5 resulted in a reduced stability of the Al-F to complex. In a study by Patel *et al*. (2018), due to the high aluminium concentration of tea that was assessed, a significantly higher fluoride concentration was recorded for TISAB III when compared to the TISAB IV. In this Chapter, the greatest interference to the fluoride ion selective electrode recorded thus far was the

hydroxide ions at the high pH above 8.1. This was evident as previous research used TISAB III and IV to determine the total fluoride. The free fluoride was first determined. The pH was measured and determined to be above 8.7 (Agarwal *et al*., 2002). The use of TISAB IV in this dissertation as a de-complexing/buffering agent with the DMEM growth medium diluents presented with a pH between 8.5 and 9.10 after 24 hours of combining the TISAB IV and the GIC-diluents. The mV readings recorded by the electrode for the GIC-diluent/TISAB IV were between -97 to -102mV (after the lapse of 24 hours de-complexing time). Therefore, the hydroxide interferences for the TISAB IV buffered GIC-diluent at these pH values would not be as accurate. Frenzel and Bratter, (1986) stated that if the pH was buffered to the point where the hydroxide ions are eliminated, it would eliminate the rationale of using TISAB IV to de-complex the aluminium (Frenzel and Bratter, 1986).

The addition of Low Level TISAB, TISAB II and TISAB III buffers (besides TISAB IV) will result in a lower pH between 4.4 and 5.6. At this pH range, the mV readings will be more stable with the fluoride ion selective electrode (Frenzel and Bratter, 1986), since the hydroxide ions are eliminated at this low pH and hydrogen ions are not present between a pH of 5 and 5.5 (Orion Research Incorporated, 2001). Then again, the fluoride will be complexed with the aluminium if the aluminium has a ratio to the fluoride of 5:1.

The GIC-diluent was mixed with TISAB III and after 24 hours the fluoride was assessed. Figures 8.4, 8.5 and 8.6 illustrate the TISAB III de-complexed fluoride for the various time periods. With the exception of FN at 21 days, FN and RSC (with their chitosan and nanodiamond modifications) at days 1, 7 and 21, the results illustrated that the de-complexed fluoride was more than the free fluoride. The free fluoride was already established to be over-estimated due to the high pH of many of the GIC-diluents. The over-estimation was due to the hydroxide interferences.

In Figures 8.4, 8.5 and 8.6, it is interesting to note that the fluoride that was de-complexed illustrated that the ppm fluoride of TISAB III is greater than TISAB IV for the control materials and their nanodiamond modifications. For most of the chitosan modifications, the TISAB IV fluoride determination was greater due to the established hydroxide interferences. Based on the indications for TISAB III and its de-complexing ability, Table 8.4 illustrates that the fluoride was underestimated based on the aluminium 5ppm:fluoride 1ppm ratio. The increased fluoride values recorded were due to the mV interferences of the additional aluminium and other ions that could either not get de-complexed or the background ionic strength could not be stabilised. Besides the pH, it was stated by Frenzel and Bratter, (1986) that accurate fluoride determination is dependent upon: 1) The use of an appropriate complexing agent 2) The absolute number of interfering elements/ ions that cause ionic strength variations and 3) The ratio between the various interfering ions and the amount of fluoride (Frenzel and Bratter, 1986).

Besides hydroxide, there are other ions that can interfere with the electrode by changing the ionic strength of the buffered medium, even if the pH is stable between 5 and 5.5. Silicon, in the form of hexafluorosilicate, only interferes with the mV at pH values well below 5. TISAB III is able to hydrolise the silicon completely at a pH of between 5 and 5.5 as TISAB III has sufficient chelating capacity. Additionally, silicon must be present in very large parts per million before it can cause any interferences (Frenzel and Bratter, 1986). Therefore silicon was not considered as an interfering ion for this study using TISAB III.

A study by Frenzel & Bratter (1986) that focussed on interferences indicated that a standardised ionic strength solution at 5ppm fluoride mixed with TISAB III showed various significant interferences as illustrated in Table 8.5. The addition of the ions above that threshold due to the ionic strength of the TISAB III/ diluent not being buffered anymore (Frenzel & Bratter, 1986), influenced the mV.

Table 8.5: Ions that provide interferences with TISAB III

Element	mV significantly influenced above:
Al^{3+}	1ppm
Ca^{2+}	>0.02ppm (converted from $0.05mol^{-1}$)
Si^{4+}	>100ppm
Na^{+}	>0.01149ppm (converted from $0.05mol^{-1}$)
Results established with a known fluoride standard of 0.5 to 5ppm, with TISAB III Frenzel and Bratter, (1986)	

As mentioned in Chapter 7, based on the ions released, the comparison of the interfering ppm values in Tables 8.4 and 8.5 supports the rationale that these aluminium and sodium ions interfered with the TISAB III fluoride values. This explains why the fluoride values were above the possible de-complexed aluminium (Table 8.4).

Lanthanum and fluoride

Lanthanum has an affinity for fluoride (Vivek and Srimurali, 2016). For this reason, the selective fluoride ion electrode has a lanthanum crystal which serves as the membrane to allow fluoride to pass through the crystal and cause an mV reading in the electrode. This dissertation therefore postulates that either the true fluoride release from KU is small, or the fluoride is tightly bound to the lanthanum and/or aluminium and cannot pass through the lanthanum crystal of the fluoride ion selective probe.

The maximum lanthanum release recorded in Chapter 7 was 0.021ppm in de-ionised water. At a pH below 7, lanthanum is present in the solution as a lanthanum ion (Cetiner and Xiong, 2008) and allows for chelation of the fluoride from the lanthanum with TISAB III. When the KU diluent is buffered with TISAB II or III and the mixed TISAB/GIC-diluent has a pH between 5 and 7, a ratio of 20 ppm of lanthanum to 1.4 ppm of fluoride can be de-complexed (Selig, 1970). With the pH between 5 and 5.5 during the combination of KU diluents with TISAB III the lanthanum will be de-complexed from the fluoride. The opposite is true for the high pH of TISAB IV and is evident since, the de-complexed fluoride readings are smaller. Once lanthanum hydroxide is formed by the combination of hydroxide ions and lanthanum ions in TISAB IV, it could have an exceptionally high fluoride absorption value of 242200ppm of fluoride at a pH≤7.5 and 24800ppm of fluoride at a pH>10. The fluoride binds to the lanthanum hydroxide by exchanging fluoride for hydroxides on the lanthanum molecule (Na and Park, 2010). The increase of hydroxides in the medium raises the pH. At a pH>8.7, the ability of the lanthanum hydroxide to adsorb fluoride sharply decreases, since the sites on the lanthanum would already be predominantly occupied by fluoride. This explains why the KU and ND modifications of TISAB IV have lower fluoride readings than the TISAB III readings.

During the initial stages of the GICs being exposed to the DMEM growth medium, the pH is 7, until the GIC elution of ions and adsorbtion of hydroxides starts to change the pH. At a pH above 7, the aluminium- and the lanthanum ions are present as salts (Vivek and Srimurali, 2016) and are able to complex with the fluoride under physiological conditions (when no chelating agents are present). In dilute acids of pH<6.5, the amino acid from chitosan can become protonated (Mandihally and Matthew, 1990). This occurs within the GIC as the moisture gets absorbed into the GIC and maturation takes place in the first 24 hours after mixing. In a study by Senthil Kumar *et al*. (2017), a more positive charge was also noted in the 10% nano-chitosan particles added to the powder of resin modified glass ionomer cement (RMGIC). A study by

Petri *et al*. (2007), indicated that a chitosan-modification made to the liquid of the GIC resulted in an increased fluoride release due to the easier movement of the fluoride through the matrix. The fluoride ion interacts with the chitosan groups and transforms a C-C bond to C-F. The replacement of the hydrogen in the chitosan with fluoride has been well established (Ando *et al*., 1995; Kealey *et al*., 2001).

This more positive charge of chitosan together with the swelling of the chitosan as it is exposed to moisture (as established in Chapter 6, 10), has also been cited to be responsible for the fast drug release in a study conducted by Park *et al*., (2010). Similarly, this swelling of the chitosan-modified GICs has resulted in a significantly higher release of fluoride (Chapter 8) and other ions (Chapter 7) in comparison with the control materials.

Chitosan and KU

The fluoride values recorded for FN as well as RSC with their respective nanodiamond modifications presented with fluoride values that were relatively in line with one another. The KU fluoride values of the free fluoride, TISAB III and TISAB IV assessment did not have a gradual increase from control material to nanodiamonds to chitosan. There was a large jump in the fluoride values for the chitosan-modifications of KU. Additionally, it was interesting that the fluoride release of KU for the free fluoride, TISAB III and TISAB IV was significantly less than FN and RSC, considering the fluoride gradient potential present within KU (Chapter 11) at 11.34% vs FN (13.3) and RSC (11.7%) The amino- and secondary hydroxyl group of CH was able to adsorb metal ions, like lanthanum (La^{3+}) and aluminium (Al^{3+}) by forming a complex. Lanthanum, aluminium and fluoride compete for the functional groups on chitosan. Anionic molecules like fluoride also bind to the amino group of the chitosan via electrostatic interaction and metal ions bond with chitosan via co-ordinate covalent bonds (Brack *et al*., 1997). KU was the only GIC that presented with lanthanum. Lanthanum has a very large fluoride adsorption

capacity of 1270ppm of fluoride. Due to the electronegativity of chitosan the electropositive lanthanum is adsorbed to the chitosan at the amino (NH_3) group. The chitosan-modified KU also released the fluoride from the material that was ionically bound to the lanthanum ion. The lanthanum-fluoride ion is released as it is exchanged for the hydroxide ion during the increasing pH>7 above 7. This exchange of fluoride in the GIC with the hydroxide was confirmed by Singh *et al*. (2016) and was additionally confirmed in this dissertation during the TISAB IV fluoride assessment. In a study for water de-fluoridation it was confirmed that when lanthanum was bound to the surface of chitosan, it was successfully used as water de-fluoridation material. The study by Jagtap *et al*. (2011) further confirmed that the fluoride bound to the lanthanum-chitosan can be liberated from the lanthanum- chitosan molecule by a 2% sodium hydroxide (Jagtap *et al*., 2011). This explains in this dissertation how the fluoride from KU is adsorbed by the lanthanum-chitosan in the chitosan-modified KU. As the sodium is released from the chitosan-KU modified materials over the various time periods (day 1, 7 and 21 KU GIC-diluents) it will result in the sodium to bind with the hydroxide ions and liberate the lanthanum-chitosan complexed fluoride. This liberation of the fluoride from the chitosan-lanthanum ions will result in a greater free fluoride concentration and total fluoride concentration (Figures 8.4, 8.5 and 8.6) and the TISAB IV buffer that was added cause the hydroxide ions to form due to the high pH due to the effect of the TISAB IV raising the pH. This then allows the fluoride to be released from the lanthanum that was adsorbed to the chitosan and allows the fluoride to be detected by the selective fluoride ion electrode. At higher pH values, whether there is a chelating agent (TISAB IV) or not, the hydroxide ions predominate and compete with the salts of aluminium and lanthanum for the fluoride. The hydroxide ions interfere with the fluoride ion selective probe and incorrect readings in mV are exacerbated. Smith and Martell, (2004) illustrated that lanthanum hydroxide ($La(OH)^{2+}$) molecule can form a wide range of ionic strengths (Smith and Martell,

2004). This adds to the incorrect mV recording of KU and its modified versions with chitosan and nanodiamonds.

Nanodiamonds and fluoride

Fluoride is well known to react with graphite to give graphite fluoride (Lagow *et al*., 1974; Kita *et al*., 1979; Hagiwara *et al*., 1986). Aluminium, barium, calcium, potassium, sodium and strontium are all inorganic salts. The GIC has three main cationic species that usually associate with fluoride namely aluminium, sodium and strontium. If the fluoride is complexed with these cations and well integrated into the matrix of the GIC, the release of fluoride will be influenced (Hadley *et al*., 2001). During the mixing of the nanodiamond-modified GICs, the cations and fluoride interact with the nanodiamond particle as previously discussed in Chapter 6 and 7 of this dissertation. The original Zeta potential (-55mV) of the nanodiamond particles (*PL-D-G01*) changes as they get hydrated and obtain a Zeta potential of 45±3mV (Yakovlev *et al*., 2015). Therefore, the Zeta potential of the nanodiamond particle changes to positive as more and more water is slowly absorbed as time passes from hours to days. The hydration results in a decrease in the release of fluoride and sodium to maintain electrical neutrality. It has been noted that the pH of the solution progressively increases as the solution is exposed to the GICs (Nicholson and Amiri, 1998). This result was confirmed by the pH that steadily increased from the original DMEM growth medium of pH7 towards the final pH (represented in Figure 8.1-8.3) for each respective material.

With nanodiamond-modified GICs, the lanthanum is ionically bound to the nanodiamonds. When the lanthanum is not adsorbed by the chitosan, the lanthanum is released into the TISAB III and IV buffered diluent to cause ionic changes in the buffered medium. This is evident when considering that KU was the only material with lanthanum. Free fluoride, TISAB III and IV de-complexed fluoride at the two different pH ranges for KU were very different to the FN and RSC materials.

For the nanodiamond-modified GICs, the nanodiamond particles react with the fluoride during the mixing process. As the nanodiamond-modified GIC increases in weight due to moisture absorption (Chapter 6), the replacement of hydrogen with fluoride results in the nanodiamond (that is usually hydrophobic) (Molian *et al*., 1993) becoming hydrophilic (Kealey, 2001). The change in hydrophilicity was confirmed by the increase of water sorption of the GICs modified with nanodiamonds (Chapter 6). The exposure of GICs to fluorides from various sources could extend the release of fluoride (Rothwell *et al*., 1998). A study where GICs were modified with bioactive glass came to the conclusion that modifying GICs could not only result in a greater leaching of fluoride but will also present with an increased adsorption of fluoride (to be discussed in Chapter 12), resulting in the long- term releasing capacity of fluoride being favourable (Yli-Urpo *et a*l., 2005).

The difference in the fluoride release between the control materials of FN and RSC and their nanodiamond-modifications are explained by the nanodiamond-modified GIC that hydrolise. During the hydrolysis, fluoride is displaced by hydroxyl, carboxyl, or amino moieties (Liu *et al*., 2004), causing the reduction of hydrolysis of the GIC that would allow the fluoride release to occur as free or complexed fluoride. Due to the chemistry of KU, the opposite is seen. The presence of lanthanum in KU and its subsequent release result in errors and underestimation of fluoride determination for the control material by the fluoride ion selective electrode. The nanodiamond and the chitosan particles readily interact with the lanthanum, allowing fluoride to enter the fluoride ion selective electrode thereby providing a larger ppm reading.

The nanodiamond modifications have a similar response to the selective fluoride ion electrode as their respective control materials. In general, there is a negative electrostatic potential on most facets of the outer layer of the nanodiamond particle in the presence of inorganic salts (Guo *et al*., 2014). An advantage of the nanodiamond modifications is that the nanodiamond particle has multiple areas where the fluoride can interact. Fluoride has an affinity for nanodiamonds and the

graphite components of the particle; hence it is relatively easy to modify the nanodiamond with fluoride (Kita *et al*., 1979).

Kealey, (2001) completed an SEM investigation where only the nanodiamond particles were exposed to fluoride at 20ºC, did not display any physical changes of the nanodiamond surfaces (Kealey, 2001). This attests to the inert nature of nanodiamonds to structural damage. Fluoride can break conjugated double bonds and change the hybridized states of carbon atoms from sp^2 to sp^3 (Ando *et al*., 1995). The interaction of fluoride with carbon can vary from individual to combinations of covalent, semi-ionic, ionic and van der Waals forces (Touhara and Okino, 2000). Fluoride has the ability to bond to C=O, C-O, O-H and C=C groups, but is first substituted at various carbonyl groups (Roeges, 1994) to form C-F groups (Siné *et al*., 2003). The specific site where fluoride substitutes the C=O functional group, is in the position of the oxygen that resides on the sp^3 diamond surface with a covalent bond (Liu *et al*., 2004). The ionisation potential of the graphite in the nanodiamond and not the atomic carbon is what governs the interaction with fluoride to form ionic graphite intercalation compounds (Touhara and Okino, 2000). Due to the negative charge on the fluoride atom, the C-C of the nanodiamond bond is influenced by inducing a dipole moment (Ando *et al*., 1995). The other local sites for fluoride ion bonding as well as the available functional groups of the nanodiamond particles on the nanodiamond surface should also be considered for the specific functionality to modify dental materials. Nanodiamonds have oxygen terminated and/or hydrogen terminating functional groups and this is where the nanodiamond reacts with the fluoride. The carbon-oxygen surface groups are more resistant to fluorination compared to the C-H surface groups. The nanodiamond -modified GICs are ideal since the C-H functional groups at the sp^3 hybridised bonding can get fluoridated at low temperatures between -10 and +35ºC. It is therefore more likely for fluoride chemisorptions into the nanodiamonds to occur at these temperatures (Ando *et al*., 1995). This is

important since fluoride dentifrices, fluoride mouthrinse and professionally applied fluoride preparations will be able to interact with the nanodiamond-modified GICs (Further discussed in Chapter 12). If a stable covalent C-F bond is not kinetically possible through the interaction of C-C (of the ND) with the fluoride, the fluoride could form weak F-F bonds with the van der Waals forces of the nanodiamond (Touhara and Okino, 2000). The nanodiamond-modified GIC materials will therefore bond fluoride at the semi-ionic (sp^3-sp^2) intermediate phase at a temperature above 20ºC change the C-C to C-F and CH_2 to C-HF. All the other interactions of the nanodiamond particles with fluoride will occur readily with the graphite and the diamond core (Touhara and Okino, 2000).

The DMEM growth medium at 4ºC therefore influences the fluoride interaction with the nanodiamond-modified GICs to a similar extent as the control materials, since the various fluoride readings between the control GICs and their nanodiamond modifications was close together.

8.7. Conclusion

TISAB III has been established as an adequate buffer medium for the adjustment of the diluent/TISAB III to a stable pH between 5 and 5.5, but the drawback is the amount of fluoride that can be released from the aluminium-fluoride complexed ions. At a pH 5-5.5, the interferences from the hydrogen and hydroxide ions are completely eliminated. The limitations with TISAB III still exist since the fluoride ppm determination with TISAB III has a degree of error as a result of the perceived interferences due to the ionic strength from the aluminium, sodium and strontium. Therefore, the appropriateness of TISAB III with the ionic strength of GIC-diluents should be replicated as the experiments of Frenzel and Bratter, (1986). This replication of the study with the GIC-diluents as the objective of determining the ionic strength

will establish the capacity of the buffer capacity by TISAB III to the ionic strength of the GIC-diluents. As shown in this Chapter the perceived ionic strength and pH are essential components to achieve an accurate mV reading. In order to establish the appropriateness of TISAB IV with the use of GIC-diluent this dissertation illustrated profound interferences with the hydroxide (OH^-) ions to the fluoride ion selective probe. Therefore the experiments of Frenzel and Bratter, (1986) should be replicated to assess the influence of the ionic strength and the fluoride readings should the pH be adjusted down to 8.1. Frenzel and Bratter, (1986) suggested that at 8.1 less interference is seen from the hydroxide ions, but how that affects the re-complexing of aluminium-fluoride would need to be investigated, since TISAB IV is stated by Orion research (2001) to function optimally for de-complexing aluminium-fluoride at a pH of 8.5. The lanthanum is not an issue with TISAB III provided that the ratio is 20 ppm lanthanum to 1.4 ppm fluoride. With regard to TISAB IV, the amount of ion released in the form of lanthanum, strontium and sodium will continue to cause the transient phenomena of drifting the mV reading due to the ionic strength variation that influences the accuracy of the determined fluoride. Additionally, the hydroxide with the use of TISAB IV is the largest contributor to the inaccuracy of the fluoride readings. Due to the hydroxide interferences, free fluoride readings for the assessed GICs in an un-buffered GIC-diluent are not accurate at all. The final conclusion from this Chapter is that much more research with TISAB III and IV is required with regard to the combination of ions seen in the GIC-diluents influencing the ionic strength as well as the variation of pH when the different TISABs are used. The author of the dissertation conclude that a new chelating and ionic strength buffer would need to be developed to accurately buffer the pH, chelate fluoride from various complexes and stabilise the ionic strength. This is based on all the multiple short comings of TISAB III and IV (noted in this Chapter); resulting in attaining an inaccurate mV reading.

8.8. References

Agarwal, M., Rai, K., Shrivastav, R. and Dass, S. (2002). A study on fluoride sorption by montmorillonite and kaolinite. *Water, Air, and Soil Pollution*, 141, pp.247-261.

Ando, T., Yamamoto, K., Kamo, M., Sato, Y., Takamatsu, Y., Kawasaki, S., Okino, F. and Touhara, H. (1995). Diffuse reflectance infrared Fourier-transform study of the direct thermal fluorination of diamond powder surfaces. *Journal of the Chemical Society, Faraday Transactions*, 91(18), p.3209.

Ariffin, Z., Ngo, H. and McIntyre, J. (2006). Enhancement of fluoride release from glass ionomer cement following a coating of silver fluoride. *Australian Dental Journal*, 51(4), pp.328-332.

Brack, H., Tirmizi, S. and Risen, W. (1997). A spectroscopic and viscometric study of the metal ion-induced gelation of the biopolymer chitosan. *Polymer*, 38(10), pp.2351-2362.

Castioni, N., Baehni, P. and Gurny, R. (1998). Current status in oral fluoride pharmacokinetics and implications for the prophylaxis against dental caries. *European Journal of Pharmaceutics and Biopharmaceutics*, 45(2), pp.101-111.

Cetiner, Z. and Xiong, Y. (2008). Chemical controls on the solubility, speciation and mobility of lanthanum at near surface conditions: A geochemical modelling study. *Applied Geochemistry*, 23(8), pp.2301-2315.

Chau, N., Pandit, S., Cai, J., Lee, M. and Jeon, J. (2015). Relationship between fluoride release rate and anicariogenic biofilm activity of glass ionomer cements. *Dental Materials*, 31(4), pp.e100-e108.

Crisp, S. and Wilson, A. (1974). Reactions in Glass Ionomer Cements: I. Decomposition of the powder. *Journal of Dental Research*, 53(6), pp.1408-1413.

Damato, F., Strang, R. and Stephen, K. (1990). Effect of Fluoride Concentration on Remineralization of Carious Enamel an in vitro pH-Cycling Study. *Caries Research*, 24(3), pp.174-180.

De Stefano, C., Gianguzza, A., Piazzese, D. and Sammartano, S. (2010). Speciation of chitosan–phosphate and chitosan–nucleotide systems in NaCI aqueous solution. *Chemical Speciation & Bioavailability*, 22(2), pp.99-107.

Featherstone, J., McIntyre, J. and Fu, J. (1987). Physico-chemical aspects of root caries progression. In: A. Thylstrup, S. Leach and V. Qvist, ed., *Dentine and Dentine Reaction in the Oral Cavity*. Oxford: IRL Press Ltd, pp.127-137.

Forss, H., Jokinen, J., Spets-Happonen, S., Seppä, L. and Luoma, H. (1991). Fluoride and Mutans Streptococci in Plaque Grown on Glass Ionomer and Composite. *Caries Research*, 25(6), pp.454-458.

Frant, M. and Ross, J. (1966). Electrode for Sensing Fluoride Ion Activity in Solution. *Science*, 154(3756), pp.1553-1555.

Frenzel, W. and Bratter, P. (1986). Fluoride ion-selective electrode in flow injection analysis Part 2. Interference Studies. *Analytica Chimica Acta*, 18(7), pp.1-16.

Guo, Y., Li, S., Li, W., Moosa, B. and Khashab, N. (2014). The Hofmeister effect on nanodiamonds: how addition of ions provides superior drug loading platforms. *Biomaterials Science*, 2(1), pp.84-88.

Hadley, P., Billington, R., Williams, J. and Pearson, G. (2001). Interactions between glass ionomer cement and alkali metal fluoride solutions: the effect of different cations. *Biomaterials*, 22(23), pp.3133-3138.

Hagiwara, R., Nakajima, T., Nogawa, K. and Watanabe, N. (1986). Properties and initial discharge behaviour of graphite fluorides decomposed under chlorine. *Journal of Applied Electrochemistry*, 16(2), pp.223-228.

Hamilton, I. (1990). Biochemical Effects of Fluoride on Oral Bacteria. *Journal of Dental Research*, 69(2_suppl), pp.660-667.

Hattab, F. and Amin, W. (2001). Fluoride release from glass ionomer restorative materials and the effects of surface coating. *Biomaterials*, 22(12), pp.1449-1458.

Hill, R., De Barra, E., Griffin, S., Henn, G., Devlin, J., Hatton, P., Brook, I., Johal, K. and Craig, G. (1995). Fluoride Release from Glass Polyalkenoate (Ionomer) Cements. *Key Engineering Materials*, 99-100, pp.315-322.

Itota, T., Al-naimi, O., Carrick, T., Yoshiyama, M. and McCabe, J. (2005). Fluoride release and neutralizing effect by resin-based materials. *Operative Dentistry*, 30(4), pp.522-527.

Itota, T., Carrick, T., Rusby, S., Al-Naimi, O., Yoshiyama, M. and McCabe, J. (2004). Determination of fluoride ions released from resin-based dental materials using ion-selective electrode and ion chromatograph. *Journal of Dentistry*, 32(2), pp.117-122.

Jagtap, S., Yenkie, M., Das, S. and Rayalu, S. (2011). Synthesis and characterization of lanthanum impregnated chitosan flakes for fluoride removal in water. *Desalination*, 273(2-3), pp.267-275.

Kauranen, P. (1977). The Use of Buffers in the Determination of Fluoride by an Ion-Selective Electrode at Low Concentrations and in the Presence of Aluminum. *Analytical Letters*, [online] 10(6), pp.451-465. Available at: http://dx.doi.org/10.1080/00032717708079390 [Accessed 7 Apr. 2019].

Kealey, C., Klapötke, T., McComb, D., Robertson, M. and Winfield, J. (2001). Fluorination of polycrystalline diamond films and powders. An investigation using FTIR spectroscopy, SEM, energy-filtered TEM, XPS and fluorine-18 radiotracer methods. *Journal of Materials Chemistry*, 11(3), pp.879-886.

Kita, Y., Watanabe, N. and Fujii, Y. (1979). Chemical composition and crystal structure of graphite fluoride. *Journal of the American Chemical Society*, 101(14), pp.3832-3841.

Koo, H., Xiao, J., Klein, M. and Jeon, J. (2010). Exopolysaccharides Produced by Streptococcus mutans Glucosyltransferases Modulate the Establishment of Microcolonies within Multispecies Biofilms. *Journal of Bacteriology*, 192(12), pp.3024-3032.

Lagow, R., Badachhape, R., Wood, J. and Margrave, J. (1974). Some new synthetic approaches to graphite–fluorine chemistry. *Journal of the Chemical Society, Dalton Transactions*, (12), pp.1268-1273.

Lewis, S., Coleman, N., Booth, S. and Nicholson, J. (2013). Interaction of fluoride complexes derived from glass-ionomer cements with hydroxyapatite. *Ceramics Silikaty*, 57(3), pp.196-200.

Liu, Y., Gu, Z., Margrave, J. and Khabashesku, V. (2004). Functionalization of Nanoscale Diamond Powder: Fluoro-, Alkyl-, Amino-, and Amino Acid-Nanodiamond Derivatives. *Chemistry of Materials*, 16(20), pp.3924-3930.

Mandihally, S. and Matthew, H. (1990). Porous scaffolds for tissue engineering. *Biomaterials*, 20, pp.1133-1142.

Massara, M., Alves, J. and Brandão, P. (2002). Atraumatic Restorative Treatment: Clinical, Ultrastructural and Chemical Analysis. *Caries Research*, 36(6), pp.430-436.

Mickenautsch, S. and Yengopal, V. (2011). Absence of carious lesions at margins of glass-ionomer cement and amalgam restorations: An update of systematic review evidence. *BMC Research Notes*, 4(1).

Molian, P., Janvrin, B. and Molian, A. (1993). Laser chemical vapor deposition of fluorinated diamond thin films for solid lubrication. *Wear*, [online] 165, pp.130-144. Available at: https://www.sciencedirect.com/science/article/pii/004316489390328 [Accessed 7 Apr. 2019].

Muzzarelli, R. (1977). *Chitin*. Oxford: Pergamon Press.

Na, C. and Park, H. (2010). Defluoridation from aqueous solution by lanthanum hydroxide. *Journal of Hazardous Materials*, 183(1-3), pp.512-520.

Nicholson, J. and Amiri, M. (1998). The interaction of dental cements with aqueous solutions of varying pH. *Journal of Materials Science*, 9, pp.549-554.

Okte, Z., Bayrak, S., Fidanci, U. and Sel, T. (2012). Fluoride and aluminum release from restorative materials using ion chromatography. *Journal of Applied Oral Science*, 20(1), pp.27-31.

Orion Research Incorporated (2001). *Fluoride Electrode Instruction Manual*. Beverly, MA, USA: Thermo Orion.

Park, J., Saravanakumar, G., Kim, K. and Kwon, I. (2010). Targeted delivery of low molecular drugs using chitosan and its derivatives. *Advanced Drug Delivery Reviews*, 62(1), pp.28-41.

Patel, S., Omid, N., Zohoori, F., Maguire, A., Waldron, K. and Valentine, R. (2018). Comparison of total ionic strength adjustment buffers III and IV in the measurement of fluoride concentration of teas. *Nutrition and Health*, 24(2), pp.111-119.

Pameijer, CH. (2012). Review article: A review of luting agents. *International Journal of Dentistry*, pp.1-7.

Petri, D., Donegá, J., Benassi, A. and Bocangel, J. (2007). Preliminary study on chitosan modified glass ionomer restoratives. *Dental Materials*, 23(8), pp.1004-1010.

Roeges, N. (1994). *Guide to the Complete Interpretation of Infrared Spectra of Organic Structures*. England: Wiley Publ.: Chichester.

Rošin-Grget, K. and Linčir, I. (2001). Current concept on the anticaries fluoride mechanism of the action. *Collegium Antropologicum*, 25(2), pp.703-712.

Rothwell, M., Anstice, H. and Pearson, G. (1998). The uptake and release of fluoride by ion-leaching cements after exposure to toothpaste. *Journal of Dentistry*, 26(7), pp.591-597.

Sanjuan, B. and Michard, G. (1987). Aluminum hydroxide solubility in aqueous solutions containing flouride ions at 50°C. *Geochimica et Cosmochimica Acta*, 51, pp.1823-1831.

Selig, W. (1970). Potentiometric micro- and semimicro-determination of fluorine in organic compounds. *Fresenius' Zeitschrift for Analytische Chemie*, 249(1), pp.30-34.

Senthil Kumar, R., Ravikumar, N., Kavitha, S., Mahalaxmi, S., Jayasree, R., Sampath Kumar, T. and Haneesh, M. (2017). Nanochitosan modified glass ionomer cement with enhanced mechanical properties and fluoride release. *International Journal of Biological Macromolecules*, 104, pp.1860-1865.

Siné, G., Ouattara, L., Panizza, M. and Comninellis, C. (2003). Electrochemical Behavior of Fluorinated Boron-Doped Diamond. *Electrochemical and Solid-State Letters*, 6(9), p.D9.

Singh, J., Singh, P. and Singh, A. (2016). Fluoride ions vs removal technologies: A study. *Arabian Journal of Chemistry*, 9(6), pp.815-824.

Smith, D. (1982). Buonocore Memorial Lecture. A milestone in dentistry. *Operative Dentistry*, 7, pp.4-25.

Smith, R. and Martell, A. (2004). *NIST Critical Selected Stability Constants of Metal Complexes Database*. Gaithersburg, MD 20899, USA: NIST Standard Reference Database 46, National Institute of Standards and Technology, US Department of Commerce.

Sutton, S., Bender, G. and Marquis, R. (1987). Fluoride inhibition of proton-translocating ATPases of oral bacteria. *Infection and Immunity*, [online] 55(11), pp.2597-2603. Available at: https://www.ncbi.nlm.nih.gov/pubmed/2889674 [Accessed 7 Apr. 2019].

Torabzadeh, H., Ghassemi, A., Janani, A., Raoofinejad, F., Naderi, H. and Akbarzadeh, B. (2015). Effect of Powder/Liquid Ratio on Fluoride Release of Glass Ionomers. *Beheshti University Dental Journal*, [online] 33(1), pp.98-105. Available at: https://www.sid.ir/En/Journal/ViewPaper.aspx?ID=530593 [Accessed 7 Apr. 2019].

Touhara, H. and Okino, F. (2000). Property control of carbon materials by fluorination. *Carbon*, 38(2), pp.241-267.

Upadhyay, S., Rao, A. and Shenoy, R. (2013). Comparison of the Amount of Fluoride Release from Nanofilled Resin Modified Glass Ionomer, Conventional and Resin Modified Glass Ionomer Cements. *Journal of Dentistry (Tehran, Iran)*, [online] 10(2), pp.134-140. Available at: https://www.ncbi.nlm.nih.gov/pubmed/23724212 [Accessed 7 Apr. 2019].

Vivek Vardhan, C. and Srimurali, M. (2016). Removal of fluoride from water using a novel sorbent lanthanum-impregnated bauxite. *SpringerPlus*, 5(1).

Wahab, F., Shellis, R. and Elderton, R. (1993). Effects of low fluoride concentrations on formation of caries-like lesions in human enamel in a sequential-transfer bacterial system. *Archives of Oral Biology*, 38(11), pp.985-995.

Wilson, A. and McLean, J. (1988). *Glass ionomer cement*. Chicago, IL, USA: Quintessence Publishing Co.

Wilson, A., Groffman, D. and Kuhn, A. (1985). The release of fluoride and other chemical species from a glass-ionomer cement. *Biomaterials*, 6(6), pp.431-433.

Yakovlev, R., Osipova, A., Solomatin, A., Kulakova, I., Murav'eva, G., Avramenko, N., Leonidov, N. and Lisichkin, G. (2015). An approach to unification of the physicochemical properties of commercial detonation nanodiamonds. *Russian Journal of General Chemistry*, 85(6), pp.1565-1574.

Yan, Z., Sidhu, S., Mahmoud, G., Carrick, T. and McCabe, J. (2007). Effects of Temperature on the Fluoride Release and Recharging Ability of Glass Ionomers. *Operative Dentistry*, 32(2), pp.138-143.

Yli-Urpo, H., Lassila, L., Närhi, T. and Vallittu, P. (2005). Compressive strength and surface characterization of glass ionomer cements modified by particles of bioactive glass. *Dental Materials*, 21(3), pp.201-209.

CHAPTER 9

CELL VIABILITY ASSAY OF 3T3 BALB/C FIBROBLASTS, EXPOSED TO DILUENTS FROM CHITOSAN- AND NANODIAMOND-MODIFIED GLASS IONOMER RESTORATIVE CEMENTS

9.1. Abstract

Background: With glass ionomer materials being considered as biomaterials, the interactions with living cells are important. Cell viability assessments provide insight to the potential cellular interaction with the dental pulp.

Materials and methods: A cell viability assay was done by exposing mouse 3T3 Balb/c fibroblast cells to diluents from fifteen glass ionomer restorative cements, Biodentine as the positive control and Dulbecco Modified Eagle's medium (DMEM) *(Hyclone, GE Healthcare Sciences, Utah, USA, Lot AD16496263)* which served as the control. The diluents were produced for the indirect contact technique on 3T3 cells by allowing sterile GIC and Biodentine specimens (6±1mm high and 4±1mm in diameter) to elude ions into sterile DMEM medium for three different time periods namely 0-1 days, 1-7 days and 7-21 days. The direct contact technique was used to evaluate the morphology of 3T3 cells on the side of the material as well as on the surface of the material. The material sample used was 3 mm in diameter and 1 mm thick. This direct contact technique allowed the visualisation and assessment of the morphology of the 3T3 cells at 24 or 72 hours with an inverted microscope at the side of the materials. Subsequent to inverted microscopy, these samples were prepared with a modified technique using sodium cacodylate trihydrate for SEM analysis. SEM images were used to evaluate the morphology of the 3T3 cells on the surface of the specimen at 150x magnification to assess the cell distribution on the surface and then at 750x for the morphology assessment of the 3T3 cells. The analysis of

the images obtained from the inverted microscope and SEM were completed by a blinded investigator.

The statistical analysis of the indirect contact technique was completed by comparing the control growth of the 3T3 cells exposed to DMEM medium with the GICs- and Biodentine diluents. The one-way ANOVA with post-hoc Holm result was completed. A p-value less than 0.05 indicated that significant differences were present.

Results: The direct contact assessment indicated the loss of stable adhesion of the 3T3 cells for the FN materials at the lamellum. Most of the 3T3 cells for KU and RSC did not present with lamellipodia or filopodia, but the nuclei of all the cells were much larger than other 3T3 cells. Lysis of the 3T3 cells on the GIC surface was present. There were significant differences in cell viability between most of the GIC-diluents and the 3T3 cells. Biodentine showed a significant increase in cell viability for all three time periods.

Conclusion: The differences in crystal precipitation were due to the interaction of the chemicals used in the fixing technique and the chemistry of the set Biodentine. The sodium cacodylate trihydrate and ethanol was not an appropriate fixing technique for the Biodentine samples. The sodium cacodylate trihydrate has been used successfully for GICs and 3T3 cells, but it is advised that the ethanol evaporation used in this dissertation, is substituted with a critical drying unit. The critical drying unit will prevent the formation of the crystals that formed as in the studies conducted in this dissertation due to the slow evaporation of the ethanol (because the critical drying unit was not used). The 3T3 cells that were investigated on the GIC materials under SEM illustrated that all the 5%ND-modified GICs had 3T3 cells with more defined lamellipodia and filopodia compared to the control materials. The cell viability for the 3T3 cells exposed to the FN diluents was greater for days 1, 7 and 21 compared to the positive control diluents of

Biodentine. Two materials i.e. RSC5%CH and RSC10%CH retained a decreased cell viability at day 21 compared to the 3T3 control cells.

Keywords: 3T3 Balb/c fibroblast; cell viability, Biodentine, Glass ionomer cement, Sodium cacodylate trihydrate, Fuji IX, Rive Self Cure, Ketac Universal.

9.2. Introduction

The use of fibroblasts (mouse 3T3 Balb/c embryo fibroblast cell line) has become one of the recommended cell lines for the assessment of cell viability and is a standard technique for dental materials (ISO 10993–10995:2008; ISO 7405). MTT (3-(4,5-dimethylthiazol-2-yl)-2,5-diphenyltetrazolium bromide) colorimetric assay has been successfully used to study the cell viability after 3T3 cells were exposed to dentine bonding agents (Moodley *et al*., 2004; Grobler *et al*., 2008) and dental composite monomers (Geurtsen *et al*., 1998).

The hypothesis of the study was that the chitosan and nanodiamond-modified glass ionomer restorative cements would have a similar cellular viability as their respective control materials.

9.3. Materials and Methods

9.3.1. Summary of procedure

In the present study, a cell viability assay with the use of MTT (3-(4,5-dimethylthiazol-2-yl)-2,5-diphenyltetrazolium bromide) was done by exposing mouse 3T3 Balb/c fibroblast cells (*The National Repository for Biological Materials, Sandringam, South Africa).* The 3T3 cells would be plated in a 96-well plate followed by the addition of the various diluents. The test diluents were fifteen GIC-diluents and the positive control was a Biodentine diluent. Sterile DMEM (*Hyclone, GE Healthcare Sciences, Utah, USA, Lot AD16496263)* was used as a control.

Five GIC and Biodentine samples of each material were made in a Teflon mould (6±0.1mm height and 4±0.1mm), sterilized with ethylene oxide gas and exposed to the 5ml of sterile DMEM medium (*Hyclone, GE Healthcare Sciences, Utah, USA, Lot AD16496263*) for three different time periods namely 0-1 days, 1-7 days and 7-21 days in sterile centrifuge tubes. At the end of each time period (end of day 1; end of day 7 and end of day 21) the centrifuge tube with diluents containing either the GIC or Biodentine samples were vortexed for 3 seconds. The GIC and Biodentine samples were removed from the centrifuge tube with sterile tweezers and the materials placed into new sterile centrifuge tubes containing 5ml of fresh sterile DMEM medium. Over the course of these three time periods (1 day, 7 days and 21 days), the exposure of the GIC or Biodentine to the DMEM medium allowed elution of ions from the GIC or Biodentine into the DMEM medium to form the diluent. 900µl of this newly formed GIC or Biodentine diluent was then used to assess the effect of the ions that eluted from the GIC or Biodentine on the 3T3 cells. In total, 900µl of the GIC or Biodentine diluent was used for the cell viability study on the fibroblasts, since it was conducted in triplicate using the MTT colimetric assay.

9.3.2. MTT colorimetric assay

The MTT (3-(4,5-dimethylthiazol-2-yl)-2,5-diphenyltetrazolium bromide) assay as described by Mosmann (1983) has been used extensively as a colorimetric assay to measure cell viability, proliferation and the activation of cells. The MTT assay works on the principle that the purple formazan formed by mitochondria is directly proportional to the amount of viable cells that are still active and proliferating (Mosmann, 1983).

9.3.3. Cell viability assay on 3T3 Balb/c fibroblasts

3T3 Balb/c fibroblasts cell culture

The 3T3 Balb/c fibroblasts were cultured under standard conditions at 37ºC with a 5% CO_2 atmosphere at 95% humidity in a sterile petri dish with sterile DMEM medium (*HyClone, SH30243.01, USA*). The medium was supplemented with a 10% fetal bovine serum, 1% penicillin and 1% streptomycin *(Sigma, P4333)* in order to retain the cell viability and prevent any growth of pathogens. The Balb/c 3T3 fibroblasts were sub-cultured as soon as a strong growth phase at approximately 80-90% confluence was reached. In order to remove the attached 3T3 cells from the bottom of petri dish they were trypsinised (*Sigma, SV30031.01*) and 100 µl plated out in each well of a 96-well plate at a concentration of $3x10^5$cells/ml. Incubation of the 3T3 cells in the 96-well plate was completed over 24 hours to allow attachment of the 3T3 cells to the well plates as cited by Basak *et al*. (2016). For each MTT assay assessment 300µl of the GIC or Biodentine diluents from each centrifuge tube was pipetted after a 3 second vortex and was equally divided between three wells. No adjustments were made to the pH values as per Chapter 8 before adding the 100µl to each well. It was essential to use the diluents with the pH as is, because in the tooth the pulp cells will be exposed to a non-adjusted pH. Fifteen control wells contained a total of 1500µl sterile DMEM medium that was equally divided between 15 wells, with each well containing 100µl. Each 96-well plate therefore consisted of a group of materials (eg. FN, FN5%ND, FN10%ND, FN5%CH and FN10%CH) as well as fifteen control wells (Figure 9.1). The 96-well plates with 3T3 cells received GIC-diluents and the control DMEM diluents. The Biodentine diluents and fifteen control wells were plated on one 96-well plate for day 1, 7 and 21. All the prepared 96-well plates with 3T3 cells exposed to diluents were incubated for 24 hours, to allow the diluent to have its effect on the 3T3 cells (Doyke and Griffiths, 1998). All the diluents and DMEM was added to the 3T3 cells once they reached room temperature, to prevent thermal shock of the 3T3 cells.

Figure 9.1: Distribution of the material diluents on the 96-well plate and the control 3T3 cells

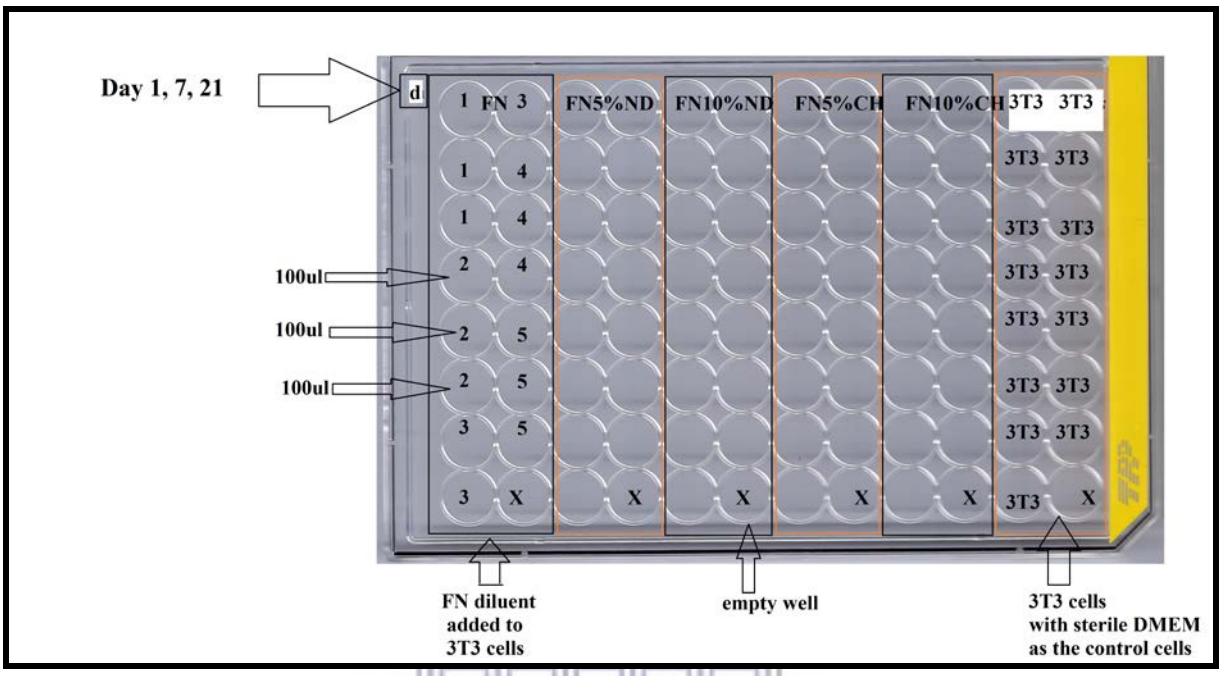

Cell viability assays

The cell viability assays was completed in accordance with an established method (Doyke and Griffiths, 1998). MTT stock solution was prepared as per the manufacturer instructions where 5mg/ml (*Sigma MTT, M5655, USA*) was prepared in phosphate buffered saline (*Merck, D8537, USA*) at a pH7.5 and filtered through a 0.22µ filter. At the end of the 24-hour incubation period, 10µl of MTT (5mg/ml) was added to the monolayer of cells that formed on the bottom of the 96-well plate to allow the mitochondria in the viable cells that were still active and proliferating to convert the yellow, water soluble MTT (3-(4,5-dimethylthiazol-2-yl)-2,5-diphenyltetrazolium bromide) into an insoluble, dark purple formazan. After 3 hours of incubation at 37ºC, 100µl of Dimethyl Sulfoxide (DMSO) (*Merck, Hibri-max D2650, USA*) was added to each well to allow the extraction of the purple/blue formazan crystals from the viable cells. Within 5 minutes of adding the DMSO, the measurements were taken with a dual wave spectrophotometer (*Smart*

Microplate Reader, Model SMR16.1. USCN life science kit Inc, Wahan, China) at a test wavelength of 570nm and a reference wavelength of 630nm (Doyke and Griffiths, 1998).

The relative cell viability of the 3T3 cells exposed to the diluents were calculated as a percentage using the following formula: [100 / (Optical density of the control 3T3 cells x Optical density of the GIC or Biodentine 3T3 cells)] –100.

This formula allowed the results to be presented as a positive percentage for cell viability above the control 3T3 cells and a negative percentage indicating a decrease of cell viability below the control 3T3 cells.

9.3.4. Direct contact evaluation

In addition to the cell viability assay with MTT, four GIC or Biodentine disc-shaped specimens (3 mm in diameter and 1 mm thick) were constructed from each material in Teflon moulds. This 3x1mm sample allowed visualisation of the material margin under inverted microscopy and was used successfully in Chapter 11 for the gradient weight percentage of the GIC materials. They were finished with a 1200 grit wet silicon carbide paper on both sides and sterilised with ethylene oxide gas (*Steri-Vac 4XL gas sterilizer, Model 400DGP, 3M centre, St Paul, MN, USA*). One sample per well in a 12-well plate was seeded with $3x10^5$ 3T3cells/ml and the remainder of the well was carefully filled with DMEM medium. It was filled with DMEM medium to allow growth of the 3T3 cell with the only variable factor being the direct contact of the 3T3 cells to the material and the medium. The effect of the material on the morphology of the 3T3 cell in direct contact with the material was the objective of this investigation. After 24 hours two samples from each material was randomly selected for visualisation and the other two retained in the incubator to be visualised at 72 hours. The light microscope (*Olympus CK2*

inverted microscope, Olympus Life Sciences, USA) at 10x magnification was used to take photos (*Zeiss Axiocam ERc5s digital camera, GmbH*) to assess the 3T3 cells at the edge of the GIC material. The GIC was removed from the well plate and prepared for SEM analysis of the 3T3 cells on the surface. The SEM images were used to evaluate the morphology of the 3T3 cells on the surface of the specimens at 150x magnification to assess the cell distribution (on the material surface) and then at 750x for the morphology assessment of the 3T3 cells. All the image analysis of the inverted microscope and SEM were completed by the blinded investigator. The image analysis of the inverted microscope and the SEM was completed by a blinded investigator. The criteria used were described in an analysis by Al-Hiyasat *et al*. (2010). Cell attachment was assessed based on the presence and shape of the filopodia (cylindrical or conical in length); lamellipodia (flat extensions or extensions that were elevated from the surface) and the density/translucency of the cells (low or high) (Al-Hiyasat *et al*., 2010).

9.3.5. Fixing technique for Scanning Electron Microscopy (SEM) of 3T3 cells

A study by Camilleri *et al*. (2004) found that the preparation of samples for SEM was important as it could influence the material as well as the cells that required investigation (Camilleri *et al*., 2004). The chemical sodium cacodylate trihydrate is also called cacodylate or cacodylic acid was used in lieu of Osmium.

For cellular investigation the buffers are normally used at 0.1 molar (https://www.laboratoryresource.com/?navaction=getitem&id=45).

To make up a 0.1 molar solution:

- 100mL of distilled water was placed in a 200mL volumetric flask and 2.15g of Sodium cacodylate trihydrate (*Merck, C4945, USA*). The powders are allowed to dissolve by adding a magnetic stirring bar at the maximum rotational speed.

- Once dissolved, the natural pH of the solution was 7.77 and adjusted with HCl to a pH of 7.2. (https://www.laboratoryresource.com/?navaction=getitem&id=45)

A modified technique with the sodium cacodylate trihydrate at a 0.1molar solution was used in lieu of Osmium. Additionally ethanol was used in lieu of a critical point dryer as described by Ibrahim *et al*. (2017). The research laboratory did not have a critical point dryer and sodium cacodylate trihydrate had a low chance of forming a precipitate on the samples if all the phosphate buffered saline was not removed completely at the rinsing steps. GICs have an affinity for phosphorus and there was a risk of precipitate formation.

The modified fixing procedure for SEM analysis:

- Multiple well plates were used between the various steps to avoid contamination with the chemicals used at different stages of the fixing procedure.
- New well plates used. GIC specimens with 3T3 cells were held (on the sides) with tweezers and gently dipped five times in sterile phosphate-buffered saline (PBS) (Ibrahim *et al*., 2017) to stabilise the cell membrane of the 3T3 cells.
- The samples were placed in new 12-well plates and completely immersed with 2.5% gluteraldehyde/PBS for 4 hours (Ibrahim *et al*., 2017) at room temperature of 25ºC.
- New well plates used. The samples were gently dipped five times in sterile PBS and left for 10 minutes in the PBS (Ibrahim *et al*., 2017).
- New well plates used. The samples were once again gently dipped five times in new sterile PBS and left for another 10 minutes (Ibrahim *et al*., 2017).
- In new 12-well plates the samples were placed in the 0.1 molar Sodium cacodylate trihydrate for one hour. Ibrahim *et al*. (2017) used 1% osmium tetroxide.

- The samples were gently dipped five times in sterile PBS and left in the 12-well plates for 10 minutes in the PBS.
- The samples were once again gently dipped five times in new sterile PBS and left in the new 12-well plates for another 10 minutes in the PBS.
- New well plates used. The samples were gently dipped five times in sterile distilled water (Ibrahim *et al*., 2017).
- In order to start the drying process because no critical dryer device was available the specimens were then exposed to a graded ethanol/distilled water dehydration at room temperature with a 25% ethanol mixture until such time that it evaporated to below the top of the specimen surface.
- The samples were removed from the well plate and placed in another well plate with 100% ethanol until it was evaporated.
- The samples were subjected to another round of 100% ethanol evaporation.
- The samples were transferred to new well plates and kept at room temperature for one week until the samples were gold sputtered to increase the electrical conductivity of the sample for SEM analysis.

9.4. Statistical analysis

In order to compare the control growth of the 3T3 cells with the GIC diluents or the Biodentine diluents, the one-way ANOVA with post-hoc Holm result was completed. A p-value < 0.05 indicated significance.

9.5. Results

Effect of different dental materials on cell viability

The control 3T3 cell growth was set at 0% and the values represented in Tables 9.1 and 9.2 therefore either indicate cell viability ("+") with a percentage greater than the control 3T3 cells or ("-")indicating cell viability at a percentage less than the control 3T3 cells.

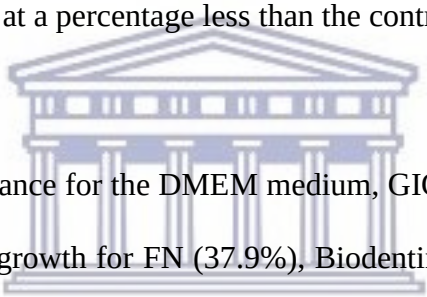

Table 9.1 indicates the significance for the DMEM medium, GICs- or Biodentine diluent for day 1 that resulted in the 3T3 cell growth for FN (37.9%), Biodentine (21.14%) and RSC (19.57%). The KU diluent resulted in a non-significant decrease in cell viability of -5.11% in relation to the control 3T3 cells. The diluent of day 7 indicated a significant ($p < 0.05$) increase in 3T3 cells for FN (49.19%), KU (42.28%) and Biodentine (18.68%) (Figures 9.2, 9.3, 9.4 and 9.5). The RSC diluent resulted in a non-significant negative cell viability of -5.08% at day 7. The KU diluent of day 21 presented with a 100.73% increase in 3T3 cell viability followed by RSC (44.56%), FN (37.29%) and Biodentine (28.9%).

Table 9.1: Cell viability percentage of the materials in relation to the 3T3 control cells

Material	Material			
	Biodentine	FN	KU	RSC
Day 1 3T3 fibroblasts	21.14^	37.90*	-5.11	19.57^
Day 7 3T3 fibroblasts	18.68*	49.19*	42.28*	-5.08
Day 21 3T3 fibroblasts	28.90*	37.29^	100.73*	44.56*
(*): Indicates significant differences ($p < 0.01$) for 3T3 cell viability percentage. (^): Indicates significant differences ($p < 0.05$) for 3T3 cell viability percentage.				

Figure 9.2: Biodentine cell viability for days 1, 7 and 21

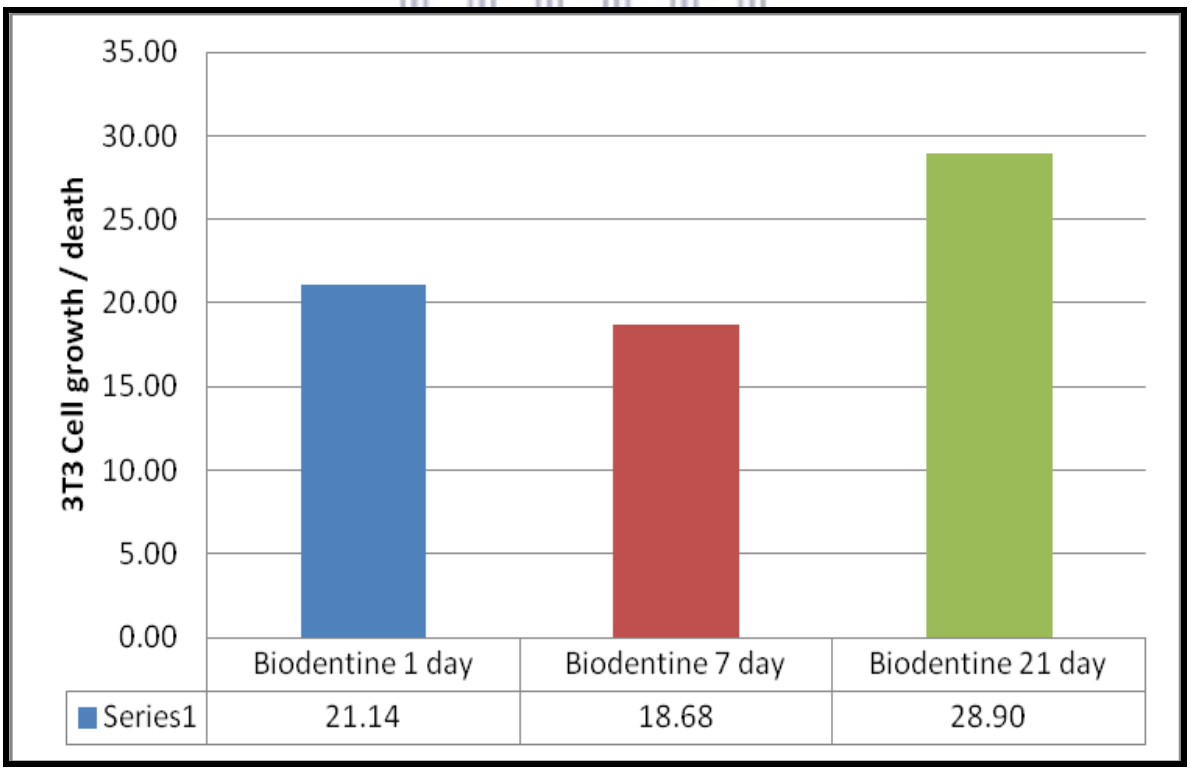

Figure 9.3: FN cell viability for days 1, 7 and 21

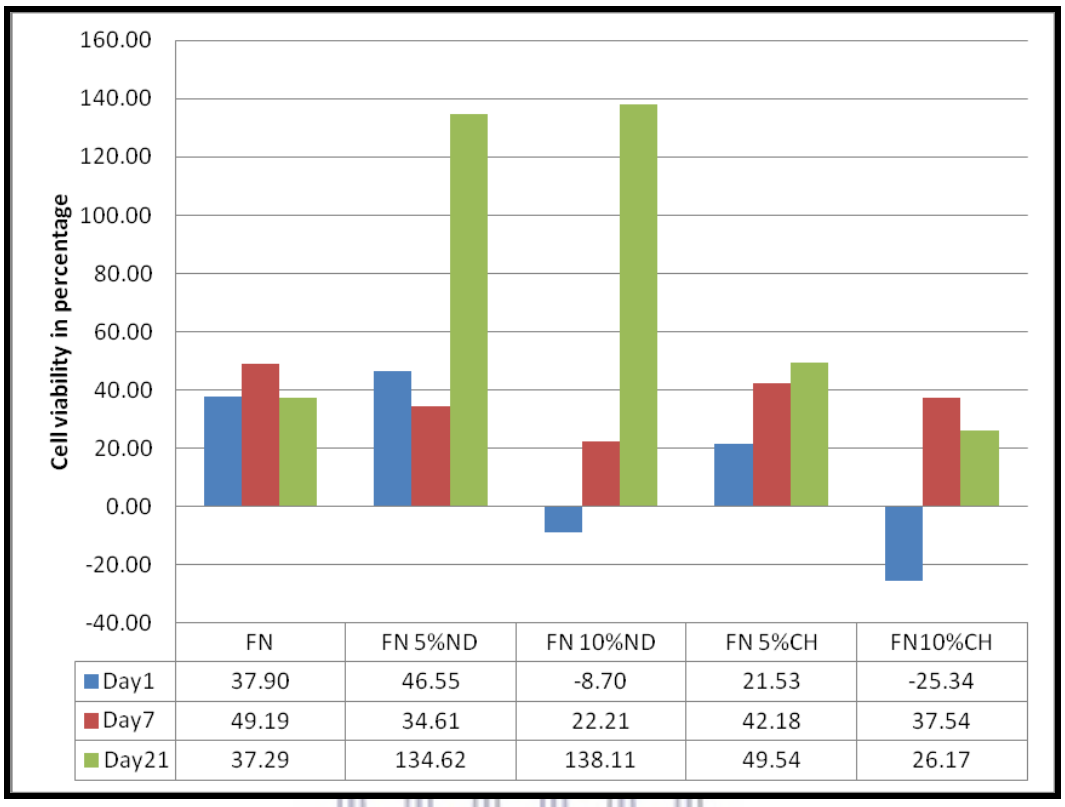

	FN	FN 5%ND	FN 10%ND	FN 5%CH	FN10%CH
Day1	37.90	46.55	-8.70	21.53	-25.34
Day7	49.19	34.61	22.21	42.18	37.54
Day21	37.29	134.62	138.11	49.54	26.17

Figure 9.4: KU cell viability for days 1, 7 and 21

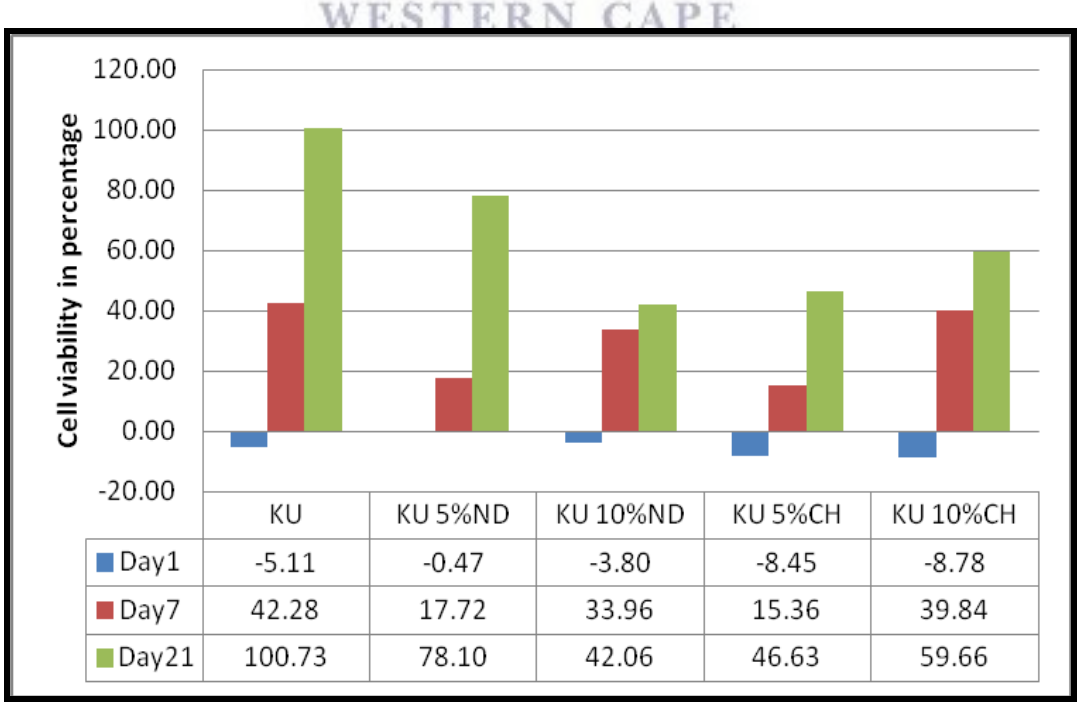

	KU	KU 5%ND	KU 10%ND	KU 5%CH	KU 10%CH
Day1	-5.11	-0.47	-3.80	-8.45	-8.78
Day7	42.28	17.72	33.96	15.36	39.84
Day21	100.73	78.10	42.06	46.63	59.66

Figure 9.5: RSC cell viability for days 1, 7 and 21

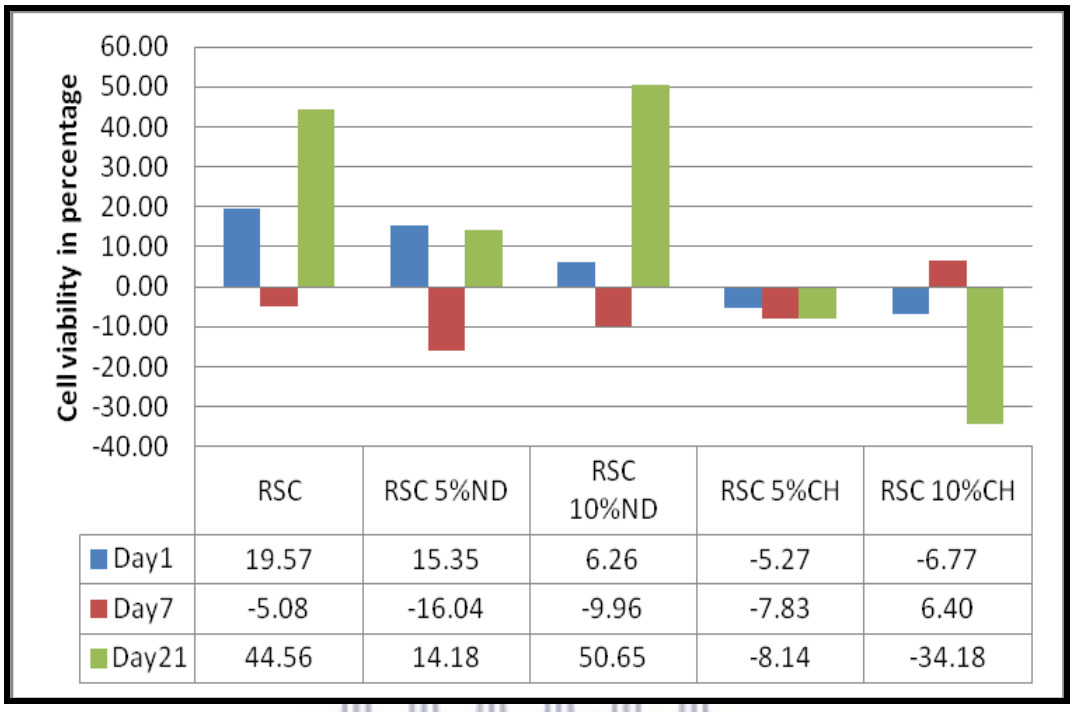

	RSC	RSC 5%ND	RSC 10%ND	RSC 5%CH	RSC 10%CH
Day1	19.57	15.35	6.26	-5.27	-6.77
Day7	-5.08	-16.04	-9.96	-7.83	6.40
Day21	44.56	14.18	50.65	-8.14	-34.18

Table 9.2: Cell viability percentage for FN, KU and RSC materials with their respective chitosan- and nanodiamond-modifications in relation to the 3T3 control fibroblasts

	Material				
	FN	**FN5%ND**	**FN10%ND**	**FN5%CH**	**FN10%CH**
Day 1 3T3 fibroblasts	37.90*	46.55*	-8.70	21.53^	-25.34^
Day 7 3T3 fibroblasts	49.19*	34.61*	22.21^	42.18*	37.54*
Day 21 3T3 fibroblasts	37.29	134.62*	138.11*	49.54^	26.17
(*): Indicates significant differences ($p < 0.01$) for 3T3 cell viability percentage. (^): Indicates significant differences ($p < 0.05$) for 3T3 cell viability percentage.					

	Material				
	KU	**KU5%ND**	**KU10%ND**	**KU5%CH**	**KU10%CH**
Day 1 3T3 fibroblasts	-5.11	-0.47	-3.80	-8.45	-8.78*
Day 7 3T3 fibroblasts	42.28*	17.72	33.96*	15.36	39.84*
Day 21 3T3 fibroblasts	100.73*	78.10*	42.06*	46.63*	59.66*
(*): Indicates significant differences ($p < 0.01$) for 3T3 cell viability percentage. (^): Indicates significant differences ($p < 0.05$) for 3T3 cell viability percentage.					

	Material				
	RSC	**RSC5%ND**	**RSC10%ND**	**RSC5%CH**	**RSC10%CH**
Day 1 3T3 fibroblasts	19.57	15.35	6.26	-5.27	-6.77^
Day 7 3T3 fibroblasts	-5.08	-16.04*	-9.96*	-7.83^	6.40
Day 21 3T3 fibroblasts	44.56*	14.18	50.65*	-8.14	-34.18^
(*): Indicates significant differences ($p < 0.01$) for 3T3 cell viability percentage. (^): Indicates significant differences ($p < 0.05$) for 3T3 cell viability percentage.					

When compared with the 3T3 control cells' viability, the results from Table 9.2 illustrate that the GIC-diluents of all the FN materials and the chitosan and nanodiamond modifications, increased the 3T3 cells viability for all the days (1, 7 and 21) except for FN on day21, FN10%ND day on 1 and FN10%CH on day 21 (Figure 9.3).

All the KU materials resulted in a decrease in the cell viability in relation to the 3T3 control cells for day 1. Day 7 indicated an increase in cell viability although only KU, KU10%ND and KU10%CH presented with significantly more viable cells in comparison to the 3T3 control cells ($p < 0.05$) (Figure 9.4).

For day 1, the diluents of RSC (19.57%) had the highest percentage of viable cells followed by RSC5%ND (15.35%) and RSC10%ND (6.26%). Both the chitosan modifications presented with a decrease in cell viability, but only RSC10%CH (-6.77) presented with a significant reduction in 3T3 cell viability in relation to the control 3T3 cells. On the contrary, for day 7, RSC10%CH was the only material from the RSC material group that presented with an increase in cell viability of the 3T3 cells. At day 21, the chitosan- modified RSC GICs presented with negative cell viability in relation to the 3T3 control cells.

Cell morphology in response to different dental materials

3T3 direct contact with materials

The interaction of the 3T3 cells were visually assessed at the margins of the GICs and Biodentine at 24 and 72 hours.

The lamellipodium is a cytoskeletal projection that is the leading edge of the cell. It is used to propel the cell forward. The “lamina” is Latin for thin sheet and the “pod” is foot (Figures 9.6 and 9.7).

The filopodium is the slender and sometimes long cytoplasmic projection that serves as an extension to the lamellipodium. The filopodium provides focal adhesions between the cell and the surface of the material (Figures 9.6 and 9.7).

Figure 9.6: 3T3 cell with annotations

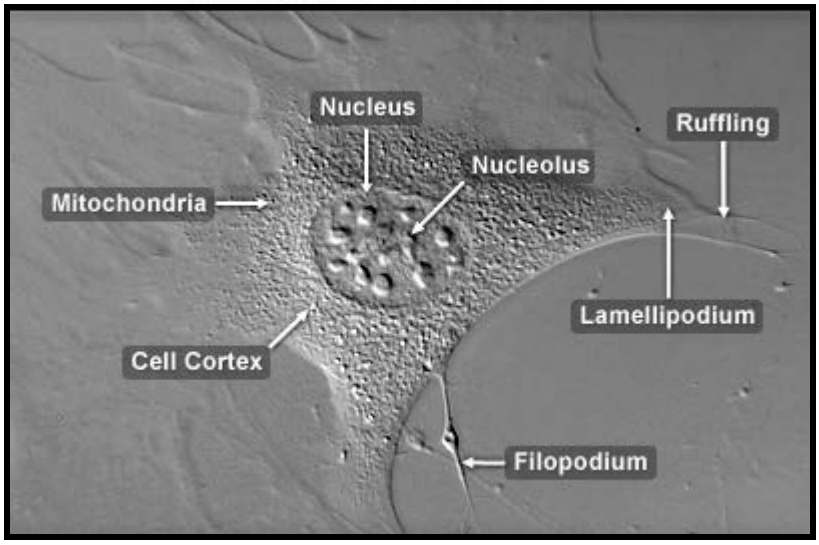

(*Image and video may be used in this dissertation courtesy of Nikon*).

Follow the link below to view the video on the motility of a 3T3 Cells

https://www.microscopyu.com/gallery-images/albino-swiss-mouse-embryo-fibroblasts-3t3-line

Figure 9.7: Graphical illustration of the structural components of a 3T3 cell

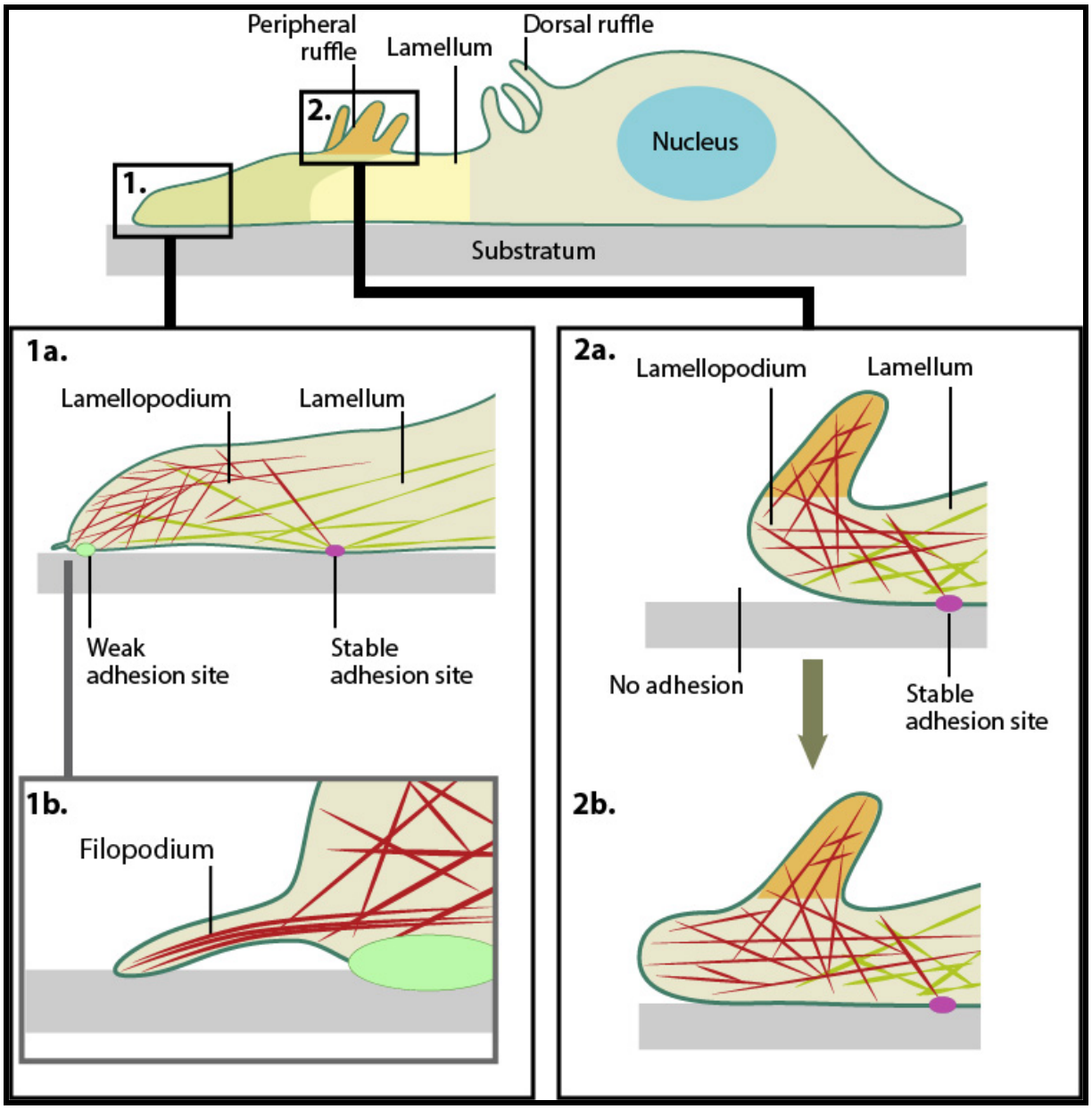

(*Image may be used in this dissertation courtesy of The National University of Singapore, 2009 – 2018. Creative Commons Attribution-NonCommercial-ShareAlike 4.0 International License.* Obtained from: https://www.mechanobio.info/cytoskeleton-dynamics/what-are-lamellipodia-and-lamella/what-is-the-role-of-the-lamellipodia-in-mechanosensing-and-cell-motility/).

Figure 9.8: Control 3T3 cells of this dissertation in subconfluent

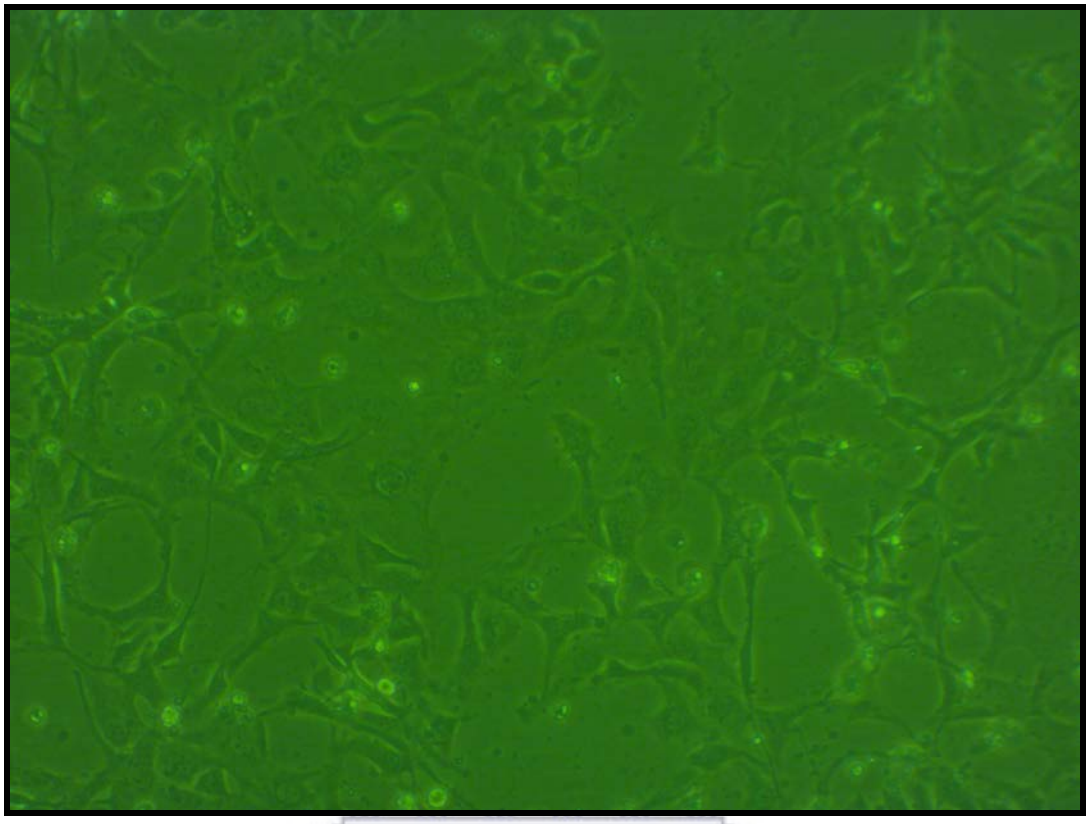

The 3T3 cells present with sheet-like extensions of the lamellipodia that are extensive and are in contact with other 3T3 fibroblasts. The filopodia have both cylindrical and conical extensions. The nucleus is visible in the sheet like cells as well as in the stellate cells. There are spindle-shaped cells present, as per the video link above. It clearly illustrates that the cells could be stellar or spindle-shaped, depending on the movement of the 3T3 cell.

Figure 9.9: Control 3T3 cells of this dissertation at postconfluent

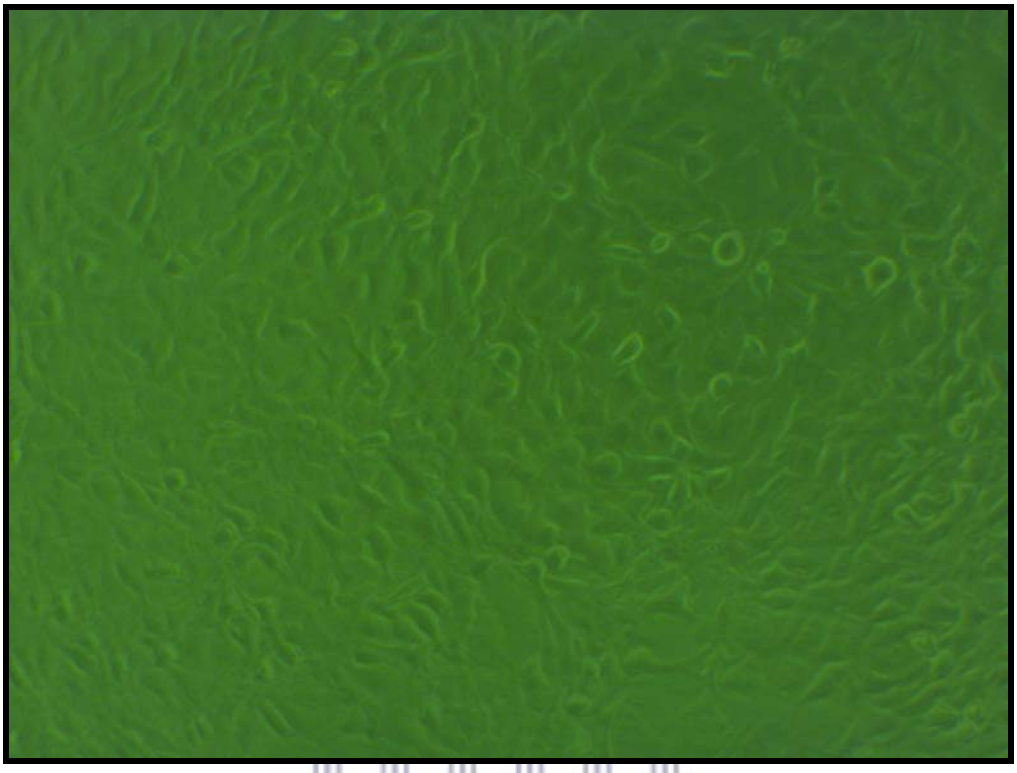

The cells do not have a spindle or stellar shape. Once the 3T3 cells reach confluence, they become epithelioid.

Figure 9.10: Control 3T3 cells of this dissertation at 24 hours with a 50x zoom

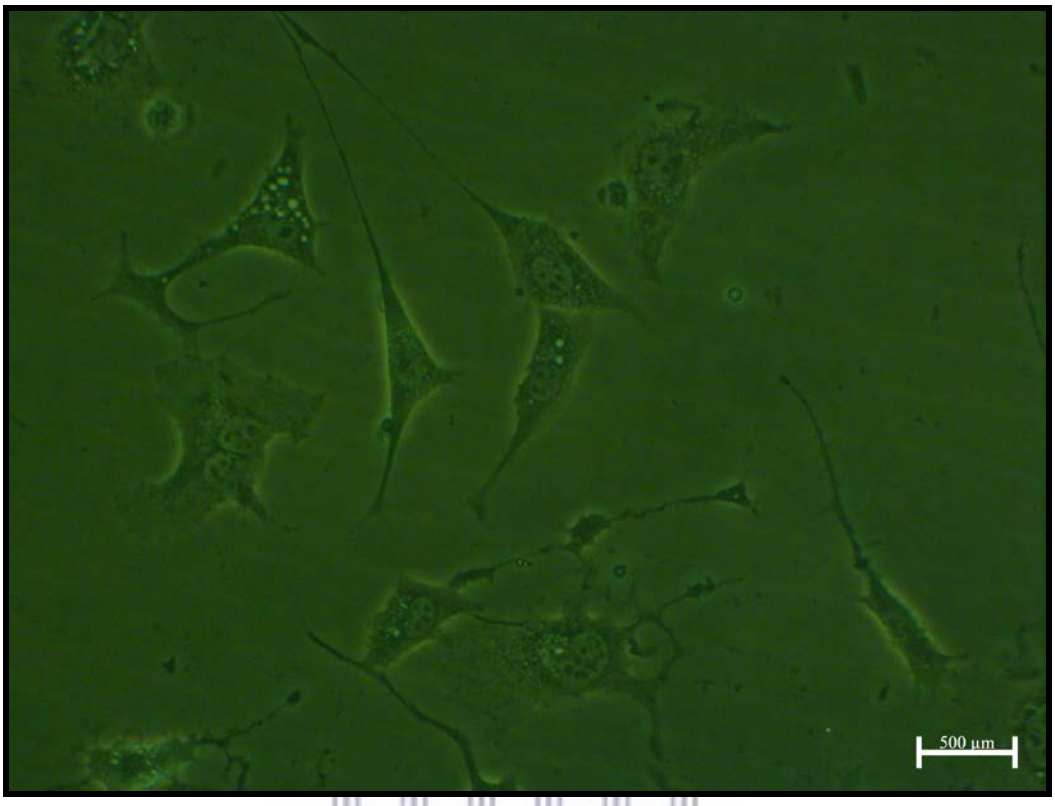

In the present study, stellate and spindle-shaped 3T3 cells with a visible nucleus could be noted. The lamellipodia and fibroblasts are well developed and 3-4 times the length of the 3T3 cell.

Figure 9.11: SEM image of 3T3 cells on the surface of FN at 24 hours

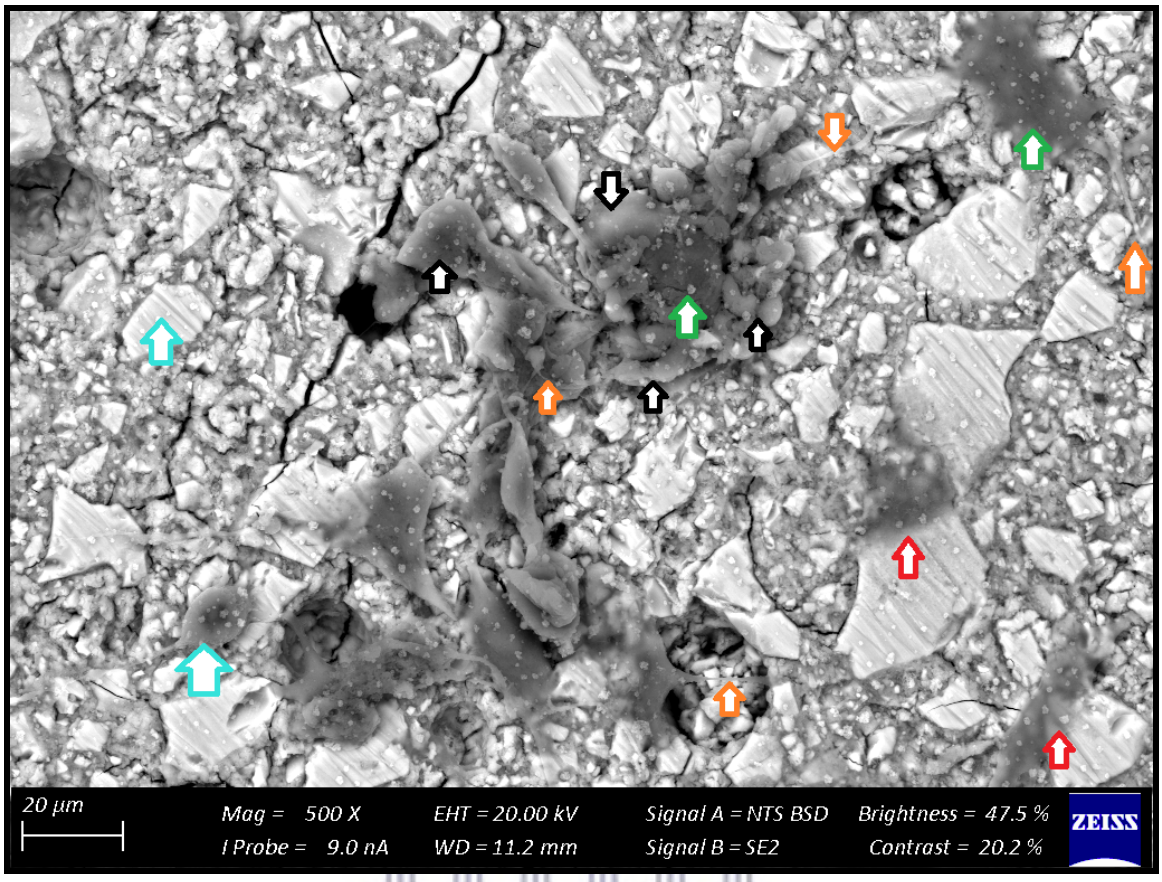

The turquoise arrows indicate the crystal precipitation from the SEM fixing process. The crystal precipitation on the samples for SEM analysis did not present with the same small crystalline contamination on all the samples and varied between the GICs and the Biodentine materials. The crystal precipitations in the GICs were due to the ethanol drying process. The small crystalline contamination of FN was equally distributed on the surface of FN as well as on the 3T3 cells. Red arrows show cells with a lower cellular density (greater translucency) compared to the green arrows that indicate a higher cell density. The black arrows indicate the loss of stable adhesion for the lamellum (see Figures 9.6 and 9.7 for annotations). They also indicate that the lamellopodium is folded inward towards the cell nucleus. The 3T3 cell on far right, indicated by the green arrow, still has a stable adhesion of the lamellum. Additionally the orange arrow indicates the filopodia are cylindrical and double the length of the 3T3 cell.

Figure 9.12: SEM image of 3T3 cells on the surface of FN at 72 hours

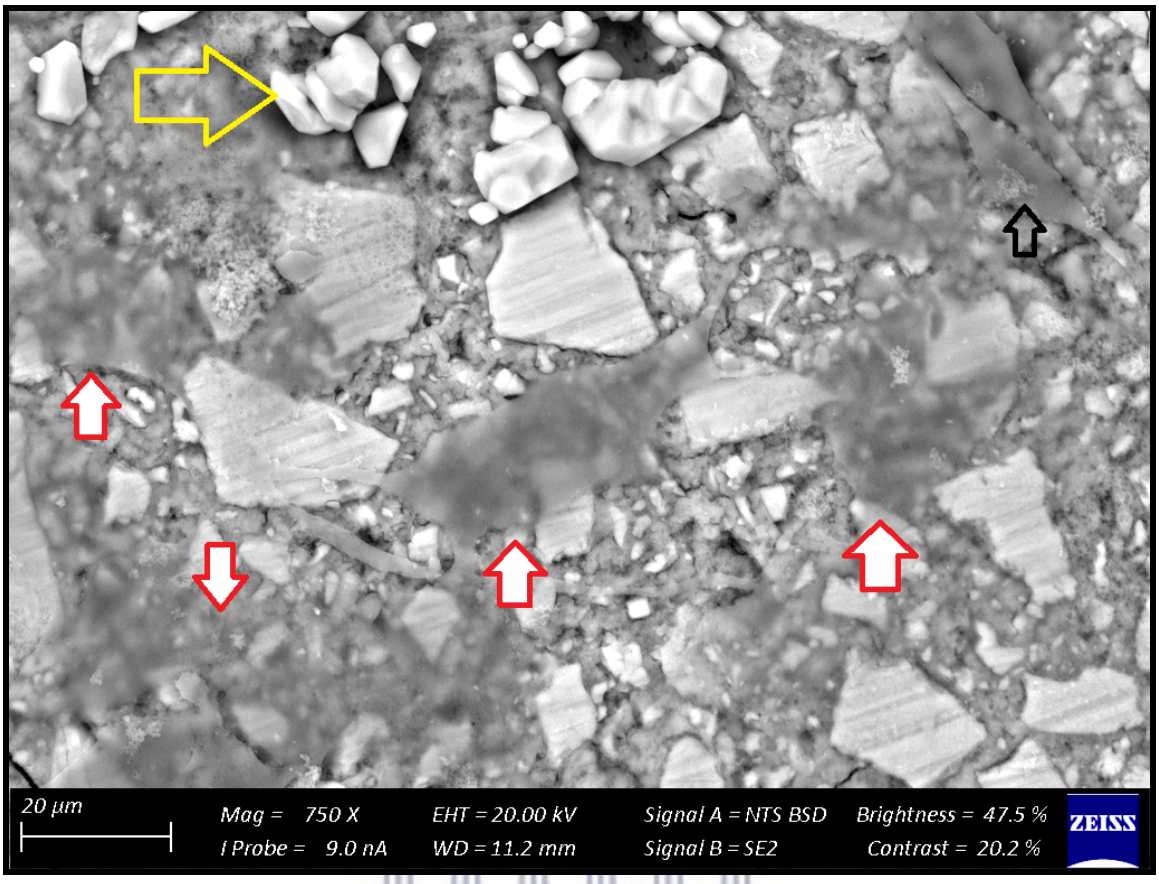

The yellow arrow represents large crystal precipitation from the ethanol drying process. At 72 hours, the 3T3 cells (indicated by the red arrows) presented with an even lower cellular density compared to the FN SEM at 24 hours (Figure 9.11). This is due to the filler particles that can be seen through the 3T3 cells. The general shape varied between stellate (red arrows) and spindle (empty black arrow), indicating that cell mobility was still present at 72 hours with the lamellopodium presenting with filopodia that joined the 3T3 cells together. This indicated that the cells had a greater viability than the 24-hour sample, despite the translucency.

Figure 9.13: Inverted microscope image of 3T3 cells on the surface of FN10%ND at 24 hours

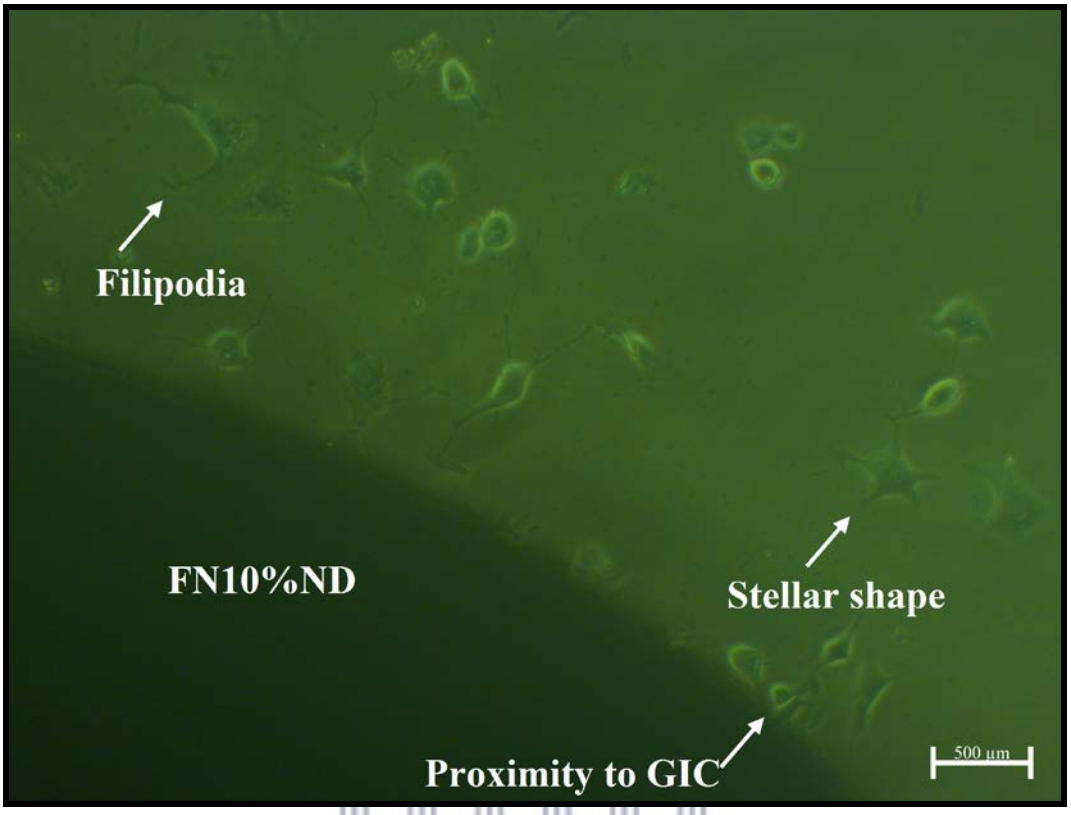

There were multiple 3T3 cells in the proximity of the FN10%ND GIC at 24 hours. Wide and long lamellopodia were present as well as conical or cylindrical filipodia up to twice the length of the 3T3 cell.

Figure 9.14: SEM image of 3T3 cells on the surface of FN10%ND at 72 hours

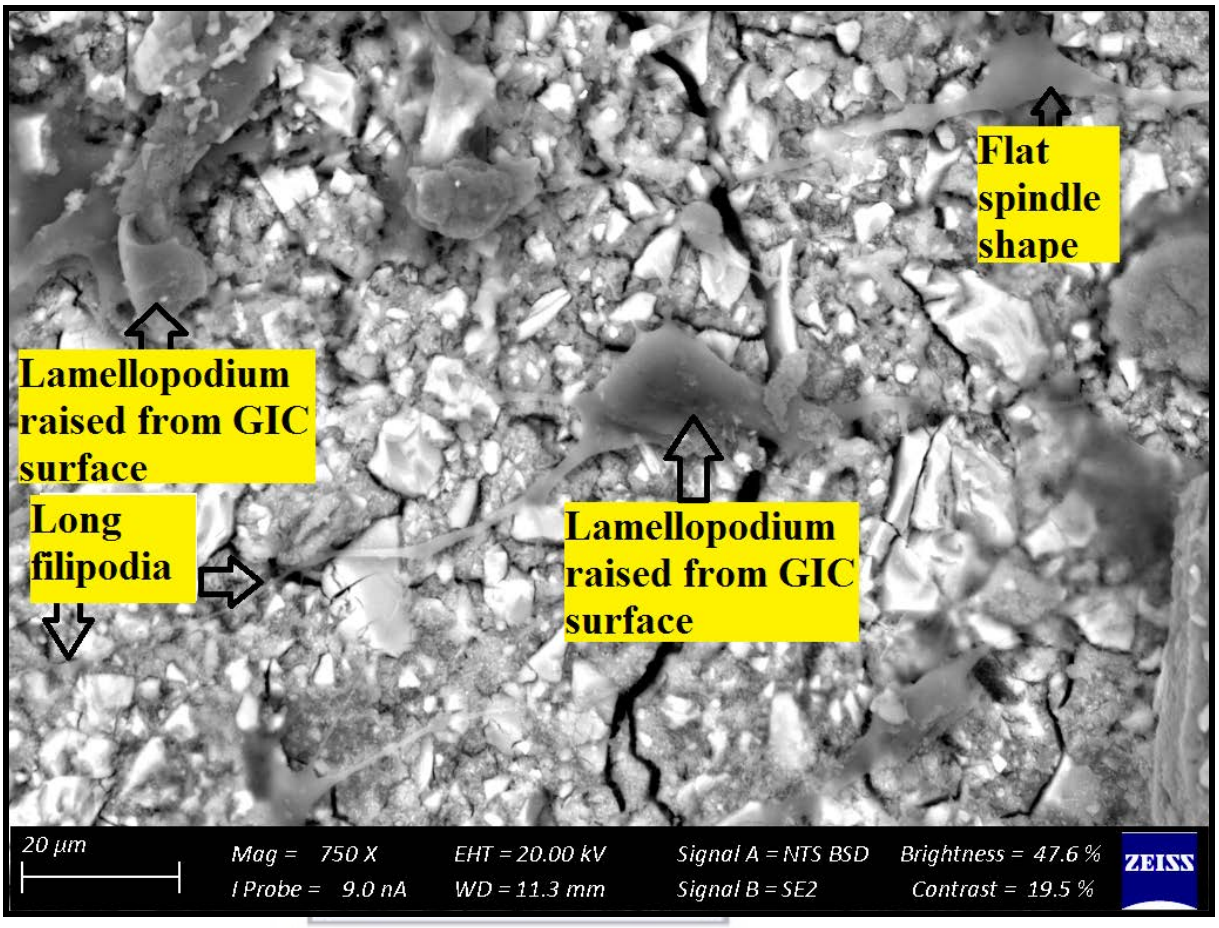

There was loss of stable attachment present of the lamellum and the lamellopodium was folded inward. A similar folded lamellipodium was noted on the FN 24-hour SEM sample (Figure 9.11). The other cells were viable with attachment and the shape was either stellar or spindle-shaped. Wide lamellipodia and filopodia up to six times the length of the 3T3 cell were present. Both high and lower cell densities were noted.

Figure 9.15: SEM image of 3T3 cells on the surface of FN5%CH at 72 hours

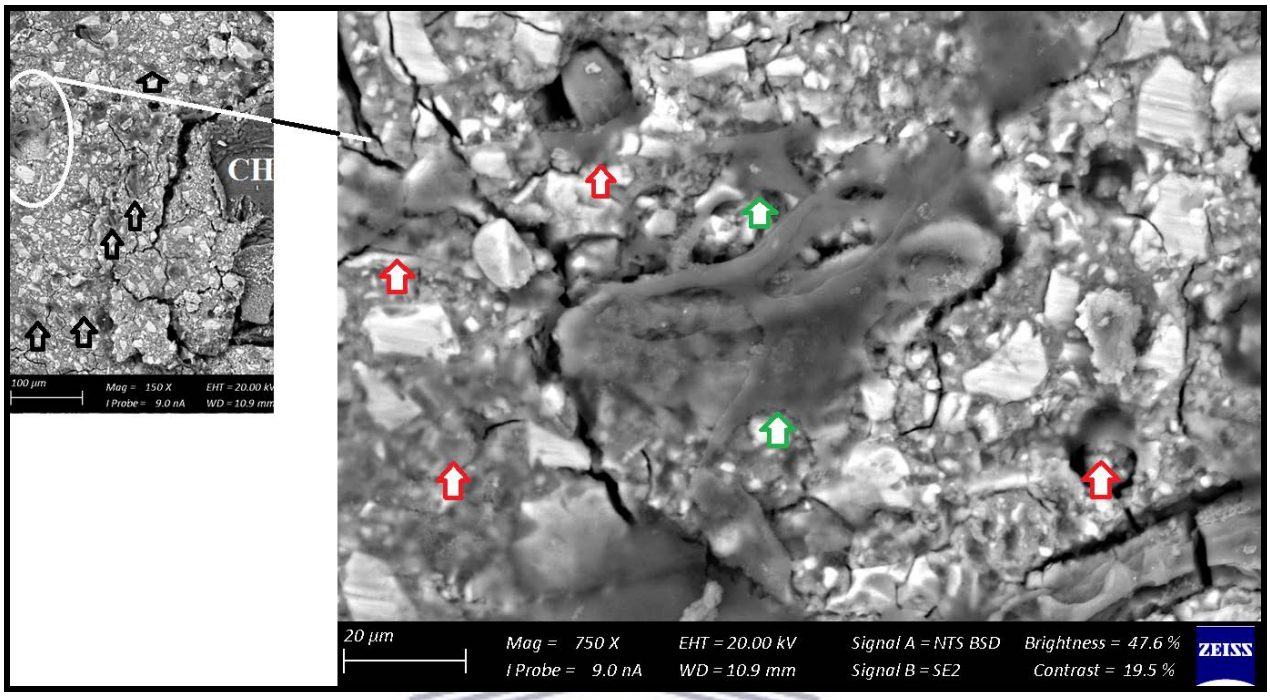

The chitosan is seen below the surface of the GIC and the expansion of the chitosan caused a crack in the GIC (Left smaller image). The empty black arrows (in the left smaller image) show the 3T3 cells far apart. Upon larger magnification, the red arrows indicate the lower cellular density of the 3T3 cells, but it extends over a much a larger surface compared to the nanodiamond SEM in Figure 9.15. The green arrows indicate a higher 3T3 cell density because there is more than one 3T3 cell in that area. It appears as though the cytoplasm of the cell has widely dispersed ruffling and neither clear lamellopodia nor filopodia are identified.

Figure 9.16: SEM image of 3T3 cells on the surface of KU at 24 hours (displaying cell lysis)

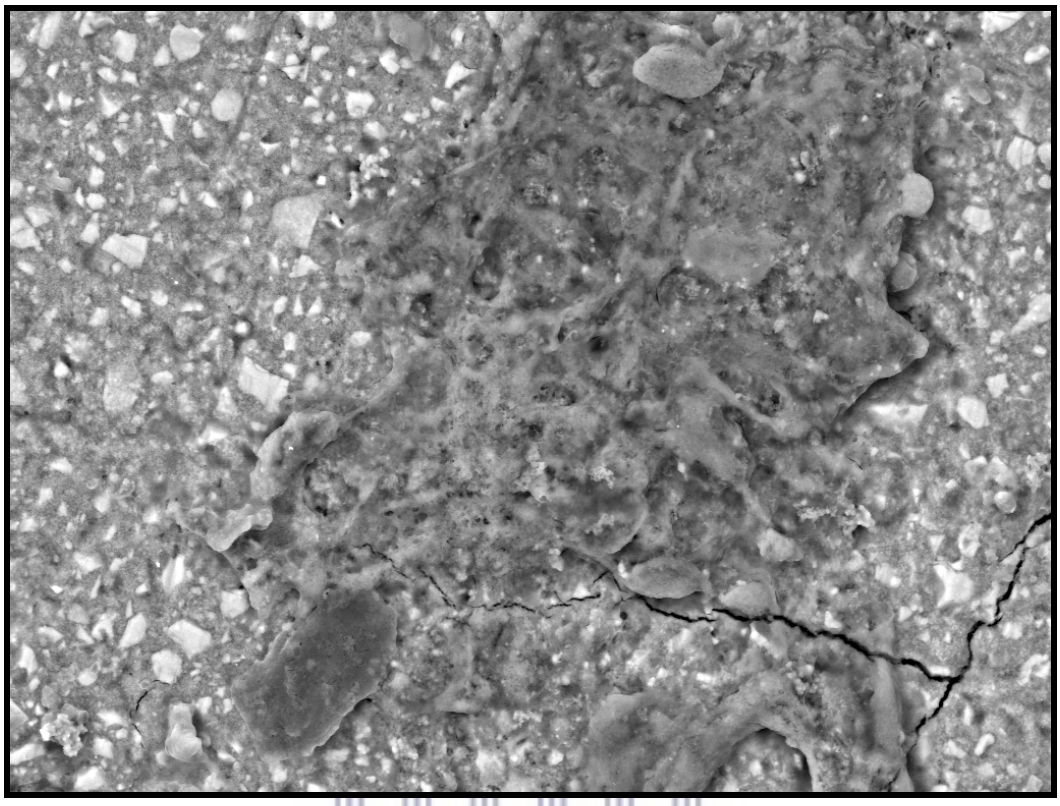

Lysis of the 3T3 cells on the surface of KU at 24 hours. At 72 hours the same trend was noted.

Figure 9.17: SEM image of 3T3 cells on the surface of RSC at 24 hours (displaying cell lysis)

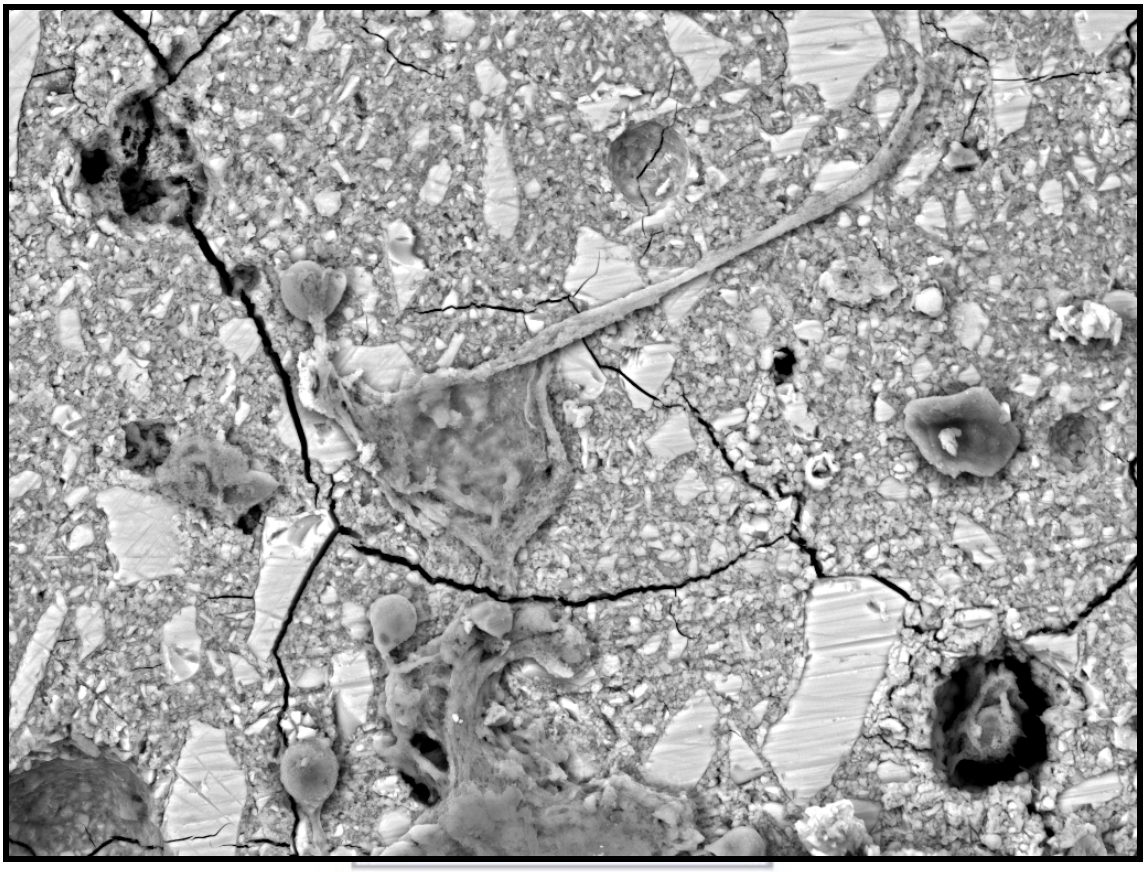

The 3T3 cells show lysis of all the cells in the field of view. The RSC GIC was the only material that seemed to have round extensions that looked like blebs. The light microscope image however showed that it was the nucleus (Figure 9.18). The filopodia were estimated to be twice the size of the 3T3 cell, but due to lysis, this is not completely accurate.

Figure 9.18: Light microscope image of 3T3 cells on the surface of RSC margin at 24 hours

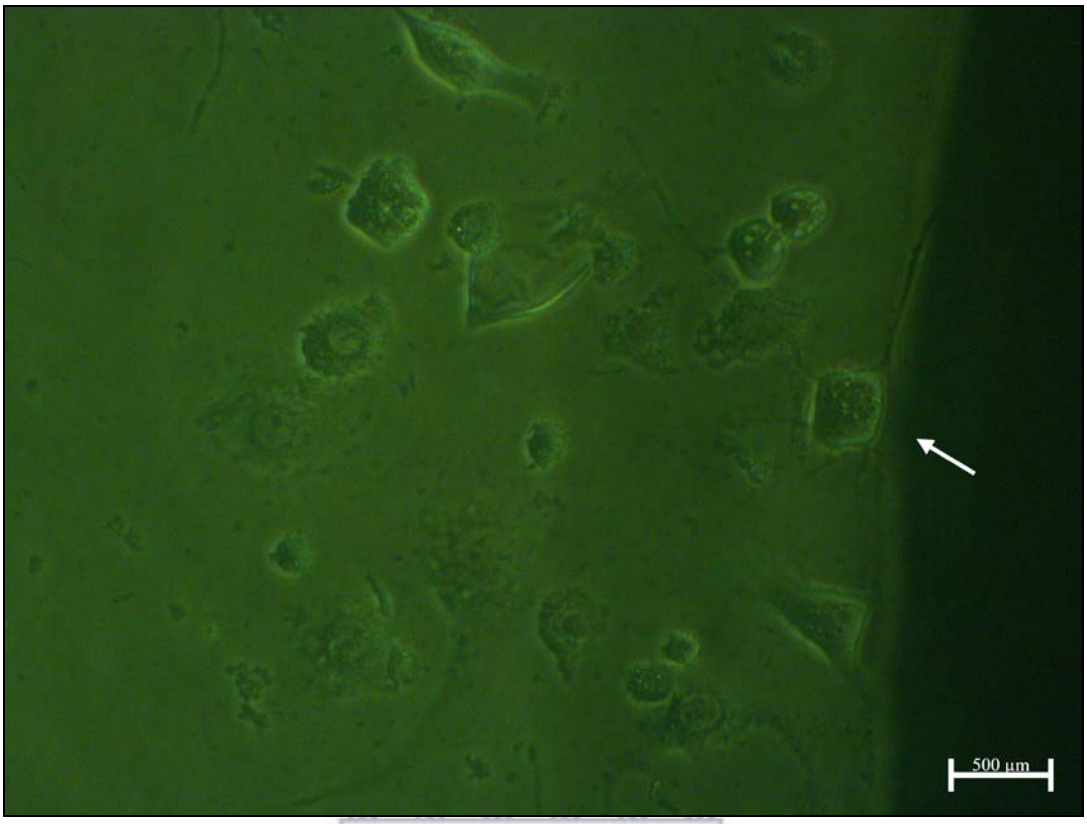

Most of the 3T3 cells did not present with lamellipodia or filopodia, but the nuclei of all the cells were much larger than other control 3T3 cells.

Figure 9.19: SEM image of 3T3 cells on the surface of RSC at 24 hours displaying no lysis

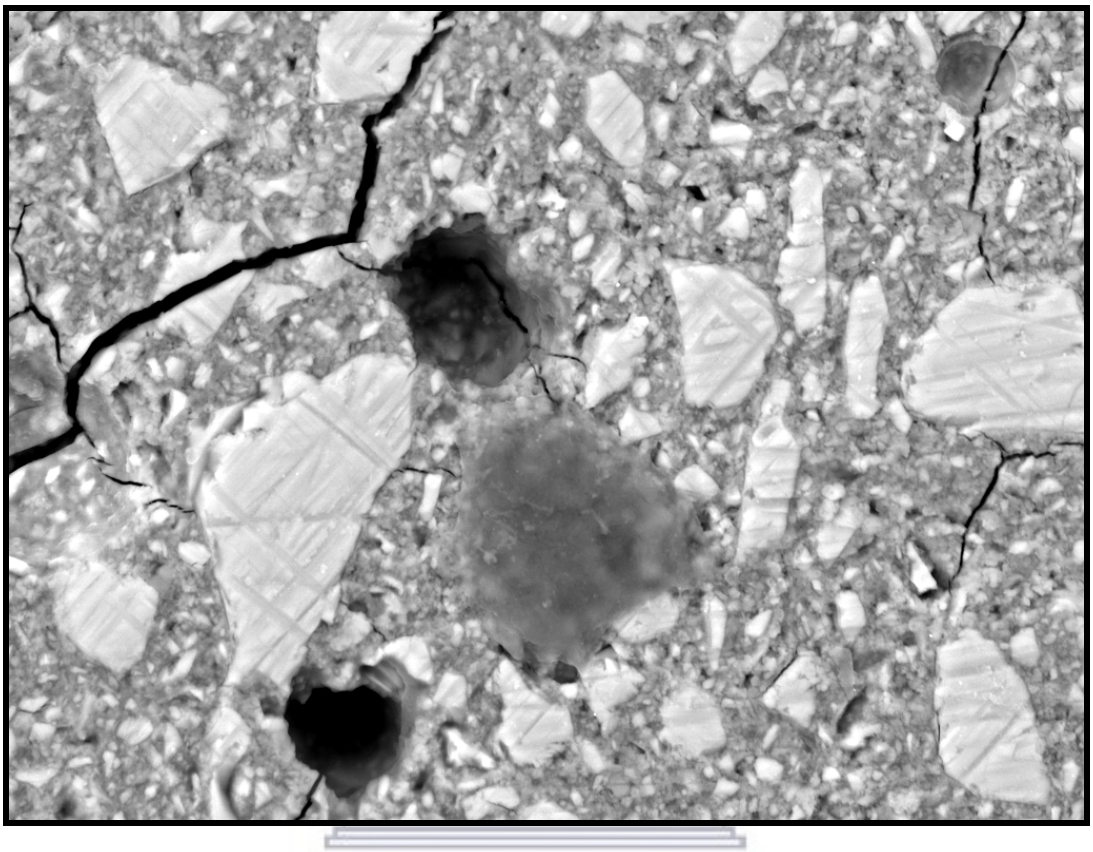

Not all the cells as illustrated in Figure 9.17 presented with lysis. Figure 9.19 present a 3T3 cell that did not display lysis. There was however no lamellipodia and very thin filopodia present on the SEM image. This matches well with the light microscope image for RSC, although filopodia can be seen on the 3T3 cell at the margin of the GIC (Figure 9.18).

Figure 9.20: Light microscope image of 3T3 cells on the surface of RSC5%ND at 24 hours

The 3T3 cells far away from the GIC margin presented with lamellipodia on the stellar 3T3 cells. The filopodia was 2-3 times longer than the 3T3 cell. The cells attached to the margin had short filopodia.

Figure 9.21: Light microscope image of 3T3 cells on the surface of RSC5%CH at 24 hours

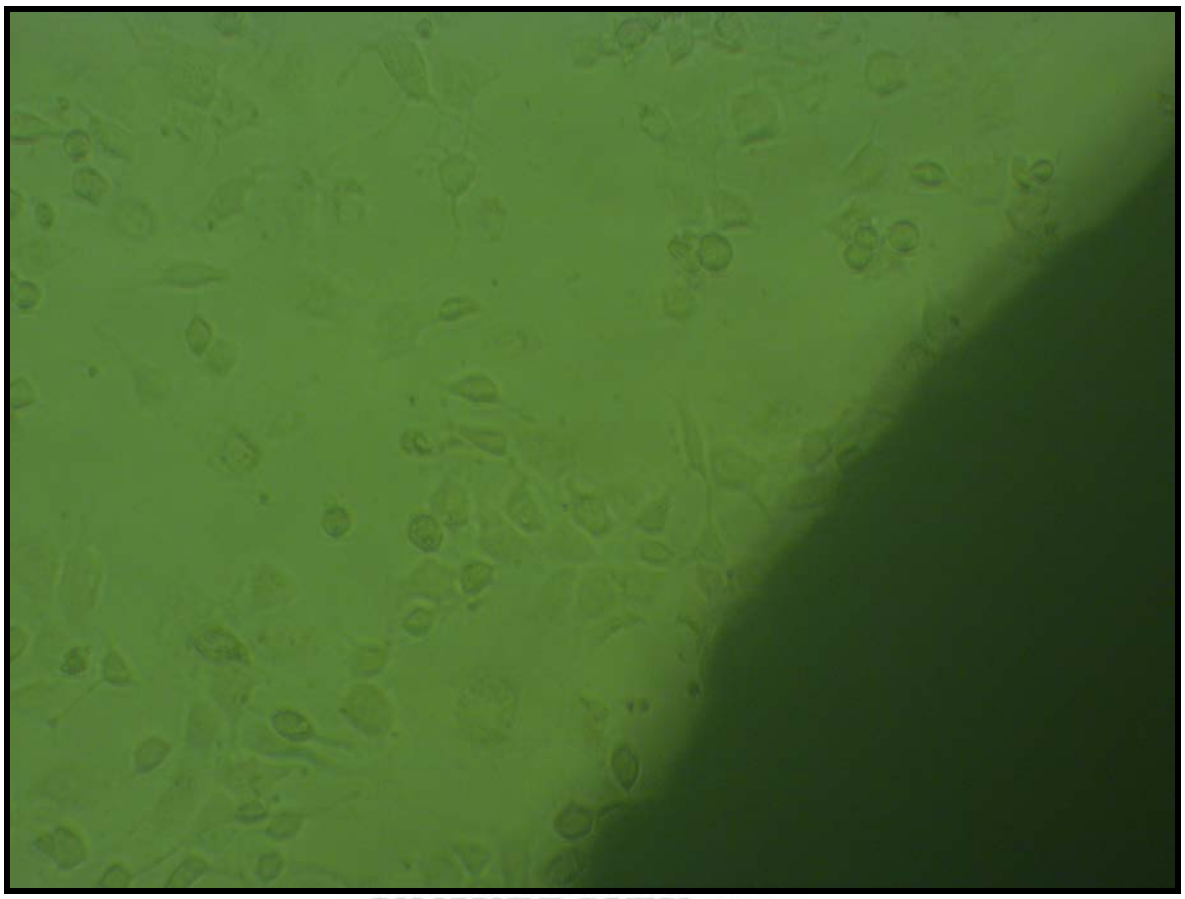

The 3T3 cells attached to the GIC had lamellipodia present as round to stellar 3T3 cells. The filopodia were the same length as the 3T3 cell or not visible at all.

Figure 9.22: SEM image of 3T3 cells on the surface of Biodentine at 24 hours

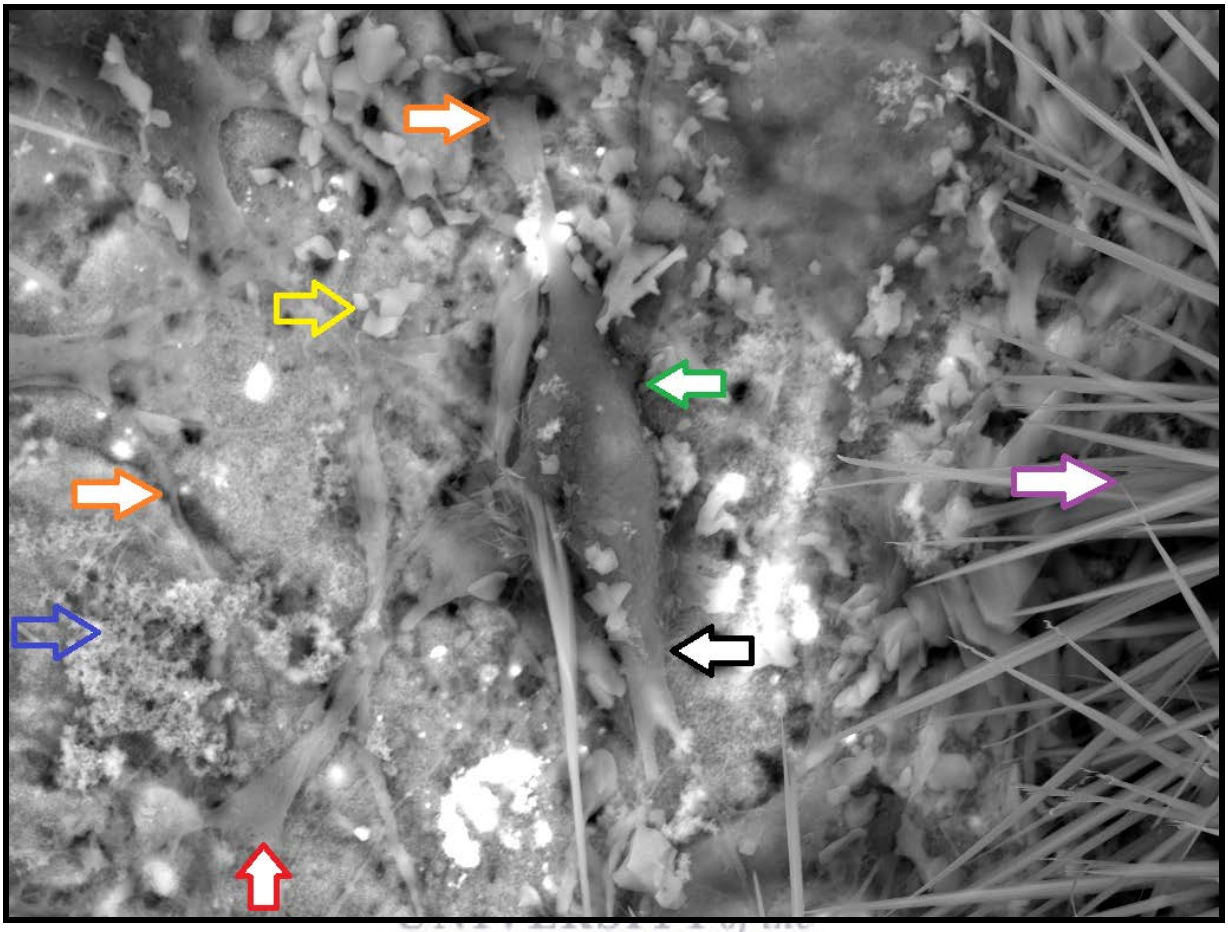

The yellow arrow represents crystal precipitation that was similar to FN (Figure 9.11). The crystalline structure illustrated in Figure 9.22 by the empty blue and the purple arrow are very different in appearance. Red arrows show cells with a lower cellular density compared to the green arrows. The black arrow indicates the lamellipodium. The 3T3 cells that still have a stable adhesion of the lamellum also present with filopodia (orange arrow) that are cylindrical and conical in shape and are double the length of the 3T3 cell. The filopodia even extend into the voids of the Biodentine material (top orange arrow).

Figure 9.23: SEM image of 3T3 cells and crystal formation on the surface of Biodentine

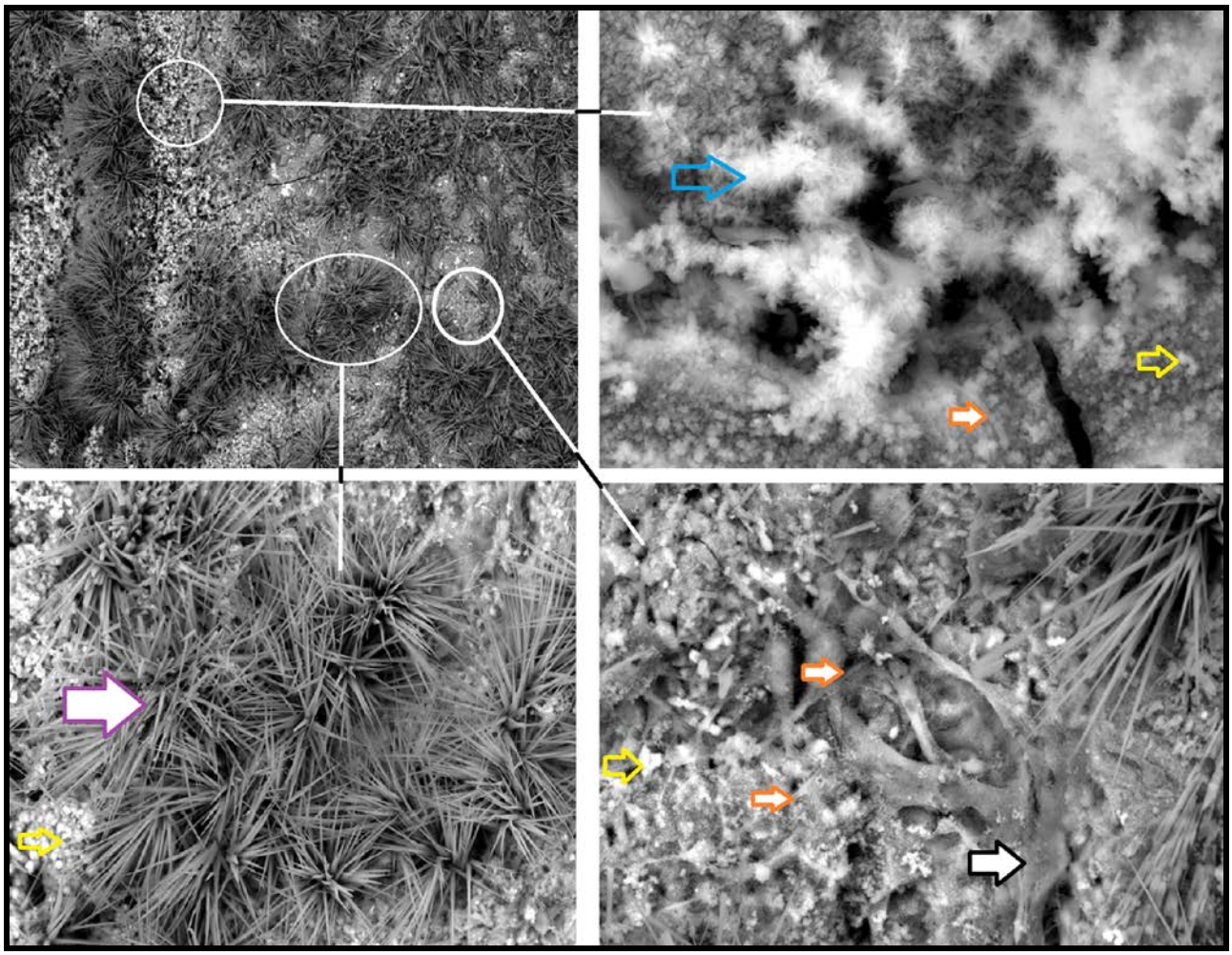

The empty yellow arrow represents large crystalline structures that were similar to the small crystals on Figure 9.23, that orginated from the ethanol drying process. The crystalline structure illustrated by the empty blue and the purple arrows are very different in appearance and orginated from the sodium cacodylate trihydrate. The black arrow indicates the lamellipodium. The 3T3 cells that still have a stable adhesion of the lamellum also present with filopodia (orange arrow). This method used for fixing the 3T3 cells on the Biodentine did not present crystallization from the use of sodium cacodylate trihydrate of the GIC materials. For Biodentine, the three different crystalline formations covered the surfaces of the Biodentine and the 3T3 cells extensively and made the discussion of the cellular structures on the Biodentine

nearly impossible. The whole surface of then GIC materials could be investigated to assess the trend of the 3T3 cells. However, for Biodentine, only a few select areas could be viewed. The cell viability assay with MTT therefore served as the confirmation of the 3T3 cell viability in relation to the control 3T3 cells.

9.6. Discussion

The hypothesis was rejected since the chitosan and nanodiamond-modified glass ionomers did not have a similar cellular viability as their respective control materials for all the time periods assessed.

The modified fixing technique used in the present study was not suitable for Biodentine as it had three distinct phases of crystal formation that obscured nearly all of the 3T3 cells, as well as the whole surface of the material. The modified technique with the use of sodium cacodylate trihydrate does however work well to visualise the 3T3 cells accurately on the GIC materials as demonstrated by comparing the images from the SEM investigation to the light microscope images. But, on some of the GIC samples, the crystalline structures that formed were either small or non-existent and originated from the ethanol evaporation technique. For GICs when using sodium cacodylate trihydrate a critical drying unit should be used to avoid the crystallization of the ethanol on the surface of the GICs. The advantage of the sodium cacodylate trihydrate for specimen preparation was that it avoids micro-precipitation of the phosphate buffers, if samples were not well rinsed (https://www.laboratoryresource.com/?navaction=getitem&id=45). As Biodentine contains phosphate, sodium cacodylate trihydrate was chosen as the fixing agent. Therefore, if the sodium cacodylate trihydrate prevents phosphate precipitation, the crystal formation was as a

result of the reaction between the sodium cacodylate trihydrate and other components in the Biodentine. The ethanol crystallization was easily seen, as it looks similar to that formed on FN. The results from an *in vivo* study on rats using FN produced moderate pulpal responses at day 8. The results at day 30 did not produce any harmful effects, since there was formation of reparative dentine similar to the control group (Six *et al*., 2000). The *in vivo* result matched with the results from the present study as the cell viability for the 3T3 cells exposed to the FN diluents was greater for days 1, 7 and 21 compared to the positive control diluents of Biodentine (Table 9.1). KU on day 1 and RSC on day 7 presented with negative cell viability. Another study on Biodentine obtained similar results to this dissertation, demonstrating an increase of cell viability in relation to the 3T3 control cells (Corral Nunez *et al*., 2014).

The two ions that are more mobile, namely sodium and free fluoride influences the pH the most. Sodium is released as the counter-ion for fluoride as the fluoride in the GIC moves into the diluent. As part of that process, the hydroxide from the diluent moves to the GIC. Additionally, sodium disrupts the cross-linking in the polysalts matrix, facilitating the ion exchange from the GIC with the hydroxide in the diluents as well (Hill *et al*., 1995). The more hydroxyl ions move into the GIC, the lower the pH of the diluent medium (Sasanaluckit *et al.*, 1993). This was confirmed by the ion release of Chapter 8. The initial pH of the DMEM medium was 7 and progressively increased. It stabilised with very little variance of the pH between the materials and the specified time intervals (1, 7 and 21 days). Only FN and its modifications presented with a wide range of pH values, compared to KU and RSC with their respective chitosan and nanodiamond modifications. Guida *et al*. (2002) partly confirmed the results from Wilson *et al*. (1985) that monovalent ions increase fluoride release and additionally suggested that most of the fluoride is present in crystalline form and therefore not available for release. Guida *et al*. (2002) also stated that the amount of fluoride released was directly proportional to the fluoride content

when the GIC is produced by the manufacturer. This is only true if the fluoride is not part of the crystalline inclusions. When the fluoride is located within the crystalline inclusions, it would be largely unavailable after the acid-base reaction is fully completed. This was confirmed by a study by Wood and Hill (1991). Therefore, as the fluoride and the various other ions have a decreased release over the various time periods, the cell viability will also increase above that of the 3T3 control cells. There was however one material (RSC10%CH) that retained a decrease in cell viability at day 21.

In vitro cytotoxicity does not merely refer to the cell viability. The direct effect on the cells should also be considered. The cell adhesion and spread of the 3T3 cells on the surface of the materials also provide insight as to how the cells react to the material. It has been suggested that the cellular function influences the cellular attachment and could thus provide insight to the cytotoxicity (Baxter *et al*., 2002; Hensten-Pettersen, 2007)

The cell morphology of the 3T3 cells in the present study was consistent with the results found by other studies (Abdullah *et al*., 2002; de Souza Costa *et al*., 2003).

The 3T3 cell attachment to the material substrate is achieved by the lamellipodium via two sites (Figure 9.7). The 3T3 cells that were investigated on the GIC materials under SEM illustrated that all the 5%ND-modified GICs presented with 3T3 cells with more defined lamellipodia and filopodia compared to the control materials. Additionally the light microscopy images all indicated that the 3T3 cells were present and attached to all the GIC materials with filopodia, although their general shape was not always stellar and spindle but more round as was the case with the RSC GICs (Figures 9.17 - 9.20).

A cell viability study with resin modified glass ionomer cement (RMGIC) materials concluded that when cells exhibited a round shape with short cellular processes that originated from their cytoplasmic membrane (lamellipodia and filopodia), they seemed to be progressing towards cell

death. The disruption of their plasma membrane seemed to be the cause of the cell death (de Souza Costa *et al*., 2003). Based on the morphology of the 3T3 cells exposed to the RSC and KU GICs, a similar result was confirmed due to the low cell viability at 24 hours (Figures 9.4 and 9.5). The 3T3 cell viability was especially low at day 1 and the SEM images (Figures 9.16 and 9.17) indicated that the 3T3 cells had severe lysis of the cytoplasm. The low cell viability continued for RSC for the diluents on day 7, but KU indicated positive cell viability in relation to the 3T3 cells.

It was postulated by de Souza Costa *et al*. (2003) that when FN was compared to various RMGICs, the release of the numerous ions like aluminium (Al^{3+}), fluoride (F^{-}), strontium (Sr^{2+}) and zinc (Zn^{2+}), did not contribute to the decrease in cell viability as much as what the unreacted resin monomers from the RMGICs (de Souza Costa *et al*., 2003). This hypothesis originated from the work done by Fujisawa *et al*. (1988) that indicated how the methacrylate monomer resins from composite (*Z100, 3M ESPE*) and RMGICs (*Vitremer and Vitrebond, 3M ESPE*) solubilise the cell membrane as it is incorporated into the lipid bilayers of the cell membrane (Fujisawa *et al*., 1988). Soheili Madj *et al*. (2003) concluded that the cytotoxicity effects from GICs could be attributed to the aluminium (Al^{3+}) and/or iron (Fe^{2+}) present in the diluent due to oxidative stress it causes within the cells. This could be a possibility, another study within this dissertation presented aluminium release after 24 hours (Chapter 7) to be the highest for KU control materials followed by RSC and then FN. This sequence also matched the cell viability sequence (Table 9.1). Based on the 5%ND modifications of the FN, KU and RSC materials, there was a greater aluminium release, but the interaction with the nanodiamond particles resulted in the formation of a covalent bond with the aluminium. FN10%ND presented with lower cell viability. Other ions released like fluoride, sodium, silicon and strontium therefore all play a role in the ionic strength of the diluent. A study with FN found no correlation after 24

hours with regard to the reduction in 3T3 cell viability and the concentration of fluoride released by FN (Selimović-Dragaš *et al*., 2013).

Radiopacifiers (such as zirconium oxide present in Biodentine) have also been found to play a role in the cell viability. Zirconium oxide was shown to be non-toxic to mouse fibroblast cells and human differentiated cells (Dion *et al*., 1994; Laurent *et al*., 2008; Zanini *et al*., 2012; Zhou *et al*., 2013). Corral Nunez *et al*., (2014) found that FN showed a decrease in cellular viability compared to Biodentine, there was no difference in gene expression IL-1α, IL-6 and 18S rNA after 24 hours between the two materials (Corral Nunez *et al*., 2014).

Lanthanum used in KU as a radiopacifier has been recognised as a phosphate binder (National Center for Biotechnology Information, 2019). Additionally lanthanum was noted to also displace calcium due to the deposition of lanthanum-phosphate in teeth (Kobayashi *et al*., 1980).

Aluminium and lanthanum can change the electrical properties of the membrane once they are adsorbed onto the phosphatidylcholine liposomes. The extent of the influence on the membrane is dependent upon the pH (Kotyńska and Figaszewski, 2018). Although the electrical activity of the 3T3 cell membrane and the Zeta potential of the diluents or the dental materials were not assessed in this dissertation it was determined that, based on the ppm of lanthanum at day 1 for KU and the modifications, a conclusion could be drawn about the effect of lanthanum on the 3T3 cells. Lanthanum is able to stimulate mitogenicity at low concentrations of 0.00003599 ppm (Smith and Smith, 1984). The release of lanthanum from the KU samples into de-ionised water (Chapter 7) was as follows: KU (0.000261ppm), KU5%ND (0.003517), KU10%ND (0.004199), KU5%CH (0.01048) and KU10%CH (0.015138). A study by Yu (2005) from the literature assessed lanthanum concentrations of 0.0007198ppm on the 3T3 cells. The 3T3 cells showed apoptotic characteristics namely: perinuclear chromatin condensation as well as fragmentation of the cell nucleus (Yu et al., 2005). In this dissertation, the lowest lanthanum release for KU into

de-ionised water at day 1 was 0.000261ppm. The magnitude of lanthanum release of KU as well as the chitosan and nanodiamond-modifications of KU at day 1 explains the contribution of lanthanum to lower cell viability below that of the control 3T3 cells of the diluents from day 1. Although the lanthanum release was not assessed for days 7 and 21, it could be deduced that the lanthanum values dropped to well below that of KU (0.000261ppm) at day 1. This deduction is plausible for the release of lanthanum into the GIC-diluents for days 7 and 21 otherwise the ppm concentration would not be low enough to stimulate the mitogenic effect based on the surging cell viability in Tables 9.1 and 9.2 for KU at days 7 and 21.

RSC with its chitosan modifications continued to decrease the cell viability well below the control 3T3 at day 21. The reason why the CH modification of RSC performed differently from FN and KU up to day 21 was due to the improved structural stability. The antibacterial study with *S. mutans* (Chapter 10) noted that after 24 hours of exposure to *S. mutans*, the chitosan-modified RSC GICs were structurally more resilient to the environment than FN and KU chitosan-modified GICs. Chitosan has a high affinity for proteins in the form of amino acids and this is provided by the DMEM medium due to the L-Glutamine in the medium that is an amino acid. The interaction of the *S. mutans* and the 3T3 cells with the amino acids will influence the chitosan-modified GIC surface. When the GICs start to disintegrate due to the environmental influence, a greater surface area is exposed to the environment which increases the release of ions into the diluent. The structural integrity of the RSC materials modified with chitosan compared to FN and KU is illustrated in Figure 9.24. This image was recorded during the dissertation study on *S. mutans* (Chapter 10) after the 24 hour exposure of the *S. mutans*/TSB medium. It is clear that the RSC10%CH surface did not disintegrate as much as the FN10%CH and KU10%CH materials, (Figure 9.24). Therefore, if the surface of the GIC remains intact for longer, there is no excessive exposure and moisture absorbtion into the material and the ion release is lower and more consistent over a longer period. In this dissertation it was clear for the

3T3 cell viability of RSC10%CH for day 1, 7 and 21 compared to the release of the ions into the diluents from RSC10%ND.

Figure 9.24: 10% Chitosan-modified GICs after 24 hours submergence with *S Mutans* tryptic soy broth medium

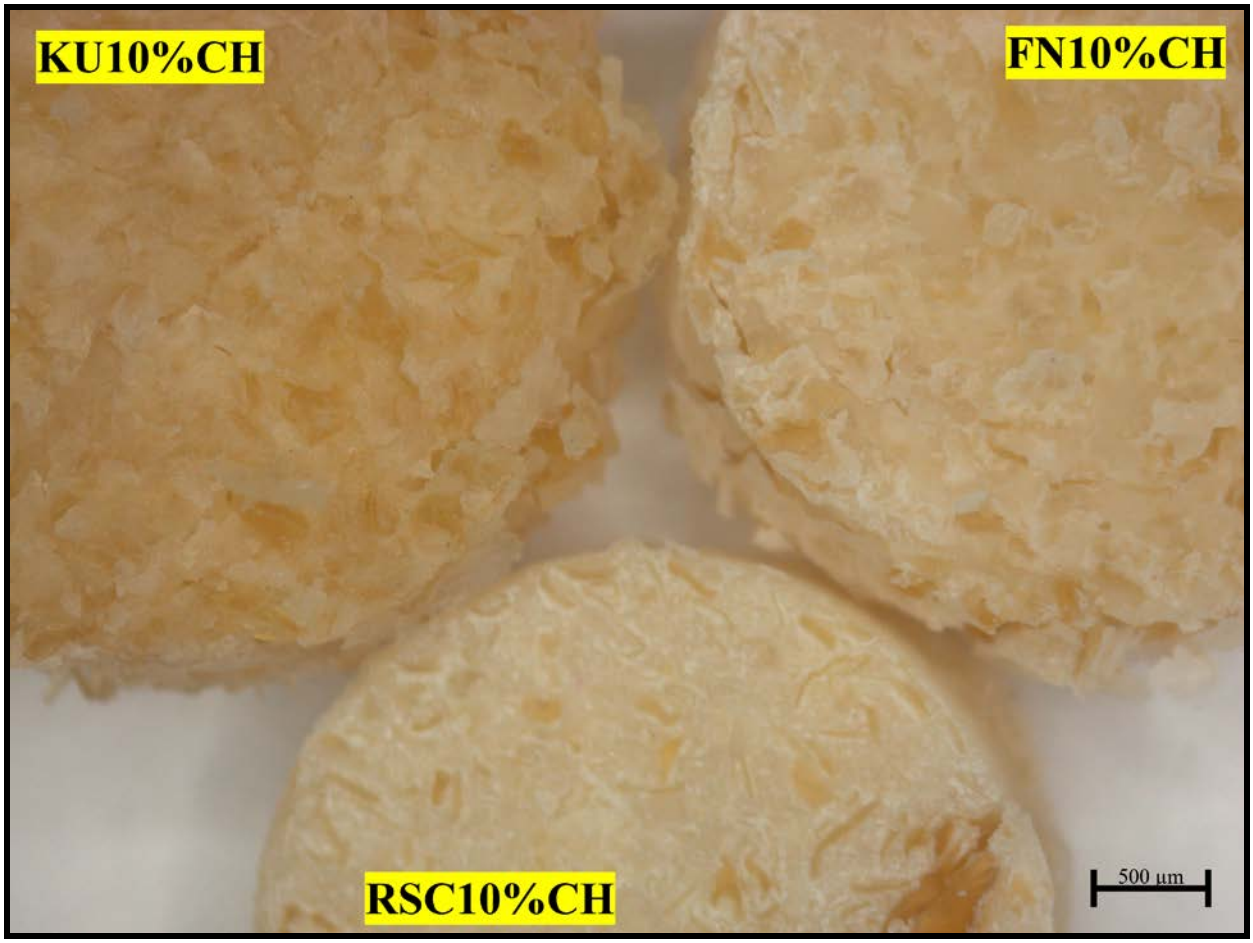

9.7. Conclusion

Fixing the 3T3 cells with a modified technique using sodium cacodylate trihydrate was adequate for the GICs but not for Biodentine. It is advised that a critical drying unit is used rather than ethanol evaporation lone. The structural integrity and the lamellopodia presenting with filopodia were variable between samples. The cell viability with MTT was the most valuable and

indicated that there was an increase in cell viability as the time period increased from 1to 21 days. This was due to the reduction of the ions present in the diluents as time passed. RSC displayed a decrease in the cell viability for the 5 and 10% chitosan materials up to day 21. This was because it was structurally more stable. FN had greater cell viability than Biodentine over all the time periods assessed.

9.8. References

Abdullah, D., Pitt Ford, T., Papaioannou, S., Nicholson, J. and McDonald, F. (2002). An evaluation of accelerated Portland cement as a restorative material. *Biomaterials*, 23(19), pp.4001-4010.

AL-Hiyasat, A., Al-Sa'Eed, O. and Darmani, H. (2012). Quality of cellular attachment to various root-end filling materials. *Journal of Applied Oral Science*, 20(1), pp.82-88.

Association for the Advancement of Medical Instrumentation/International Organization for Standardization. Biological evaluation of medical devices (2009). Part 5: test for *in vitro* cytotoxicity (ISO 10993–10995:2009). *Association for the Advancement of Medical Instrumentation*.

Basak, V., Bahar, T., Emine, K., Yelda, K., Mine, K., Figen, S. and Rustem, N. (2016). Evaluation of cytotoxicity and gelatinases activity in 3T3 fibroblast cell by root repair materials. *Biotechnology & Biotechnological Equipment*, 30(5), pp.984-990.

Baxter, L., Frauchiger, V. and Textor, M. (2002). Fibroblast and osteoblast adhesion and morphology on calcium phosphate surfaces. *European Cells and Materials*, 30(4), pp.1-17.

Camilleri, J., Montesin, F., Papaioannou, S., McDonald, F. and Pitt Ford, T. (2004). Biocompatibility of two commercial forms of mineral trioxide aggregate. *International Endodontic Journal*, 37(10), pp.699-704.

Corral Nuñez, C., Bosomworth, H., Field, C., Whitworth, J. and Valentine, R. (2014). Biodentine and Mineral Trioxide Aggregate Induce Similar Cellular Responses in a Fibroblast Cell Line. *Journal of Endodontics*, 40(3), pp.406-411.

De Souza Costa, C., Hebling, J., Garcia-Godoy, F. and Hanks, C. (2003). *In vitro* cytotoxicity of five glass-ionomer cements. *Biomaterials*, 24(21), pp.3853-3858.

Dion, I., Bordenave, L., Lefebvre, F., Bareille, R., Baquey, C., Monties, J. and Havlik, P. (1994). Physico-chemistry and cytotoxicity of ceramics. *Journal of Materials Science: Materials in Medicine*, 5(1), pp.18-24.

Doyke, A. and Griffiths, J. (1998). *Cell and Tissue Culture - Laboratory Procedures in Biotechnology*. John Wiley and Sons Ltd, pp.62-65.

Fujisawa, S., Kadoma, Y. and Komoda, Y. (1988). 1H and 13C NMR Studies of the Interaction of Eugenol, Phenol, and Triethyleneglycol Dimethacrylate with Phospholipid Liposomes as a Model System for Odontoblast Membranes. *Journal of Dental Research*, 67(11), pp.1438-1441.

Geurtsen, W., Lehmann, F., Spahl, W. and Leyhausen, G. (1998). Cytotoxicity of 35 dental resin composite monomers/additives in permanent 3T3 and three human primary fibroblast cultures. *Journal of Biomedical Materials Research*, 41(3), pp.474-480.

Grobler, S., Olivier, A., Moodley, D. and Van Wyk Kotze, T. (2008). Cytotoxicity of recent dentin bonding agents on mouse fibroblast cells. *Quintessence International*, 39(6), pp.511-516.

Guida, A., Hill, R., Towler, M. and Eramo, S. (2002). *Journal of Materials Science: Materials in Medicine*, 13(7), pp.645-649.

Hensten-Pettersen, A. (2007). Comparison of the methods available for assessing cytotoxicity. *International Endodontic Journal*, 21(2), pp.89-99.

Hill, R., De Barra, E., Griffin, S., Henn, G., Devlin, J., Hatton, P., Brook, I., Johal, K. and Craig, G. (1995). Fluoride Release from Glass Polyalkenoate (Ionomer) Cements. *Key Engineering Materials*, 99-100, pp.315-322.

Ibrahim, M., Meera Priyadarshini, B., Neo, J. and Fawzy, A. (2017). Characterization of Chitosan/TiO2 Nano-Powder Modified Glass-Ionomer Cement for Restorative Dental Applications. *Journal of Esthetic and Restorative Dentistry*, 29(2), pp.146-156.

International Organisation for Standardisation (2008). Preclinical evaluation of biocompatibility of medical devices used in dentistry—test methods for dental materials. *International Standard ISO 7405*.

Kobayashi, Y., Ozeki, M., Yagi, T., HosoI, T. and Takei, M. (1980). X-ray Diffraction Analysis of the Reaction Products of Hydroxyapatite and Lanthanum. *Journal of Dental Health*, 29(4), pp.354-360.

Kotyńska, J. and Figaszewski, Z. (2018). Binding of trivalent metal ions (Al3+, In3+, La3+) with phosphatidylcholine liposomal membranes investigated by microelectrophoresis. *The European Physical Journal E*, 41(5).

Laurent, P., Camps, J., De Méo, M., Déjou, J. and About, I. (2008). Induction of specific cell responses to a Ca3SiO5-based posterior restorative material. *Dental Materials*, 24(11), pp.1486-1494.

Moodley, D., Grobler, S. and Olivier, A. (2004). Cytotoxicity of a dentine bonding agent on four different cell-lines. *South African Dental Journal (SADJ)*, 60(6), pp.101-105.

Mosmann, T. (1983). Rapid colorimetric assay for cellular growth and survival: Application to proliferation and cytotoxicity assays. *Journal of Immunological Methods*, 65(1-2), pp.55-63.

Pubchem.ncbi.nlm.nih.gov. (2019). *Lanthanum(3+)*. [online] Available at: https://pubchem.ncbi.nlm.nih.gov/compound/104897 [Accessed 4 Apr. 2019].

Sasanaluckit, P., Albustany, K., Doherty, P. and Williams, D. (1993). Biocompatibility of glass ionomer cements. *Biomaterials*, 14(12), pp.906-916.

Selimović-Dragaš, M., Hasić-Branković, L., Korać, F., Đapo, N., Huseinbegović, A., Kobašlija, S., Lekić, M. and Hatibović-Kofman, Š. (2013). *In vitro* fluoride release from a different kind of conventional and resin modified glass-ionomer cements. *Bosnian Journal of Basic Medical Sciences*, 13(3), p.197.

Six, N., Lasfargues, J. and Goldberg, M. (2000). In vivo study of the pulp reaction to Fuji IX, a glass ionomer cement. *Journal of Dentistry*, 28(6), pp.413-422.

Smith, J. and Smith, L. (1984). Initiation of DNA synthesis in quiescent Swiss 3T3 and 3T6 cells by lanthanum. *Bioscience Reports*, 4(9), pp.777-782.

Soheili Madj, E., Goldberg, M., Stanislawski, L. (2003). *In vitro* effect od ascorbate and Trolox on the biocompatibility od dental restorative materials. *Biomaterials*, 24(1), pp.3-9.

Wilson, A., Groffman, D. and Kuhn, A. (1985). The release of fluoride and other chemical species from a glass-ionomer cement. *Biomaterials*, 6(6), pp.431-433.

Wood, D. and Hill, R. (1991). Glass ceramic approach to controlling the properties of a glass-ionomer bone cement. *Biomaterials*, 12(2), pp.164-170.

Yu, S., Yuan, L., Yang, X., Wang, K., Ke, Y. and Qian, Z. (2005). La3+-promoted proliferation is interconnected with apoptosis in NIH 3T3 cells. *Journal of Cellular Biochemistry*, 94(3), pp.508-519.

Zanini, M., Sautier, J., Berdal, A. and Simon, S. (2012). Biodentine Induces Immortalized Murine Pulp Cell Differentiation into Odontoblast-like Cells and Stimulates Biomineralization. *Journal of Endodontics*, 38(9), pp.1220-1226.

Zhou, H., Shen, Y., Wang, Z., Li, L., Zheng, Y., Häkkinen, L. and Haapasalo, M. (2013). *In Vitro* Cytotoxicity Evaluation of a Novel Root Repair Material. *Journal of Endodontics*, 39(4), pp.478-483.

CHAPTER 10

STREPTOCOCCUS MUTANS ACTIVITY AND THE CHANGE IN SURFACE ROUGHNESS OF CHITOSAN AND NANODIAMOND-MODIFIED GLASS IONOMER RESTORATIVE CEMENT

10.1. Abstract

Introduction: The aims of the present study were to investigate the change in the *Streptococcus Mutans (S. mutans)* optical density at 450nm (OD450nm) as well as the change in surface roughness of three chitosan and nanodiamond-modified glass ionomers.

Materials and Methods: The chitosan (CH) and nanodiamonds (ND) were mixed with glass ionomer powder at 5% and 10% weight per weight percentage. The surface roughness was assessed with a contact surface roughness tester before and after the antibacterial study. The antibacterial activity of *S. mutans* was assessed in terms of the optical density (OD450nm) with a spectrophotometric technique over various time periods of 0, 2, 4, 6 and 24 hours of *S. mutans* incubation.

Results: The *S. mutans* OD450nm decreased significantly ($p < 0.0001$) from zero hours through 2 hours to 4 hours for each material. At 24 hours, there were significant differences between all three control materials ($p < 0.0001$). The lowest bacterial OD450nm was noted for FN followed by KU. RSC had the largest *S. mutans* OD450nm. The *S. mutans* OD450nm seemed to stabilise as the growth significantly increased at 6 hours compared to the preceding time periods (2 and 4 hours) for all the materials and their respective chitosan and nanodiamond modifications. There was no significant reduction in the *S. mutans* OD450nm between the control material and their respective chitosan or nanodiamond modifications for any time period ($p > 0.05$).

The *S. mutans* OD450nm in relation to the control bacteria indicated significant reduction ($p < 0.01$) for FN (Fuji IX GP), FN5%ND, FN10%CH and KU10%CH. The *S. mutans* growth was less in the control compared to the FN10%ND material at 2, 4 and 6 hours. The materials modified with chitosan indicated an increase in surface roughness.

Conclusion: Although the surface roughness did not change after 24 hours for the control materials or the nanodiamond modifications, the SEM images illustrated clearly that the chitosan and the nanodiamond modifications disrupted the biofilm and changed the surface adherence as well as the quorum grouping of the *S. mutans.*

Keywords: Glass Ionomer, Antimicrobial effect, *Streptococcus Mutans*, Surface roughness, Nanodiamonds, Chitosan, Quorum sensing.

Abbreviations and acronyms:

Optical density: OD450nm

Streptococcus Mutans: *S. mutans*

10.2. Introduction

Streptococcus Mutans (*S. mutans*) has been identified as one of the main role players in the development of dental caries (van Houte *et al*., 1982). *S. mutans* forms part of the phylogenetic tree of 34 species of *Streptococcus species* that have been classified into five phylogenic groups per viridians (Kawamura *et al*., 1995). *S. mutans* has been presented to be one of the most virulent bacterial species in the caries process (Banas, 2004; Kuramitsu and Wang, 2006) and has been implicated in the progression of dental caries (van Houte *et al*., 1982; Carlsson *et al*., 1985; Loeshe, 1986). *S. mutans* has the ability to adhere to tooth structure. The metabolism of carbohydrates (Ajdic *et al*., 2002) by *S. mutans* results in its high aciduricity (Welin-Neilands and Svensater, 2007) and acidogenecity (Hamada and Slade, 1980; Loeshe, 1986; Khoo *et al*., 2005). Plaque samples have been shown to contain high levels of L–lactic isomer i.e. lactic acid (Geddes, 1972). The role of lactic acid was identified as one of the main acids produced by *S. mutans* (Geddes 1972). GICs are known to have an inhibitory influence on *S. mutans* (Palenik *et al*., 1992) and reduce the acid production (Nakajo *et al*., 2009; Wiegand *et al*., 2007).

Various antibacterial materials have been incorporated into GICs in order to increase their antibacterial activity. These included benzalkonium chloride (Dimkov *et al*., 2012), cetrimide (Botelho, 2003), cetylpyridinium chloride (Botelho, 2003), chlorhexidene (Ribeiro and Ericson, 1991), zinc sulfate (Osinaga *et al*., 2003) and silver or zinc zeolites (Mabrouk *et al*., 2013) to name a few.

The literature on the various modifications of glass ionomer cements (GICs) to enhance the antibacterial activity was reviewed by Ching *et al*. (2018). According to their search parameters, 22 appropriate studies were identified (Ching *et al*., 2018). Many of these studies did not demonstrate a significant improvement in the antibacterial properties, but they still illustrated an effect on the *S. mutans* OD450nm. The studies where the chitosan (CH) was incorporated into the liquid showed favourable results (Ibrahim *et al*., 2015; Debnath *et al*., 2017; Ibrahim *et al*.,

2017). Favourable results were demonstrated with 5 and 10% volume per volume percent (v/v%) in relation to the control material (Ibrahim *et al*., 2015; 2017).

There are however various factors that influence the interaction of the micro-organisms with tooth structure and the restorative materials. The bacterial adherence, colonization and growth of bacteria on the restoration and tooth structure have been linked to the surface roughness. Bacterial colonization on surfaces with a surface roughness (Ra) of more than 0.2µm has been detected to be significant (Bollen, 1997). High levels of *S. mutans* were detected in plaque from saliva and the surfaces of carious teeth as well as sound teeth (van Houte *et al*., 1982). The interaction of *S. mutans* with dental materials has been of importance for dental research. Although glass ionomer cements (GICs) have been identified to have antibacterial properties, a bacterial biofilm can form on the GIC surface (Auschill, 2002). A nanodiamond modification of GICs has never been assessed and this study will investigate the changes in *S. mutans* OD450nm and surface roughness of these GICs when exposed to *S. mutans*.

The aims of the study were to investigate the change in surface roughness and the *S. mutans* OD450nm of *S. mutans* at different time intervals. The hypothesis was that chitosan and nanodiamond-modified GICs would reduce the *S. mutans* OD450nm with no effect on the surface characteristics of the GICs.

10.3. Materials and Methods

10.3.1. Material modification

Three commercially available GICs namely FN: Fuji IX GP hand-mix (*GC Corp, Tokyo, Japan; Batch: 1503231*); KU: Ketac Universal hand-mix; (*3M ESPE, Seefeld, Germany; Batch: 583514*) and RSC: Riva Self Cure hand-mix (*SDI Limited, Australia; Batch: 62657V*) were used in this study. These GICs were modified in the powder phase with 5% or 10% chitosan (CH) or nanodiamond particles (ND)

The nanodiamond particles used were from detonated synthesized nanodiamonds (*PlasmaChem, item: PL-D-G01*). The average particle size is 4-6 nm and the particles generally present in non-fused diamond clusters. The carbon purity of >98% has an enhanced stability (5w/v%) in a water suspension and carries a -55 ±5 mV Zeta potential. The three GICs were modified in the powder phase per weight percentage (w/w%) by adding 5% or 10% of a commercially available chitosan powder (*Merck, item 448877*) and the same percentages followed for the nanodiamond particles. The modified experimental materials were produced by placing the GIC powder in an airtight high density polyethylene (HDPE) container. The containers were subsequently clamped in a beaker shaker for two hours to ensure complete mixing of the two powders.

Fifteen GICs were prepared in accordance with the manufacturers' powder/ liquid ratios: (1) FN GIC powder [FN]; (2) FN GIC powder modified with 5-wt% chitosan powder [FN5%CH]; (3) FN10%CH; (4) FN5%ND; (5) FN10%ND; (6) KU; (7) KU5%CH; (8) KU10%CH; (9) KU5%ND; (10) KU10%ND; (11) RSC; (12) RSC5%CH; (13) RSC10%CH; (14) RSC5%ND; (15) RSC10%ND.

10.3.2. Sample preparation

The powder/ liquid ratio prescribed by the manufacturer was followed and confirmed on a desktop analytical balance (*Metler AE240 analytical balance, Columbus, Ohio, USA*) by first dispensing the powder followed by the liquid. This ensured that the manufacturer's recommended powder/ liquid ratio was maintained for all the GICs used in this study (Mulder, 2018). Disc-shaped specimens of GIC were prepared (7±0.1mm diameter and 2±0.1mm thickness) by packing the GICs into a Teflon mould and covering it with a polyester strip under the glass slide and leaving it to set at room temperature (±23ºC) for 1 hour. After setting, the polyester strip and glass slide were removed and the specimens were stored for 24 hours at 37ºC and 100% humidity in a temperature controlled chamber. Samples were treated with sandpaper on both sides (1200 grit sand paper as ISO9917-1:2007 page, as per the acid erosion test). This standard surface preparation was chosen to provide consistency in accordance with the ISO. Carlén *et al*., (2001) illustrated that after the polishing of a GIC restoration, the protein/bacterial binding and the surface roughness did not change in relation to the GIC prior to polishing.

10.3.3. Surface roughness

The contact surface roughness (Ra) of the materials was measured with a Leeb contact surface roughness tester with a standard sensor (*Model Leeb432, Chongqing Leeb Instrument co Ltd*). Two surface roughness (Ra) measurements were recorded namely, before exposure to *S. mutans* (known as "Ra 0 (zero) hours) and after exposure to *S. mutans* (known as Ra 24 hours).

The Leeb contact surface roughness tester has a measuring range of 0.005-16µm for surface roughness. The testing parameters were: surface roughness (Ra), the filter option was adjusted to the Gauss setting, the assessment length (λc) at 0.8mm x n5 (assessment length (*L*n=*l*r x n); *L*n=3.2mm) (International Organization for Standardization. ISO 4288: Rules and Procedures for

Assessment of Surface Texture. Geneva: ISO; 1998). The standard stylus has a natural diamond at a 90º cone angle with a 5µm tip radius. The stylus applied a force to the sample of <4mN. The travelling speed (Vt) for the above parameters was 0.135mm/s and the measurement accuracy was ±10%.

Two parallel lines were recorded 2mm apart with two lines perpendicular to that (n = 4) per sample. The aforementioned measurements (n = 4) were therefore recorded per side and the average of the eight measurements was used as the mean Ra per specimen for time period Ra 0 (zero) hours. The GIC samples were re-assessed after 24 hours subsequent to the 24 hour exposure to the tryptic soy broth containing *S. mutans* (TSB/ *S. mutans* broth) at Ra 24 hours. Subsequent to removing the GIC samples from the TSB/ *S. mutans* growth medium, a 10 second vortex in 5ml de-ionised water was completed to remove any *S. mutans* biofilm and bacteria from the surface of the GICs. The aforementioned samples (n = 4) for Ra readings were then repeated. The mean percentage difference was calculated for the five samples per GIC group in relation to the Ra 0 hour value. A positive percentage value indicated an increase in Ra from Ra 0 hours to Ra 24 hours.

10.3.4. Sterilization

Sterilization of the GIC samples was completed after the first surface roughness readings (Ra 0 hours) was completed. The GIC specimens and the 5ml cryotube bottles were sterilized with ethylene oxide gas (*Steri-Vac 4XL gas sterilizer, Model 400DGP, 3M centre, St Paul, MN, USA*). The ethylene oxide gas was used, since the rise in temperature to 120ºC in the autoclave could alter the surface due to moisture absorption and the high temperature causing cracks in the GIC that was not part of normal maturation. UV light was impractical due to the large number of specimens.

10.3.5. Reconstitution of Streptococcus Mutans

Streptococcus Mutans bacteria (*ATCC 25175)* was reconstituted in brain heart infusion (BHI broth) for 24 hours at 37ºC and streaked on a contact plate (*TSA LTHth-ICR, Merck Life Science GmbH; Eppelheim; Germany; Batch 140477*) in order to isolate a single *S. mutans* colony.

10.3.6. Incubation of the GIC samples to ascertain changes in the S. mutans OD450nm over time

The single *S. mutans* colony (*ATCC 25175*) taken from the agar plate was grown overnight at 37ºC under 5% CO_2 conditions in a BHI broth. The overnight culture was added in 5µl at a time to the sterile phosphate buffered saline (PBS). The McFarland 0.5 was established and assessed with the DensiCHECK plus measuring device at a 580nm wavelength (*BioMerieux Inc, Hazelwood, Missouri, USA*). The McFarland 0.5 was equivalent to a concentration of $1.5x10^8$ *S. mutans* cells/mL in the PBS solution. One thousand millilitres of tryptic soy broth (TSB) was manufacture using 30 grams of TSB (*TSB CM0129; Oxoid Ltd; Basingstoke; Hampshire; UK*) mixed with 1000ml of de-ionised water and sterilized in an autoclave at 121ºC for 15 minutes. After the broth had cooled to 23ºC (ISO 9917-1:2007), 50µl of the McFarland standard 0.5 *S. mutans*/PBS suspension ($1.5x10^8$ *S. mutans* cells/mL in PBS) was added to 5ml of TSB in the sterile cryotube bottles (TSB/ *S. mutans).* The inoculated 5ml TSB/*S. mutans* and the five GIC samples per material were placed in an orbital shaking incubator (*MRC, Holon, Israel*) at 37ºC with a speed of 120 rotations per hour.

10.3.7. Colorimetric assay (XTT based) of cell proliferation and viability

The changes in the *S. mutans* OD450nm of *S. mutans* was measured at 0, 2, 4, 6 and 24 hours. The 5ml cryotube bottle was tipped twice at 180º and 300µl was equally divided between three wells on a 96-well plate from the 5ml cryotube TSB/ *S. mutans* bottle at 37ºC (Ma, 1997) (Figure 10.1). For the XTT analysis, each well of the 96-well plate would contain 100µl TSB/ *S. mutans* and 50µl of a XTT Cell Proliferation kit II (*Roche Diagnostics GmbH, Mannheim, Germany*). The XTT labelling reagent and coupling agent were mixed in accordance with the manufacturers' instructions (*Roche Diagnostics GmbH, Mannheim, Germany*). The spectrophotometer measurements were taken after 4 hours of incubation at 450nm (*Smart Microplate Reader, Model SMR16.1. USCN life science kit Inc, Wahan, China*). At optical density of 450nm, the mitochondrial activity was determined with the aid of formazan dye.

Figure 10.1: 96-well plate of the TSB/*S. mutans* and control *S. mutans.*

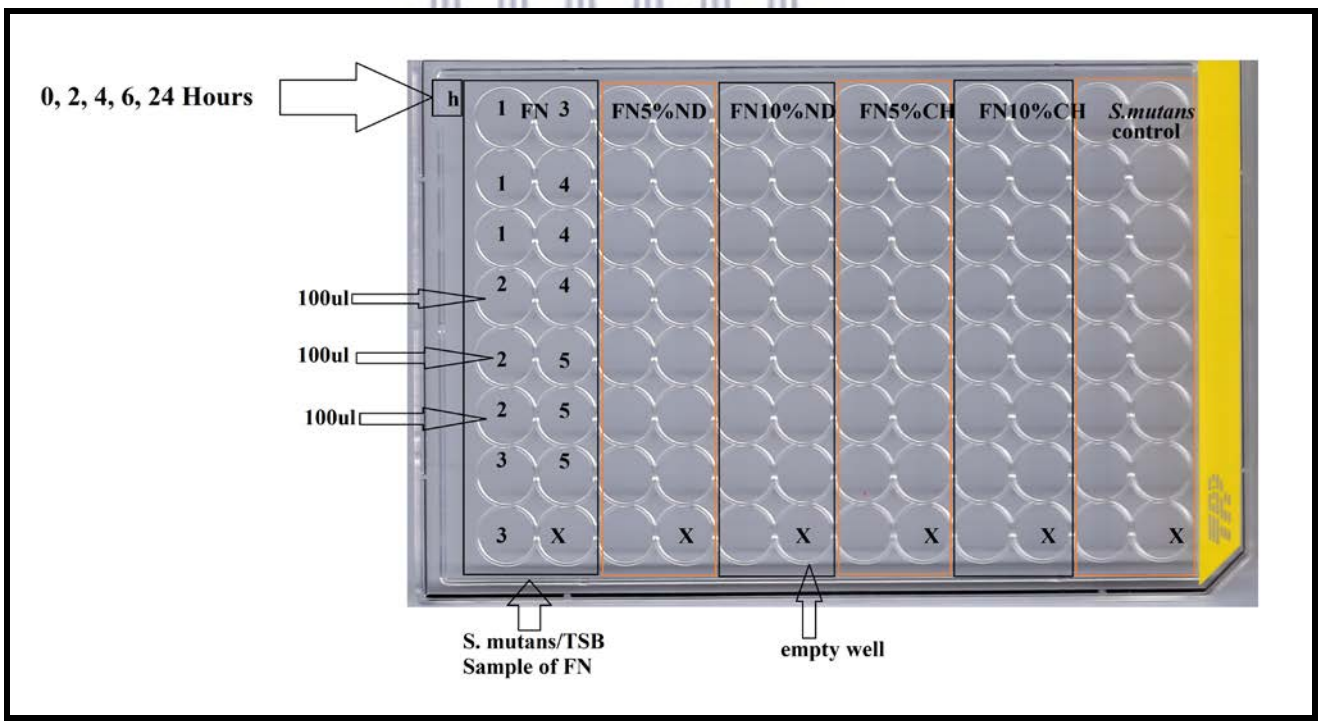

10.4. Statistical analysis

The statistical analysis for the *S. mutans* bacterial OD450nm was completed in two stages. Stage 1: The change in the bacterial OD450nm for 2, 4, 6 and 24 hours was assessed against the 0 hour *S. mutans* OD450nm within the three materials (FN, KU and RSC) and then with their respective chitosan and nanodiamond modifications. The one way ANOVA with linear mixed modelling was completed. The data was considered to be longitudinal for which the linear mixed effects models have been developed (Modern Applied Statistics with S, by W.N. Venables and B.D. Ripley).

Stage 2: One-way ANOVA was used with the p-value corresponding to the F-statistic of one-way ANOVA $p < 0.05$. This suggests that one or more treatments for *S. mutans* OD450nm were significantly different between the control and the three materials (FN, KU and RSC) and their chitosan and nanodiamond modifications. The post hoc Holm-Bonferroni formula for the first-ranked p-value was used to determine the true significance for hours 0, 2, 4, 6 and 24 in relation to the control *S. mutans* OD450nm for the same time periods.

10.5. Results

Statistical results from Stage 1: Within-group analysis for the time periods 0 hours vs 2, 4, 6 and 24 hours.

S. mutans OD450nm for the control materials FN, KU, RSC

Table 10.1 and Figure 10.2 illustrate the *S. mutans* growth incubated with the GIC material over time (the circles in Figure 10.2 represent the mean value from Table 10.1). The *S. mutans* OD450nm decreased significantly ($p < 0.0001$) from zero (0) hours through 2 hours to 4 hours for each material. At 6 hours, the *S. mutans* OD450nm increased when compared to 0, 2 and 4 hours. There were no significant differences in the OD450nm at any time period (0, 2, 4, 6

hours) between the three control GIC materials with p = 0.9969. At 24 hours there were significant differences between all three control materials (p < 0.0001). The lowest *S. mutans* OD450nm was noted for FN followed by KU. RSC had the largest *S. mutans* OD450nm.

Table 10.1: Mean *S. mutans* OD450nm of the control materials

Material	Hours				
	0	**2**	**4**	**6**	**24**
FN	0.726	0.563	0.571	0.658	0.783
KU	0.620	0.570	0.588	0.608	0.927
RSC	0.587	0.536	0.515	0.618	1.056
***S. mutans* control**	0.717	0.607	0.601	0.680	0.944
The circles in Figure 10.2 represent the mean value from Table 10.1					

Figure 10.2: Mean *S. mutans* OD450nm of the control materials

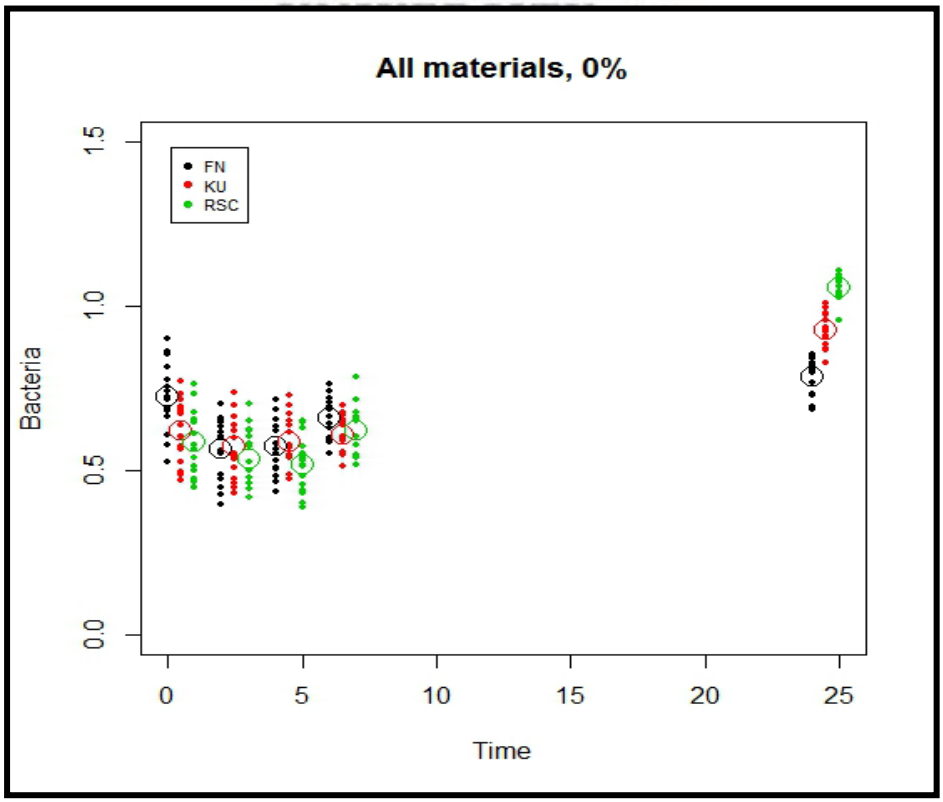

***S. mutans* OD450nm for FN and its ND modifications**

Table 10.2 and Figure 10.3 illustrate the *S. mutans* growth incubated for FN with its ND modification over time (the circles in Figure 10.3 represent the mean values from Table 10.2). The *S. mutans* OD450nm decreased significantly ($p < 0.0001$) from 0 hours through 2 hours to 4 hours for each material. At 6 hours the *S. mutans* OD450nm increased when compared to 2 and 4 hours. At 24 hours there were significant increases in *S. mutans* OD450nm compared to 0 hours ($p < 0.0001$). There were no significant differences in the *S. mutans* OD450nm at any time period (0, 2, 4, 6 and 24 hours) between FN vs FN5%ND ($p = 0.275$) and FN vs FN10%ND ($p = 0.363$).

Table 10.2: Mean *S. mutans* OD450nm of FN with its chitosan and nanodiamond modifications

Material	Hours				
	0	**2**	**4**	**6**	**24**
FN	0.726	0.563	0.571	0.658	0.783
FN5%CH	0.593	0.555	0.542	0.653	0.762
FN10%CH	0.635	0.553	0.552	0.625	0.689
FN5%ND	0.623	0.567	0.528	0.629	0.759
FN10%ND	0.686	0.711	0.670	0.753	0.831
***S. mutans* control**	0.717	0.607	0.601	0.680	0.944
The circles in Figure 10.3 and 10.4 represent the mean values from Table 10.2.					

Figure 10.3: Mean *S. mutans* OD450nm of FN with its nanodiamond modifications

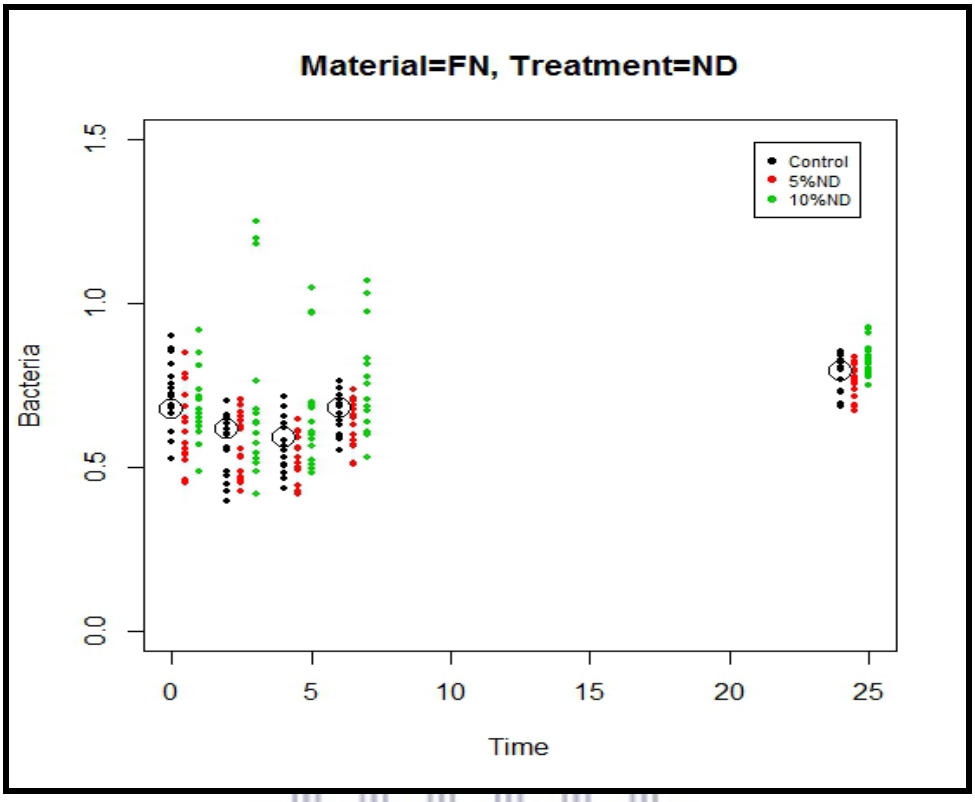

***S. mutans* OD450nm for FN and its chitosan modifications**

Table 10.2 and Figure 10.4 illustrate the *S. mutans* growth incubated for FN with its chitosan modification over time (the circles in Figure 10.3 represent the mean values from Table 10.2). At time 0 hours the 5% and 10% chitosan modifications of FN had already reduced the *S. mutans* OD450nm during the first 20 minutes of material exposure to the *S. mutans* (Table 10.2). The *S. mutans* OD450nm decreased significantly ($p < 0.0001$) from 0 hours through 2 hours to 4 hours for all three materials. At 6 hours, the *S. mutans* OD450nm increased compared to at 2 and 4 hours. At 24 hours, there was a significant increase in *S. mutans* OD450nm compared to 0, 2 and 4 hours ($p < 0.0001$). There were no significant differences in the OD450nm at any time period (0, 2, 4, 6 and 24 hours) between the three control GIC materials with $p = 0.2393$ for FN vs FN5%CH and $p = 0.1469$ for FN vs FN10%CH.

Figure 10.4: Mean *S. mutans* OD450nm of FN with its chitosan modifications

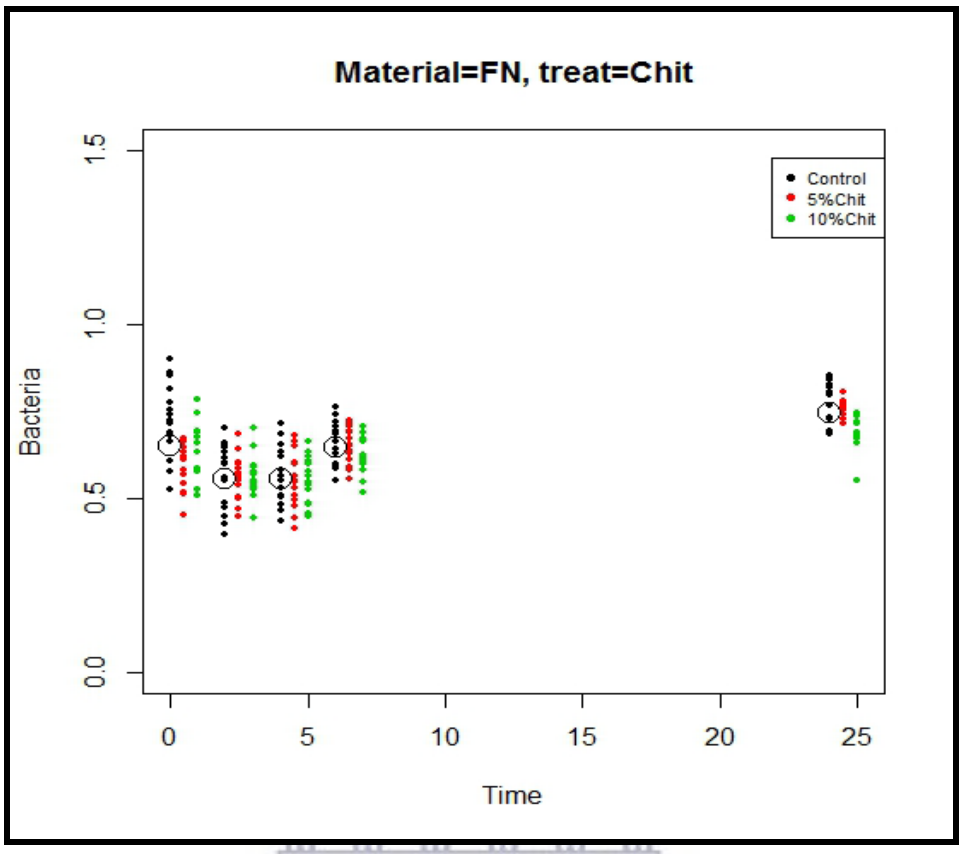

***S. mutans* OD450nm for FN modifications of chitosan vs nanodiamonds.**

Table 10.2 and Figure 10.4 illustrate the *S. mutans* growth incubated for FN with its 10%CH and 10%ND modification over time (the circles in Figure 10.5 represent the mean values from Table 10.2). There were no significant differences between the 5%CH vs 5%ND or the 10%CH vs the 10%ND modification of FN ($p = 0.1639$).

Figure 10.5: Mean *S. mutans* OD450nm of the FN modifications: 10%CH vs 10%ND modifications

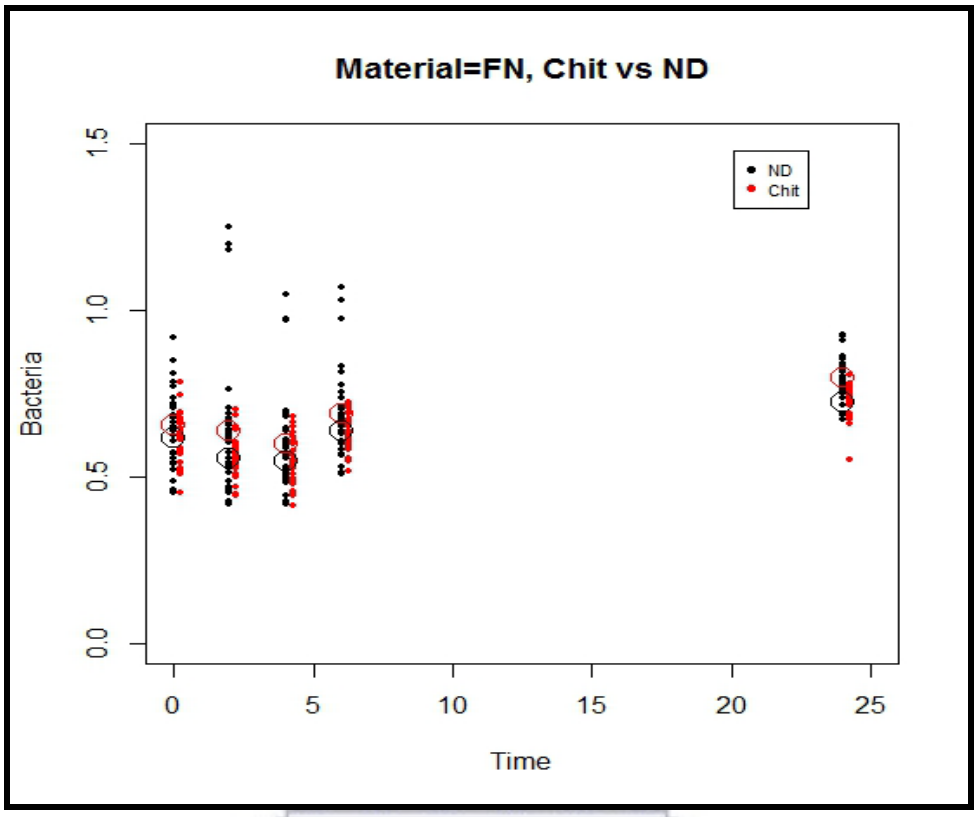

***S. mutans* OD450nm for KU and its nanodiamond modifications**

Table 10.3 and Figure 10.6 illustrate the *S. mutans* growth incubated for KU with its nanodiamond modification over time (the circles in Figure 10.6 represent the mean values from Table 10.3). The *S. mutans* OD450nm decreased significantly ($p < 0.0001$) from 0 hours to 2 hours for each nanodiamond-modified KU material. At 6 hours, the *S. mutans* OD450nm increased compared to at 2 and 4 hours. At 24 hours there was a significant increase in *S. mutans* OD450nm compared to 0, 2, 4, 6 and 24 hours ($p < 0.0001$). There were no significant differences in the *S. mutans* OD450nm at any time period (0, 2, 4, 6 and 24 hours) between KU vs KU5%ND ($p = 0.8262$) and KU vs KU10%ND ($p = 0.5497$).

Table 10.3: Mean *S. mutans* OD450nm of KU with its chitosan and nanodiamond modifications

Material	Hours				
	0	**2**	**4**	**6**	**24**
KU	0.620	0.570	0.588	0.608	0.927
KU 5%CH	0.616	0.548	0.569	0.617	0.903
KU 10%CH	0.597	0.531	0.611	0.678	0.842
KU 5%ND	0.635	0.566	0.565	0.577	0.930
KU 10%ND	0.570	0.539	0.536	0.650	0.906
***S. mutans* control**	0.717	0.607	0.601	0.680	0.944
The circles in Figure 10.6 and 10.7 represent the mean values from Table 10.3.					

Figure 10.6: Mean *S. mutans* OD450nm of KU with its nanodiamond modifications

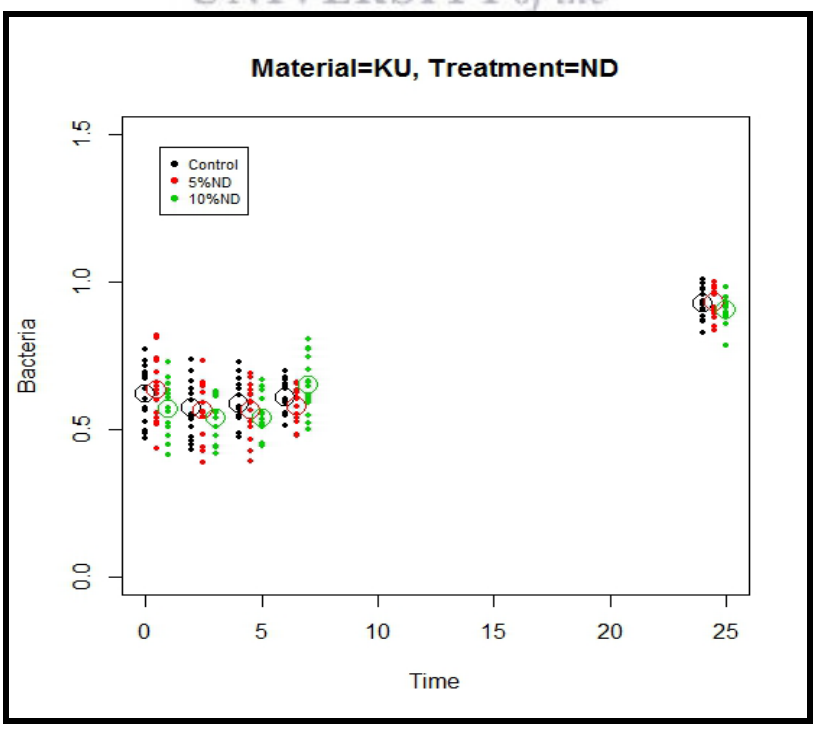

S. mutans OD450nm for KU and its chitosan modifications

Table 10.3 and Figure 10.7 illustrate the *S. mutans* growth incubated for KU with its chitosan modification over time. The circles in Figure 10.7 represent the mean value from Table 10.3. At time 0 hours, the 5% and 10% chitosan modifications of KU already reduced the *S. mutans* OD450nm during the first 20 minutes of material exposure to the *S. mutans* (Table 10.3). The *S. mutans* OD450nm decreased significantly ($p < 0.0001$) from 0 hours through 2 hours to 4 hours for all three materials. At 6 hours, the *S. mutans* OD450nm increased compared to at 2 and 4 hours. At 24 hours there was a significant increase in *S. mutans* OD450nm compared to 0, 2 and 4 hours ($p < 0.0001$). There were no significant differences in the *S. mutans* OD450nm at any time period (0, 2, 4, 6 and 24 hours) between the three control GIC materials with $p = 0.7363$ for KU vs KU5%CH and $p = 0.1469$ for KU vs KU10%CH.

Figure 10.7: Mean *S. mutans* OD450nm of KU with its chitosan modifications

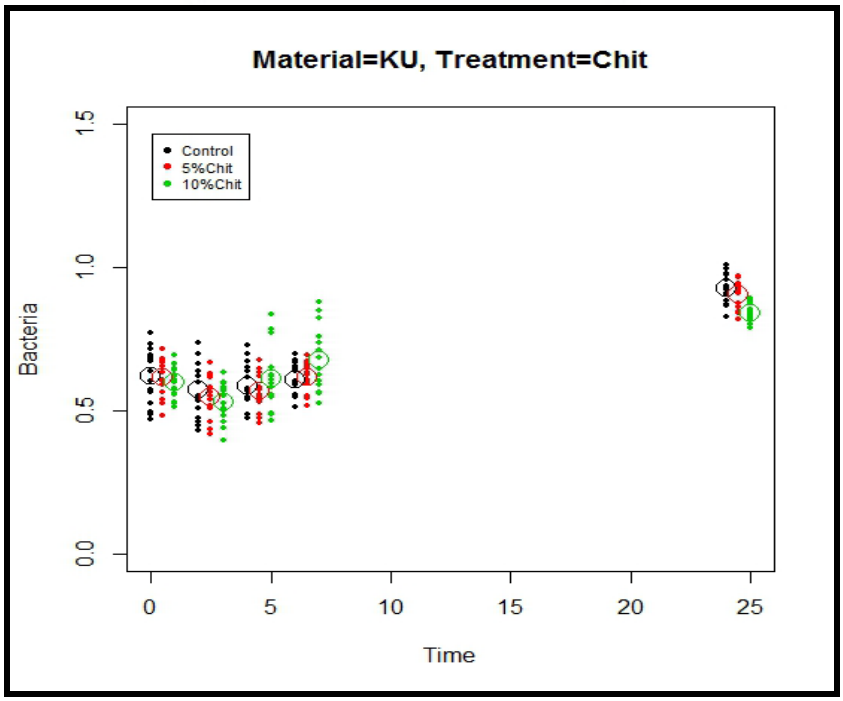

***S. mutans* OD450nm for KU modifications of chitosan vs nanodiamonds**

Table 10.3 and Figure 10.7 illustrate the *S. mutans* growth incubated for KU with its 10%CH and 10%ND modification over time. The circles in Figure 10.7 represent the mean values from Table 10.3. There were no significant difference between the 5%CH vs 5%ND or the 10%CH vs 10%ND modification of KU ($p = 0.8411$).

Figure 10.8: Mean *S. mutans* OD450nm of the KU modifications: 10%CH vs 10%ND modifications

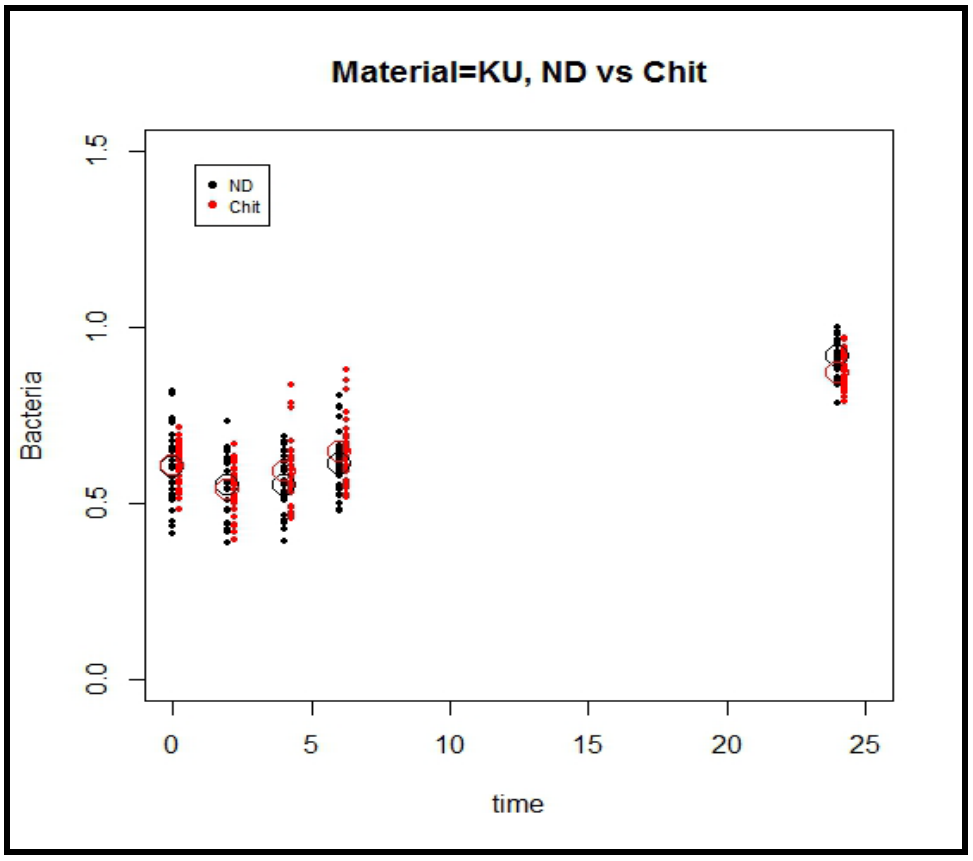

***S. mutans* OD450nm for RSC and its nanodiamond modifications**

Table 10.4 and Figure 10.9 illustrate the *S. mutans* growth incubated for RSC with its nanodiamond modification over time. The circles in Figure 10.9 represent the mean values from Table 10.4. The *S. mutans* OD450nm decreased significantly ($p < 0.0001$) from 0 hours to 2 hours through to 4 hours for each nanodiamond-modified RSC material. At 6 hours, the *S. mutans* OD450nm increased compared to at 2 and 4 hours. At 24 hours there was a significant

increase in *S. mutans* OD450nm compared to 2, 4, 6 and 24 hours ($p < 0.0001$). There were no significant differences in the OD450nm at any time period (0, 2, 4, 6 and 24 hours) between RSC vs RSC 5%ND ($p = 0.7965$) and RSC vs RSC 10%ND ($p = 0.3490$).

Table 10.4: Mean *S. mutans* OD450nm of RSC with its chitosan and nanodiamond modifications

Material	Hours				
	0	**2**	**4**	**6**	**24**
RSC	0.587	0.536	0.515	0.618	1.056
RSC 5%CH	0.586	0.535	0.552	0.630	1.045
RSC 10%CH	0.558	0.525	0.547	0.633	1.021
RSC 5%ND	0.533	0.543	0.557	0.598	0.973
RSC 10%ND	0.668	0.592	0.516	0.635	1.081
***S. mutans* control**	0.717	0.607	0.601	0.680	0.944
The circles in Figure 10.9 and 10.10 represent the mean value from Table 10.3.					

Figure 10.9: Mean *S. mutans* OD450nm of RSC with its nanodiamond modifications

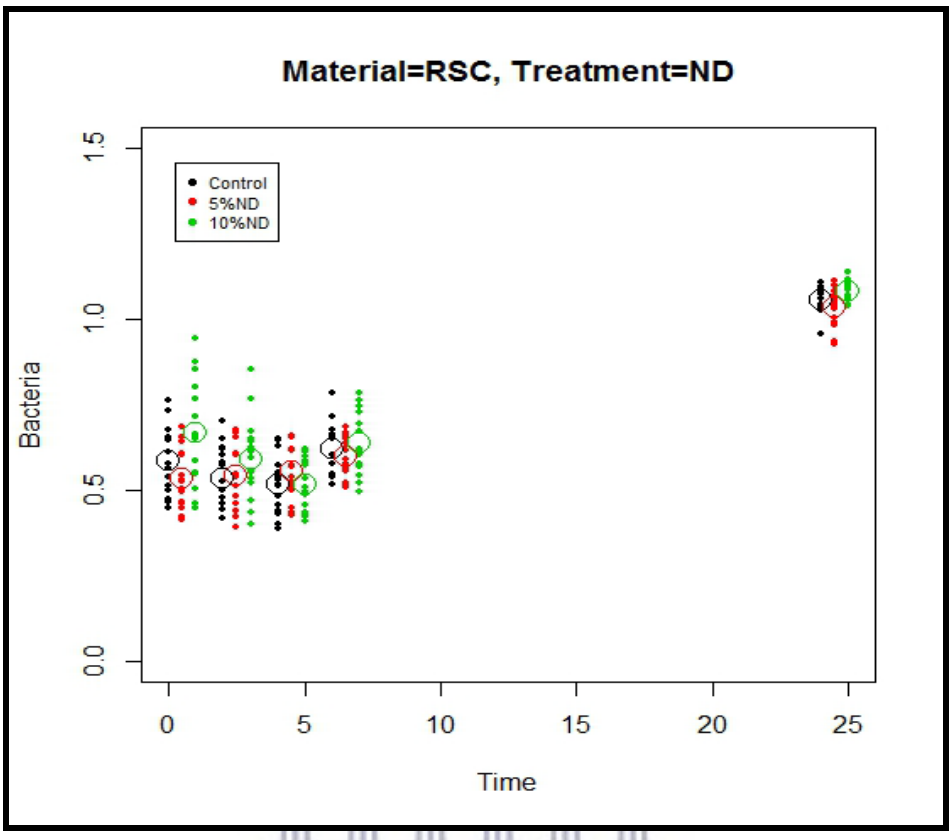

***S. mutans* OD450nm for RSC and its CH modifications**

Table 10.4 and Figure 10.10 illustrate the *S. mutans* growth incubated for RSC with its chitosan modifications over time. The circles in Figure 10.10 represent the mean values from Table 10.4. At zero hours, the 5% and 10%CH modifications of RSC already had reduced the *S. mutans* OD450nm during the first 20 minutes of material exposure to the *S. mutans* (Table 10.4). The *S. mutans* OD450nm decreased significantly ($p < 0.0001$) from 0 hours through 2 hours to 4 hours for all three materials. At 6 hours, the *S. mutans* OD450nm increased compared to at 2 and 4 hours. At 24 hours, there was a significant increase in *S. mutans* OD450nm compared to at 2 and 4 hours ($p < 0.0001$). There were no significant differences in the OD450nm at any time period (0, 2, 4, 6 and 24 hours) between the three control GIC materials with $p = 0.8409$ for RSC vs RSC 5%CH and $p = 0.8803$ for RSC vs RSC 10%CH.

Figure 10.10: Mean *S. mutans* OD450nm of RSC with its chitosan modifications

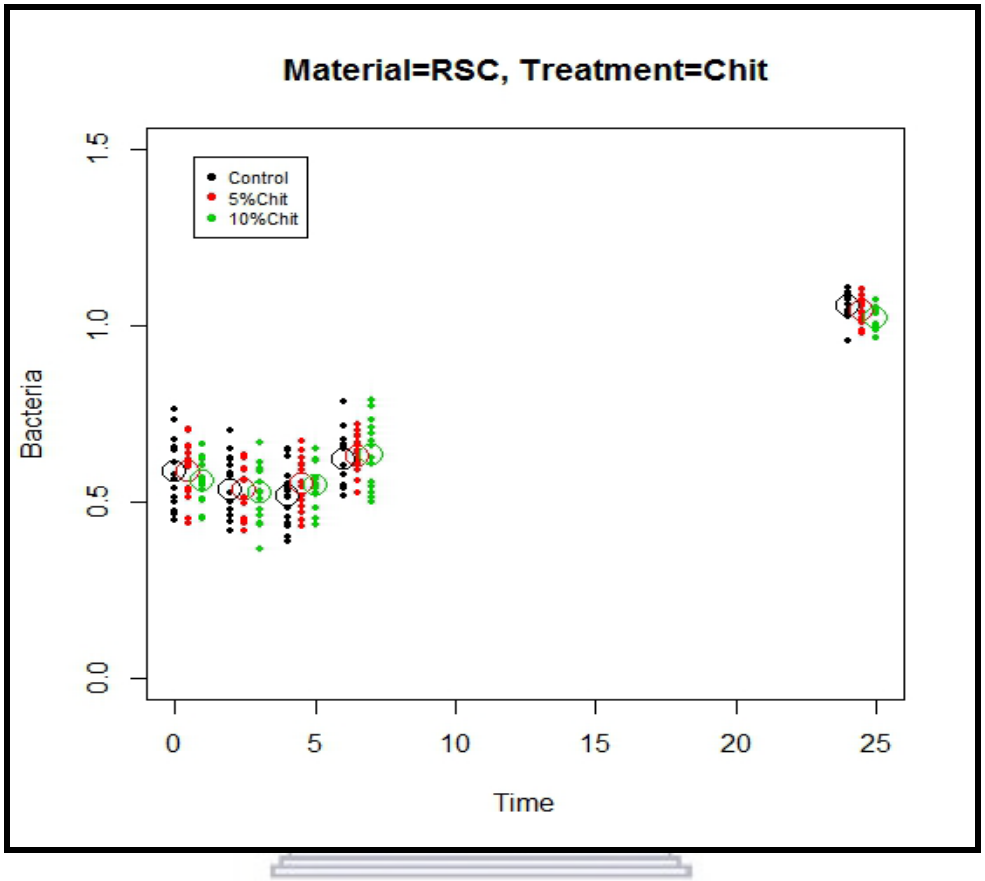

***S. mutans* OD450nm for RSC modifications of CH vs ND**

Table 10.4 and Figure 10.10 illustrate the *S. mutans* growth incubated for RSC with its 10%CH and 10%ND modification over time. The circles in Figure 10.10 represent the mean values from Table 10.4. There were no significant differences between the 5%CH vs 5%ND or the 10%CH vs 10%ND modification of RSC (p = 0.1936).

Figure 10.11: Mean *S. mutans* OD450nm of the RSC modifications: 10%CH vs 10%ND modifications

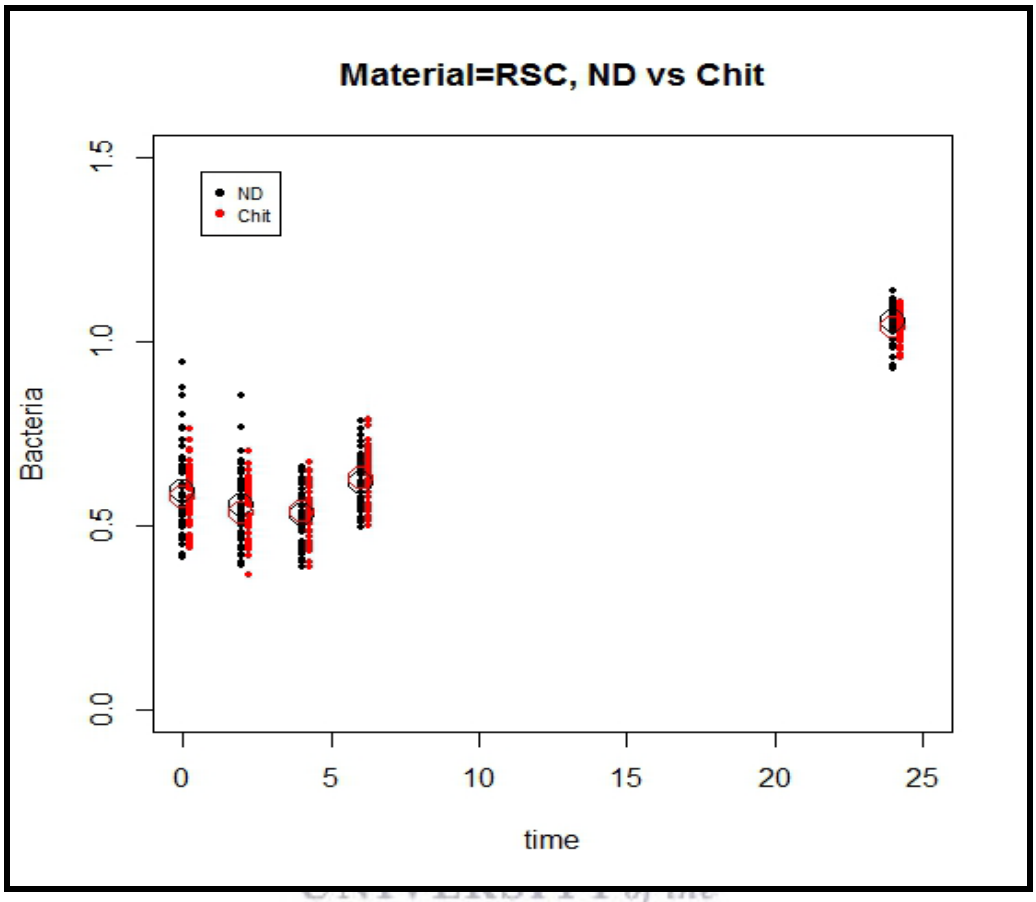

Comparison of the RSC modifications chitosan and the nanodiamond

Statistical results from Stage 2*: S. mutans* OD450nm of the control *S. mutans* vs the control materials and their modifications

Figures 11, 12 and 13 indicate the significant reduction of the *S. mutans* OD450nm within the material group. Only FN, FN5%ND, FN10%ND, FN10%CH and KU10%CH demonstrated a significant ($p < 0.01$ (indicated by "*") reduction compared to the *S. mutans* control OD450nm at 24 hours. A significant difference of $p < 0.05$ is indicated by "^".

FN, KU, RSC and all their modifications had lower *S. mutans* OD450nm than the *S. mutans* control OD450nm (except for FN10%ND at 2, 4 and 6 hours). However, this was not significant for all the time periods (Figure 10.12).

Figure 10.12: Mean *S. mutans* OD450nm of FN and the respective modifications in relation to the control *S. mutans* OD450nm

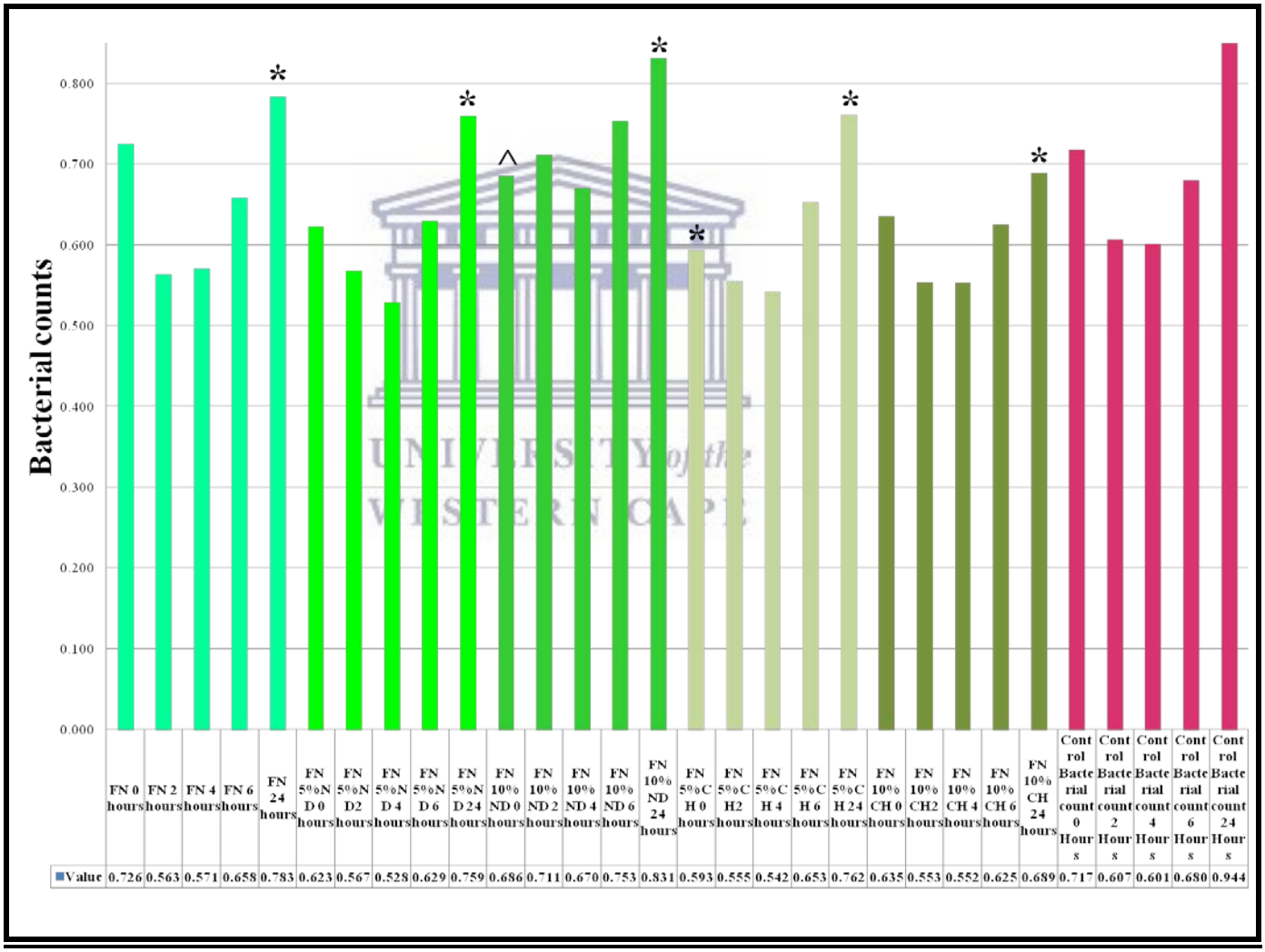

Figure 10.13: Mean *S. mutans* OD450nm of KU and the respective modifications in relation to the control *S. mutans* OD450nm

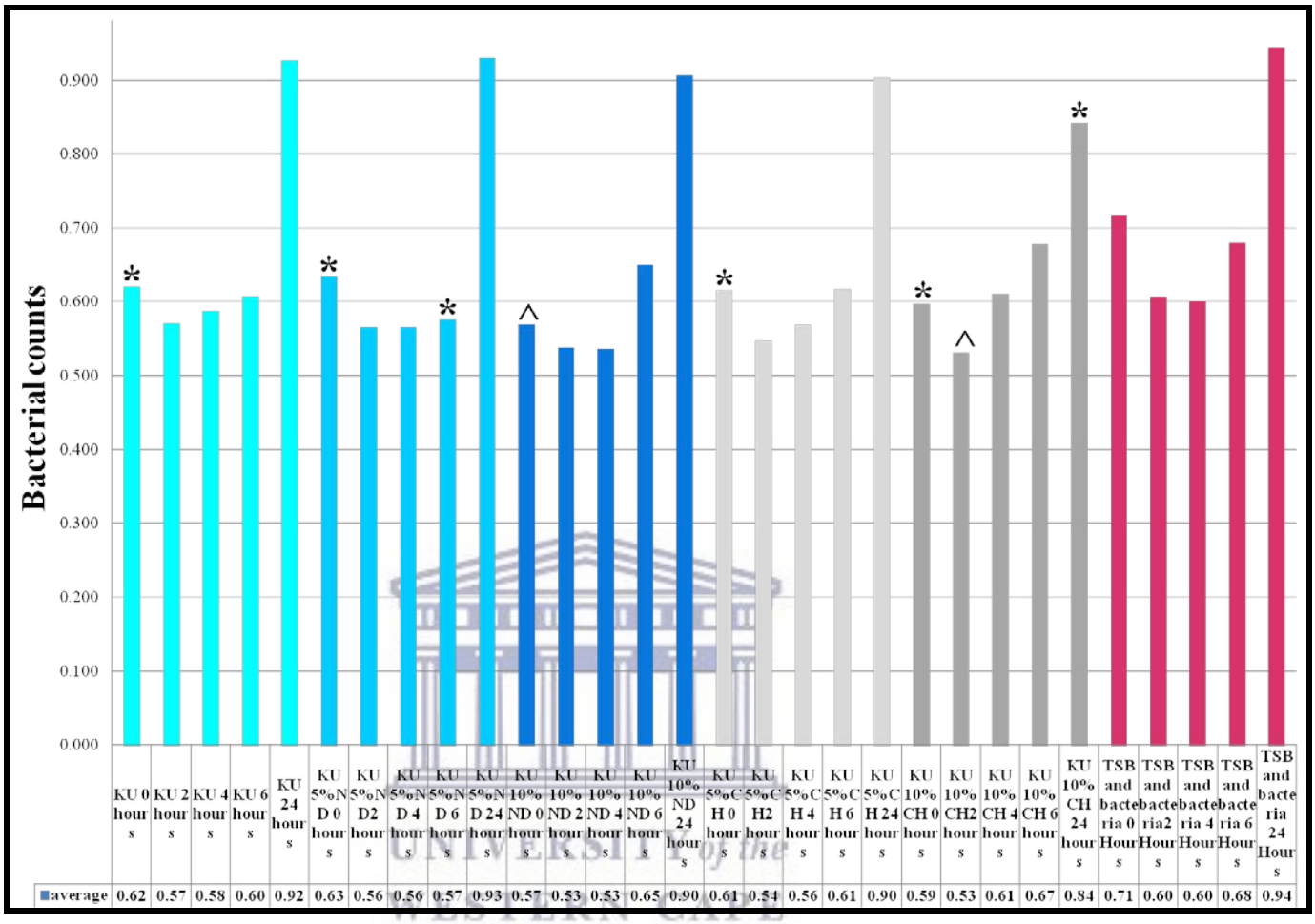

Figure 10.14: Mean *S. mutans* OD450nm of RSC and its respective modifications in relation to the control *S. mutans* OD450nm

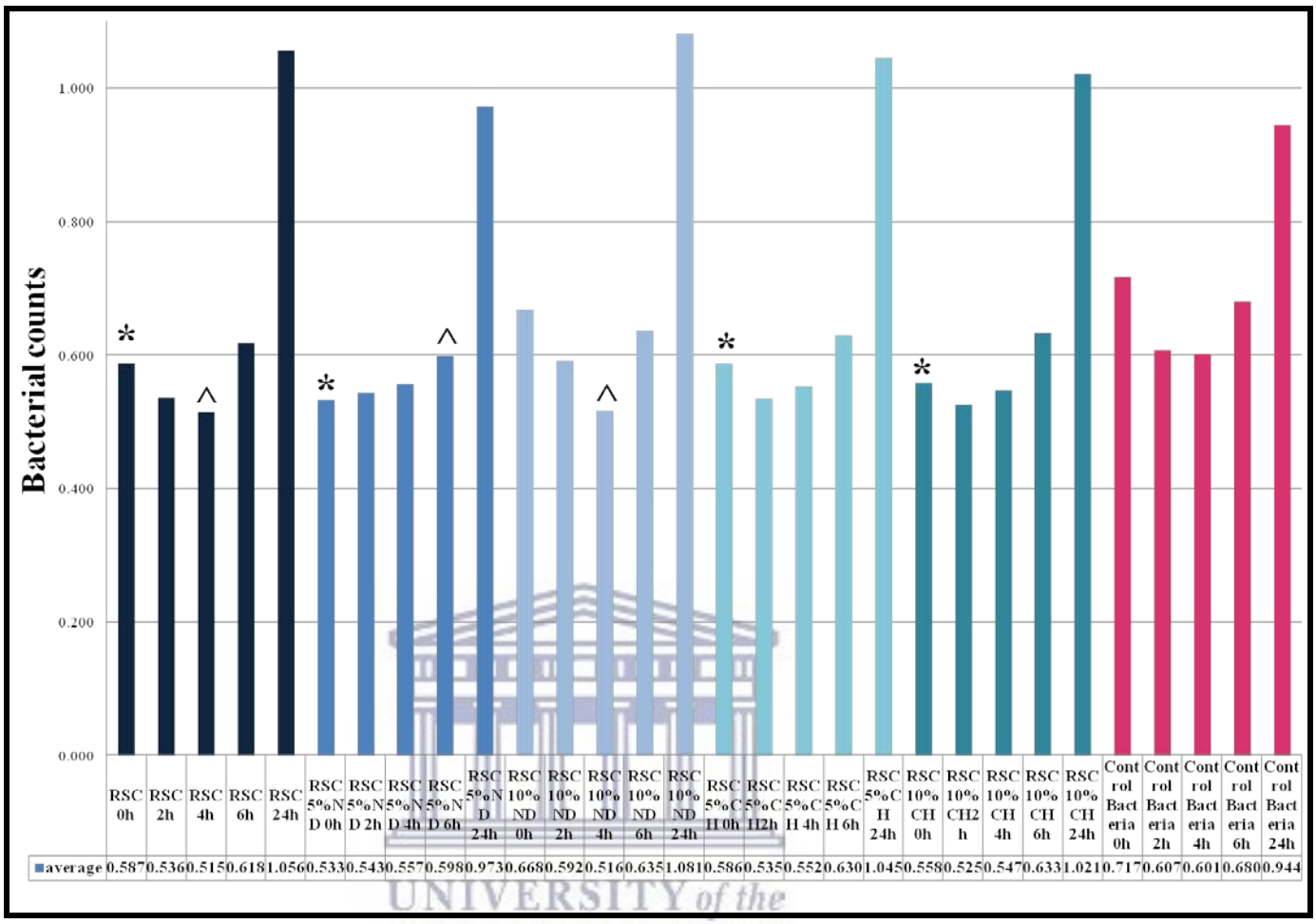

Surface roughness change

Figure 10.15 illustrates the difference in the surface roughness between the start of the experiment (0 hours) and the end of the study (24 hours). The difference in percentage was calculated by using the following formula: [(100 / Ra 0 hours) x (Ra 24 hours)] – [100].

A positive percentage change of the surface roughness from 0 hours to 24 hours represents an increase in surface roughness. Table 10.5 indicates the precise surface roughness values as recorded for each material at 0 hours and at 24 hours. $p < 0.05$ indicates significant differences.

Table 10.5: Change in surface roughness values from 0 hours to 24 hours for each material

	FN	FN5%ND	FN10%ND	FN5%CH	FN10%CH
Ra 0 hours	0.971	1.371	0.990	1.023	1.650
Ra 24 hours	1.116	1.333	1.187	2.085^	3.447^
	KU	**KU5%ND**	**KU10%ND**	**KU5%CH**	**KU10%CH**
Ra 0 hours	0.833	0.736	0.924	1.196	1.581
Ra 24 hours	0.871	0.751	0.774	2.021^	2^
	RSC	**RSC5%ND**	**RSC10%ND**	**RSC5%CH**	**RSC10%CH**
Ra 0 hours	1.366	1.163	1.244	1.617	1.797
Ra 24 hours	1.338	1.115	1.301	2.528^	2.716^
(^): Indicates significant change $p < 0.05$ for the respective material.					

Figure 10.15: Percentage of surface roughness change from 0 hours to 24 hours

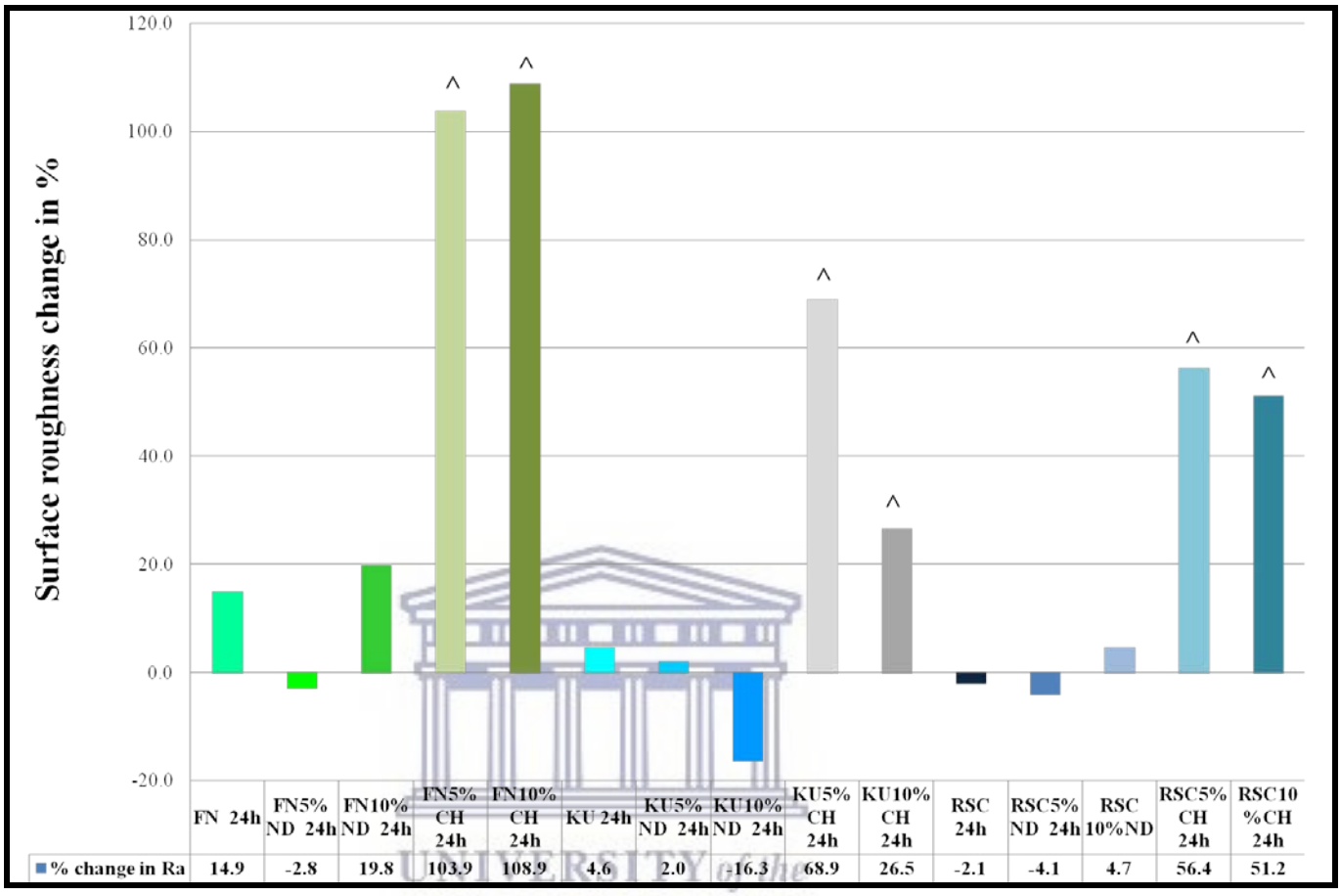

10.6. Discussion

The hypothesis that chitosan- and nanodiamond-modified GICs would significantly reduce the *S. mutans* OD450nm in relation to the control bacteria as well as not influence the surface roughness was rejected for all the chitosan and nanodiamond modifications.

Being a dominant bacterial species in the dental plaque and its importance in the caries process, research of dental materials and the impact of *S. mutans* continually needs to be investigated (Gambhir *et al*., 2013). The colonization of plaque in the oral cavity and on various surfaces is complicated and occurs in phases. Firstly, the various components of saliva, crevicular fluid and colonizing bacteria play a role in pellicle formation (Scannapieco, 1994; Bollen *et al*., 1996).

Nanodiamonds (NDs) combined with GICs provide the potential for enhancing the antibacterial activities of the GIC. Nanodiamonds are predominantly manufactured through a process of detonation synthesis. The nanodiamonds are produced by detonating 60% weight percentage TNT ($C_6H_2(NO_2)_3CH_3$) and a 40% weigh percentage of hexogen ($C_3H_6N_6O_6$) in a negative oxygen environment. The detonation occurs inside a metallic chamber with an atmosphere of N_2, CO_2 and liquid or solid water (Danilenko, 2004). The nanodiamond particles that form have a graphitized outer layer where the various functional groups are present. Carboxylic groups are among the most common and abundant functional groups (Ullah et al., 2015) (Figure 10.16). The carboxylic groups present on the nanodiamond surface participate with ion exchange during the GIC acid-base reactions. The ion exchange occurs specifically with Al^{3+} and Sr^{2+} to form various metal salts which can be released upon hydrolysis (Panich *et al.*, 2011). This was noted and discussed in detail previously (Chapter 7).

Figure 10.16: Possible functional groups on the graphitized outer layer of a nanodiamond

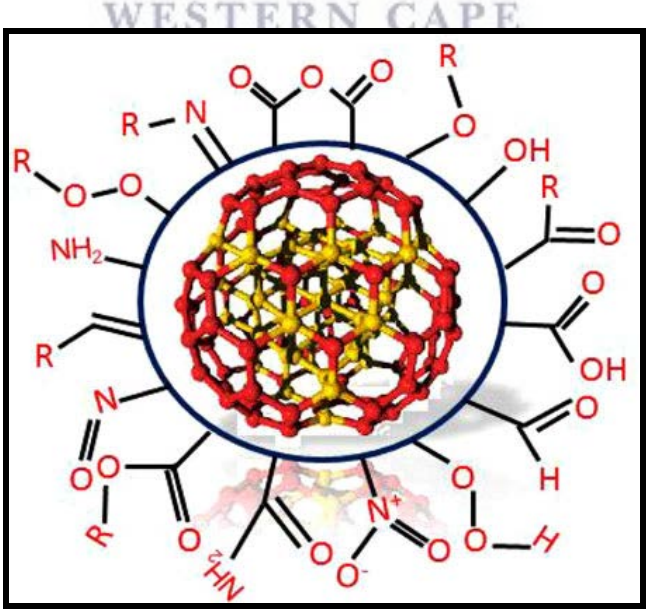

Image used with permission from: (Ullah *et al.*, 2015)

After the initial manufacture of the nanodiamond particles, they undergo a purification process. At this stage, the oxidation of the nanodiamond removes various functional groups from the surface. The resultant nanodiamond particle has multiple oxygen-containing surface species like carboxylic acids and anhydrides (Osswald *et al*., 2006). It has been shown that the nanodiamond particles used in this dissertation (*PL-D-G01*) exhibit a variety of reactive oxygen groups like acid anhydrides (Figure 10.18). The acid anhydrides have two acyl groups joined together by an oxygen atom (Figures 10.18 and 10.19). The other oxygen-containing functional groups such as hydroxyl-, alkyl- (derived from sp^3-carbon), carboxylic- (C=O) and aromatic groups (C=C) (Mochalin *et al*., 2011; Wehling *et al*., 2014) have been noted by other researchers. The various oxygen-containing functional groups add to the antibacterial activities of the nanodiamond particle. The major surface groups of the nanodiamond particles used in this dissertation (*PL-D-G01*) are therefore carboxylic acid (COOH) and hydroxide (OH) (Yoshida *et al*., 2000).

Figure 10.17: $ND_{raw\ n.u}$ illustration of the nanodiamond particles used in this dissertation

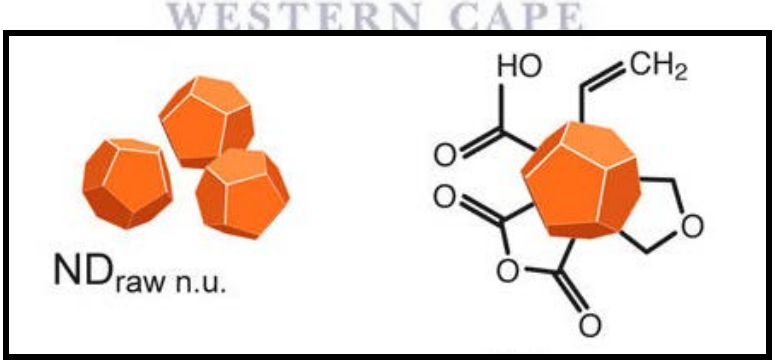

Image used with permission from: (Wehling *et al*., 2014)

Figure 10.18: Functional group namely: acid anhydrate

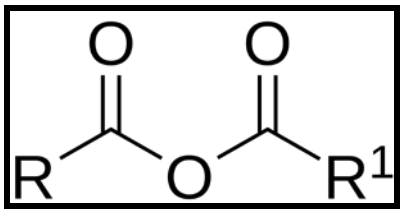

Figure 10.19: Acid anhydride and the reactions that are possible

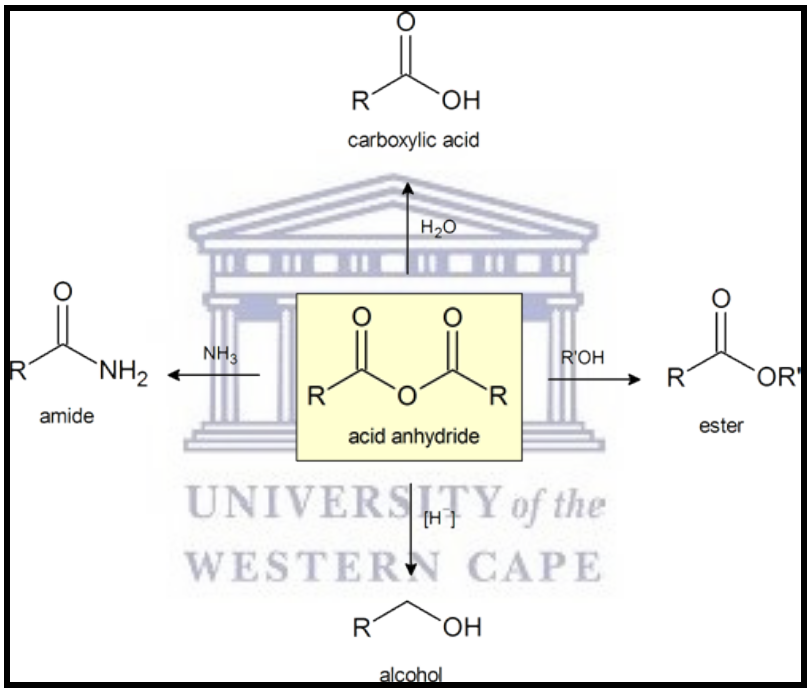

Image 17 and 18 obtained from:

https://chem.libretexts.org/Courses/Athabasca_University/Chemistry_360%3A_Organic_Chemistry_II/Chapter_21%3A_Carboxylic_Acid_Derivatives%3A_Nucleophilic_Acyl_Substitution_Reactions/21.05_Chemistry_of_Acid_Anhydrides

The antibacterial effect of the nanodiamond particles as represented in Figure 10.17 has been tested against various bacterial species. The reduction of ATP production of gram-negative *E. coli* to less than 10% was achieved with nanodiamond particles in a concentration of 50- and

500mg/L within 15 minutes when compared to the control. Similar results were noted with the gram-positive bacterium of *B. subtilis* (Wehling *et al*., 2014). In this study, a similar trend was observed with the nanodiamond modifications of FN, KU and RSC where many of the GIC modifications had a significant reduction at 0 hours (after 20 minutes of exposure to *S. mutans*) compared to the *S. mutans* control (Figures 10.12-10.4). Wehling *et al*. (2014) further identified that nanodiamond particles with *E. coli* at a non-lethal dose (0.5mg/L) were phagocytosed by the bacterium. The irregular shape of the bacterium in Figure 10.20 indicates stress within the bacterium.

Figure 10.20 Nanodiamond particle inside *E. coli.*

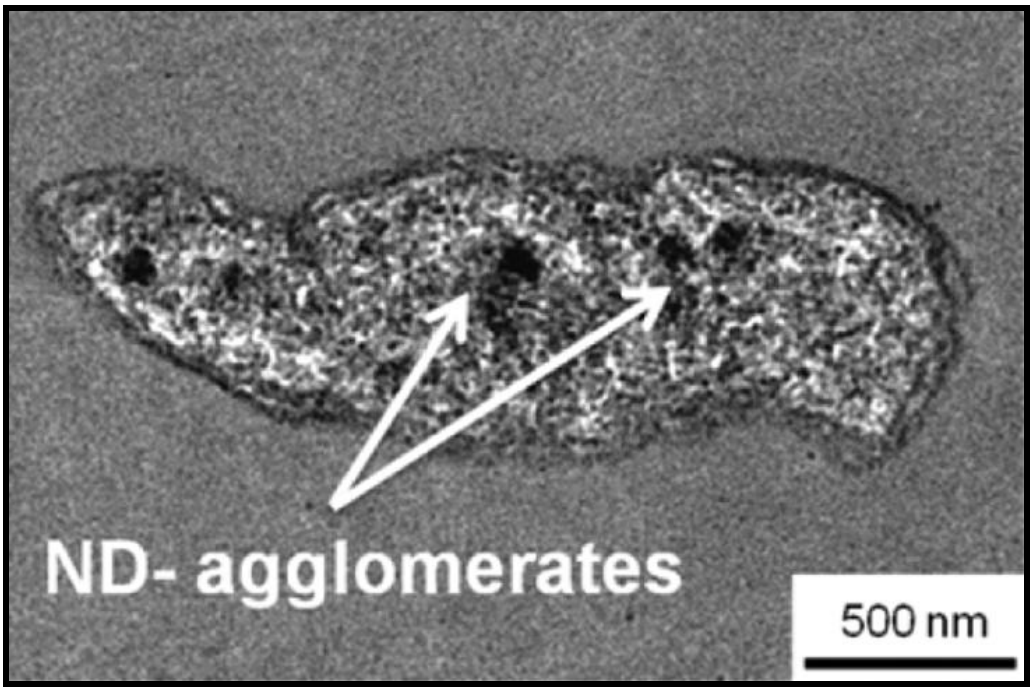

Image used with permission from: Wehling *et al*., 2014

Wehling *et al*. (2014) concluded that the antibacterial property of the nanodiamond (*PL-D-G01*) was not only due to the surface functional groups of the nanodiamond, but also to the change in the Zeta potential. The loss of the surface reactive functional groups resulted in reduction of the negative Zeta potential to become more positive. The acid anhydrate functional group (Figures 10.18 and 10.19) was established to be the distinguishing antibacterial group of the nanodiamond particle (Chng and Pumera, 2013; Wehling *et al*., 2014). In the nanodiamond-

modified GICs used in this dissertation, non-covalent interactions occurred between the nanodiamond particles, the ions of the GIC and the polyacrylic liquid (Huang and Chang, 2004). This type of non-covalent interaction would therefore include ionic interactions, hydrogen bonding and dipole-dipole bonding to the nanodiamond particles' (*PL-D-G01*) terminated carboxyl groups and the other oxygen-containing groups (Mochalin *et al*., 2011; Wehling *et al*., 2014).

The bacterial adherence to the inhabiting environment is essential to their survival in the oral cavity (Fejerskov and Kidd, 2005). Thus if the adherence can be influenced, the tongue, saliva flow and swallowing action will remove the loose bacteria from the oral cavity. Studies on the bacterial adherence to GICs and the subsequent biofilm formation on the surface have shown that GICs do influence the bacterial adherence as well as the biofilm formation (Hayacibara *et al*., 2003; Nakajo *et al*., 2009). The biofilm comprises of the initial adsorption of glucan-binding proteins produced from the saliva (Scannapieco, 1994) by *S. mutans* (Banas and Vickerman, 2003) and pioneer bacterial colonies within the pellicle. *S. mutans* synthesise an adhesive glycan from sucrose (Yamashita *et al*., 1993) and in combination with the van der Waals electrostatic forces, create a reversible adherence to teeth. As the various microbes of especially *S. sangius* and *S. mutans* anchor to the pellicle, the plaque becomes visible after 12 to 24 hours. The extra-cellular polysaccharides (EPSs), glucosyltransferases (GTFs) (Schilling and Bowen, 1992) and the various proteins produced by bacteria (Hannig, 1997) can all be vulnerable to the influence of the nanodiamond particles incorporated into the GICs. FN has been extensively used for *in vitro* studies for various aspects of research on its properties and clinical success (Da Silva *et al*., 2007) and is therefore an ideal material to have as a control material. Table 10.2 and Figure 10.2 illustrate that all the commercial GICs (FN, KU and RSC) showed a reduction in the *S. mutans* OD450nm in relation to the control bacteria. Although it was not significantly reduced for FN

when compared to the control for 2, 4 and 6 hours, there was a significant reduction at the 24 hour growth period. This was the general trend for the chitosan and nanodiamond modifications as well. KU and RSC showed similar trends with a significant reduction in *S. mutans* OD450nm for 0 and 4 hours compared to the control bacteria. This study therefore illustrates that when the GICs are exposed to the *S. mutans* for various time periods 2, 4, 6 hours there was a decrease in the *S. mutans* OD450nm in relation to the control bacteria. At 0 and 24 hours, the *S. mutans* OD450nm were variable between the various chitosan and nanodiamond modifications in relation to the control. With significant differences ($p < 0.0001$) noted between the three control materials at 24 hours, it became clear from Figures 10.21-10.23 why the *S. mutans* OD450nm of FN (0.783), KU (0.927) and RSC (1.056) differed. The white arrows indicate the *S. mutans* that formed biofilms at various thicknesses. The *S. mutans* for the material samples of FN and KU were smaller and more individually spread, with the filler particles of the GICs still visible. For RSC the biofilm ranges from transparent biofilm to very thick biofilm coverage of the filler particles and matrix of the GIC and many quorum forming *S. mutans.* Figures 10.21-10.23 correlate well with the result of Figure 10.2 at 24 hours in that the biofilm that formed was the thickest and best developed for RSC followed by KU and then FN.

Figure 10.21: *S. mutans* on the surface of FN

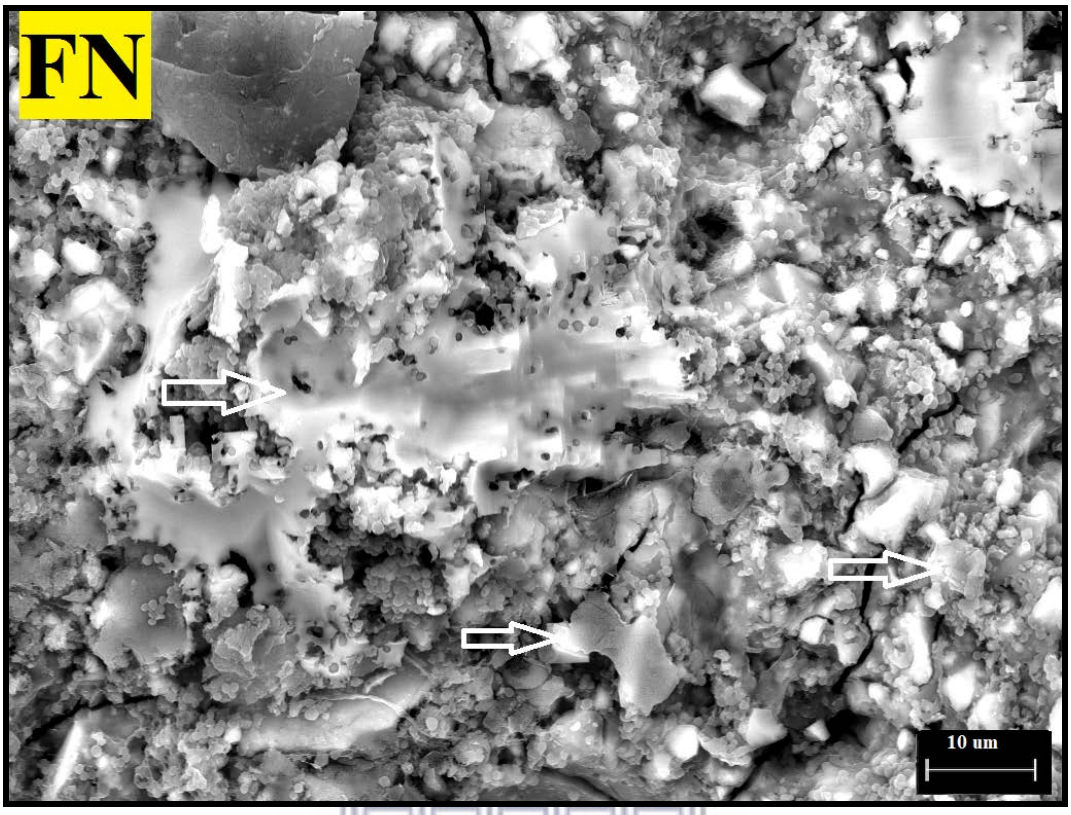

Figure 10.22: *S. mutans* on the surface of the KU

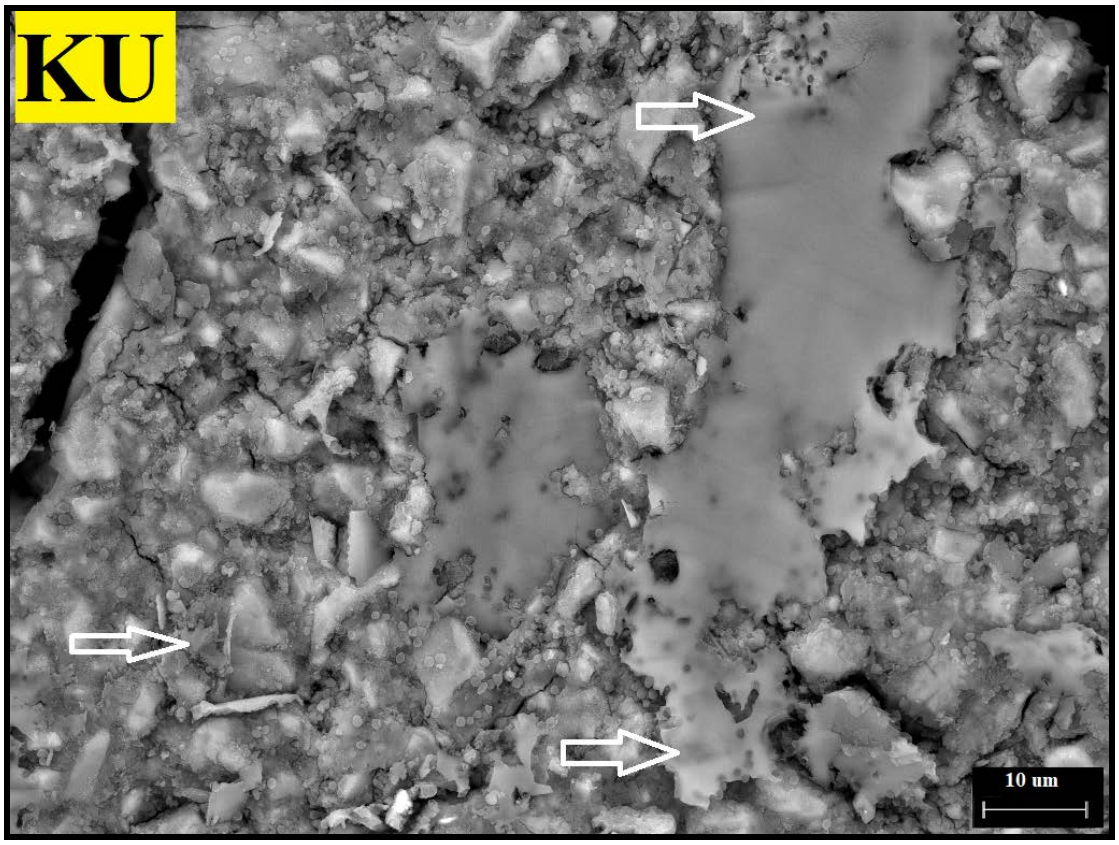

Figure 10.23: *S. mutans* on the surface of the RSC

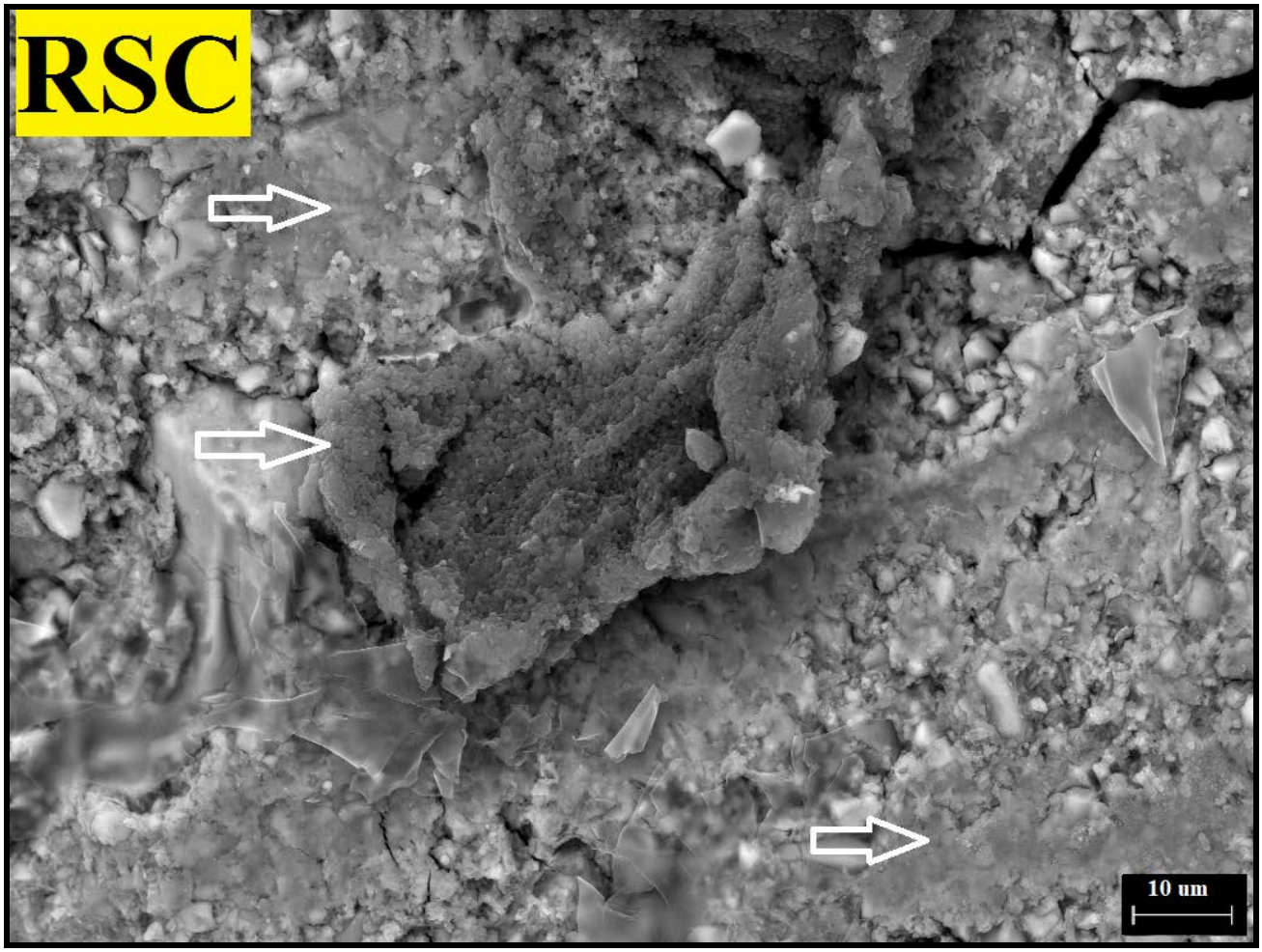

Nanodiamonds (ND) are ideal particles for integration with GICs because they retain many of the true diamond properties like thermal conductivity, stiffness, hardness and Young's modulus of elasticity (Mochalin *et al*., 2011). Due to the nano size, the dispersion of the nanodiamond particles should be more ideal if it were to have a random dispersion. Random dispersion will allow the exploitation of the large surface area of the nanoparticles and therefore the many exposed functional groups of these nanodiamond particles. The nanodiamond particles used are supplied by the manufacturer as non-clustered. Unfortunately the clustering (or rather agglomeration) of the nanodiamond particles did however occur due to various cohesive and adhesive forces between the nanodiamond particles (Bika *et al*., 2001) while they are stored in

their packaging. These clusters form due to capillary forces pulling the individual nanoparticles together during the drying of the nanodiamonds (for storage) at the manufacturer (Mochalin *et al*., 2011). When combining the nanodiamond particles with the GIC powder, the problem with the nanodiamonds was that although it appeared as if the GIC and the nanodiamond particles were homogeneously mixed, during the hand-mixing process, seemingly small clusters of agglomerated nanodiamond particles were noted. Fortunately, the spatulation process separated many of them into micro-sized agglomerated clusters. The advantages of nanodiamonds are the large surface area due to the nanoparticles. When the nanoparticles agglomerate to form a larger "microdiamond agglomerated particle", there will be less functional groups around the circumference of the particle that can interact with the ions from the GIC and the forming matrix. The interaction of these agglomerated nanodiamond particles and the substrate (e.g. GIC), might not be suitable if the powder and liquid do not integrate completely during the mixing process (Chapter 6). This integration occurs to a point, but the agglomerated nanodiamond particle interaction with the GIC is based on the wetting ability and the rate of polyacrylic acid absorption during mixing. This resulted in the need to assess the surface roughness (Ra) after *S. mutans* exposure. Figure 10.24 illustrates the interaction of the edge of an agglomerated nanodiamond particle (grey surface on the left) to the GIC matrix (right) with the red/white arrow indicating the nanodiamond. It can be clearly seen that the edge of the agglomerated nanodiamond particle was bound to the GIC matrix. The *S. mutans* at the white arrow is clearly visible on the GIC filler particle with only a few individual *S. mutans* seen on the nanodiamond agglomerated particle indicated by the red/white arrow (Figure 10.24).

Figure 10.24: KU5%ND nanodiamond agglomerate and the GIC matrix

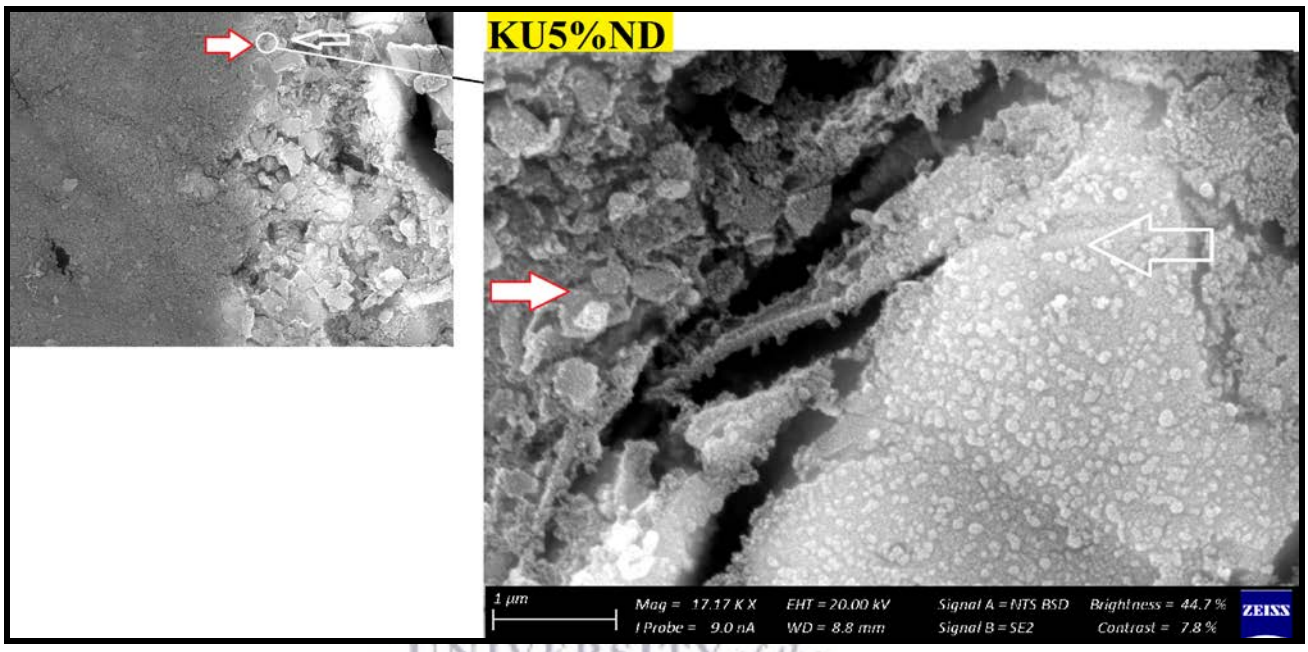

The integrity of the nanodiamond agglomerated particle is dependent upon: 1) the size of the agglomerated nanodiamond particles. 2) The volume of absorbed polyacrylic acid into the agglomerated nanodiamond particle. 3) Interaction with the GIC matrix and 4). The strength of the forces keeping these agglomerated ND particles together (that were not hydrated with polyacrylic acid). Based on these aforementioned factors the development of voids of various sizes in the centre of the nanodiamond agglomerated particles will occur as the centre (Ullah *et al*., 2015) nanodiamond particles are lost, exposing the GIC surface (black arrows) The nanodiamond particles are lost from the centre of the agglomerated nanodiamond particle (white arrows), since they are loosely bound with van der Waals forces if the liquid from the GIC did not penetrate into the agglomerated particle (Figure 10.25). The loss of the nanodiamond

agglomerated particles from the surface of the GIC (black arrow) additionally confirmed that the outer margin of the smaller nanodiamond agglomerated particles (that were moistened by the matrix and the polyacrylic acid) are well fused with the matrix of the GIC (Figures 10.24 and 10.25).

Figure 10.25: Nanodiamond particles lost after surface preparation with 1200 grit wet silicon carbide paper

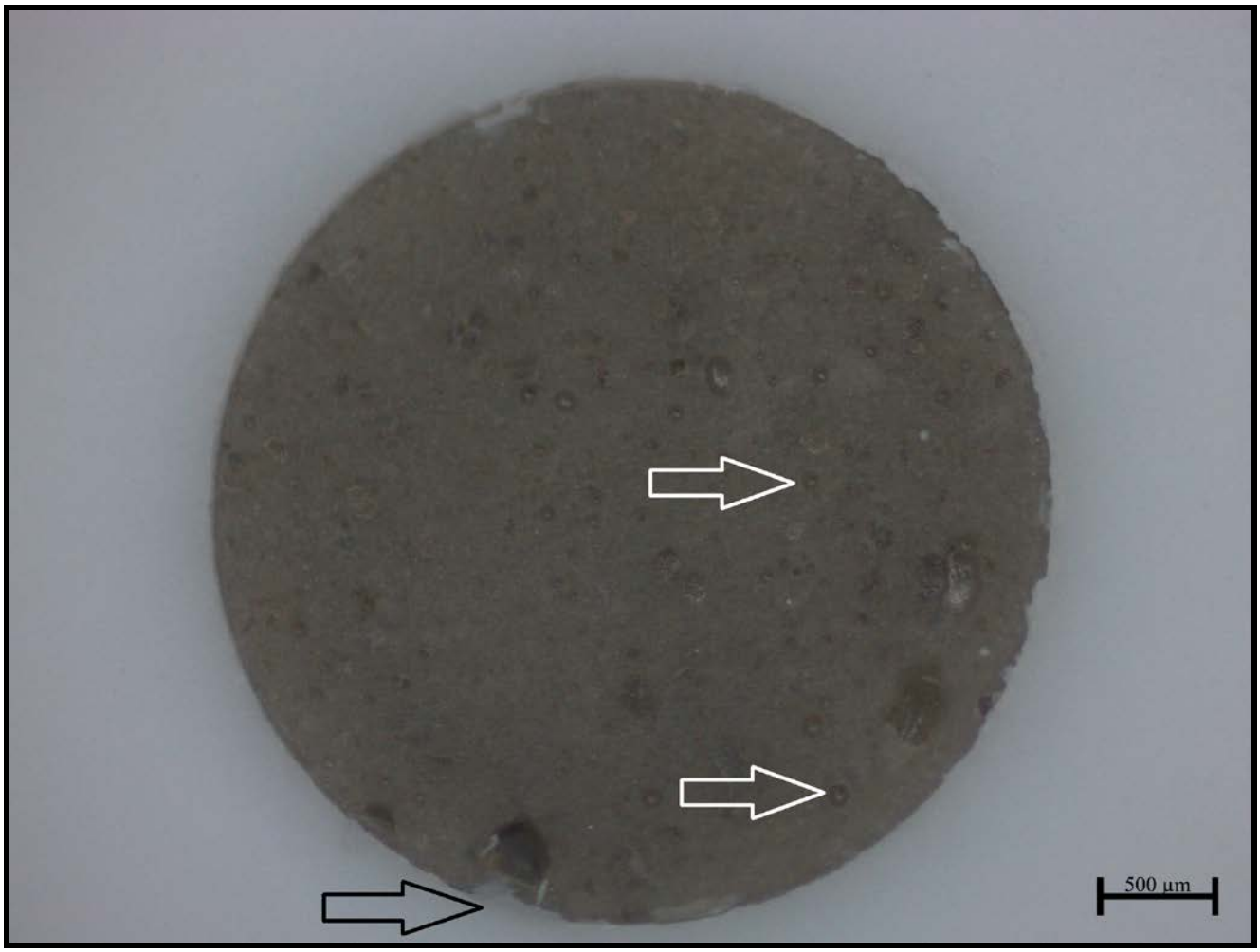

Surface irregularities like cracks and pits on teeth are the ideal area for early plaque formation on the enamel (Nyvad and Fejerskov, 1987). It has been well documented that the increase of the surface roughness of the material results in a deterioration of the material surface (Yip *et al*., 1999; Yip *et al*., 2001). The surface roughness (Ra) from 0 to 24 hours presented with the lowest

surface roughness for the 5%ND modification of FN, KU and RSC compared to the 10%ND modifications and all the chitosan modifications (Table 10.5 and Figure 10.15). The original particle size of the chitosan material as received from the manufacturer clearly influenced the surface roughness, due to 1) The larger chitosan particles (Figures 10.27-10.30) which already increase the surface roughness at 0 hours compared to the nanodiamond-modified GICs (Figure 10.25). 2) The difference in the chitosan particle distribution (Bala *et al*., 2012) within the GIC material (Figures 10.29, 10.30). 3) The increase in volume of the CH as it is exposed to moisture and 4). The increase in *S. mutans* OD450nm producing lactic acid that interacts with the chitosan surface (Figures 10.26 and 10.30) and 4) The irregular shape (Figures 10.28 and 10.30) and non-fusion of the chitosan particle with the GIC (Figures 10.26 and 10.28).

The chitosan materials seem to have fewer singular *S. mutans* as illustrated by the white arrows highlighting the quorum function in the thick biofilm growth from the chitosan particle (Figure 10.26).

Figure 10.26: FN5%CH where the chitosan swelled above GIC surface

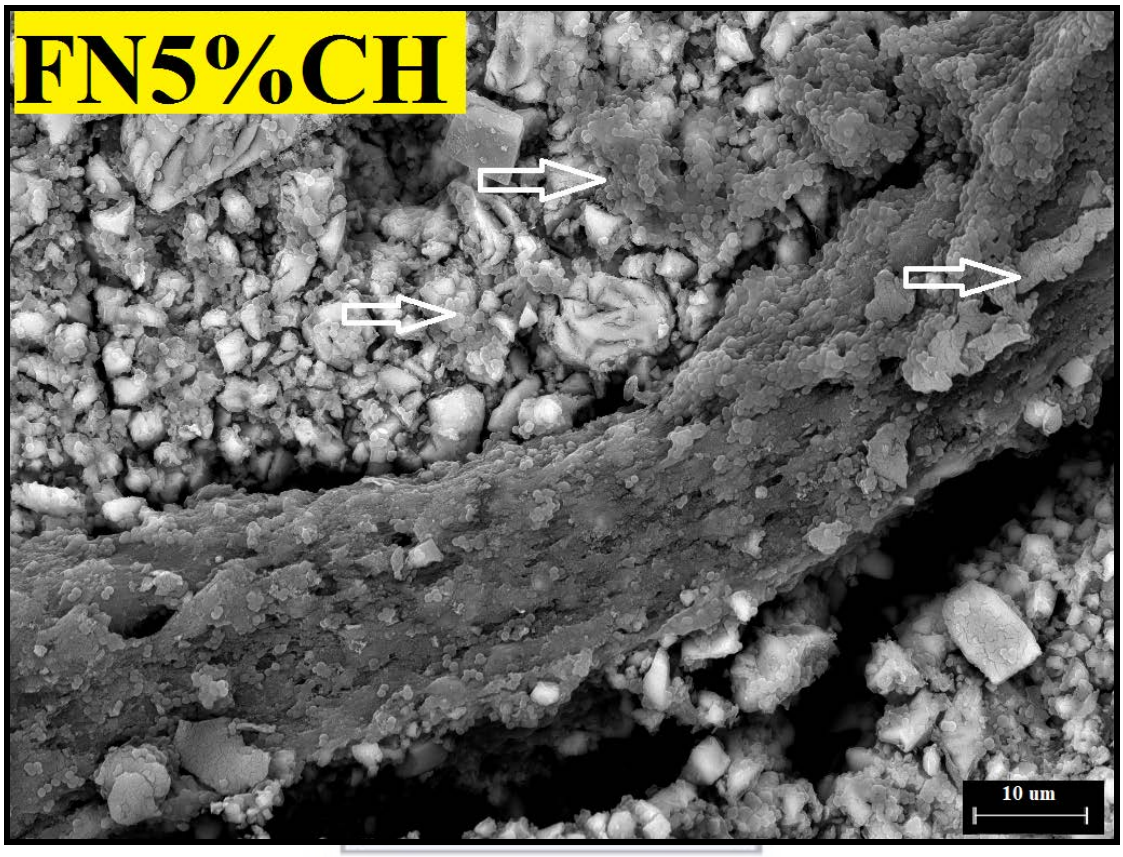

Figure 10.27: Chitosan particles at 6x magnification

Figure 10.28: SEM illustrating the irregular shape of the chitosan particles

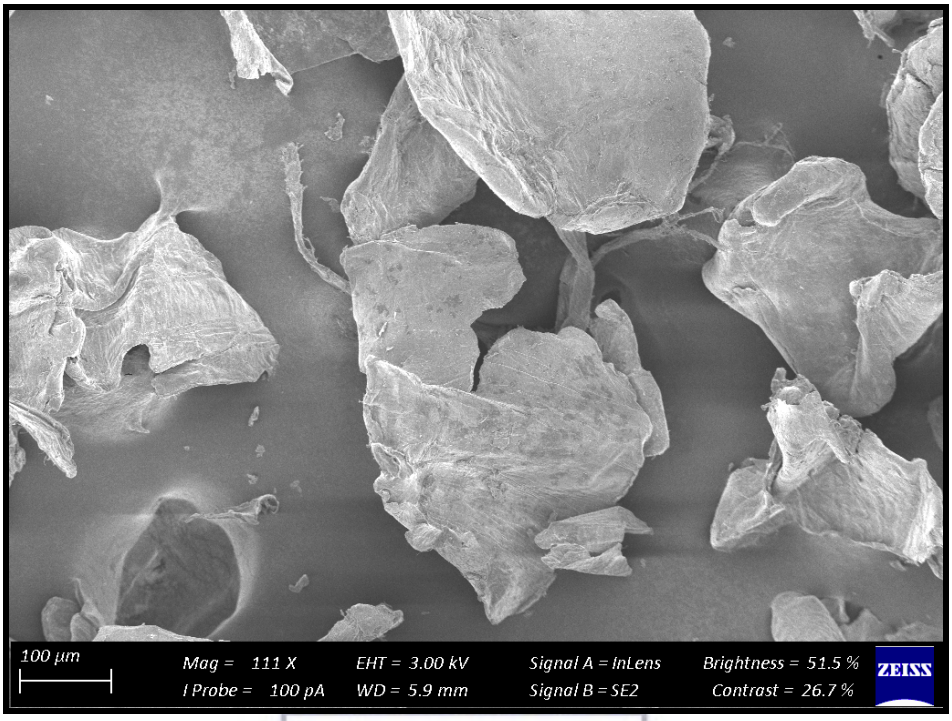

Figure 10.29: Chitosan particles clearly visible as whitish flakes

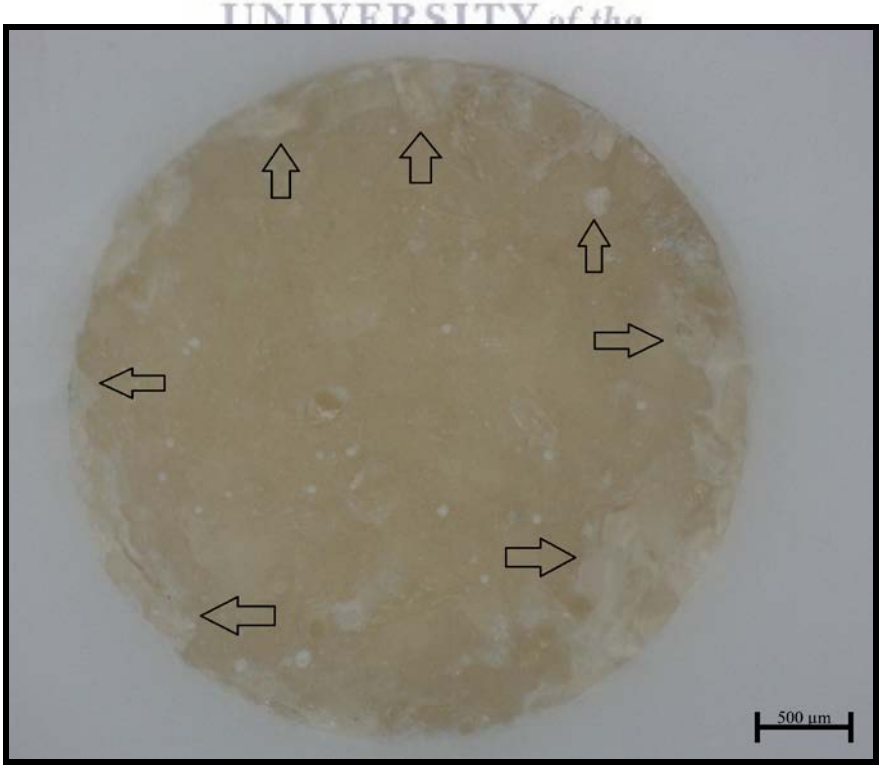

Figure 10.30: SEM image of KU10%CH illustrating irregular chitosan particle shape and non-fusion with GIC

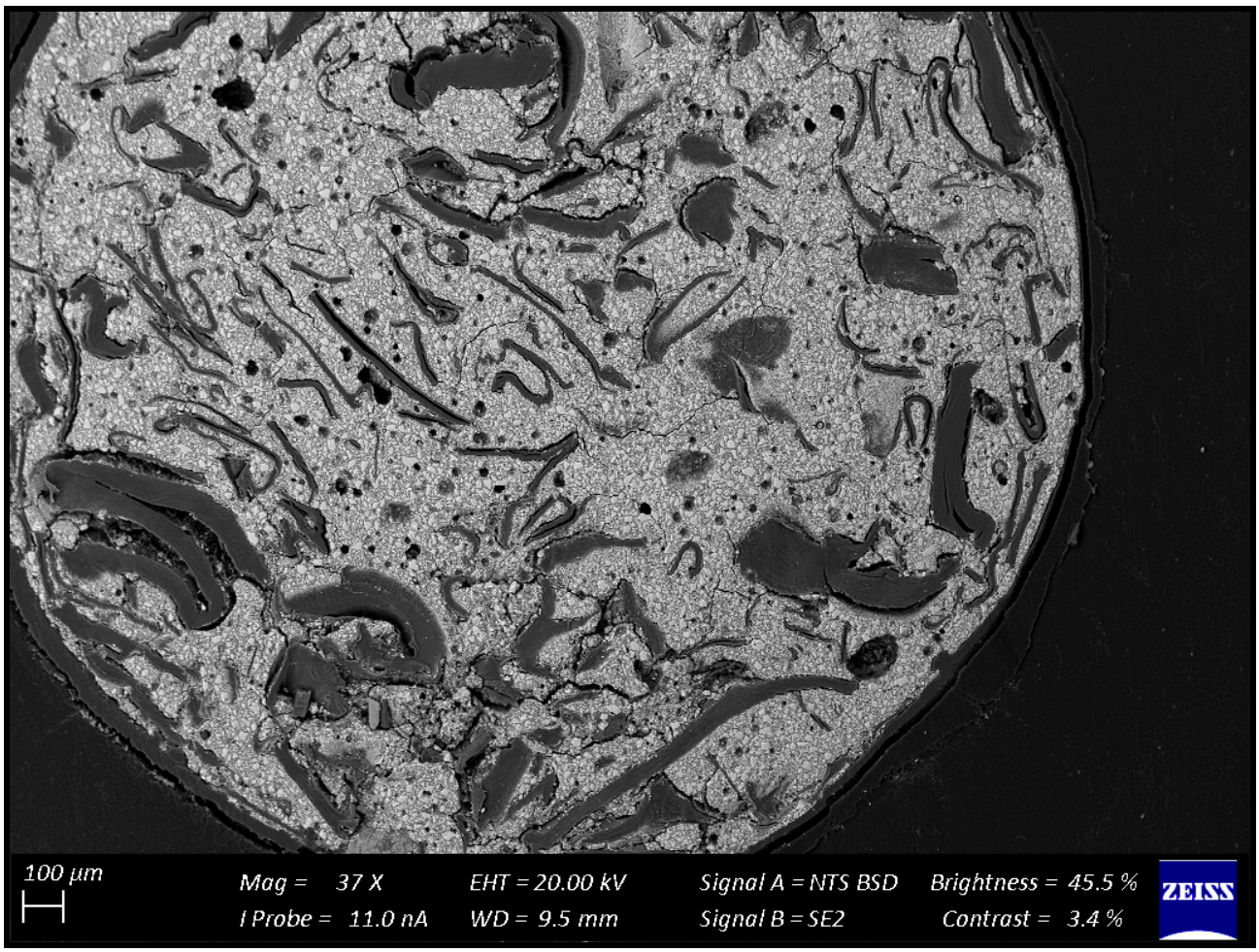

The antibacterial and haemorrhage control properties of chitosan (Figure 10.27 and 10.28) was first noted and applied as a wound dressing for skin and other trauma in 2005 according to the Food and drug administration registration (*Hemcon bandage, Portland, Oregan, USA*). Colonization of the chitosan with *S. mutans* is expected to some extent considering that an *in vivo* study has shown that *S. mutans* colonization for various restoration margins is always present, even in different patients (van Houte *et al*., 1982). The surfaces of crowns, amalgams and composites have shown consistent *S. mutans* colonization, although the amount of colonization had great variability when the OD450nm between restorations and the OD450nm of

saliva from the same patients were compared (Wallman and Krasse, 2009). Although the chitosan modifications had significant increases in the surface roughness, it was attributed to the swelling effect and the interaction of *S. mutans* with the chitosan particles. The 24 hour exposure of the *S. mutans* to the control materials and their respective nanodiamond modifications did not significantly change their surface roughness (Figure 10.15).

The adhesion level of *S. mutans* to the FN glass ionomer was higher than other regularly used non-GIC dental materials (Poggio *et al*., 2009). Even with the ion release from GICs the adhesion of the *S. mutans* did not seem to be influenced when compared to the other materials (Eick *et al*., 2004). This led the research group of Eick *et al*. (2004) to question the effectiveness of GICs against *S. mutans*. It was well accepted that fluoride release could influence the *S. mutans* (Seppä *et al*., 1992), but Montanaro *et al*. (2004) rejected this due to the lack of change in the adhesion of *S. mutans* in relation to other materials tested (Montanaro *et al*., 2004). To this effect, Figures 10.21- 10.23 illustrate the adherence of *S. mutans* to the various aspects of the GICs covering the matrix as well as the filler particles. The chitosan (Figure 10.26) and the nanodiamond agglomerated particles also showed *S. mutans* adherence (Figure 10.31). The white arrow indicates the presence of *S. mutans* on the nanodiamond agglomerated particle as well as on the rest of the nanodiamond-modified GIC surface. The red/white arrows at the nanodiamond/GIC interface indicate that for FN10%ND, the nanodiamond agglomerate separated from the GIC matrix. This did not occur during the sample preparation for the SEM investigation since the *S. mutans* can be seen well within the space between the nanodiamond agglomerated particle and the GIC surface. *S. mutans* had therefore been noted to have adherence capabilities and this study confirmed that even in the absence of an initial pioneer pellicle, *S. mutans* as a mono-species was also able to adhere to all the GICs.

Figure 10.31: FN10%ND and KU10%ND with *S. mutans* present

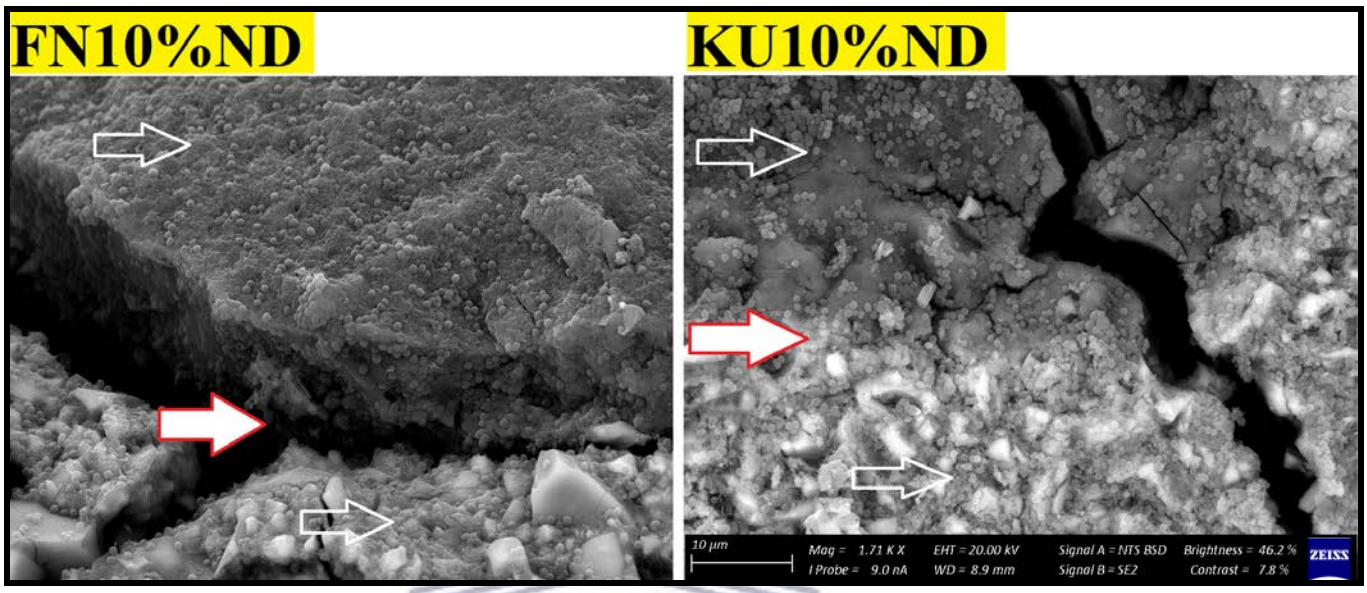

With regard to FN, differences were seen between the surface growth of the biofilm and the *S. mutans* at 24 hours although there was no significant difference in the *S. mutans* OD450nm at 24 hours between the chitosan and ND modification and their controls for FN (0.783), FN10%CH (0.831) and FN5%ND (0.759) (Figures 10.21, 10.32 and 10.33).

Figure 10.32: FN5%ND with the white arrows indicating the *S. mutans* biofilm

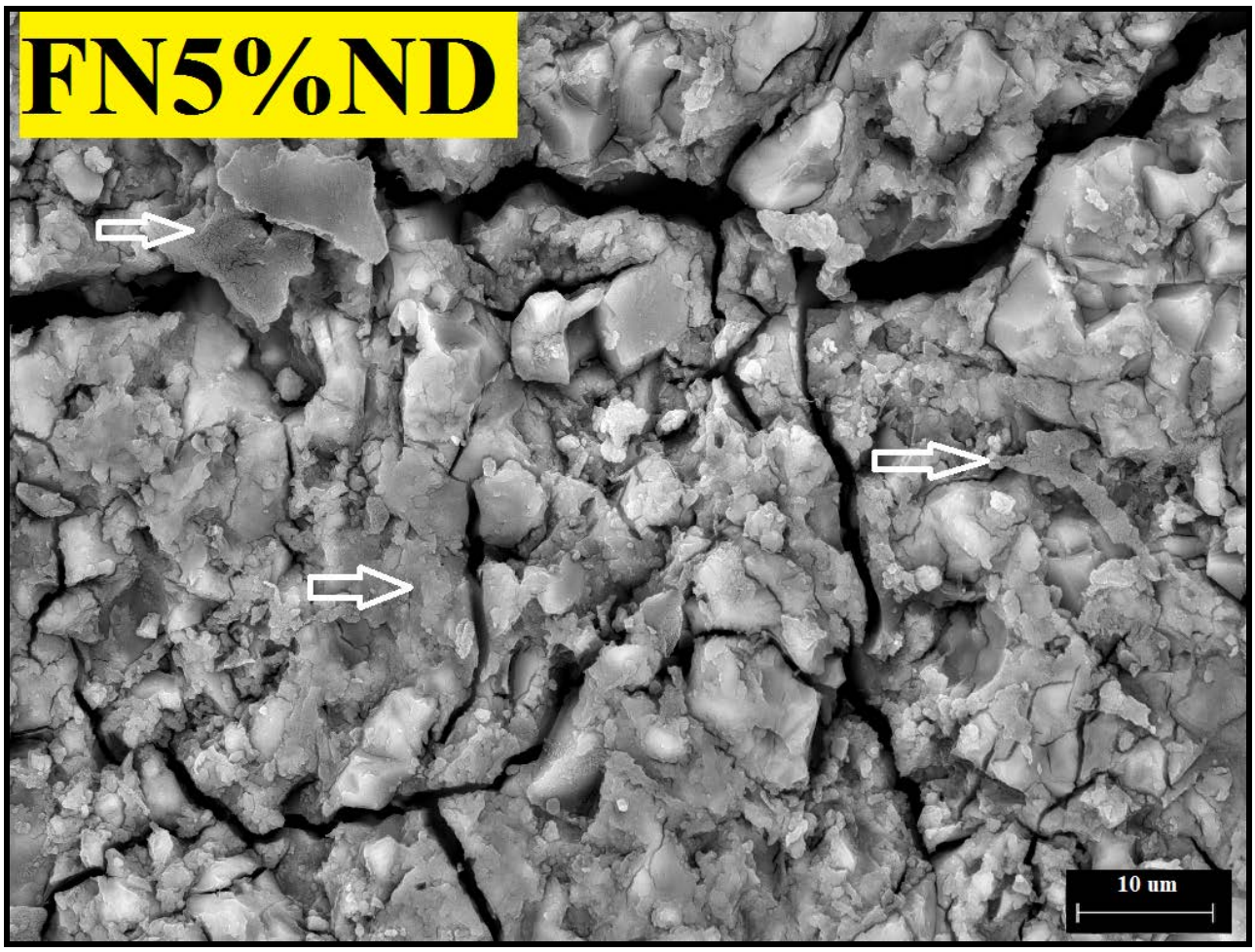

Figure 10.33: FN10%CH with the white arrows indicating the *S. mutans* biofilm

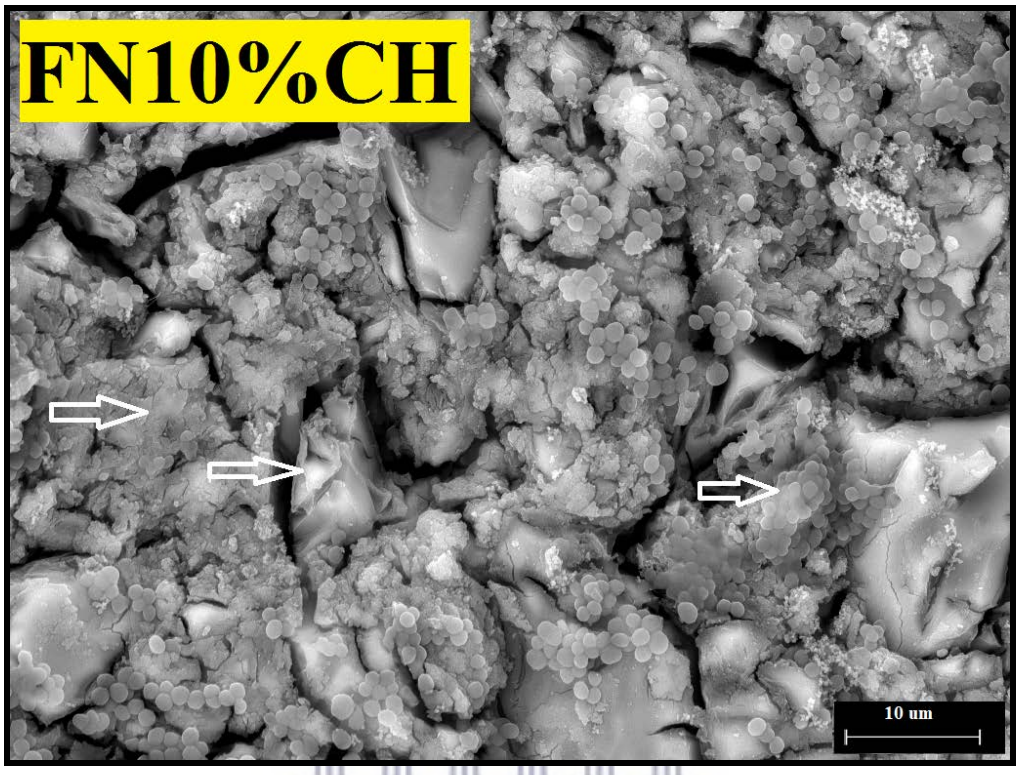

The individual, quorum forming and various appearances of the biofilm produced by the *S. mutans* appear different on each surface. This could be due to the fact that chitosan was derived from aminopolysaccharide copolymers of glucosamine and N-acetylglucosamine. The chitosan particles contain primary amino groups in the main backbone of the molecule, resulting in the positive charge of the surface (Sonia and Sharma, 2011). *S. mutans* has a negative charge and is therefore attracted to the surface of the chitosan particle. Further to the amino acids (acetamino acetamide (CH_3CONH_2) (Yang *et al*., 2010), there are hydroxyl groups at the C2 positions of the glucose ring as well as D-glucosamine that has features like its ability to biodegrade and interact with the biological surfaces (Sonia and Sharma, 2011). Chitosan particles contain many active hydroxyl groups and amino acids that have been attributed to its ability to scavenge hydroxide radicals (Guo *et al*., 2005). This strong scavenging ability of the hydroxyl radicals are important,

since it is known to damage amino acids, DNA and proteins (Halliwell and Gutteridge, 1990). Upon contact with the positively charged chitosan and the negatively charged *S. mutans*, the bacterial cell wall and the protonated ammonia (NH_3^+) from chitosan will compete for the calcium (Ca^{2+}). The calcium usually stabilises the bacterial cell wall and with the reduction of it, there are two interferences that occur as cited by a review article by Goy *et al*. (2009) namely: 1) Bacterial cell wall membrane permeability change causing an inhibition of *S. mutans* growth. 2) Hydrolysis of the cell wall leading to the leakage of potassium, proteins, nucleic acids, glucose and lactate dehydrogenase from *S. mutans* (Goy *et al*., 2009) explaining the varied appearance between FN (Figure 10.21), FN5%ND (Figures 10.32) and FN10%CH (Figures 10.33). The chitosan particles used in this dissertation with a 75-85% deacetylated physical form illustrated significant antibacterial action against *S. mutans* (Fernandes *et al*., 2009; Costa *et al*., 2013). However, in those studies, the chitosan particles were dissolved in the acetic acid and in this dissertation; it was used in particle powder form. The only protonation that can occur on chitosan is therefore during the mixing stage as well as the acid-base reaction with the polyacrylic liquid.

During the increased *S. mutans* growth over the incubation period the lactic acid interacts with the chitosan (Figures 10.33 and 10.34) that can be readily seen on the surface of the chitosan-modified GICs of how the chitosan particle has changed when compared to Figure 10.26 and 10.28. There is subsequent formation of polyelectrolyte complexes by the chitosan particles (Berger *et al*., 2004) that provide the required physicochemical properties needed to also increase the ion release as seen in the Chapter 7 causing the chitosan-modified GIC to reduce the *S. mutans* OD450nm.

The significant reduction of the *S. mutans* OD450nm at 2 hours and 24 hours (Figures 10.12-10.14) in relation to the control *S. mutans* was in line with a study completed with dissolved chitosan and *S. mutans* biofilm growth that was continuously assessed over a 24-hour period (Pasquantonio *et al*., 2008).

It has been noted from the research completed by Wehling *et al*. (2014) that there could be potential interaction with the growth medium for the *S. mutans* that could inhibit the effects of the chitosan and the nanodiamond particles. The concepts are described in detail below. Nanodiamond particles have shown to be non-toxic to eukaryotic cells (Xing and Dai, 2009). The non-toxic effect of the nanodiamond particles could have been due to the affinity of nanodiamond particles to the essential amino acids and proteins. If the nanodiamond particles interact with the essential amino acids and proteins, it would not be able to have a toxic effect on the eukaryotic cells. The interaction of the amino acids and the proteins with the nanodiamond particle could possibly reduce the toxic effects of the nanodiamond particles. It has been documented that biological fluids rapidly cover nanoparticles (Monopoli *et al*., 2012). These terminated carboxyl groups and other oxygen-containing groups of the NDs readily interact with amino groups of proteins (Huang and Chang, 2004). Bovine serum albumin (BSA) interactions with nanodiamond particles have shown a strong association to form nanodiamond-BSA., With the variances in pH, the adsorption of the nanodiamond particle onto the BSA, the agglomerated nanodiamond particles can be reduced in size due to the strong binding force and association between nanodiamond and BSA (Wang *et al*., 2011).

This is why the antibacterial assessment by Wehling *et al*. (2014) on *E. coli* was done with 4-(2-hydroxyethyl) piperazine-1-ethanesulfonic acid buffer (HEPES) (pH 7.2) (Wehling *et al*., 2014). Wehling *et al*. (2014) showed that the addition of only 10% fetal bovine serum (FBS) containing 38mg/ml protein (60% albumin) resulted in the disappearance of the antibacterial activity against *E. coli* and *B. subtilis*. Bovine serum albumin (BSA) and Dulbecco's modified Eagle medium

(containing glucose, ions and amino acids) were also assessed against *E. coli* and *B. subtili*s with a very similar result (Wehling *et al*., 2014)

The Tryptic soy broth (TSB) that was used in this dissertation was selected due to the high nutritional requirements of *S. mutans.* The high nutritional requirements for *Steptococcus* were confirmed in the literature (Ogawa *et al*., 2011; Wang and Kuramitsu, 2005). Oral streptococci require glucose to facilitate the sugar transport system called phosphoenolpyruvate (PEP) - dependent sugar phosphotransferase transport system (PTS) (Thompson, 1988). In the present study, the TSB at a pH of 7.3 contained pancreatic digest of casein (source of amino acids), Soy (protein), Di-basic potassium phosphate, sodium chloride and glucose (monosaccharide carbohydrate). At the end of the study regarding inhibitory affects of various bacterial growth media, it was found that even protein-free cell media decreased the antibacterial effects of nanodiamond particles to some extent (Wehling *et al*., 2014). Although the antibacterial effect could potentially be overshadowed by the interaction of the growth medium, the *in vivo* situation for nanodiamond particles would be similar since its carboxylic acid groups in the acid anhydride form are highly reactive toward nucleophilic additions (Cloete *et al*., 2013) with the biofilm and cell membrane of all bacteria. Wehling *et al.* (2014) suggested that the carboxylic acid groups can form covalent bonds with the proteins and molecules on the cell walls or even bind to the intracellular components if the nanodiamond particle is phagocytised. This binding of the ND would subsequently inhibit vital enzyme and protein production, decreasing metabolism and resulting in eventual cell death of the bacteria (Wehling *et al*., 2014). Due to the negative Zeta potential of nanodiamond particles there is usually high dispersion stability in basic aqueous pH solutions. This feature further indicates that there is a presence of carboxylic groups on the surface of the nanodiamond particles (Osswald *et* al., 2006). With the surface chemistry of the nanodiamond particles creating a high affinity for amino acid protein adsorption (Wang *et al*., 2011), the carboxylate groups promote the electrostatic breaking of hydrogen bonds between

the water molecules. The interaction of water molecules with the carboxylate group results in fewer water molecules in the double hydrogen bond donor configuration and more in a single hydrogen bond configuration (Petit *et al*., 2015). Increased water sorption and the nanodiamond particle becoming more positive as the water sorption occurs, results in an increased antibacterial activity as time passes. This matches well with the 24 hour reduction of the *S. mutans* OD450nm compared to the control materials.

The antibacterial effect of chitosan (CH) may be attributed to its chemical structure, with the presence of deacetylated C2 amino groups which become protonated and positively charged at pH < 6.5. Thus, chitosan binds to the membrane of bacterial cells leading to: 1) an increase in membrane permeability with a concomitant increase in the outward flow of ions and proteins from the microbial cell. 2) The inhibition of mRNA transcription and 3) the alteration of protein translation (Blecher *et al*., 2011; Adams *et al*., 2006). The molecular weight of chitosan appears to be strongly related to the antibacterial activity of chitosan (Huh and Kwon, 2011; Fernandes, 2010). The molecular weight may be correlated with the mechanism of destabilisation of the bacterial membrane. The lipoteichoic acid that is present in gram-positive bacteria acts as a binding site for chitosan, causing alteration of membrane functionality (Raafat *et al*., 2008). In gram-negative bacteria, the chitosan polycations compete with divalent cations and interact with the bacterial cell membrane through electrostatic interactions (Kong *et al*., 2008). It is well known that magnesium (Mg^{2+}) or calcium (Ca^{2+}) stabilise the outer membrane of the bacteria. When these ions are replaced with chitosan, modification of the cell wall occurs together with the alteration of the activity of enzymes. There has been a low level of cytotoxicity for chitosan nanoparticles (Friedman *et al*., 2013) and attention must be paid to the purification and processing methods employed for the production of these chitosan nonmaterial, mainly because of the possible incorporation of toxins and other residues from chemicals used during production

of the nanochitosan that could have influenced the antibacterial effects of the nanochitosan particles. Even in its purest particle form from the manufacturer (without any additional processing), chitosan showed a *S. mutans* OD450nm reduction and an alteration to the biofilm that developed on chitosan-modified GICs. The white arrows indicate where the *S. mutans* attached to the biofilm (Figure 10.34).

Figure 10.34: KU and KU5%CH *S. mutans* biofilm comparison

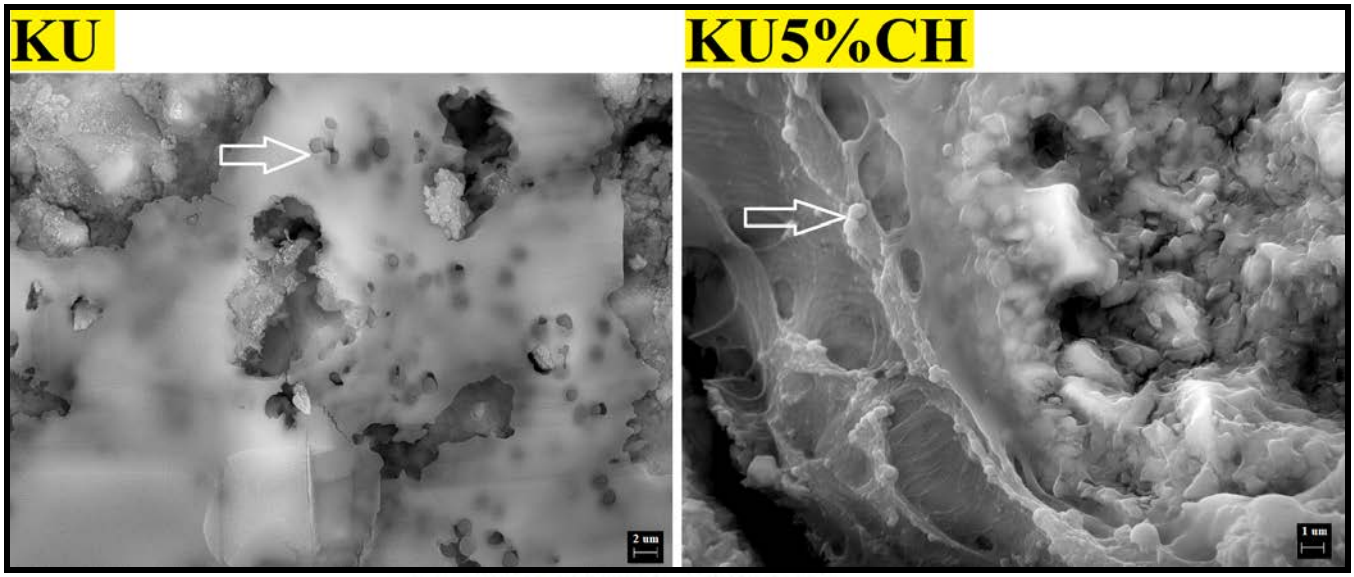

The nanodiamond particles provided a greater disruption of the *S. mutans* as illustrated in Figure 10.35 even though the *S. mutans* OD450nm was not as low as the chitosan modifications for each material. Nanodiamond particles with the positive influence clearly visible on the nanodiamond-modified GIC surface had reduced surface biofilm compared to the RSC. The biofilm on the nanodiamond-modified GIC is disrupted and not multi-layered. There are also more single *S. mutans* present on the nanodiamond-modified GIC rather than a thick multi-cell quorum of *S. mutans* bacteria

Figure 10.35: RSC and RSC5%ND *S. mutans* biofilm comparison

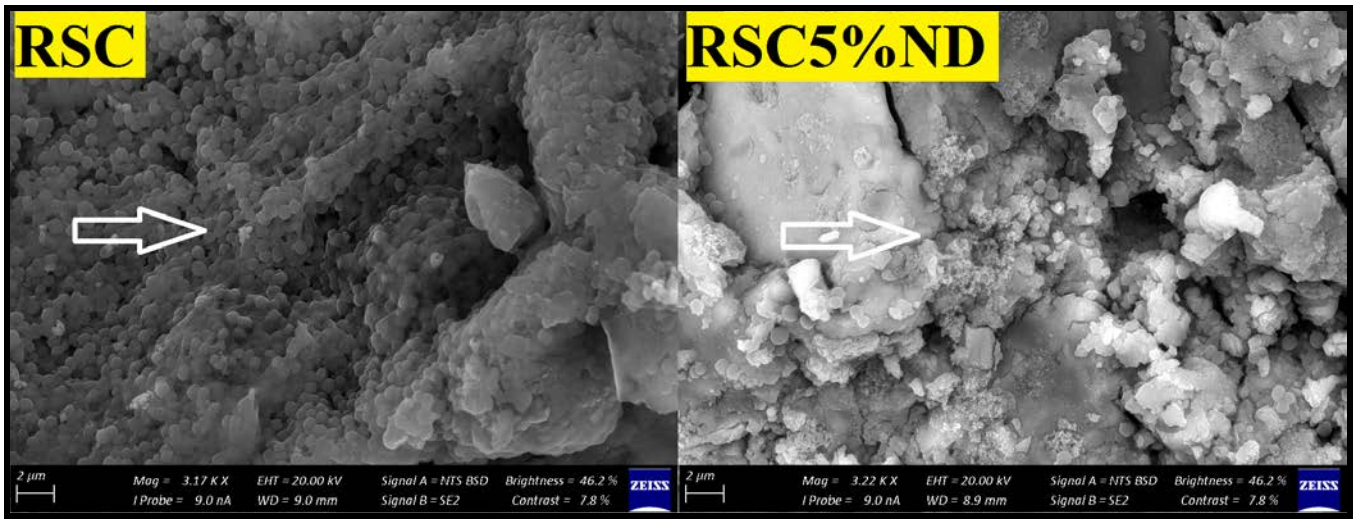

The oral cavity and the diets of patients present with a variety of proteins, amino acids and biological fluids that could alter the chitosan and nanodiamond particles. If chitosan and nanodiamond particles are to be added to restorative materials, the assessment of such modified materials must be done in relation to how GICs have been assessed in the past literature, using a variety of growth mediums that formed the base of known knowledge on the antibacterial effect of GICs. Because the assessment of the antibacterial effect of GICs has been assessed with the various mediums in the literature, the chitosan and nanodiamond GIC modifications should be assessed with the same methodology.

With the biofilm clearly disrupted in the nanodiamond-modified materials, the *S. mutans* would be more loosely bound. This would therefore provide an opportunity for the daily oral hygiene practices of patients to remove the loosely bound *S. mutans*.

10.7. Conclusion

The presence of the bacterial biofilm on the margins of restorations had been cited as a promoter of secondary caries (Kawai *et al*., 1997; Seixas *et al*., 2004). *S. mutans* use quorum sensing by binding together in order to regulate their physiological processes (Bassler, 1999). Based on the SEM images it became clear that the chitosan and nanodiamond modifications disrupted the biofilm and changed the surface adherence and quorum grouping of the *S. mutans*. GICs and all their modifications have illustrated a similar reduction in the *S. mutans* OD450nm from 0, 2 and 4 hours. At the end of this study in the dissertation at 24 hours the *S. mutans* OD450nm for FN at 0 and 24 hours were similar, with KU and RSC indicating an increase in the *S. mutans* OD450nm. The *S. mutans* OD450nm seem to stabilise as the growth significantly increased at 6h, compared to the preceding time periods (2 and 4h). Interestingly all the chitosan and nanodiamond modifications caused a reduction for the *S. mutans* OD450nm at the 0h time period compared to the control bacteria. The chitosan and nanodiamond modifications for FN made no difference in the *S. mutans* OD450nm for any stage of growth 2, 4, 6 and 24.

10.8. References

Adams, L., Lyon, D. and Alvarez, P. (2006). Comparative eco-toxicity of nanoscale TiO2, SiO2, and ZnO water suspensions. *Water Research*, 40(19), pp.3527-3532.

Ajdic, D., McShan, W., McLaughlin, R., Savic, G., Chang, J., Carson, M., Primeaux, C., Tian, R., Kenton, S., Jia, H., Lin, S., Qian, Y., Li, S., Zhu, H., Najar, F., Lai, H., White, J., Roe, B. and Ferretti, J. (2002). Genome sequence of Streptococcus mutans UA159, a cariogenic dental pathogen. *Proceedings of the National Academy of Sciences*, 99(22), pp.14434-14439.

Auschill, T., Arweiler, N., Brecx, M., Reich, E., Sculean, A. and Netuschil, L. (2002). The effect of dental restorative materials on dental biofilm. *European Journal of Oral Sciences*, 110(1), pp.48-53.

Bala, O., Arisu, H., Yikilgan, I., Arslan, S. and Gullu, A. (2012). Evaluation of surface roughness and hardness of different glass ionomer cements. *European Journal of Dentistry.*, 6(1), pp.79-86.

Banas, J. (2004). Virulence properties of Streptococcus Mutans. *Frontiers in Bioscience*, 9(1-3), pp.1267.

Banas, J. and Vickerman, M. (2003). Glucan-binding Proteins of the Oral Streptococci. *Critical Reviews in Oral Biology & Medicine*, 14(2), pp.89-99.

Bassler, B. (1999). How bacteria talk to each other: regulation of gene expression by quorum sensing. *Current Opinion in Microbiology*, 2(6), pp.582-587.

Berger, J., Reist, M., Mayer, J., Felt, O. and Gurny, R. (2004). Structure and interactions in chitosan hydrogels formed by complexation or aggregation for biomedical applications. *European Journal of Pharmaceutics and Biopharmaceutics*, 57(1), pp.35-52.

Bika, D., Gentzler, M. and Michaels, J. (2001). Mechanical properties of agglomerates. *Powder Technology*, 117(1-2), pp.98-112.

Blecher, K., Nasir, A. and Friedman, A. (2011). The growing role of nanotechnology in combating infectious disease. *Virulence*, 2(5), pp.395-401.

Bollen, C., Papaioanno, W., Van Eldere, J., Schepers, E., Quirynen, M. and van Steenberghe, D. (1996). The influence of abutment surface roughness on plaque accumulation and peri-implant mucositis. *Clinical Oral Implants Research*, 7(3), pp.201-211.

Bollenl, C., Lambrechts, P. and Quirynen, M. (1997). Comparison of surface roughness of oral hard materials to the threshold surface roughness for bacterial plaque retention: A review of the literature. *Dental Materials*, 13(4), pp.258-269.

Botelho, M. (2003). Inhibitory Effects on Selected Oral Bacteria of Antibacterial Agents Incorporated in a Glass Ionomer Cement. *Caries Research*, 37(2), pp.108-114.

Carlén, A., Nikdel, K., Wennerberg, A., Holmberg, K. and Olsson, J. (2001). Surface characteristics and *in vitro* biofilm formation on glass ionomer and composite resin. *Biomaterials*, 22(5), pp.481-487.

Carlsson, P., Olsson, B. and Bratthall, D. (1985). The relationship between the bacterium Streptococcus mutans in the saliva and dental caries in children in Mozambique. *Archives of Oral Biology*, 30(3), pp.265-268.

Ching, H., Luddin, N., Kannan, T., Ab Rahman, I. and Abdul Ghani, N. (2018). Modification of glass ionomer cements on their physical-mechanical and antimicrobial properties. *Journal of Esthetic and Restorative Dentistry*, 30(6), pp.557-571.

Chng, E. and Pumera, M. (2013). The Toxicity of Graphene Oxides: Dependence on the Oxidative Methods Used. *Chemistry - A European Journal*, 19(25), pp.8227-8235.

Cloete, W., Verwey, L. and Klumperman, B. (2013). Permanently antimicrobial waterborne coatings based on the dual role of modified poly(styrene-co-maleic anhydride). *European Polymer Journal*, 49(5), pp.1080-1088.

Costa, E., Silva, S., Tavaria, F. and Pintado, M. (2013). Study of the effects of chitosan upon Streptococcus mutans adherence and biofilm formation. *Anaerobe*, 20, pp.27-31.

Da Silva, R., Zuanon, A., Spolidorio, D. and Campos, J. (2007). Antibacterial activity of four glass ionomer cements used in atraumatic restorative treatment. *Journal of Materials Science: Materials in Medicine*, 18(9), pp.1859-1862.

Danilenko, V. (2004). On the history of the discovery of nanodiamond synthesis. *Physics of the Solid State*, 46(4), pp.595-599.

Debnath, A. (2017). Comparative Evaluation of Antibacterial and Adhesive Properties of Chitosan Modified Glass Ionomer Cement and Conventional Glass Ionomer Cement: an *In vitro* Study. *Journal of Clinical and Diagnostic Research*, 11(3),pp.ZC75-ZC78.

Dimkov, A., Nicholson, J. and Gjorgievska, E. (2012). Compressive strength and setting time determination of glass-ionomer cements incorporated with cetylypyridinium chloride and benzalkonium chloride. *Macedonian Academy of Sciences and Arts, Section of Biological and Medical Sciences (Prilozi)*, 33, pp.243-263.

Eick, S., Glockmann, E., Brandl, B. and Pfister, W. (2004). Adherence of Streptococcus mutans to various restorative materials in a continuous flow system. *Journal of Oral Rehabilitation*, 31(3), pp.278-285.

Fejerskov, O. and Kidd, E. (2005). Cárie Dentária: A doença e seu tratamento clínico. *São Paulo: Santos*, [online] pp.350-353. Available at: https://unasus.unifesp.br/biblioteca_virtual/pab/4/unidades_casos_complexos/unidade27/unidade27_ft_etiologia.pdf [Accessed 25 Mar. 2019].

Fernandes, J. (2010). *In Vitro* Screening for Antimicrobial Activity of Chitosans and Chitooligosaccharides, Aiming at Potential Uses in Functional Textiles. *Journal of Microbiology and Biotechnology*, 20(2), pp.311-318.

Fernandes, J., Eaton, P., Gomes, A., Pintado, M. and Xavier Malcata, F. (2009). Study of the antibacterial effects of chitosans on Bacillus cereus (and its spores) by atomic force microscopy imaging and nanoindentation. *Ultramicroscopy*, 109(8), pp.854-860.

Friedman, A., Phan, J., Schairer, D., Champer, J., Qin, M., Pirouz, A., Blecher-Paz, K., Oren, A., Liu, P., Modlin, R. and Kim, J. (2013). Antimicrobial and Anti-Inflammatory Activity of Chitosan–Alginate Nanoparticles: A Targeted Therapy for Cutaneous Pathogens. *Journal of Investigative Dermatology*, 133(5), pp.1231-1239.

Gambhir, R., Sujlana, A. and Pannu, P. (2013). Correlation between the salivary Streptococcus mutans levels and dental caries experience in adult population of Chandigarh, India. *European Journal of Dentistry*, 7(2), pp.191.

Geddes, D. (1972). The production of l(+) and d(−) lactic acid and volatile acids by human dental plaque and the effect of plaque buffering and acidic strength on pH. *Archives of Oral Biology*, 17(3), pp.537-545.

Goy, R., Britto, D. and Assis, O. (2009). A review of the antimicrobial activity of chitosan. *Polímeros*, 19(3), pp.241-247.

Guo, Z., Xing, R., Liu, S., Yu, H., Wang, P., Li, C. and Li, P. (2005). The synthesis and antioxidant activity of the Schiff bases of chitosan and carboxymethyl chitosan. *Bioorganic & Medicinal Chemistry Letters*, 15(20), pp.4600-4603.

Halliwell, B. and Gutteridge, J. (1990). Role of free radicals and catalytic metal ions in human disease: An overview. *Methods Enzymology*, 186, pp.1-85.

Hamada, S. and Slade, H. (1980). Biology, immunology, and cariogenicity of streptococcus mutans. *Microbiolgy and Molecular Biology Reviews*, 44, pp.331-384.

Hannig, M. (1997). Transmission electron microscopic study ofin vivopellicle formation on dental restorative materials. *European Journal of Oral Sciences*, 105(5P1), pp.422-433.

Hayacibara, M., Rosa, O., Koo, H., Torres, S., Costa, B. and Cury, J. (2003). Effects of Fluoride and Aluminum from Ionomeric Materials on S. mutans Biofilm. *Journal of Dental Research*, 82(4), pp.267-271.

Huang, L. and Chang, H. (2004). Adsorption and Immobilization of Cytochromecon Nanodiamonds. *Langmuir*, 20(14), pp.5879-5884.

Huh, A. and Kwon, Y. (2011). "Nanoantibiotics": A new paradigm for treating infectious diseases using nanomaterials in the antibiotics resistant era. *Journal of Controlled Release*, 156(2), pp.128-145.

Ibrahim, M., Meera Priyadarshini, B., Neo, J. and Fawzy, A. (2017). Characterization of Chitosan/TiO2 Nano-Powder Modified Glass-Ionomer Cement for Restorative Dental Applications. *Journal of Esthetic and Restorative Dentistry*, 29(2), pp.146-156.

Ibrahim, M., Neo, J., Esguerra, R. and Fawzy, A. (2015). Characterization of antibacterial and adhesion properties of chitosan-modified glass ionomer cement. *Journal of Biomaterials Applications,* 30(4), pp.409-419.

Kawai, K., Heaven, T. and Retief, D. (1997). *In vitro* dentine fluoride uptake from three fluoride-containing composites and their acid resistance. *Journal of Dentistry*, 25(3-4), pp.291-296.

Kawamura, Y., Hou, X., Sultana, F., Miura, H. and Ezaki, T. (1995). Determination of 16S rRNA Sequences of Streptococcus mitis and Streptococcus gordonii and Phylogenetic Relationships among Members of the Genus Streptococcus. *International Journal of Systematic Bacteriology,* 45(4), pp.882-882.

Khoo, G., Hoover, C. and Featherstone, J. (2005). Cariogenic virulence characteristics of mutans streptococci isolated from caries-active and caries-free adults. *Journal of the California Dental Association,* 33, pp.973-980.

Kong, M., Chen, X., Liu, C., Liu, C., Meng, X. and Yu, L. (2008). Antibacterial mechanism of chitosan microspheres in a solid dispersing system against E. coli. *Colloids and Surfaces B: Biointerfaces*, 65(2), pp.197-202.

Kuramitsu, H. and Wang, B. (2006). Virulence properties of cariogenic bacteria. *BMC Oral Health*, 6(S1):11

Loeshe, W. (1986). Role of streptococcus mutans in human dental decay. *Microbiological Reviews*, 50, pp.353-380.

Mabrouk, M., Selim, M. and Beherei, H. (2013). Incorporation effect of silver and zinc zeolites into commercial glass ionomer cements. *Interceram-International ceramics review*, 62, pp.50-54.

Mochalin, V., Shenderova, O., Ho, D. and Gogotsi, Y. (2011). The properties and applications of nanodiamonds. *Nature Nanotechnology*, 7(1), pp.11-23.

Monopoli, M., Åberg, C., Salvati, A. and Dawson, K. (2012). Biomolecular coronas provide the biological identity of nanosized materials. *Nature Nanotechnology*, 7(12), pp.779-786.

Montanaro, L., Campoccia, D., Rizzi, S., Donati, M., Breschi, L., Prati, C. and Arciola, C. (2004). Evaluation of bacterial adhesion of Streptococcus mutans on dental restorative materials. *Biomaterials*, 25(18), pp.4457-4463.

Nakajo, K., Imazato, S., Takahashi, Y., Kiba, W., Ebisu, S. and Takahashi, N. (2009)a. Fluoride released from glass-ionomer cement is responsible to inhibit the acid production of caries-related oral streptococci. *Dental Materials*, 25(6), pp.703-708.

Nyvad, B. And Fejerskov, O. (1987). Scanning electron microscopy of early microbial colonization of human enamel and root surfaces in vivo. *European Journal of Oral Sciences*, 95(4), pp.287-296.

Ogawa, A., Furukawa, S., Fujita, S., Mitobe, J., Kawarai, T., Narisawa, N., Sekizuka, T., Kuroda, M., Ochiai, K., Ogihara, H., Kosono, S., Yoneda, S., Watanabe, H., Morinaga, Y., Uematsu, H. and Senpuku, H. (2011). Inhibition of Streptococcus mutans Biofilm Formation by Streptococcus salivarius Fru A. *Applied and Environmental Microbiology*, 77(5), pp.1572-1580.

Osinaga, P., Grande, R., Ballester, R., Simionato, M., Delgado Rodrigues, C. and Muench, A. (2003). Zinc sulfate addition to glass-ionomer-based cements: influence on physical and antibacterial properties, zinc and fluoride release. *Dental Materials*, 19(3), pp.212-217.

Osswald, S., Yushin, G., Mochalin, V., Kucheyev, S. and Gogotsi, Y. (2006). Control of sp2/sp3Carbon Ratio and Surface Chemistry of Nanodiamond Powders by Selective Oxidation in Air. *Journal of the American Chemical Society*, 128(35), pp.11635-11642.

Palenik, C., Behnen, M., Setcos, J. and Miller, C. (1992). Inhibition of microbial adherence and growth by various glass ionomers *in vitro*. *Dental Materials*, 8(1), pp.16-20.

Panich, A., Altman, A., Shames, A., Osipov, V., Aleksenskiy, A. and Vul', A. (2011). Proton magnetic resonance study of diamond nanoparticles decorated by transition metal ions. *Journal of Physics D: Applied Physics*, 44(12), p.125303.

Pasquantonio, G., Greco, C., Prenna, M., Ripa, C., Vitali, L., Petrelli, D., Di Luca, M. and Ripa, S. (2008). Antibacterial Activity and Anti-Biofilm Effect of Chitosan against Strains of Streptococcus Mutans Isolated in Dental Plaque. *International Journal of Immunopathology and Pharmacology*, 21(4), pp.993-997.

Petit, T., Yuzawa, H., Nagasaka, M., Yamanoi, R., Osawa, E., Kosugi, N. and Aziz, E. (2015). Probing Interfacial Water on Nanodiamonds in Colloidal Dispersion. *The Journal of Physical Chemistry Letters*, 6(15), pp.2909-2912.

Poggio, C., Arciola, C., Rosti, F., Scribante, A., Saino, E. and Visai, L. (2009). Adhesion of Streptococcus Mutans to Different Restorative Materials. *The International Journal of Artificial Organs*, 32(9), pp.671-677.

Raafat, D., von Bargen, K., Haas, A. and Sahl, H. (2008). Insights into the Mode of Action of Chitosan as an Antibacterial Compound. *Applied and Environmental Microbiology*, 74(12), pp.3764-3773.

Ribeiro, J. and Ericson, D. (1991). *In vitro* antibacterial effect of chlorhexidine added to glass-ionomer cements. *European Journal of Oral Sciences*, 99(6), pp.533-540.

Scannapieco, F. (1994). Saliva-Bacterium Interactions in Oral Microbial Ecology. *Critical Reviews in Oral Biology & Medicine*, 5(3), pp.203-248.

Schilling, K. and Bowen, W. (1992). Glucans synthesized in situ in experimental salivary pellicle function as specific binding sites for Streptococcus mutans. *Infection and Immunity*, 60, pp.284-295.

Seixas, L., Seixas, F., Ciccone, J., Souza, W. and Palma-Dibb, R. (2004). Demineralization around restorations with different restorative materials containing fluoride. *Materials Research*, 7(2), pp.235-240.

Seppä, L., Torppa-Saarinen, E. and Luoma, H. (1992). Effect of Different Glass Ionomers on the Acid Production and Electrolyte Metabolism of Streptococcus mutans Ingbritt. *Caries Research*, 26(6), pp.434-438.

Sonia, T. and Sharma, C. (2011). Chitosan for Biomaterials I. *Advances in Polymer Science*, pp.30.

Thompson, J. (1988). Lactic acid bacteria: model systems for in vivo studies of sugar transport and metabolism in gram-positive organisms. *Biochimie*, 70(3), pp.325-336.

Ullah, M., Kausar, A., Siddiq, M., Subhan, M. and Abid Zia, M. (2015). Reinforcing Effects of Modified Nanodiamonds on the Physical Properties of Polymer-Based Nanocomposites: A Review. *Polymer-Plastics Technology and Engineering*, 54(8), pp.861-879.

van Houte, J., Gibbs, G. and Butera, C. (1982). Oral Flora of Children with "Nursing Bottle Caries." *Journal of Dental Research*, 61(2), pp.382-385.

Wallman, C. and Krasse, B. (1992). Mutans streptococci in margins of fillings and crowns. *Journal of Dentistry*, 20(3), pp.163-166.

Wang, B. and Kuramitsu, H. (2005). Interactions between Oral Bacteria: Inhibition of Streptococcus mutans Bacteriocin Production by Streptococcus gordonii. *Applied and Environmental Microbiology*, 71(1), pp.354-362.

Wang, H., Niu, C., Yang, Q. and Badea, I. (2011). Study on protein conformation and adsorption behaviors in nanodiamond particle–protein complexes. *Nanotechnology*, 22(14), pp.145703.

Wehling, J., Dringen, R., Zare, R., Maas, M. and Rezwan, K. (2014). Bactericidal Activity of Partially Oxidized Nanodiamonds. *ACS Nano*, 8(6), pp.6475-6483.

Welin-Neilands, J. and Svensater, G. (2007). Acid Tolerance of Biofilm Cells of Streptococcus mutans. *Applied and Environmental Microbiology*, 73(17), pp.5633-5638.

Wiegand, A., Buchalla, W. and Attin, T. (2007). Review on fluoride-releasing restorative materials—Fluoride release and uptake characteristics, antibacterial activity and influence on caries formation. *Dental Materials*, 23(3), pp.343-362.

Xing, Y. and Dai, L. (2009). Nanodiamonds for nanomedicine. *Nanomedicine*, 4(2), pp.207-218.

Yamashita, Y., Bowen, W., Burne, R. and Kuramitsu, H. (1993). Role of the Streptococcus mutans gtf genes in caries induction in the specific pathogen free rat model. *Infection and Immunity*, 61(9), pp.3811-3817.

Yang, S., Guo, Z., Miao, F., Xue, Q. and Qin, S. (2010). The hydroxyl radical scavenging activity of chitosan, hyaluronan, starch and their O-carboxymethylated derivatives. *Carbohydrate Polymers*, 82(4), pp.1043-1045.

Yip, H., Peng, D. and Smales, R. (2001). Effects of APF gel on the physical structure of compomers and glass ionomer cements. *Operative Dentistry.*, 26(3), pp.231-238.

Yip, K., Lam, W. and Smales, R. (1999). Fluoride release, weight loss and erosive wear of modern aesthetic restoratives. *British Dental Journal*, 187(5), pp.265-270.

Yoshida, Y., Van Meerbeek, B., Nakayama, Y., Snauwaert, J., Hellemans, L., Lambrechts, P., Vanherle, G. and Wakasa, K. (2000). Evidence of Chemical Bonding at Biomaterial-Hard Tissue Interfaces. *Journal of Dental Research*, 79(2),pp.709-714.

CHAPTER 11

ION MOVEMENT ADJACENT TO THE INTER-DIFFUSION ZONE OF NANODIAMOND-MODIFIED GLASS IONOMER RESTORATIVE CEMENTS

11.1. Abstract

Background and objective: Immediately after mixing the powder and liquid components of the glass ionomer restorative cements (GICs), the water as well as the polycarboxcylic acid liquid, hydrate the glass filler particles. This results in the release of the cation combinations depending on the formulation of the GIC. The release of aluminium (Al^{3+}) and calcium (Ca^{2+}) are associated with the release of sodium (Na^{+}). In GICs that do not contain calcium but rather strontium (Sr^{2+}), the strontium will perform all the same functions as the calcium. The carboxylic parts of the GIC liquid interact with the tooth structure and an inter-diffusion zone is established between the GIC and the tooth surface. The ion exchange between the tooth and the GIC results in the tooth-restoration surface becoming more resistant to demineralisation (Berg, 2002). It has been established that the assessment of the ions present in the tooth structure and more specifically the inter-diffusion zone which forms between the restoration and the tooth is difficult. The difficulty stems from the variability of the ion concentrations that differ between teeth, especially the variation of calcium and phosphorus (Gjorgievska *et al*., 2012). Calcium and phosphorus play an integral role in maintaining neutrality during ion movement between the tooth and the GIC restoration (Wilson *et al*., 1983). Utilising the same tooth to compare the ion movement from the GIC to the tooth structure would remove the aforementioned variability in tooth structure and would allow a more accurate comparison between the various GIC material modifications.

The aim of the study was to compare the ion exchange of the inter-diffusion zone adjacent to the tooth using three GICs modified with nanodiamonds.

Materials and Methods: A caries-free primary molar was sectioned and polished to 1200 grit with silicon carbide paper under de-ionised water. The dimensions of the sectioned tooth were confirmed with a micrometer to 2mm thick x 5mm wide x 8mm long. The three GICs, namely Fuji IX GP (FN) *(GC Corp)* Ketac Universal (KU) *(3M ESPE)* and Riva Self Cure (RSC) *(SDI Ltd),* were hand-mixed according to the manufacturers' recommended powder/liquid ratio. Nanodiamond modifications to the GICs were made in a 5% or 10% nanodiamond substitution weight to weight percentage (w/w%). Three samples of each GIC were assessed with SEM-EDS for the gradient weight percentage (wt%) of the ions present in the control materials. For the inter-diffusion zone assessment, the mixed GICs were placed on the 2mm thick x 8mm long side of the dentine, without the use of any dentine conditioners. After the initial 10 minutes of bench curing, the specimens were smoothed on the 1200 wet silicon carbide paper under de-ionised water and wrapped in 5 x 5cm filter paper moistened with 500µl of de-ionised water and left for 14 days at 25ºC in an airtight high density polyethylene (HDPE) container. The GIC/tooth specimens were invested in clear acrylic and the specimens were prepared with 4000 grit wet silicon carbide paper followed by diamond polishing paste under de-ionised water irrigation to remove 0.5mm in order to polish the surface. SEM-EDS line scan analysis was completed progressing from the tooth to the restoration while analysing the ions: The ions assessed were: Aluminium (Al^{3+}), Carbon (C^{4+}), Calcium (Ca^{2+}), Fluoride (F^{-}), Iron ($Fe^{2+\&3+}$), Lanthanum (La^{3+}), Oxygen (O^{2-}), Phosphorus (P^{3+}), Potassium (K^{+}), Silicon (Si^{4+}), Sodium (Na^{+}), Strontium (Sr^{+}) and Zinc (Zn^{2+}).

Results: There were significant differences ($p < 0.05$) between the control materials according the one-way ANOVA and the Scheffé multiple comparison post-hoc test. The gradient wt% ion analysis of the control materials revealed that FN had the highest gradient wt% potential for aluminium, fluoride, calcium, phosphorus, silicon and strontium. KU had the highest wt% for aluminium, fluoride, sodium and silicon diffusion from the restoration into the tooth. The 5%ND modifications except for RSC10%ND, presented with the highest aluminium, fluoride, silicon and strontium ion movement into the dentine compared to their respective controls and their other nanodiamond modifications.

Conclusion: The assessment of ion movement between the various GICs and the tooth sections from the same tooth provided crucial information regarding ion exchange and the formation of the inter-diffusion zone. The GICs with the highest gradient wt% potential of various ions did not necessarily produce the greatest ion movement into the tooth. The movement of strontium into the tooth is however dependent on the movement of calcium and phosphorus from the tooth to the restoration and not the gradient wt% potential present in the material. The exceptionably low fluoride wt% of both the GICs/tooth in the SEM-EDS assessed 29.1µm of the tooth and indicated that the fluoride ion is in fact a free ion that moves out of the GICs readily upon contact with moisture from the environment. With regard to the nanodiamond modification of the three GIC control materials, the ion interaction with the tooth structure for FN5%ND, KU5%ND and RSC10%ND were preferable to their respective control materials.

Key words: Glass ionomer cement, ion movement, inter-diffusion zone, ion rich layer, SEM-EDS, glass ionomer cement, nanodiamonds.

Abbreviations and acronyms

FN: Fuji IX GP

GICs: Glass-ionomer cements

Gradient wt% potential: Ions present in the GICs

KU: Ketac Universal

ND: Nanodiamond particles

RSC: Riva Self Cure

SEM-EDS: Scanning Electron Microscopy and Energy Dispersive X-Ray Spectrometry Microanalysis

wt%: weight percentage

11.2. Introduction

Glass polyalkenoate cements also known as glass-ionomer restorative cements (GICs) (ISO 9917–1, 2007) are one of the key materials utilised by the paediatric dentist. The physical properties (Kerby and Knobloch, 1992) and survival rates of GICs are lower than more commonly used restorative materials like resin modified glass ionomers and compomers (Hickel *et al*., 2000). GICs have been cited to have a caries inhibitory and / or anticariogenic effect (Guida *et al*., 2002) and are considered to be bioactive due to the presence of silicates (SiO_4) and fluorides (Anusavice *et al*., 2012). The bioactive interactions of GICs include the ionic interaction and adherence of the material to enamel and dentine (Wilson *et al*., 1983; Erickson and Glasspoole, 1994). Even in the presence of a smear layer GICs have illustrated the ability to bond directly to dentine and enamel (Powis *et al*., 1982; Glasspoole *et al*., 2002). The dentine conditioner used with most GICs acts as a chelating agent which partly removes and modifies

the smear layer. The dentine conditioner, usually a 10-20% polyalkenoic acid, can penetrate the dentine surface layer to a depth of up to 1 μm (Van Meerbeek *et al*., 2003) and enhance the chemical bonding of the GIC to the tooth. Ketac Universal (KU, *3M ESPE*) has been developed to be used without a dentine conditioner. The GICs like Fuji IX (FN), Ketac Universal (KU) and Riva Self Cure (RSC) draw their favourable features from the constituents of alumina (Al_2O_3), soda (Na_2O), strontium fluoride (SrF_2), silica (SiO_2) and strontium oxide (SrO) (Wilson and McLean, 1988). The most notable feature of GICs is the release of fluoride (Mount, 2002). Souto and Donly (1994) recognized that secondary caries can partly be prevented due to the fluoride release. Fluoride is however not the only ion that is readily released from GICs (Chapter 7 and 8). Before ions can be released into a moist environment or into the tooth structure, there should first be a release of ions from the glass filler particles initiated by the mixing of the powder and the liquid of the GICs. The ion release after the powder and the liquid is mixed results in the setting process and subsequent strength development (Nicholson, 2018). Ions like calcium, sodium and strontium followed by aluminium are released in the form of complexes during mixing of the GIC and take part in the salt bridge formation. During the final setting- and maturation phase of the GIC, strontium ions form the cross-linked matrix followed by aluminium ions that will contribute to the strength enhancement of the cross-linked matrix. As the acid-base reaction continues more aluminium becomes available. Aluminium (Al^{3+}) has a higher ionic charge and therefore aluminium is essential for the development of a stronger polycarboxylate matrix. Aluminium has the ability to displace strontium ions (Nicholson, 1998). As the GIC matrix mature aluminium (Al^{3+}) polycarboxylate converts into Al(IV). This transformation occurs at a slower rate than the strontium polycarboxylate. The interactions of the ions are also responsible for the adherence to tooth structure in the form of the inter-diffusion zone. Aluminium, sodium and strontium complexes precipitate with fluoride and phosphorus in the matrix of the GIC. If calcium or strontium form part of the GIC formulation these calcium or

strontium polysalts will develop first. The aforementioned polysalts release faster from the CaF_2 or SrF_2 followed by aluminium polysalts, since aluminium is usually in the form of aluminosilicate (Al_2SiO^5) (Xie *et al*., 2000). These ions and their release into the tooth structure by way of ion exchange have been established as the mechanism that enables GICs to remineralise the demineralised dentine (Ngo *et al*., 2006).

Gjorgievska *et al.* (2012) indicated that aluminium, fluoride, magnesium, silicon and strontium were incorporated into the dentine from FN. Although the distance of ion movement was not assessed using line scans as in the present study, Gjorgievska *et al*.(2012) could conclude that the variation of the ion movement between different teeth would be limited by the dense crystalline nature of tooth structure (Gjorgievska *et al*., 2012). In order to assess the true effect of the nanodiamond particles modification on the commercial GICs, the same tooth had to be utilised to eliminate the potential variability of especially the calcium and phosphorus ions present in the composition of different teeth.

The bioactivity of GICs allows the ions from GICs to move towards and incorporate into the tooth structure. This is termed the ion-rich layer, better known as the ion diffusion zone (Ngo *et al*., 1997).

This ion movement and ion exchange with the tooth structure was the objective of the present study in the dissertation. The hypothesis was that the ions from the GICs modified with nanodiamonds would increase the bioactivity of the modified GICs to allow more ion exchange and a wider inter-diffusion zone between the GIC and the tooth.

11.3. Pilot study

The pilot study was completed using second primary molar teeth. Three teeth received single Class I cavity preparations and three other teeth received multiple Class I cavity preparations. The teeth were restored with the various GICs and an example in Figure 11.1 illustrates KU and KU5%ND. A tooth with multiple restorations indicated erratic ion percentages, as the ion diffusion from the adjacent restorations of various materials reached one another. The five line scans (yellow lines on Figure 11.1) illustrated irregular results in terms of the data comparison between different teeth; this confirmed the research of Gjorgievska *et al*. (2012). The assessment showed variability especially for the ions moving into the teeth due to calcium and phosphorus weight percentage (wt%) differences. This could result in inaccurate deductions being made with regard to the movement of the ions from the GICs, especially the movement of calcium, fluoride, phosphorus and strontium to and from the restoration and the tooth.

Figure 11.1: Pilot study of GIC/tooth interface

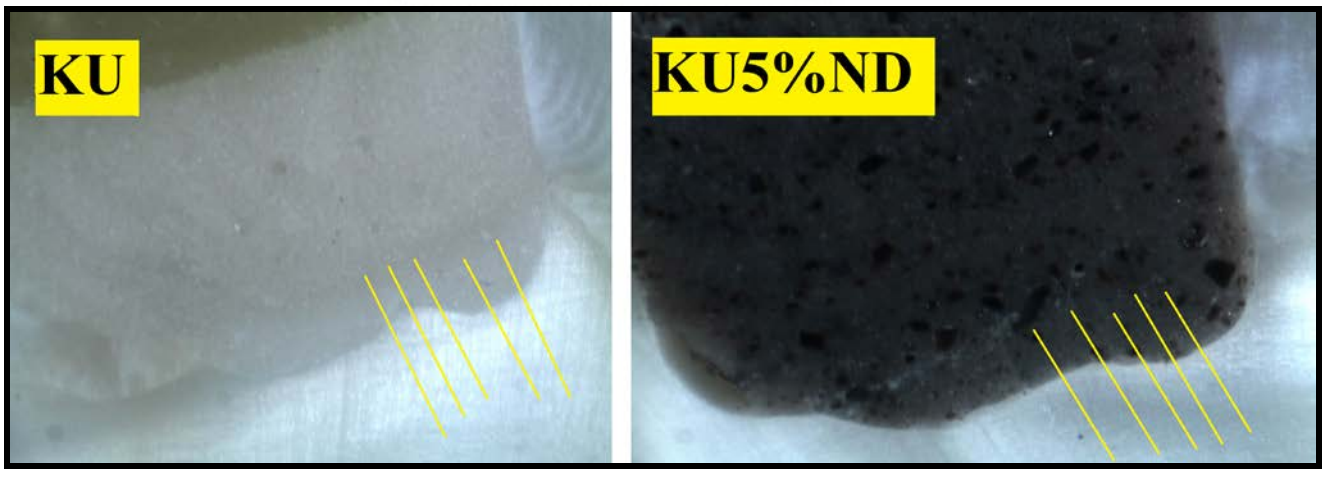

11.4. Materials and Methods

11.4.1. Materials and tooth preparation

The GICs used as the control materials were Fuji IX (FN: *GC Corp, Tokyo, Japan, Batch: 1503231*); Ketac Universal (KU: *3M ESPE, Seefeld, Germany, Batch: 583514*) and Riva Self Cure (RSC: *SDI Limited, Australia, Batch: 62657V*). The three GICs were modified in the powder phase weight per weight percentage (w/w%) by replacing 5% or 10% of the GIC with a commercially available nanodiamond particles (*PlasmaChem, item: PL-D-G01)* (GIC95%:ND5%; GIC90%:ND10%). The chosen primary second molar tooth exfoliated naturally and was placed in 1% thymol in de-ionised water solution for 24 hours. The remaining roots were sectioned off at the cemento enamel junction of the primary second molar with a 25mm diamond disc at 200 RPM cooled with de-ionised water (*Isomet 11-1180 low speed saw, Buehler LTD, IL USA*). The buccal and lingual curvature of enamel was removed, followed by sectioning through the central fissure from a mesial to distal direction. These two halves were subsequently sectioned into specimens from a buccal to ligual direction to obtain a 2mm buccal dimension by 5mm bucco-lingual dimension and 8mm in height (Figure 11.2).

Figure 11.2: Flow diagram to illustrate tooth preparation and GIC placement prior to SEM-EDS

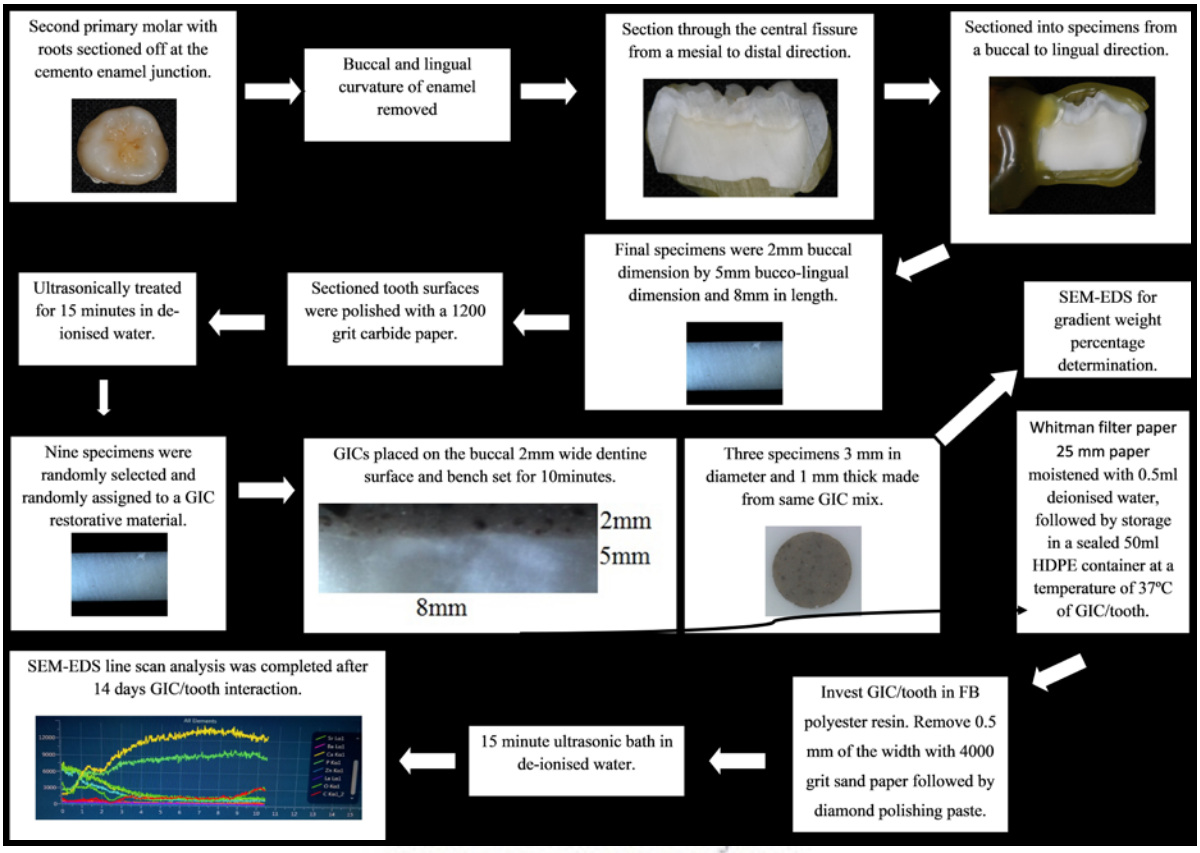

The sectioned tooth surfaces were polished with 1200 grit, wet silicon carbide paper under de-ionised water irrigation on all the surfaces in order to standardise the surface roughness. The specimens were ultrasonically treated for 15 minutes in de-ionised water to remove any loose silicon particles originating from the wet silicon carbide paper. Nine specimens were randomly selected and randomly assigned to one of the 15 GIC restorative materials. The material was mixed in accordance with the manufacturer's instructions. The powder/liquid ratios were followed and confirmed with an analytical balance (Mulder, 2018). No dentine conditioner was used on the tooth surfaces for any of the GICs, since the surface was similarly prepared with the wet silicon carbide paper. Additionally, to truly determine the influence of the nanodiamond

modifications on the GICs, the use of no surface treatment was justified. Only a cotton pellet was used to blot dry the dentine surface prior to the GIC placement. A cellulose strip was placed between the GIC/tooth and a microscope slide. In order to obtain a standard volume of GIC material a custom made Teflon die was used into which the dentine specimen fitted. The final volume of GIC was placed on the buccal 2mm wide and 8mm long dentine surface and allowed to bench-set for 10 minutes. 2500 grit wet carbide paper was used to level out the surface of the GIC with the tooth. The final dimensions of the GIC that adhered to the tooth was 2mm thick x 2mm wide x 8mm long. The GIC/tooth sections were subsequently stored in 25 mm paper Whitman filter paper (*Whitman no1, GE Healthcare, Illinois, USA*) which was made with a punch (*Upikit HCP-110 craft punch, circle shape size one, Upikit International PTY Ltd, Tainan, Taiwan*) and moistened with 500µl of de-ionised water. Storage of the samples was completed for 14 days in a sealed HDPE container at a temperature of 37ºC. The tooth surface and GIC was therefore kept moist in this sealed environment, since ion exchange from the GIC can only occur with moist dentine (Watson, 1992).

The interaction between the tooth and the GIC was allowed to continue for 14 days and then the GIC/tooth specimen was invested in polyester resin (*FB polyester resin, Folks Brothers, South Africa*). The GIC/tooth specimen was oriented with the 5mm bucco-lingual surface and 2mm GIC to the top to allow the removal of 0.5mm using 4000 grit carbide paper under de-ionised water irrigation and this was confirmed with a calliper. This was then followed by a final polish with EVE DP1 Once diamond paste (*Ernst Vetter GmbH, Lot 191213; Rorstatter Str30, D-75179 Pforzheim*) and a silk cloth for 5 minutes on each sample. The loose debris from the polishing process was removed by a 15 minute ultrasonic bath in de-ionised water.

The samples were blot dry with Whitman filter paper and placed in a sealed plastic bag until gold sputtered to increase the electrical conductivity of the sample for SEM-EDS analysis. The line scan analysis was completed after 14 days of GIC/tooth interaction (Knight *et al*., 2006).

11.4.2. SEM-EDS ion analysis for gradient wt% potential on discs

Scanning Electron Microscope (*Carl Zeiss Microscopy, Munchen, Germany*) and Zeiss Smart SEM software were used to generate images, while quantitative Energy Dispersive X-Ray Spectrometry (EDS) using an X-Max 20 mm^2 detector (*Oxford Instruments, Oxfordshire OX13 5QX, United Kingdom*) and Oxford Aztec software (*Oxford Instruments, Oxfordshire OX13 5QX, United Kingdom*) chemically quantified the samples. Analyses were also completed on the three commercial GICs and their respective nanodiamond disc shaped specimens (3±0.1mm in diameter and 1±0.1mm thick). This analysis was essential to establish a baseline weight percentage of the ions present in the 15 GICs used as restorations on the dentine slices. Three randomly selected slices were selected for the baseline ion analyses of the dentine. Each dentine slice received 10 spectrums in order to determine an average ion weight percentage per sample. The baseline weight percentage of the ions present in the GICs will further be known as the "gradient wt% potential". Point and ID analysis on the Aztec Software allow the operator to manually choose individual areas and analyse where the focussed electron beam is placed. Hill *et al*., (1995) confirmed that the fluoride release from GICs were complex and originated from the three material phases within the GIC (Hill *et al*., 1995). Thirty points in total was selected (spectrum points) where the ID analyses would be taken for each disc shaped GIC specimen. The 30 points were divided between the three different areas in the matured GIC that was established under magnification. Figure 11.3 illustrates the three different areas where each set of ten points with their ID analyses were done on: 1) areas of glass clusters (glass), 2) area of dissolved glass (silica gel) and the 3) areas of less glass and more polyacrylic acid / glass slurry dominated by polyacrylic acid (polysalt matrix) (Figure 11.3). The average of the 90 analyses from the three samples of each material provided the gradient wt% potential of the ion wt% for the GICs (Table 11.1). The spectrum of the ID analysis distribution between the three distinct phases in the GICs was essential to allow for sufficient quantification, since it has been shown

that the glass filler particle and matrix have different ion concentrations (Hatton and Brook, 1992; Hill *et al*., 1995).

Figure 11.3: SEM-EDS spectrums of the various restoration phases

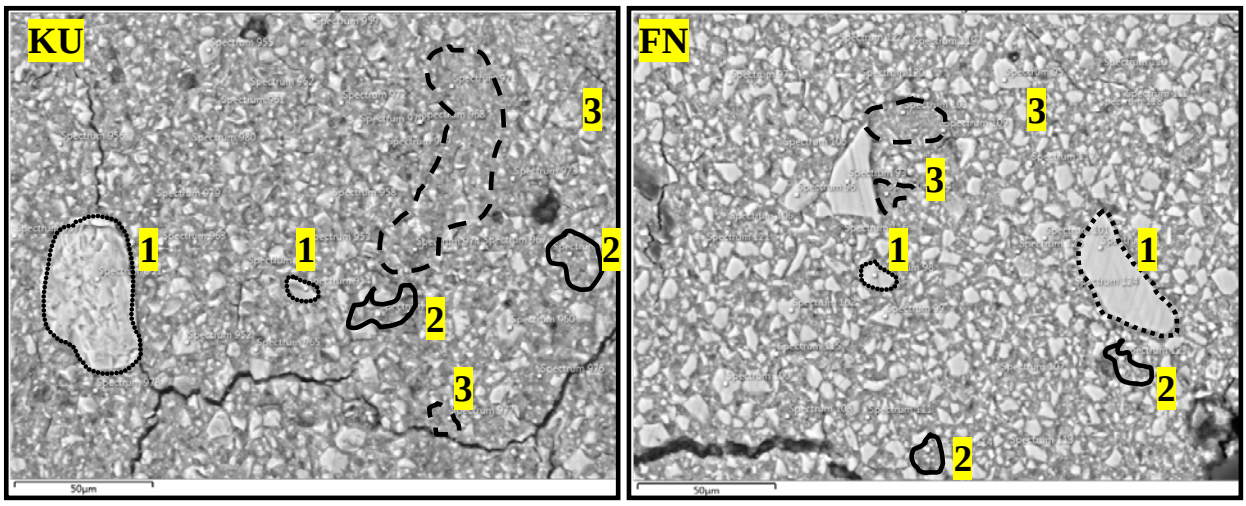

1) Areas of glass clusters (glass),

2) Area of dissolved glass (silica gel) and

3) Areas of less glass and more polyacrylic acid / glass slurry dominated by polyacrylic acid (polysalt matrix)

In order to increase the electrical conductivity of the GIC specimens for SEM analysis, the specimens were first gold sputter-coated (*Edwards S150A Sputter Coater*) at 40 mA. SEM-EDS of the outer surfaces was then performed (*Zeiss MERLIN Field Emission SEM; Carl Zeiss Microscopy, Munchen, Germany*) at 200x magnification. The ions assessed were: Aluminium (Al^{3+}), Carbon (C^{4+}), Calcium (Ca^{2+}), Fluoride (F^{-}), Iron ($Fe^{2+\&3+}$), Lanthanum (La^{3+}), Oxygen (O^{2-}), Phosphorus (P^{3+}), Potassium (K^{+}), Silicon (Si^{4+}), Sodium (Na^{+}), Strontium (Sr^{+}) and Zinc (Zn^{2+}).

Backscatter Electron detection combined with EDS was collected from the central field of view for each specimen. For Backscattered Electron detection coupled with EDS, operating conditions of 20 kV accelerating voltage, 11 nA beam current with a working distance of 9.5

mm, 10s acquisition time and 30-45% detector dead time were used for this application. For this SEM unit a pressure of 10^6 Torr (high-vacuum) was present. The ion analyses (in weight percentage (wt%) of the specimens were performed against the factory standards in normalized mode and the PROZA (Phi-Rho-Z) correction method was applied. A Zeiss 5-diode Back Scattered Electron Detector (*Zeiss NTS BSD*) and Zeiss Smart SEM software generated the BSE images. The Semi-quantitative Energy Dispersive X-Ray Spectrometry (EDS) using an X-Max $20mm^2$ detector (*Oxford Instruments, Oxfordshire OX13 5QX, United Kingdom*) and Oxford Aztec software were used to chemically quantify the specimens. Images were obtained at 200 and 500nm (Chapter 7).

11.4.3. SEM-EDS line scan of inter-diffusion zone on the GIC/tooth specimen

SEM-EDS line scans were performed with the same settings as the aforementioned SEM-EDS analysis of the gradient wt% potential of the GIC discs. Line scan analysis on the Aztec Software allowed the operator to manually choose a start and end point. A connecting line drawn by the software could be optimised as follows: 1) the software allow the operator to choose the amount of points along the line 2) and the separation between the points. The final settings for the line scans with EDS analyses were set at 266 individual points at a distance of 0.746µm apart. The scan started in the tooth (167.14µm from the GIC/tooth interface, total of 226 points) and continued towards the restoration. The line scan had 40 points in the restoration to a total distance of 29.1µm. The exact GIC/tooth contact point was determined during the placement of the 197µm line with its 266 individual points. Five line scans were performed per GIC/tooth taking care to avoid areas of air voids, lost filler particles and cracks wider than 0.746µm. This was essential; as these imperfections affect the beam focus alter the true detection of the ion weight percentage. The averages of the scans per spectrum point were calculated. The statistical analysis of the 5 line scans per specimen was completed on the 29.1µm adjacent of the GIC and

29.1µm adjacent to the tooth interface. The statistics was therefore completed with the ion wt% per spectrum point at the two 29.1µm distances, resulting in 40 spectrums spaced 0.746µm apart. In the areas where a crack was unavoidable, the distance of the crack was added to the line scan length, in order to remove those spectrums in the crack (Figure 11.4).

Figure 11.4: SEM-EDS line scan from the tooth towards the restoration

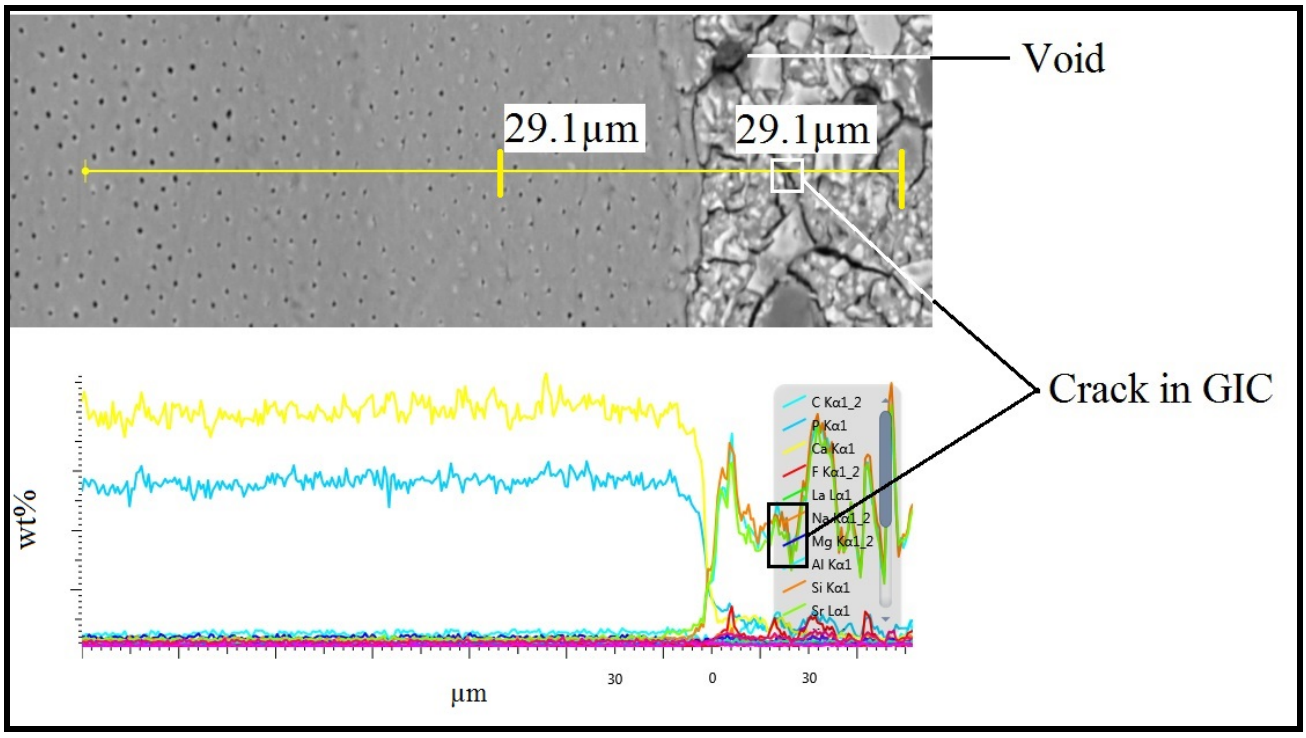

11.4.4. Weight percentage (wt%) interpretation of ion movement

In order to have a fair representation of the bioavailability and the ability of the ions to move between the tooth and the restoration, the weight percentage of ions were recorded from of the SEM-EDS results. The line scan of the GIC/tooth wt% was compared to the gradient wt% potential of the various GICs using comparative tables (Tables 11.1 and 11.2).

11.5. Statistical analysis

The data sheet with 266 spectrum points derived from the GIC/tooth line scans were fitted with a Logarithmic trendline for each ion and the intersection point of between 20-25µm was determined as the intersection of where the ions reached the same percentage per weight in the restoration and tooth (Figure 11.4). Atmeh *et al*. (2012) determined a dye penetration due to ion exchange of 14.5±1.9µm wide. Therefore, for the statistical analysis, the ion weight percentage points for 29.10µm of the line scan into the GIC and 29.10µm of the line scan into the tooth was selected to allow an equally divided 80 spectrum points between the GIC/tooth interfaces. A p-value lower than 0.05 corresponding to the F-statistic for the one-way ANOVA, would suggest that there were one or more significant differences located between ion wt% for that 29.10µm line scan. The Scheffé multiple comparison test followed as the post-hoc test to identify which of the pairs of materials were significantly different from each other.

11.6. Results

The ion analysis of the GIC control and nanodiamond-modified materials are presented in Table 11.1 This represents the gradient weight percentage (wt%) potential of the present wt% of ions for the various GICs and the tooth. The nanodiamond particles contain many of the ions assessed in this study (Volkov *et al*., 2014). These ions are however presented in parts per million (ppm) and did not contribute to a higher gradient wt% potential of the nanodiamond-modified GICs

(Tables 11.1 and 11.2) due to the ions being retained in the nanodiamond nuclei. The ions in the nanodiamond nuclei were not released from the nanodiamond due to their resistance to acid attack (Volkov *et al*., 2014).

Table 11.1: Gradient weight percentage: Ion analysis of the material discs and tooth in weight percentage

Material name	Al	Ba	Ca	F	Fe	La	Na	P	Si	Sr	Zn
Nanodiamond particles (in ppm)	10500	22	300	Not assessed	2680	0	25	100	1260	3	90
Tooth	0.18	0.78	49.24	0.49	0.2	0	0.64	20.66	0.08	0.44	0.47
FN	11.2	0.1	0.2	13.3	0	0	0.9	3.1	10.2	3.9	0.1
FN5%ND	10.7	0.2	0.2	11.9	0	0	0.8	3	9.9	3.7	0
FN10%ND	9.5	0.1	0.2	12.3	0	0	0.8	2.7	8.5	3.2	0
KU	8.2	0.1	0.2	11.4	0	2.6	1.8	2.5	10.5	2.8	0
KU5%ND	7.8	0	0.2	9.8	0.1	2.6	1.6	2.4	10.1	2.7	0
KU10%ND	7.7	0.1	0.2	10.2	0	2.5	1.6	2.3	9.8	2.6	0
RSC	9.8	0.5	0.1	11.7	0	0	1.3	2.3	9.9	3	0
RSC5%ND	10.4	0.5	0.1	10.9	0	0	1.2	2.6	10.6	3.3	0
RSC10%ND	9.3	0.4	0.1	11.1	0	0	1.1	2.3	9.3	3	0

After the ion movement between the tooth and the GICs have taken place, the resultant ion weight percentages are represented in Table 11.2 illustrate the average ion wt% in the tooth versus the restoration for the 40 spectrums in the two 29.1µm areas of the line scan that was statistically assessed.

Table 11.2: Average ion weight percentage in the tooth or GIC restoration adjacent to the inter-diffusion zone (29.10µm dentine and 29.10µm GIC)

Comparison	Average ion weight percentage in the Dentine								Average ion weight percentage in the GIC restoration							
	Al	Ca	F	La	Na	P	Si	Sr	Al	Ca	F	La	Na	P	Si	Sr
FN	0.59	39.14	0.64	0	0.43	17.64	0.41	1.15	11.51	4.83	1.03	0	0.32	7.26	15.42	21.63
FN5%ND	4.10	26.89	4.21	0	0.64	12.09	3.50	5.06	11.08	3.66	0.86	0	0.24	6.44	15.18	21.39
FN10%ND	0.65	39.68	0.68	0	0.46	17.28	0.50	1.57	9.55	5.16	0.88	0	0.24	5.21	12.00	17.51
KU	0.72	43.33	1.07	0.84	0.53	19.22	0.65	1.15	9.60	6.65	1.53	6.99	0.8	4.77	17.47	18.97
KU5%ND	2.64	34.37	1.84	1.33	0.52	13.07	3.92	3.87	10.44	3.75	0.24	5.86	0.77	6.08	18.68	19.89
KU10%ND	1.96	35.67	1.74	1.64	0.62	15.01	2.66	3.38	9.22	4.0	0.57	5.43	0.69	6.12	16.31	16.75
RSC	0.28	41.63	0.61	0	0.47	18.46	0.18	0.82	10.98	3.15	0.68	0	0.44	5.16	16.01	18.87
RSC5%ND	0.68	53.97	0.66	0	0.74	21.84	0.61	0.56	11.45	2.02	1.01	0	0.46	5.79	18.07	22.54
RSC10%ND	0.75	38.56	0.67	0	0.39	17.00	0.82	1.36	10.34	3.97	0.51	0	0.35	5.87	15.19	19.06

The statistical analysis illustrated in Table 11.3 provides the significance of the analysis on the wt% for a distance of 29.10µm into the restoration and the tooth structure (Figure 11.3). The line scans (Figures 11.4 to 11.13) illustrate the tooth on the left and the GIC on the right.

Table 11.3: Multiple comparisons of the ion percentage present in the tooth vs the GIC restoration percentage

Comparison	Significance in the Dentine								Significance in the GIC restoration							
	Al	Ca	F	La	Na	P	Si	Sr	Al	Ca	F	La	Na	P	Si	Sr
FN vs KU		*	^	///	^	*			*			///	*	*	^	^
FN vs RSC		^		///								///		*		*
KU vs RSC			^	///					^	^	^	///	*			
FN vs FN5%ND	*	*	*	///	^	*	*	*				///	*	^		
FN vs FN10%ND				///					*			///	*	*	*	*
FN5%ND vs FN10%ND	*	*	*	///		*	*	*	*			///		^	*	*
KU vs KU5%ND	*	*				*	*	*		*	*			*		
KU vs KU10%ND		*		*		*		^			*	*		*		*
KU5%ND vs KU10%ND									*						*	*
RSC vs RSC5%ND		*		///	*	*						///			*	*
RSC10%ND vs RSC				///		^						///	^			
RSC5%ND vs RSC10%ND		*		///	*	*			*	^		///	*		*	*

(*) indicates a significant difference in the ion percentage between the materials per group ($p < 0.01$).

(^) indicates a significant difference in the ion percentage between the materials per group ($p < 0.05$)

(**grey blocks**) no significance, (////) not present in material

The movement of calcium and phosphorus dictate the neutrality of the ion movement across the inter-diffusion zone. For the three control materials, the calcium of KU (43.33wt%) had a significantly higher wt% than FN (39.14wt%) in the dentine (Tables 11.2 and 11.3). KU also had significantly greater wt% of calcium present in the restoration than RSC (3.15wt%). KU had significantly more wt% of calcium, fluoride, sodium and phosphorus than FN and RSC in the

dentine (with the exception of fluoride for KU vs RSC). No significance in the wt% was noted for aluminium, silicon and strontium between the three control materials. The lanthanum therefore aided in moving the calcium, fluoride and phosphorus between the GIC restoration and the tooth (Table 11.3).

FN within-group comparison

The calcium and phosphorus of FN and FN10%ND had a significantly higher wt% over the 29.1µm in the dentine. At the inter-diffusion zone (Figure 11.5), the wt% was higher and a continuously higher wt% was maintained until the ions reached the same wt% equilibrium at 23.13µm for calcium and 18.65µm for phosphorus compared to FN5%ND (Tables 11.2, 11.3 and Figure 11.5).

Figure 11.5: Average line scan representing the diffusion of calcium and phosphorus of FN

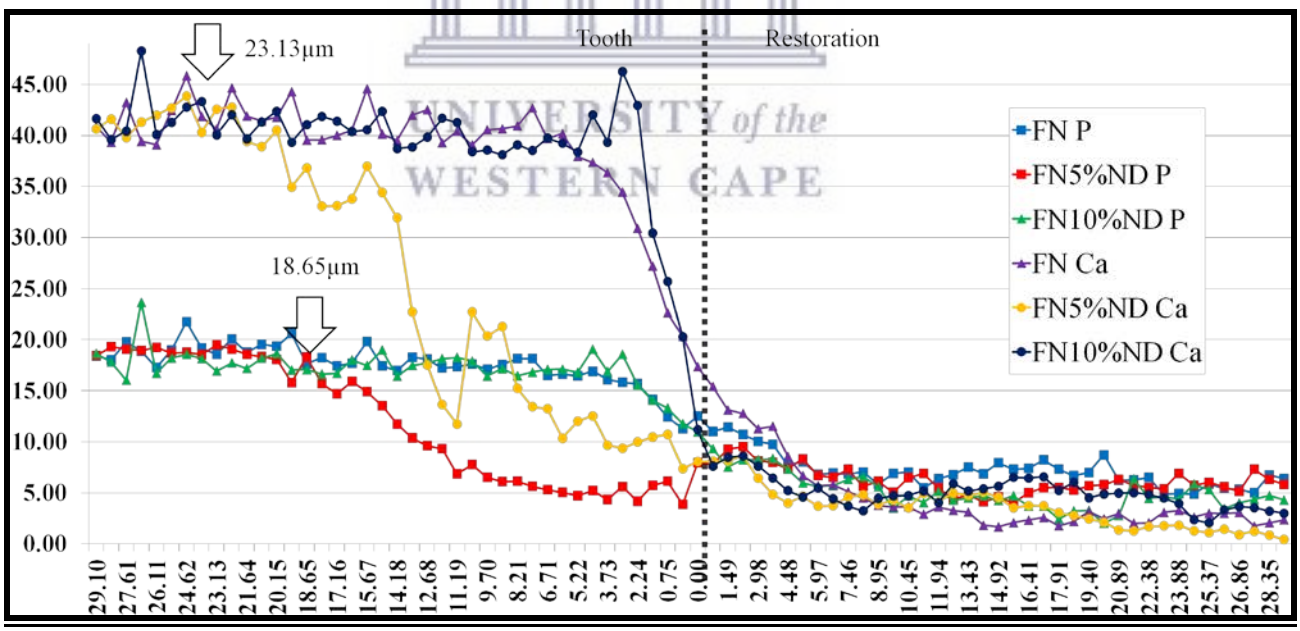

FN5%ND had a significantly higher aluminium, fluoride, silicon and strontium wt% in the tooth than FN and FN10%ND, although the gradient wt% potential in the material (Table 11.1) was lower than FN. FN10%ND also had a lower gradient wt% potential than FN, yet there were no

significant differences in the wt% ion penetration in terms of the dentine for any of the ions (Table 11.3). FN had significantly more aluminium, sodium, phosphorus, silicon and strontium remaining in the restoration than the FN10%ND. It was however noted that at the inter-diffusion zone, there was a much higher wt% for the aluminium and silicon ions for FN5%ND (Figure 11.6).

Figure 11.6: Average line scan representing the diffusion of aluminium and silicon of FN

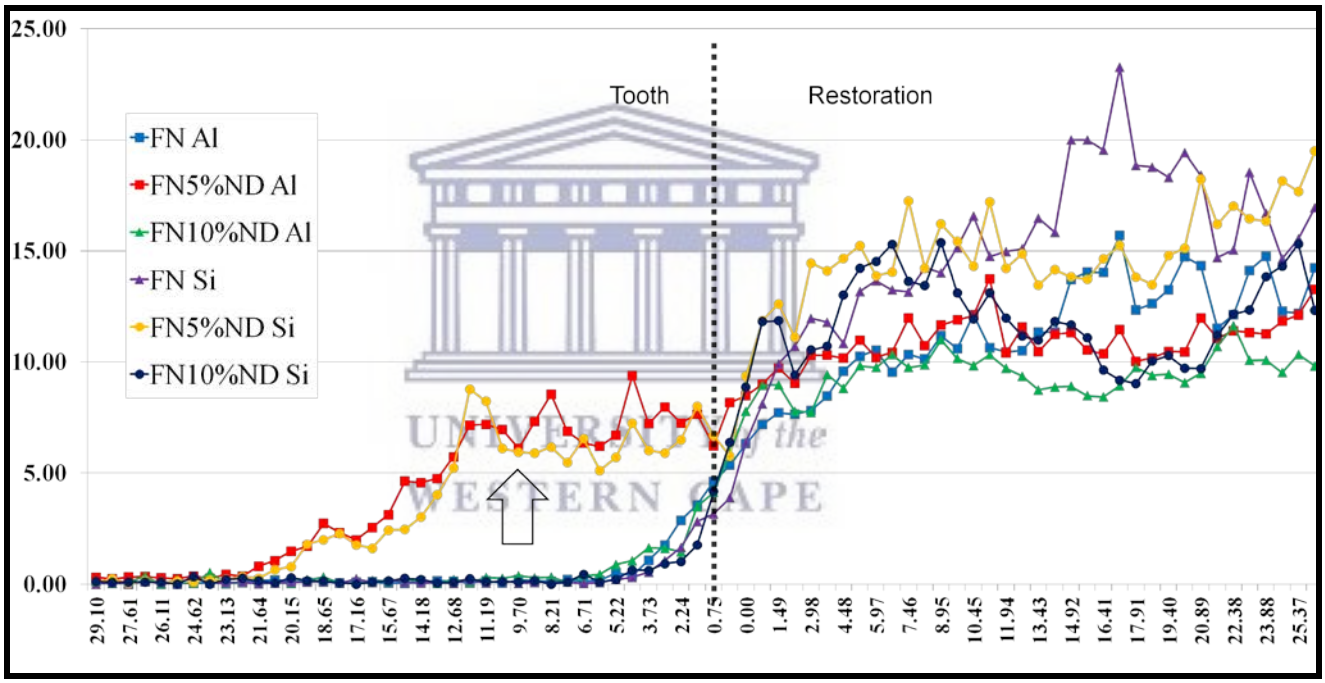

KU within-group comparison

The calcium and phosphorus of KU had a significantly higher wt% than KU5%ND and KU10%ND over the 29.1µm in the dentine. The aluminium, silicon and strontium of KU5%ND had a significantly higher wt% than KU (Table 11.3) over the 29.1µm in the dentine. At the inter-diffusion zone (Figure 11.7), the wt% was higher and a continuously higher wt% was maintained in the dentine until the ions reached the same wt% equilibrium at 15.67µm for strontium and between 23.13 and 24.62µm for fluoride in the tooth (Figure 11.7). With regard to

aluminium and silicon for KU5%ND the highest concentration was retained up to 14.18µm (Figure 11.8). KU contains lanthanum and sodium that also diffuse into the tooth. Based on the large wt% at the 0.00-5.97µm of the restoration, KU exhibited lanthanum moving towards the dentine. It is clear that KU5%ND and KU10%ND allowed a greater wt% of lanthanum to diffuse into the tooth structure up to 8.21µm (Figure 11.9).

Figure 11.7: Average line scan representing the diffusion of fluoride and strontium for KU

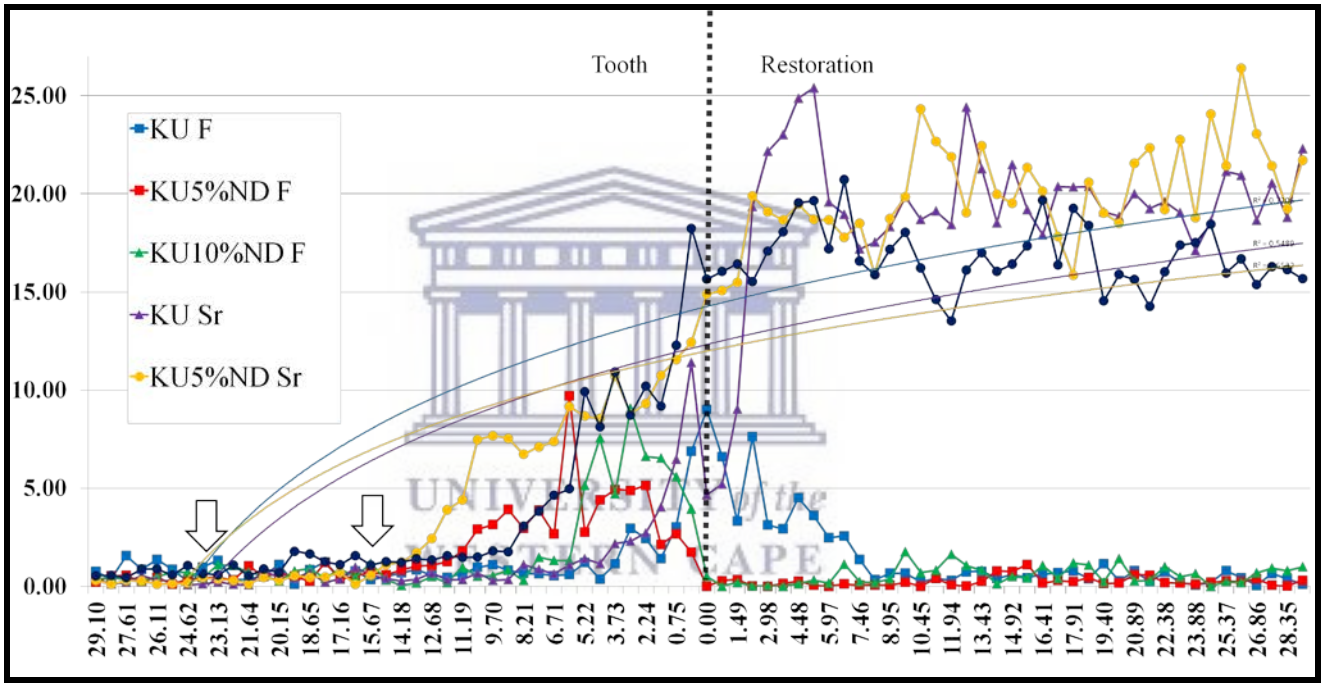

Figure 11.8: Average line scan representing the diffusion of aluminium and silicon for KU

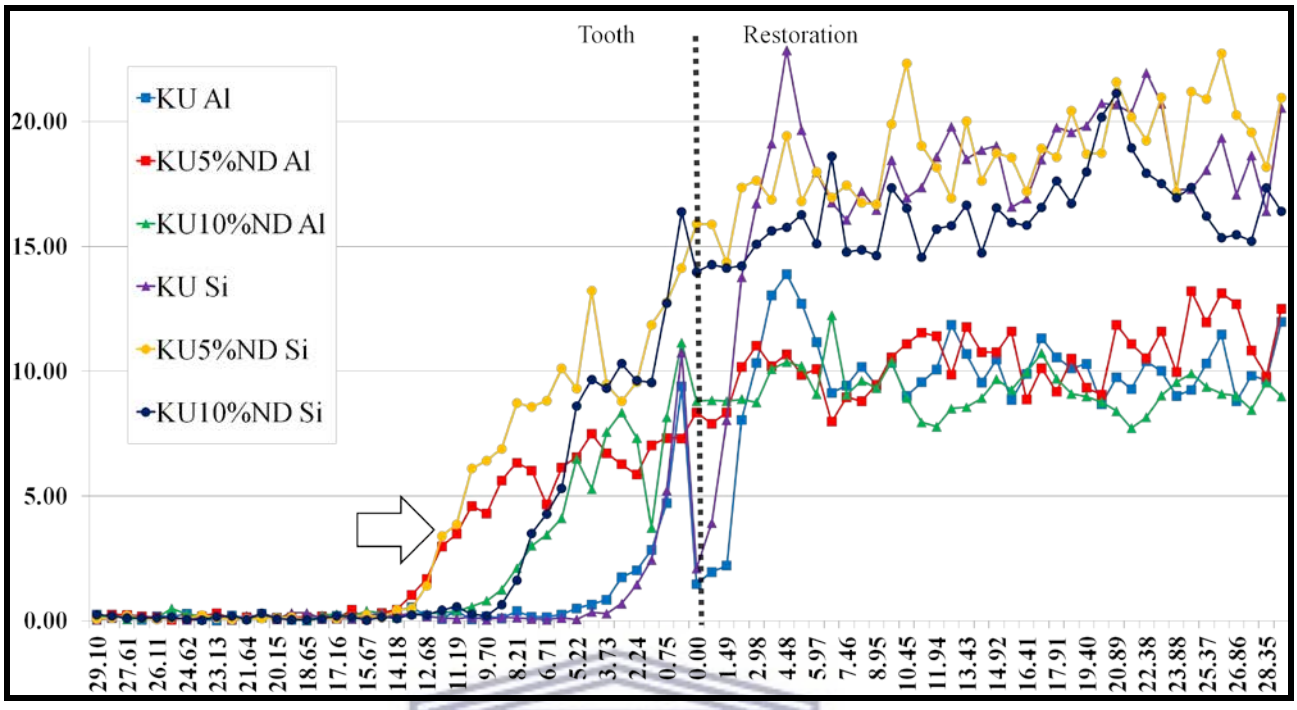

Figure 11.9: Average line scan representing the diffusion of lanthanum and sodium for KU

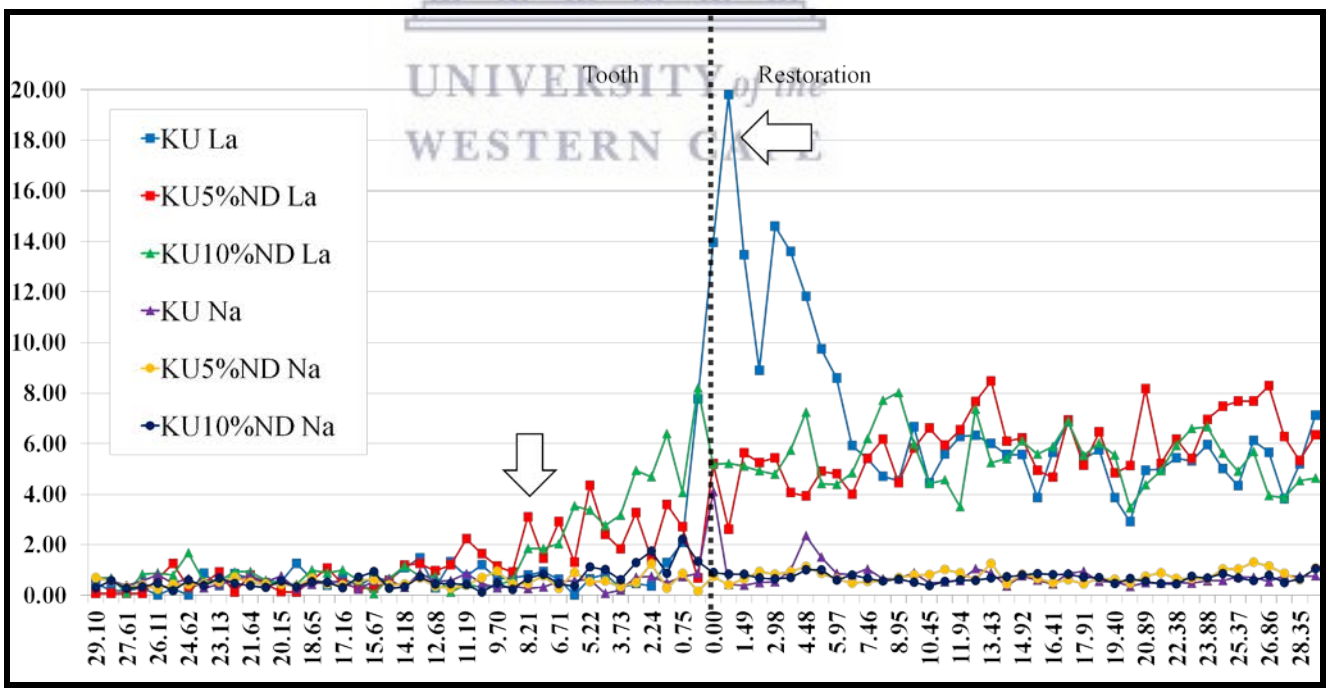

RSC within-group comparison

The calcium, sodium and phosphorus of RSC5%ND had a significantly higher wt% than RSC and RSC10%ND over the 29.1µm in the dentine. The aluminium, fluoride, silicon and strontium of RSC and all the nanodiamond modifications presented with no significant differences in the dentine (Table 11.3, Figures 11.10-11.12).

Figure 11.10: Average line scan representing the diffusion of calcium and phosphorus of RSC

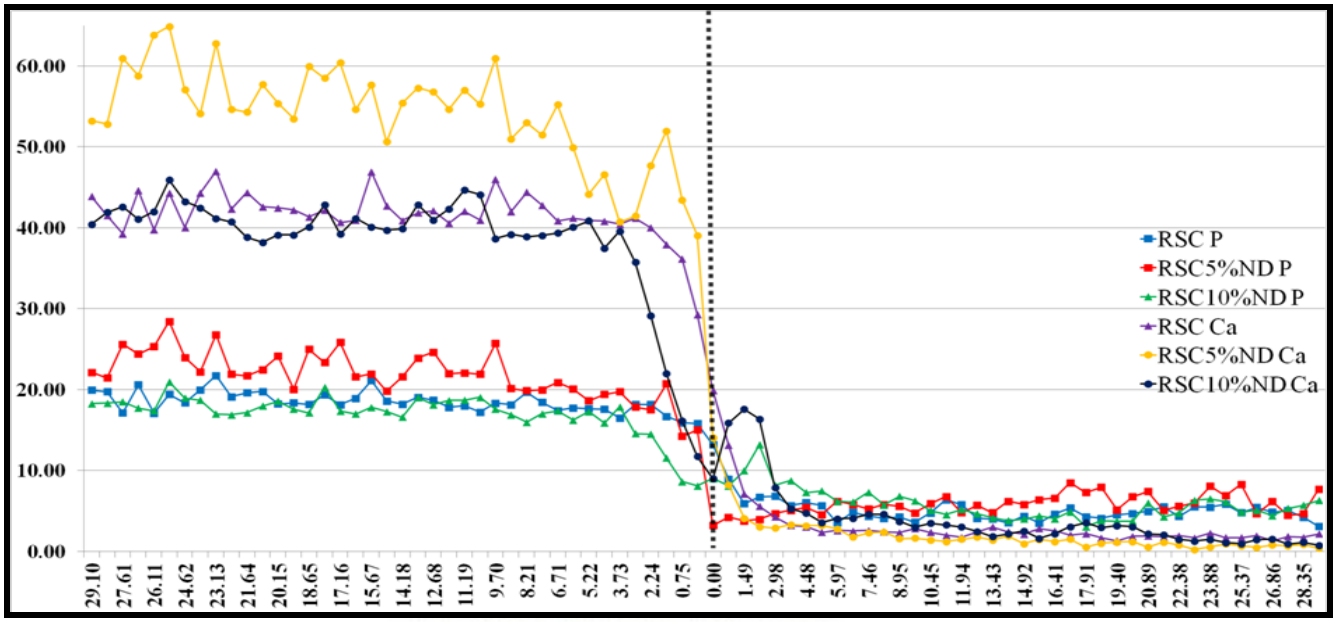

Figure 11.11: Average line scan representing the diffusion of aluminium and silicon of RSC

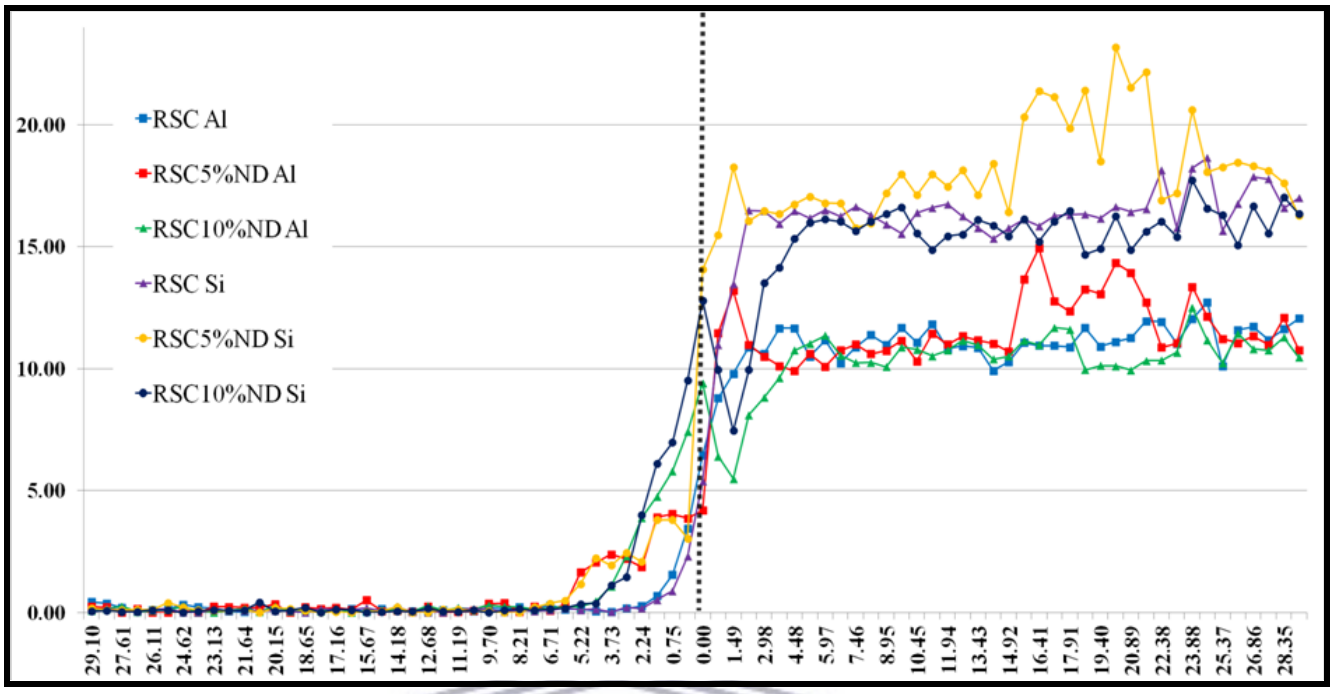

Figure 11.12: Average line scan representing the diffusion of fluoride and strontium of RSC

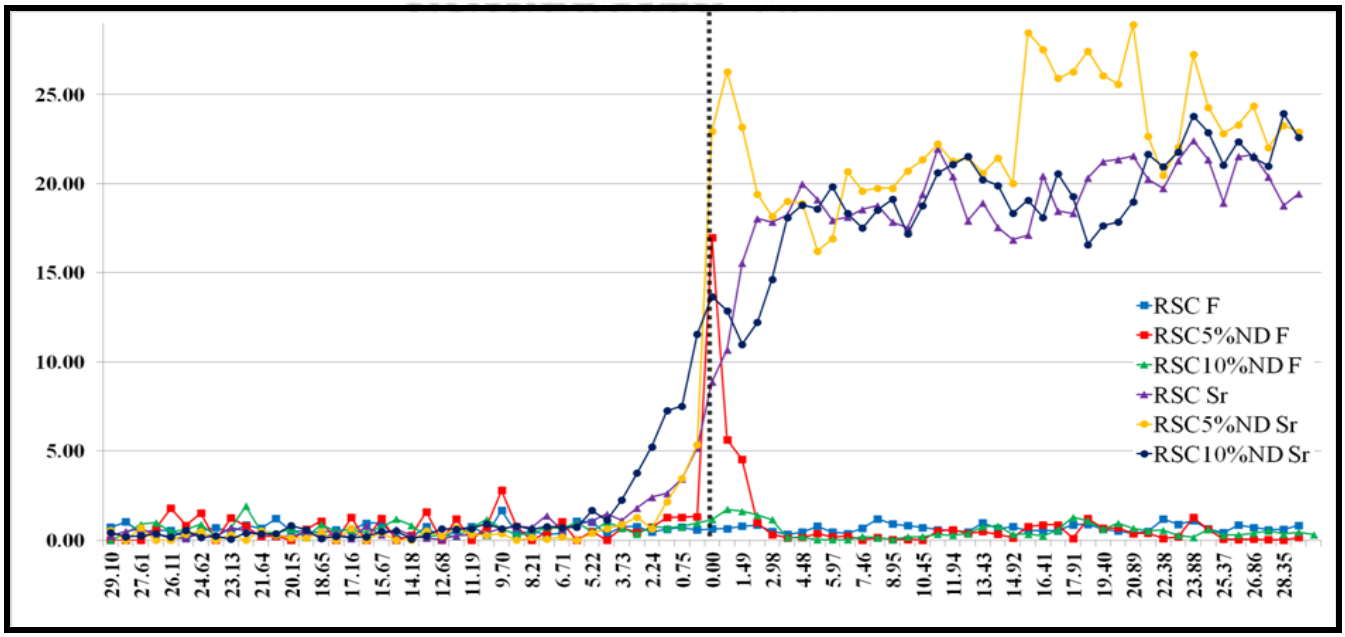

11.7. Discussion

The hypothesis that ions from the nanodiamond-modified GICs would increase the bioactivity of the modified GICs and allow more ion exchange with a wider inter-diffusion zone between the GIC and the tooth was accepted.

The use of conventional GICs in stress-bearing Class II restorations has been limited due to the restricted indications of convention GICs. A newer glass ionomer, namely, Ketac Universal (*3M ESPE*) has expanded indications and the manufacturer imposes no limitations for primary teeth (3M ESPE, Ketac Universal technical profile). As Class II stress-bearing cavities are predominantly restored with RMGI's or compomers, there is scope for the improvement of GICs to be used in these restorations. Ion release from GICs promotes the diffusion of ions into the tooth structure in areas that are in close proximity to the restoration. The use of GICs for restorations where inter-proximal areas are involved can therefore be advantageous at the tooth margin in the proximal box (Ten Cate and van Duinen, 1995). An *in vitro* analysis indicated that FN displayed an antibacterial effect towards *Streptococcus Mutans* (Tiwari, 2016).

The composition of GICs plays a role in the ion wt% potential of the material (Table 11.1). The ion movement and resultant ion exchange between the restoration and the tooth interface is one of the key features of a GIC. The ionic interaction between the carboxylate groups of the GIC liquid and the tooth has already been confirmed in the early years of GIC use (Beech, 1973). Wilson *et al*. (1983) later postulated that a physical bonding of the GIC to the tooth structure took place by way of the aforementioned ionic interaction. X-ray photoelectron spectroscopy (XPS) of the GIC/dentine interface indicated that various ions bound together within the dentine namely calcium and silicon as well as calcium and carbon (Sennou *et al*., 1999). This ion exchange between the tooth and the GIC restoration results in the formation of an ion rich layer known as the inter-diffusion zone. In carious teeth restored with a GIC, the inter-diffusion zone can be 1-2µm wide (Ngo *et al*., 1997). For conditioned healthy dentine an inter-diffusion zone of

6µm wide was noted for FN (Ferrari and Davidson, 1997) and a 2-3µm zone was noted after 48 hours (Yiu *et al*., 2004). It has been found that an acid resistant zone can be 5-7mm wide due to the ion movement into the tooth (Ferrari and Davidson, 1997). In order to obtain a constant wt% of ions for this and future research studies, a precise PLR was used (Mulder, 2018). This standardisation resulted in accurate results of the gradient wt% potential being obtained (11.1) and can serve as a comparable gradient wt% potential between the GIC and tooth to enable more accurate deductions to be made. The wt% of ions present in FN was previously ascertained using the magnetic nuclear-magnetic resonance (MAS-NMR) technique. The values obtained for the various ions differed with this dissertation where the gradient wt% potential was determined with SEM-EDS. The differences between MAS-NMR and SEM-EDS in percentage were: a higher release was found for the MAS-NMR technique for aluminium (+15%), silicon (+ 12%), sodium (+11%, and strontium (+43%). Lower values were obtained for fluoride (-6%) and phosphorus (-54%) using MAS-MNR (Stamboulis *et al*., 2004). The reason for the differences in gradient wt% potential between values recorded in Table 11.1 and those obtained by Stamboulis *et al*. (2004) could be that in this dissertation, the gradient wt% potential was calculated on the set cement 15 days after setting whereas Stamboulis *et al*. (2004) calculated the wt% on the powder alone. Water plays a role in allowing the mobility of ions between the tooth and the restoration and therefore moisture is always essential to form an inter-diffusion zone especially in GICs. The cumulative wt% of the ion movement illustrated in Table 11.2 could be used to determine the mobility of the ions. The mobility of the ions is dependent on the interaction with the tooth structure. The effect of this variable was completely eliminated by producing specimens from the same primary second molar. This single tooth technique provided a true reflection of the interaction of the tooth and the GIC, thereby allowing comparable results.

Nanodiamond modifications of the GICs and their influence on the ion release from the glass particles and the ion movement during the salt-bridge formation resulted in the nanodiamond-modified material setting within 2–3 minutes after mixing. The control materials set within 4-5 minutes. The setting time of the nanodiamond-modified materials was thus shortened. Ionic interactions within the setting GICs are dependent upon one another in order for the GICs to achieve setting, maturation and formation of the inter-diffusion zone with tooth structure. Sodium and strontium are added to the glass filler particle to achieve a more basic character which would make the glass filler particle more susceptible to acid attack. The role of aluminium and silicon are greatly influenced by the nanodiamond modifications. In order to understand the ion movement, the role of aluminium and silicon needs to be explained in detail. If silicon was present in the GIC (and aluminium was absent), it would have to be tetrahedra linked (SiO_4) with oxygen and carry no charge. This formation would have no influence on the maturing GIC. Silicon is dependent upon aluminium and the combination of the two in the GIC allows aluminium to achieve a 4-fold tetrahedral geometry with silicon (Sidhu and Nicholson, 2016). The changes that the aluminium ions undergo during the setting and maturation of the FN GIC were reported on by Munhoz *et al*. (2010). During the first 5 minutes after mixing, the aluminium present in FN is predominantly in a tetrahedral state with four coordination [Al(IV)] and continues to change to an octahedral state with six coordination [Al(VI)] as crosslinking in the polymeric chains occurs to form the final set GIC. This change to Al(VI) has been reported to occur over a period of a year (Munhoz *et al*., 2009). Upon mixing the GIC powder with its liquid, the first step is the reaction with hydrated protons from the polyacid at basic sites on the surface of the glass particles. The dissolution of the glass filler particles by the GIC liquid occurs until the silicon rich layer is formed around the filler particle. This results in the movement of ions such as sodium and calcium (or strontium) from the glass into the polyacid solution, followed quickly by aluminium (Al^{3+}) ions. After about ten minutes and continuing to 24 hours,

interaction with the polyacid chain molecules occur to form ionic cross-linkages and subsequently forms the rigid framework of aluminium, calcium and strontium carboxylate salts for the set cement (Crisp and Wilson, 1974). The nanodiamond particles present in the GIC powder interact with the polyacid faster leaving less space on the polyacid for the ions released from the glass powder. The interaction of the released aluminium, sodium and strontium will therefore have a reduced interaction within the forming salt bridge reaction. The GICs that contain nanodiamond particles presented with an increased setting reaction. When less aluminium is bound to the polyacid and less aluminium was able to form part of the matrix the result is that less Al(IV) can change to Al(VI), due to the polyacid of the matrix being partly occupied by the nanodiamond particles. In the control GICs with no nanodiamond modifications, aluminium is the primary ion to interact with the carboxylate groups of the GIC liquid (Nicholson, 2018) with the changes from Al(IV) to Al(VI) gradually occurring as maturation progresses (Stamboulis *et al*., 2004) and it is exposed to moisture (Tsomaia *et al*., 2003). It has been calculated that more than 10% of the Al(IV) converts to Al(VI) within the first 5 minutes after mixing (Stamboulis *et al*., 2004). Due to the zeta potential of the nanodiamond particles being negative, the aluminium, sodium and strontium interact with the nanodiamond particles and become absorbed into the nanodiamond clusters. Some of the converted Al(VI) will therefore take part in the matrix formation of the nanodiamond function groups in the nanodiamond-modified GICs. If the setting reaction of nanodiamond-modified GICs with the released sodium and strontium occurs faster, their influence on the pH will continue. Sodium and strontium interact with the nanodiamond agglomerates (Figure 11.14), resulting in less Al(VI) polyacrylate forming and insufficient aluminium (Al^{3+}) will be extracted from the condensed aluminium oxide (Al_2O_3) (Wasson and Nicholson, 1991). The hydration of the GIC matrix over the initial 0-24 hours is an essential part of the maturation process. The hydration of the GIC slowly sheaths the unreacted glass as the siloxane groups (-Si-O-Si-) dissociate into silanol

groups (-Si-OH) (Czarnecka *et al*., 2015). This process is known as stoichiometrically. Aluminium interacts with the silicon around the unreacted glass filler particles to form a silica gel around the glass particle. The aluminium, silicon and phosphorus that do not form part of the silica gel (silaceous bonds) around the glass filler particles will be present in the matrix in the form of Si-O-Al and phosphorus. The phosphorus wt% was relatively low in the GICs and the matrix achieved a higher wt% due to phosphorus from the tooth moving into the restoration. The final GIC matrix contains the carboxylate groups (COO^-) of polyacrylic acid, hydrated calcium-, strontium- and aluminium polysalts as well as the glass filler particles covered with the silica gel, all bound together (Skinner and Phillips, 1982). With aluminium and strontium binding to the polyacrylate as well as the tartrate (Potts, 1987; Sidhu and Nicholson, 2016), in this *in vitro* experiment (in this dissertation), this allowed for a greater interaction with the hydroxide groups of the nanodiamond particles as the hydration of the nanodiamond-modified GIC occurred and therefore resulted in a greater ion release. This increased ion release was confirmed in Chapter 7 and 8. The free ions released from the glass filler particle (aluminium, calcium, fluoride, sodium and strontium) that did not bind to the amorphous matrix during the first 10 minutes of the setting process or during the 24-hour maturation, moves towards the tooth structure to form the inter-diffusion zone (Czarnecka *et al*., 2002). The aforementioned process explains why the RSC10%ND showed a drop in the gradient wt% potential in relation to the control as well as the 5% and 10% nanodiamond-modified FN and KU materials with a slight drop in the gradient wt% potential of most ions in relation to the control materials as outlined in Table 11.1. RSC5%ND, however, had an increase in the gradient wt% potential for aluminium, phosphorus, silicon and strontium in relation to the RSC control material. This is because the nanodiamond particles were well dispersed into the powder and liquid upon mixing for the RSC5%ND mixtures. During the mixing of the RSC5%ND a greater dispersion of the agglomerated

nanodiamond particles and spread in the matrix of the GIC was noted. FN and KU nanodiamond modifications had a similar and firmer mixing consistency (Chapter 6, Figure 6.26).

The COOH- group is primarily responsible for the calcium and strontium cross-linking with the tooth (Skinner and Phillips, 1982). The aluminium, fluoride and strontium ions increase the resistance of the tooth structure to the environmental changes impacting on the tooth surface. The aluminium is then leached from the glass filler particle as hydration of the GIC occurs. This leaching and release into de-ionised water was shown to have no significant difference in the release of aluminium and silicon compared to the nanodiamond-modified GICs. Figures 11.6, 11.8 and 11.11 illustrate the gradient wt% potential of aluminium and silicon in the various control materials (presented in Table 11.1). The black arrow indicates the data points on the far right of the graph (Figure 11.13). The data points of all three control materials achieved a much higher wt% in the GIC material closer to the tooth/GIC interface than the gradient wt% of the control material where the gradient weight percentage was determined. This greater gradient weight percentage of the GICs in contact with tooth structure illustrates the leaching of ions from the restoration towards and into the tooth and not just into the moist environment as illustrated in Chapter 7 where the ions was allowed to move into the de-ionised water and Chapter 9/10 where the ions moved into the DMEM medium.

Figure 11.13: Average line scan representing the diffusion of aluminium and silicon for FN, KU and RSC

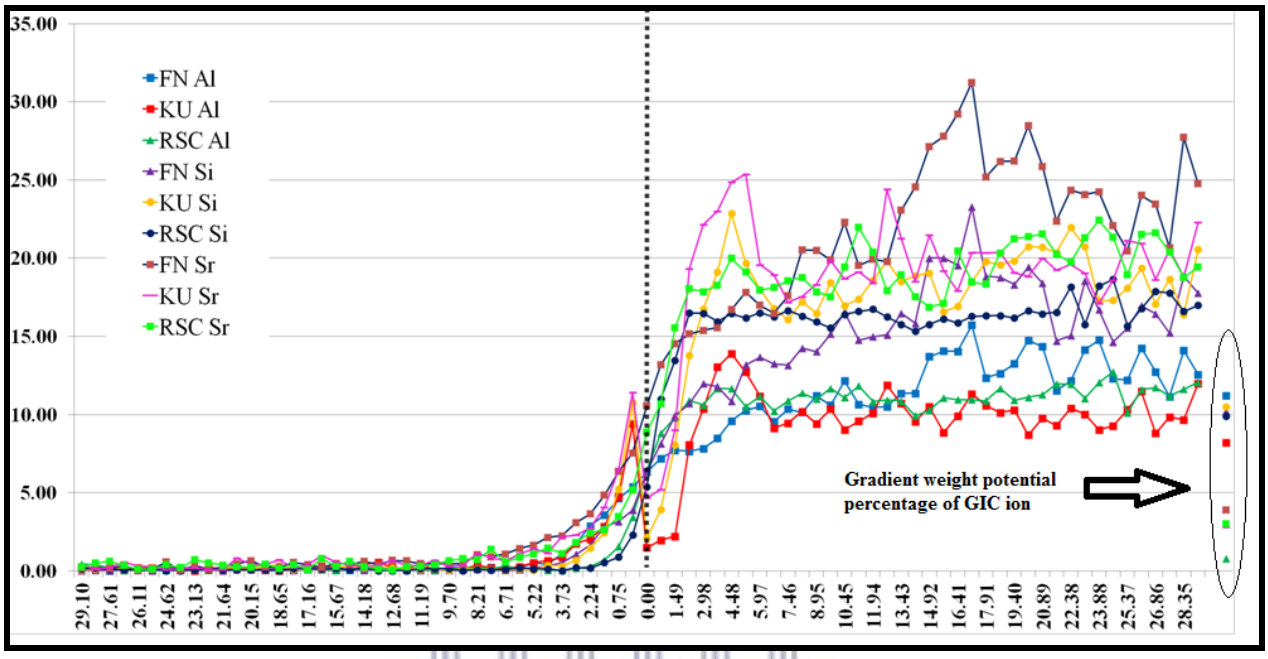

The movement and incorporation of ions from the GICs was suggested to be driven by the gradient wt% potential between the GIC and the tooth structure (Ngo *et al*., 2006). This has been established for the fluoride ions with the amount of fluoride present in the GIC being proportional to the amount of fluoride released (Hill *et al*., 1995; Guida *et al*., 2002) over time. The release of fluoride does not increase when strontium is replaced with calcium in the GICs (Guida *et al*., 2003) but sodium could play a role in increasing the fluoride by serving as a soluble counter-ion (Billington *et al*., 1998).

The GICs in the present study were considered high in aluminium, silicon and strontium based on the ion analysis represented in Table 11.1. The control GIC materials therefore contain strontium-aluminium-fluorosilicate-glasses. These ion release results are in accordance with the *in vitro* analysis results (Chapter 7) of this dissertation where the gradient wt% potential was

also assessed prior to ion release in de-ionised water. It was noted that the ion gradient wt% potential of the nanodiamond-modified GICs were lower in terms of the weight percentage (wt%). This was due to the nanodiamond clusters (Figure 11.14), that interacted with the cations as they were released from the glass filler particles and were retained until the water sorption of the GICs occurred (Figure 6.3). The nanodiamond particles in Figure 11.14 are an example of their agglomeration. This porous agglomeration absorbs the released ions from the early stages of ion release and then becomes shielded from the SEM-EDS analysis. The SEM-EDS assessed the spectrums of the matured GIC in 500nm spot size.

Figure 11.14: Agglomerated nanodiamond particles

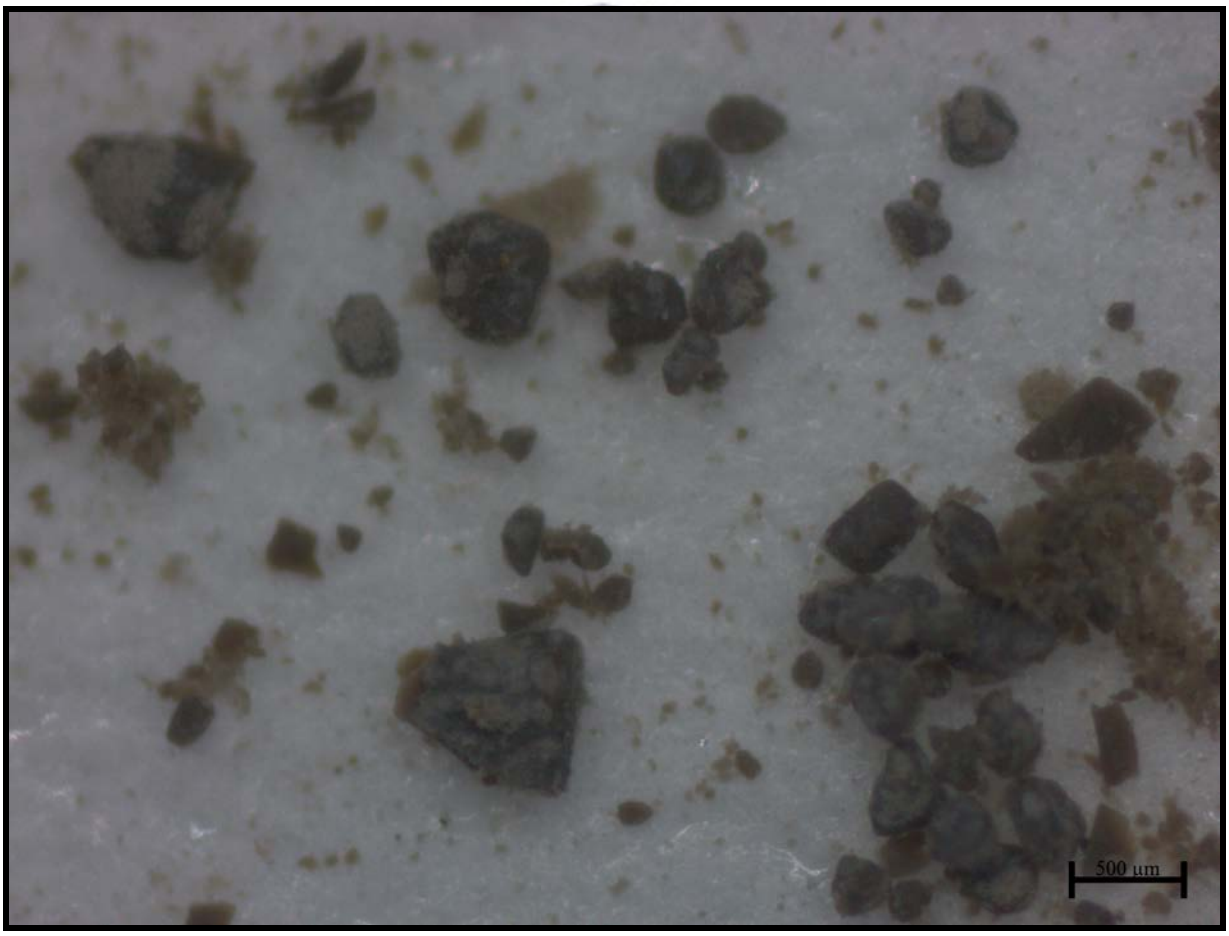

As mentioned earlier, Ngo *et al*. (1997) suggested that the inter-diffusion zone can be 1-2µm wide in carious dentine. Although the inter-diffusion zone is narrow, there is a much deeper penetration of ions into the tooth structure from the restoration. The ion movement from FN and RSC was also assessed by Knight *et al*. (2006). Their investigation illustrated movement of ions into the tooth up to 75µm for FN and RSC, but their graphs illustrated a sharp decline of ion wt% after 20µm (Knight *et al*., 2006).

In the present study, the GIC KU achieved the largest wt% in the tooth as well as in the restoration for fluoride and sodium compared to FN and RSC (11. 2). The largest gradient wt% potential was present for FN (13.3wt%) and RSC (11.7wt%). This illustrated that KU was therefore more active for the aluminium, fluoride, sodium ions than FN. It also illustrated that the highest gradient wt% potential (Table 11.1) of FN for aluminium and fluoride in the GIC does not necessarily mean a higher concentration in the tooth structure (Table 11.2). It is more dependent on whether the ions are able to move from within the GIC towards the tooth. Increasing the gradient wt% potential could very well be driving the ions towards the tooth to form the ion rich inter-diffusion zone. An ideal inter-diffusion zone should extend well into the tooth with a wt% of ions moving into the tooth structure with the highest wt% of ions possible. This is illustrated by comparing Table 11.1 to the average ion wt% in the restoration (Table 11.2). When looking at aluminium, fluoride, lanthanum, silicon and strontium, there is a clear trend towards the ions moving through the restoration towards the tooth. This is evident by the increased wt% of ions in the restoration at the closest contact with tooth the structure, illustrating that within 29.10µm from the inter-diffusion zone, the wt% is much higher than the wt% of ions determined in Table 11.1. These ions are derived from the restoration based on the relative wt% present within the tooth (Table 11.1). This is proof that the ions are moving from within the GIC material towards the inter-diffusion zone and replenishing the gradient wt% potential of ions that

move towards the inter-diffusion zone. In order for the polycarboxcylic acid to react completely, a 1:1 ratio of polycarboxcylic acid to water ratio is required. FN has 1.2g of polycarboxcylic acid to 1g of water (Young *et al*., 2000). This explains the large increase of aluminium and silicon release from FN and RSC, as they contain an insufficient amount of water. This secondary diffusion mechanism occurs upon hydration (Munhoz *et al*., 2010). The dissolution of the ions from the GICs increases in the nanodiamond-modified GICs, as many of the available ions interact with the nanodiamond particles (Chapter 7).

Fluorides have the ability to incorporate into the hydroxyapatite, but the results from Table 11.2 illustrated a very low wt% in the tooth compared to the gradient wt% potential of all the materials (Table 11.1). The wt% of F was much lower than that reported by Knight *et al*. (2006) for FN and RSC. The volume of the material for Knight *et al*. (2006) was much more than what was used in this study. Also, the influence of Whitman filter paper moistened with de-ionised water on the restoration could have made the environment more favourable to the fluoride moving into the filter paper rather than the tooth. This difference in the research methodologies therefore supports and proves that fluoride should rather be considered a mobile ion which does not contribute strongly to the aluminium in the matrix responsible for the formation of the GIC (Chapters 7 and 8). It has been cited that the fluoride replaces hydroxide in mature enamel and strontium replaces calcium (Robinson *et al*., 1995). Fluoride is an ion that is exclusively bound to aluminium (Stamboulis *et al*., 2004) although it is added to the GIC in strontium-fluoride complex (Sr-F_2) (Shahid *et al*., 2014). Fluoride in FN for example, is mainly present in the matrix of the GIC in the form of Sr-F_3. Fluoride is also associated with fluoro-aluminostrontium (Al-F-Sr) in the matrix. Aluminium and silicon are able to form new species during maturation. There are however no new fluoride species that develops between 5 minutes and 24 hours after mixing (Munhoz *et al*., 2010). Fluoride is a smaller particle than calcium (Guida *et al*., 2002;

Gjorgievska *et al*., 2012) and in theory should incorporate easily into the tooth structure. This was clearly not the situation, based on the low wt% of the fluoride that moved into the tooth structure (Table 11.2, Figures 11.7 and 11.12). Fluoride has been detected in relatively large gradient wt% percentages within the restoration in this dissertation for FN (13.3wt%), KU (11.4wt%) and RSC (11.7wt%) (Table 11.1), as well as large parts per million release (ppm) (Chapter 8).This would suggest that F is more readily released to the moist environment rather than diffusing into the tooth surface, since the wt% of F in the tooth was so small for all the GICs assessed (Table 11.2, Figures 11.7 and 11.12). Based on the ^{19}F NMR spectrums analysis, Munhoz *et al*. (2010) suggested that for FN, only 1% of the fluoride could be detected due to the fact that the fluoride is present deep within the glass filler particle spectrums. In a moist environment, the free fluoride ion would be diffused from the restoration to the moist environment. The fluoride and sodium ions are generally released in large mg/L and the moist filter paper could have played a role in this low wt% in the tooth and the restoration (Table 11.2), since the remaining wt% of fluoride in the restoration was as low as the fluoride in the tooth (Chapters 7 and 8).

Nickolson (2016), reiterated that although the GIC sets relatively fast by an acid-base reaction, the immature outer surface is susceptible to water exchange (Nicholson, 2016). Therefore, based on the present research illustrating the low fluoride wt% content of the dentine, GIC restorations would require surface protection in order to prevent the leaching of fluoride ions from the restoration immediately after placement until full maturation of the GIC is reached. Based on the time taken for the inter-diffusion zone to form, the surface protective layer should stay intact for at least 14 days. Surface protective layers limit the ingress of water (Hotta *et al*., 1992). As moisture can ingress into the restoration from the dentine, the prevention of the ingress of water from the outer surface of the restoration does not pose a risk to the maturation of the GICs which

is reliant on the water sorption (Watson *et al*., 1991; Watson *et al*., 1998). The only possible drawback is that if the GIC draws moisture from the tooth structure too fast, possible post-operative sensitivity can occur (Christensen, 1990). This possible increase in sensitivity would need to be investigated with the more modern GICs, as this conclusion was reached in 1990 based on luting GICs with high liquid and low powder contents. Surface protective layers with micro- and nano-filled particles have shown to significantly reduce the fluoride ion release. Additionally, surface protective layers like Single bond universal (*3M ESPE*) and G-Goat (*GC Corp*) allow a slow and steady fluoride release from the GIC compared to the non-filled surface protective layers like Riva coat (*SDI Ltd*). GICs without a filled surface protective layer will release similar fluoride concentrations as a GIC coated with a non-filled surface protective layer (Shatat *et al*., 2018). It has been postulated that fluoride does not function on its own. Fluoride together with other ions like aluminium and strontium, boosts the remineralisation effect of enamel, compared to fluoride alone (Thuy *et al*., 2008). Fluoride is also more bactericidal when strontium is present (Guida *et al*., 2003). Thus, the retention of these ions during maturation to allow further ion movement into the tooth due to the gradient potential, is advantageous to the formation of the inter-diffusion zone. Even without the use of surface protective layers, the other ions achieved comparable movement into the tooth (Knight *et al*., 2006). The higher values of aluminium, fluoride and strontium were found in RSC followed by FN and the lowest value for KU. These higher values of ions in RSC should allow a greater inter-diffusion zone than FN and KU, based on the gradient wt% potential (Table 11.1 and Figure 11.13). When compared to FN and RSC, KU has the most significant movement of fluoride towards the inter-diffusion zone and wt% in the restoration based on the wt% adjacent to it. In terms of strontium there were no significant differences between the three materials, but KU did have the highest wt% in the 0.00 to 0.75µm section of the tooth structure and the lowest (0.00 to 1.49µm) in the restoration, illustrating the ready transfer of strontium from KU. The strontium gradient wt% potential of

KU was the lowest (2.8wt%), yet the highest wt% concentration was present in the restoration from 2.24 to 6.71µm (Figure 11.7). The fluoride movement into the dentine for FN5%ND, KU5%ND and RSC5%ND was associated with higher strontium ion movement and the presence of less calcium and phosphate wt% in the tooth as well in relation to their control materials (Table 11.2). These nanodiamond percentage modifications are therefore the most favourable for FN, KU and RSC.

Koletsi-Kounari *et al*. (2012) showed that an aluminium and strontium solution compared to distilled water, retarded demineralization and accelerated the remineralisation of an artificial enamel lesion. Furthermore, the combination ion solutions with fluoride (AlF_3 and SrF_2) also showed a remineralisation potential of softened enamel and prevention of acid demineralization (Koletsi-Kounari *et al*., 2012). Strontium has an anticariogenic property by way of remineralisation of hydroxyapatite (Brudevold *et al*., 1985). Strontium moves towards the hydroxyapatite by replacement of the calcium in the tooth (Billington *et al*., 2006). The role of calcium and phosphorus from the tooth are inter-connected in order to allow ion exchange with the restoration. The carboxylic group of the GIC interacts and replaces the phosphorus in the tooth. The calcium ion in the hydroxyapatite then follows the phosphorus (Yoshida *et al*., 2000) in order to ensure ionic neutrality. These interactions of the carboxylic group therefore prompt the formation of the ionic bonds between the GIC and the tooth. Higher calcium and phosphorus wt% levels were noted in the dentine of teeth restored with the two control materials FN and KU, compared to the FN5%ND and KU5%ND materials. This discrepancy in calcium and phosphorus wt% is explained by the associated higher concentration of fluoride and strontium for FN5%ND and KU5%ND in the tooth structure (Table 11.2). Based on the trait of strontium to replace calcium, the present *in vitro* investigation can therefore postulate that the remineralisation effect of strontium is directly dependent on the movement of calcium and P

from the tooth as well. This property of strontium has been known for many years, since strontium and fluoride were considered as important trace ions in water and have been identified to be responsible for the lower caries prevalence noted in several populations (Barmes, 1969; Curzon *et al*., 1970; Curzon *et al*., 1978; Vbrič and Štupar, 1980).

Calcium and P are derived from the tooth structure and as a result, move from the tooth towards the restoration. This movement of calcium and phosphorus from the tooth occurs at a much lower wt% than the other ions from the restoration towards the tooth. This is clear for calcium and phosphorus from the gradient wt% potential of the tooth (Table 11.1) to the sum of these ions (Table 11.2) for the restoration as well as the tooth interface. Calcium in the tooth had a gradient wt% potential of 49.24wt% and the sum from Table 11.1 and 11.2 for FN (0.2+39.14+4.83=44.17wt%); KU (50.09wt%) and RSC (44.88wt%). KU, followed by RSC were the most active with regard to the calcium and phosphorus interaction, with more calcium and phosphorus moving into the restoration. More strontium was also present in the tooth for KU and RSC in relation to FN. KU clearly allows more movement of calcium into the restoration with FN and RSC to a lesser extent. The control materials contain very little calcium (Table 11.2) as the gradient wt% illustrates that the calcium movement occurs from the tooth to the restoration. Table 11.2 illustrates that KU had more calcium remaining in the tooth and the restoration followed by FN and then RSC (KU had more than FN and FN had more than RSC). Table 11.2 and Figures 11.5 and 11.10 illustrates that the wt% points of calcium at point “0.00” tooth/restoration was KU (Tooth 29.75wt% / restoration 40.24wt%); RSC (Tooth 29.26wt% / restoration 19.86wt%); FN (Tooth 20.36wt% / restoration 17.32wt%) and for phosphorus at point “0.00” tooth/restoration was RSC (Tooth 15.79wt% / restoration 13.19wt%); FN (Tooth 11.28wt% / restoration 12.50wt%); KU (Tooth 12.19wt% / restoration 2.05wt%). Tables 11.2 and 11.3 illustrate that KU (19.22wt%) and RSC (18.46wt%) had significantly more phosphorus

in the tooth than FN (17.64wt%). Therefore, KU is able to render calcium from deeper in the tooth to move towards the inter-diffusion zone, to such a wt% that the calcium wt% close to the inter-diffusion zone was also high.

All three materials render the movement of phosphorus from the tooth towards the inter-diffusion zone, as the sum of phosphorus was FN (17.64+7.26+3.1=28wt%), KU (26.49wt%) and RSC (25.92wt%) with the tooth having a gradient wt% potential of 20.66wt%. Figure 11.13 illustrates the gradient wt% potential as well as the ion movement into the tooth of the three control materials for the ions aluminium, silicon and strontium. The wt% of the ions were not significantly different (Table 11.3), yet the wt% per spectrum point and the depth of ion penetration into the tooth vary greatly for KU compared to FN and RSC. Although this high wt% between 0.00 to 0.75µm (for ions like aluminium, silicon and strontium from KU) had a large percentage difference compared to the aluminium, silicon and strontium of FN and RSC, the mean value for the ions over the full 29.10µm distance showed no significance with FN and RSC. Point 30 is the gradient wt% potential of the GICs (as per Table 11.1 and Figure 11.13) when compared to the wt% of the ions in the restoration from 29.10µm towards the tooth, was much higher, supporting the movement of ions towards the inter-diffusion zone from within the GIC material. Strontium was present in the GIC materials to a much lower gradient wt% potential than aluminium (Table 11.1). Calcium, fluoride, phosphorus and strontium have been identified as apatite forming ions (Losee and Bibby, 1970). The aforementioned ions and Si incorporate well into the hydroxyapatite (Qiu *et al*., 2013). It has already been noted that strontium is the ideal ion for movement into the tooth, since it has the ability to replace calcium in the tooth with no alteration to the restoration. Initially, strontium was added for radiopacity (Billington *et al*., 2006), but now its addition to GICs has become essential. Silicon can incorporate into tooth structure without any changes to the crystalline structure of the

hydroxyapatite (Qiu *et al*., 2013). Fluoride and the metal ion such as strontium, in the presence of phosphorus, results in the formation of a calcium-strontium complex with the tooth structure (Dedhiya *et al*., 1973). This calcium-strontium complex occurs as a direct result of the ion exchange of four calcium ions being replaced by four strontium ions in the healthy tooth structure ($Ca_{10}(PO_4)_6OH_2$) to form $Ca_6Sr_4(PO_4)_6(OH)_2$) (Newman *et al*., 1963). The present study showed that the calcium ion is not completely lost as it moved into the restoration to the full 29.1µm that was assessed. These replacements of the calcium with strontium ions result in a reduction of the total surface area of the tooth structure, since the strontium is much smaller (Legeros *et al*., 1976). This phenomenon was also cited as the reason why the strontium had such a deep penetration into the demineralised dentine (Knight *et al*., 2006; Ngo *et al*., 1997; Ngo *et al*., 2006). When healthy dentine is considered as in this investigation, fluoride and strontium displayed a large increase in the wt% within the tooth structure for FN and KU modified with 5% ND when compared with their respective control materials. It is important to note that without the ND modifications, the FN and KU materials increased in fluoride and strontium between 0.5-1wt% compared to the fluoride and strontium present in the tooth (Table 11.1 and 11.2). In this *in vitro* study on healthy dentine, strontium penetrated further and at a much higher wt% than aluminium and silicon for all three control materials into the tooth structure (Table 11.2, Figures 11.6, 11.8 and 11.11). This is also echoed with fluoride where KU (11.4wt%) had the lowest gradient wt% potential in relation to FN (13.3wt%) and RSC (11.7wt%), but a significantly higher wt% in the tooth structure at 1.07wt% (Tables 11.1-11.3). The ability of strontium to replace calcium has increased its indications. Strontium has been incorporated into silica-based dentifrices and was shown to be effective in decreasing dentinal hypersensitivity (Addy *et al*., 1987).

Aluminium is another important ion, not only for its cross-linking and incorporation into the polyalkenoate groups to form the matrix of the GIC (Griffin and Hill, 1999; Fennell and Hill,

2001), but it has also been shown to incorporate into and resist demineralization of sound or demineralised tooth structure (Kleber and Putt, 1985; Kleber and Putt, 1994). GIC is also a bioactive glass. Hydroxycarbonate apatite is formed upon exposure to body fluids (Wallace *et al*., 1999). Knight *et al*. (2006) detected strontium percentages between 10-17wt% for FN and RSC. There was a lower aluminium wt% than for strontium in a study by Knight *et al*., (2006). In the present study, the strontium in the dentine at 0.00µm was FN (7.54wt%), KU (11.40wt%) and RSC (5.18wt%). The results mirrored that of Knight *et al*., (2006) in terms of the aluminium at 0.00 µm in the dentine was FN (5.36wt%), KU (9.39wt%) and RSC (3.45wt%) being lower than that of strontium. As the aluminium continues to leach from the GIC towards the tooth structure or into the moist environment (Chapter 7) the internal conversion of Al(IV) to Al(VI) continues to increase (Tsomaia *et al*., 2003). The gradient potential for aluminium and silicon in this study was therefore confirmed by the research completed by Tsomaia *et al*. (2003). The gradient wt% of FN (11.2wt%) and RSC (9.8wt%) was higher than KU (8.2wt%). The aluminium moving towards the area of depletion, i.e. the restoration surface adjacent to the inter-diffusion zone, was FN (11.51wt%) and RSC (10.98wt%) being higher than KU (9.60wt%) (Figure 11.13). The gradient wt% potential determines the movement of the ions, but not necessarily the absorption of the ions into the tooth. This is apparent with the 5% nanodiamond modifications of FN, KU and RSC where the gradient potential in the 29.1µm of the restoration was lower than that of the control materials in the restoration. The ion movement into the tooth was however greater with the 5% nanodiamond modifications (Table 11.2).

The nanodiamond modifications achieved a greater inter-diffusion zone into the tooth than the respective control materials (although the wt% was not necessarily significant for all the ions Table 11.3). The initial intimate contact of the GIC on the tooth structure occurs due to its hydrophilic nature (Nicholson, 2016). The tooth provides the hydrogen bonds from the moisture

on the tooth surface that interact with the carboxylate groups of the GIC (Hinoura *et al*., 1991). The nanodiamond particles also interact with the tooth due to a high amount of hydrogen ions introduced into the GICs from the 5 and 10% wt% nanodiamond particles that interact with the COO- of the GIC. The carboxylate groups in the GIC that bond to the aluminium, fluoride, sodium, strontium and silicon start to interact with the tooth by way of ionic interaction (exchange) with the calcium and phosphorus from the tooth structure (Wilson, 1974; Yoshida *et al*., 2000). In this instance the nanodiamond-modified GICs have an advantage based on the multiple hydrogen bonds available in the GICs that can provide the initial hydrogen bonds, preceding ionic interaction. Figure 11.15 illustrate the GIC (white arrow), GIC/tooth contact point (yellow arrow) and the inter-diffusion zone (orange) of where the ions released from the glass filler particle and the carboxylate component from the GIC (KU5%ND) have modified the tooth structure and changed the dentine surface (orange bracket). A similar change in the inter-diffusion zone and the dentine surface was noted with SEM and Confocal microscopy for FN by other authors (Ngo *et al*.,1997; Atmeh *et al*., 2012).

Figure 11.15: Inter-diffusion zone of KU5%ND

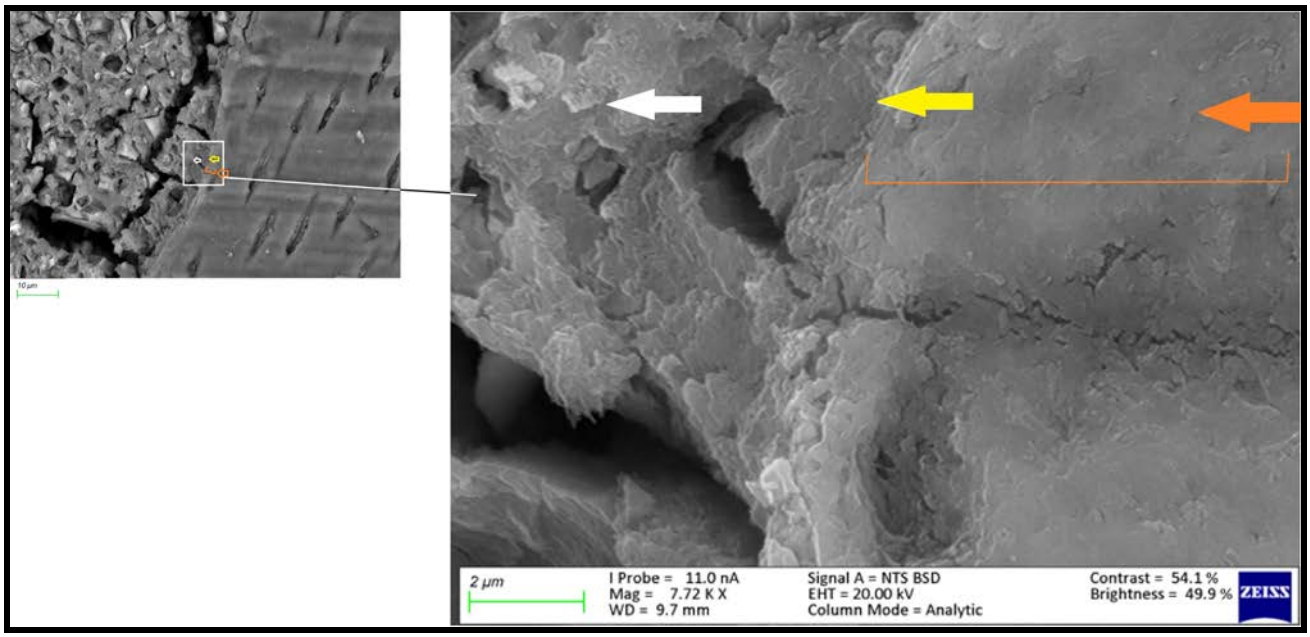

11.8. Conclusion

- For the control materials, FN had the highest gradient wt% potential for aluminium, calcium, fluoride, phosphorus, silicon and strontium.
- KU had the highest wt% for aluminium, calcium, fluoride and silicon from the restoration into the tooth.
- The 5% nanodiamond modifications (except for RSC10%ND) presented with the highest aluminium, fluoride, silicon and strontium ion movement into the dentine compared to their respective controls and other nanodiamond modifications. Therefore, with regard to the GIC material interaction with the tooth structure, the nanodiamond modifications for FN5%ND, KU5%ND and RSC10%ND are preferred over their respective control materials.
- When it comes to the average wt% of the ions present in the restoration, the higher the wt% the better the gradient wt% potential and the more prone the restoration was to move the ions towards the tooth interface in the 29.1µm zone. On the contrary, the other ions namely aluminium, silicon and strontium increased their wt% in the restoration over the depth of 29.1µm from the tooth surface to a much higher wt% than what was initially available in the gradient wt% determination materials. These ion movement phenomena from the restoration towards the tooth interface illustrate the affinity of these ions to move towards the tooth structure. Therefore, the gradient wt% potential must be used together with aluminium, silicon and strontium as they have the ability to move into tooth structure through the restoration.
- The movement of strontium into the tooth is however dependent on the movement of calcium and phosphorus from the tooth to the restoration and not on the gradient wt% potential present in the material.

- The exceptionably low fluoride wt% of both the GIC/tooth 29.1µm analysis indicated that the fluoride ion is in fact a free ion that moves out of the GIC readily upon contact with moisture from the environment if no barrier (like a surface protective layer) is present.
- A surface protective layer would result in moisture being obtained from the tooth and should drive the fluoride movement into the tooth. This movement would coincide with strontium moving towards the tooth. During this Sr-F movement, calcium and phosphorus moves into the restoration. This was evident from the wt% across the measured 29.1µm restoration surface being much higher than the calcium and phosphorus initially present at the gradient wt% determination.

11.8. References

3M ESPE. *3M ESPE, Ketac Universal technical profile*. [online] Available at: http://multimedia.3m.com/mws/media/1090408O/ketac-universal-aplicap-technical-product-profile-pdf.pdf [Accessed 5 Mar. 2019].

Addy, M., Mostafa, P. and Newcombe, R. (1987). Dentine hypersensitivity: a comparison of five toothpastes used during a 6-week treatment period. *British Dental Journal*, 163(2), pp.45-51.

Anusavice, K., Shen, C. and Rawls, H. (2012). *Phillip's Science of Dental Materials*. St. Louis, MO, USA: Elsevier Health Sciences.

Atmeh, A., Chong, E., Richard, G., Festy, F. and Watson, T. (2012). Dentin-cement Interfacial Interaction. *Journal of Dental Research*, 91(5), pp.454-459.

Barmes, D. (1969). Caries Etiology in Sepik Villages – Trace Ion, Micronutrient and Macronutrient Content of Soil and Food. *Caries Research*, 3(1), pp.44-59.

Beech, D. (1973). Improvement in the adhesion of polyacrylate cements to human dentine. *British Dental Journal*, 135(10), pp.442-445.

Berg, J. (2002). Glass ionomer cements. *Pediatric Dentistry*, 24(5), pp.430-438.

Billington, R., Towler, M., Hadley, P. and Pearson, G. (1998). Effects on glass ionomer of NaF addition. *Journal of Dental Res*earch, 77, pp.1226.

Billington, R., Williams, J. and Pearson, G. (2006). Ion processes in glass ionomer cements. *Journal of Dentistry*, 34(8), pp.544-555.

Brudevold, F., Tehrani, A., Attarzadeh, F., Goulet, D. and Van Houte, J. (1985). Effect of Some Salts of Calcium, Sodium, Potassium, and Strontium on Intra-oral Enamel Demineralization. *Journal of Dental Research*, 64(1), pp.24-27.

Christensen, G. (1990). Glass Ionomer as a Luting Material. *The Journal of the American Dental Association*, 120(1), pp.59-62.

Crisp, S. and Wilson, A. (1974). Reactions in Glass Ionomer Cements. *Journal of Dental Research*, 53(6), pp.1408-1413.

Curzon, M., Adkins, B., Bibby, B. and Losee, F. (1970). Combined Effect of Trace Ions and Fluorine on Caries. *Journal of Dental Research*, 49(3), pp.526-528.

Curzon, M., Spector, P. and Iker, H. (1978). An association between strontium in drinking water supplies and low caries prevalence in man. *Archives of Oral Biology*, 23(4), pp.317-321.

Czarnecka, B., Klos, J. and Nicholson, J. (2015). The effect of ionic solutions on the uptake and water-binding behaviour of glass-ionomer dental cements. *Journal Ceramics-Silikaty*, 59, pp.102-108.

Czarnecka, B., Limanowska-Shaw, H. and Nicholson, J. (2002). Buffering and ion-release by a glass-ionomer cement under near-neutral and acidic conditions. *Biomaterials*, 23(13), pp.2783-2788.

Dedhiya, M., Young, F. and Higuchi, W. (1973). Mechanism for the Retardation of the Acid Dissolution Rate of Hydroxyapatite by Strontium. *Journal of Dental Research*, 52(5), pp.1097-1109.

Erickson, R. and Glasspoole, E. (1994). Bonding to Tooth Structure: A Comparison of Glass-Ionomer and Composite-Resin Systems. *Journal of Esthetic and Restorative Dentistry*, 6(5), pp.227-244.

Fennell, B. and Hill, R. (2001). The influence of poly(acrylic acid) molar mass and concentration on the properties of polyalkenoate cements. Part I—compressive strength. *Journal of Materials Science*, 36(21), pp.5193-5202.

Ferrari, M. and Davidson, C. (1997). Interdiffusion of a tradition glass ionomer cement into conditioned dentin. *American Journal of Dentistry*, 10, pp.295-297.

Gjorgievska, E., Nicholson, J. and Grcev, A. (2012). Ion migration from fluoride-releasing dental restorative materials into dental hard tissues. *Journal of Materials Science: Materials in Medicine*, 23(7), pp.1811-1821.

Glasspoole, E., Erickson, R. and Davidson, C. (2002). Effect of surface treatments on the bond strength of glass ionomers to enamel. *Dental Materials*, 18(6), pp.454-462.

Griffin, S. and Hill, R. (1999). Influence of glass composition on the properties of glass polyalkenoate cements. Part I: influence of aluminium to silicon ratio. *Biomaterials*, 20(17), pp.1579-1586.

Guida, A., Hill, R., Towler, M. and Eramo, S. (2002). Fluoride release from model glass ionomer cements. *Journal of Materials Science: Materials in Medicine*, 13(7), pp.645-649.

Guida, A., Towler, M., Wall, J., Hill, R. and Eramo, S. (2003). Preliminary work on the antibacterial effect of strontium in glass ionomer cements. *Journal of Materials Science Letters*, 22(20), pp.1401-1403.

Hatton, P. and Brook, I. (1992). Characterisation of the ultrastructure of glass-ionomer (poly-alkenoate) cement. *British Dental Journal*, 173(8), pp.275-277.

Hickel, R., Manhart, J. and Garcia-Godoy, F. (2000). Clnical results and new developments of direct posterior restorations. *American Journal of Dentistry*, 13, pp.41-54.

Hill, R., De Barra, E., Griffin, S., Henn, G., Devlin, J., Hatton, P., Brook, I., Johal, K. and Craig, G. (1995). Fluoride Release from Glass Polyalkenoate (Ionomer) Cements. *Key Engineering Materials*, 99-100, pp.315-322.

Hinoura, K., Miyazaki, M. and Onose, H. (1991). Dentin Bond Strength of Light-cured Glass-ionomer Cements. *Journal of Dental Research*, 70(12), pp.1542-1544.

Hotta, M., Hirukawa, H. and Yamamoto, K. (1992). Effect of coating materials on restorative glass-ionomer cement surface. *Operative Dentistry*, 17, pp.57-61.

International Organization for Standardization (2007). *ISO 9917-1- Dentistry-Water based cements Part 1: Powder/liquid acid-base cements*, 1st ed.; (pages1–21).

Kerby, R. and Knobloch, L. (1992). Strength characteristics of glass ionomer cements. *Operative Dentistry*, 17, pp.172-174.

Kleber, C. and Putt, M. (1985). Uptake and Retention of Aluminum by Dental Enamel. *Journal of Dental Research*, 64(12), pp.1374-1376.

Kleber, C. and Putt, M. (1994). Aluminum Uptake and Inhibition of Enamel Dissolution by Sequential Treatments with Aluminum Solutions. *Caries Research*, 28(6), pp.401-405.

Knight, G., Mclntyre, J., Craig, G. and Mulyani (2006). Ion uptake into demineralized dentine from glass ionomer cement following pretreatment with silver fluoride and potassium iodide. *Australian Dental Journal*, 51(3), pp.237-241.

Koletsi-Kounari, H., Mamai-Homata, E. and Diamanti, I. (2012). An *In Vitro* Study of the Effect of Aluminum and the Combined Effect of Strontium, Aluminum, and Fluoride Ions on Early Enamel Carious Lesions. *Biological Trace Ion Research*, 147(1-3), pp.418-427.

Legeros, R., Miravite, M., Quirolgico, G. and Curzon, M. (1976). The effect of some trace ions on the lattice parameters of human and synthetic apatites. *Calcified Tissue Research*, 22(S1), pp.362-367.

Mount, C. (2002). *Color atlas of Glass Ionomer Cement*. 2nd ed. London, UK: Martin Dunitz.

Mulder, R. (2018). Variation in the Dispersions of Powder Liquid Ratios in Hand-Mix Glass Ionomers. *The Open Dentistry Journal*, 12(1), pp.647-654.

Munhoz, T., Karpukhina, N., Hill, R., Law, R. and De Almeida, L. (2010). Setting of commercial glass ionomer cement Fuji IX by 27Al and 19F MAS-NMR. *Journal of Dentistry*, 38(4), pp.325-330.

Neuman, W., Bjornerstedt, R. and Mulryan, B. (1963). Synthetic hydroxy apatite crystals. II. Aging and strontium incorporation. *Archives of Biochemistry and Biophysics*, 101(2), pp.215-224.

Ngo, H., Mount, G. and Peters, M. (1997). A study of glass ionomers cement and its interface with enamel and dentine using a low temperature, high resolution scanning electron microscopic technique. *Quintessence International*, 28, pp.63-69.

Ngo, H., Mount, G., Mc Intyre, J., Tuisuva, J. and Von Doussa, R. (2006). Chemical exchange between glass-ionomer restorations and residual carious dentine in permanent molars: An in vivo study. *Journal of Dentistry*, 34(8), pp.608-613.

Nicholson, J. (1998). Chemistry of glass-ionomer cements: a review. *Biomaterials*, 19(6), pp.485-494.

Nicholson, J. (2016). Adhesion of glass-ionomer cements to teeth: A review. *International Journal of Adhesion and Adhesives*, 69, pp.33-38.

Nicholson, J. (2018). Maturation processes in glass-ionomer dental cements. *Acta Biomaterialia Odontologica Scandinavica*, 4(1), pp.63-71.

Potts, P. (1987). *Handbook of Silicate Rock Analysis*. Glasgow, London, UK: Blackie and Son.

Powis, D., Follerås, T., Merson, S. and Wilson, A. (1982). Materials Science - Improved adhesion of a glass ionomer cement to dentine and enamel. *Journal of Dental Research*, 61(12), pp.1416-1422.

Qiu, Z., Noh, I. and Zhang, S. (2013). Silicate-doped hydroxyapatite and its promotive effect on bone mineralization. *Frontiers of Materials Science*, 7(1), pp.40-50.

Robinson, C., Kirkham, J., Brookes, S. and Shore, R. (1995). *Chemistry of mature enamel. Dental enamel: formation to destruction*. Boca Raton: CRC, pp.170-175.

Sennou, H., Lebugle, A. and Grégoire, G. (1999). X-ray photoelectron spectroscopy study of the dentin–glass ionomer cement interface. *Dental Materials*, 15(4), pp.229-237.

Shahid, S., Hassan, U., Billington, R., Hill, R. and Anderson, P. (2014). Glass ionomer cements: Effect of strontium substitution on esthetics, radiopacity and fluoride release. *Dental Materials*, 30(3), pp.308-313.

Shatat, F., Peerbhay, F. and Adam, R. (2018). *The effect of resin based coatings on fluoride release of glass ionomer cement, an in vitro study*. Masters Degree In Pediatric Dentistry. Univeristy of the Western Cape (UWC) South Africa.

Sidhu, S. and Nicholson, J. (2016). A Review of Glass-Ionomer Cements for Clinical Dentistry. *Journal of Function Biomaterials*, 7(3), p.16.

Skinner, E. and Phillips, R. (1982). *Skinner's Science of dental materials*. 8th ed. Philadelphia: Saunders.

Souto, M. and Donly, K. (1994). Caries inhibition of glass ionomers. *American Journal of Dentistry*, 7, pp.122-4.

Stamboulis, A., Law, R. and Hill, R. (2004). Characterisation of commercial ionomer glasses using magic angle nuclear magnetic resonance (MAS-NMR). *Biomaterials*, 25(17), pp.3907-3913.

Ten Cate, J. and van Duinen, R. (1995). Hypermineralization of Dentinal Lesions Adjacent to Glass-ionomer Cement Restorations. *Journal of Dental Research*, 74(6), pp.1266-1271.

Thuy, T., Nakagaki, H., Kato, K., Hung, P., Inukai, J., Tsuboi, S., Nakagaki, H., Hirose, M., Igarashi, S. and Robinson, C. (2008). Effect of strontium in combination with fluoride on enamel remineralisation *in vitro*. *Archives of Oral Biology*, 53(11), pp.1017-1022.

Tiwari, S. (2016). Antibacterial Activity and Fluoride Release of Glass-Ionomer Cement, Compomer and Zirconia Reinforced Glass-Ionomer Cement. *Journal of clinical and diagnostic research*, 10(4), pp.ZC90-3.

Tsomaia, N., Brantley, S., Hamilton, J., Pantano, C. and Mueller, K. (2003). NMR evidence for formation of octahedral and tetrahedral Al and repolymerization of the Si network during dissolution of aluminosilicate glass and crystal. *American Mineralogist*, 88(1), pp.54-67.

Van Meerbeek, B., De Munck, J., Yoshida, Y., Inoue, S., Vargas, M., Vijay, P., Van Landuyt, K., Lambrechts, P. and Van Herle, G. (2003). Buonocore Memorial lecture - Adhesions to Enamel and Dentin: Current status and Future challenges. *Operative Dentistry*, 28(3), pp215-235.

Volkov, D., Proskurnin, M. and Korobov, M. (2014). Ion analysis of nanodiamonds by inductively-coupled plasma atomic emission spectroscopy. *Carbon*, 74, pp.1-13.

Vrbič, V. and Štupar, J. (1980). Dental Caries and the Concentration of Aluminium and Strontium in Enamel. *Caries Research*, 14(3), pp.141-147.

Wallace, K., Hill, R., Pembroke, J., Brown, C. and Hatton, P. (1999). Influence of sodium oxide content on bioactive glass properties. *Journal of Materials Science: Materials in Medicine*, 10(12), pp.697-701.

Wasson, E. and Nicholson, J. (1991). Studies on the setting chemistry of glass-ionomer cements. *Clinical Materials*, 7(4), pp.289-293.

Watson TF. (1992). Bonding glass-ionomer cements to tooth structure. In: Davidson CL, Mjor IA, eds. Advances in glass-ionomer cements. Chicago: Quintessence, pp.121-135.

Watson, T., Billington, R. and Williams, J. (1991). The interfacial region of the tooth/glass-ionomer restoration: a confocal optical microscope study. *American Journal of Dentistry*, 4, pp.303-310.

Watson, T., Pagliari, D., Sidhu, S. and Naasan, M. (1998). Confocal microscopic observation of structural changes in glass-ionomer cements and tooth interfaces. *Biomaterials*, 19(6), pp.581-588.

Wilson, A. (1974). Alumino-silicate polyacrylic acid and related cements. *British Polymer Journal*, 6(3), pp.165-179.

Wilson, A. and McLean, J. (1988). *Glass-ionomer cement*. Berlin, Germany: Quintessence Publishing Co.

Wilson, A., Prosser, H. and Powis, D. (1983). Mechanism of Adhesion of Polyelectrolyte Cements to Hydroxyapatite. *Journal of Dental Research*, 62(5), pp.590-592.

Xie, D., Brantley, W., Culbertson, B. and Wang, G. (2000). Mechanical properties and microstructures of glass-ionomer cements. *Dental Materials*, 16(2), pp.129-138.

Yiu, C., Tay, F., King, N., Pashley, D., Sidhu, S., Neo, J., Toledano, M. and Wong, S. (2004). Interaction of Glass-ionomer Cements with Moist Dentin. *Journal of Dental Research*, 83(4), pp.283-289.

Yoshida, Y., Van Meerbeek, B., Nakayama, Y., Snauwaert, J., Hellemans, L., Lambrechts, P., Vanherle, G. and Wakasa, K. (2000). Evidence of Chemical Bonding at Biomaterial-Hard Tissue Interfaces. *Journal of Dental Research*, 79(2), pp.709-714.

Young, A., Sherpa, A., Pearson, G., Schottlander, B. and Waters, D. (2000). Use of Raman spectroscopy in the characterisation of the acid–base reaction in glass-ionomer cements. *Biomaterials*, 21(19), pp.1971-1979.

CHAPTER 12

NEUTRAL SODIUM FLUORIDE GEL UPTAKE OF NEWLY PLACED NANODIAMOND-MODIFIED GLASS IONOMER RESTORATIVE CEMENTS

12.1. Abstract

Purpose: Three commercial restorative glass-ionomer restorative cements (GICs) were modified by the incorporation of 5% and 10% nanodiamond particles (ND) with a weight by weight percentage (w/w%) into the powder of the GICs. The aim of the study was to assess the percentage of surface fluoride percentage increase on the surface of the materials, following neutral sodium fluoride gel application.

Materials and Methods: The commercial GICs were FN: Fuji IX GP (*GC Corp*); KU: Ketac Universal (*3M ESPE*) and RSC: Riva Self Cure (*SDI Ltd*). Nanodiamond particles (ND) (*PlasmaChem*) were used. Six specimens of each material were prepared using precise powder/liquid ratios. After a 10-minute set time, the GICs were polished. The specimens were randomly divided into two groups i.e. control (Group A) and test groups (Group B). The samples were blot dried and Group B received the neutral sodium fluoride gel for 2 minutes. The excess was wiped off with gauze and both groups analysed with SEM-EDS.

Results: Data analysis revealed that all the GICs and their respective nanodiamond modifications had a significant increase ($p < 0.0001$) in the surface fluoride percentage compared to the GICs in Group B. The addition of ND10% w/w to FN ($p < 0.001$) and RSC ($p = 0.029$) resulted in significant increases in the surface fluoride percentage. There were no significant difference between the increase of the surface fluoride between KU and the nanodiamond-modified KU materials.

Conclusion: The ability of GICs to absorb the neutral sodium fluoride gel immediately after finishing of the restoration significantly increases the fluoride percentage of the surface layer.

Keywords: Glass ionomer cement; Neutral sodium fluoride; Nanodiamonds; Elemental analysis; SEM-EDS.

Abbreviations and acronyms:

FN: Fuji IX GP

GICs: Glass-ionomer cements

KU: Ketac Universal

ND: Nanodiamond particles

NSF: Neutral sodium fluoride

RSC: Riva Self Cure

SEM-EDS: Scanning Electron Microscopy and Energy Dispersive X-Ray Spectrometry Microanalysis

w/w%: weight/weight%

12.2. Introduction

Glass ionomer restorative cements (GICs) have anicariogenic properties due to the release of fluoride which have also been suspected of influencing the biofilm metabolism (Xie *et al*., 2000; Chau *et al*., 2015). Fluorides play a role in reducing the demineralisation of tooth structure (Watson *et al*., 2014). The effectiveness of GICs is therefore partly related to the fluoride release (Wiegand *et al*., 2007; Nakajo *et al*., 2009; Trairatvorakul *et al*., 2010). Initially, after the placement of the GICs, there is an increase in fluoride release over the initial 24 hours (El Mallakh and Sarkar, 1990). Although the GICs serve as fluoride reservoirs (Walls, 1986) they have the ability to replenish the fluoride potential from various fluoride sources. The replenishment of fluoride is essential in order to maintain a fluoride potential that can sustain a continuous release for the aforementioned biofilm modification and tooth structure mineralization (Walls, 1986). GICs previously exposed to high fluoride concentrations have shown an enhanced fluoride release in deionised water (Forsten, 1990; De Witte *et al*., 2003).

Nanodiamond particles (ND) have been identified for this dissertation as a potential material that could be explored for the modification of GICs due to the presence of various functional groups located on the surface of the nanodiamond particles. Nanodiamond are made by the detonation of an explosive mixture of carbon-containing compounds such as trinitrotoluene (1,3,5-trinitro-1,3,5-triazinane) and hexogen in a gaseous environment (Dolmatov, 2001; Danilenko, 2004). The resultant nanodiamonds have a sp^3-carbon diamond core and a graphite outer layer presenting with a sp^2-hybridized carbon (Roy *et al*., 2013). The grade 1 nanodiamond particles used in this study have oxygen-containing functional groups such as hydroxyl groups, alkyls derived from sp^3-carbon, carboxylic groups (C=O) and Aromatic groups (C=C) (Mochalin *et al*., 2011; Wehling *et al*., 2014). Due to these surface functional groups nanodiamonds have been explored in various biomedical applications for many years (Mochalin *et al*., 2011) and have been successfully researched for their application in medicine for biosensing electrodes (Zhang *et al*., 2014) and nanodiamond films (Kealey et al, 2001).

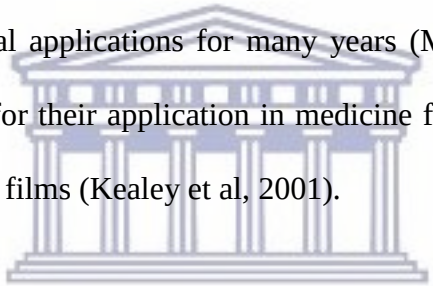

The aim of this study was to determine the percentage of change in the surface fluoride in the nanodiamonds modified GICs after a neutral sodium fluoride application. The hypothesis was that the newly placed nanodiamond-modified GICs would have an increased surface fluoride percentage compared with their respective GICs used as the control.

12.3. Materials and Methods

Aim: To determine the change in the surface fluoride percentage of nanodiamonds modified GICs after a neutral sodium fluoride application.

Objectives:

- To compare the percentage of change of fluoride between three commercial GICs from Groups A and B i.e. Fuji IX (FN), Ketac Universal (KU) and Riva Self Cure (RSC).
- To compare the percentage of change of fluoride between 5% or 10% nanodiamonds modified GICs from Group A and B.

Six disc shaped specimens (3 mm in diameter and 1 mm thick) were constructed for each material. Three commercially available hand-mix GICs namely FN: Fuji IX GP (*GC Corp, Tokyo, Japan; Batch: 1503231*); KU: Ketac Universal; (*3M ESPE, Seefeld, Germany; Batch: 583514*) and RSC: Riva Self Cure (*SDI Limited, Australia; Batch: 62657V*) were used in this study. The three GICs were additionally modified with 5% and 10% weight by weight percentage (w/w%) nanodiamond particles *(PlasmaChem*) incorporated into the powder phase of the GICs. The GIC powder and nanodiamond particles were placed in an air tight HDPE container and clamped in a beaker shaker for two hours to ensure complete mixing prior to dispensing with the manufacturer's powder spoon. The GICs were mixed in accordance with the powder and liquid ratios as provided by the manufacturer (Mulder; 2018). The precise weights were confirmed on a desktop analytical balance (*Metler AE240 analytical balance, Columbus, Ohio, USA*) by first dispensing the powder, followed by the liquid. The mixed GICs were applied into Teflon moulds. Cellulose acetate sheets were placed on either surface of the mould with a glass slide over the top cellulose acetate sheet. The GICs were allowed to bench-set at 37ºC for 10-minutes in a temperature controlled incubator (Pawluk *et al*., 2008) at 80% humidity. The surface of all the specimens were smoothened with 2500 grit wet silicon carbide

paper, followed with 4000 grit (*3M, Massachusetts, USA*) under de-ionised water. The polishing ensured an adjustment to the surface of ±100µm (as measured within a micrometer). The application of the silicon carbide paper simulated the restoration polishing that would be performed by the clinician in the clinical setting (Menne-Hap and Ilie, 2013). Lastly, the specimens were polished with diamond polishing paste (*Eve Ernest Vetter GmbH; Keltern, Germany*) and the polished samples were subsequently rinsed with de-ionised water for 30 seconds and blot dried with filter paper (*Whitman no.1, Cat No 1001125; GE Healthcare UK Limited, Buckinghamshire, UK*). The neutral sodium fluoride (*Topex Neutral pH Sodium fluoride gel; Sultan Healthcare Inc, New Jearsey, USA*) was applied to the Group B samples for two minutes and then wiped off with dry gauze.

12.3.1. SEM-EDS micro-analysis

Scanning Electron Microscopy (SEM) and Energy Dispersive X-Ray Spectrometry (EDS) Microanalysis (SEM-EDS) analysis was completed on control Group A, to establish the baseline percentage of fluoride and other elements. The process was repeated for Group B. In order to increase the electrical conductivity of the GIC specimens for SEM analysis, the specimens were first gold sputter-coated (*Edwards S150A Sputter Coater*) at 40 mA. SEM-EDS of the outer surfaces to enhance the electrical conductivity of the samples from Groups A and B (*Zeiss MERLIN Field Emission SEM; Carl Zeiss Microscopy, Jena, Germany*) at 200x magnification. Five points were chosen in the central field of view on the filler particles and five points in the matrix of the GIC for EDS analyses (providing ten spectrums per specimen). This was essential since it has been shown that there are varying ions in the GICs. The results from the SEM-EDS had to be representative of the GICs since the “glass particle” has more ions compared to the ”matrix” (Wasson and Nicholson, 1993). The EDS spectrums were collected from the central field of view from each specimen under the following conditions: The accelerating voltage of 20kV and a working distance of 9.5mm were used for this application, an 11nA beam current at

10^6 Torr pressure (high-vacuum), with a 10s acquisition time and 30-45% detector dead time. The elemental analyses (in weight percentage) of the specimens were performed in non-standard analysis mode, applying the PROZA (*Phi-Rho-Z*) correction method. A Zeiss 5-diode Back Scattered Electron (*BSE*) Detector (*Zeiss NTS BSD*) and Zeiss Smart SEM software generated the BSE images. The Semi-quantitative Energy Dispersive X-Ray Spectrometry (EDS) using an Oxford Instruments® (*Abingdon, UK*) X-Max 20mm^2 detector and Oxford Aztec software were used to chemically quantify the specimens. Images were obtained at 200 and 500nm.

12.4. Statistical analysis

The SEM-EDS spectrums from each material specimen were used to determine the average fluoride percentage for that specimen. No statistically significant outliers were present in the data as assessed by box plots and the studentized residuals were less than 3.0. The assessment of homogeneity of variances and covariances were not required, since the group sizes were equal. The data was assessed for normality by Shapiro-Wilk test ($p > 0.05$) and homogeneity of variances by Levene's test ($p > 0.05$). A one-way analysis of variance and the Tukey post hoc analysis or the one-way Welch's ANOVA with a Games-Howell post hoc analysis was used for the analysis of the data, based on the Shapiro-Wilk and Levene's tests.

12.5. Results

Surface fluoride percentage of three commercial materials before NaF application (Group A)

The data from FN, KU and RSC had no statistically significant outliers, the data was normally distributed (Shapiro-Wilk test; $p > 0.05$) and homogeneity of variances (Levene's test; $p > 0.05$) was present.

The one-way analysis of variance and the Tukey post hoc analysis revealed that the surface fluoride percentage of FN in Group A had the highest fluoride percentage of 13.29 (±0.42)%,

followed by RSC 11.71 (±0.16)% and finally KU 11.35 (±0.35)%. The differences in the surface fluoride percentages of the commercial materials in Group A were statistically different ($p < 0.0001$). The Tukey post hoc analysis revealed that the largest difference of the surface fluoride percentage was between FN that had a significantly larger percentage of surface fluoride compared to KU ($p < 0.001$) and RSC ($p < 0.0001$) (Table 12.1).

Table 12.1: Multiple comparison of the fluoride percentage difference between materials

Comparison	Significance before NaF (Group A)	Significance after NaF (Group B)
FN vs KU	p < 0.001*	p < 0.001* (KU vs FN)
FN vs RSC	p < 0.0001*	p = 0.856
FN vs FN5%ND	p < 0.001*	p = 0.087
FN vs FN10%ND	p = 0.002*	p < 0.001* (FN 10%ND vs FN)
FN 10%ND vs FN 5%ND	p = 0.228	p < 0.001*
KU vs RSC	P = 0.03* (RSC vs KU)	p < 0.001*
KU vs KU5%ND	p < 0.001*	p < 0.0001*
KU vs KU10%ND	p = 0.001*	p = 0.035*
KU5%ND vs KU10%ND	p = 0.214	p > 0.066 (KU10%ND vs KU5%ND)
RSC vs RSC5%ND	p < 0.001*	p < 0.001*
RSC10%ND vs RSC	p < 0.016*	p = 0.029*
RSC10%ND vs RSC5%ND	P = 0.337	p < 0.001*
(*) indicates a significant difference in the fluoride percentage between the materials per group.		

Surface fluoride percentage of three commercial materials after NaF application (Group B)

The one-way Welch's ANOVA was used for the analysis of Group B for the three commercial products since there was no homogeneity of the variances as assessed by Levene's test ($p < 0.05$). The data for the three commercial materials in Group B was normally distributed, as assessed by Shapiro-Wilk test ($p > 0.05$). The differences between KU and FN as well as KU and RSC were statistically different, Welch's F ($p < 0.0001$). For the materials from Group B; KU had the highest surface fluoride percentage after the NaF treatment at 20.32 (±0.88)%; followed by FN 16.91 (±1.07)% and RSC 16.32 (±0.69)% (Table 12.2). Games-Howell post hoc analysis revealed that the difference between KU and RSC as well as KU and FN were statistically significant ($p < 0.001$). No significant difference ($p = 0.856$) was noted between FN and RSC.

Table 12.2: Significance of the change in the fluoride percentage from Groups A to B

Material	[F%] before NaF (Group A)	[F%] after NaF (Group B)	Difference in [F%] (Group B-Group A)
FN	13.29 (0.42)	16.91 (1.07)	3.61 (0.67) ^
KU	11.35 (0.35)	20.32 (0.88)	8.96 (0.79) ^
RSC	11.71 (0.16)	16.32 (0.69)	4.6 (0.53) ^
FN5%ND	11.94 (0.14)	16.39 (0.53)	4.44 (0.40) ^
FN10%ND	12.31 (0.69)	19.75 (0.07)	7.44 (0.74) ^
KU5%ND	9.77 (0.62)	19.01 (0.37)	9.24 (0.53) ^
KU10%ND	10.18 (0.76)	19.62 (0.87)	9.44 (0.32) ^
RSC5%ND	10.85 (0.45)	14.85 (0.85)	4 (1.25) ^
RSC10%ND	11.09 (0.45)	16.88 (0.72)	5.79 (1.13) ^
(^) indicates a significant difference in the change of the fluoride percentage between Group A and Group B with a $p < 0.0001$.			

Surface fluoride percentage of the ND modified GICs

Data analysis revealed that the surface fluoride percentage difference for the three commercial GICs as well as the 5%ND and 10%ND modifications from Group A to B had a significant ($p < 0.0001$) surface fluoride increase on the surface of the GICs (Table 12.2).

In Group B, after the application of the neutral sodium fluoride, the addition of 10% w/w ND to FN resulted in FN10%ND having a significant ($p < 0.001$) increase in the surface fluoride percentage for FN. Additionally RSC10%ND had a significantly greater surface fluoride percentage than RSC ($p = 0.029$). The modification of KU with both 5% and 10%ND showed no significant increase in the surface fluoride of the ND modified KU materials when compared with the commercial KU material in Groups A or B (Table 12.1).

Table 12.2 represents the increase in the surface fluoride percentage between Group A and B with 3.61(0.67)% in FN, 4.44(0.40)% in FN5%ND and 7.44(0.74)% in FN10%ND. The surface fluoride percentage in Group B was significantly different between FN and FN10%ND ($p < 0.001$), as well as a significant difference between FN10%ND and FN5%ND ($p < 0.001$). However, the difference between FN and FN5%ND ($p = 0.12$), was not statistically significant.

The surface fluoride percentage increase between Group A and B for KU by 8.96 (±0.79)%, KU5%ND by 9.24(±0.53)% and KU by 10%ND 9.44(±0.32)%. The KU surface fluoride percentage increase was statistically larger than KU10%ND ($p = 0.035$) followed with KU5%ND ($p < 0.0001$).

For RSC, the surface fluoride percentage increased by 4.00(±1.25)% for RSC5%ND; RSC by 4.6(±0.53)% and RSC10%ND by 5.79 (±1.13)% ($p < 0.001$). RSC10%ND resulted in a significant increase between Groups A and B that was also larger than the fluoride increase of RSC ($p = 0.029$) followed by RSC5%ND ($p < 0.001$).

12.6. Discussion

The hypothesis was accepted that a significant increase in the surface fluoride percentage will occur following a neutral sodium fluoride application immediately after finishing the GICs. As noted in a SEM study of GICs using 1.1% neutral sodium fluoride gel, the use of a neutral sodium fluoride gel did not change in the surface roughness of FN (Ozdemir-Ozenen *et al*., 2003) and no damage to the GICs surface was noted (El-Badrawy and McComb, 1998). This was confirmed in the present *in vitro* study of the dissertation (Figure 12.1).

Figure 12.1: Percentage of fluoride before and after neutral sodium fluoride treatment (from Groups A to B)

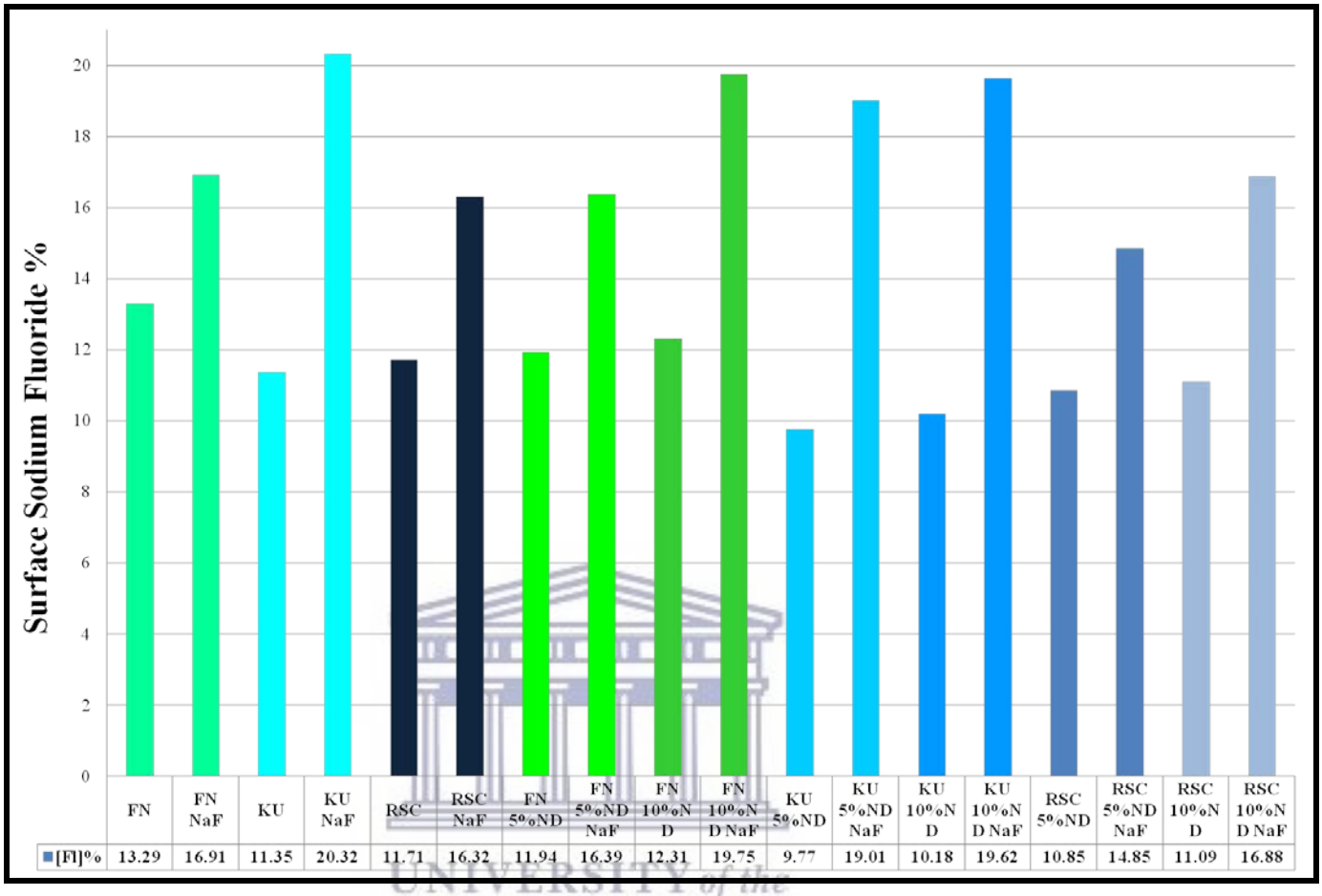

Upon further investigation of the surface (Figure 12.2) of the GICs with SEM at a greater magnification (Figure 12.3) it became clear how the neutral sodium fluoride gel interacted with the surface of the matrix and filler particles.

Figure 12.2: KU from Group B at 200X magnification

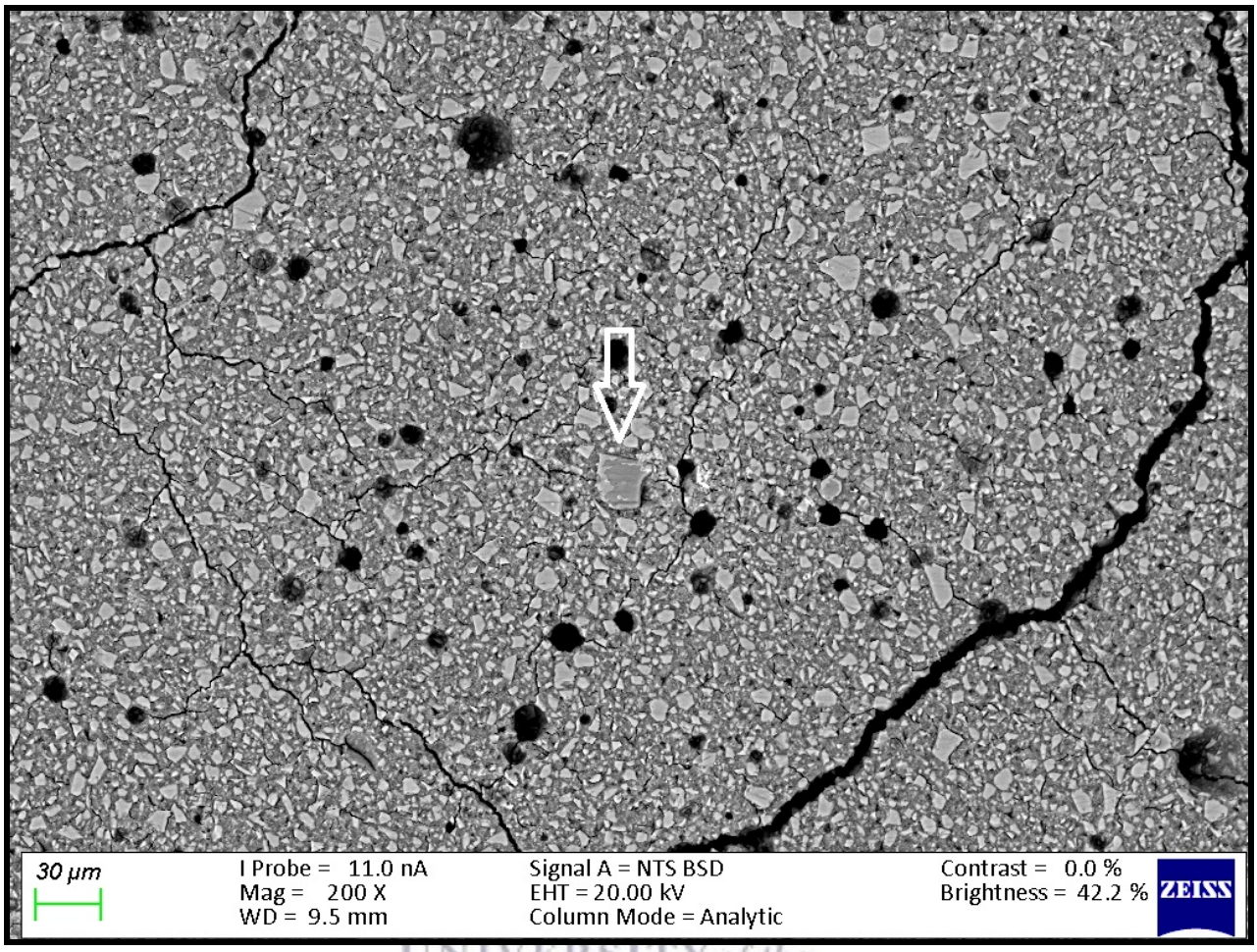

A well covered GIC surface was noted with a small film of the dried neutral sodium fluoride gel which flaked off the filler particle (Figure 12.3).

Figure 12.3: KU from Group B at 500X magnification

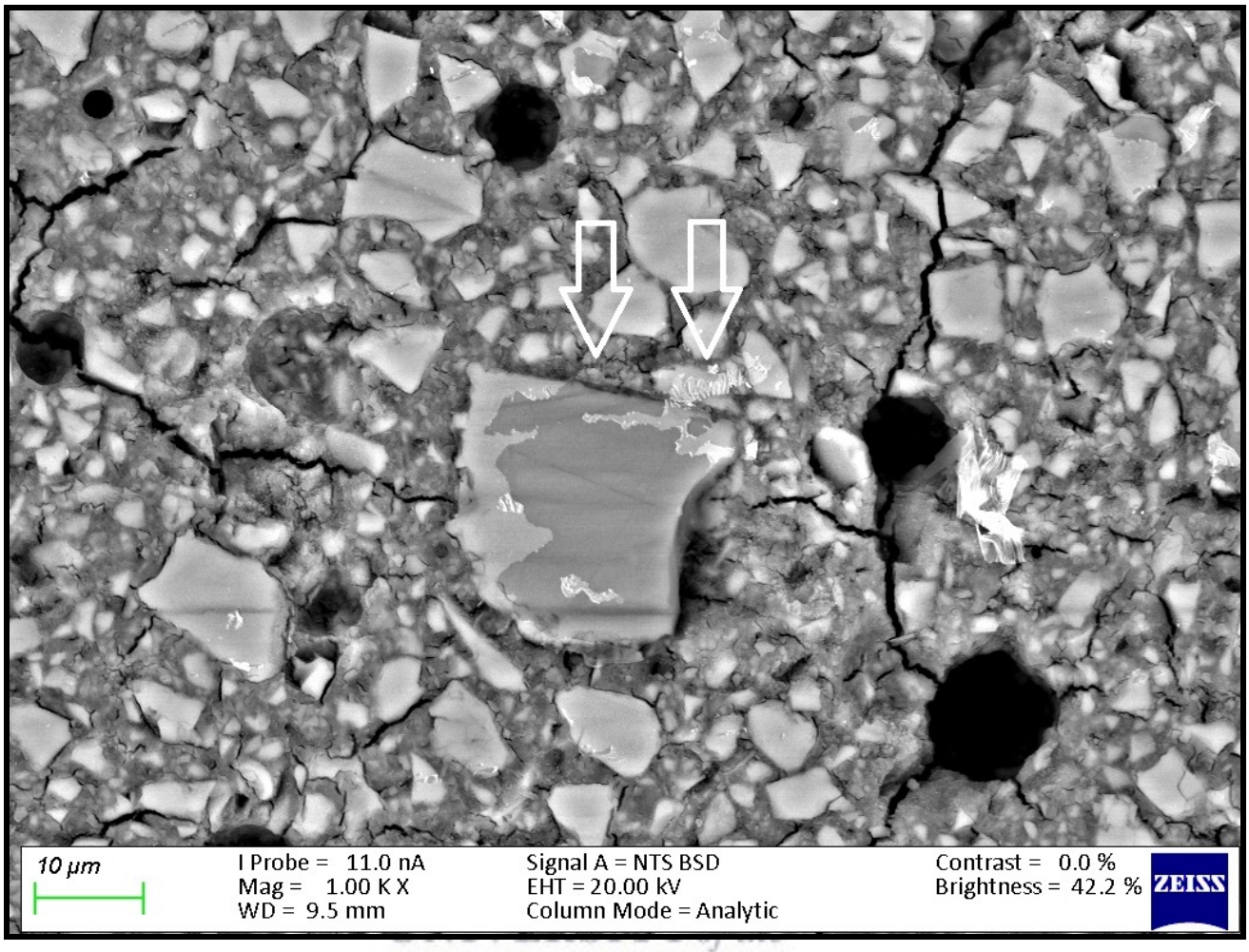

The addition of nanodiamonds to GICs is therefore more important if it is considered that the fluoride ion is able to interact and retain a greater percentage of fluoride in FN10%ND and RSC10%ND. Kealey., *et al*. (2001) illustrated that these PL-ND-G01 nanodiamond particles exposed to fluoride did not show any physical changes. The incorporation of the nanodiamond particles with the GIC powder was easily achieved, since the nanodiamond particles has a coherent scattering region size of 4nm (Figure 12.4) with an aggregate size of 5-15nm (Yakovlev *et al*., 2015) (Figure 12.5).

Figure 12.4: Nanodiamonds *PL-D-G01* particle of 4nm

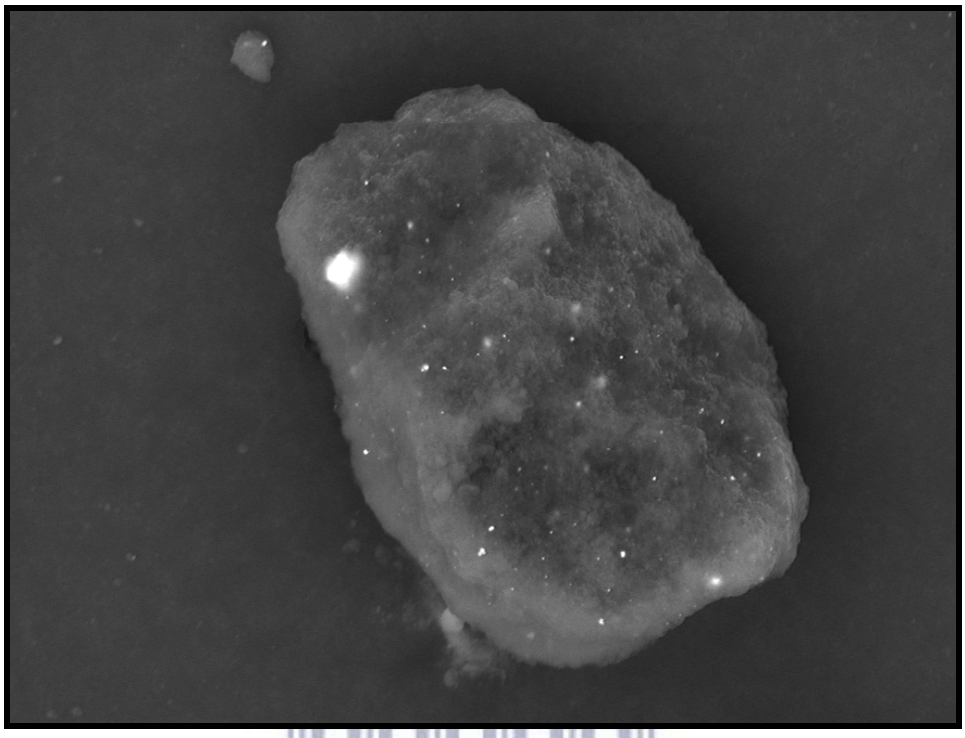

Figure 12.5: Nanodiamonds *PL-D-G01* aggregate of 5-15nm

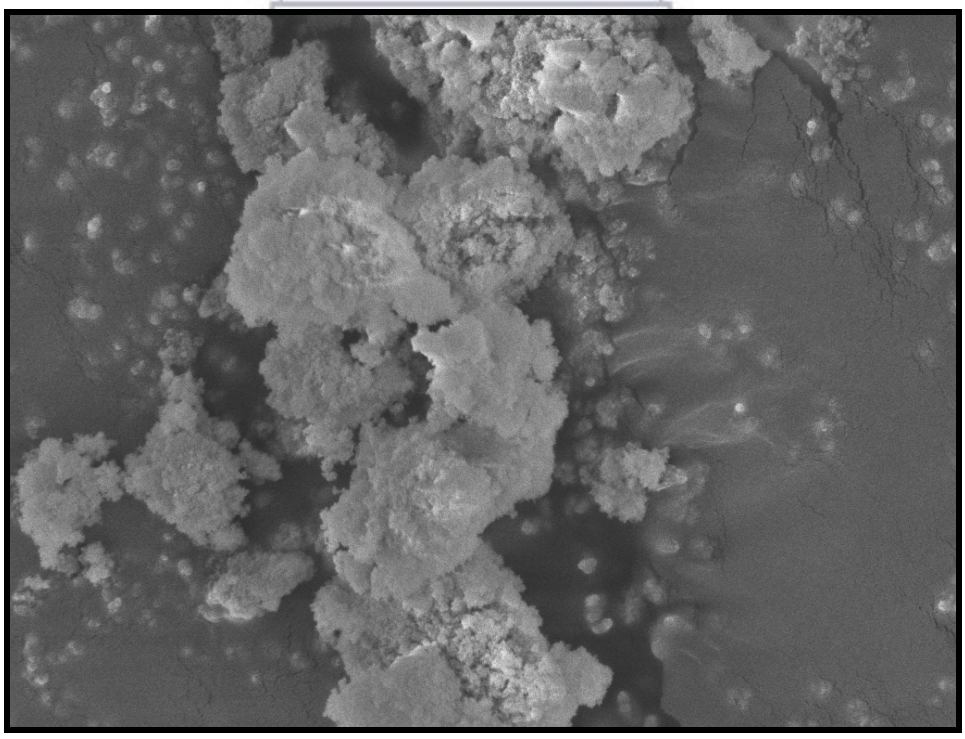

The interaction of fluoride with the nanodiamonds was considered to be favourable, since fluoride has an affinity for the graphite components of the nanodiamonds particle (Kita *et al*.,

1979) and also interacts with the van der Waals forces. Therefore, the GICs modified with nanodiamonds continuously recharge upon fluoride exposure, retaining the recharge functionality of the commercial GICs. The long-term fluoride release from GICs is mitigated through the matured matrix (Matsuya *et al*., 1996; Verbeeck *et al*., 1998). Although the commercial GICs had a significant increase in fluoride on the surface, the nanodiamond-modified GICs (with the exception of KU) illustrated a significant increase in the fluoride percentage. With this increased fluoride percentage demonstrated by all the GICs and the ND modified GICs, the gradient potential of fluoride available for release to the tooth structure and the oral environment has an important clinical application. The nanodiamond particles with its functional group also interact with the aluminium, fluoride, lanthanum, silica, sodium and strontium of the commercial GICs (Table 12.3).

Table 13.3: Elemental analysis of the surface elemental percentage of the commercial GICs of Group A

	Aluminium	Calcium	Fluoride	Lanthanum	Phosphate	Silica	Sodium	Strontium
FN	11.181	0.223	13.294	0.000	3.104	10.183	0.906	3.854
KU	8.151	0.172	11.357	2.586	2.494	10.464	1.813	2.782
RSC	9.793	0.096	11.719	0.000	2.349	9.911	1.266	3.048

This interaction of the aforementioned elements interacts during the acid-base reaction and occupies many bonding sites on the nanodiamonds. This is illustrated with the initial drop in the fluoride percentage in the nanodiamond-modified GICs compared to the commercial GICs in Group A (Figure 12.1). Fluoride is a free ion after the acid-base reaction of the maturing GICs are completed fluoride with its negative charge does however have a strong interaction with aluminium, calcium ions, sodium and strontium linked in the polyalkenoate chains of the silica matrix of the mature restoration. This interaction is why fluoride has a slow and continuous movement through the matured matrix (Wilson *et al*., 1985). The application of the neutral

sodium fluoride after the finishing of the GICs is advantageous. Even after the GICs have matured, the fluoride will be able to substitute the available terminating hydrogen (H) or hydroxyl (OH) species on the ND surface (Badea and Kaur, 2013) as the GIC absorbs moisture.

12.7. Conclusion

In order for the tooth and the restoration to benefit from the fluoride ions, it is advisable to apply neutral sodium fluoride directly after finishing GIC restorations. This is where the ND modified GICs namely FN10%ND and RSC10%ND indicated a significantly larger percentage of surface fluoride than the FN and RSC commercial material. All the ND modified GICs (besides RSC5%ND) had a larger surface fluoride percentage increase than their respective commercial materials. ND particle incorporation into GICs can therefore improve the fluoride adsorption of FN and RSC in 10% w/w integration with the GIC powder.

12.8. References

Badea, I. and Kaur, R. (2013). Nanodiamonds as novel nanomaterials for biomedical applications: drug delivery and imaging systems. *International Journal of Nanomedicine*, pp.203.

Chau, N., Pandit, S., Cai, J., Lee, M. and Jeon, J. (2015). Relationship between fluoride release rate and anicariogenic biofilm activity of glass ionomer cements. *Dental Materials*, 31(4), pp.e100-e108.

De Witte, A., De Maeyer, E. and Verbeeck, R. (2003). Surface roughening of glass ionomer cements by neutral NaF solutions. *Biomaterials*, 24(11), pp.1995-2000.

Danilenko, V. (2004). On the history of the discovery of nanodiamond synthesis. *Physics of the Solid State*, 46(4), pp.595-599.

Dolmatov, V. (2001). Detonation synthesis ultradispersed diamonds: properties and applications. *Russian Chemical Reviews*, 70(7), pp.607-626.

El Mallakh, B. and Sarkar, N. (1990). Fluoride release from glass-ionomer cements in de-ionized water and artificial saliva. *Dental Materials*, 6(2), pp.118-122.

El-Badrawy, W. and McComb, D. (1998). Effect of home-use fluoride gels on resin-modified glass ionomer cements. *Operative Dentistry*, 23(1), pp.2-9.

Forsten, L. (1990). Short- and long-term fluoride release from glass ionomers and other fluoride-containing filling materials *in vitro*. *European Journal of Oral Sciences*, 98(2), pp.179-185.

Kealey, C., Klapötke, T., McComb, D., Robertson, M. and Winfield, J. (2001). Fluorination of polycrystalline diamond films and powders. An investigation using FTIR spectroscopy, SEM, energy-filtered TEM, XPS and fluorine-18 radiotracer methods. *Journal of Materials Chemistry*, 11(3), pp.879-886.

Kita, Y., Watanabe, N. and Fujii, Y. (1979). Chemical composition and crystal structure of graphite fluoride. *Journal of the American Chemical Society*, 101(14), pp.3832-3841.

Matsuya, S., Maeda, T. and Ohta, M. (1996). IR and NMR Analyses of Hardening and Maturation of Glass-ionomer Cement. *Journal of Dental Research*, 75(12), pp.1920-1927.

Menne-Happ, U. and Ilie, N. (2013). Effect of heat application on the mechanical behaviour of glass ionomer cements. *Clinical Oral Investigations*, 18(2), pp.643-650.

Mochalin, V., Shenderova, O., Ho, D. and Gogotsi, Y. (2011). The properties and applications of nanodiamonds. *Nature Nanotechnology*, 7(1), pp.11-23.

Mulder, R. (2018). Variation in the Dispersions of Powder Liquid Ratios in Hand-Mix Glass Ionomers. *The Open Dentistry Journal*, 12(1), pp.647-654.

Nakajo, K., Imazato, S., Takahashi, Y., Kiba, W., Ebisu, S. and Takahashi, N. (2009). Fluoride released from glass-ionomer cement is responsible to inhibit the acid production of caries-related oral streptococci. *Dental Materials*, 25(6), pp.703-708.

Ozdemir-Ozenen, D., Sungurtekin, E., Issever, H. and Sandalli, N. (2003). Surface roughness of fluoride-releasing restorative materials after topical fluoride application. *European Journal of Paediatric Dentistry*, 14(1), pp68-72.

Pawluk, K., Booth, S., Coleman, N. and Nicholson, J. (2008). The kinetics of fluoride uptake from aqueous solutions by immature glass-ionomer dental cements. *Dental Forum*, 36.

Roy, S., Mitra, K., Desai, C., Petrova, R. and Mitra, S. (2013). Detonation Nanodiamonds and Carbon Nanotubes as Reinforcements in Epoxy Composites—A Comparative Study. *Journal of Nanotechnology in Engineering and Medicine*, 4(1), pp.011008.

Trairatvorakul, C., Itsaraviriyakul, S. and Wiboonchan, W. (2010). Effect of Glass-ionomer Cement on the Progression of Proximal Caries. *Journal of Dental Research*, 90(1), pp.99-103.

Verbeeck, R., De Maeyer, E., Marks, L., De Moor, R., De Witte, A. and Trimpeneers, L. (1998). Fluoride release process of (resin-modified) glass-ionomer cements versus (polyacid-modified) composite resins. *Biomaterials*, 19(6), pp.509-519.

Walls, A. (1986). Glass polyalkenoate (glass-ionomer) cements: a review. *Journal of Dentistry*, 14(6), pp.231-246.

Wasson, E. and Nicholson, J. (1993). New Aspects of the Setting of Glass-ionomer Cements. *Journal of Dental Research*, 72(2), pp.481-483.

Watson, T., Atmeh, A., Sajini, S., Cook, R. and Festy, F. (2014). Present and future of glass-ionomers and calcium-silicate cements as bioactive materials in dentistry: Biophotonics-based interfacial analyses in health and disease. *Dental Materials*, 30(1), pp.50-61.

Wehling, J., Dringen, R., Zare, R., Maas, M. and Rezwan, K. (2014). Bactericidal Activity of Partially Oxidized Nanodiamonds. *ACS Nano*, 8(6), pp.6475-6483.

Wiegand, A., Buchalla, W. and Attin, T. (2007). Review on fluoride-releasing restorative materials—Fluoride release and uptake characteristics, antibacterial activity and influence on caries formation. *Dental Materials*, 23(3), pp.343-362.

Wilson, A., Groffman, D. and Kuhn, A. (1985). The release of fluoride and other chemical species from a glass-ionomer cement. *Biomaterials*, 6(6), pp.431-433.

Xie, D., Brantley, W., Culbertson, B. and Wang, G. (2000). Mechanical properties and microstructures of glass-ionomer cements. *Dental Materials*, 16(2), pp.129-138.

Yakovlev, R., Osipova, A., Solomatin, A., Kulakova, I., Murav'eva, G., Avramenko, N., Leonidov, N. and Lisichkin, G. (2015). An approach to unification of the physicochemical properties of commercial detonation nanodiamonds. *Russian Journal of General Chemistry*, 85(6), pp.1565-1574.

Zhang, W., Patel, K., Schexnider, A., Banu, S. and Radadia, A. (2014). Nanostructuring of Biosensing Electrodes with Nanodiamonds for Antibody Immobilization. *ACS Nano*, 8(2), pp.1419-1428.

CHAPTER 13

CONCLUSION AND RECOMMENDATIONS

Chapter 2 confirmed the result from the literature that the clinician can increase the surface hardness of a GIC by applying the heat set technique with a LED curing unit. A command set can be achieved with the electronic piezo or the air piezo. However a new contribution to the literature was that the air piezo and finger pressure will not increase the surface hardness. A profound discovery was that combining the electronic piezo with a setting above 17Hz followed by heat generated with a LED curing light will significantly reduce the surface hardness of a GIC.

Chapter 3 highlighted that although the powder/liquid ratio in the GIC and carbomer capsules are not exactly as the manufacturers indicate on the side of the packaging, the variation does not affect the surface micro-hardness (Vickers Hardness) or the compressive strength significantly.

Chapter 4 explored the variability in hand-mix GIC dispensing of the powder and liquid ratios. The final conclusion was that it is relatively rare that the clinician can dispense the powder/liquid ratio as recommended by the manufacturer. Due to the possibility of the variation in the GIC powder and liquid dispensing, the clinician should focus on the consistent dispensing of especially the liquid. There should be no air bubbles in the dispensed drop. For this reason it was advised that for dental material research an analytical balance should be used to dispense the material in the prescribed ratio, to ensure the validity of the powder/liquid ratio. This was further confirmed in Chapter 5 where it was shown that the manufacturers' recommendations achieved significantly higher compressive strength values than those obtained based on the "preferences" of the clinician to have a "smooth" yet "workable mix", as these concepts are subjective between clinicians. The acceptable variation of the powder/liquid ratio of ±10% from the manufacturer's recommendation has been found to be acceptable.

Chapter 6 coined the term “popcorn effect” where the GIC powder encapsulates the chitosan completely. This resulted in the liquid from the GICs not immediately interacting with the chitosan and dissolving it to expose the protonated properties of chitosan. These protonated properties of nano-chitosan have been cited to have a strong bond with the GIC matrix. As a direct result of using the manufacturer supplied chitosan particles without modification in this dissertation, the chitosan-modified GICs presented with the lowest compressive strength, proportional limit and surface micro-hardness values.

Overall, the nanodiamond particles either had no significant differences with their respective control materials although the compressive strength (CS) test resulted in only FN, KU, RSC, FN10%ND and KU5%ND retaining a compressive strength above 100MPa. This is essential to conform to the ISO 9917-1, 2007 of a minimum of 100MPa compressive strength. Based on the water contact angle (θ) below 65º and the calculated water adhesion tension (τ^o) above 30dyn/cm, FN and KU with their respective chitosan and nanodiamond modifications were all hydrophilic. RSC and its nanodiamond modifications were hydrophobic. The KU and RSC contact angle and water adhesion tension has never been reported on in the literature.

Chapter 7 investigated the ion release from GICs. It is a neglected part of GIC research, based on the very limited number of studies that have assessed it. The ion release of KU has never been assessed and the result indicated no significant difference after 24 hours for aluminium, silicon and strontium ions from FN and RSC. The nanodiamonds followed by chitosan, presented with a greater ion release than the control materials. The release of these ions was essential to highlight the shortcomings of fluoride analysis.

Chapter 8 continued with the fluoride release assessment of the control materials and the chitosan and nanodiamond modifications. A critical review of the available literature on fluoride release from glass ionomers highlighted that only a handful of authors reported on the pH of the GIC-diluents combined with their TISAB of choice. The free fluoride was determined to be

inaccurate for most materials. This was due to the pH being above 8.1, so hydroxide interferences play a role with the mV reading obtained from the fluoride ion selective probe. If the free fluoride were to be determined it would need to be buffered to 8.1. The volume of liquid added to buffer the GIC diluent must be recorded and the parts per million need to be calculated based on the original volume of diluent. As the GIC-diluents were assessed for their fluoride content for use with TISAB III, it presented as the better medium for the de-complexing of fluoride. Although the pH was correct between 5 and 5.5 to eliminate interferences from the hydroxide and hydrogen ions, the ionic strength and low aluminium de-complexing capacity made fluoride assessment inaccurate. TISAB IV was initially thought to solve the aluminium de-complexing problem, but the pH above 8.1 presented with interfering hydroxide ions. As the total fluoride could not be accurately determined and most of the free fluoride values were incorrect, the true de-complexed fluoride could not be determined. This leads the author of the dissertation to agree with Frenzel and Bratter, (1986) that the buffering of the TISAB IV/GIC-diluent mixture down to a pH where the hydroxides will not interfere, defeats the objective of the high aluminium de-complexing. In addition to the pH and the de-complexing of aluminium, other ions like lanthanum, silicon, sodium and strontium can all to some extent influence the ionic strength. It is the conclusion from this chapter that TISAB III and IV are not ideal for determining the total fluoride concentration in GICs. For truly accurate GIC fluoride determination, the development and assessment techniques as pioneered by Frenzel and Bratter, (1986) should be used to further investigate the diluent ion concentrations and their influence on the ionic strength that cannot be buffered completely by TISAB III and TISAB III. Until then, TISAB II and TISAB III are the buffer/chelating agents of choice although the fluoride content due to 1) aluminium not being de-complexed could result in an underestimation of the fluoride or 2) over-estimation of the fluoride due to ionic strength (that could not be stabilised by the TISAB II or III) interferences on the selective fluoride ion probe.

Chapter 9 indicated that the GIC-diluents made by allowing the GICs to elude their ions into the DMEM growth medium was a reproducible indirect contact assessment with 3T3 cells. Biodentine as the positive control presented with significant growth for all the diluent time periods. FN was the most consistent in maintaining positive cell viability and even performed better than Biodentine. KU and RSC have never been assessed for cell viability and for RSC the diluent produced for day 7 presented with a non-significant reduction in cell viability compared to the 3T3 control cells. KU presented with a non-significant reduction in cell viability compared to the 3T3 control cells for the diluent of day 1. The diluents from days 7 and 21 on the other hand presented with greater cell viability than all the materials accept for FN (day7). The use of 5% nanodiamonds presented with an overall acceptable cell viability for FN and KU in relation to the FN and KU control materials, but RSC should not be modified with nanodiamonds due to reduced cell viability.

Chapter 10 showed that the *S. mutans* growth did not differ between the chitosan and nanodiamond modifications of the three control GICs. The chitosan and nanodiamond modifications did not have a significant reduction in *S. mutans* growth compared to their respective control materials. The lowest bacterial growth was noted for FN followed by KU. Although the surface roughness of the GICs (due to 24 hours of *S. mutans* growth) did not change after 24 hours for FN, KU and RSC materials or their nanodiamond modifications, the SEM images illustrated clearly that the chitosan and the nanodiamond modifications disrupted the biofilm and changed the surface adherence as well as the quorum grouping of the *S. mutans.* Degradation of the chitosan particles occurred and the swelling disrupted the surface of the chitosan-modified GICs.

Chapter 11 assessed the gradient weight percentage of the FN, KU and RSC materials to determine of what their gradient potential was. The study further showed that a large gradient potential did not translate into the most ion movement into the dentine. A novel technique was

presented in this Chapter where a single primary molar was used for the study in order to eliminate the variability of the ion movement due to calcium and phosphorous differences between teeth. For fluoride retention in the GIC, a surface protective layer would be advantageous to retain the fluoride in the GIC and allow a greater gradient potential percentage to move into the dentine. The diffusion of fluoride documented in this study further indicated that fluoride cannot act alone when it comes to protecting the primary tooth due to the low to no fluoride penetration. The other ions like aluminium, strontium, sodium and lanthanum all penetrated the tooth structure to a much deeper penetration. Fluoride presented with a very poor penetration into the primary tooth, compared to the other ions released from the GICs. The conclusion was that the fluoride was predominantly in fact a free ion that released into the moist filter paper. The fluoride that entered into the tooth structure was therefore the fluoride complexed to the aluminium, strontium, silicon and lanthanum ions. This Chapter illustrated that all the ions in the GIC play a role in the diffusion of the ions from the GICs into healthy dentine. The study by Ngo *et al*., (1997 and 2007) detected strontium ions in the demineralised and the decomposed dentine. This Chapter indicated that strontium and other ions can diffuse into the healthy dentine. With regard to the nanodiamond modification of the three GIC control materials, the ion interaction with the tooth structure for FN5%ND, KU5%ND and RSC10%ND were preferable to their respective control materials.

Chapter 12 correlated with the established literature that GICs had the ability to absorb the neutral sodium fluoride gel immediately after finishing. This increase in fluoride significantly increased the fluoride percentage in the surface layer of the restoration. For the three control materials the surface fluoride for KU was significantly greater than FN and RSC. The 5% nanodiamond modifications did not present with a significant increase in the surface fluoride in

relation to their respective control materials after the neutral sodium fluoride was applied to the nanodiamond-modified GICs.

Concluding remarks

The recommended powder liquid ratio of the manufacturer should be used for nanodiamond and chitosan modifications in order to obtain the largest compressive strength. Overall, chitosan as supplied by the manufacturer is not suitable for restorative treatment due to the low physical properties achieved in this dissertation. The nano-chitosan modifications and chitosan modification in the liquid is a more viable technique for incorporating chitosan into the GICs as cited in this dissertation.

Overall, the 5% nanodiamond modifications presented with physical properties close to that of the control and for that reason the 10% nanodiamond modification is not a suitable modification. The cell viability was increased and the biofilm integrity disrupted with GICs that contained a 5% nanodiamond modification. The 5% nanodiamond addition presented with an ion release (aluminium, lanthanum, silicon, sodium and strontium) into the de-ionised water that increased significantly for most ions in KU and RSC, but no significant difference was demonstrated for FN. The fluoride release as assessed with TISAB III in the GIC-diluents of DMEM liquid was improved for KU and RSC with a 5% nanodiamond modification but no significant effect for the fluoride release of FN. The ion movement into the healthy dentine for the 5% nanodiamond-modified materials presented with the highest weight percentages of each ion for all three GIC materials (FN, KU and RSC). The surface fluoride percentage increased for the 5% nanodiamond GICs, but did not increase the surface fluoride percentage significantly in relation to their control materials.

There is no perfect material but there are advantages to FN and RSC with the inclusion of 5% nanodiamonds depending on the various results considered in this dissertation and the intended

rationale for use of he material. But, it is the conclusion of the author that based on the following categories: physical properties, all the ions released, cell viability compared to the control 3T3 cells, *S. mutans* biofilm disruption and the ion movement from the 5% nanodiamond GIC into the dentine, only KU5%ND is a viable option as a restorative material. This 5% nanodiamond modification of KU meets all the needs for an improvement of the above-mentioned categories. The only current disadvantage would be the greyer appearance of the material and whether that is acceptable to the patient.

Turnitin report

Similarity of 19% of the dissertation as a whole.

The full reference lists accounted for 3% and the published article of Chapter 4 for 3% of the 19%. Therefore, the final similarity could be considered to be 13%.